Investigation of circulating biomarkers in combination with computer tomography (CT) and magnetic resonance imaging (MRI) markers to improve diagnosis of ischaemic stroke

Meaad Mohammed A Almusined

Submitted in accordance with the requirements for the degree of Doctor of Philosophy.

The University of Leeds

School of Medicine and Health

December 2022

Intellectual Property and Publication Statements

The candidate confirms that the work submitted is her own and that appropriate credit has been given where reference has been made to the work of others.

Acknowledgements

First and foremost, I thank and worship God for the inexhaustible blessings he has bestowed upon me. I am grateful to him for giving me the courage, patience, and power to finish what I started, as well as for tolerating me to get to where I am. I would like to thank all my supervisors; Professor Sikha Saha, Professor Steven Sourbron and Professor Tufail Patankar.

My first and deepest appreciation goes to my wonderful supervisor, Professor Sikha Saha, for admitting me as a PhD student in her lab. I would like to thank her for leading me through my PhD, as well as for her advice and guidance. She was always there for me during both my professional and personal matters. I sincerely thank her for giving me this opportunity to conduct this project. She was always kind when I knocked on her door with a question, and I appreciated her tolerance and understanding while I revised my thesis. The completion of my PhD could not have been possible without her guidance. I am really grateful for Professor Sikha Saha who was the leader of my project besides being the main supervisor. She taught me a variety of techniques such as immunohistochemistry staining, cell counting, participated in the design of the experiments, and taught me presentation skills, in addition to her time and effort and comments on my thesis. Professor Sikha Saha is the ideal example of a good scientist who is also kind and generous.

I am really grateful to Professor Steven Sourbron for being one of my wonderful supervisors. He taught me how to use PMI software, which I used for CT and MRI data analysis, in addition to his time, effort, and comments on the imaging chapters of my thesis. I thank him for all of his help during my PhD and for his insightful remarks on my thesis. Thanks to Professor Tufail Patankar for being one of my finest supervisors. I am grateful to him for his kindness, understanding and support.

I would like to express my gratitude to Professor Laura Hardie, my postgraduate teacher, for her kind assistance during my PhD.

My heartfelt thanks go to Miss Helen McPherson for teaching me ELISA.

I would like to thank Dr Neil Turner for helping me with the ELISA data analysis, Dr Fiona Platt, who taught me how to use the cryostat and Dr Hema Viswambharan for all her help with the western blot work.

My sincere thanks to Dr Nadira Yuldasheva for providing me with mice brain tissues and mice blood samples.

My sincere thanks to the Stroke Centre Surgery Core, Department of Neurosurgery, University of Kentucky in the USA, for the collaboration in providing me with middle cerebral artery occlusion (MCAO) mice brain tissues and mice blood samples.

My sincere thanks to Dr Darren Greenwood for his help in correlation data analysis.

My heartfelt thanks go to the Neurosciences Clinical Research Team for stroke in Leeds Teaching Hospitals; Dr Ahamad Hassan, Dr Kirti Kain, Prof. Tufail Patankar, Linetty Makawa, Nathan Douglas, Michelle Simpson, Emelda Veraque for all the help and support in my cross-sectional clinical study.

I would like to thank all my colleagues in Professor Sikha Saha's group namely Dr Tarun Kakkar, Dr Pragati Kakkar, Dr Padmaja Vasudev for their helps and supports during my PhD period. Working in this group has been a fantastic experience. I am really grateful for every encouraging word they said to me. In simple words, they were always there whenever I needed them. I would like to thank Dr Tarun Kakkar and Dr Pragati Kakkar for helping me with the proofreading of my thesis.

I would like to thank all my friends, Dr Sumia Bageghni, Dr Naima Endesh, Dr Heba Shawer, Basmah Asayejh, Reem Alotaibi, Altaf Almutairi, Rawan Abuzinadah, and Ghadir Alkarithi, for their unwavering support during the challenging period of completing my thesis.

I would like to express my gratitude to all LICAMM members for any and all assistance they may offer in the lab.

My research would have been impossible without the aid and support of my sponsor King Saud University in Riyadh and Saudi Cultural Bureau in London.

I would like to express my special thanks to my husband Abdulaziz, for whom I cannot express my gratitude and appreciation in simple words for supporting me, always being by my side and providing constant encouragement to reach the highest peak throughout my research period. He is my closest friend, my loudest supporter and a wonderful husband and parent. Without him, I would not have been able to finish this journey; I would not have the same level of optimism; I would not have reached this level of success; I would be lost without his help and support. Thank you for your

patience and understanding. Thank you for always believing in me and helping me achieve my goals. Thank you for all your wise input, for always making me laugh, and for the countless little things you did to make me happy. I am thankful to him for all he has sacrificed to make me complete my studies. He has been with me throughout this incredible adventure.

I would also like to thank my kids; Faisal and Aljawharah, who had to deal with all the difficult times away from home, family and friends. I was busy, stressed and moody all the time, but they were there for me.

Finally, for my parents; Mohammed and Qumashah, there are no words to express how grateful I am for all of their love and even financial assistance. Thank you for their blessings, support and encouragement. Thanks for believing in me and helping me achieve my dreams. By earning my degree, I hope to bring joy to their hearts and smiles to their lips. My brother Dr. Mohannad, Mutaz, and Majd, as well as my sister Mada, for their unwavering encouragement and support throughout my PhD journey.

I'll never forget to appreciate my Husband's family for their blessings and support.

Last but not least, thank you to any other members of my family or friends who might wish me the best of luck.

Publications and presentations

Publications

- Investigation of blood-brain barrier proteins as potential biomarkers in a murine model of ischaemic stroke

Meaad Almusined[1], Nadira Y Yuldasheva[2], Hema Viswambharan[2], Pragati Kakkar[2], Tarun Kakkar[2], Sikha Saha[1](to be submitted to JCI insight journal)

- Circulating biomarkers in differentiating ischaemic stroke from mimics

Meaad Almusined[1], Pragati Kakkar[1], Tarun Kakkar[1], Linetty Makawa[1,2], Kirti Kain[2], Ahamad Hassan[2], Tufail Patankar[2], Sikha Saha[1](to be submitted to Stroke AHA journal)

Oral Presentations

- Investigation of blood brain barrier damage in stroke

Meaad Almusined, Nadira Y Yuldasheva, Sikha Saha

The 12th MCRC Retreat Webinar, Leeds Cardiovascular Research, Leeds, UK, 2020.

Poster Presentations

- Investigation of blood brain barrier damage in a murine model of Stroke

Meaad Almusined, Nadira Y Yuldasheva, Sikha Saha

11th MCRC Retreat, Leeds Cardiovascular Research, Glenridding, UK, 2019.

(Best poster Award)

- Investigation of blood brain barrier damage in a murine model of Stroke

Meaad Almusined, Nadira Y Yuldasheva, Sikha Saha

27th Northern Cardiovascular Research Group Meeting, Leeds, UK, 2019.

- Investigation of blood brain barrier damage in a murine model of Stroke

Meaad Almusined, Nadira Y Yuldasheva, Sikha Saha

Showcase Poster Conference Leeds, UK, 2019.

- Investigation of blood brain barrier damage in a murine model of Stroke

Meaad Almusined, Nadira Y Yuldasheva, Sikha Saha

The Faculty of Medicine & Health Postgraduate Researcher Conference, Leeds, UK, 2019.

- Investigation of blood brain barrier damage and changes in amyloid beta peptide in a murine model of cerebral ischaemia

Meaad Almusined, Mohammad Ali, Nadira Y Yuldasheva, Sikha Saha

The Alzheimer's Research UK(ARUK)Yorkshire Regional Meeting, Bradford, UK, 2019.

- Can quantitative CT perfusion improve prediction of outcomes after mechanical thrombectomy? A cross-sectional pilot study.

Meaad Almusined, Tufail Patankar, Sikha Saha, Steven Sourbron

British Society of neuroradiologist Annual Conference, Cardiff, UK, 2019.

- Investigation of pericytes on blood brain barrier damage after Stroke

Meaad Almusined, Mosan Rashid, Nadira Y Yuldasheva, Sikha Saha

Leeds Doctoral College Showcase, Leeds, UK, 2020.

- Circulating biomarkers in differentiating stroke from stroke mimics

Meaad Almusined, Pragati Kakkar, Tarun Kakkar, Linetty Makawa, Kirti

Europhysiology 2022 Conference, Copenhagen, Denmark, 2022.

Abstract

Background: The current diagnosis of stroke remains largely clinical but widely used stroke scoring systems do not allow differentiation between stroke patients and mimics (e.g., migraine, seizures). Computed tomography (CT) can confirm haemorrhage, but many patients with suspected stroke are subsequently found to have alternative pathologies. Magnetic resonance imaging (MRI) distinguishes between acute strokes and mimics, but the majority of patients do not tolerate longer scanning time. Recently, the blood biomarker strategy showed a promising diagnostic method, however, there are limited studies examining circulating biomarkers in acute stroke patients compared to mimics as defined by both neurological scores and imaging data.

Hypothesis: The combination of circulating biomarkers in acute stroke patients with neurological scores, CT and MRI data can improve the diagnosis of stroke.

Methods: Two murine stroke models were used to examine cellular and blood brain barrier (BBB) tight junctional (TJ) markers in the brain by immunohistochemistry and western blotting and assess circulatory biomarkers by ELISA. The serum biomarker levels were measured in stroke patients and mimics identified by both neurological scores and imaging data.

Results: Neuronal, glial cell and BBB damage in the brain and changes in circulatory biomarkers were observed in stroke mice compared to shams. The clinical study showed the levels of glial fibrillary acidic protein (GFAP), Neurofilament light chain (NfL) and TJ proteins can differentiate between strokes and mimics. GFAP level is correlated with CT data and Neuron-specific enolase level is correlated with MRI data.

Conclusion: The preclinical studies for the first-time demonstrated brain damage together with changes in circulatory markers in two murine models of stroke. The novel clinical study confirmed the preclinical results and suggested that biomarkers in combination with stroke scales and imaging might offer valuable tools for differentiation between ischaemic stroke and mimics and assessing the severity of ischaemic stroke.

Table of Contents

Acknowledgements ..... **II**

Publications and presentations ..... **V**

Abstract ..... **VII**

Table of Contents ..... **VIII**

List of Figures ..... **X**

List of Tables ..... **XXXI**

List of Abbreviations ..... **XXXIII**

Chapter 1 Introduction and background **1**

1.1 General background 5

1.2 Hypothesis 48

1.3 Aim 48

1.4 Objectives 48

Chapter 2 Materials and methods **50**

2.1 Preclinical study 50

2.2 Clinical study (retrospective study- pilot study) 64

2.3 Clinical study (Cross sectional study) 68

Chapter 3 Results - Biomarkers in preclinical models **78**

3.1 Changes in neuronal, glial cell and blood brain barrier proteins in bilateral common carotid artery occlusion (BCCAO) 79

3.2 Changes in neuronal, glial cell and blood brain barrier proteins in middle cerebral artery occlusion (MCAO) 134

Chapter 4 CT and MRI imaging biomarkers in clinical samples **186**

4.1 Retrospective study - Can quantitative CT and MRI biomarkers improve the prediction of outcomes after mechanical thrombectomy? A cross-sectional pilot study 186

Chapter 5 Biomarkers in clinical samples **207**

5.1 Cross-Sectional study – Comparison of circulating biomarkers between stroke and stroke mimics 207

5.2 Cross sectional study - Comparison of CT and MRI imaging biomarkers between stroke and stroke mimics 222

5.3 Cross sectional study – Added value of imaging biomarkers to circulating biomarkers for improving stroke diagnosis 240

Chapter 6 Discussion, conclusions and future work **263**

6.1 Overview on the results 263

6.2 General Discussion 266

6.3 Final Conclusions 278
6.4 Project limitations..... 278
6.5 Clinical relevance and future direction 280
References..... 282
Chapter 7 Appendices 318

List of Figures

Figure 1.1 Schematic diagram of current clinical pathway for suspected stroke starting from time of stroke onset until treatment and outcomes (Dias et al., 2021). IS—ischaemic stroke; HS—haemorrhagic stroke; CSC—Comprehensive stroke centre; mRS—modified Rankin Score: functional outcomes score. 2

Figure 1.2 The two categories of stroke (Heart & Stroke, 2022)..... 5

Figure 1.3 Diagrammatic representation of circle of Willis, adopted from (Ashish, 2017)..... 7

Figure 1.4 Schematic diagram of the mechanisms of Stroke, information adopted from (Lo et al., 2003). 10

Figure 1.5 The cell types within the BBB. PC: pericytes, AE: astrocytes, EC: endothelial cells and TJ: tight junction (Daneman and Prat, 2015).11

Figure 1.6 A CT scanner (The Leeds Teaching Hospitals, 2022)..... 14

Figure 1.7 Representative cross-sections through the brain, adopted from (My-MS.org, 2022). 15

Figure 1.8 An illustration of the basic principle of CT (The Leeds Teaching Hospitals, 2022)..... 15

Figure 1.9 An MRI scanner (The Leeds Teaching Hospitals, 2022)..... 18

Figure 1.10 An illustration of interventional therapy (MT) for the treatment of an ischaemic stroke patient , information adopted from: (CIRSE, 2022). 21

Figure 2.1Schematic diagram for cerebral ischaemia induction using transient BCCAO model. The arterial scheme was adopted from (León-Moreno et al., 2020)..... 51

Figure 2.2 Schematic diagram for production of cerebral ischaemia with transient (1 h) MCAO model. (The arterial scheme was adopted from (Rousselet et al., 2012). ECA: external carotid artery, ICA: internal carotid artery, MCA: middle cerebral artery and PPC: pterygopalatine artery. 52

Figure 2.3 A)The level of extracted sections in the project (adapted from the Mouse Brain Library (The Mouse brain Library, 2003), (B) Dorsal view of a stroke model and a control model and (C) Frontal view of a stroke model and a control model..... 53

Figure 2.4 A diagram of the patient selection criteria. (mRS): modified Rankin Score which is functional outcomes score..... 64

Figure 2.5 Flow diagram of the Design of the Study and patients' Routine Clinical pathways. 68

Figure 2.6 Blood sample collection tubes. From left to right: a gel clot active tube, heparin tube, sodium citrate tube, EDTA tube and acid citrate dextrose tube (Fisher Scientific, 2022)..... 71

Figure 2.7 An initial CT head at two different levels, (left: basal ganglia level) and (right: corona radiata level). Both images show where a 10 ASPECTS ROIs are drawn manually. Right side areas (solid outline) represent the ischaemic side while the left areas (dashed outline) represent the non-ischaemic one. L = lentiform nucleus; C = caudate head; I = insular ribbon; IC = internal capsule; M1 = anterior MCA cortical region; M2 = MCA cortical region located lateral to insular ribbon; M3 = posterior MCA cortical region; M4, M5 and M6 about 2 cm superior to M1, M2, and M3 ROIs respectively. 75

Figure 2.8 This ADC image shows where the ROIs in WM& GM are drawn. Right side areas (solid outline) represent the ischaemic side while the left areas (dashed outline) represents the non-ischaemic side.... 76

Figure 3.1 Representative photomicrographs showing cresyl violet staining of neuron cell nuclei in the hippocampus in control (A) and BCCAO (B) brains. The staining shows chromatolytic changes in the stroke brain compared to the control brain due to cellular damage following BCCAO induced stroke (arrowheads). (Scale bar=20um). (The images are taken at the level of Bregma -2.06mm). 80

Figure 3.2 Representative photomicrographs showing immunofluorescence staining of NeuN labelled cell nuclei in the M1 motor cortex (A-B), M2 motor cortex (C-D), granular insular Cortex (E-F), 2nd somatosensory cortex (G-H) and hippocampus (CA1) (I-J) of control (left column) and BCCAO stroke brains (right column). NeuN labelled cells are fewer in stroke models than in the controls due to neuronal cells death following stroke (arrowheads). (Scale bar=50um). (The images are taken at the level of Bregma 1.54 or -2.06mm). (Slice thickness=50um)..... 82

Figure 3.3 Representative photomicrographs showing immunofluorescence staining of NeuN labelled cell nuclei in the M1 motor cortex (A-B), M2 motor cortex (C-D) ,granular insular Cortex (E-F), 2nd somatosensory cortex (G-H) and hippocampus (CA1) (I-J) of control (left column) and BCCAO stroke brains (right column). NeuN labelled cells are fewer in stroke mice than in the controls due to neuronal cells death following stroke (arrowheads). (Scale bar=50um). (The images are taken at the level of Bregma 1.54 or -2.06mm). (Slice thickness=20um)..... 83

Figure 3.4 Quantitative analysis shows significant differences (*p< 0.05, **p ≤ 0.01, ****p ≤ 0.0001-Unpaired Student's t-test, n=6) in the number of NeuN-positive nuclei between sham-operated and BCCAO stroke mice in the M1 motor cortex(A-B, p=0.0019), M2 motor cortex (C-D, p= 0.0024), granular insular cortex (E-F, p=0.0194), 2nd somatosensory cortex (G-H, p=0.0019) and hippocampus (CA1) (I-J, p<0.0001)..... 85

Figure 3.5 Representative photomicrographs showing immunofluorescence staining of GFAP labelled astrocytes in the hippocampus area of control (A, C) and BCCAO stroke (B, D) brains. The GFAP labelled cells and processes are thicker and higher in number in stroke mice than in the controls due to astrocytes activation following stroke (arrowheads). (Scale bar=50um:A,B and 20um:C,D). (The images are taken at the level of Bregma -2.06mm). (Slice thickness=50um). 86

Figure 3.6 Representative photomicrographs showing immunofluorescence staining of GFAP labelled astrocytes in the hippocampus area of control (A, C) and BCCAO stroke (B, D) brains. The GFAP labelled cells and processes are thicker and higher in number in stroke mice than in the controls due to astrocytes activation following stroke (arrowheads). (Scale bar=50um:A,B and 20um:C,D). (The images are taken at the level of Bregma -2.06mm). (Slice thickness=20um). 87

Figure 3.7 Quantitative analysis shows significant increases (p ≤ 0.01, ***p ≤ 0.001- Unpaired Student's t-test, n=6) in the number of GFAP labelled astrocyte cells (A-B, p=0.0036) and profiles processes (C,D-p=0.0003) in BCCAO mice compared to sham in hippocampus (CA1). 88**

Figure 3.8 Representative photomicrographs showing immunofluorescence staining for PDGFR with anti-PDGFR and Alexa488 conjugated secondary antibodies with DAPI stained nuclei in the hippocampus area in sham (A, C, E) and BCCAO stroke brains (B, D, F). The labelled pericytes show morphological changes with some dilatation and loss in the stroke brain (arrowheads) compared to control (arrows). (Scale bar=50um:A,B and 20um:C,D,E,F). (The images are taken at the level of Bregma -2.06mm). (Slice thickness=20 um). 90

Figure 3.9 Representative photomicrographs showing immunofluorescence staining for PDGFR with anti-PDGFR and Alexa488 conjugated secondary antibodies with DAPI stained nuclei in the cortex in sham (A, C, E) and BCCAO stroke brains (B, D, F). The labelled pericytes show morphological changes and some loss in the stroke brain (arrowheads) compared to control (arrows). (Scale bar=50um:A,B and 20um:C,D,E,F). (The images are taken at the level of Bregma 1.54mm). (Slice thickness=50 um). 91

Figure 3.10 Quantitative analysis shows significant differences (**p ≤ 0.0001- Unpaired Student's t-test, n=6) in the number of PDGFR positive pericytes between sham-operated and stroke mice in the hippocampus (****p<0.0001)..... 92**

Figure 3.11 Representative photomicrographs showing immunofluorescence staining for NG2 with anti-NG2 and Alexa488 conjugated secondary antibodies with DAPI stained nuclei in the hippocampus area in sham (A, C, E) and BCCAO stroke brains (B, D, F). The labelled pericytes show morphological changes with some loss and dilatation in the stroke brain (arrowheads) compared to control (arrows). (Scale bar=50um:A,B and 20um:C,D,E,F). (The images are taken at the level of Bregma -2.06mm). (Slice thickness=20 um). 93

Figure 3.12 Representative photomicrographs showing immunofluorescence staining for NG2 with anti-NG2 and Alexa488 conjugated secondary antibodies with DAPI stained nuclei in the cortex in sham (A, C, E) and BCCAO stroke brains (B, D, F). The labelled pericytes show morphological changes with some loss and dilatation in the stroke brain (arrowheads) compared to control (arrows). (Scale bar=50um:A,B and 20um:C,D,E,F). (The images are taken at the level of Bregma 1.54mm). (Slice thickness=50 um). 94

Figure 3.13 Quantitative analysis shows significant differences (**p ≤ 0.0001- Unpaired Student's t-test, n=6) in the number of NG2 positive pericytes between sham-operated and stroke mice in the hippocampus (****p<0.0001)..... 95**

Figure 3.14 Representative photomicrographs showing immunofluorescence staining for IBA-1 using anti-IBA-1 in the hippocampus area of control (A, C) and stroke (B, D). The IBA-1 labelled cells and processes are more in stroke mice than in the controls following stroke (arrowheads). (Scale bar=50um:A,B and 20um:C,D). (The images are taken at the level of Bregma -2.06mm). (Slice thickness=20 um). 96

Figure 3.15 Representative photomicrographs showing immunofluorescence staining for IBA-1 using anti-IBA-1 in the cortical area of control (A, C) and stroke (B, D). The IBA-1 labelled cells and processes are more in stroke mice than in the controls following stroke (arrowheads). (Scale bar=50um:A,B and 20um:C,D). (The images are taken at the level of Bregma 1.54mm). (Slice thickness=50 um)..... 97

Figure 3.16 Quantitative analysis shows the significant differences (p ≤ 0.01, ***p ≤ 0.001, - Unpaired Student's t-test, n=6) in the number of IBA-1 positive microglia cells and processes between sham-operated and stroke mice in the hippocampus (A,B-p=0.0021) and (C,D-p=0.0002) respectively. 98**

Figure 3.17 Representative photomicrographs showing immunofluorescence staining using anti-CD31 in the hippocampus of control (A, C) and stroke (B, D). The labelled endothelial cells with anti-CD31 showing morphological changes with some dilatation in the stroke brain (arrowheads) compared to control (arrows). (Scale bar=50um:A,B and 20um:C,D). (The images are taken at the level of Bregma -2.06mm). (Slice thickness=20um)..... 99

Figure 3.18 Representative photomicrographs showing immunofluorescence staining using anti-CD31 in the cortical area of control (A, C) and stroke (B, D). The labelled endothelial cells with anti-CD31 showing morphological changes with some dilatation in the stroke brain (arrows) compared to control (arrows). (Scale bar=50um:A,B and 20um:C,D). (The images are taken at the level of Bregma 1.54mm). (Slice thickness=50um)..... 100

Figure 3.19 Representative photomicrographs showing immunofluorescence staining for ZO-1 with anti-ZO-1 and Cy3-conjugated secondary antibodies with DAPI stained nuclei in the hippocampus in sham (A, C, E) and BCCAO stroke brains (B, D, F). The labelled TJs are disrupted in stroke brain (arrowheads) compared to the intact ones in the control (arrows). (Scale bar=10um). (The images are taken at the level of Bregma-2.06mm). (Slice thickness=50um). 102

Figure 3.20 Representative photomicrographs showing immunofluorescence staining for Occludin with anti-Occludin and Cy3-conjugated secondary antibodies with DAPI stained nuclei in the hippocampus in sham (A, C, E) and BCCAO stroke brains (B, D, F). The labelled TJs are disrupted in stroke brain (arrowhead) compared to the intact ones in the control (arrow). (Scale bar=10um). (The images are taken at the level of Bregma-2.06mm). (Slice thickness=50um). 104

Figure 3.21 Representative photomicrographs showing immunofluorescence staining for Claudin-5 with anti-Claudin-5 and Cy3-conjugated secondary antibodies with DAPI stained nuclei in the hippocampus in sham (A, C, E) and BCCAO stroke brains (B, D, F). The labelled TJs are disrupted in stroke brain (arrowheads) compared to the intact ones in the control (arrows). (Scale bar=10um). (The images are taken at the level of Bregma-2.06mm). (Slice thickness=50um). 106

Figure 3.22 Representative photomicrographs showing double immunofluorescence staining for Occludin and CD31 with anti-Occludin (A,B-red) and anti-CD31 (C, D-green) and DAPI stained nuclei (E, F-blue) in the hippocampus area in BCCAO model of stroke (B,D,F,H) compared to control (A,C,E,G). The labelled TJs with anti-Occludin showing disruption of TJs in stroke brain (arrowheads) compared to the intact ones in the control (arrows). The labelled endothelial cells with anti-CD31 showing morphological changes with some dilatation in the stroke brain (arrowheads) compared to control (arrows). (Scale bar=10um). (The images are taken at the level of Bregma-2.06mm). (Slice thickness=20um). 108

Figure 3.23 Representative photomicrographs showing double immunofluorescence staining for Occludin and CD31 with anti-Occludin (A,B-red) and anti-CD31(C,D-green) and DAPI stained nuclei (E,F-blue) in the cortical area in BCCAO model of stroke (B,D,F,H) compared to control (A,C,E,G). The labelled TJs with anti-Occludin showing disruption of TJs in stroke brain (arrowheads) compared to the intact ones in the control (arrows). The labelled endothelial cells with anti-CD31 showing morphological changes with some dilatation in the stroke brain (arrowheads) compared to control (arrows). (Scale bar=10um). (The images are taken at the level of Bregma 1.54 mm). (Slice thickness=20um). 109

Figure 3.24 Representative photomicrographs showing double immunofluorescence staining for ZO-1 and CD31 with anti-ZO-1 (A,B-red) and anti-CD31(C,D-green) and DAPI (E,F-blue) stained nuclei in the hippocampus area in BCCAO model of stroke (B,D,F,H) compared to control (A,C,E,G). The labelled TJs with anti-ZO-1 showing disruption of TJs in stroke brain (arrowheads) compared to the intact ones in the control (arrows). The labelled endothelial cells with anti-CD31 showing morphological changes with some dilatation in the stroke brain (arrowheads) compared to control (arrows). (Scale bar=10um). (The images are taken at the level of Bregma-2.06mm). (Slice thickness=20um)..... 111

Figure 3.25 Representative photomicrographs showing double immunofluorescence staining for ZO-1 and CD31 with anti-ZO-1 (A,B-red) and anti-CD31(C,D-green) and DAPI (E,F-blue) stained nuclei in the cortical area in BCCAO model of stroke (B,D,F,H) compared to control (A,C,E,G). The labelled TJs with anti-ZO-1 showing disruption of TJs in stroke brain (arrowheads) compared to the intact ones in the control (arrows). The labelled endothelial cells with anti-CD31 showing morphological changes with some dilatation in the stroke brain (arrowheads) compared to control (arrows). (Scale bar=10um). (The images are taken at the level of Bregma 1.54 mm). (Slice thickness=20um)..... 112

Figure 3.26 Representative photomicrographs showing double immunofluorescence staining for Claudin-5 and CD31 with anti-Claudin-5 (A,B-red) and anti-CD31(C,D-green) and DAPI (E,F-blue) stained nuclei in the hippocampus area in BCCAO model of stroke (B,D,F,H) compared to control (A,C,E,G). The labelled TJs with anti-Claudin-5 showing disruption of TJs in stroke brain (arrowheads) compared to the intact ones in the control (arrows). The labelled endothelial cells with anti-CD31 showing morphological changes with some dilatation in the stroke brain (arrowheads) compared to control (arrows). (Scale bar=10um). (The images are taken at the level of Bregma-2.06mm). (Slice thickness=20um)..... 114

Figure 3.27 Representative photomicrographs showing double immunofluorescence staining for Claudin-5 and CD31 with anti-Claudin-5 (A,B-red) and anti-CD31(C,D-green) and DAPI (E,F-blue) stained nuclei in the cortical area in BCCAO model of stroke (B,D,F,H) compared to control (A,C,E,G). The labelled TJs with anti-Claudin-5 showing disruption of TJs in stroke brain (arrowheads) compared to the intact ones in the control (arrows). The labelled endothelial cells with anti-CD31 showing morphological changes with some dilatation in the stroke brain (arrowheads) compared to control (arrows). (Scale bar=10um). (The images are taken at the level of Bregma 1.54 mm).(Slice thickness=20um)..... 115

Figure 3.28 Representative photomicrographs showing double immunofluorescence staining for NeuN and ZO-1 using anti-NeuN (A,B-red) and anti-ZO-1 (C,D-green) in the hippocampus in BCCAO model of stroke (B,D,F,H) compared to control (A,C,E,G). The labelled TJs with anti-ZO-1 are disrupted in stroke brain (arrowheads) compared to the control (arrows). The labelled neuron cells with anti-NeuN show neuronal death following stroke (arrowheads) compared to control (arrows). (Scale bar= 20um and 50um). (The images are taken at the level of Bregma -2.06mm). (Slice thickness=20um). 117

Figure 3.29 Representative photomicrographs showing double immunofluorescence staining for NeuN and ZO-1 with using anti-NeuN (A,B-red) and anti-ZO-1 (C,D-green) in the cortical area in BCCAO model of stroke (B,D,F,H) compared to control (A,C,E,G). The labelled TJs with anti-ZO-1 are disrupted in stroke brain arrowheads) compared to the control (arrows). The labelled neuron cells with anti-NeuN show neuronal death following stroke (arrowheads) compared to control (arrows). (Scale bar=20um and 50um). (The images are taken at the level of Bregma 1.54mm). (Slice thickness=20um). 118

Figure 3.30 Representative photomicrographs showing double immunofluorescence staining for GFAP and ZO-1 with anti-GFAP (A,B-red) and anti-ZO-1 (C,D-green) in the hippocampus in BCCAO model of stroke (B,D,F,H) compared to control (A,C,E,G). The labelled TJs with anti-ZO-1 are disrupted in stroke brain (arrowheads) compared to the control (arrows). The labelled astrocytes and processes with anti-GFAP become more and thicker due to astrocytes activation following stroke (arrowheads) compared to control (arrows). (Scale bar=20um and 50um). (The images are taken at the level of Bregma -2.06mm). (Slice thickness=20um). 120

Figure 3.31 Representative photomicrographs showing double immunofluorescence staining for GFAP and ZO-1 with anti- GFAP (A,B-red) and anti- ZO-1 (C,D-green) in the cortical area in BCCAO model of stroke (B,D,F,H) compared to control (A,C,E,G). The labelled TJs with anti-ZO-1 are disrupted in stroke brain (arrowheads) compared to the control (arrows). The labelled astrocytes and processes with anti-GFAP become more and thicker due to astrocytes activation following stroke (arrowheads) compared to control (arrows). (Scale bar=20um and 50um). (The images are taken at the level of Bregma 1.54mm). (Slice thickness=20um). 121

Figure 3.32 Bicinchoninic acid assay (BCA) standard dilution..... 122

Figure 3.33 Quantitative analysis shows a very significant increase of proteins level (**p<0.0001, Unpaired Student's t-test, n=6) in BCCAO as compared to control mice individually (n=6) (A) and as mean ± SD (B). 122**

Figure 3.34 WB analysis of GFAP expression in the hippocampus of sham-operated and BCCAO mice. A) GFAP band density is greatly increased in the hippocampus of BCCAO models as compared to control. B) Quantitative analysis of GFAP band density relative to ß-actin shows a significant increase (p=0.002, Mann-Whitney U test, n= 6/group) in GFAP expression in BCCAO mice as compared to control. (Data presented as mean ± SD). (Control group was set as 1.0 as comparison to BCCAO). 123**

Figure 3.35 WB analysis of Occludin expression in the hippocampus of sham-operated and BCCAO mice. A) Occludin band density is greatly decreased in the hippocampus of BCCAO models as compared to control. B) Quantitative analysis of Occludin band density relative to ß-actin shows a significant decrease (p=0.002, Mann-Whitney U test, n= 6/group) in Occludin expression in hippocampus of BCCAO mice as compared to control. (Data presented as mean ± SD). (Control group was set as 1.0 as comparison to BCCAO). 125**

Figure 3.36 WB analysis of ZO-1 expression in the hippocampus of sham-operated and BCCAO mice. A) ZO-1 band density is greatly decreased in the hippocampus of BCCAO models as compared to control. B) Quantitative analysis of ZO-1 band density relative to ß-actin shows a significant decrease (p=0.002, Mann-Whitney U test, n = 6/group) in ZO-1 expression in hippocampus of BCCAO mice as compared to control. (Data presented as mean ± SD). (Control group was set as 1.0 as comparison to BCCAO). 125**

Figure 3.37 WB analysis of Claudin-5 expression in the hippocampus of sham-operated and BCCAO mice. A) Claudin-5 band density is greatly decreased in the hippocampus of BCCAO models as compared to control. B) Quantitative analysis of Claudin-5 band density relative to ß-actin shows a significant decrease (p=0.002, Mann-Whitney U test, n = 6/group) in Claudin-5 expression in hippocampus of BCCAO mice as compared to control. (Data presented as mean ± SD). (Control group was set as 1.0 as comparison to BCCAO). 126**

Figure 3.38 ELISA analysis showing serum GFAP levels between control and BCCAO stroke models. A) Mouse GFAP serial standard dilution vs optimal density in 450nm. B) Serum GFAP levels in control and BCCAO ischaemic models (n=8) individually. C) Significant increase in the serum protein levels in BCCAO ischaemic serum group compared to the control group (p=0.0002 - Unpaired Student's t-test)..... 128

Figure 3.39 ELISA analysis showing serum Occludin levels between control and BCCAO stroke models. A) Mouse Occludin serial standard dilution vs optimal density in 450nm. B) Serum Occludin levels in control and BCCAO ischaemic models (n=8) individually. C) Significant increase in the serum protein levels in BCCAO ischaemic serum group compared to the control group (p<0.0001 - Unpaired Student's t-test). 129

Figure 3.40 ELISA analysis showing serum ZO-1 levels between control and BCCAO stroke models A) Mouse ZO-1serial standard dilution vs optimal density in 450nm. B) Serum ZO-1 levels in control and BCCAO ischaemic models (n=8) individually. C) Significant increase in the serum protein levels in BCCAO ischaemic serum group compared to the control group (p<0.0001- Unpaired Student's t-test). 130

Figure 3.41 ELISA analysis showing serum Claudin-5 levels between control and BCCAO stroke models. A) Mouse Claudin-5 serial standard dilution vs optimal density in 450nm. B) Serum Claudin-5 levels between control and BCCAO ischaemic models (n=8) individually. C) Significant increase in the serum protein levels in BCCAO ischaemic serum group compared to the control group (p<0.0001- Unpaired Student's t-test). 131

Figure 3.42 Correlation analysis between serum A: GFAP, B: Occludin, C: ZO-1 and D: Claudin-5 levels and these proteins' expressions in hippocampal tissue of the brain in BCCAO using Spearman correlation and simple linear regression. Proteins expressions in hippocampal brain tissue of the brain were quantitatively assessed by WB. Serum proteins levels were quantified by ELISA. A: Spearman correlation showing a significant very strong positive correlation between GFAP expression in the brain and serum GFAP level; (r=0.943, p=0.017). Linear regression analysis showing non-significant association GFAP expression in the brain and serum GFAP level ;(R SQUARED = 0.319, p=0.243). B: Spearman correlation and linear regression showing a significant very strong negative correlation between Occludin expression in the brain and serum Occludin level; (r = -0.886, p=0.033) and (95% confidence interval, R SQUARED = 0.545, p=0.009) respectively. C: Spearman correlation analysis and simple linear regression analysis showing no association between serum ZO-1 level and ZO-1 expression in hippocampal tissue of the brain; (r = 0.029, *p*>0.999) and (R SQUARED = 0.004, p=0.912) respectively. D: Spearman correlation analysis and simple linear regression analysis showing no association between serum Claudin-5 level and Claudin-5 expression in hippocampal tissue of the brain; (r = 0.435, p=0.389) and (R SQUARED = 0.197, p=0.378) respectively. 133

Figure 3.43 Representative photomicrographs showing cresyl violet staining of neuron cell nuclei in the hippocampus in control (A) and MCAO (B) brains. The staining shows chromatolytic changes in the stroke brain compared to the control brain due to cellular damage following MCAO induced stroke (arrowheads). (Scale bar=20um). (The images are taken at the level of Bregma -2.06mm). 135

Figure 3.44 Representative photomicrographs showing immunofluorescence staining of NeuN labelled cell nuclei in the M1 motor cortex (A-B), the M2 motor cortex (C-D), granular insular Cortex (E-F), hippocampus (CA1) (G-H) and striatum area (I-J) of control (left column) and MCAO stroke (right column). NeuN labelled cells are fewer in stroke mice than in the controls due to neuronal cells death following stroke (arrowheads). (Scale bar=50um). (The images are taken at the level of Bregma 1.54 or -2.06mm). (Slice thickness=20um). 136

Figure 3.45 Quantitative analysis shows significant differences (*p< 0.05, ,p ≤ 0.01 - paired Student's t-test, n=3) in the number of NeuN-positive nuclei between sham-operated and MCAO mice in the M1 motor cortex (A-B, p=0.0392), the M2 motor cortex (C-D, p=0.0017) and striatum area (I-J, p=0.0010), but not in granular insular Cortex (E-F, p=0.080) and hippocampus (CA1) (G-H, p=0.1141). 138**

Figure 3.46 Representative photomicrographs showing immunofluorescence staining of GFAP labelled astrocytes in the hippocampus of control (A, C) and MCAO stroke (B, D) brains. The GFAP labelled cells and processes becomes thicker and more due to astrocytes activation following stroke (arrowheads). (Scale bar=50um:A,B and 20um:C,D). (The images are taken at the level of Bregma -2.06mm). (Slice thickness=20um). 139

Figure 3.47 Quantitative analysis shows significant increases (*p < 0.05 - paired Student's t-test, n=3) in the number of GFAP labelled astrocyte cells (A,B-*p=0.0497) and profiles processes (C,D-*p=0.0485) in MCAO mice compared to sham in hippocampus (CA1). 140

Figure 3.48 Representative photomicrographs showing immunofluorescence staining for ZO-1 using anti-ZO-1 and Cy3-conjugated secondary antibodies with DAPI stained nuclei in the hippocampus in sham (A, C, E) and MCAO stroke brains (B, D, F). The labelled TJs are disrupted in stroke brain (arrowheads) compared to the intact ones in the control (arrows). (Scale bar=10um). (The images are taken at the level of Bregma-2.06mm). (Slice thickness=20um). 141

Figure 3.49 Representative photomicrographs showing immunofluorescence staining for Occludin using anti-Occludin and Cy3-conjugated secondary antibodies with DAPI stained nuclei in the hippocampus in sham (A,C,E) and MCAO stroke brains (B,D,F). The labelled TJs are disrupted in stroke brain (arrowhead) compared to the intact ones in the control (arrow). (Scale bar= 10um). (The images are taken at the level of Bregma-2.06mm). (Slice thickness=20um). 143

Figure 3.50 Representative photomicrographs showing immunofluorescence staining for Claudin-5 using anti-Claudin-5 and Cy3-conjugated secondary antibodies with DAPI stained nuclei in the hippocampus in sham (A, C, E) and MCAO stroke brains (B, D, F). The labelled TJs are disrupted in stroke brain (arrowhead) compared to the intact ones in the control (arrow). (Scale bar=10um). (The images are taken at the level of Bregma-2.06mm). (Slice thickness=20um). 145

Figure 3.51 Representative photomicrographs showing immunofluorescence staining for NeuN using anti-NeuN in the hippocampus of MCAO stroke model and BCCAO stroke model. For both models, the left panel side represents the control brains, while the right panel side represents the stroke brains. NeuN labelled cells are fewer in stroke models (arrowheads) than in the controls (arrows). (Scale bar=100um: upper row,50um:middle row and 20um:lower row). (The images are taken at the level of Bregma -2.06mm). (Slice thickness = 20 um). 146

Figure 3.52 Representative photomicrographs showing immunofluorescence staining for GFAP using anti-GFAP in the hippocampus area of MCAO stroke model and BCCAO stroke model. For both models, the left panel side represents the control brains, while the right panel side represents the stroke brains. In the stroke brains, the GFAP labelled cells and processes are thicker and higher in number due to astrocytes activation following stroke (arrowheads). (Scale bar=100um: upper row,50um:middle row and 20um:lower row). (The images are taken at the level of Bregma -2.06mm). (Slice thickness=20um). 147

Figure 3.53 Representative photomicrographs showing immunofluorescence staining for Occludin using anti-Occludin in the hippocampus area of MCAO stroke model and BCCAO stroke model. For both models, the left panel side represents the control brains, while the right panel side represents the stroke brains. In the stroke brains, the labelled TJs are disrupted (arrowheads) compared to the intact ones in the control brains (arrows). (Scale bar= 50um:upper row and 20um:lower row). (The images are taken at the level of Bregma -2.06mm). (Slice thickness=20um).148

Figure 3.54 Representative photomicrographs showing immunofluorescence staining for ZO-1 using anti-ZO-1 in the hippocampus area of MCAO stroke model and BCCAO stroke model. For both models, the left panel side represents the control brains, while the right panel side represents the stroke brains. In the stroke brains, the labelled TJs are disrupted (arrowheads) compared to the intact ones in the control brains (arrows). (Scale bar= 50um:upper row and 20um:lower row). (The images are taken at the level of Bregma-2.06mm). (Slice thickness=20um)..... 149

Figure 3.55 Representative photomicrographs showing immunofluorescence staining for Claudin-5 using anti-Claudin-5 in the hippocampus area of MCAO stroke model and BCCAO stroke model.For both models, the left panel side represents the control brains, while the right panel side represents the stroke brains. In the stroke brains, the labelled TJs are disrupted (arrowheads) compared to the intact ones in the control brains (arrows). (Scale bar= 50um:upper row and 20um:lower row). (The images are taken at the level of Bregma-2.06mm). (Slice thickness=20um).149

Figure 3.56 Representative photomicrographs showing immunofluorescence staining for CD-31 using anti-CD31 in the hippocampus area of MCAO stroke model and BCCAO stroke model. For both models, the left panel side represents the control brains, while the right panel side represents the stroke brains. In the stroke brains, the endothelial labelled cells showing morphological changes with some dilatations (arrowheads) compared to control (arrows). (Scale bar= 50um:upper row and 20um:lower row). (The images are taken at the level of Bregma -2.06mm). (Slice thickness=20um). 150

Figure 3.57 Representative photomicrographs showing immunofluorescence staining for IBA-1 using anti-IBA-1 in the hippocampus area of MCAO stroke model and BCCAO stroke model. For both models, the left panel side represents the control brains, while the right panel side represents the stroke brains. The IBA-1 labelled cells and processes are more in stroke brains than in the control brains following stroke (arrowheads). (Scale bar= 50um:upper row and 20um:lower row). (The images are taken at the level of Bregma -2.06mm). (Slice thickness=20 um)..... 151

Figure 3.58 Representative photomicrographs showing immunofluorescence staining for PDGFR using anti-PDGFR and Alexa488 conjugated secondary antibodies with DAPI stained nuclei in the hippocampus of MCAO stroke model and BCCAO stroke model. For both models, the left panel side represents the control brains, while the right panel side represents the stroke brains. The labelled pericytes show morphological changes with some reduction in the stroke brains (arrowheads) compared to control (arrows). (Scale bar= 50um:upper row and 20um:middle and lower rows). (The images are taken at the level of Bregma -2.06mm). (Slice thickness=20 um). 152

Figure 3.59 Representative photomicrographs showing immunofluorescence staining for NG2 using anti-NG2 and Alexa488 conjugated secondary antibodies with DAPI stained nuclei in the hippocampus of MCAO stroke model and BCCAO stroke model. For both models, the left panel side represents the control brains, while the right panel side represents the stroke brains. The labelled pericytes show morphological changes and some reduction in the stroke brains (arrowheads) compared to control (arrows). (Scale bar= 50um:upper row and 20um:middle and lower rows). (The images are taken at the level of Bregma -2.06mm). (Slice thickness=20 um)..... 153

Figure 3.60 Representative photomicrographs showing double immunofluorescence staining for Occludin and CD31 with anti-Occludin (A,B-red) and anti-CD31(C,D-green) and DAPI (E,F-blue) stained nuclei in the hippocampus area in MCAO model of stroke (B,D,F,H) compared to control (A,C,E,G). The labelled TJs with anti-Occludin showing disruption of TJs in stroke side (arrowheads) compared to the intact ones in the control (arrows). The labelled endothelial cells with anti-CD31 showing morphological changes in the stroke brain (arrowheads) compared to control (arrows). (Scale bar=10um). (The images are taken at the level of Bregma -2.06mm). (Slice thickness=20um)..... 155

Figure 3.61 Representative photomicrographs showing double immunofluorescence staining for Occludin and CD31 with anti-Occludin (A,B-red) and anti-CD31(C,D-green) and DAPI (E,F-blue) stained nuclei in the cortical area in MCAO model of stroke (B,D,F,H) compared to control (A,C,E,G). The labelled TJs with anti-Occludin showing disruption of TJs in stroke side (arrowheads) compared to the intact ones in the control (arrows). The labelled endothelial cells with anti-CD31 showing morphological changes in the stroke brain (arrowheads) compared to control (arrows). (Scale bar= 10um). (The images are taken at the level of Bregma 1.54 mm). (Slice thickness=20um)..... 156

Figure 3.62 Representative photomicrographs showing double immunofluorescence staining for ZO-1 and CD31 with using anti-ZO-1 (A,B-red) and anti-CD31(C,D-green) and DAPI (E,F-blue) stained nuclei in the hippocampus area in MCAO model of stroke (B,D,F,H) compared to control (A,C,E,G). The labelled TJs with anti-ZO-1 showing disruption of TJs in stroke side (arrowheads) compared to the intact ones in the control (arrows). The labelled endothelial cells with anti-CD31 showing morphological changes in the stroke brain (arrowheads) compared to control (arrows). (Scale bar=10um). (The images are taken at the level of Bregma -2.06mm). (Slice thickness=20um). 158

Figure 3.63 Representative photomicrographs showing double immunofluorescence staining for ZO-1 and CD31 with anti- ZO-1 (A,B-red) and anti-CD31(C,D-green) and DAPI (E,F-blue) stained nuclei in the cortical area in MCAO model of stroke (B,D,F,H) compared to control (A,C,E,G). The labelled TJs with anti-ZO-1 showing disruption of TJs in stroke side (arrowheads) compared to the intact ones in the control (arrows). The labelled endothelial cells with anti-CD31 showing morphological changes in the stroke brain (arrowheads) compared to control (arrows). (Scale bar=10um). (The images are taken at the level of Bregma 1.54 mm). (Slice thickness=20um)..... 159

Figure 3.64 Representative photomicrographs showing double immunofluorescence staining for Claudin-5 and CD31 with anti-Claudin-5 (A,B-red) and anti-CD31(C,D-green) and DAPI (E,F-blue) stained nuclei in the hippocampus area in MCAO model of stroke (B,D,F,H) compared to control (A,C,E,G). The labelled TJs with anti-Claudin-5 showing disruption of TJs in stroke side (arrowheads) compared to the intact ones in the control (arrows). The labelled endothelial cells with anti-CD31 showing morphological changes in the stroke brain (arrowheads) compared to control (arrows). (Scale bar=10um). (The images are taken at the level of Bregma -2.06mm). (Slice thickness=20um)..... 161

Figure 3.65 Representative photomicrographs showing double immunofluorescence staining for Claudin-5 and CD31 with anti-Claudin-5 (A,B-red) and anti-CD31(C,D-green) and DAPI (E,F-blue) stained nuclei in the cortical area in MCAO model of stroke (B,D,F,H) compared to control (A,C,E,G). The labelled TJs with anti-Claudin-5 showing disruption of TJs in stroke side (arrowheads) compared to the intact ones in the control (arrows). The labelled endothelial cells with anti-CD31 showing morphological changes in the stroke brain (arrowheads) compared to control (arrows). (Scale bar=10um). (The images are taken at the level of Bregma 1.54 mm). (Slice thickness=20um)..... 162

Figure 3.66 Representative photomicrographs showing double immunofluorescence staining for NeuN and ZO-1 with using anti- NeuN (A,B-red) and anti-ZO-1 (C,D-green) in the hippocampus in MCAO model of stroke (B,D,F,H) compared to control (A,C,EG). The labelled TJs with ant-ZO-1 are disrupted in stroke side (arrowheads) compared to the control (arrows). The labelled neuron cells with anti-NeuN show neuronal death following stroke (arrowheads) compared to control (arrows). (Scale bar=20um and 50um). (The images are taken at the level of Bregma-2.06mm). (Slice thickness=20um). 164

Figure 3.67 Representative photomicrographs showing double immunofluorescence staining for NeuN and ZO-1 with anti-NeuN (A,B-red) and anti-ZO-1 (C,D-green) in the cortical area in MCAO model of stroke (B,D,E,H) compared to control (A,C,EG). The labelled TJs with anti-ZO-1 are disrupted in stroke side (arrowheads) compared to the control (arrows). The labelled neuron cells with anti-NeuN show neuronal death following stroke (arrowheads) compared to control (arrows). (Scale bar= 20um and 50um). (The images are taken at the level of Bregma 1.54mm). (Slice thickness=20um). 165

Figure 3.68 Representative photomicrographs showing double immunofluorescence staining for GFAP and ZO-1 with anti-GFAP (A,B-red) and anti-ZO-1 (C,D-green) in the hippocampus in MCAO model of stroke (B,D,F,H) compared to control (A,C,E,G). The labelled TJs with anti-ZO-1 showing disruption of TJs in stroke side (arrowheads) compared to the intact ones in the control (arrows). The labelled astrocytes and processes with anti-GFAP become more and thicker due to astrocytes activation following stroke (arrowheads) compared to control (arrows). (Scale bar= 20um and 50um). (The images are taken at the level of Bregma-2.06mm). (Slice thickness=20um). 167

Figure 3.69 Representative photomicrographs showing double immunofluorescence staining for GFAP and ZO-1 with anti-GFAP (A,B-red) and anti-ZO-1 (C,D-green) in the cortical area in MCAO model of stroke (B,D,F,H) compared to control (A,C,E,G). The labelled TJs with anti-ZO-1 showing disruption of TJs in stroke side (arrowheads) compared to the intact ones in the control (arrows). The labelled astrocytes and processes with anti-GFAP become more and thicker due to astrocytes activation following stroke (arrowheads) compared to control (arrows). (Scale bar=20um and 50um). (The images are taken at the level of Bregma 1.54mm). (Slice thickness=20um).168

Figure 3.70 Standard dilution curve of bicinchoninic acid assay (BCA).169

Figure 3.71 Quantitative analysis shows a very significant increase of proteins level (p=0.0001- paired Student's t-test, n=6) in MCAO as compared to control mice individually (n=6) (A) and as mean ± SD (B). 169

Figure 3.72 WB analysis of GFAP expression in the hippocampus of sham-operated and MCAO mice. A) GFAP band density is greatly increased in the hippocampus of MCAO models as compared to control. B) Quantitative analysis of GFAP band density relative to ß-actin shows a significant increase (*p=0.031, Wilcoxon matched-pairs signed rank test, n= 6/group) in GFAP expression in MCAO mice as compared to control. (Data presented as mean ± SD). (Control group was set as 1.0 as comparison to MCAO). 170

Figure 3.73 WB analysis of Occludin expression in the hippocampus of sham-operated and MCAO mice. A) Occludin band density is greatly decreased in the hippocampus of MCAO models as compared to control. B) Quantitative analysis of Occludin band density relative to ß-actin shows a significant decrease (*p=0.031, Wilcoxon matched-pairs signed rank test, n= 6/group) in Occludin expression in hippocampus area of MCAO mice as compared to control. (Data presented as mean ± SD). (Control group was set as 1.0 as comparison to MCAO). 171

Figure 3.74 WB analysis of ZO-1 expression in the hippocampus of sham-operated and MCAO mice. A) ZO-1 band density is greatly decreased in the hippocampus of MCAO models as compared to control. B) Quantitative analysis of ZO-1 band density relative to ß-actin shows a significant decrease (*p=0.031, Wilcoxon matched-pairs signed rank test, n = 6/group) in ZO-1 expression in hippocampus of MCAO mice as compared to control. (Data presented as mean ± SD). (Control group was set as 1.0 as comparison to MCAO). 172

Figure 3.75 WB analysis of Claudin-5 expression in the hippocampus of sham-operated and MCAO mice. A) Claudin-5 band density is greatly decreased in the hippocampus of MCAO models as compared to control. B) Quantitative analysis of Claudin-5 band density relative to ß-actin shows a significant decrease (*p=0.031, Wilcoxon matched-pairs signed rank test, n = 6/group) in Claudin-5 expression in hippocampus area of MCAO mice as compared to control. (Data presented as mean ± SD). (Control group was set as 1.0 as comparison to MCAO). 172

Figure 3.76 ELISA analysis showing serum GFAP levels between control and MCAO stroke models. A) Mouse GFAP serial standard dilution vs optimal density in 450nm. B) Serum GFAP levels in control and MCAO ischaemic models (n=10) individually. C) Significant increase in the serum protein levels in MCAO group compared to the control group (p=0.0060 - Unpaired Student's t-test). 174

Figure 3.77 ELISA analysis showing serum Occludin levels between control and MCAO stroke models. A) Mouse Occludin serial standard dilution vs optimal density in 450nm. B) Serum Occludin levels in control and MCAO ischaemic models (n=10) individually. C) Significant increase in the serum protein levels in MCAO group compared to the control group (p=0.0051-Unpaired Student's t-test). 175

Figure 3.78 ELISA analysis showing serum ZO-1 levels between control and MCAO stroke models. A) Mouse ZO-1serial standard dilution vs optimal density in 450nm. B) Serum ZO-1 levels in control and MCAO ischaemic models (n=10) individually. C) Significant increase in the serum protein levels in MCAO group compared to the control group (p=0.0136-Unpaired Student's t-test). **176**

Figure 3.79 ELISA analysis showing serum Claudin-5 levels between control and MCAO stroke models. A) Mouse Claudin-5 serial standard dilution vs optimal density in 450nm. B) Serum Claudin-5 levels in control and MCAO ischaemic models (n=10) individually. C) Significant increase in the serum protein levels in MCAO group compared to the control group (p=0.0137-Unpaired Student's t-test). **177**

Figure 3.80 Correlation analysis between serum A: GFAP, B: Occludin, C: ZO-1 and D: Claudin-5 levels and these proteins' expressions in hippocampal tissue of the brain in MCAO using Spearman correlation and simple linear regression. Proteins expressions in hippocampal brain tissue of brain were quantitatively assessed by WB. Serum proteins levels were quantified by ELISA. A: Spearman correlation analysis and simple linear regression analysis showing no association between serum GFAP level and GFAP expression in hippocampal tissue of the brain; (r = -0.257, *p*=0.658) and (R SQUARED = 0.028, p=0.771) respectively. B: Spearman correlation and simple linear regression showing a significant negative correlation between serum Occludin level and the Occludin expression in hippocampal tissue in the brain; (r =-1.00, p=0.003) and (95% confidence interval, R SQUARED = 0.950, p=0.001) respectively. C: Spearman correlation analysis and simple linear regression analysis showing no association between serum ZO-1 level and ZO-1 expression in hippocampal tissue of the brain; (r = 0.086, p=0.919) and (R SQUARED = 1.157e-006, p=0.998) respectively. D: Spearman correlation analysis and simple linear regression analysis showing no association between serum Claudin-5 level and Claudin-5 expression in hippocampal tissue of the brain; (r = 0.200, p=0.714).and (R SQUARED = 0.323, p=0.239) respectively. **179**

Figure 4.1 CTP CBF (left), CBV (middle) and MTT (right) maps in a typical ischaemic stroke patient. Red areas show the location of ROIs in WM ischaemic (upper row) and non-ischaemic areas (bottom row).. 187

Figure 4.2 CTP CBF (A), CBV (B) and MTT(C) values in ischaemic and non-ischaemic WM and GM areas in the MT group (n=15), (Paired Student's t-test - A: CBF in WM p=0.0001 and in GM p<0.0001), (C: MTT in GM p=0.0003). **188**

Figure 4.3 A) CTP images of right-side MCA infarct in a patient, who received MT directly after the CTP scan. Also, CBF, CBV and MTT maps are shown. B) CBF, CBV and MTT values for the ischaemic and non-ischaemic sides in WM and C) CBF, CBV and MTT values for the ischaemic and non-ischaemic sides in GM. **189**

Figure 4.4 CTP CBF (A), CBV (B) and MTT (C) values in ischaemic and non-ischaemic WM and GM areas in the non-MT group (n=15), (Paired Student's t-test - A: CBF in WM p=0.0031 and in GM p<0.0001), (B: CBV in WM p = 0.0269 and CBV in GM p= 0.0350) and (C: MTT in GM p=0.0011). 191

Figure 4.5 A) CTP images for a patient with a massive right MCA territory ischaemia who couldn't receive MT after the CTP scan due to delay from stroke onset to hospital arrival. Also, CBF, CBV and MTT maps are shown. B) CBF, CBV and MTT values for the ischaemic and non-ischaemic sides in WM and C) CBF, CBV and MTT values for the ischaemic and non-ischaemic sides in GM. 191

Figure 4.6 The analysis of WM CBF (A), CBV (B) and MTT (C) ratio between the MT group (n=15) and the non-MT group (n=15). No significant difference was seen between the two groups (Mann-Whitney U test). 192

Figure 4.7 The analysis of GM CBF (A), CBV (B) and MTT (C) ratio between the MT group (n=15) and the non-MT group (n=15). Only CBV ratio showed significant difference between the two groups (Mann-Whitney U test - p=0.041)..... 193

Figure 4.8 ADC map values in MRI DWI in ischaemic and non-ischaemic WM and GM areas in the MT group (n=7). 194

Figure 4.9 A) MRI ADC map and fluid-attenuated inversion recovery (FLAIR) of left hemisphere anterior circulation stroke in a patient, who received MT. B) ADC values for the ischaemic and non-ischaemic areas in WM and GM. The stroke is shown as hyperintense in the ADC map as the scan has done after more than a month from the stroke onset.. 195

Figure 4.10 ADC map values in MRI DWI in ischaemic and non-ischaemic WM and GM areas in the non-MT group (n=8), (Paired Student's t-test - in WM p=0.047 and in GM p=0.0016). 196

Figure 4.11 A) MRI ADC map and fluid-attenuated inversion recovery (FLAIR) of pons infarct and right cerebral infarct in a patient, who couldn't receive MT. B) ADC values for the ischaemic and non-ischaemic areas in WM and GM. The stroke is shown as hyperintense in the ADC map as the scan has done after more than a month from the stroke onset.. 196

Figure 4.12 The analysis of ADC WM and GM ratio between the MT group (n=7) and the non-MT group (n=8), (Mann-Whitney U test – in GM p=0.009). 197

Figure 4.13 A comparison between the infarct volume in ml between the MT group (n=7) and the non-MT group (n=8). 198

Figure 4.14 CTP and ADC images for a patient with acute stroke in the right MCA occlusion who received MT directly after the CTP scan (left panel). The middle panel represents an ADC map on follow-up MRI. The volume of infarct was calculated in ml according to the ROI volume (right panel, red). The histogram shows the number of pixels in the infarct area with been used to calculate the volume of infarct in ml (11.80ml)..... 198

Figure 4.15 CTP and ADC images for a patient case with acute stroke with a massive infarction in the right MCA occlusion who couldn't receive MT after the CTP scan (left panel). The middle panel represents an ADC map on follow-up MRI. The volume of infarct was calculated in ml according to the ROI volume (right panel, red). The histogram shows the number of pixels in the infarct area with been used to calculate the volume of infarct in ml (110.79ml). 199

Figure 4.16 A) A comparison between the number of patients with "good oucome" (mRS≤2) and "bad outcome" (mRS>2) in the MT group (left) and the non-MT group (right). B) Individual mRS at 3 months in the MT group in the left (n=15) and the non-MT group in the right (n=15).201

Figure 5.1 The difference in (A) GFAP, (B) NSE, (C) Occludin, (D) Claudin-5 and (E) ZO-1 levels between serum and plasma in the ischaemic group (n=25) and the mimics group (n=5). No significant changes were found, (Paired Student's t-test)..... 210

Figure 5.2 The levels of serum (A) GFAP, (B) NSE, (C) NfL, (D) Occludin, Claudin-5 (E) and ZO-1 (F) levels in the ischaemic patients (n=70) compared to the mimics (n=24). A significant increase has been observed in the concentrations of biomarkers except NSE in the ischaemic group compared to the mimics. GFAP: p<0.0001, NfL: p<0.0001, Occludin: p<0.0001, Claudin-5: p<0.0001 and ZO-1: p<0.0001. (Mann-Whitney U test, p≤0.0001: **). 213**

Figure 5.3 The difference in serum (A) GFAP, (B) NSE, (C) NfL, (D) Occludin, Claudin-5 (E) and ZO-1(F) levels between the ischaemic group and the mimics group based on the gender. (Mann-Whitney U test, p≤0.001: ***, p≤0.0001: **). (Ischaemic male: n=48 and female: n=22) (Mimics male: n=15 and female: n=9). 214**

Figure 5.4 The difference in serum (A) GFAP, (B) NSE, (C) NfL, (D) Occludin, Claudin-5 (E) and ZO-1(F) levels between the ischaemic group and the mimics group based on the day of blood collection. (Mann-Whitney U test, p≤0.001: ***, p≤0.0001: **). (Ischaemic $\leq$2 days: n=44 and >2 days: n=26) (Mimics $\leq$2 days: n=13 and >2 days: n=11).... 216**

Figure 5.5 The difference in serum (A) GFAP, (B) NSE, (C) NfL, (D) Occludin, Claudin-5 (E) and ZO-1(F) levels based on the severity of stroke. (Mann - Whitney U test, p≤0.01: **, p≤0.001: ***, p≤0.0001: **). (NIHSS $\leq$ 7: n=60, NIHSS >7:n=10 and mimics: n=24). 217**

Figure 5.6 The difference between serum (A) GFAP, (B) NSE ,(C) NfL, (D) Occludin, Claudin-5 (E) and ZO-1(F) levels in the ACO (n=45) and the PCO (n=25) in a comparison with the mimics (n=24). (Mann-Whitney U test, p≤0.001: ***, p≤0.0001: **)..... 219**

Figure 5.7 The ratio of serum A) GFAP/NSE, B) GFAP/NfL C) GFAP/Occludin D) GFAP/Claudin-5 and E) GFAP/ZO-1 in the ischaemic patients (n=70) compared to the mimics (n=24). (Mann-Whitney U test, p≤0.001: ***, p≤0.0001: **)..... 220**

Figure 5.8 The difference in HU values (densities) of 10 regions of ASPECTS between the ischaemic side and the non-ischaemic side in the ischaemic stroke patients (n=49), (Paired Student's t-test; p<0.0001: **).. 225**

Figure 5.9 A) initial axial CT head images at two different levels, (left: basal ganglia level) and (right: corona radiata level) show where the 10 ASPECTS ROIs are drawn manually. Solid line regions represent the ischaemic side, and the dashed line regions represent the non-ischaemic side. L = lentiform nucleus; C = caudate head; I = insular ribbon; IC = internal capsule; M1 = anterior MCA cortical region; M2 = MCA cortical region located lateral to insular ribbon; M3 = posterior MCA cortical region; M4, M5 and M6 about 2 cm superior to M1, M2, and M3 regions respectively. B) NCCT head for a patient with chronic lacunar infarction in the right caudate head. C) (HU) values of the 2 hemispheres (Rt: the ischaemic side and Lt: the non-ischaemic side). 226

Figure 5.10 The difference between HU values (densities) of 10 regions of ASPECTS in the right and the left side of brain in the mimics (n=16). No statistical difference was seen (Paired Student's t-test). 228

Figure 5.11 A) initial axial CT head images at two different levels, (left: basal ganglia level) and (right: corona radiata level) show where the 10 ASPECTS ROIs are drawn manually. Solid line regions represent the right side, and the dashed line regions represent the left side. L = lentiform nucleus; C = caudate head; I = insular ribbon; IC = internal capsule; M1 = anterior MCA cortical region; M2 = MCA cortical region located lateral to insular ribbon; M3 = posterior MCA cortical region; M4, M5 and M6 about 2 cm superior to M1, M2, and M3 regions respectively. B) NCCT head for a stroke mimics. This patient has a generalised hyperdensity of intracranial vessels which could be due to dehydration. C) (HU) values of the 2 hemispheres (right side and left side).... 229

Figure 5.12 The difference between serum (A) GFAP, (B) NSE, (C) NfL, (D) Occludin, Claudin-5 (E) and ZO-1(F) levels according to ASPECT score in the ischaemic group in a comparison with the mimics. (ASPECTS ≤ 7, n=33), (ASPECTS > 7, n=16) and mimics (n=24). (Mann-Whitney U test, p>0.05: *, p≤0.01: **, p≤0.0001: **). 230**

Figure 5.13 ADC values in MRI DWI in the ischaemic and the non-ischaemic WM and GM areas in the ischaemic patients (n=9), (Paired Student's t-test, in WM p=0.002 and in GM p=0.002). 232

Figure 5.14 An MRI head scan for a patient with acute right MCA territory infarct. A) MRI ADC map (left) and fluid-attenuated inversion recovery (FLAIR)(right). B) ADC values of the 2 hemispheres (the ischaemic side and the non-ischaemic side) in both WM and GM..... 232

Figure 5.15 ADC map values in the left side and the right side WM and GM areas in the mimics (n=13). No significant difference was observed between the two sides (Paired Student's t-test)..... 233

Figure 5.16 An MRI head scan for a stroke mimics A) MRI ADC map (left) and fluid-attenuated inversion recovery (FLAIR)(right). B) ADC values of the 2 hemispheres (the right side and the left side) in both WM and GM. 234

Figure 5.17 Ratio of T2 signal intensity different from 1 in WM and GM areas in the ischaemic patients (n=9). (One sample t-test, in WM p=0.05 and in GM p=0.05). 234

Figure 5.18 Follow-up MRI head scan for a patient with atypical ischaemic in the left thalamus. A) T2-weighted image. B) the ratio of T2 signal intensity (the ischaemic side / the non-ischaemic side) in both WM and GM. 235

Figure 5.19 Ratio of T2 signal intensity different from 1 in WM and GM areas in mimics (n=16). No significant difference was observed between the two sides of the brain. 236

Figure 5.20 Follow-up MRI head scan for stroke mimics. A) T2-weighted image. B) the ratio of T2 signal intensity (the left side / the right side) in both WM and GM. 236

Figure 5.21 Difference of A) ADC values and B) ratio of T2 signal intensity between (ACO:n=5) and (PCO:n=4) in WM and GM. No significant difference was observed in both groups, (Unpaired Student's t-test t). 237

Figure 5.22 An individual volume of infarct volume ml in each patient.237

Figure 5.23 A comparison between the volume of infarct and NIHSS ($NIHSS \leq 7$, n=7) ($NIHSS > 7$, n=2). (Mann-Whitney U test- p=0.884). 238

Figure 5.24 A comparison of the volume of infarct volume in ml between the anterior circulation occlusion (ACO:n=5) and the posterior circulation occlusion (PCO:n=4). (Mann-Whitney U test- p=0.713). 238

Figure 5.25 Correlation analysis between serum A: GFAP, B: NSE C: NfL, D: Occludin, E: Claudin-5 and F: ZO-1 levels and ASPECTS using Spearman correlation and simple linear regression (n=49). Only GFAP level (A) showed a significant negative association with ASPECTS (r= - 0.273, p =0.023). 242

Figure 5.26 Correlation analysis between serum A: GFAP, B: NSE C: NfL, D: Occludin, E: Claudin-5 and F: ZO-1 levels and ADC values in MRI using Spearman correlation and simple linear regression (n=9). None of the biomarkers were correlated with ADC values. 246

Figure 5.27 Correlation analysis between serum A: GFAP, B: NSE C: NfL, D: Occludin, E: Claudin-5 and F: ZO-1 levels and the of T2 signal intensity in MRI using Spearman correlation and simple linear regression (n=9). NSE level (B) and NfL level (C) were correlated positively with T2 signal intensity in both WM and GM. 249

Figure 5.28 Correlation analysis between serum A: GFAP, B: NSE C: NfL, D: Occludin, E: Claudin-5 and F: ZO-1 levels and the volume of infarct in MRI using Spearman correlation and simple linear regression (n=9). Only NSE level (B) showed a significant positive association with the volume of infarct (r =0.717; p=0.037)..... 251

Figure 5.29 Correlation analysis between serum A: GFAP, B: NSE C: NfL, D: Occludin, E: Claudin-5 and F: ZO-1 levels and NIHSS at arrival using Spearman correlation and simple linear regression (n=70). Only NfL levels (C) showed a significant positive correlation with NIHSS (r =0.441; p=0.0001)..... 253

List of Tables

Table 1-1 The normal perfusion CT parameter values (Rostrup et al., 2005; Mu et al., 2013; Kaneko et al., 2004). 17

Table 1-2 The normal ADC values of WM and GM regions of the brain (Helenius et al., 2002)..... 19

Table 1-3 Changes of imaging biomarkers after an ischaemic stroke noticed in previous studies. 24

Table 1-4 Variations of blood circulating biomarkers after an ischaemic stroke noticed in earlier A: clinical studies and B: preclinical studies.... 29

Table 2-1 The used specific primary antibodies..... 55

Table 2-2 Different used dilutions for specific antibodies in the optimisation process. 57

Table 2-3 Specific antibodies with dilutions for double labelling. 58

Table 2-4 The detection range, sensitivity and specificity for the used mouse ELISA kits in this study. 62

Table 2-5 Linear relationship strength (Chan, 2003). 63

Table 2-6 The detection range, sensitivity and specificity for the used human ELISA kits in this study. 73

Table 4-1 A comparison of CTP parameters between ischaemic and non-ischaemic WM and GM areas in the MT group (n=15). Data are shown as mean (SD). 188

Table 4-2 A comparison of CTP parameters between ischaemic and non-ischaemic WM and GM areas in the non-MT group (n=15). Data are shown as mean (SD). 190

Table 4-3 A comparison of ADC map values in MRI DWI between ischaemic and non-ischaemic WM and GM areas in the MT group (n=7). Data are shown as mean (SD). 194

Table 4-4 A comparison of ADC map values in MRI DWI between ischaemic and non-ischaemic WM and GM areas in the non-MT group (n=8). Data are shown as mean (SD)..... 195

Table 4-5 Individual mRS at 3 months in the MT group (n=15) and the non-MT group (n=15), "good outcome" (mRS≤2) or "bad outcome" (mRS>2). 200

Table 5-1 Baseline characteristics of the included patients including age, gender, type of stroke, time difference between stroke and blood sample collection, NIHSS on arrival. Data are presented as mean (SD).. 208

Table 5-2 The range, mean and median of serum GFAP, NSE, NfL, Occludin, ZO-1 and Claudin-5 concentrations in the ischaemic stroke group (n=70) and the mimics group (n=24). 211

Table 5-3 The mean (SD) of HU values (densities) obtained from 10 regions of ASPECTS in the ischaemic side and the non-ischaemic side in the ischaemic stroke patients (n=49)..... 223

Table 5-4 The mean (SD) of HU values (densities) obtained from 10 regions of ASPECTS in the left side and the right side of brain in the mimics (n=16). 226

Table 5-5 ADC values of the ischaemic and the non-ischaemic WM and GM areas in the ischaemic patients (n=9). Data are shown as mean (SD). 231

Table 5-6 ADC values in the left side and the right side WM and GM areas in the mimics (n=13). Data are shown as mean (SD)..... 233

Table 5-7 Ratio of T2 signal intensity (ischaemic side/non-ischaemic side) in WM and GM in the ischaemic group (n=9). Data are shown as mean (SD). 234

Table 5-8 Ratio of T2 signal intensity (left side of brain/right side of the brain) in WM and GM in the mimics (n=13). Data are shown as mean (SD). 235

List of Abbreviations

ACA	Anterior cerebral arteries
ACO	Anterior circulation occlusion
ASPECTS	Alberta Stroke Program Early CT Score
ADC	Apparent diffusion coefficient
ATP	Adenosine triphosphate
AVMs	Arteriovenous malformations
BBB	Blood brain barrier
BCCAO	Bilateral common carotid artery occlusion
CBF	Cerebral blood flow
CBV	Cerebral blood volume
CD31	Cluster differentiation 31
CNS	Central nervous system
CSF	Cerebrospinal fluid
CT	Computed tomography
CTA	Computed tomography angiography
CTP	Computed tomography perfusion
DCE	Dynamic Contrast–Enhanced
DSC	Dynamic Susceptibility Contrast
DWI	Diffusion-weighted Imaging
ELISA	Enzyme-linked immunosorbent assay
FDA	Food and Drug Administration
GFAP	Glial fibrillary acidic protein
GM	Grey matter
HU	Hounsfield unit
IBA-1	Ionized calcium-binding adaptor protein-1

ICA	Internal carotid artery
IF	Intermediate filament
IMS	Industrial Methylated Spirits
L.A.B. Solution	Liberate Antibody Binding Solution
LVO	Large vessel occlusion
MCA	Middle cerebral artery
MCAO	Middle cerebral artery occlusion
MRI	Magnetic resonance imaging
mRS	Modified Rankin Score
MT	Mechanical thrombectomy
MTT	Mean transit time
NCCT	Non-contrast computed tomography
NeuN	Neuronal nuclei protein
NfL	Neurofilament light chain
NG2	Neural/Glial Antigen 2
NIHSS	National Institutes of Health Stroke Scale
NSE	Neuron-specific enolase
NVU	Neurovascular unit
OCT	Optimal cutting temperature compound
PBS	Phosphate buffer solution
PBS-T	Phosphate buffer solution Triton
PCA	Posterior cerebral arteries
PCO	Posterior circulation occlusion
PDGFR	Platelet-derived growth factor
PWI	Perfusion weighted imaging
RF	Radio frequency

ROI	Region of interest
r-tPA	Recombinant tissue plasminogen activator
TJ	Tight junction
TTP	Time to peak
WB	Western blotting
WM	White matter
ZO-1	Zonula occludens-1

Chapter 1 Introduction and background

Stroke is the most common cerebrovascular disease leading to a sudden neurological dysfunction caused by a disturbance in the cerebral blood flow due to ischaemia or haemorrhage. In the UK, stroke is the fourth leading cause of death and a leading cause of disability (Stroke Association, 2018). According to the Stroke Association UK, there are over 100,000 stroke cases each year in the UK. This is equivalent to one case every five minutes and about two-thirds of stroke survivors leave the hospital with a disability (Stroke Association, 2018). In the UK, there are more than 1.2 million stroke survivors (Stroke Association, 2018). The cost of stroke to society is approximately £26 billion a year (Stroke Association, 2018).

The current management of stroke patients relies on rapid assessment of the two types of strokes, ischaemic stroke or haemorrhagic stroke (Glushakova et al., 2016). Thrombolytic therapy with recombinant tissue plasminogen activator (r-tPA) is the only effective treatment for ischaemic stroke approved by the Food and Drug Administration (FDA) (Roth, 2011), whereas no treatment has been shown to be effective for haemorrhagic stroke. However, a narrow therapeutic window within 4.5 hours of symptom onset (Adams et al., 2007; Saver et al., 2013) and intracranial haemorrhage related r-tPA treatment (Whiteley et al., 2016) make many clinicians to avoid using this treatment. Therefore, objective and rapid assessments of the types of stroke at admission would increase the number of patients with ischaemic stroke receiving r-tPA treatment and thereby, improve functional outcomes for many additional stroke patients (Roth, 2011).

Endovascular therapy such as mechanical thrombectomy (MT) utilizing stent retriever devices allows emergent reperfusion with great recanalisation, which provides cure for acute ischaemic stroke with a large artery occlusion (LVO) in the anterior circulation who can be treated within 24 hours of the time onset (Mokin et al., 2019).

A primary aim in acute stroke therapy is quick, early diagnosis and targeted acute treatment (Maas et al., 2020). Because the effectiveness of reperfusion therapies like intravenous thrombolysis and MT is time-dependent, there is a pressing need to improve techniques for a quicker and more precise diagnosis (Hacke et al., 2008; Sandercock et al., 2012; Lever et al., 2013; Emberson et al., 2014).

Current clinical pathway for suspected stroke (as shown in schematic Figure 1.1) depends on neurological assessment by a stroke consultant and neuroimaging by computer tomography (CT) and/or magnetic resonance imaging (MRI) in-hospital, requiring patients to be sent to surrounding medical facilities for an initial assessment. Neuroimaging by CT scan and MRI plays a critical role in the stroke workup and diagnosis (Tatlisumak, 2002). This clinical based investigation consumes time especially with MRI. Moreover, when a patient is deemed eligible for thrombectomy, he/she should be sent to a comprehensive stroke unit.

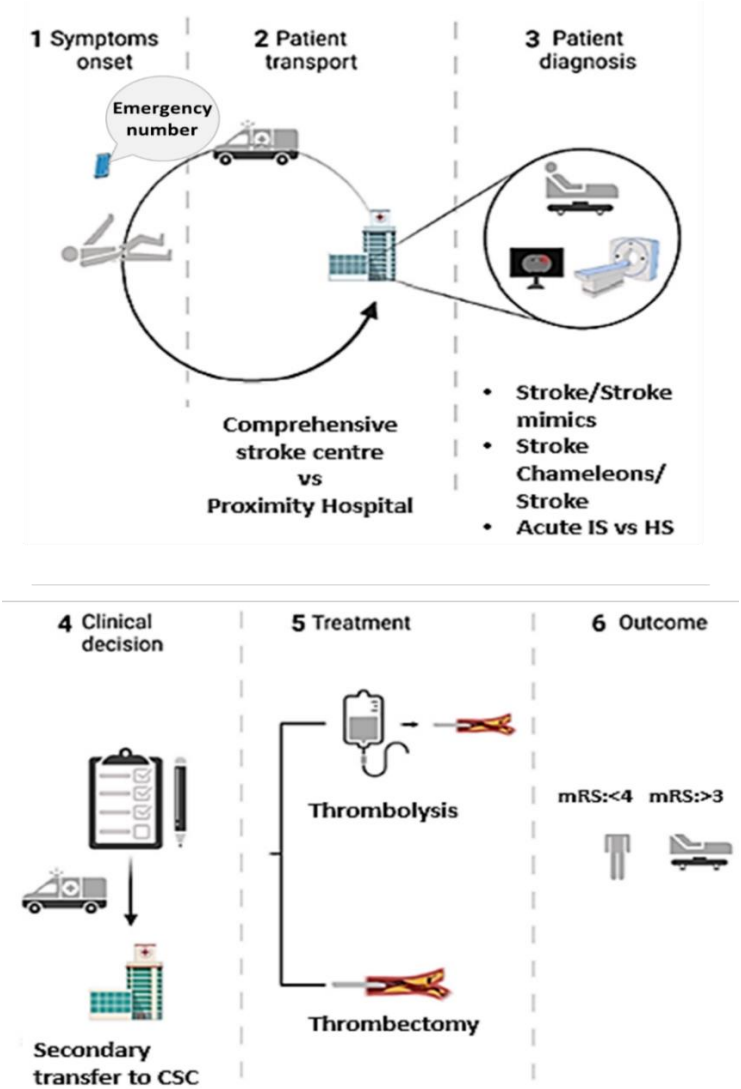

Figure 1.1 Schematic diagram of current clinical pathway for suspected stroke starting from time of stroke onset until treatment and outcomes (Dias et al., 2021). IS—ischaemic stroke; HS—haemorrhagic stroke; CSC—Comprehensive stroke centre; mRS—modified Rankin Score: functional outcomes score.

However, CT and MRI modalities have drawbacks. For examples, CT is relatively expensive and requires a high radiation dose (Tsalafoutas and Koukourakis, 2010) and many patients with suspected stroke are subsequently confirmed to have alternative pathologies (Buck et al., 2021). MRI is expensive, inaccessible and unavailable in many places like remote areas. It also needs long scanning time and susceptible to motion artifacts (Zaitsev et al., 2015). Moreover, in the presence of pacemakers, or other metallic implants, an MRI cannot be performed (Fred, 2004; Shaikh et al., 2019). In point of fact, early acute ischaemic changes within the initial three hours following symptom might be difficult to detect on non-contrast computed tomography (NCCT) scan alone (Gao et al., 2017). Although MRI known to be more sensitive than CT in terms of the diagnosis of acute ischaemic stroke, it takes longer scanning time and is not accessible in every medical institution (Zaitsev et al., 2015). Furthermore, MRI may not be appropriate for claustrophobic patients (Ghadimi and Sapra, 2022). Thus, the current diagnostic tests for stroke primarily rely on the neurological assessment in the absence of a practical and generally available radiological diagnostic (Musuka et al., 2015).

Early and accurate stroke diagnosis are extremely important in order to reach a good outcome and improved functional recovery. The diagnosis could be challenging especially within the hyperacute and acute phases that are relied on clinical investigations in combination with neuroimaging techniques. Moreover, there is a lack of immediate diagnostic tool at 'point of care' in the community near the patient. While imaging biomarkers have played significant role in determining acute therapies, the use of sensitive and specific blood-based biomarkers of stroke-associated brain injuries could significantly improve the current diagnosis of stroke, treatment and functional outcomes (Katan and Elkind, 2018). This points to the necessity for an additional accurate and rapid clinical test to offer ischaemic diagnostic information in addition to clinical assessments.

Blood Biomarkers could improve the care of stroke by allowing early stroke diagnosis even by clinical providers without extensive neurological training as well as by facilitating patients monitoring and assessment of the brain injury severity (Glushakova et al., 2016). In addition, a panel of brain damage markers in blood might be used to compliment current neuroimaging tools for stroke diagnosis (Glushakova et al., 2016). These blood biomarkers would be particularly important in patients with transient

neurological symptoms or those who are not easily diagnosed by imaging (Glushakova et al., 2016). The biomarker assessment could be performed during initial triage by ambulance staff at or near patient's home, avoiding delays in transporting stroke patients to appropriate care centres and permitting treatment of patients at high risk for early stroke recurrence (Glushakova et al., 2016).

Stroke affects and damages brain cells (Lo et al., 2003). Multiple experimental studies have found that cerebral ischaemia caused by stroke leads to changes in neurons, astrocytes, oligodendrocytes, and microglia and these changes are reflected in proteins released into the blood due to post-stroke damage of the blood brain barrier (BBB) (Li et al., 2018). Recently, different blood-based biomarker panels have been investigated for human stroke (Whiteley et al., 2008; Hasan et al., 2012; Glushakova et al., 2016). Some biomarkers, such are neuron-specific enolase (NSE) (Bharosay et al., 2012; Lu et al., 2015) and glial fibrillary acidic protein (GFAP) (Luger et al., 2017; Ren et al., 2016) have shown promising results.

Despite progress in research about biomarkers in blood serum during the past years, there is no single circulating biomarker for tracking stroke onset and progression in the clinical settings. Moreover, correlating these biomarkers levels with MRI and CT imaging results as well as clinical outcomes remains inconclusive. Therefore, the main aims of this PhD project are first to determine the circulating biomarkers in mouse models of stroke compared to sham operated mice and then to examine these circulating biomarkers in acute stroke patients compared to mimics defined by clinical scoring systems as well as CT and MRI scans. This chapter defines stroke classifications, stroke types, blood supply of the brain and areas affected by stroke, cellular damage and mechanism of stroke and BBB. This chapter also describes current clinical stroke diagnostic methods, stroke treatment and stroke mimics. Finally, an insight into imaging technologies and principles of using CT scan and MRI as well as current advances and gap in circulatory biomarker studies in both preclinical and clinical settings is provided.

1.1 General background

1.1.1 Stroke Classifications

Stroke is classified into two broad categories: ischaemic stroke and haemorrhagic stroke (Stroke Association, 2018). More than 87% percent of all strokes are cerebral ischaemic strokes, which are caused by a blood clot (obstruction of the brain blood vessel). On the other hand, haemorrhagic strokes are caused by rupture of brain blood vessels (Maas and Furie, 2009), Figure 1.2.

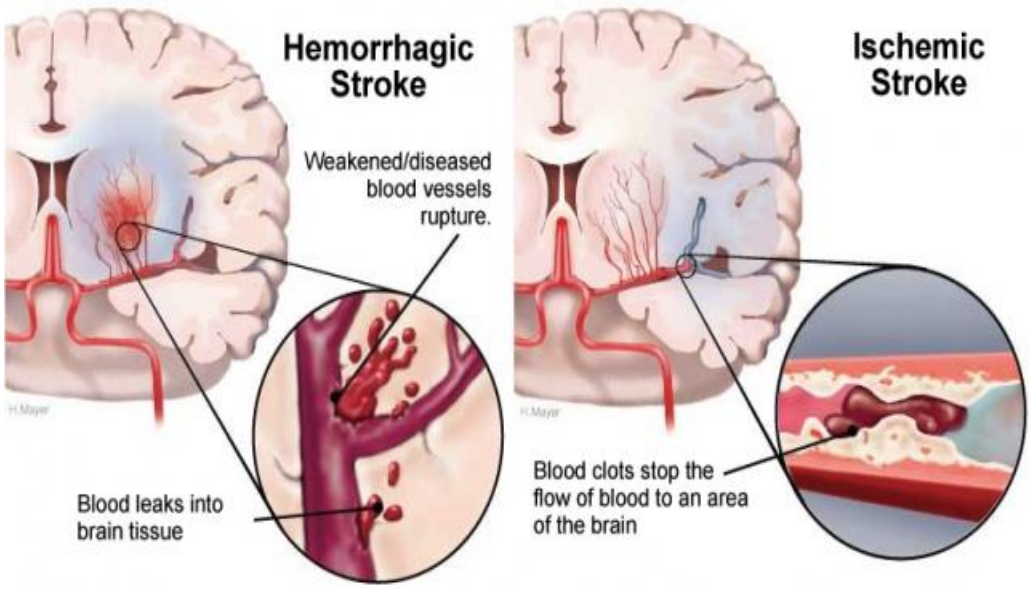

Figure 1.2 The two categories of stroke (Heart & Stroke, 2022).

1.1.2 Types of ischaemic stroke: Global and focal

Ischaemic stroke or cerebral ischaemia is known as an insufficient blood flow to the brain to complete metabolic demands (Stroke Association, 2018), causing loss of brain function and cell death, and can be divided into two types: Global ischaemia and focal ischaemia (Hossmann, 1991). Global ischaemia is where there is no blood flow to the entire brain leading to neuronal injury to susceptible areas of the brain or neuronal death if global ischaemia persists (Hossmann, 1991). On the other hand, focal ischaemia is where there is no blood flow to a portion of the brain (Hossmann, 1991). It involves an occlusion of one major cerebral blood artery such as the middle cerebral artery (MCA), distal internal carotid artery (ICA), and basilar artery. Ischaemic stroke

can further be classified into two categories: (a) Thrombotic stroke and (b) Embolic stroke (Hossmann, 1991). Thrombotic stroke onsets when a thrombus (blood clot) forms within the blood vessel of the brain, whereas, an embolic stroke happens when a blood clot travels from the other parts of the body to the blood vessels of the brain (Hossmann, 1991). The most common cerebral vessels that are affected in human ischaemic stroke are MCA and its branches, which accounting for about 70% of infarcts (Tamura et al., 1981).

Different models of focal and global cerebral ischaemia have been established over the past years to mimic ischaemic stroke in patients. Middle cerebral artery occlusion (MCAO) model of ischaemia has widely been used for induction of focal ischaemia in small animals (Takizawa et al., 1991) and two-vessel bilateral common carotid artery occlusion (BCCAO) has been used for induction of global ischaemia (Speetzen et al., 2013).

1.1.3 Haemorrhagic stroke

Haemorrhagic strokes are caused by rupture of weakened vessel that bleeds into the surrounding brain (Stroke Association, 2020). There are two types of weakened blood vessels that usually cause haemorrhagic stroke: aneurysms and arteriovenous malformations (AVMs). An aneurysm is a dilating of a weakened area of a blood vessel that might leads to rupture if left untreated whereas the AVMs are defined as a collection of abnormally formed blood vessels which might rupture leading to bleeding in the brain (Stroke Association, 2020).

There are two major types of haemorrhagic strokes: intracerebral haemorrhage (bleeding within the brain) or subarachnoid haemorrhage (bleeding within the skull but outside the brain tissue) (Stroke Association, 2020). Intracerebral haemorrhage is the most common type of haemorrhagic stroke and can occurs in the lobes, pons and cerebellum of the brain (Stroke Association, 2020).

However, the bleeding within the brain could happen between the skull bone and the dura mater, which is called epidural haemorrhage; or between the dura mater and the arachnoid membrane (subdural haemorrhage); or between the arachnoid membrane and the pia mater (subarachnoid haemorrhage) (Tenny and Thorell, 2022).

1.1.4 Blood Supply of the brain and areas affected by stroke

There are two main arteries that supply blood to the brain: the internal carotid arteries and the vertebral arteries (Purves et al., 2001), Figure 1.3. The internal carotid arteries arise from the common carotid arteries at the level of the neck to form two main cerebral arteries, the anterior cerebral arteries (ACA) and the MCA. These two arteries form the anterior circulation which supplies blood to the forebrain (Purves et al., 2001). The MCA is a large artery that supplies the cortical areas with the corpus striatum (the caudate nucleus and lentiform nucleus) within the basal ganglia. MCA is the most commonly vessel affected by ischaemia. Therefore, any MCA occlusion will affect these areas (Nogles and Galuska, 2022). On the other hand, ACA supply the medial cortex, parietal, basal ganglia anterior portion and frontal lobe of the brain with blood. Thus, any ACA occlusion will affect these areas. The posterior cerebral arteries (PCA) arise from the basilar artery and supply the occipital lobe of the brain (Purves et al., 2001). All these arteries are joined by Circle of Willis (Purves et al., 2001), as shown in Figure 1.3.

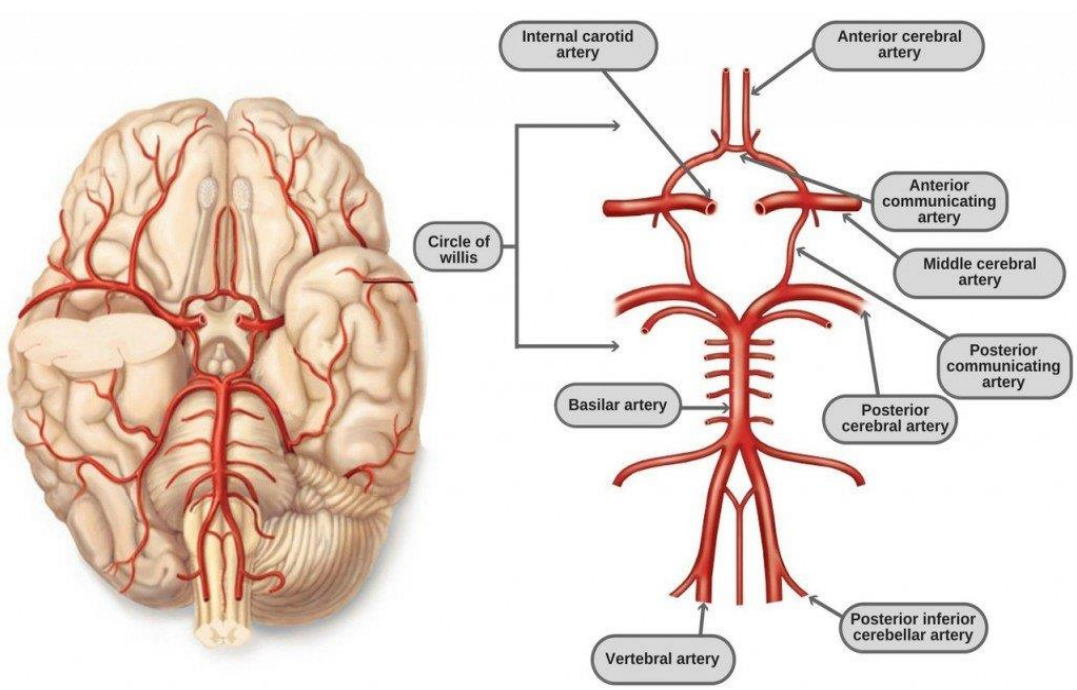

Figure 1.3 Diagrammatic representation of circle of Willis, adopted from (Ashish, 2017).

1.1.5 Cellular damage of stroke

Stroke affects all brain cells including neurons, glial cells (astrocytes, microglia, and oligodendrocytes), BBB cells, and cells linings of the ventricles of the brain that produce and recycle cerebrospinal fluid (CSF) (Pekny et al., 1999). Stroke also disturbs the CSF production, distribution, and reabsorption and leads to variations in the cells metabolism and function to the dying tissue and remote regions correlated to the stroke area (Pekny et al., 1999).

Stroke also affects neuronal extensions (dendrites and axons) through which neurons send and receive signals by molecules known as neurotransmitters (Pekna and Pekny, 2012). Stroke often causes increased accumulation of neurotransmitters in the brain tissue, specially glutamate, which may cause neurons overstimulation and neuronal death (Pekny et al., 1999).

The brain can reduce the spread of damage by producing a glial scar that seals off the region of damage (Wang et al., 2018). Glial cells are significantly essential in this mechanism. Astrocytes are responsible for glucose and other nutrients production in addition to supporting the surviving cells viability (Pekny et al., 1999). After stroke, astrocytes are activated. This phenomenon is called reactive gliosis which occurred by variation of many genes leading to profound variations in the astrocytes function and properties (Zamanian et al., 2012). The reactive gliosis cellular hallmarks include proliferation of astrocytes, thickening of astrocyte processes, (hypertrophy) and increased amount of the intermediate filaments. These intermediate filaments produce a scaffold-like network in the cell cytoplasm, a significant dynamic structure included in cell signalling, migration and adhesion that can be as a signalling platform, assisting cells deal with stress in health and injury (Pekny et al., 1999).

GFAP is the hallmark intermediate filament (IF) protein present in cytoskeleton of the astrocytes (Hol and Pekny, 2015). GFAP shows a great role in ischaemic diagnosis (Foerch et al., 2006). Recently, numerous studies focused on the role of GFAP in differentiating between intracerebral haemorrhage and cerebral ischaemia in the early phase of stroke (Xiong et al., 2015; Ren et al., 2016; Luger et al., 2017; Katsanos et al., 2017). Accordingly, these clinical studies found that GFAP level measured by sandwich enzyme-linked immunosorbent assays (ELISA), {a technique to detect the presence of antigens in samples (Alhajj and Farhana, 2022)} increased early after

stroke, suggesting that serum GFAP level can be a tool for early prediction of internal cerebral haemorrhage (Ren et al., 2016; Luger et al., 2017). However, these studies need correlation with imaging biomarkers results.

In the central nervous system (CNS), during neuroinflammation condition, the first responding cells microglia are considered the resident immune cells (Puig et al., 2018). Multiple studies have reported the important role of microglia in maintaining normal brain function in addition to pathogenesis and neuroinflammation in neurological diseases (Ma et al., 2017; Colonna and Butovsky, 2017). Following a stroke when the blood flow is reduced, microglia become activated, leading to microgliosis (an abnormal increase in the number of activated microglia number) (Masuda et al., 2011; Li and Zhang, 2016). This microglia activation is considered to have participated in the pathological progression of stroke, the role of microglia in stroke is still not fully known (Zhang, 2019).

Pericytes cells are widely diffused within the body. About 80% of blood microvessels are mounted by pericytes (Winkler et al., 2012). Particularly, the highest pericytes density is located in the CNS (Winkler et al., 2012). One of the pericytes' functions is to control the microvessels blood flow. Platelet-derived growth factor receptor (PDGFR) is a pericytes receptor that is responsible for controlling the pericytes contractility (Arimura et al., 2012). Arimura et al. (2012) stated that the PDGFR level is elevated during stroke and this endothelial PDGFR elevation dilates pericytes to increase the diameter of microvessels (Arimura et al., 2012).

1.1.6 Mechanism of stroke

Studies on stroke models mimicking the pathophysiology of human stroke are important to understand the mechanism of stroke and developing effective therapeutic measures for stroke patients (Lo et al., 2003). During the first few hours, the primary ischaemic stroke is caused by a clot in the blood vessel. This clot causes an inadequate supply of energy to the brain tissue leading to neuronal death and neurological damage. Decreased oxygen supply affects mitochondrial function and causes increase in lactic acid levels leading to a reduction in adenosine triphosphate (ATP) production and decreased activity of ion pumps on the cell membrane (Lo et al., 2003). Consequently, calcium, protons and sodium ions concentrations are elevated in the cells leading to water influx into the cells, cell

swelling and death, (Lo et al., 2003). These critical events happen quickly in the stroke site and needs to be treated within minutes to hours. In stroke the BBB integrity is compromised, permitting uncontrolled molecules entry into the brain parenchyma leading to vascular oedema, cell swelling and death, which are associated with worse stroke outcome (Lo et al., 2003). This damaged tissue can partially be salvageable within hours to few days (Lo et al., 2003). Therefore, it is important to identify brain and BBB damage to start early treatment. Figure 1.4. shows the mechanisms of stroke.

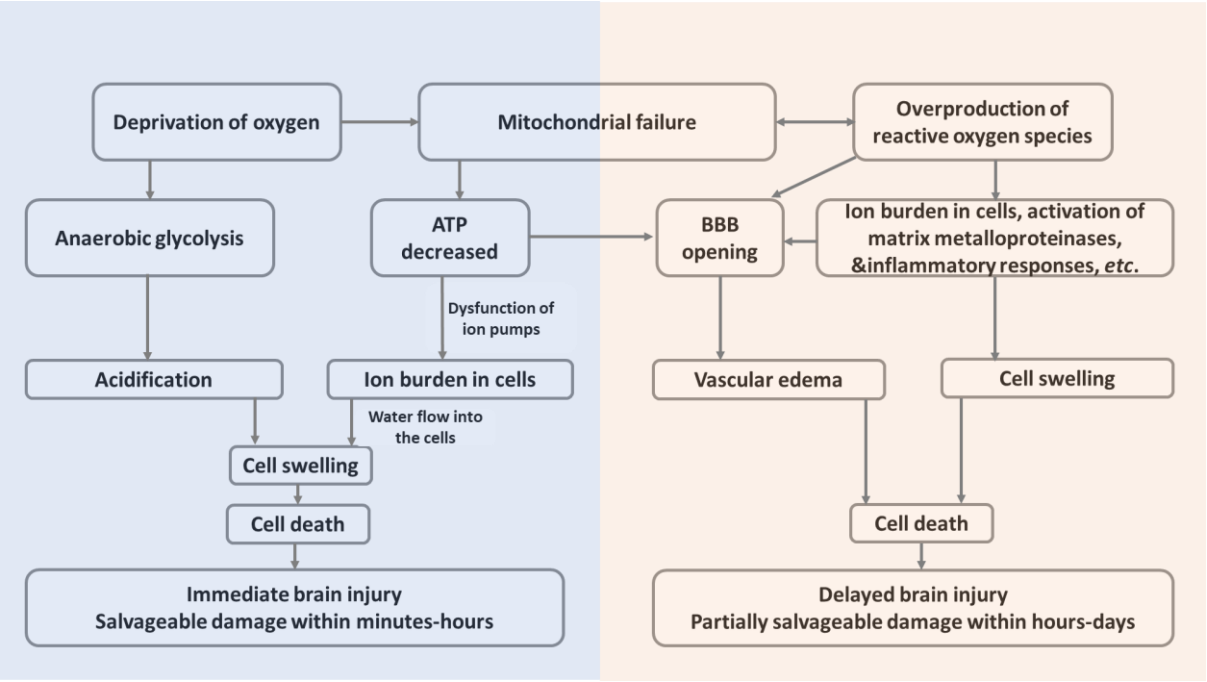

Figure 1.4 Schematic diagram of the mechanisms of Stroke, information adopted from (Lo et al., 2003).

1.1.7 Blood-brain barrier (BBB)

The BBB is formed by endothelial cells surrounding the brain blood vessels. The BBB's endothelial cells are unique in comparison with endothelial cells in different tissues since they have continuous intercellular tight junctions (TJ), which highly restrict the transcellular and paracellular molecules move through the endothelial cells layer (Liebner et al., 2018), Figure 1.5. The BBB is essential in maintaining the CNS microenvironment that allows neurones to function properly (Liebner et al., 2018). It

also preserves the influx and efflux mechanisms by tightly regulating the molecules and ions passage, delivering oxygen and nutrients depending on neuronal needs, protecting the brain from toxins as well as maintaining a suitable brain functional environment (Liebner et al., 2018).

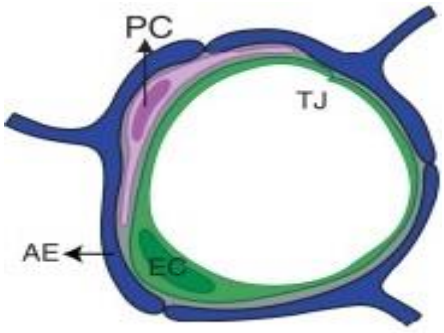

Figure 1.5 The cell types within the BBB. PC: pericytes, AE: astrocytes, EC: endothelial cells and TJ: tight junction (Daneman and Prat, 2015).

The neurovascular unit (NVU) is a complex interaction of endothelial cells, neurons, pericytes, astrocytes and the extracellular matrix (Zlokovic, 2008). Astrocytes are required for the creation and maintenance of the BBB because they release substances that allow for proper cell interaction and the establishment of robust TJ (Cabezas et al., 2014). Pericytes have mostly been linked to blood vessel stability and hemodynamic activities (Bergers and Song, 2005).

One of the signs of stroke pathology is BBB damage, which is represented by changes in TJ protein complexes leading to an increased paracellular solute leak. TJ is formed by the transmembrane proteins: Occludin, Claudin-5 and peripheral membrane proteins such as Zonula occludens-1 (ZO-1) (Keep et al., 2008; Prakash and Carmichael, 2015; Kassner and Merali, 2015).

Occludin is one of the BBB's TJ components (Zhao et al., 2020). Occludin degradation has been observed in human and animal studies with acute ischaemic stroke leading to BBB breakdown (Yuan et al., 2020). Recently, in a rat ischaemic stroke model, it has been seen the rapid loss of Occludin from ischaemic cerebral microvessels (Liu et al., 2012). Pan et al. (2017) showed correlations between Occludin levels and the extent of BBB damage in a rat ischaemic stroke model. Moreover, they measured the Occludin level in blood by ELISA and found a significant increase at 4.5 hours after

MCAO. Additionally, they examined the loss of Occludin from microvessels in a brain slice of a rat model of MCAO by using immunostaining and found that blood Occludin levels correlate well with the BBB damage suggesting that Occludin may work as a clinically relevant stroke biomarker for ischaemic stroke (Pan et al., 2017).

Claudin-5, is another TJ component of endothelial cells of brain (Jia et al., 2014). Fundamental role of Claudin-5 is to selectively reduce ions (Jia et al., 2014). It is been found that Claudin-5 is expressed in the early stages of development (Lv et al., 2018). However, Pan et al. (2017) and Shi et al. (2017) have found that the blood Claudin-5 concentrations did not change significantly after cerebral ischaemia.

ZO-1 is one of the BBB's TJ component that reduces the cerebral vessels permeability by restricting the free molecular exchange between brain tissues and blood (Itoh and Bissell, 2003). Disarrangement of ZO-1 has been shown to reduce BBB integrity and is an indicator of BBB damage (Petty and Wettstein, 2001). However, these TJ proteins findings in blood need to be correlated with CT and MRI imaging biomarkers and neurological outcomes to increase the efficiently of diagnosis.

A positive correlation between astrocytes and the maintenance or improvement of BBB characterisation has been well established. Several studies have shown a relationship between astrogliosis and the dysfunction of BBB (Liebner et al., 2011; Liu and Chopp, 2016). Following stroke, astrocytes proliferates and release of GFAP leading to a reactive astrogliosis process (Sofroniew and Vinters, 2010). This is followed by a decrease in the expression of Occludin and Claudin-5 in endothelial cells, BBB damage, and infiltration of immune cells as shown by both in vitro and in vivo studies (Proescholdt et al., 2002; Argaw et al., 2009; 2012).

Pericytes are essential cellular components of the BBB and are actively related to other NVU cells. Several studies have reported that pericytes constrict capillaries resulting in fast closure of the capillary causing a long-lasting blood flow restriction (Brown et al., 2019). Moreover, it has been shown that capillary pericytes are quickly lost following a stroke in both human and animal stroke (Fernández-Klett et al., 2013a). Compatible with these results, a recent study reported that pericyte constriction or loss causes an increase in cerebral blood flow and subsequent damage of BBB in stroke (Hall et al., 2014). Overall, this subsequent BBB damage leads to

development of the most common ischaemic stroke complication i.e., intracerebral haemorrhage.

1.1.8 Current stroke diagnostic methods

Most hospitals make the diagnosis of acute ischaemic stroke entirely on the neurological assessment by clinical stroke consultants in conjunction with neuroimaging scans. Neuroimaging plays a critical role in the management of stroke patients beginning from their initial diagnosis to providing suitable medical interventions for further treatment (Akbarzadeh et al., 2021).

The common clinical neurological assessment scoring systems are: FAST test – (Face, arms, speech, time), CPSS – (Cincinnati Prehospital Stroke Scale) and NIHSS score – (National Institutes of Health Stroke Scale).

The FAST test is useful to identify the most common stroke signs. It assists to notice the three most common stroke symptoms (facial weakness, arm weakness and speech problems) (Stroke Association, 2018).

CPSS is an approved stroke screening tool used during triage. It was established to quickly evaluate patients with suspected stroke in the prehospital setting (De Luca et al., 2019). It includes an assessment of facial drop, arm drift and abnormal speech.

NIHSS score, which runs from 0 to 42, is the total of 15 separately assessed components. The severity of a stroke can be classified as follows: 0 means no symptoms; 1–4 means small stroke; 5–15 means moderate stroke; 16–20 means moderate to severe stroke; and 21–42 means severe stroke (Khan et al., 2017).

In a patient with a suspected ischaemic stroke, neuroimaging is used to rule out the existence of other forms of CNS abnormalities and to differentiate between stroke and stroke mimics and also between ischaemic stroke and haemorrhagic stroke (Yew and Cheng, 2009). Furthermore, when assessing a patient with a suspected stroke, doctors must evaluate a wide range of possibilities including stroke mimics such as seizures, mass lesions and migraines (Buck et al., 2021), (as per section 1.1.10).

The following section presents a brief introduction to the role of CT and MRI in stroke diagnosis.

1.1.8.1 Computed Tomography (CT)

CT is a widely used imaging modality in the stroke diagnosis because of its comparatively lower cost, ease in availability, and faster data acquisition (Tsalafoutas and Koukourakis, 2010) (Figure 1.6).

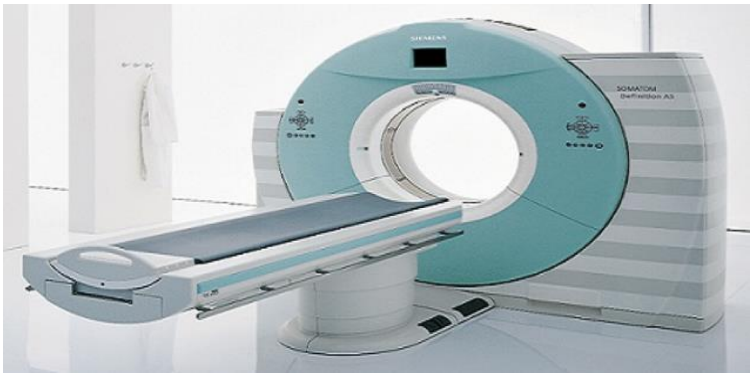

Figure 1.6 A CT scanner (The Leeds Teaching Hospitals, 2022).

1.1.8.2 Basic principle of CT

CT uses an x-ray source and a digital detector system that rotates around the patient's body to create horizontal or axial section images of the region under diagnosis (Pitkanen et al., 2006) Figure 1.7. The x-ray source is located opposite to an x-ray detector, and the pair rotates around the patient in the centre as shown in Figure 1.8. As the x rays pass through the body, they get attenuated. The attenuation depends on the tissue type and tissue density from which the beam of x-ray passes (Caldemeyer and Buckwalter, 1999). Furthermore, the alterations in the attenuation between adjacent tissues give rise to contrast in images. The tissues with less attenuation e.g., air and water appear dark in CT images, whereas tissues with high attenuation e.g., bone appear as bright (Caldemeyer and Buckwalter, 1999).

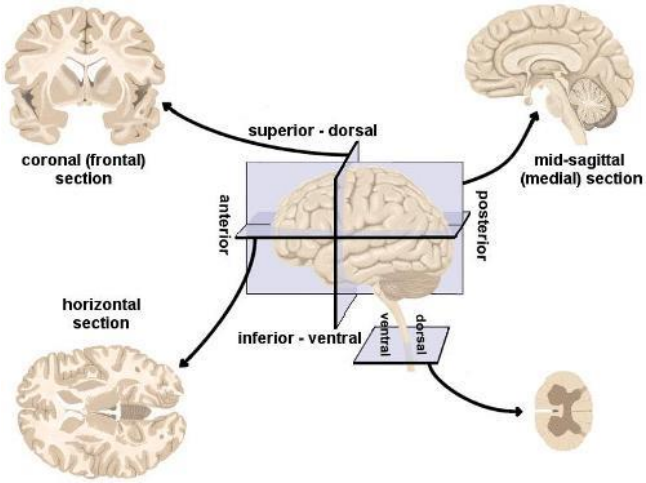

Figure 1.7 Representative cross-sections through the brain, adopted from (My-MS.org, 2022).

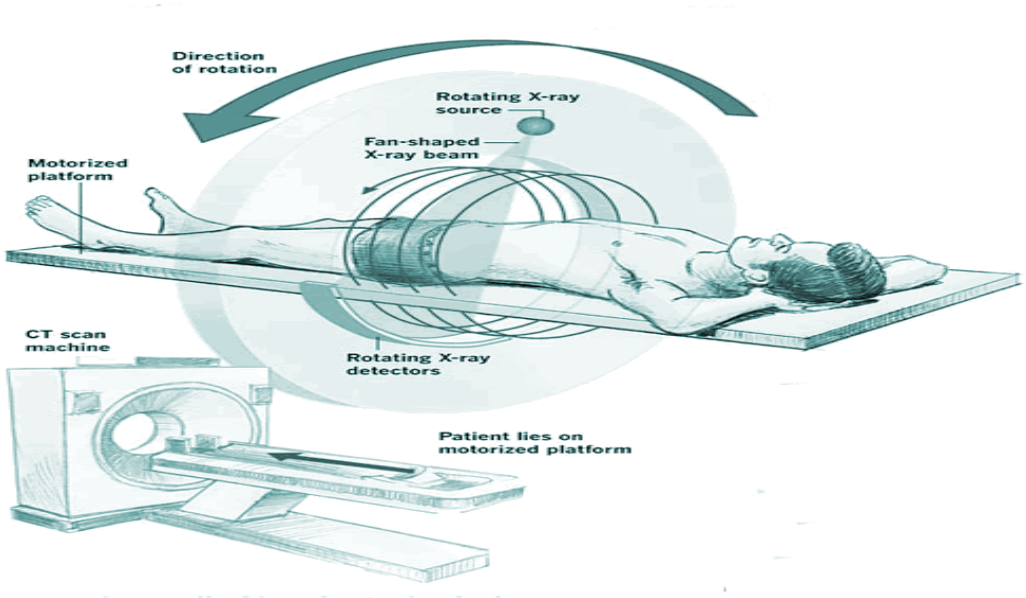

Figure 1.8 An illustration of the basic principle of CT (The Leeds Teaching Hospitals, 2022).

1.1.8.3 CT imaging to characterise immediate primary brain injury

An initial clinical step in the management of suspected stroke patients is the NCCT examination since it can quickly exclude the possibility of a cerebral haemorrhage (Birenbaum et al., 2011). Furthermore, CT angiography (CTA) is an adjunctive procedure used to investigate neurovascular anatomy and blood vessel abnormalities such as stenosis and occlusion (Birenbaum et al., 2011). In a clinical stroke protocol,

an addition of CTA with NCCT provides cerebral information about thrombus extension and type of clinical intervention required (Menon and Demchuk, 2011). Besides, CT perfusion (CTP) imaging is also an excellent imaging modality for neuro-interventionists. CTP relies on the tracking of a single bolus of intravenously injected contrast agent (iodinated) through the cerebral circulation by consecutive spiral scanning (Munich et al.,2016). Iodine-containing intravenous radio-contrast agent increases the visibility of vascular organs and structures during radiographic procedures (Andreucci et al., 2014). CTP technique provides detailed blood flow information in the brain by showing the extent of salvageable tissue that can get benefit from endovascular intervention treatment (Campbell et al., 2015; Munich et al., 2016). CTP also provides relative and absolute information regarding brain perfusion parameters, which are detailed in the following section.

1.1.8.4 CTP biomarkers or parameters

Perfusion biomarkers are known as cerebral hemodynamic perfusion parameters (Engedal et al., 2018) such as cerebral blood volume (CBV), cerebral blood flow (CBF), mean transit time (MTT) and time to peak (TTP) (Khandelwal, 2008). CBV refers to the blood volume per unit of brain tissue and is usually measured as millilitres per 100 gm of blood (Khandelwal, 2008). CBF refers to the rate of blood to brain tissue per minute and is usually measured as millilitres per minute per 100 gm of blood (Khandelwal, 2008). MTT can be defined as the time between the venous outflow and the arterial inflow, and TTP is the time taken by the contrast agent to achieve maximum enhancement Hounsfield unit (HU) {a quantitative value of the radio density of the tissue (DenOtter and Schubert, 2022)} in the region of interest (ROI) prior its value starts reducing (Khandelwal, 2008). It is possible to measure these quantitative perfusion parameters from different modalities such as CTP and MRI perfusion.

Latchaw et al. (2003) in the guidelines and recommendations for perfusion imaging in cerebral ischaemia have stated that CT scan can quantify the change in the density of tissue following administration of a contrast agent to calculate the perfusion parameters; CBF, CBV and MTT. Additionally, they have been recommended that perfusion techniques are capable of identifying reversible and irreversible ischaemic tissues (Latchaw et al., 2003). Multiple clinical studies also have mentioned the quantitative perfusion parameters percentage (Abels et al., 2010). The normal perfusion parameters values in white matter (WM) and grey matter (GM) are shown in

Table 1-1 (Kaneko et al., 2004; Rostrup et al., 2005; Mu et al., 2013). According to a study by Rostrup et al. (2005), in normal perfusion case, a symmetric sided perfusion is observed with higher CBV and CBF in the GM than in the WM due to the variation between their physiological hemodynamic properties. However, in the case of stroke, the prediction of penumbra (the brain tissue at risk) or core (a tissue within the ischaemic area which is irreversibly damaged) (Yu et al., 2016), is based on the resulting changes in cerebral blood perfusion parameters.

The change in perfusion parameters aids in the patient's treatment. Multiple studies have shown that CTP parameters help to differentiate salvageable and unsalvageable tissue, and in the identification of patients with salvageable tissue for their reperfusion therapy. The quantitative measurement of CTP parameters indicates that abnormal cerebral hemodynamics can offer an efficient basis for clinical diagnosis and decision-making process for patient selection in MT (Rostrup et al., 2005; Borst et al., 2015). Also, according to a study by Xu et al. (2019) on acute ischaemic stroke patients, the patient's prognosis is significantly related to the value of CTP parameters.

Table 1-1 The normal perfusion CT parameter values (Kaneko et al., 2004; Rostrup et al., 2005; Mu et al., 2013) .

	CBF (ml/min/100g)	**CBV (ml/100g)**	**MTT (sec)**
White Matter	20	1-2	4-5
Grey Matter	60-80	4-5	4-5

In principle, slightly decreased CBF refers to a decompensated cerebral circulation reserve. However, a significant CBF reduction denotes the probability of a cerebral infarction development (Yu et al., 2016). Severe reduction in CBV (30-40% in comparison with CBV in the normal condition) indicates core infarct (Munich et al., 2016; Flottmann et al., 2017) . A delayed MTT indicates an impaired perfusion reserve and this relates to collateral circulation (Yu et al., 2016). Moreover, a delayed MTT is an easy way to measure the cerebral circulation which assists in dealing with the lack of CTA anatomic resolution for collateral evaluation. Also, ischaemic stroke patients with raised MTT delay are considered at high risk of getting infarct in the future (Keedy et al., 2012).

1.1.8.5 Magnetic resonance imaging (MRI)

MRI also known as nuclear magnetic resonance imaging, is a multimodal imaging technique that generates detailed anatomical images of the diagnosed organ of the patient by utilizing the magnetic properties of hydrogen nuclei (protons) from water molecules present in the body (Berger, 2002). As shown in Figure 1.9 , a ring-shaped structure produces a strong magnetic field that aligns the hydrogen nuclei along its direction. Further, a brief radio frequency (RF) signal (90º to the magnetic field) flips the aligned spin of the protons. When the RF signal is turned off, the spins of the protons relax back to their original states and realign with the static magnetic field. In the relaxation process, the protons emit energy at the same radio frequency which is further detected by the receiver coil to generate an image (Roth et al., 2005). In contrast to CT, MRI offers a non-invasive diagnostic platform as it doesn't expose the patients to ionizing X-ray rations. It is very suitable for the diagnosis of soft tissues rather than bony structures (Caldemeyer and Buckwalter, 1999).

Figure 1.9 An MRI scanner (The Leeds Teaching Hospitals, 2022).

1.1.8.6 Role of MRI in acute ischaemic stroke

MRI is more sensitive than CT in distinguishing the secondary ischaemic lesions and the stroke mimics (Vymazal et al., 2012). Diffusion-weighted imaging (DWI) has a great role in providing valuable information on brain tissue viability. It is one of the sequences of MRI which uses the water molecules' diffusion to produce contrast in images. The diffusion process alters markedly by a neurological disorder such as stroke (Schaefer et al., 2006). The DWI sequence calculates the water molecules'

diffusion speed in different parts of the brain and illustrates where the motion of water is restricted which indicates the area of brain damage (Linfante et al., 2001). Besides, DWI, which is faster than other imaging techniques, can detect ischaemic stroke within a few minutes of stroke onset (Linfante et al., 2001).

Apparent diffusion coefficient (ADC) map is a calculated map of the water molecular diffusion within tissue and is clinically generated using DWI sequence (Yang et al., 1999). The ADC can be used as a brain ischaemia biomarker as it shows an increased DWI signal in acute stroke with a decrease in the ADC value (Yang et al., 1999). The normal ADC values of WM and GM regions of the brain are shown in Table 1-2.

Table 1-2 The normal ADC values of WM and GM regions of the brain (Helenius et al., 2002).

	ADC ($*10^{-6}$ mm ^{2}/s)
White Matter	670-800
Deep Grey Matter	700-850
Cortical Grey Matter	800-1000

Additionally, Magnetic resonance angiography (MRA) is a technique that is used to image the blood vessels to evaluate their vascular flow dynamics (Vu et al., 2006). Furthermore, the administration of a contrast agent aids in the enhancement of the image and specificity of the ischaemic region (Vymazal et al., 2012). This can be done by performing MR perfusion or Perfusion weighted imaging (PWI) which shows perfusion in tissues through blood (Vymazal et al., 2012). Using PWI, perfusion parameters: CBF, CBV and MTT could be measured as mentioned previously.

Three methods are widely used to measure perfusion using MRI: Dynamic Susceptibility Contrast (DSC) perfusion MRI, Dynamic Contrast–Enhanced (DCE) perfusion MRI and Arterial spin labelling (ASL) (Jahng et al., 2014). DSC and DCE require a gadolinium intravenous bolus administration whereas ASL is performed without exogenous contrast. DSC and DCE are the commonly used techniques for the diagnosis of ischaemic stroke (Jahng et al., 2014). DSC perfusion imaging starts with injecting a gadolinium bolus intravenously followed by a rapid series of gradient or spin-echo images over the organ of interest. As the gadolinium contrast agent passes

through the area of circulation, it stays in the intravascular space. Its paramagnetic properties cause a local magnetic field distortion around the blood vessels with T2 (T2*) dephasing and signal loss (Jahng et al., 2014). The different parameters can be calculated with signal intensity as a function of time such as CBF, CBV and MTT. Besides, the time of image acquisition is very short which is around 2 min (Tofts, 2010; Jahng et al., 2014).

While DCE also requires an exogenous gadolinium administration like DSC imaging. However, DCE uses the T1 shortening effects of gadolinium to acquire repeated T1-weighted images within 5-10 minute of interval. The gadolinium contrast agent accumulates in the tissue extracellular space at an amount defined by perfusion, surface area and capillary permeability during this time frame (Jahng et al., 2014). The images can be analysed quantitatively, semi-quantitatively or visually (Sourbron et al., 2009).

1.1.9 Stroke treatment

Stroke has four main stages or phases: hyperacute, acute, subacute and chronic (Tong et al., 2014). In the last two decades, the medical interventions for the treatment of ischaemic stroke patients have been enhanced by using a clot-buster drug, r-tPA (Bansal et al., 2013) or the endovascular thrombectomy. The haemorrhagic transformation is a very frequent complication in ischaemic stroke patients after the r-tPA treatment (Yang et al., 2007). The temporary reperfusion would restore the permeability of BBB, however, late reperfusion may lead to aggressive BBB injury (Yang et al., 2007; Jickling et al., 2014). Recent randomized trials have shown the implementation of MT (an endovascular interventional treatment using stent retrievers in a distal ICA or a proximal MCA) for reperfusion and improve functional outcomes (Evans et al., 2017) (Figure 1.10).

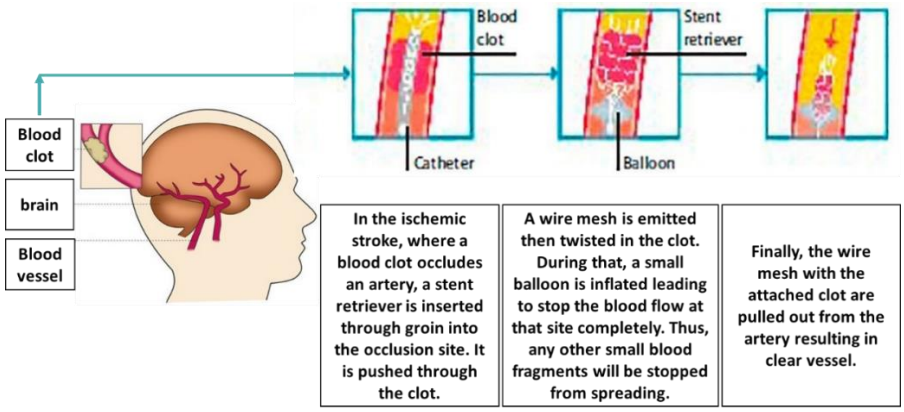

Figure 1.10 An illustration of interventional therapy (MT) for the treatment of an ischaemic stroke patient , information adopted from: (CIRSE, 2022).

MT as mentioned previously is indicated for acute ischaemic stroke with a LVO in the anterior circulation who can be treated within 24 hours of the time onset (Mokin et al., 2019). On 2012, new-generation stent retriever devices (the Solitaire FR Revascularisation Device and Trevo ProVue Retriever) have been invented and then studied (Saver et al., 2012). Saver et al. (2012) showed significant benefits of these devices in terms of better recanalization in a comparison with the older MERCI (Mechanical Embolus Removal in Cerebral Ischaemia) device. As a consequence, the SWIFT (Solitaire with the intention for thrombectomy) study has stopped the use of MERCI device early due to the significant recanalization results with Solitaire compared to MERCI (83% vs 48.1%) respectively. Moreover, the comparison results showed a significant decrease in mortality rate at 3 months (17.2% vs 38.2%) respectively and better neurological outcome at 3 months (Saver et al., 2012).

In order to define whether patient is indicated for MT, severity of stroke should be evaluated using the NIHSS (as per section 1.1.8). The recent trials on MT independently established a low initial NIHSS as an inclusion criterion of stroke severity during MT selection in acute ischaemic stroke patients with LVO in the anterior circulation (Mokin et al., 2019).

MT improves the clinical outcome in combination with intravenous thrombolysis within six hours of symptom onset (Derex and Cho, 2017). However, additional detailed studies are necessary to ascertain this hypothesis. Therefore, one objective of this study was to determine if absolute values of imaging biomarkers (CBV, CBF and MTT) obtained from CTP have the potential to improve prediction of clinical outcomes in MT

(2.2). Then, this study aims to assess the role of blood biomarkers and imaging biomarkers in acute stroke patients compared to stroke mimics patients undergoing all treatment for stroke diagnosis improvement.

1.1.10 Stroke mimics

Stroke mimics are false positive stroke cases and can be defined as non-vascular disorders that present with an acute neurological disorder simulating acute ischaemic stroke and represent a high percentage of all acute ischaemic hospital admissions (Vilela, 2017).

The aetiologies of mimics were separated into neurological (55.1%) and non-neurological (44.9%) aetiologies (Buck et al., 2021). In details, the most common neurological mimics includes seizures (19.7%), migraines (18.8%) as well as peripheral neuropathies (11.2%). While, the most common non-neurological mimics are cardiovascular (15.9%), psychiatric (11.9%) and infections (8.9%) (Buck et al., 2021). These conditions can imitate stroke, especially during the acute phase. According to Hand et al. (2006), up to 20% to 30% of stroke code activations at the prehospital level are caused by these conditions.

In the very early stages of stroke, an alternative test with sufficient sensitivity and specificity in distinguishing between real strokes and stroke mimics, and also between different types of strokes, might be useful to guide the management of prehospital stroke, including patient's allocation and prehospital reperfusion treatments such as r-tPA in the very early stroke phase. Blood biomarkers have been presented as a method to aid in the diagnosis of acute stroke (Dagonnier et al., 2021). They are an objective measurement of molecular features. In a study including 1005 patients with suspected stroke, a blood biomarkers panel had a prediction accuracy of 0.759 in distinguishing between strokes and stroke mimics within the first 24 hours (Montaner et al., 2011). On 2017, a panel of 21 biomarkers has examined (Bustamante et al., 2017). However, the predictive model's accuracy rates are still away from those needed (Bustamante et al., 2017). Therefore, the need of new valuable biomarkers remains the upcoming challenges to fulfil the molecular stroke diagnosis.

1.1.11 Current evidence of using biomarkers for stroke diagnosis

This section will mention the current evidence of applying biomarkers to diagnose stroke. The biomarkers were focused on this research are imaging biomarkers and blood circulating biomarkers.

1.1.11.1 Imaging biomarkers

Imaging biomarkers are the characteristic parameters that are objectively acquired from the radiological medical images (deSouza et al., 2019). These parameters illustrate and measure the characteristic of a tissue (functional, structural or biological) after performing signal processing as well as computational models to images in the space and time domains. Additionally, these imaging biomarkers help in the detection of disease, abnormalities characterisation, and treatment response (deSouza et al., 2019). Recently, in acute stroke neuroimaging, huge attention has been given to imaging biomarkers for their assistance in providing a much better understanding of acute stroke pathophysiology, improving diagnostic precision, patients selection for clinical trials, clinical outcomes prediction, monitoring disease prognosis, and defining new therapeutic targets (Henriksen et al., 2014). Moreover, these biomarkers can also be utilized to enhance inclusion/exclusion criteria for patient selection by focusing on the patients with a target disease and excluding the patients who are likely at risk for bad outcomes (Kidwell, 2013). According to a study by Kidwell (2013), these biomarkers also predict the prospect of ischaemic interventional treatment response. Specifically, imaging biomarkers could precisely predict non-aneurysmal rupture risk and risk of subarachnoid haemorrhage (Achrol and Steinberg, 2016). These parameters allow radiologists to draw curves of time versus concentration and then obtain the perfusion parameters (Gordon et al., 2014).

The most commonly used imaging biomarkers are: Alberta Stroke Program Early CT Score (ASPECTS) which is a score that quantifies the early ischaemic changes extent (Mokin et al., 2017), infarct volume, CT HU, ADC value, T2 signal intensity value (the value of the signal intensity obtained from the T2 image in MRI (Bloem et al., 2018)), and perfusion parameters (CBF, CBV and MTT). Some of these biomarkers have been explained in detail previously in section 1.8. A brief review regarding the variations of these imaging biomarkers following an ischaemic stroke which has been reported in earlier studies is shown in the following Table 1-3.

Table 1-3 Changes of imaging biomarkers after an ischaemic stroke noticed in previous studies.

Imaging markers	Sample size / method used	Marker levels	Results	Authors
ADC values.	14 patients with acute ischaemic stroke / MRI-DWI	**Control:** ADC=702 $\times10^{-6}$ mm ^{2}/s **Stroke:** ADC=605 $\times10^{-6}$ mm ^{2}/s for the infarct	Infarct areas have much lower ADC values than non-infarct locations. **Strengths:** In a prospective cohort of acute stroke patients, sequential MR imaging was collected at baseline, 6 hours after r-tPA, and 30 days after r-tPA. **Limitations:** Small number of sample. The work has not been correlated with blood biomarkers.	(Purushotham et al., 2015)
Hounsfield units (HU) of ASPECTS.	100 of middle cerebral aretery occlusion / CT imaging	**Control:** the HU values in all the 10 regions of ASPECTS in normal side were higher than the one stroke side **Stroke:** the HU values in stroke side were	A reduction in HU values in ischaemic side compared to normal side. Control: lentiform nucleus (L)=34.7; caudate head (C)=33; insular ribbon (I)=32; internal capsule (IC)=29.2; anterior MCA cortical region (M1) =35.4; MCA cortical region located lateral to insular ribbon (M2) =33.6; posterior MCA cortical region (M3) =34.3; M4 superior to M1=33.2; M5 superior M2=32.7 and M6 superior to M3=33.2 Stroke: lentiform nucleus (L)=32.6; caudate head (C)=31.6; insular ribbon (I)=29; internal capsule (IC)=28.1; anterior MCA cortical region (M1) =33.4; MCA cortical region located lateral to insular ribbon (M2) =33; posterior MCA cortical region (M3) =33.2; M4 superior to M1=33; M5 superior M2=32.7 and M6 superior to M3=33.1	(Maegerlein et al., 2019)

		lower than the one in control side.	**Strengths:** Good sample size. **Limitations:** The work has not correlated with blood biomarkers.	
ADC value T2 value	103 Acute ischaemic stroke / MRI-DWI and MRI T2	**Control:** ADC= 0.88 X 10^{-3} mm^2/sec **Stroke:** below 8 hours = 0.29 X 10^{-3} mm^2/sec and up to 5 months= 1.60X 10^{-3} mm^2/sec The mean T2 ratio below 8 hours =1.16 The mean T2 ratio at 0.75 to 5 months = 2.04	ADCs have been reported to stay low after stroke for up to ten days before increasing. ADC values and T2 values are increased significantly after 5 months from stroke onset. **Strengths:** The study analysed two MRI parameters (ADC values and T2). **Limitations:** The study did not separate the GM and WM zones which would allow for more accurate stroke duration calculations. ADC values in an infarct are heterogeneous. Lack of blood biomarkers correlation with imaging biomarkers.	(Lutsep et al., 1997)
Infarct lesion volume in	120 ischaemic stroke	**Control:** -	Estimated volumes of infarct obtained from CTP were significantly smaller than the one obtained	(Hoving et al., 2018)

CT and MRI	patients / CTP and follow-up MRI-DWI	**Stroke:** CTP estimated lesion volume = 7.8 mL DW lesion volume at 24 hrs = 30.8 mL	follow-up MRI-DWI at 24 hours. This may be due to infarct growth. **Strengths:** The study compared the lesion volume of a relatively good sample size from 2 modalities; from initial CTP and the follow-up MRI **Limitations:** The possibility for infarct development beyond 24 hours as it is known that the ischaemic infarct continues to grow in the days following onset of stroke. The study lack correlation with blood biomarkers.	
CBV, CBF, MTT and infarct volume.	161 acute ischaemic patients treated with recanalization. (A)- 93 individuals were successfully treated and (B)-68 individuals were not successfully treated /	**Control:** Optimal cutoff in non-successfully treated group CBF=34 ml × 100 g −1 × min−1 CBV= 2.4 ml × 100 g−1 MTT=9sec Volume of infarct(B) =113.4 ml **Stroke:** Optimal cutoff values in	Significant decrease in CBV and CBF in ischaemic patients. Successfully treated patients had significantly smaller volumes of infarct compared to non-successfully treated group. **Strengths:** A first study to evaluate the anticipation ability of perfusion thresholds versus threshold free infarct anticipation. **Limitations:** The study only included patients who were treated endovascularly with major vessel blockage. Patients who are intravenously treated should be included in future therapy. Final infarction was measured on follow-up imaging from 48 hours until 7 days following stroke, which could be affected by brain shift from oedema. The study lacks correlation with blood biomarkers.	(Flottmann et al., 2017)

	CTP	successfully treated group CBF=33 ml×100g^{-1} × min^{-1} CBV= 2.4 ml×100g^{-1} MTT=10sec Volume of infarct =35.7 ml		

Principally CT scans are thought to be sensitive enough to detect mass lesions, such as a brain tumour or abscess, as well as acute bleeding. However, CT scans may be insufficiently sensitive to identify an early ischaemic alterations, especially if it is small, acute, or occurs in the posterior fossa (Mullins et al., 2002).

Several multimodal MRI sequences have shown promise in the early detection of ischaemic stroke particularly DWI (Fiebach et al., 2002). DWI sequence can detect parenchymal alterations early in the course of a stroke, thus, has a higher sensitivity than CT for identifying acute ischaemic stroke (Schaefer et al., 2000). Even though MRI scans have a higher sensitivity and resolution than CT scans (Müller, 2002), MRI scanners are less common in the acute environment due to a practical challenge and are more expensive. In addition, MRI scans are contraindicated for people who have implanted electronic devices (e.g., pacemakers) or who have claustrophobia (Ghadimi and Sapra, 2022). As a result, the diagnosis of stroke is essentially a clinical choice in the absence of practical and generally available radiological and imaging diagnostics.

All in all, ischaemic stroke patients are currently assessed using a combination of the extensive clinical neurological examination and neuroimaging approaches. Furthermore, clinical conditions that mimic the signs and symptoms of a stroke may make it more difficult to diagnose and treat stroke sufferers quickly. Thus, it is

important to find a quick, accurate and simple technique that can rapidly identify and differentiate stroke from stroke mimics.

1.1.11.2 Circulating biomarkers

A stroke circulating biomarker can be defined as any measurable physiological substance in the body which indicates a stroke-related process, risk and/or manifestation (Maas and Furie, 2009). Presently, the research on stroke biomarkers is of immense interest in the field of medical diagnostics. Any development in this direction will contribute to the understanding of stroke pathophysiology, diagnosis, and treatment approach (Maas and Furie, 2009). According to Saenger and Christenson (2010), the characteristics of an ideal stroke biomarker are specificity, sensitivity, predictable clearance, differentiation between haemorrhagic vs ischaemic stroke, stable and early release shortly after infarction, the potential for risk assessment and guidance of therapies, and ability to be measured rapidly by affordable methodologies (Saenger and Christenson, 2010).

Despite the role of current imaging modalities in the diagnosis of acute stroke, early stroke diagnosis and treatment is still much needed for making quick decisions and relevant medical interventions without any objective input. The images do not provide enough objective data of pathologic events at the required time (Peacock, 2017). Although CT imaging is beneficial in detecting intracranial bleeding, it exposes patients to radiation. MRI distinguishes between acute stroke and mimics, but many patients do not tolerate the longer scanning time. The circulating biomarkers can help in the decision-making process as to which patient further needs to undergo CT or MRI scan thus avoiding the patient from exposure to unnecessary radiation (Saenger and Christenson, 2010). Besides, circulating biomarkers would help differentiate stroke patients from stroke mimics.

The following table (Table 1-4) summarises the changes in the blood circulating biomarkers following an ischaemic stroke observed in some earlier studies.

Table 1-4 Variations of blood circulating biomarkers after an ischaemic stroke noticed in earlier A: clinical studies and B: preclinical studies.

A: Clinical studies biomarkers

Circulating biomarkers	Sample size / method used	Biomarker levels in serum	Results	Authors
Neuron Specific Enolase (NSE)	67 acute ischaemic stroke patients / ELISA	**Control:** No control **Stroke:** (15.60ng/ml)	NSE concentrations at 24hours after r-tPA bolus were highly correlated with the severity of the corresponding neurological deficit as quantified by the NIHSS score at 24 hours. NSE level is correlated with favourable outcomes and stroke volume. **Strengths:** They looked at the levels of NSE from clinical samples and correlate the results with favourable outcome, stroke volume and NIHSS. **Limitations:** The findings come from individuals who had an acute ischaemic stroke and were given r-tPA treatment without a control group or stroke mimics. Relatively small sample size. Lack of correlation with imaging biomarkers.	(Lu et al., 2015)
NSE	251 subjects : 101 control & 150 stroke patients / ELISA	**Control:** (7.48 ng/ml) **Stroke:** (22.68 ng/ml)	Higher levels of NSE in serum in stroke patients in a comparison with controls. The increase in NSE level within 72 hours of admission was significantly correlated with greater disability at admission. NSE levels were significantly correlated with bad neurological outcomes. **Strengths:** Large sample size.	(Bharosay et al., 2012)

			Correlate the levels of NSE with disability and functional neurological outcomes. **Limitations:** Lack of correlation with imaging biomarkers. The study did not compare the levels of NSE between stroke with stroke mimics.	
NSE	75 acute ischaemic stroke patients / ELISA	**Control:** No control **Stroke:** (64.36 ng/ml on Day 1).	Largest infarct volumes have the highest mean's NSE levels. The worst clinical outcome has the highest mean's NSE levels. The higher stroke severity the higher mean's NSE levels. **Strengths:** The study showed findings consistent with majority of the recent published studies with NSE. Correlate the levels of NSE with stroke severity, infarct volume and clinical outcomes. **Limitations:** Sample size was relatively modest. The study lack of stroke mimics inclusion. It would be better if the results were correlated with imaging biomarkers.	(Zaheer et al., 2013)
NSE	n=88 stroke & n=50 controls / ELISA	**Control:** (7.48 ng/l) **Stroke:** (22.6ng/l)	The mean NSE in stroke patients was significantly higher compared to controls and correlated with higher degree of disability. **Strengths:** According to their knowledge, the work is the first in India to measure NSE levels in stroke patients and link the results with the NIHSS. **Limitations:** It would be better if they include stroke mimics.	(Pandey et al., 2014)

			Lack of imaging biomarkers correlation with the blood biomarkers.	
NSE	n=44 ischaemic & n=79 controls / ELISA	**Control:** (9.5 µg/L) **Stroke:** (11.2 µg/L)	Higher concentrations of NSE were measured in stroke patients compared to controls. NSE works as functional outcomes predictor. **Strengths:** Correlate the levels of NSE with functional outcomes. **Limitations:** It would be better if they include stroke mimics beside haemorrhagic and ischaemic stroke patients. Relatively small sample size. Lack of correlation with imaging biomarkers.	(González-García et al., 2012)
Glial fibrillary acidic protein (GFAP)	79 ischaemic patients & 57 controls / ELISA	**Control:** (0.004ng/ml) **Stroke:** (0.02 ng/ml)	GFAP increases early after stroke. **Strengths:** The study presents the diagnostic usefulness of GFAP as a potential biomarker in the acute care situation. **Limitations:** Sample size was relatively modest. The study did not include stroke mimics. Lack of correlation with imaging biomarkers.	(Ren et al., 2016)
GFAP	146 ischaemic stroke & 45 haemorrhagic stroke & & 11 stroke mimics / ELISA	**Control:** No control but mimics (0.01µg/L) **Stroke:** (0.16µg/L)	GFAP concentrations were significantly higher in haemorrhagic stroke patients compared to ischaemic stroke or stroke mimics patients. **Strengths:** The findings support earlier research that has found a strong link between GFAP levels and haemorrhage volumes. The study includes haemorrhagic stroke patients, ischaemic stroke and stroke mimics **Limitations:**	(Luger et al., 2017)

			Few numbers of mimic's patients were included. Patients who had previously experienced a stroke were excluded, resulting in a selection bias in research population. Lack of correlation with imaging biomarkers.	
GFAP	64 acute ischaemic stroke patients / ELISA	**Control:** No control **Stroke:** (0.113 ng/ml)	GFAP was correlated positively with severity of stroke on 72 hours and day 7 after stroke. **Strengths:** The study correlates the GFAP levels with NIHSS at different time points. **Limitations:** The study only includes ischaemic patients without other comparable groups. Sample size was relatively small. Stroke mimics group lack. Lack of correlation with imaging biomarkers.	(Puspitasari et al., 2019)
GFAP	286 acute stroke patients / ELISA	**Control:** No control **Stroke:** (0.18 ng/ml)	GFAP levels were correlated with higher risk of stroke severity (NIHSS>6). GFAP levels were associated with bad outcome. **Strengths:** The study correlates the levels of GFAP with NIHSS and outcomes. Large sample size. **Limitations:** The study only includes ischaemic patients without control or other comparable groups such as stroke mimics Lack of correlation with CT or MRI biomarkers	(Liu and Geng, 2018)
Claudin-5	458 consecutive	**Control:** No control but	Claudin-5 concentrations were higher in patients with haemorrhagic transformation who	(Kazmierski et al., 2012)

	ischaemic stroke patients (Ischaemic stroke without worsening n = 373 & Ischaemic stroke with worsening, without haemorrhagic transformation n= 52 & clinically evident haemorrhagic transformation n= 33 / ELISA	ischaemic stroke without worsening (0.69ng/ml) **Stroke:** Ischaemic stroke with worsening, without haemorrhagic transformation (0.0ng/ml) & clinically evident haemorrhagic transformation (1.75ng/ml)	were admitted more than 3 hours after stroke onset. **Strengths:** The study examined a number of biomarkers such as: Occludin, Claudin-5 and zonula occludens 1 (ZO-1). Large sample size. **Limitations:** No correlation with imaging results. It would be better if the study included stroke mimics group.	
Claudin-5	8 patients with acute ischaemic stroke & 8 healthy people /	**Control:** (5 ng/ml) **Stroke:** (Less than 6 ng/ml)	There was a rise in Claudin-5 levels in ischaemic patients without significant changes. **Strengths:** The findings from this small pilot study provide a solid foundation for further research into similar field. **Limitations:**	(Shi et al., 2017)

	ELISA		Very small sample size and no stroke mimics patients included in the study. Lack of correlation with imaging biomarkers.	
Zonula occludens 1 (ZO-1)	458 consecutive ischaemic stroke patients (Ischaemic stroke without worsening n = 373 & Ischaemic stroke with worsening, without haemorrhagic transformation n= 52 & clinically evident haemorrhagic transformation n= 33 / ELISA	**Control:** No control but ischaemic stroke without worsening (1.08ng/ml) **Stroke:** Ischaemic stroke with worsening, without haemorrhagic transformation (0.57 ng/ml) & Clinically evident haemorrhagic transformation (1.48 ng/ml)	Elevated ratio of Claudin-5/ZO-1 is associated with haemorrhagic transformation. **Strengths:** The study examined a number of biomarkers such as: Occludin, Claudin-5 and zonula occludens 1 (ZO-1). Large sample size. **Limitations:** Lack of correlation with imaging biomarkers. It would be better if the study includes with these larger sample size stroke mimics group.	(Kazmierski et al., 2012)
Occludin	458 consecutive ischaem	**Control:** No control but	Elevated Occludin is associated with HT. **Strengths:**	(Kazmierski et al., 2012)

	ic stroke patients (Ischaemic stroke without worsening n = 373 & Ischaemic stroke with worsening, without haemorrhagic transformation n= 52 & clinically evident haemorrhagic transformation n= 33 / ELISA	ischaemic stroke without worsening (0 ng/ml) **Stroke:** Ischaemic stroke with worsening, without haemorrhagic transformation (0.01ng/ml) & Clinically evident haemorrhagic transformation (0.08 ng/ml)	The study examined a number of biomarkers such as: Occludin, Claudin-5 and zonula occludens 1 (ZO-1). Large sample size. **Limitations:** Lack of correlation with imaging biomarkers. It would be better if the study includes with these larger sample size stroke mimics group.	
Occludin	8 patients with acute ischaemic stroke and 8 healthy people / ELISA	**Control:** 4ng/ml **Stroke:** About less than 6 ng/ml	The levels of Occludin in patients with acute ischaemic stroke are significantly increased at admission. **Strengths:** The findings from this small pilot study provide a solid foundation for further research into similar field. **Limitations:** Very small sample size and no mimics patients include in the study.	(Shi et al., 2017)

			Lack of correlation with imaging biomarkers	
Neurofilagent Light (NfL)	23 stroke patient (40.31 pg/ml) & 16 control (7.70 pg/ml) / Simoa	**Control:** (7.70 pg/ml) **Stroke:** (40.31 pg/ml)	NfL levels in stroke patients were higher than the healthy group. **Strengths:** The study provides for future research that might use NfL to determine prognostic and therapeutic potential. **Limitations:** Small sample size. The study measured NfL concentrations using Simoa and did not used conventional ELISA. Lack of correlation with imaging biomarkers.	(Zheng et al., 2021)
Circulating biomarkers	**Sample size / method used**	**Biomarker levels in plasma**	**Results**	**Authors**
NfL	14 acute ischaemic patients & 33 controls / digital ELISA	**Control:** (~14 pg/mL) **Stroke:** (~40 pg/mL)	NfL levels were significantly elevated in stroke individuals compared to controls. **Strengths:** The results suggests that NfL might be used as blood biomarker of ischaemic stroke during triage. **Limitations:** Small sample size. Rather of using individuals with disorders that mimicked stroke as controls, the study used people who were neurologically normal. It would be better if the study includes stroke mimics. Lack of correlation with imaging biomarkers. The study measured the NfL levels in plasma only but not in serum as serum lacks some	(O'Connell et al., 2020)

			proteins that interferes with the other parameters.	
NfL	314 stroke & 79 control / Simoa	**Control:** (~13 pg/mL) **Stroke:** (less than 100 pg/mL)	Following stroke, an increase in NfL level was seen and peaked at 9 days after stroke. **Strengths:** Good sample size. **Limitations:** Lack of correlation with imaging biomarkers. The study did not include stroke mimics. The study measured the NfL levels in plasma only but not in serum as serum lacks some proteins that interferes with the other parameters.	(Gendron et al., 2020)
Claudin-5	88 stroke patients / ELISA	**Control:** No control **Stroke:** (The posterior cerebral infarct group= 0.21 ng/ml) (The partial anterior cerebral infarct group= 0.37ng/ml)	The Claudin-5 concentration was significantly higher in partial anterior cerebral infarct patients in a comparison with posterior cerebral infarct to patients. **Strengths:** The study showed that Claudin-5 concentrations are associated with the stroke type and location of stroke. The study measured other TJ proteins such as Occludin and ZO-1. **Limitations:** Relatively modest patient's sample size. The study measured the Claudin-5 levels in plasma only but not in serum as serum lacks some proteins that interferes with the other parameters. Lack of imaging biomarkers correlation and lack of stroke mimics inclusion group.	(Lasek-Bal et al., 2020)

ZO-1	88 stroke patients / ELISA	**Control:** No control **Stroke:** (The patients younger than 65 years group= 0.48ng/ml) & (The patients older than 65 years group= 0.59ng/ml)	The ZO-1 concentration was significantly higher in patients older than 65 years of age in a comparison with younger patients **Strengths:** The study showed that ZO-1 concentrations are associated with the age of patients. The study measured other TJ proteins such as Occludin and Claudin-5. **Limitations:** Relatively modest patient's sample size. The study measured the ZO-1 levels in plasma only but not in serum as serum lacks some proteins that interferes with the other parameters. Lack of imaging biomarkers correlation and lack of stroke mimics inclusion group.	(Lasek-Bal et al., 2020)

B: Preclinical studies biomarkers

Biomarker	Species / method used	Results	Authors
Glial fibrillary acidic protein (GFAP)	Rats / Immuno histoche mistry (IHC)	Substantial increase in GFAP processes immuno-positive density at 3 and 7 days after stroke with a more than three-fold rise at 7 days compared to sham animals. **Strengths:** The study correlated the GFAP histology results with MRI. **Limitations:** The study only examined GFAP using IHC but not using western blotting (WB) and ELISA.	(Weber et al., 2017)
GFAP	Rats / WB	Increased in GFAP expression after ischaemia. **Strengths:** The study is prospective design and the prognostic usefulness of GFAP serum levels for long-term outcomes were discovered. The study examined Occludin and Claudin-5 as well. **Limitations:** The study has no data on when as well as how long biomarkers were high in tested animals since there was no monitoring of circulating GFAP. The study did not examine GFAP using IHC.	(Liu et al., 2018)
GFAP	Mice / IHC	GFAP astrocytes in cortex rose after 5 days. **Strengths:** The study examined GFAP, NeuN and IBA-1 using IHC. **Limitations:** The only used method was IHC but they did not use WB or ELISA.	(Ahn et al., 2019)
Neuronal Nuclei	Mice / IHC	NeuN immunoreactive neurons was significantly decrease in specific fields of brain compared to contralateral side.	(Ahn et al., 2019)

(NeuN)		**Strengths:** The study examined GFAP, NeuN and IBA-1 using IHC. **Limitations:** The only used method was IHC but they did not use WB or ELISA.	
Occludin	Rats / ELISA	A sharp rise in level of Occludin after 4.5 hours of MCAO. Occludin is a potential early BBB damage biomarker. **Strengths:** Occludin levels in the blood might be used as a biomarker to determine the risk of haemorrhage after thrombolysis. The study used IHC, WB beside ELISA. The study tested Claudin-5 as well. **Limitations:** The study did not include ZO-1.	(Pan et al., 2017)
Occludin	Rats / WB	Decrease in expressions levels of Occludin after ischaemia. **Strengths:** The study examined GFAP and Claudin-5 as well. **Limitations:** The study has no data on when as well as how long biomarkers were high in tested animals since there was no monitoring of circulating Occludin using ELISA. The study did not examine Occludin using IHC.	(Liu et al., 2018)
Occludin	Rats / WB ELISA	WB for Occludin revealed that sham rats have significant high Occludin level. The Occludin levels were doubled following 4 hours of ischaemia then slightly decrease following reperfusion but still remain significant higher compared to sham group. **Strengths:** The work discovered that higher blood Occludin levels might be a useful biomarker for assessing BBB during ischaemia in rats. The study used WB and ELISA. **Limitations:** The study lack of IHC staining results.	(Shi et al., 2017)

Claudin-5	Rats / WB ELISA	Significant reduction in the Claudin-5 expression after stroke. No significant changes were observed regarding Claudin-5 levels in blood. **Strengths:** The study used WB and ELISA. **Limitations:** The study lack of IHC staining results.	(Shi et al., 2017)
Claudin-5	Rats / ELISA	Blood Claudin-5 concentrations did not vary significantly during the initial 4.5 hours of cerebral ischaemia. **Strengths:** The study used IHC, WB beside ELISA. The study tested Occludin as well. **Limitations:** The study did not include ZO-1.	(Pan et al., 2017)
platelet-derived growth factor receptor beta **(PDGFR)**	Mice / IHC	Quantification of positive PDGFR cells reveals a significant difference in the cells number in the ischaemic area after MCAO versus control. **Strengths:** Series of IHC images were done at different time point. The study includes PDGFR staining results using human stroke tissues samples. The study of human stroke showed similar pattern of results compared with the animal results in terms of pericytes loss and the PDGFR proliferation cells. **Limitations:** The study did not include the other pericytes marker (NG2).	(Fernández-Klett et al., 2013b)
Neuron-glial antigen-2 **(NG2)**	Rats / IHC	NG2 expressed in cells in the hippocampus had some morphological changes such as scarcely branched processes and shortened after stroke. **Strengths:** The study did double labelling of NG2 with NeuN, IBA-1 and GFAP. **Limitations:** The study did not study the levels of GFAP in blood.	(Jin et al., 2020)

		The study did not include the other pericytes marker (PDGFR).	
Ionized calcium binding adaptor molecule 1 (IBA-1)	Mice / IHC	The numbers of IBA-1 positive cells were significantly increased in different area of brains after stroke. **Strengths:** The study examined GFAP, NeuN and IBA-1 using IHC. **Limitations:** The only used method was IHC but they did not use WB or ELISA.	(Ahn et al., 2019)
Cluster differentiation 31 (CD31)	Mice / IHC	CD31 endothelium loss after ischaemia. **Strengths:** The study included PDGFR staining as well. **Limitations:** The study lacks double labelling of CD31 with TJ of endothelial cells.	(Fernández-Klett et al., 2013b)

1.1.12 Circulating biomarkers for ischaemic stroke so far

As evident from Table 1-4, different specific circulating biomarkers have been studied in the last decade in preclinical models (Table 1-4-B) and also in small number of stroke patients (Table 1-4-A). However, these studies have produced variable results, which were not systemically correlated with imaging parameters.

As mentioned in the previous clinical table (Table 1-4-A), most of the studies have shortcomings such as: lack of correlation between circulating biomarkers with CT and MRI imaging biomarkers, shortcomings of inclusion of stroke mimics group alongside ischaemic stroke, lack of studies on circulating biomarkers panel comprising neuronal biomarkers {NSE and Neurofilament light chain (NfL)}, glial cell biomarker (GFAP) and BBB TJ proteins (Occludin, Claudin-5 and ZO-1) in stroke patients compared to mimics and correlate the results with CT scan and MRI results. Moreover, as per the preclinical table (Table 1-4-B), multiple shortcomings have been identified such as a lack of combined brain and BBB damage using neuronal, glial, microglial, pericytes, endothelial cells and TJ specific markers following ischaemic stroke. Additionally, there are not enough studies examining the expressions of these markers in the brain

and the concentration of these biomarkers in blood in the ischaemic model. Moreover, the majority of studies used rat models of ischaemic stroke.

The present study examined the changes in neuronal, glial cells, microglial, pericytes, endothelial cells and BBB TJ proteins in two murine models of stroke to assess brain cells changes and BBB damage and determine the level of circulatory biomarkers in these models. Then, examined the level of these circulating biomarkers in stroke patients as compared to stroke mimics and correlated the blood results with CT and MRI imaging biomarkers.The present study used two cerebral ischaemia and reperfusion models: BCCAO and MCAO. BCCAO produces global ischaemia which is occurring more than the other type of stroke in cardiovascular diseases like cardiac arrest (Wahul et al., 2018). Also, the common carotid artery is a large artery which is involved in most stroke conditions (Stroke Association, 2018). Moreover, this type of stroke specifically effects the astrocytes in the hippocampus where astrogliosis mostly was seen (Soria et al., 2013). MCAO model produces focal ischaemia which occluded the MCA (Jin et al., 2014); one of the most affected vessels in human stroke (Nogles and Galuska, 2022).

The selected markers for preclinical work in this study are : Neuronal nuclei protein (NeuN), GFAP, Neural/Glial Antigen 2 (NG2), Platelet-derived growth factor receptor (PDGFR), Ionized calcium-binding adaptor protein-1 (IBA-1), Cluster differentiation 31 (CD31) and TJ proteins: {ZO-1, Occludin and Claudin-5}. The biomarkers for the clinical study in the present study were based on the results of the preclinical work.

The following section introduces in brief the biomarkers that has been looked at in this study.

NeuN is one of the specific proteins that are present in the nucleus of neurons. Neurons are extremely sensitive to ischaemic stroke. Buscemi et al. (2019) have examined the neuronal damage following MCAO model using an antibody to NeuN and found that the number of NeuN labelled nuclei in MCAO is decreased reflecting the evidence of neuronal death following stroke. Therefore, the neuronal marker NeuN works as a useful marker for stroke diagnosis.

NSE is another neuron specific biomarker that is found mainly in the neuronal cytoplasm (Anand and Stead, 2005). NSE has been used in multiple studies to investigate its role in stroke disease. According to Bharosay et al. (2012), NSE level

is elevated in stroke patients compared to the control suggesting the presence of neuronal injury. Additionally, they stated that higher NSE levels were related to greater disability degree and neurological worsening as seen after 7 days in stroke patients providing the role of NSE in evaluating the neurobehavioral outcome following ischaemic stroke (Bharosay et al., 2012). González-García et al. (2012) have stated that NSE was associated with functional outcomes at 60 days as well as with the degree of recovery of stroke patients. Furthermore, Lu et al. (2015) states that NSE has a significant role in evaluating stroke severity, infarct volume, and functional neurological outcome after stroke. This present study examined the neuronal damage in stroke by measuring levels of NSE in stroke patients and mimics and check its ability to differentiate between them.

GFAP is widely utilized in neuropathology as a glial cell marker. A previous study has showed the elevation of serum GFAP level is a significant evidence for neurological injury (Maas and Furie, 2009). As it was shown in the (Table 1-4-A), most of the GFAP studies have been done on stroke patients (Ren et al., 2016; Puspitasari et al., 2019) and reported a significant correlation between GFAP serum levels with stroke severity (Puspitasari et al., 2019) as well as associated with stroke characteristics and type (Ren et al., 2016; Liu and Geng, 2018). Liu and Geng (2018) stated that serum levels of GFAP and NIHSS are novel and complementary biomarker to predict patients' outcomes 1 year after acute ischaemic stroke. While few works have examined the changes in astrocytes after ischaemia using preclinical models of ischaemia with multiple methods such as IHC, quantitative methodology, ELISA and WB and correlate the results with ELISA and WB, this study carried out this work initially on BCCAO and MCAO models to compare and confirm the results. Additionally, the correlation between changes in GFAP expression in brains tissues and the serum GFAP circulating biomarkers were investigated. Then, the work carried out human samples obtained from stroke patients and mimics to confirm the preclinical results since GFAP is known to be a standard stroke biomarker.

TJ proteins: ZO-1, Occludin and Claudin-5 play essential roles in the maintenance of TJ function and structure. Transmembrane proteins Claudin-5 and Occludin are involved in BBB integrity regulation and proper functions (Feldman et al., 2005; Piorntek et al., 2008). The membrane spanning TJ specific protein, Occludin acts as an adhesion molecule on the endothelial cell surface, linking the two cells together.

Also, it has been shown that Occludin is linked to the complex of cytoplasmic proteins via the ZO-1 (Furuse et al., 1994). Occludin release in blood with almost double the levels of control is observed in preclinical acute ischaemic stroke due to BBB breakdown (Shi et al., 2017) as mentioned in (Table 1-4,B). It has been observed that Occludin releases in blood in preclinical MCAO rat model due to BBB breakdown (Pan et al., 2017).

Claudin-5 is an important component of TJ particularly in brain's endothelial cells (Jia et al., 2014). Claudin-5's primary function is to decrease ions in a certain manner (Jia et al., 2014). Kazmierski et al. (2012) found that patients with haemorrhagic transformation who were hospitalised more than 3 hours after the stroke had higher Claudin-5 concentrations. In contrast , Pan et al. (2017) and Shi et al. (2017) have not found any significant changes in the blood Claudin-5 concentrations after cerebral ischaemia.

ZO-1 is one of TJ protein of endothelial cells (Itoh and Bissell, 2003). It limits the free molecular exchange between brain tissues and blood, hence reducing the permeability of cerebral arteries (Wang et al., 2016).

Interestingly, despite the significant role of ZO-1 in the integrity of BBB, there aren't enough studies concentrating on the investigating of its role in BBB damage after focal and global cerebral ischaemia in animals using IHC, WB and ELISA methods. Thus, in this study, the changes in TJ proteins in murine stroke models as compared to sham operated mice using single and double labelling were investigated. Additionally, the expressions of ZO-1, Occludin and Claudin-5 proteins in BCCAO, as well as MCAO brain tissues compared to the control brain tissues, were examined. Furthermore, the correlation between changes in TJ proteins expression in brains tissues and the serum circulating biomarkers were investigated. Moreover, since there is a lack of further studies investigating the TJ biomarkers' role in clinical samples especially ZO-1, this study investigated these proteins in acute stroke patients and mimics after carrying on the work initially on cerebral ischaemia and reperfusion models. Then correlate the circulating biomarkers with CT and MRI imaging biomarkers results.

Neurofilament light chain (NfL) is a cytoskeletal protein known to be specific for neurons and axons (Barro et al., 2020). This biomarker has developed as a blood biomarker that can detect neuronal damage in a wide range of neurological disorders

(Barro et al., 2020). Following injury to both central (Khalil et al., 2018) and peripheral neurons (Antje et al., 2018; Sandelius et al., 2018), NfL is released into the CSF and blood. Blood NfL was validated as a biomarker of neuronal damage , and it was discovered that neuronal damage assessed by NfL reflected clinical and imaging measurements of illness across different neurological diseases (Khalil et al., 2018). The value of serum NfL in patients with ischaemic stroke has been linked to subcortical hyperintensities (Jonsson et al., 2010) and small vessel disease (Tiedt et al., 2018 ; Duering et al., 2018), both of which are linked to recurrent stroke (Fu et al., 2010; Wang et al., 2021) and mortality (Debette et al., 2015). Most of the previous studies evaluated NfL blood samples by Simoa methods (Zheng et al., 2021; Uphaus et al., 2019). Thus, this study investigated the ability of serum NfL level to diffrentiate between ischaemic stroke patients and mimic using ELISA.

NG2 is a protein expressed on the surface of pericytes during vasculogenic and angiogenic processes (Stallcup, 2002). Moreover, PDGFR is a pericyte specific protein (Bjarnegård et al., 2004). Several preclinical studies reported the morphological changes on pericytes following stroke as they become hyper dilated, irregularly shaped and enlarged (Bergers and Song, 2005; Roth et al., 2019). However, further studies need to be done to examine the changes on pericytes following stroke compared to control as they are part of BBB components. Thus, this study studied the changes in pericytes in murine stroke models compared to controls using IHC.

IBA-1 is a protein that is expressed in all microglia (Ahmed et al., 2007). It has been reported that, the IBA-1 cells were significantly higher in stroke brains compared to controls as shown in (Table 1-4, B). Due to the importance of microglia cells in CNS health, this study targeted the changes in microglia in BCCAO and MCAO models of stroke and reperfusion using IHC.

CD31 is also known as a platelet–endothelial cell adhesion molecule (PECAM 1) (Delisser et al., 1993). It was detected primarily from endothelial cells and platelets (Mourik et al., 1985), then was detected latterly from blood leucocytes (Stockinger et al., 1990). In this project, the changes on endothelial cells in a relation with the changes on TJ proteins in cerebral ischaemia models of stroke and reperfusion using single and double labelling was examined.

In conclusion, the previous works of the mentioned biomarkers have been conducted preclinically on stroke models without examining the correlation of these changes in the brain and the blood or on stroke patients without correlating with CT and MRI imaging techniques. Hence, this study carried out to assess the levels of these biomarkers in acute stroke patients and mimics patients after confirming the results preclinically on animal stroke and reperfusion models. Additionally, the same circulating biomarkers were correlated with CT and MRI imaging biomarkers. The selected blood biomarkers for the project's clinical work are: GFAP, NSE, NfL and BBB TJ specific biomarkers: (ZO-1, Occludin and Claudin-5). This selection is based on the reviews of the previous studies done on potential stroke biomarkers as detailed in Table 1-4,A. Moreover, glial marker (GFAP) and BBB TJ specific biomarkers were examined initially on murine stroke models to investigate the ability of these biomarkers to diagnose stroke in these models.

1.1.13 Gap in research

Currently, an expert stroke clinician's evaluation of the stroke patient, reinforced by the results of brain imaging besides clinical assessment, is used to diagnose ischaemic stroke (Dias et al., 2021). Thus, the diagnosis of stroke remains largely clinical, yet widely used stroke scoring systems (e.g., FAST test or CPSS) do not allow distinction of patients with acute stroke from those with mimics. CT scan can confirm haemorrhage, but it is not sensitive enough in minor stroke (Mullins et al., 2002) as well as many patients with suspected stroke are subsequently confirmed to have alternative pathologies. DWI helps to distinguish between acute stroke and mimics but requires a longer scanning time (Zaitsev et al., 2015). Recently, the circulating blood biomarkers strategy showed a promising stroke diagnostic method in the research field. In the clinical scenario of suspected myocardial ischaemia, this method is well-established. The myocardial isoform of creatinine phosphokinase and troponin are significant in both therapy decisions and clinical studies in acute coronary syndromes (Al-Otaiby et al., 2011). However, there are no definite blood biomarkers to distinguish between stroke and stroke mimics at the point of care. Thus, a quick test based on simple, accurate and low-cost technology to confirm the clinical and neuroimaging diagnosis of ischaemic stroke would be tremendously beneficial to provide the best possible treatment to stroke patients. Furthermore, few studies have correlated circulating biomarkers data obtained from ischaemic stroke samples with CT and MRI

biomarkers. To my knowledge, there are limited studies examining the correlation between the concentration of circulating biomarkers (GFAP, Claudin-5, Occludin and ZO-1) in blood serum and the expression of these biomarkers in the brain in both BCCAO and MCAO stroke models. This study aimed to examine the circulating biomarkers in mouse models of stroke compared to sham operated mice. Also, aimed to assess the circulating biomarkers in acute stroke patients compared to mimics as defined by clinical scoring systems as well as CT and MRI scans.

1.2 Hypothesis

The combination of circulating biomarkers in acute stroke patients with neurological scores, CT and MRI imaging data can improve the diagnosis of stroke.

Aim and objectives

1.3 Aim

- To determine the circulating biomarkers in mouse models of stroke compared to sham operated mice.
- To examine the circulating biomarkers in acute stroke patients compared to mimics as defined by clinical scoring systems as well as CT and MRI scans.

1.4 Objectives

To address the aims of this project, the preclinical study was conducted using two murine models of stroke to examine the changes in neuronal, glial cell and BBB TJ markers in the brain and concentrations of these biomarkers in blood. After that, a retrospective pilot clinical study on stroke patients was performed to identify imaging markers that can inform a longitudinal study design in the future. Finally, a cross-sectional clinical study of ischaemic stroke and stroke mimics was done to confirm the preclinical results. Additionally, the CT and MRI data of these patients were analysed to measure imaging biomarkers. Then correlations between circulating biomarkers with CT and MRI imaging biomarkers were performed.

The specific objectives in the studies were:

1.4.1 Preclinical study

- To determine brain damage using antibodies of specific neuronal and glial cells (NeuN, GFAP and IBA-1), pericytes cells (PDGFR and NG2) and endothelial cells (CD31) as well as to assess BBB marker of specific TJ (Occludin, Claudin-5 and ZO-1) in murine stroke model as compared to sham operated mice using single and double labelling.
- To determine the expressions of some biomarkers (GFAP, Claudin-5, Occludin and ZO-1) in the brain using WB are significantly different between control and stroke mice.
- To determine if circulating biomarkers (GFAP, Claudin-5, Occludin and ZO-1) determined by the ELISA method are significantly different between control and stroke mice.
- To determine if the expressions of biomarkers in brain tissues are correlated with the levels of these biomarkers in blood.

1.4.2 Clinical study

- To assess the ability of the diagnostic circulating biomarkers in distinguishing between ischaemic stroke and stroke mimics to improve stroke diagnosis.
- To determine the CT and MRI biomarker's ability in distinguish between stroke and mimics.
- To correlate the circulating biomarkers with CT and MRI imaging biomarkers to improve stroke diagnosis.

Chapter 2 Materials and methods

2.1 Preclinical study

2.1.1 Animal

All experiments used male C57BL/6J mice that were 10 to 12 weeks old and weighed 25 to 30 g (Harlan-Olac, Bicester, UK). They were conducted in accordance with the U.K. Animals (Scientific Procedures) Act of 1986 and under the proper personal and project licences issued by the United Kingdom Home Office. The Animal Research: Reporting of In Vivo Studies (ARRIVE) standards were followed in all experiments.

2.1.2 Induction of stroke or Cerebral ischaemia and reperfusion

Strokes in mice were induced by either transient (15 min) bilateral common carotid artery occlusion (BCCAO) as described in (Khan et al., 2018) or transient (1 hour) middle cerebral artery occlusion (MCAO) as described previously in (McColl et al., 2007). BCCAO surgical procedures were performed by Dr Nadira Yuldasheva. MCAO surgical procedures were performed by Stroke Centre Surgery Core, Department of Neurosurgery, University of Kentucky, USA.

In BCCAO, (Figure 2.1) mice were anaesthetised using isoflurane (1-1.5%) followed by buprenorphine HCL (0.25 mg/ kg) injection intraperitoneally. Through a midline neck incision, both carotid arteries were exposed and occluded using microserrefines for 15 min occlusion period and anaesthesia was stopped when the wound was sutured. Following surgery, sterile saline was administered intraperitoneally to each mouse (0.4 ml). Sham-operated mice underwent the same procedure except no occlusion was performed for carotid arteries. Throughout the procedure and following it until the mouse came awake from anaesthesia, a warming plate maintained the rodent's core body temperature at 37 ± 0.5°C. Then, reperfusion was permitted for 5 days as it has routinely found in a pilot study in our lab that this occlusion protocol generates reproducible hippocampus and cortical damage 5 days after BCCAO. The pilot results also showed very little ischaemic damage following occlusion of carotid arteries for less than 10 min.

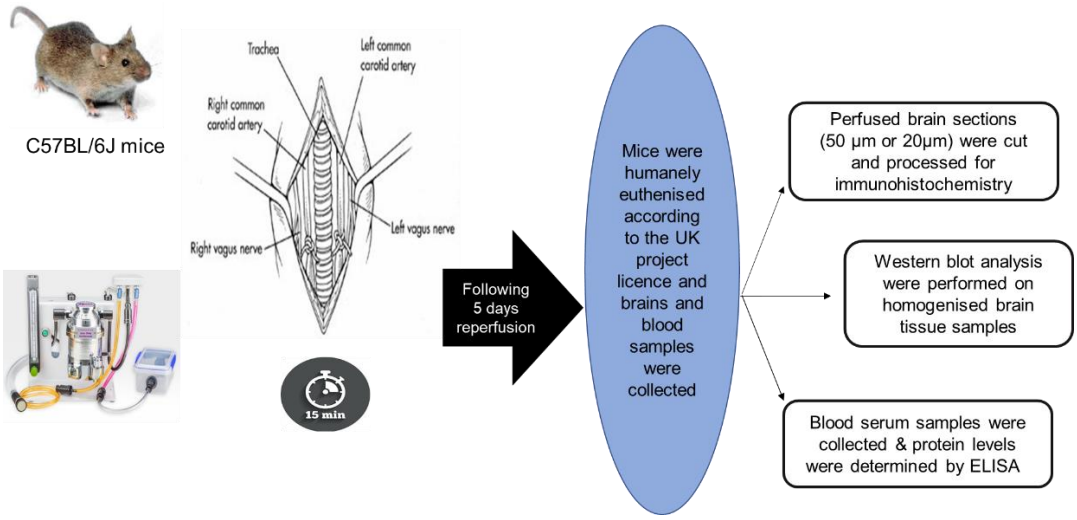

Figure 2.1Schematic diagram for cerebral ischaemia induction using transient BCCAO model. The arterial scheme was adopted from (León-Moreno et al., 2020)

In MCAO, (Figure 2.2) mice were anaesthetised using isoflurane (1-1.5% in 30% O2 / 70% N2O) followed by buprenorphine HCL (0.25 mg/ kg) injection intraperitoneally. Then, the carotid arteries were separated and a 6-0 nylon monofilament (Dermalon) with a 2 mm tip (180 µm diameter) that was waxed in thermo-melting glue (Jet Melt) was inserted along the external carotid artery and forward along the ICA to block the origin of the MCA. Throughout the process, a heating blanket with feedback control kept the patient's core body temperature at 37°C ± 0.5°C. The filament was removed after one hour to achieve reperfusion. Following surgery, sterile saline was injected intraperitoneally into each mouse (0.4 ml). Sham-operated mice went through the exact procedure except that the filament was inserted into the ICA and then removed immediately. Then, reperfusion was permitted for 1 day (24 hours), as it has been found in a pilot study in our lab that this occlusion protocol generates reproducible striatal and cortical damage 24 hours after MCAO.

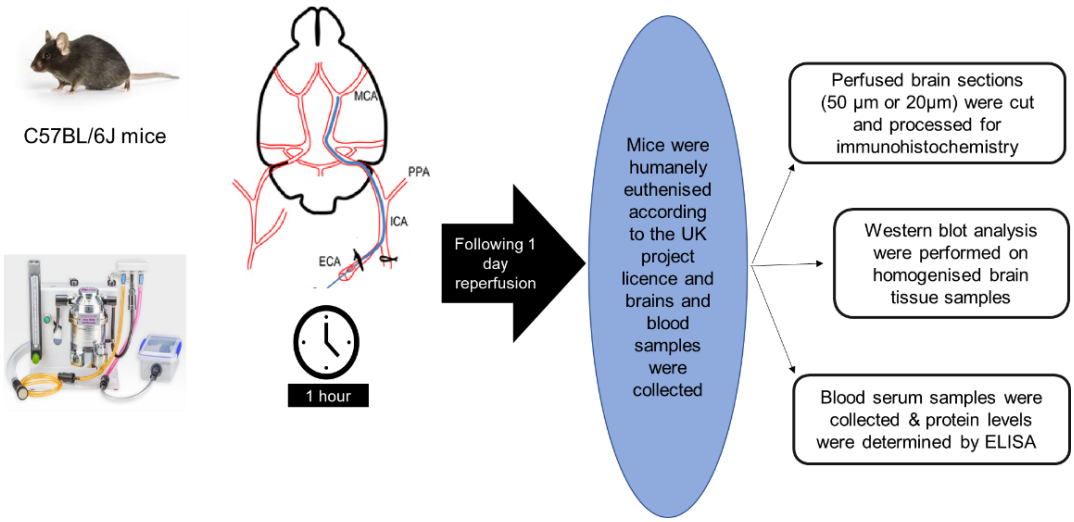

Figure 2.2 Schematic diagram for production of cerebral ischaemia with transient (1 h) MCAO model. (The arterial scheme was adopted from (Rousselet et al., 2012). ECA: external carotid artery, ICA: internal carotid artery, MCA: middle cerebral artery and PPC: pterygopalatine artery.

2.1.3 Neurological deficit Assessment

Neurological deficit assessment was performed in BCCAO operated animals and sham operated animals using neurological deficit signs including disturbances of consciousness, drowsiness and circling, torsion of the neck and seizure (Yang et al., 1997) i.e., 0, no observable deficit; 1, drowsiness and circling; 2, torsion of the neck and disappearance of the righting reflex; 3, seizure; 4, coma or no spontaneous movement.

Whereas the assessment of neurological deficit in the MCAO operated animals was confirmed by neurological deficit tests that were performed using a neurological grading score of increasing the severity of deficit (Bederson et al., 1986) i.e. 0, no observable deficit; 1, forelimb flexion; 2, reduced resistance to lateral push but no circling; 3, similar to grade 2 with additional circling; 4, no spontaneous movement.

2.1.4 Collection, processing and storing of brain tissue

For WB, following reperfusion, both MCAO and BCCAO mice and sham operated mice were humanely euthanised according to the UK project licence by decapitation under anaesthesia, brains extracted and rapidly frozen on dry ice and stored at − 80 °C.

For IHC, following reperfusion, stroke induced, and sham-operated control mice were perfused transcardially with 0.9% saline followed by 4% paraformaldehyde. Brains were post-fixed overnight and stored in phosphate buffered saline (PBS, PH7.4, Sigma-Aldrich) at 4°C. Sections (20 µm) cut on cryostat (Leica, Bensheim, Germany) or sections (50 µm) cut on a vibrating microtome (Leica Microsystems, Germany) were processed for histochemistry and IHC (Figure 2.3), mounted on gelatinised slides and stored at − 20 °C. Tissues from the sham operated animals and the stroke induced animals were harvested and processed in parallel and in similar condition.

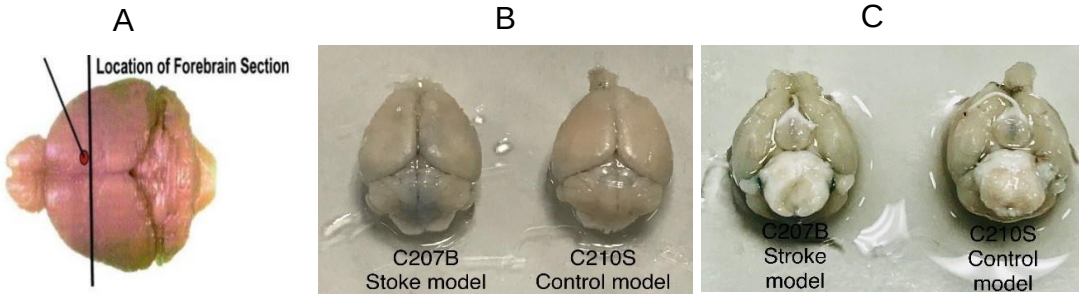

Figure 2.3 A)The level of extracted sections in the project (adapted from the Mouse Brain Library (The Mouse brain Library, 2003), (B) Dorsal view of a stroke model and a control model and (C) Frontal view of a stroke model and a control model.

2.1.5 Assessment of cerebral ischaemia injury using immunohistochemistry and histochemistry

2.1.5.1 Histochemistry- Cresyl violet staining

Brain sections were stained with cresyl violet solution (1% in water). These sections were incubated in 95% Industrial Methylated Spirits (IMS) for 2 min and washed quickly with running water. Following that, sections were incubated in 1% cresyl violet solution for 5 min and then rinsed in running water until the water is clear. After that, sections were incubated in graded ethanol (75%, 95%, 99%) each for 2 min. Finally, sections were cleared in Xylene for 2 min then the cover slipped with DPX mounting medium (Sigma-Aldrich) and kept drying in air. The slides that have been used in this staining process were coated previously with chrome gelatinized to avoid falling of sections from the slide.

2.1.5.2 Cryostat sectioning and immunohistochemistry staining

To detect the death of neurons, changes in glial, pericytes, microglia, endothelial cells and specific BBB TJ proteins more specifically, immunohistochemical stainings were performed with thinner sections (20 µm). Briefly, the brain tissue was kept in 15% sucrose in PBS for 2 days until it becomes sunk. The brain tissue was embedded in an optimal cutting temperature compound (OCT) and 20 µm thin brain sections were cut using a cryostat (Leica, Bensheim, Germany). The immunohistochemical staining with antibodies specific to neurons, glial cells, pericytes, microglia, endothelial cells markers and BBB TJ proteins on brain sections was performed as described in the following section.

2.1.5.3 Immunohistochemistry

Brain sections were placed in PBS (Sigma-Aldrich) into WHO plate wells. The sections were treated with Liberate Antibody Binding Solution (L.A.B. Solution) (antigen retrieval solution, Polysciences Inc) for 10 min in order to wipe off excessive fixative and minimize protein cross-linking. Then, the sections were washed with PBS containing 0.1% Triton-X100 (PBS-T) for 5 min followed by incubation in 10% horse or donkey serum (Sigma-Aldrich, Poole, Dorset, UK) diluted in PBS-T at room temperature on a shaker table (Bio Dancer, New Brunswick scientific, Edison N.J U.S.A) for 30 min with gentle agitation to block any nonspecific binding and decrease background staining. Following that, sections were transferred to the appropriate primary antibody (details of antibodies and dilutions used for IHC are listed in Table 2-2) diluted in PBS-T and incubated overnight at 4^{0}C. Sections were then washed in PBS-T three times for 5 min each using the shaker table for gentle agitation. Sections were transferred to the appropriate (rabbit or mouse) red fluorescence Cy3-conjugated secondary antibody (Jackson Immunoresearch Laboratories) or green fluorescence Alexa^{488} secondary antibody (Molecular Probes, Leiden, Netherlands) (diluted 1/1000 in PBS-T) and incubated at room temperature on the shaker table for 4 hours. Since, the secondary antibodies are light sensitive, the plate was covered with foil. Lastly, sections were washed in PBS-T three times each for 5 min, then mounted on slides and coverslipped with Vectashield mounting medium with or without DAPI (Vector Laboratories, Inc, Burlingame, CA 94010).

2.1.5.4 Primary antibodies

Multiple antibodies specific for the detection of neurons, glial cells, pericytes, microglia, endothelial cells and specific BBB TJ proteins were used. The details of these antibodies are shown in Table 2-1. Specificity of all the antibodies was defined according to the suppliers.

Table 2-1 The used specific primary antibodies.

Antibody	Code no	Supplier	Species	Specificity data (Immunogen) according to supplier
NeuN	ab104224	Abcam	Mouse	Monoclonal antibody against NeuN was prepared by immunising mouse with N terminal peptide 1B7. Recombinant fragment corresponding to NeuN aa 1-100 (N terminal). Sequence: MAQPYPPAQYPPPPQNGIPAEYAPPPPHPTQDYSGQTPV PTEHGMTLYTP AQTHPEQPGSEASTQPIAGTQTVPQTDEAAQTDSQPLHP SDPTEKQQPKR The antibody was raised, purified, and extensively characterised according to supplier data sheet.
GFAP	131-17719	Invitrogen (A21282)	Mouse	Monoclonal antibody against GFAP was prepared by immunising mouse with 131-17719. The antibody was raised, purified, and extensively characterised according to supplier data sheet.
Occludin	OC-3F10	Life technologies (331511)	Mouse	Monoclonal antibody against Occludin was prepared by immunising mouse with C terminal peptide OC-3F10. The antibody was raised, purified, and extensively characterised according to supplier data sheet.
ZO-1	40-2200	Invitrogen (40-2200)	Rabbit	Polyclonal antibody against ZO-1 was prepared by immunising rabbit with synthetic peptide found in the ZO-1 protein's middle region. The antibody was raised, purified, and extensively characterised according to supplier data sheet.
IBA-1	ab5076	Abcam	Goat(sheep)	Polyclonal antibody against IBA-1 was prepared by immunising goat with peptide synthesised to match IBA-1

				aa 135–147 (C terminal). The isoforms represented by Accession Number(s): NP 001614.3; NP 116573.1, sequence: C-TGPPAKKAISELP are anticipated to be recognised by IBA-1. The antibody was raised, purified, and extensively characterised according to supplier data sheet.
NG2	ab50009	Abcam	Mouse	Monoclonal antibody against NG2 was prepared by immunising mouse with 132.38. The antibody was raised, purified, and extensively characterised according to supplier data sheet.
PDGFR	ab124392	Abcam	Rabbit	Polyclonal antibody against PDGFR was prepared by immunising rabbit with synthetic peptide with keyhole limpet haemocyanin linked to PDGFR alpha aa 1035–1053. Sequence cGKRNRHSSQTSEESAIETG, matching to Human PDGFR alpha aa 1035–1053, was used to detect specificity. The antibody was raised, purified, and extensively characterised according to supplier data sheet.
CD31	ab28364	Abcam	Rabbit	Polyclonal antibody against CD31 was prepared by immunising rabbit with synthetic peptide from aa 700 to the C-terminus (C terminal). The antibody was raised, purified, and extensively characterised according to supplier data sheet.
CD31	PECAM-1	Invitrogen (14-0311-82)	Mouse	Monoclonal antibody against CD31 was prepared by immunising mouse with 390. The antibody was raised, purified, and extensively characterised according to supplier data sheet.
Claudin-5	34-1600	Invitrogen (34-1600)	Rabbit	Polyclonal antibody against Claudin-5 was prepared by immunising rabbit with synthetic peptide from the Claudin-5 C-terminus. The antibody was raised, purified, and extensively characterised according to supplier data sheet.

2.1.6 Optimization of concentration

In order to find the best IHC staining results for the following antibodies: Occludin, ZO-1, CD31, Claudin-5, IBA-1, PDGFR and NG2, different dilutions have been tried to find out the optimal dilution for specific staining with low non-specific background staining. The details of these antibodies, the different dilutions have been used and

the optimal dilutions are shown in Table 2-2. Regarding NeuN's and GFAP's working dilutions were (NeuN,1:4000) and (GFAP,1:1000) respectively based on earlier work in our lab.

Table 2-2 Different used dilutions for specific antibodies in the optimisation process.

Antibody	Species	Different dilutions	Optimal dilution
Occludin	Mouse	1/1000, 1/200,1/400, 1/100, 1/50	1/50
ZO-1	Rabbit	1/1000, 1/200,1/400, 1/100, 1/50	1/100
IBA-1	Goat	1/100, 1/500, 1/1000, 1/200,1/400	1/200
NG2	Mouse	1/600 1/200 ,1/500, /1000 ,1/800	1/600
PDGFR	Rabbit	1/1000,1/800,1/500 ,1/400 ,1/600	1/600
CD31	Rabbit	1/100, 1/500	1/100
CD31	Mouse	1/100, 1/200,1/500,1/1000	1/200
Claudin-5	Rabbit	1/100, 1/200,1/500,1/1000	1/500

2.1.7 Double labelling Immunohistochemistry

For dual immunolabelling, brain sections were incubated in a mixture of two antibodies raised in different species as listed in Table 2-3 overnight at 4°C. All antibodies were diluted in PBS-T. After 3 washes (5 min each) in PBS-T, sections were incubated for 4 hours in a mixture of species-specific secondary antibodies raised against rabbit or mouse immunoglobulins (as appropriate) conjugated to Cy3 (Jackson ImmunoResearch) and Alexa^{488} (Molecular Probes, Leiden, Netherlands) to visualise the bound primary antibodies in the double labelling. The immunolabelled sections were dried overnight onto glass slides at 4 °C in the dark and coverslipped with Vectashield mounting medium with DAPI or without DAPI (Vector Laboratories, Inc, Burlingame, CA 94010).

Table 2-3 Specific antibodies with dilutions for double labelling.

Combined antibodies	Dilution in PBS-T
GFAP (mouse) + ZO-1 (rabbit)	GFAP =1/500 + ZO-1 = 1/50
NeuN (mouse) + ZO-1 (rabbit)	NeuN=1/2000 + ZO-1 = 1/50
CD31 (mouse) +ZO-1 (rabbit)	CD31=1/100 + ZO-1=1/50
CD31 (rabbit) +Occludin (mouse)	CD31=1/50 + Occludin= 1/25
CD31 (mouse) +Claudin-5 (rabbit)	CD31=1/100 + Claudin-5 =1/250

2.1.8 Microscopic imaging analysis of histochemical and immunohistochemical data

Histochemical or immunohistochemical stained sections were imaged using an AxioImager Z.1 epifluorescence microscope (Carl Zeiss, Welwyn Garden City, UK). Multiple digital images were taken with the imaging system AxioVision (AxioImager.Z1). Bright field images also were taken using a Zeiss AxioVision Imaging System. Then, all captured images were imported into ImageJ for contrast and brightness, minor amendment, cropping or resizing and collecting into figures. Finally, the images were saved as TIFF files.

2.1.9 Stereological method for immunolabelled profiles quantification

The number of NeuN immunoreactive neuronal cells, GFAP immunoreactive glial cells, PDGFR immunoreactive and NG2 immunoreactive pericytes cells and IBA-1 immunoreactive microglia cells per unit volume of brain tissue in outlined brain areas were estimated using a three-dimensional counting method based on the well-established optical dissector method (Williams and Rakic, 1988). This method has been tested earlier in our lab (Khan et al., 2018). Areas of the hippocampus, M1 (primary motor cortex) and M2 (2nd motor cortex), secondary somatosensory cortex, striatum and granular insular cortex region to be sampled in BCCAO were located by examining immunolabelled brain sections under the fluorescence microscope at low magnification (x 10 objectives). Since BCCAO mice in this study revealed cortical and

hippocampal damage in both hemispheres, histological analysis in the stroke mouse brain and sham operated mouse brain was conducted unilaterally. In MCAO mice, the hippocampus, M1 and M2 motor cortex, the granular insular cortex and striatum damage was evident in one hemisphere. So histological analysis was conducted bilaterally (stroke side and non-stroke side). Analysis was achieved from each brain at two sectioning levels: interaural line (5.34mm to 1.74mm); bregma (1.54mm to -2.06mm) (Paxinos and Franklin, 2012). Using the x10 objective, images were taken into Axiovision. Each image corresponded to a 450 x 350 um measured area of tissue. To create a counting box for the image, an acetate sheet with a conventional, unbiased counting frame (Gundersen, 1977), each side corresponding to 200 um at this magnification, was placed over the image on the monitor. Using the measurement module's "event counting" feature, all immunopositive cells that fell inside the counting frame were noted on the image, and the images were checked to make sure that each cell's nucleus was counted only once. A single observer conducted each count blindly on coded slides. A normality test was performed to test data distribution. Data were analysed using Unpaired Student's t-test to determine statistical significance with exception of MCAO counting cells comparison in the two hemispheres of the same mouse brain where paired Student's t-test was used. $P \leq 0.05$ was considered statistically significant.

2.1.10 Tissue preparation for western blotting

Western blotting analyses were conducted in hippocampal regions in both models. In brief, the mice were killed by decapitation under anaesthesia, and their brains were extracted and quickly frozen on dry ice. From the forebrain (over dry ice), approximately 1 mm thickness of coronal slices were cut with a scalpel blade. Following that, about (25-35 mg) hippocampal tissue samples from both brain sides were collected at the level identical to bregma (−0.22 to −2.06 mm) (Paxinos and Franklin, 2012) under a × 5 dissecting microscope, using a 1 mm corer.

2.1.11 Protein extraction

Blunt 20-gauge blunt needle was used for brain tissue homogenisation and 300 µl of Lysis buffer (ThermoScientific) was used for protein extraction. Harvested brain tissues were sonicated in an ice bath and centrifuged (Eppendorf FBS29112 Centrifuge 5340 R) for 30 min at 13 000 rpm at 4 ^{0}C. Then, the standard bicinchoninic

acid (BCA) assay (Pierce Protein Quantification Kit) (ThermoScientific, Pierce™ BCA Protein Assay Kit, Catalog number: 23225) was performed using the supernatant to measure protein concentration in samples. Instructions are followed according to manufacture. Standard Test Tube Protocol provided was followed to prepared standards. Nine vials are labelled from A to I. Standards A (2mg/ml) to I (water) were taken out which provide concentrations (A=2000µg/ml) to (I=0µg/ml). 25 µl of each standard and actual samples are filled in each well in duplicate. Since each well needs 200µl of protein assay, thus wells were filled with Reagent A: Reagent B = 50:1. Lid was placed over the plate and incubated in 37 ºC oven for 30 min. Finally, the plate was read using a plate reader.

2.1.12 Western Blotting

For an experiment, 30-50 µl of actual samples were used. Any shortfall should be made up with lysis buffer++. Loading dye was added to achieve a 1:4 dilution. A reducing buffer was added to achieve a 1:10 dilution then transferred all into a fresh Eppendorf. Eppendorfs were put into the heating block at 95 ºC for 5 min. 12 % SDS polyacrylamide gel (Invitrogen) was washed with tap water and placed into a tank facing the worker and other gel/dummy gel was placed on the opposite side facing the opposite way. Buffer was prepared by adding 25 ml MES buffer with making up to 500 ml of distilled water. The prepared buffer was poured into the tank. 20 µl of each sample and 3.5-4 µl of Western C marker were added into separate wells. Power pack machine was switched on and gel was run at 180V for 80 min. Transferring gel process was carried out by removing gels and washing them out upside down. Transferring buffer solution includes (200 ml 10x transfer buffer + 200 ml Methanol + 600 ml distilled water) which was prepared and placed in a white tray. The gel was picked up carefully and placed face down in white tray until submerged. Sandwich was prepared on the black side of the cassette according to the following order (sponge after soaking, filter after soaking in transfer buffer, then roll, gel then roll, polyvinylidene difluoride membrane (Millipore) then roll, filter after soaking then roll, sponge). Cassette was closed and the stirrer was switched on (100V for 15 min). Membrane/blot was moved to the pot and washed with methanol followed by distilled water. Blocking buffer was prepared - milk buffer 5% (10 ml TBSTween (TBST {Tris-buffered saline and 0.1% Tween 20}) + 0.5 g BSA powder or skimmed milk powder). 5 ml was added to each of the pots and put on the roller for 20 min. Membrane/blot was washed with PBST twice

for 10 min. Membranes were then immunoblotted and incubated overnight at 4°C with appropriate primary antibodies GFAP, ZO-1, Occludin or Claudin-5 (diluted 1:1000) against B-Actin (diluted 1:1000). Membranes were washed in TBS-T three times 15 min each on a shaker and incubated for 1 hour at room temperature with corresponding HRP-conjugated anti-rabbit or anti-mouse antibodies (Santa Cruz Biotechnology; 1:5000). Then, the membranes were washed in TBS-T once (15 min). 1:25,000 of Anti-western - C marker (Precision Protein Streptactin HRP) in TBST (1 µL in 25 ml) was prepared and added into pots for incubation on the shaker for 10 min. Pots were covered with foil as anti-western - C marker is light sensitive. Then pots were washed with TBST twice for 15 min on a shaker. Finally, the camera was prepared for imaging. The membranes were developed with 600 µL of Immobilon Western HRP substrate luminol reagent and 600 µL of peroxide reagent (Millipore) and placed on camera. The Syngene densitometry (Syngene Gel Documentation) system which is called GeneSys application was used to photograph the immunoblots. Densitometric quantification analysis of blots was performed using GeneTools analysis software along with Excel software. Statistical analyses were performed using GraphPad Prism software. Normality test was performed to test data distribution. Unpaired Mann-Whitney U test was used to compare the control and BCCAO. Paired Wilcoxon matched pairs signed rank test were used to compare control and MCAO.

2.1.13 Blood sample collection

Blood samples were collected from the inferior vena cava from stroke and sham-operated mice with an amount of 1 ml (1000 µl) of blood from each mouse. Blood samples were collected after 5 days from BCCAO whereas, the blood samples were collected after 24 hours from MCAO. Serum samples were centrifuged at 13000 rpm for 10 min within two hours of collection and then kept at room temperature until processing. After that, samples were saved in aliquots in Eppendorf tubes (1.5ml micro tubes; Sarstedt; Leicester, UK, Ref: 72.690), flash frozen in liquid nitrogen and stored at −80°C until analysis.

2.1.14 Analysis and measurement of blood biomarkers using ELISA method

A mouse GFAP ELISA Kit (Fine test, EM0335), a mouse Occludin ELISA Kit (AVIVA Systems Biology, OKEH 07095), a mouse Claudin-5 ELISA kit (DL EVELOP, DL-

CLDN5-Mu) and a mouse TJP1 (Tight junction protein ZO-1) ELISA Kit (Elabscience, E-EL-M1161) were used, and the protocols were followed according to the attached guidance of the companies. Table 2-4 shows the detection range, sensitivity and specificity for each previously mentioned ELISA kits. In brief, firstly, 100 µL of serially standard, sample (serum) and control (zero) solutions were added to each well and incubated for 90 min in GFAP and ZO-1 assay and 2 hours in Occludin and Claudin-5 assay at 37 °C. The liquid was removed and 100 µL of Biotin-detection antibody was added to each well for 60 min at 37°C. Following that, plate was washed three times and 100µL of HRP Conjugate (SABC) was added to each well and incubated for 30 min in GFAP, Occludin and ZO-1 assay and for 1 hour in Claudin-5 assay at 37 °C. Then, the plate was washed five times and 90 µL of TMB substrate was added to each well for 20 min at 37 °C covered with foil as the substrate is known to be light sensitive. Finally, 50 µL of Stop Solution was added followed by immediate optimal density determination at 450 nm (Bio-Tek Powerwave 1). Normality test was performed to test data distribution. Accordingly, serum concentration comparison between the two experimental groups was analysed by Unpaired Student's t-test. P≤0.05 is considered significantly high or different.

Table 2-4 The detection range, sensitivity and specificity for the used mouse ELISA kits in this study.

ELISA kit name and catalogue number	Detection range	Sensitivity	Specificity
Mouse GFAP ELISA Kit (Fine test, EM0335)	15.625 -1000 pg/ml	<9.375pg/ml	For GFAP quantitative detection in plasma, serum, tissue homogenates and other biological fluids.
Mouse Occludin ELISA Kit (AVIVA Systems Biology, OKEH 07095),	156.0 – 10000 pg/ml	<78.0 pg/ml	Mouse Occludin UniProt ID: Q61146 GeneID: 18260 Target Alias: AI503564, Occludin, Ocl.
Mouse Claudin-5 ELISA kit (DL EVELOP, DL-CLDN5-Mu)	312.0-20000pg/ml	<127.0pg/ml	This kit has excellent specificity and high sensitivity for detection of CLDN5.

Mouse TJP1 (Tight junction protein ZO-1) ELISA Kit (Elabscience, E-EL-M1161)	78.13-5000pg/ml	46.88pg/ml	This kit recognizes Mouse TJP1 in samples.

2.1.15 Statistical analysis

Excel program and GraphPad Prism 9 software (GraphPad, San Diego, California) were used for statistical analysis and graph production. All continuous measurements are shown as mean (SD). A value of $p \leq 0.05$ was considered statistically significant. Spearman rank correlation test was achieved to assess the correlation between ELISA results and WB results. Spearman rank correlation is a non-parametric test that is usually performed to measure the association degree between two variables (Schober et al., 2018). Linear regression analysis was performed to evaluate the linear relationship between two variables. The significance of the correlation was obtained by performing the 2-tailed Student's t- test against the null hypothesis that the correlation coefficient was zero. Table 2-5 provides a recommendation for the linear relationship's strength based on the correlation coefficient value (Chan, 2003).

Table 2-5 Linear relationship strength (Chan, 2003).

Correlation Coefficient value	Strength of linear relationship
At least 0.8	Very strong
0.6 up to 0.8	Moderately strong
0.3 to 0.5	Fair
Less than 0.3	Poor

2.2 Clinical study (retrospective study- pilot study)

2.2.1 Patient selection

Retrospective data analysis was conducted from 30 consecutive acute ischaemic adult strokes cases who received a brain CTP scan at Leeds Teaching Hospitals NHS Trust, UK, between 2017 and 2018. Data were divided into two groups: a group treated with MT and another non-treated with MT. Altogether, 15 cases out of the 30 consecutive acute ischaemic stroke cases received a follow-up brain MRI with stroke protocol.

In brief, an audit identified 30 patients divided into two groups at Leeds Teaching Hospitals NHS Trust (Figure 2.4). .

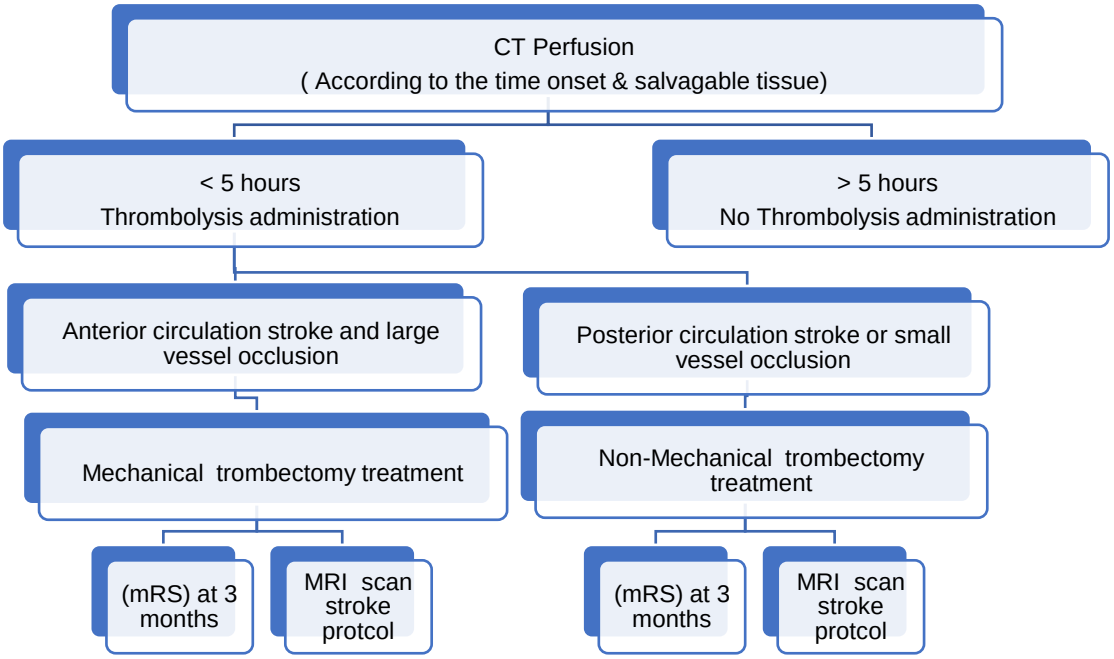

Figure 2.4 A diagram of the patient selection criteria. (mRS): modified Rankin Score which is functional outcomes score.

2.2.1.1 Inclusion criteria

MT treated group inclusion criteria (n=15)

- Patients with anterior circulation occlusion / large vessel occlusion (LVO) were included as MT was indicated for acute stroke patients with Anterior circulation occlusion / large vessel occlusion (LVO)
- Patients received MT treatment.

Non-MT treated group inclusion criteria (n=15)

- Patients with posterior circulation occlusion / small vessel occlusion were included as MT was not indicated for acute stroke patients with posterior circulation occlusion and small vessel occlusion
- Patients didn't receive MT treatment.

2.2.1.2 Exclusion criteria

- Tumour cases
- Extreme motion artifacts scans.

2.2.2 CT scan protocol

The CT protocol included NCCT, CTA and CTP (axial or horizontal sections). Patients received a contrast bolus of 50 ml of Omnipaque 300 mg/ml with an injection rate of at least 5 ml/sec via power injector through the 18-gauge intravenous line. Scanning parameters: slice thickness= 5mm, space between slices= 1mm, tube voltage= 80 KV (peaks), x-ray tube current= 125 mAs, scanning delay= 4-5 sec, scanning time= 88 sec and temporal resolution= 1 sec.

2.2.3 CT Image processing

Patient data have been anonymised using DicomCleaner software (PixelMed, 2019). CBF, CBV and MTT maps were calculated off-line from CTP using in-house software; Platform for Research in Medical Imaging (PMI) (Ledsam, 2021). An arterial input function (AIF) was selected semi-automatically and partial-volume effects were corrected with a venous outflow function (VOF) in the sagittal sinus. CBF, CBV and MTT maps were calculated by model-free deconvolution. First of all, small, rounded

ROIs were generated on the CBF map on both the right and left side on WM and GM (Basal ganglia). These were used as a reference only. WM and GM identical small, rounded ROIs were defined on the CBF map on the penumbra by an Interventional Neuroradiologist to define the salvageable tissue of the ischaemic area and in mirrored contralateral non-ischaemic area. Similar analysis was conducted in both groups.

2.2.4 CT Statistical analysis

Mean (SD) values over each ROI were determined for CBF, CBV and MTT in the two groups. Normality test was performed initially to test the data distribution using GraphPad. A paired Student's t-test was used to identify significant difference in CT imaging biomarkers between ischaemic and contralateral areas in WM and GM in the same patient brain. For statistical comparison between MT treated group and non-MT treated group values, the Mann-Whitney U test was performed. For statistical analysis and the creation of graphs, the Excel programme, and GraphPad Prism 9 software (GraphPad, San Diego, California) were used.

2.2.5 Follow-up MRI scan protocol

Altogether, 15 cases out of the 30 consecutive acute ischaemic strokes cases who received brain CTP scan were collected. The 15 patients (7 patients from MT group and 8 patients from non-MT group) received MRI follow-up stoke protocol. In all cases, the MRI protocol included T1 and T2 weighted images, FLAIR sequence images and DWI images. All brain MRI studies were done on a Siemens 1.5 T magnet in an axial plane. Data analyses were obtained from DWI sequence, specifically, the ADC map. The imaging parameters for the DWI sequence is (sequence type: Echo planner imaging (EPI), transmitting coil: body, patient position: head first, Spin-echo repetition time (TR): 3300 ms, echo time (TE): 89 ms, A 192 * 192 matrix with 100 percent phase field of view and one excitation was used. percent sampling:100, pixel bandwidth: 1240, acquisition number: 1, sample per pixel: 1, rows:192, colums:192. Slices were 5 mm thick with an intervening 6.5 mm gap. Number of averages was 4, imaging frequency: 63.68, echo number: 1, flip angle: 90-degree, echo train length: 1, acquisition number :1, region changed flap: 1, group length: 188, number of phase encoding steps: 143, phase encoding direction: coronal, Specific absorption rate (SAR): 0.10 Watt/kg. No contrast agent was injected.

2.2.6 MRI Image processing

Patient's scans have been anonymised using DicomCleaner (PixelMed, 2019). Data analysis was performed on the DWI sequence of the MRI scan using PMI software (Ledsam, 2021). On the ADC map, small, rounded ROIs matched the exact location of ROIs in CTP map which were generated in WM and GM by an Interventional Neuroradiologist. On the ADC map, the volume of infarct of each patient was measured by calculating the number of pixels in ROI that were generated around the infarction. The volume of the infarct was calculated by multiplying the number of pixels by the volume of the voxel. It is worth mentioning that, the volume of the voxel is identical for all patients as the protocol parameters were identical for all patients. The volume of voxel can be calculated using the following formula:

The volume of voxel (mm^3)= slice thickness(mm) * pixel spacing(mm) * pixel spacing (mm)

As the slice thickness= 5 mm and the pixel spacing= 1.18 mm, the voxel volume is equal to 6.962 mm^3. Lastly, the volume of infarct was calculated in ml by dividing by 1000.

2.2.7 MRI Statistical analysis

Mean (SD) values over each ROI were determined for ADC in the two groups. Normality test was performed to test the data distribution. A paired Student's t-test was used to identify significant difference in imaging biomarkers between ischaemic and contralateral areas in WM and GM in the same patient. The Mann-Whitney U test was used for statistical comparison between the MT group and the non-MT group values. Excel software and GraphPad Prism 9 software (GraphPad, San Diego, California) were used for statistical data analysis and graph generation.

2.2.8 Clinical Outcomes

Clinical outcome was derived from Patient Pathway Manager (PPM+) records or clinical notes. The primary outcome measure: modified Rankin Score (mRS) which is functional outcomes score at 3 months (90 days) was collected. Functional outcomes at 90 days was divided into "good outcome" (mRS≤2) or "bad outcome" (mRS>2). mRS was compared between the two groups using Mann-Whitney U test.

2.3 Clinical study (Cross sectional study)

2.3.1 Method Design

This study is an observational cross sectional acute stroke study of suspected ischaemic stroke patients (n=70) and stroke mimics (n=24) recruited as soon as possible on the Wards or Stroke unit in Leeds Teaching Hospitals NHS Trust. Figure 2.5 shows a flow diagram of the design of the study and patient's routine clinical and research pathways. The study was approved by Yorkshire & The Humber - Leeds East Research Ethics Committee, NHS REC reference 19/YH/0232, IRAS reference No: 50831.

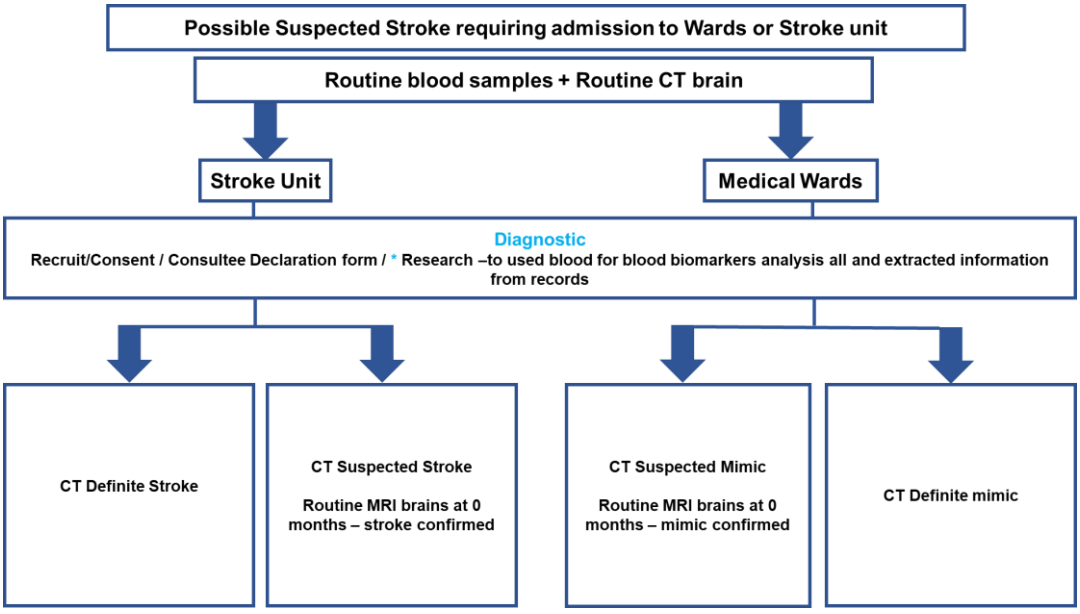

Figure 2.5 Flow diagram of the Design of the Study and patients' Routine Clinical pathways.

2.3.1.1 Patient selection

Participants who met the following selection criteria were included in this study:

Inclusion Criteria:

- Age 18 + years.
- Patients with suspected acute stroke admitted to hospital.

- Patients with confirmed stroke admitted in the acute stroke unit or medical wards.
- Stroke mimics in medical wards or the acute stroke unit.

Exclusion Criteria:

- The patient has capacity but refuses consent.
- The patient lacks capacity and informed consent from consultee cannot be obtained.

2.3.2 Recruitment Procedures

- The researched nurses who are good clinical practice (GCP) trained has taken the consent from the patients (A copy is available in Appendices in Chapter 7).
- Patients with acute stroke lose capacity frequently and it is also important to include acute stroke patients in the study. Therefore, if the patient lacks capacity, a consent from consultee has been obtained to make sure the research does not pose any significant risk to the patient and has the potential to benefit other patients with stroke in the future.
- A written information leaflet was provided to the patient or consultee.
- The study was discussed, and every relevant question was addressed.
- The patient or the consultee was given up to 24 hours on the ward to decide whether they want to take part in the study or not.
- No specific attempt was made to ascertain whether the patient has regained or lost capacity in the future as this would be overly intrusive and potentially upsetting for the patient.
- All populations with suspected stroke were approached. Patients in the research were not included if unable to obtain informed consent or consultee declaration from a relative.

2.3.3 Clinical Evaluation

- Information on all patients was retrieved from NHS Trust paper and electronic medical health records (Patient Pathway Manager PPM+). All patient identifiable data were stored on a password protected database on the NHS

Trust network drive. Data taken offsite to the University for analysis were linked-pseudo-anonymised format.

- The following data were collected at baseline:
  - Centre Number
  - Demographic information (age, gender, ethnicity and occupation)
  - Height, weight, waist circumference, blood pressure
  - Comorbidities
  - Date of stroke/admission/discharge
  - Vital signs
  - Specimens to be obtained and frequency
- Clinical data:

Patients who were included in the study were subjected to the following protocol: type of stroke, time difference between stroke and blood sample collection, NIHSS on arrival, medical history, medication on admission and clinical procedure were obtained from clinical records. Patients were divided into acute ischaemic stroke and mimics.

The NIHSS was used by the neurologist to assess the severity of the stroke on arrival. The NIHSS score is made up of 11 elements as mentioned previously (Refer to section 1.1.8). Patients were divided into two groups; a group with NIHSS scores less or equal than 7 and a group with NIHSS more than 7 and blood biomarkers level has been compared accordingly. Data analysis was carried out also into divided patients into a group where blood has been collected on less or equal 2 days from stroke onset and a group where blood has been collected on more than 2 days from stroke onset with blood biomarkers comparison.

2.3.4 Blood sample collection

Blood samples (15 ml) from 70 ischaemic stroke patients and 24 stroke mimics were collected to measure the concentration of biomarkers GFAP, ZO-1, Occludin, Claudin-5, NSE, and NfL using ELISA technique. For serum samples, 5 ml of whole blood was collected in a gel clot active tube (Gold Hemogard closure) (Figure 2.6). After the collection, the blood was left undisturbed at room temperature for 30 min to be allowed

to clot. The clot was then removed by centrifuging at 1500 x g for 10 min in a cold centrifuge. The supernatant (serum) was pipetted out into a sterile aliquot tube.

For the plasma samples, whole blood was collected into anticoagulant-treated tubes i.e., heparin (green, 4 ml), sodium citrate (blue, 2 ml), EDTA (purple, 2 ml), and acid citrate dextrose (yellow conventional closure, 2 ml) tubes (Figure 2.6). The cell components were removed by centrifuging at 2000 x g for 10 min in a cold centrifuge. The supernatant was pipetted out i.e., plasma into a sterile tube.

All samples were maintained at 2–8°C while transporting them. Samples were aliquoted into 500 µl – 2 ml Eppendorf centrifuge vials and each 1 ml was stored in a separate vial to avoid freeze-thaw cycles. The vials were labelled with patient's ID, date of blood collection / time of collection. The samples were flash frozen using liquid nitrogen and stored at – 80 °C or lower until analysis. For ELISA, only serum and plasma collected in heparin tubes have been analysed.

Figure 2.6 Blood sample collection tubes. From left to right: a gel clot active tube, heparin tube, sodium citrate tube, EDTA tube and acid citrate dextrose tube (Fisher Scientific, 2022).

2.3.5 Analysis and measurement of blood biomarkers

The quantitative analysis of blood-based biomarkers in blood has been performed using the well-established method, ELISA technique. A human GFAP (Glial fibrillary acidic protein) ELISA Kit (Fine test, EH0410), a human TJP1(Tight junction protein ZO-1) ELISA Kit (Fine test, EH15434), a human OCLN (Occludin) ELISA Kit (Fine test, EH1674), a human CLDN5 (Claudin-5) ELISA Kit (Fine test, EH2839), a human NSE (neuronal-specific enolase) ELISA kit (R&D Systems, DENL20), a human Neurofilament, Light Polypeptide (NEFL) ELISA Kit (Abbexa, abx152468) was used.

Assay procedure was followed according to the protocol provided by the manufacturer. All the samples and reagents were prepared as instructed in the protocol. Table 2-6 reveals the detection range, sensitivity and specificity for the used human ELISA kits in this study.

For GFAP, ZO-1, Occludin and Claudin-5 experiments, the plate was washed with washing buffer twice and 100 µL of serially added standard, sample (serum or plasma), and control (zero) solutions were added into wells and incubated for 90 min at 37 °C. After that, the liquid was sucked out and the plate was washed twice. Each well received 100 µL of Biotin-detection antibody, which was incubated at 37 °C for 60 min. The plate was then washed three times more. Each well received 100 µL of HRP Conjugate (SABC) and was incubated for 30 min at 37 °C. The plate was then washed five times before adding 90 µL of TMB substrate to each well for 20 min at 37 °C with covering with foil as the substrate is light sensitive. Lastly, about 50 µL of stop solution was added, then immediate optimal density was determined at 450 nm using plate reader (Bio-Tek Powerwave 1).

With regard to NSE measurement, it was measured according to the supplier's instructions.100 µL of Assay Diluent RD1-9 was added to each well followed by 50 µL of standard, control and sample was added per well. The plate was covered with the provided adhesive strip and incubated for 2 hours at room temperature on a shaker. Then, each well was aspirated and washed with 400 µL of washing buffer for 4 times. Following that, 200 µL of Human Enolase 2 Conjugate was added to each well and incubated for 2 hours on the shaker at room temperature. The plate was washed after that for 4 times. 200 µL of Substrate Solution was added to each well and protected from light the incubated for 30 min on the benchtop. Lastly, 50 µL of Stop Solution was added followed by immediate optical density determination using a microplate reader set to 450 nm (Bio-Tek Powerwave 1).

Finally, the measurement of NfL using ELISA was done according to the manufacturer’s protocol. 100 µL of diluted standard, samples and control (zero) was aliquoted into the well and incubated with a sealed cover for 1 hour at 37 °C. Following that, the cover was removed and 100 µl of Detection Reagent A working solution was aliquoted to each well and incubated for 1 hour at 37 °C. The plate was washed after that for 3 times with washing buffer. Then,100 µl of Detection Reagent B working solution was added to each well and incubated for 30 min at 37 °C followed by washing

of the plate for 5 times. After that, 90 µl of TMB Substrate was aliquoted into each well with plate coving with foil for 20 min. Finally, 50 µL of Stop Solution was aliquoted into each well and optical density was measured immediately using a microplate reader set to 450 nm (Bio-Tek Powerwave 1).

Table 2-6 The detection range, sensitivity and specificity for the used human ELISA kits in this study.

ELISA kit name and catalogue number	Detection range	Sensitivity	Specificity
Human GFAP (Glial fibrillary acidic protein) ELISA Kit (Fine test, EH0410)	0.313-20ng/ml	0.188ng/ml	For GFAP quantitative detection in plasma, serum, tissue homogenates as well as other biological fluids.
Human TJP1(Tight junction protein ZO-1) ELISA Kit (Fine test, EH15434)	0.156-10ng/ml	0.094ng/ml	For ZO-1 quantitative detection in plasma, serum, tissue homogenates as well as other biological fluids.
Human OCLN (Occludin) ELISA Kit (Fine test, EH1674)	0.156-10ng/ml	0.094ng/ml	For Occludin quantitative detection in plasma, serum, tissue homogenates as well as other biological fluids.
Human CLDN5 (Claudin-5) ELISA Kit (Fine test, EH2839)	0.156-10ng/ml	0.094ng/ml	For Claudin-5 quantitative detection in plasma, serum, tissue homogenates as well as other biological fluids.
Human NSE (neuronal specific enolase) ELISA kit (R&D Systems, DENL20)	0.013-0.038 ng/mL	0.020 ng/mL	This assay recognizes natural and recombinant human Enolase 2.
Human Neurofilament Light Polypeptide (NEFL) ELISA Kit (Abbexa, abx152468)	0.0156 ng/ml - 1 ng/ml	<0.0057 ng/ml	The NfL quantitative detection in human plasma, serum, tissue homogenates, cell lysates, cell culture supernatant and other biological fluids.

2.3.6 Statistical blood data analysis

All data are presented as mean (SD). Data were statistically analysed by Excel program and all analysis and graphs were performed using GraphPad Prism 9 software (GraphPad, San Diego, California). Statistical significance was determined when $p \leq 0.05$. Normality test was performed to test the data distribution. For statistical analysis comparison of circulating biomarkers values, the Mann–Whitney U test was used.

2.3.7 CT and MRI data recording and transferring

- CT and MRI data were recorded using the patient ID in the secure Picture Archiving and Communication system (PACS) of the radiology department.
- The researcher retrieved the routine radiology reports and included them in the participants anonymous study file.
- The CT and MRI images were transferred anonymously from the scanner to the university Digital Imaging and Communications in Medicine (DICOM) database, using an encrypted and secure protocol, where they were analysed to extract imaging biomarkers.
- The results were uploaded in the participant's study file once the analysis was completed
- The original CT and MRI data has been retained in a separate DICOM image database in the University's system to enable future secondary analysis.

2.3.8 CT scan protocol

All patients had NCCT imaging including CTA for large vessel occlusion confirmation. The Brilliance 64 PHILIPS scanner was used to provide 5-mm baseline head NCCT imaging on all patients, with the following standard parameters: tube voltage, 80 kV; tube current, 125 mA; and space between slices=1mm.

2.3.9 CT data analysis

Anonymised scans were analysed using in-house software; PMI (Ledsam, 2021). The Alberta Stroke Program Early CT Score (ASPECTS) was used in CT data analysis. It is a quantitative score that assesses the severity and extent of early ischaemic alterations in hyperacute ischaemic stroke (Barber et al., 2000). Two standardised axial CT cuts; basal ganglia level and corona radiata level as shown in Figure 2.7 were used to determine the ASPECTS. Ten different ROIs corresponding to the MCA territory ASPECTS were manually delineated using baseline NCCT scans as shown in Figure 2.7.

The MCA territory received 10 points for these two portions, which were not continuous by definition. For each of the identified locations, a single point was subtracted for an area of early ischaemia changes which is shown as parenchymal hypoattenuation on

the CT image. A normal CT head scan scored as ten on the ASPECTS scale. A zero ASPECTS indicated diffuse ischaemia within the MCA territory. A region with abnormally low attenuation relative to the same region on the contralateral side was considered parenchymal hypoattenuation. A specialized Neuroradiologist was asked to review the drawing of the ASPECTS regions. Hounsfield unit (HU) values of the ten ROIs were reported from the ischaemic side and the non-ischaemic contralateral side of the scan and then compared.

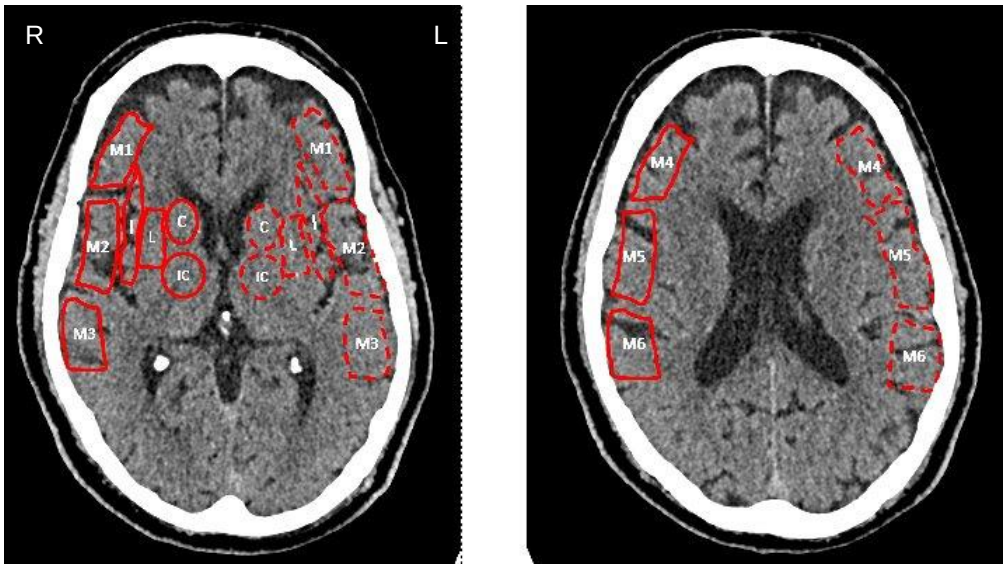

Figure 2.7 An initial CT head at two different levels, (left: basal ganglia level) and (right: corona radiata level). Both images show where a 10 ASPECTS ROIs are drawn manually. Right side areas (solid outline) represent the ischaemic side while the left areas (dashed outline) represent the non-ischaemic one. L = lentiform nucleus; C = caudate head; I = insular ribbon; IC = internal capsule; M1 = anterior MCA cortical region; M2 = MCA cortical region located lateral to insular ribbon; M3 = posterior MCA cortical region; M4, M5 and M6 about 2 cm superior to M1, M2, and M3 ROIs respectively.

2.3.10 CT scan statistical Analysis

Patients were divided into two groups: ischaemic patients and mimics. In the ischaemic patients, the mean (SD) of HU value for the 10 ASPECTS regions obtained from the ischaemic side were compared with the respective HU values of non-ischaemic side. Similarly, in the stroke mimics, mean (SD) of HU for the 10 ASPECTS regions obtained from the right and left sides of the head scan were compared. Statistical analysis and graph production was carried out using Excel program and GraphPad Prism 9 software (GraphPad, San Diego, California). To compare

significant trend of HU values between the two hemispheres, paired Student's t-test was used. P≤0.05 was taken into consideration as statistically significant. ASPECTS data were correlated with the blood circulating biomarkers.

2.3.11 MRI scan protocol

Protocol was achieved identically to the retrospective study method as in section 2.2.5. In addition, the imaging parameters for the T2 weighted image sequence are (sequence type: spin echo (SE), repetition time (TR): 5530 ms , echo time (TE) : 98 ms ,echo number: 1, number of average:1, echo train length: 11, percent sampling: 75, pixel bandwidth: 100 and flip angle: 150. Slices were 5 mm thick. No contrast agent was given.

2.3.12 MRI image processing

Data analysis was achieved identically to the retrospective study method as in section 2.2.6. and in Figure 2.8. Additionally, identical ROIs were determined from T2 weighted images in WM and GM areas to measure the ratio of T2 signal intensity. Furthermore, a comparison between the volume of infarct and the NIHSS was done.

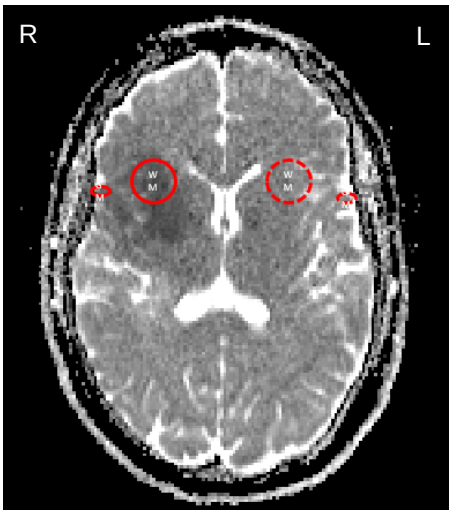

Figure 2.8 This ADC image shows where the ROIs in WM& GM are drawn. Right side areas (solid outline) represent the ischaemic side while the left areas (dashed outline) represents the non-ischaemic side.

2.3.13 MRI Statistical analysis

Mean (SD) values for each region were determined from ADC and T2 images in each case. Normality test was performed to examine the data distribution. To test the

significant trend between two variables, paired Student's t-test or Unpaired Student's t-test were used as appropriate. MRI imaging biomarkers were correlated with the blood circulating biomarkers.

2.3.14 Statistical correlation analysis

Linear regression and correlation analyses were performed using the nonparametric Spearman rank correlation test to analyse the extent of relationships between circulating biomarkers and imaging biomarkers. Statistical analysis and graphs production were achieved using GraphPad Prism 9 software (GraphPad, San Diego, California). Statistical significance was determined when $p \leq 0.05$.

Chapter 3 Results - Biomarkers in preclinical models

The overall aim of the study was to assess brain cells and BBB damage and determine the level of circulatory biomarkers following ischaemic stroke. Two preclinical murine models [bilateral carotid artery occlusion (BCCAO) model and middle cerebral artery occlusion (MCAO) model] of ischaemic stroke were used to assess detailed brain damage and relevant proteins released in the blood circulation.

Initially, BCCAO model was used as this model produces consistent cell damages in the brain, which are very important to assess brain damage related proteins released in the blood serum or plasma. Furthermore, patients with BCCAO have a particularly poor prognosis as a result of a high subsequent stroke prevalence rate (66% in bilateral ICA occlusion and 71% in BCCAO) (Lai et al., 2005). BCCAO produces global cerebral ischaemia which is the most occurring type of stroke in cardiovascular diseases like cardiac arrest, small vessel infarctions or lacunar stroke (Wahul et al., 2018). The common carotid artery is also a big artery that is implicated in the majority of strokes (Stroke Association, 2018). Moreover, this type of stroke damages neurones and astrocytes, particularly in the cortex and hippocampus, where neurodegeneration and astrogliosis are most common (Soria et al., 2013).

Once I established and optimised all techniques including IHC, WB and ELISA in the BCCAO model , I used MCAO model as this model produces focal ischaemia which occluded the MCA (Jin et al., 2014); one of the most affected vessels in human stroke (Nogles and Galuska, 2022). These accounting for about 70% of infarcts (Bogousslavsky et al., 1988). MCAO model is known to produce neuronal damage in the cortex, hippocampus and striatum both in mice and rats (McColl et al., 2007; Rao et al., 2001; Ketheeswaranathan et al., 2011).

3.1 Changes in neuronal, glial cell and blood brain barrier proteins in bilateral common carotid artery occlusion (BCCAO)

In this part of the study, murine model of ischaemic stroke induced by the BCCAO was used to determine changes in neuronal, glial cells, pericytes and BBB junctional proteins (ZO-1, Occludin and Claudin-5) in the forebrain. The levels of brain and BBB damaged proteins were then measured in blood serum to find out if these proteins can be used as potential biomarkers of ischaemic stroke.

C57BL/6 mice have been used as previous studies in our lab (Khan et al., 2018) and others (Yang et al., 1997; Murakami et al., 1998) showed BCCAO in these mice developed consistent and selective neuronal death in the hippocampus, the motor and somatosensory cortex with a higher survival rate.

To determine brain damage in the cortex and hippocampus, antibodies of specific neuronal (NeuN), glial cell (GFAP), microglial cell (IBA-1), pericytes cell (PDGFR and NG2) and endothelial cells (CD31) were used. Additionally, antibodies to specific BBB TJ proteins (Occludin, Caludin-5 and ZO-1) were used to assess BBB damage. Quantifications of NeuN, GFAP, NG2, PDGFR and IBA-1 immunolabelled profiles were done using the method described in section 2.1.9.

Furthermore, this study used quantitative WB analysis to determine if the expressions of GFAP, Claudin-5, Occludin and ZO-1 in the hippocampus are significantly different between control and BCCAO mice as detailed in section 2.1.12.

Finally, the levels of GFAP, Claudin-5, ZO-1 and Occludin were assessed in the blood serum of BCCAO and control mice using ELISA method (section 2.1.14.). Correlation analysis between WB analysis of brain markers and ELISA of blood biomarkers was done as per section 2.1.15.

3.1.1 Histochemistry - Cresyl violet staining results

The extent of cerebral damage following ischaemia was first assessed by using cresyl violet staining, which is a routinely used method to define cellular damage in the cerebral infarction areas. Light microscopy imaging with cresyl violet staining revealed ischaemic damage, as assessed by chromatolytic changes (reactive variations that happen in the damaged neuron's cell body including the dispersal of Nissl bodies (Bradley et al., 2018)) in the hippocampus in the BCCAO group (n=3) as compared to the control group (n=3) following BCCAO and reperfusion (Figure 3.1).

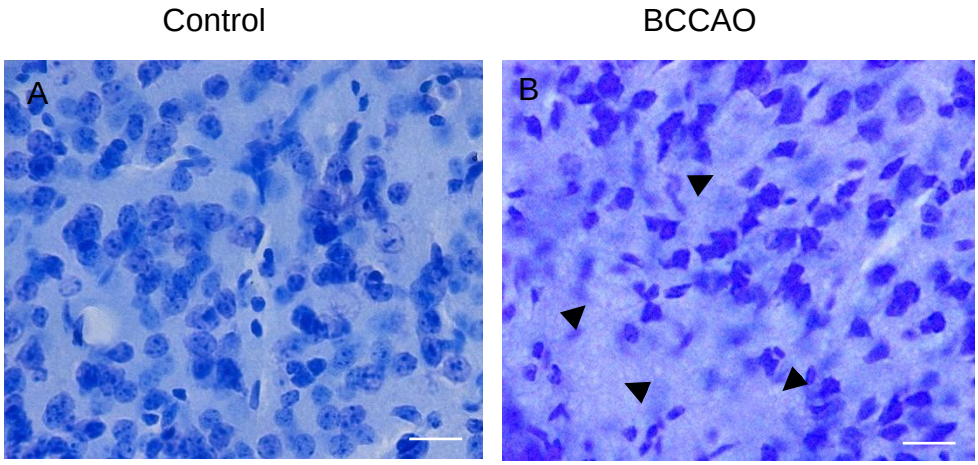

Figure 3.1 Representative photomicrographs showing cresyl violet staining of neuron cell nuclei in the hippocampus in control (A) and BCCAO (B) brains. The staining shows chromatolytic changes in the stroke brain compared to the control brain due to cellular damage following BCCAO induced stroke (arrowheads). (Scale bar=20um). (The images are taken at the level of Bregma -2.06mm).

3.1.2 NeuN immunostaining and quantitative analysis

Immunohistochemical staining using antibodies to NeuN was utilised to investigate neuronal death in ischaemic brains compared to the sham operated brains. Immunostained coronal brain sections were examined under a fluorescent microscope. NeuN is a neuronal specific nuclear protein that is commonly used as a marker of mature neurones (Gusel'nikova and Korzhevskiy, 2015). The antibody to NeuN was selected to immunostain neuronal cells in ischaemic and sham brains as it labels nuclei of neuronal cell in the brain (Gusel'nikova and Korzhevskiy, 2015). Cell counting method was used to count the number of immunostained cells in the

hippocampus and the cortex, areas known to be greatly affected by cerebral ischaemia or stroke. Also, it was used to determine specifically the extent of neuronal death in the hippocampus and cortex. In the course of the study, it was realised that optimal dilutions of antibodies are important to get specific immunolabeling in the brain. The optimal working dilution for NeuN was found to be 1:4000, diluted in PBS-T buffer. This NeuN dilution showed the strongest and best specific antigen labelling with low non-specific background labelling. Negative controls, which show a low degree of non-specific staining, were used to assess the primary and secondary antibodies' binding specificity. The brain sections were seen using 20 X magnification objectives, concentrating on the following specific areas of brains: hippocampus (CA1), 2nd somatosensory cortex, M1 (primary motor cortex), M2 (2nd motor cortex) and granular insular cortex, areas affected most in the BCCAO model. These areas of the brain were determined according to mouse brain atlas (Paxinos and Franklin., 2012).

Data from NeuN IHC showed that BCCAO and reperfusion induce considerable loss of neurones in the hippocampus (CA1), 2nd somatosensory cortex, M1 (primary motor cortex) , M2 (2nd motor cortex) and the granular insular cortex area as shown in Figure 3.2 using 50um microtome brain sections thickness (fixed brain tissue) and in Figure 3.3 using 20um cryostat brain sections thickness (fixed and frozen brain tissue). Both thick and thin brain sections were used initially to see if there is any difference in staining between the two different thicknesses of brain sections. To detect the loss of neurons more specifically and accurately, quantitative analysis was performed on thin sections (20 µm). Quantitative analysis showed that the NeuN positive cells were significantly decreased in ischaemic brains (n=6) when compared to the sham-operated group (n=6). The highest significant decrease was shown in the hippocampus (Unpaired Student’s t-test, $p<0.0001$), followed by M1 primary motor cortex ($p=0.0019$) and 2nd somatosensory cortex ($p=0.0019$) then M2 2nd motor cortex ($p=0.0024$) and lastly the granular insular cortex area with ($p=0.0194$) as shown in Figure 3.4.

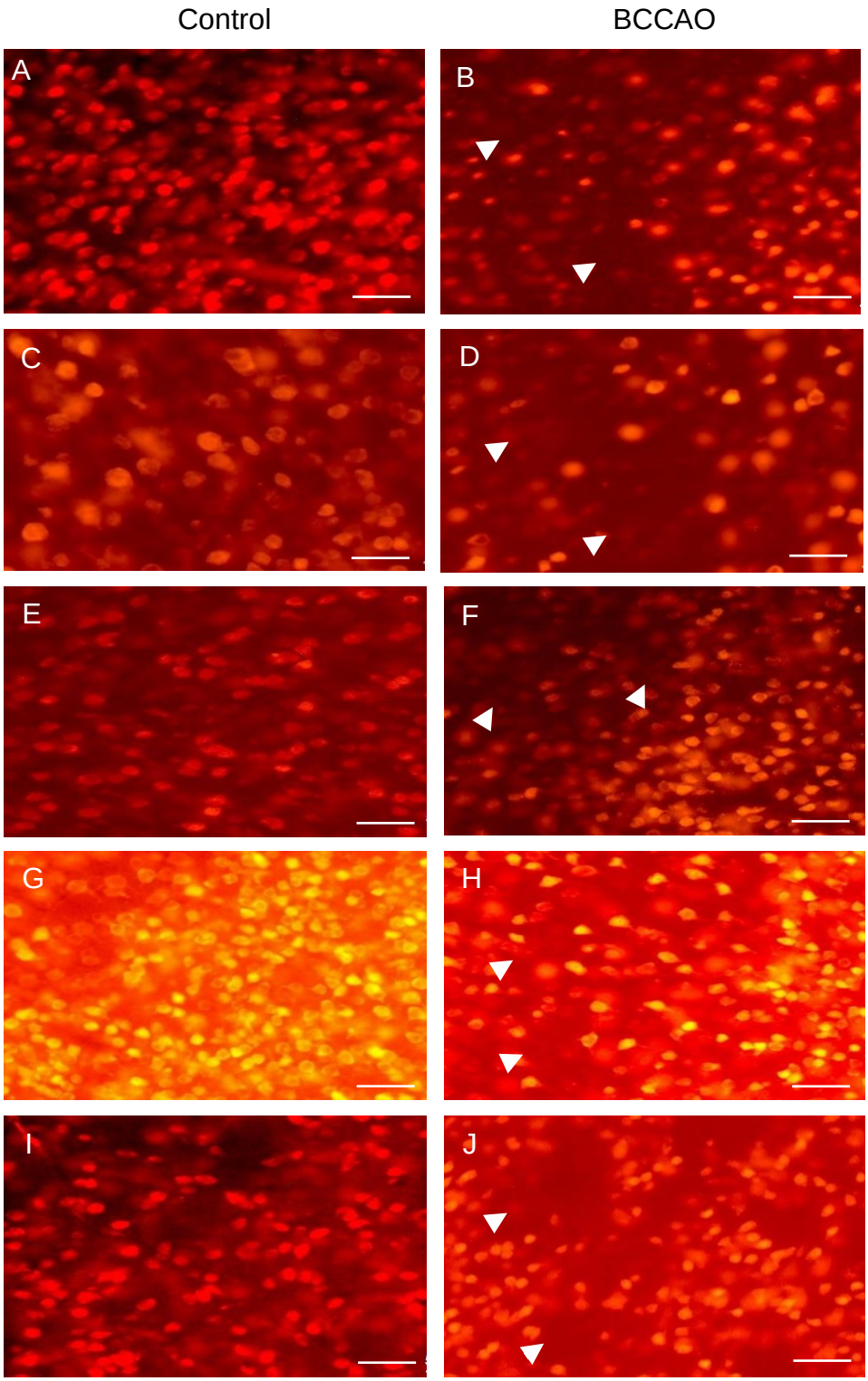

Figure 3.2 Representative photomicrographs showing immunofluorescence staining of NeuN labelled cell nuclei in the M1 motor cortex (A-B), M2 motor cortex (C-D), granular insular Cortex (E-F), 2nd somatosensory cortex (G-H) and hippocampus (CA1) (I-J) of control (left column) and BCCAO stroke brains (right column). NeuN labelled cells are fewer in stroke models than in the controls due to neuronal cells death following stroke (arrowheads). (Scale bar=50um). (The images are taken at the level of Bregma 1.54 or -2.06mm). (Slice thickness=50um).

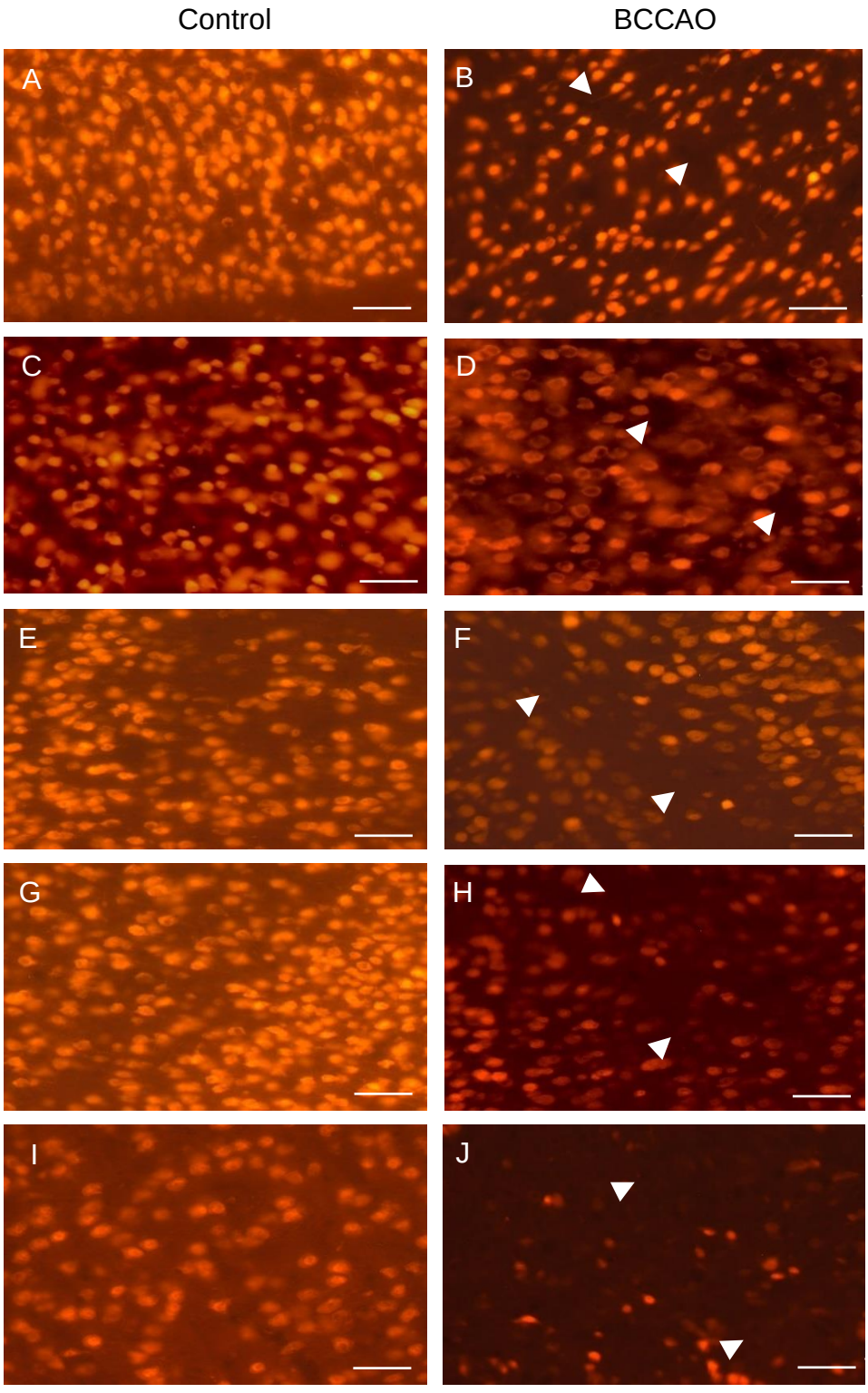

Figure 3.3 Representative photomicrographs showing immunofluorescence staining of NeuN labelled cell nuclei in the M1 motor cortex (A-B), M2 motor cortex (C-D) ,granular insular Cortex (E-F), 2nd somatosensory cortex (G-H) and hippocampus (CA1) (I-J) of control (left column) and BCCAO stroke brains (right column). NeuN labelled cells are fewer in stroke mice than in the controls due to neuronal cells death following stroke (arrowheads). (Scale bar=50um). (The images are taken at the level of Bregma 1.54 or -2.06mm). (Slice thickness=20um).

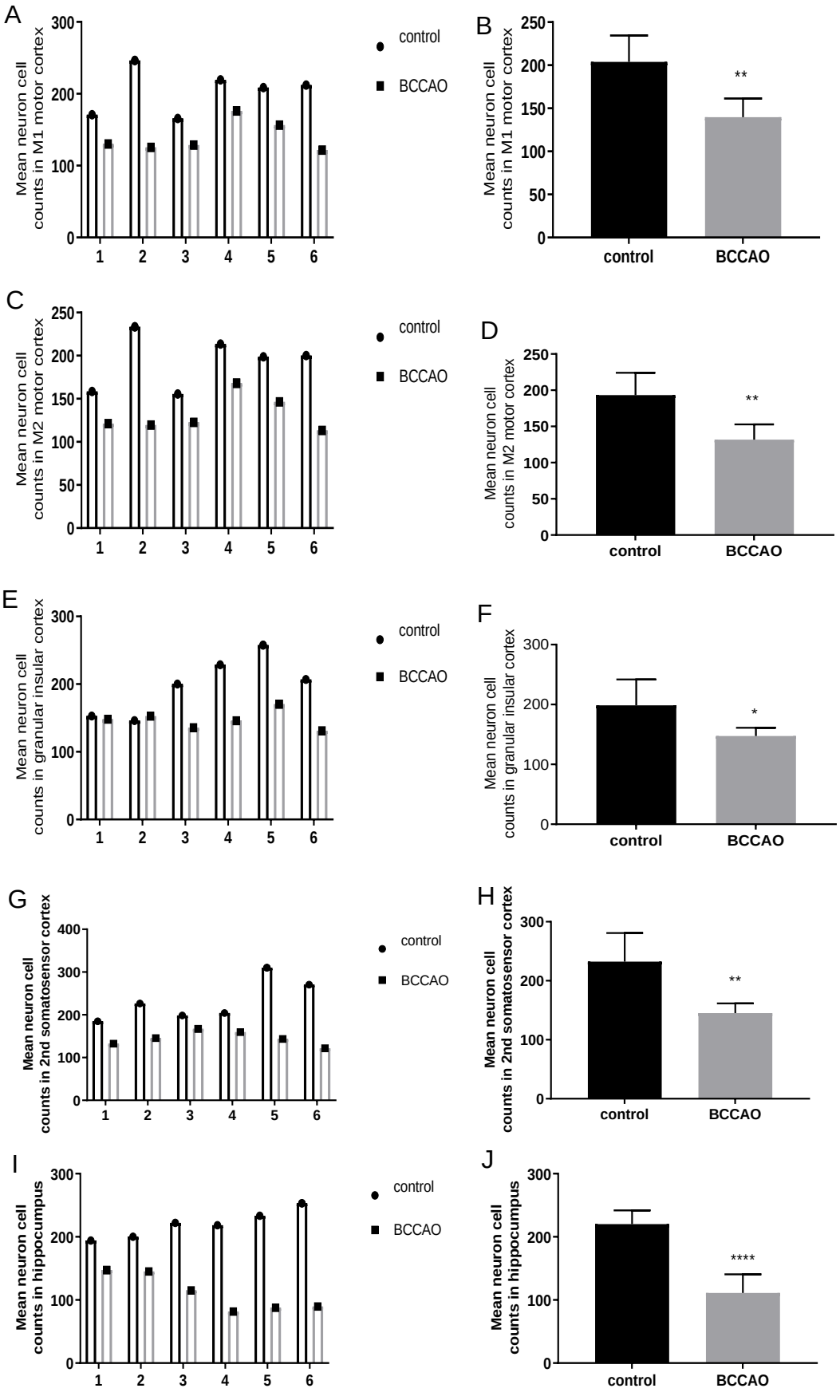
A
Mean neuron cell counts in M1 motor cortex
300
200
100
0
1 2 3 4 5 6
control
BCCAO
B
Mean neuron cell counts in M1 motor cortex
250
200
150
100
50
0
**
control
BCCAO
C
Mean neuron cell counts in M2 motor cortex
250
200
150
100
50
0
1 2 3 4 5 6
control
BCCAO
D
Mean neuron cell counts in M2 motor cortex
250
200
150
100
50
0
**
control
BCCAO
E
Mean neuron cell counts in granular insular cortex
300
200
100
0
1 2 3 4 5 6
control
BCCAO
F
Mean neuron cell counts in granular insular cortex
300
200
100
0
*
control
BCCAO
G
Mean neuron cell counts in 2nd somatosensor cortex
400
300
200
100
0
1 2 3 4 5 6
control
BCCAO
H
Mean neuron cell counts in 2nd somatosensor cortex
300
200
100
0
**
control
BCCAO
I
Mean neuron cell counts in hippocumpus
300
200
100
0
1 2 3 4 5 6
control
BCCAO
J
Mean neuron cell counts in hippocumpus
300
200
100
0
****
control
BCCAO

Figure 3.4 Quantitative analysis shows significant differences (*p< 0.05, **p ≤ 0.01, ****p ≤ 0.0001-Unpaired Student's t-test, n=6) in the number of NeuN-positive nuclei between sham-operated and BCCAO stroke mice in the M1 motor cortex(A-B, p=0.0019), M2 motor cortex (C-D, p= 0.0024), granular insular cortex (E-F, p=0.0194), 2nd somatosensory cortex (G-H, p=0.0019) and hippocampus (CA1) (I-J, p<0.0001).

3.1.3 GFAP immunostaining and quantitative analysis

GFAP is an intermediate filament (IF) protein that is predominantly expressed by astrocytes in the CNS (Hol and Pekny, 2015). IHC staining for GFAP is known to be standard for labelling reactive astrocytes in white matter in the brain such as hippocampus (Schmidt-Kastner et al., 1993). Thus, specific antibody to specific glial cell marker, GFAP was used for immunolabelling of astrocytes in sections obtained from both stroke and control mice. The GFAP optimal working dilution was found to be 1:1000, diluted in PBS-T buffer as it gave the strongest antigen staining with low non-specific background labelling. Moreover, negative controls were performed to examine the primary and secondary antibodies' binding specificity. The coronal brain sections at the level of Bregma -2.06mm were visualized using 20 and 40 X magnification objectives, focusing on the hippocampus.

Data from astrocytes cells and processes labelled by GFAP IHC in BCCAO ischaemic model compared to sham brain showed an increase in astrocytes cells and processes in the hippocampus both in microtome sections (50um thickness) and cryostat sections (20um thickness) as shown in (Figure 3.5 and Figure 3.6) respectively. Quantitative analysis showed that the GFAP positive glial cells numbers and GFAP positive glial processes numbers were significantly increased in cerebral ischaemic brains in the hippocampus (CA1) in a comparison with the correspondent area of the sham operated animals. The data showed a significant elevation in the numbers of both astrocyte's cells and processes in the BCCAO stroke models (n=6) compared to the control models (n=6) with (Unpaired Student's t-test, p=0.0036, p=0.0003 respectively) Figure 3.7.

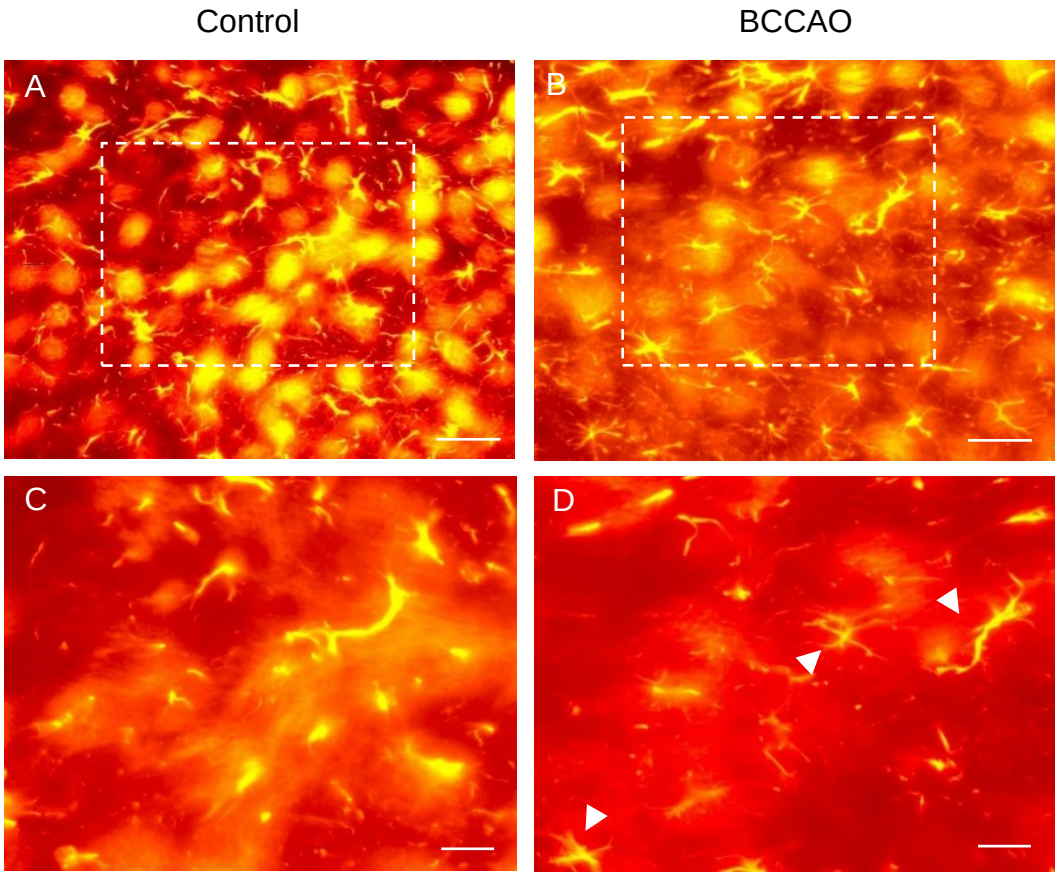

Figure 3.5 Representative photomicrographs showing immunofluorescence staining of GFAP labelled astrocytes in the hippocampus area of control (A, C) and BCCAO stroke (B, D) brains. The GFAP labelled cells and processes are thicker and higher in number in stroke mice than in the controls due to astrocytes activation following stroke (arrowheads). (Scale bar=50um:A,B and 20um:C,D). (The images are taken at the level of Bregma -2.06mm). (Slice thickness=50um).

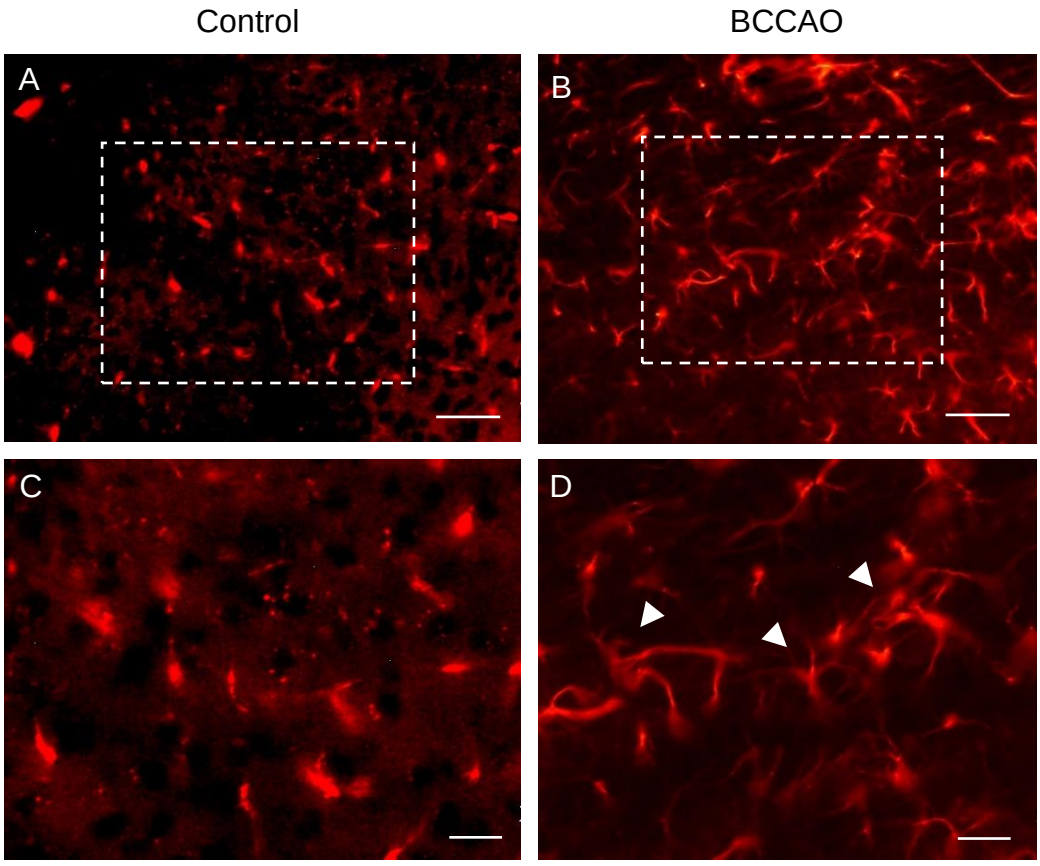

Figure 3.6 Representative photomicrographs showing immunofluorescence staining of GFAP labelled astrocytes in the hippocampus area of control (A, C) and BCCAO stroke (B, D) brains. The GFAP labelled cells and processes are thicker and higher in number in stroke mice than in the controls due to astrocytes activation following stroke (arrowheads). (Scale bar=50um:A,B and 20um:C,D). (The images are taken at the level of Bregma -2.06mm). (Slice thickness=20um).

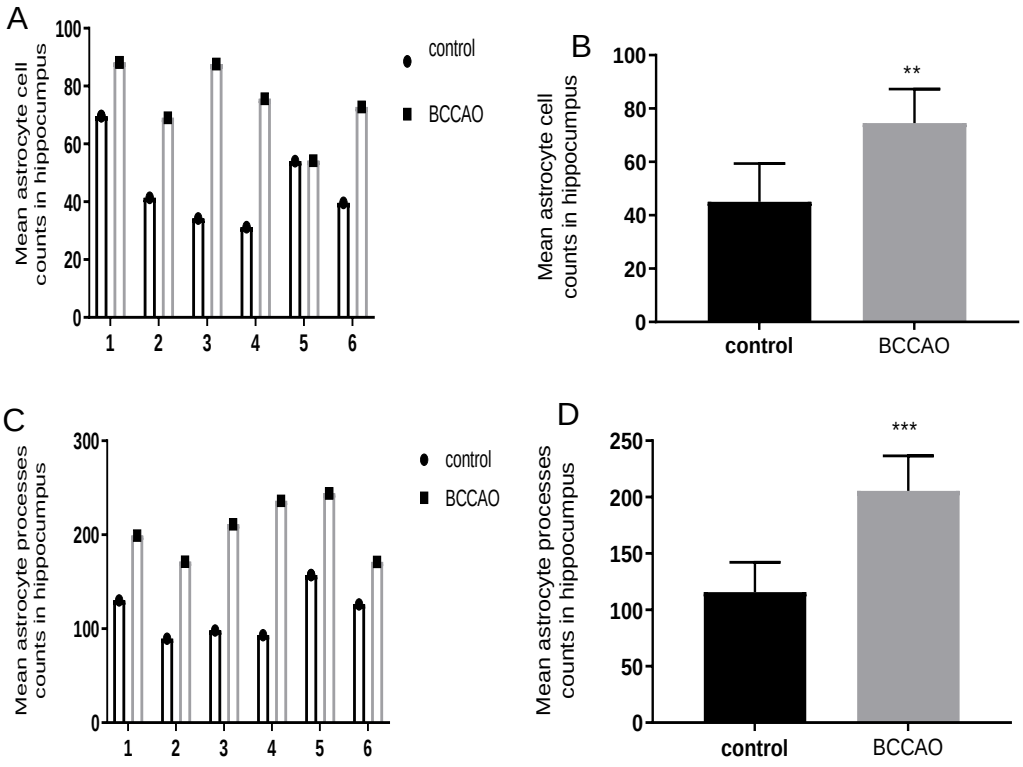

Figure 3.7 Quantitative analysis shows significant increases (p ≤ 0.01, ***p ≤ 0.001- Unpaired Student's t-test, n=6) in the number of GFAP labelled astrocyte cells (A-B, p=0.0036) and profiles processes (C,D-p=0.0003) in BCCAO mice compared to sham in hippocampus (CA1).**

3.1.4 Immunostaining and quantitative analysis of pericytes

The effects of cerebral ischaemia injury on the pericytes were investigated following BCCAO and reperfusion using specific antibodies to pericytes. To examine changes in pericytes cells after stroke, pericyte specific proteins were selected using IHC staining. Antibodies to NG2 and PDGFR were used in this study. The best optimal dilution for NG2 and PDGFR which showed the best specific antigen labelling was 1:600, diluted in PBS-T. Multiple sections of brain tissues at the cortical and hippocampal levels (at the level of bregma 1.54mm and -2.06mm respectively) were imaged at 20 and 40 X magnification objectives. Pericytes stained with PDGRF antibody showed morphological changes with loss of cell bodies in both hippocampal and cortical areas of the stroke brain compared to the control, as shown in (Figure 3.8 and Figure 3.9). Moreover, pericytes stained with NG2 antibody in both hippocampal

and cortical areas in stroke brain compared to control showed similar damage that observed with PDGRF, as shown in Figure 3.11 and Figure 3.12.

Quantitative analysis of the PDGFR immunoreactive profiles demonstrated that, the BCCAO and reperfusion significantly decreased the PDGFR immunoreactive pericytes profiles with almost three-fold reduction following the ischaemic insult in comparison to the control operated mice (n=6/ group, ****p<0.0001-Unpaired Student's t-test ,Figure 3.10). Similarly, pericytes reduction was observed with the numbers of NG2 positive cells with about twice and a half fold significant reduction in the cerebral ischaemia group (n=6/ group ****p<0.001- Unpaired Student's t-test, Figure 3.13) compared to the sham group.

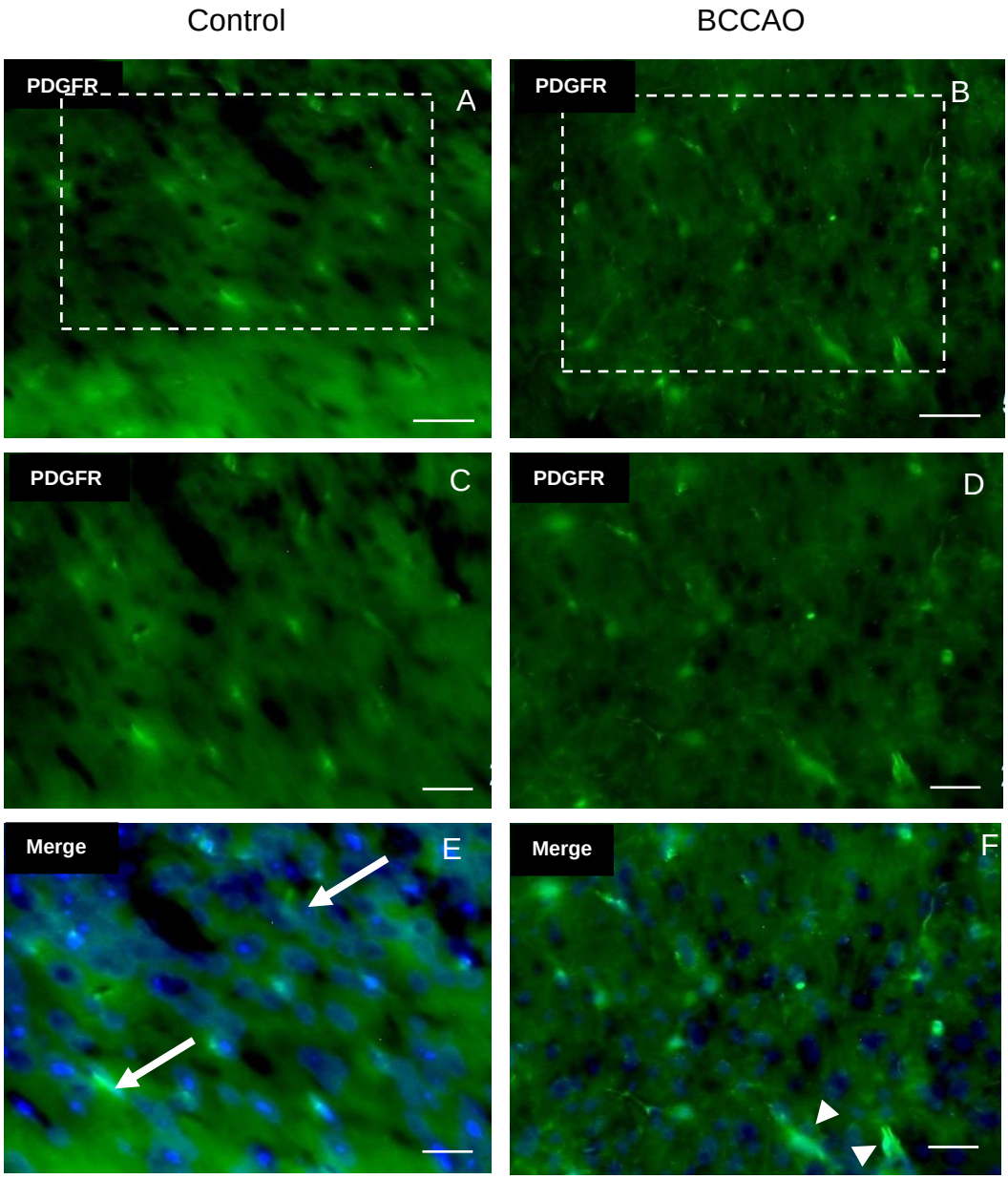

Figure 3.8 Representative photomicrographs showing immunofluorescence staining for PDGFR with anti-PDGFR and Alexa488 conjugated secondary antibodies with DAPI stained nuclei in the hippocampus area in sham (A, C, E) and BCCAO stroke brains (B, D, F). The labelled pericytes show morphological changes with some dilatation and loss in the stroke brain (arrowheads) compared to control (arrows). (Scale bar=50um:A,B and 20um:C,D,E,F). (The images are taken at the level of Bregma -2.06mm). (Slice thickness=20 um).

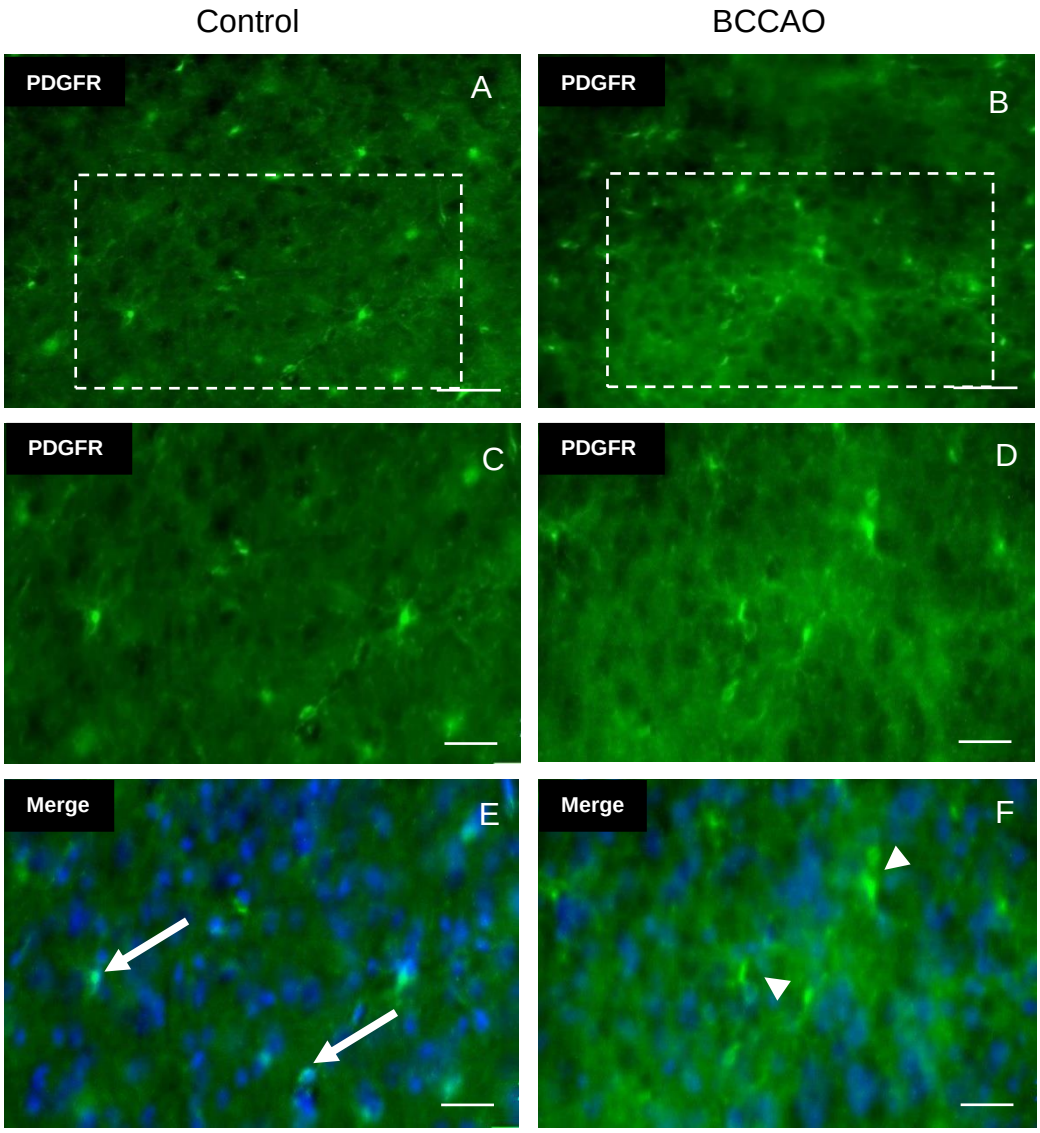

Figure 3.9 Representative photomicrographs showing immunofluorescence staining for PDGFR with anti-PDGFR and Alexa488 conjugated secondary antibodies with DAPI stained nuclei in the cortex in sham (A, C, E) and BCCAO stroke brains (B, D, F). The labelled pericytes show morphological changes and some loss in the stroke brain (arrowheads) compared to control (arrows). (Scale bar=50um:A,B and 20um:C,D,E,F). (The images are taken at the level of Bregma 1.54mm). (Slice thickness=50 um).

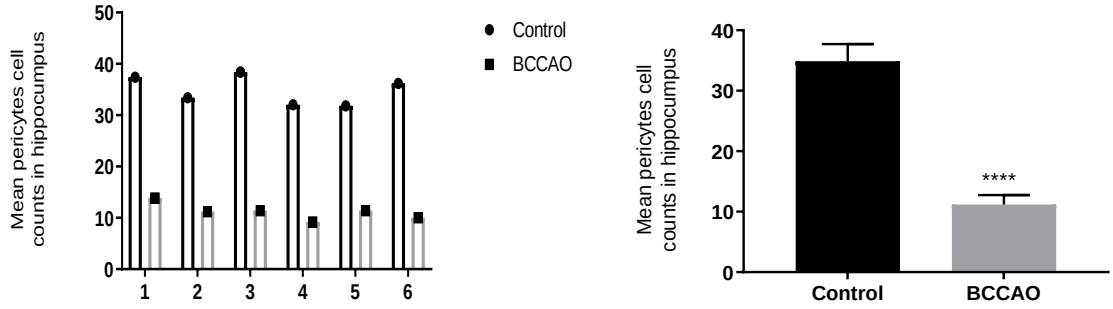

Figure 3.10 Quantitative analysis shows significant differences (**p ≤ 0.0001- Unpaired Student's t-test, n=6) in the number of PDGFR positive pericytes between sham-operated and stroke mice in the hippocampus (****p<0.0001).**

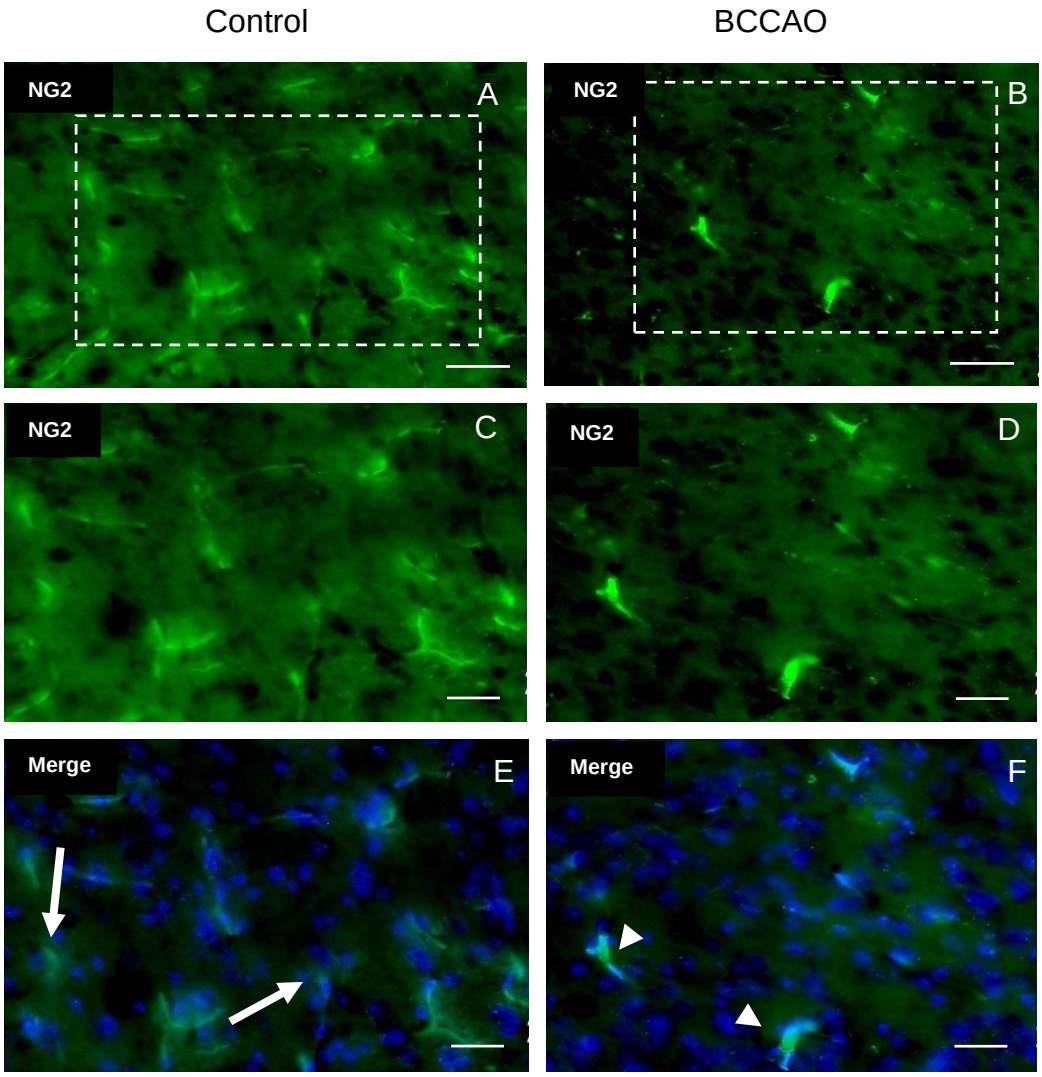

Figure 3.11 Representative photomicrographs showing immunofluorescence staining for NG2 with anti-NG2 and Alexa488 conjugated secondary antibodies with DAPI stained nuclei in the hippocampus area in sham (A, C, E) and BCCAO stroke brains (B, D, F). The labelled pericytes show morphological changes with some loss and dilatation in the stroke brain (arrowheads) compared to control (arrows). (Scale bar=50um:A,B and 20um:C,D,E,F). (The images are taken at the level of Bregma -2.06mm). (Slice thickness=20 um).

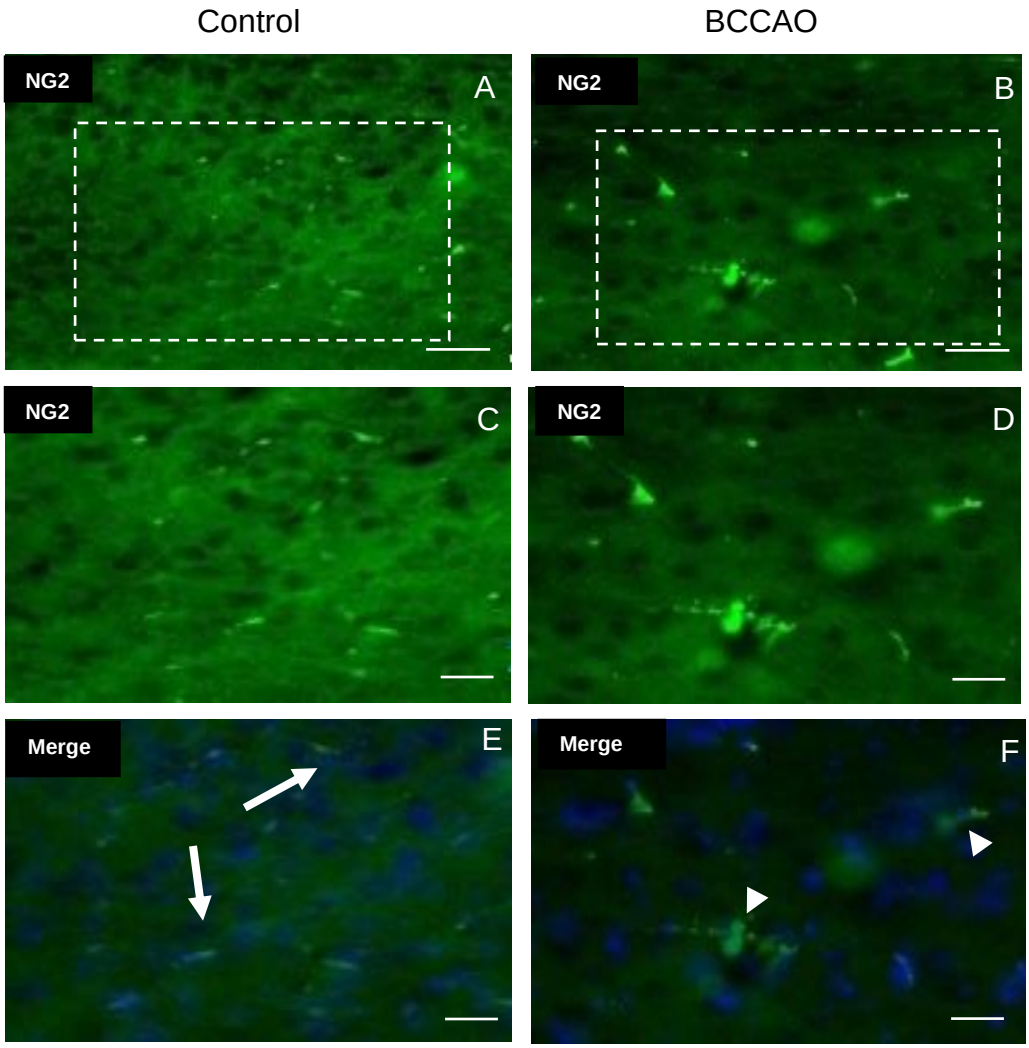

Figure 3.12 Representative photomicrographs showing immunofluorescence staining for NG2 with anti-NG2 and Alexa488 conjugated secondary antibodies with DAPI stained nuclei in the cortex in sham (A, C, E) and BCCAO stroke brains (B, D, F). The labelled pericytes show morphological changes with some loss and dilatation in the stroke brain (arrowheads) compared to control (arrows). (Scale bar=50um:A,B and 20um:C,D,E,F). (The images are taken at the level of Bregma 1.54mm). (Slice thickness=50 um).

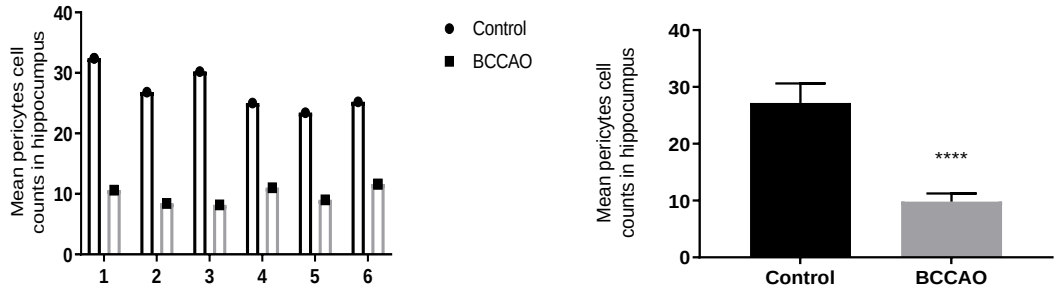

Figure 3.13 Quantitative analysis shows significant differences (**p ≤ 0.0001- Unpaired Student's t-test, n=6) in the number of NG2 positive pericytes between sham-operated and stroke mice in the hippocampus (****p<0.0001).**

3.1.5 Immunostaining and quantitative analysis of microglia

Immunohistochemical staining for IBA-1, a microglia specific protein was used to localize microglial cells in the cortex and the hippocampus of stroke and control brains. The optimal IBA-1 dilution was 1:200, diluted in PBS-T. IBA-1 immunoreactive cells were increased in both the hippocampus area and the cortex area after stroke as shown in Figure 3.14 and Figure 3.15 respectively. There was also an increase in microglia processes in the stroke brains compared control brains. Quantitative analyses of microglia cells and processes in ischaemic and sham brains (n=6) showed significant increases of both microglia cells and processes in the hippocampal area (Unpaired Student's t-test, p=0.0021 and p=0.0002) respectively in the ischaemic group compared to the corresponding control group, Figure 3.16.

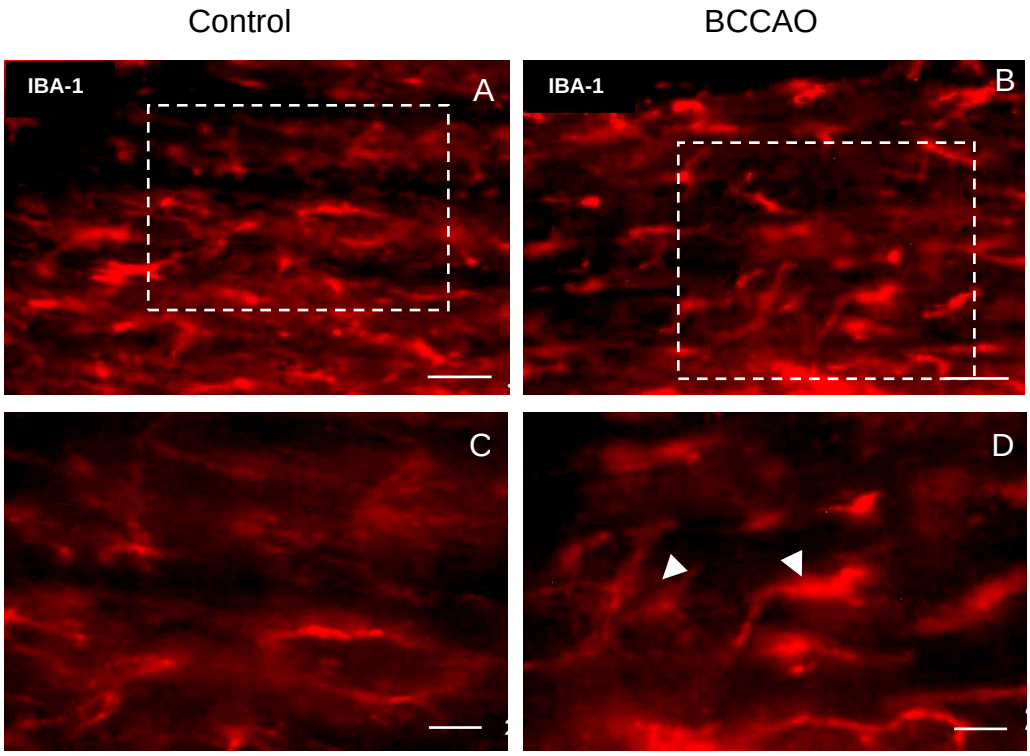

Figure 3.14 Representative photomicrographs showing immunofluorescence staining for IBA-1 using anti-IBA-1 in the hippocampus area of control (A, C) and stroke (B, D). The IBA-1 labelled cells and processes are more in stroke mice than in the controls following stroke (arrowheads). (Scale bar=50um:A,B and 20um:C,D). (The images are taken at the level of Bregma -2.06mm). (Slice thickness=20 um).

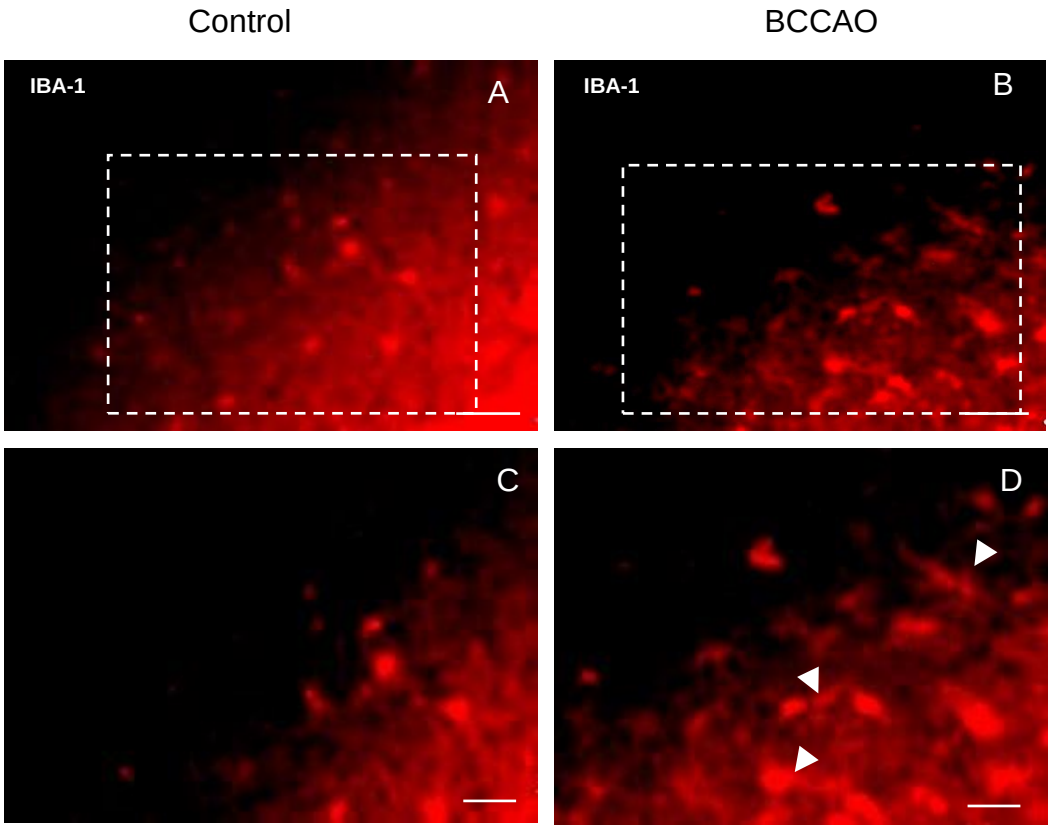

Figure 3.15 Representative photomicrographs showing immunofluorescence staining for IBA-1 using anti-IBA-1 in the cortical area of control (A, C) and stroke (B, D). The IBA-1 labelled cells and processes are more in stroke mice than in the controls following stroke (arrowheads). (Scale bar=50um:A,B and 20um:C,D). (The images are taken at the level of Bregma 1.54mm). (Slice thickness=50 um).

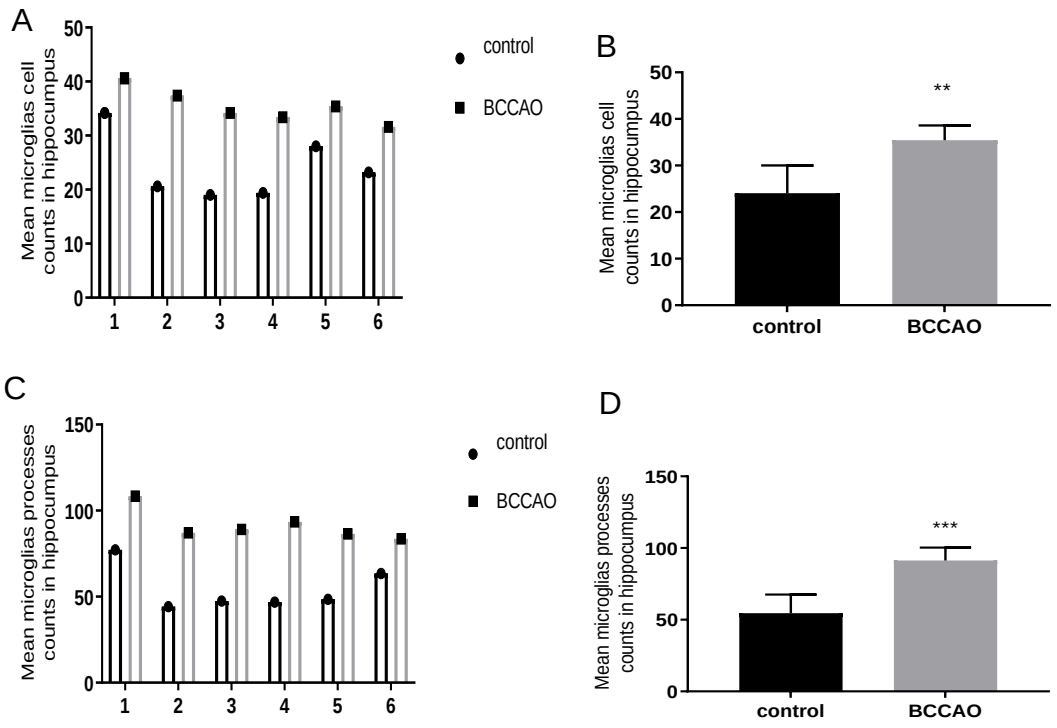

Figure 3.16 Quantitative analysis shows the significant differences (p ≤ 0.01, ***p ≤ 0.001, - Unpaired Student's t-test, n=6) in the number of IBA-1 positive microglia cells and processes between sham-operated and stroke mice in the hippocampus (A,B-p=0.0021) and (C,D-p=0.0002) respectively.**

3.1.6 Immunostaining of endothelial cells

To examine the changes in endothelial cells of blood vessels following stroke, antibody to CD31 was used for IHC staining. The optimal CD31 working dilution was 1:100, diluted in PBS-T buffer. CD31 immunoreactivity was present in the cortical and hippocampal areas and imaged at 20 and 40 X magnification objectives. CD31 immunoreactivity was present in the endothelial cells. Endothelial cells labelled with anti-CD31 showed distortion in morphology and dilatation in the ischaemic brain compared to sham brain, particularly in the hippocampus and cortex as shown in Figure 3.17 and Figure 3.18 respectively.

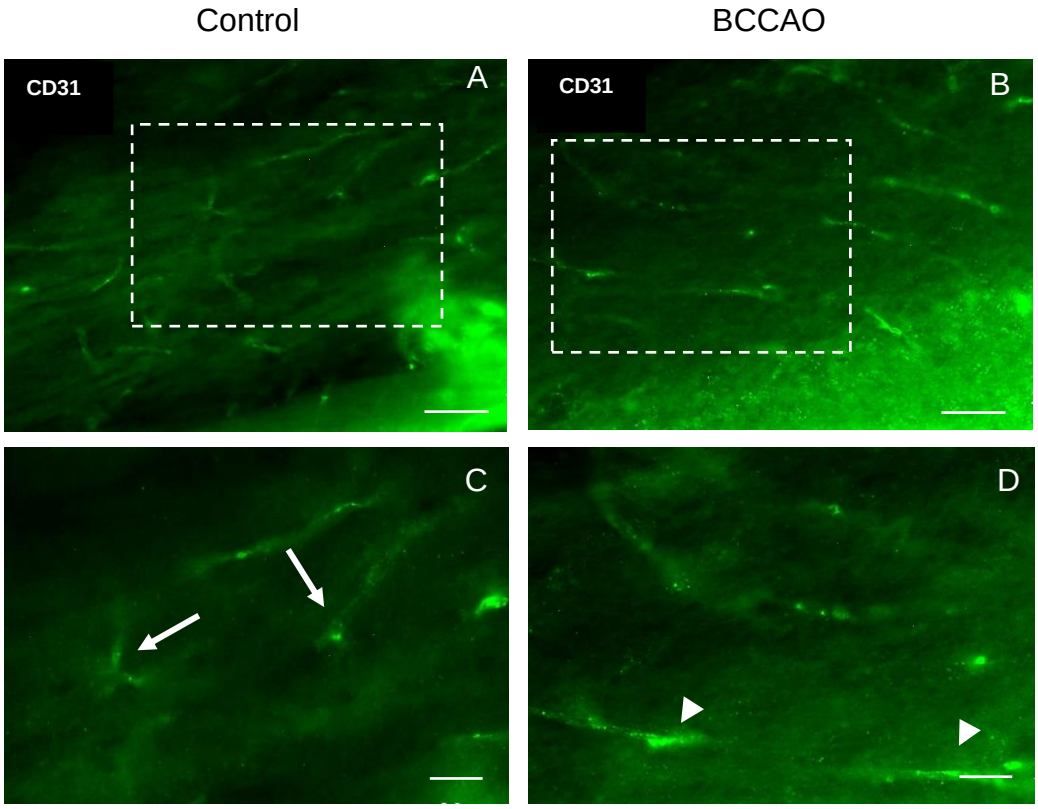

Figure 3.17 Representative photomicrographs showing immunofluorescence staining using anti-CD31 in the hippocampus of control (A, C) and stroke (B, D). The labelled endothelial cells with anti-CD31 showing morphological changes with some dilatation in the stroke brain (arrowheads) compared to control (arrows). (Scale bar=50um:A,B and 20um:C,D). (The images are taken at the level of Bregma -2.06mm). (Slice thickness=20um).

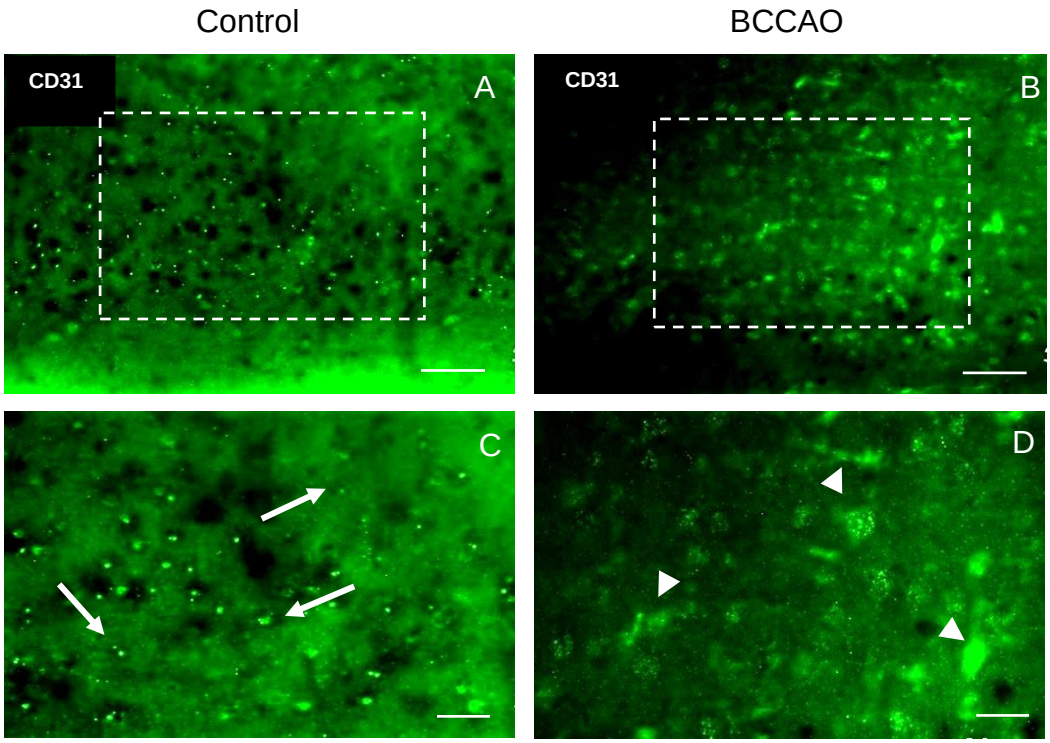

Figure 3.18 Representative photomicrographs showing immunofluorescence staining using anti-CD31 in the cortical area of control (A, C) and stroke (B, D). The labelled endothelial cells with anti-CD31 showing morphological changes with some dilatation in the stroke brain (arrows) compared to control (arrows). (Scale bar=50um:A,B and 20um:C,D). (The images are taken at the level of Bregma 1.54mm). (Slice thickness=50um).

3.1.7 Disruption of TJ of BBB

To investigate BBB damage in murine model of cerebral ischaemia, immunohistochemical staining of BBB TJ proteins were performed using specific antibodies to these proteins. Antibodies to three TJ proteins were used: ZO-1, Occludin and Claudin-5 and the immunostaining results are shown in the following section.

3.1.7.1 ZO-1 immunostaining results

ZO-1 is one of the main TJ proteins that reduces the cerebral vessels permeability by restricting the free molecular exchange between blood and brain tissues (Itoh and Bissell, 2003). The optimal working dilution was found after multiple optimisation processes to be 1:100, diluted in PBS-T. This working dilution resulted in strong specific antigen staining along with low non-specific staining for the background. Furthermore, negative controls were achieved to assess the binding specificity of primary and secondary antibodies. Brain sections at the level of Bregma -2.06mm (the hippocampus) were imaged using 60 X magnification objective. The immunostaining results illustrated disruption of ZO-1 labelled profiles in the hippocampus following BCCAO and reperfusion compared to the intact ones in the control as shown in Figure 3.19.

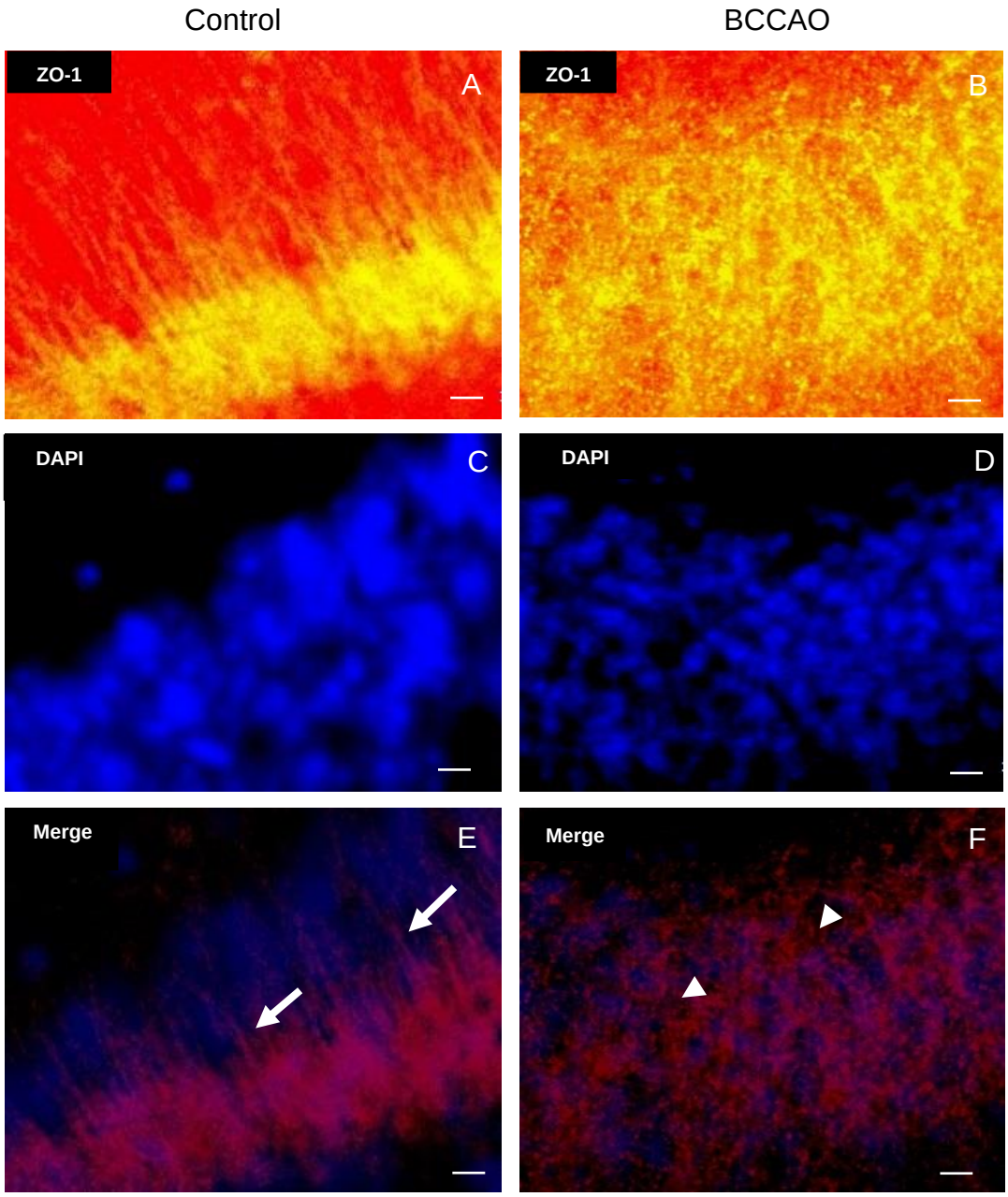

Figure 3.19 Representative photomicrographs showing immunofluorescence staining for ZO-1 with anti-ZO-1 and Cy3-conjugated secondary antibodies with DAPI stained nuclei in the hippocampus in sham (A, C, E) and BCCAO stroke brains (B, D, F). The labelled TJs are disrupted in stroke brain (arrowheads) compared to the intact ones in the control (arrows). (Scale bar=10um). (The images are taken at the level of Bregma-2.06mm). (Slice thickness=50um).

3.1.7.2 Occludin immunostaining results

Occludin is also one of the main TJ proteins that are an integral part of the BBB's structure (Hawkins and Davis, 2005). Antibody to Occludin, one of the TJ proteins was used to immunostain the Occludin-immunoreactive profiles in the BBB TJ. The optimal working dilution was found 1:50 diluted in PBS-T after several optimising experiments. This dilution gave the best labelling of specific antigen with low non-specific staining for the background. Negative controls were done to determine the specificity of the binding of primary and secondary antibodies. Immunofluorescence images using 60 X magnification objective at the level of hippocampus showed disruption of Occludin immunoreactive profiles in the hippocampus of ischaemic mice as compared to sham-operated mice (Figure 3.20).

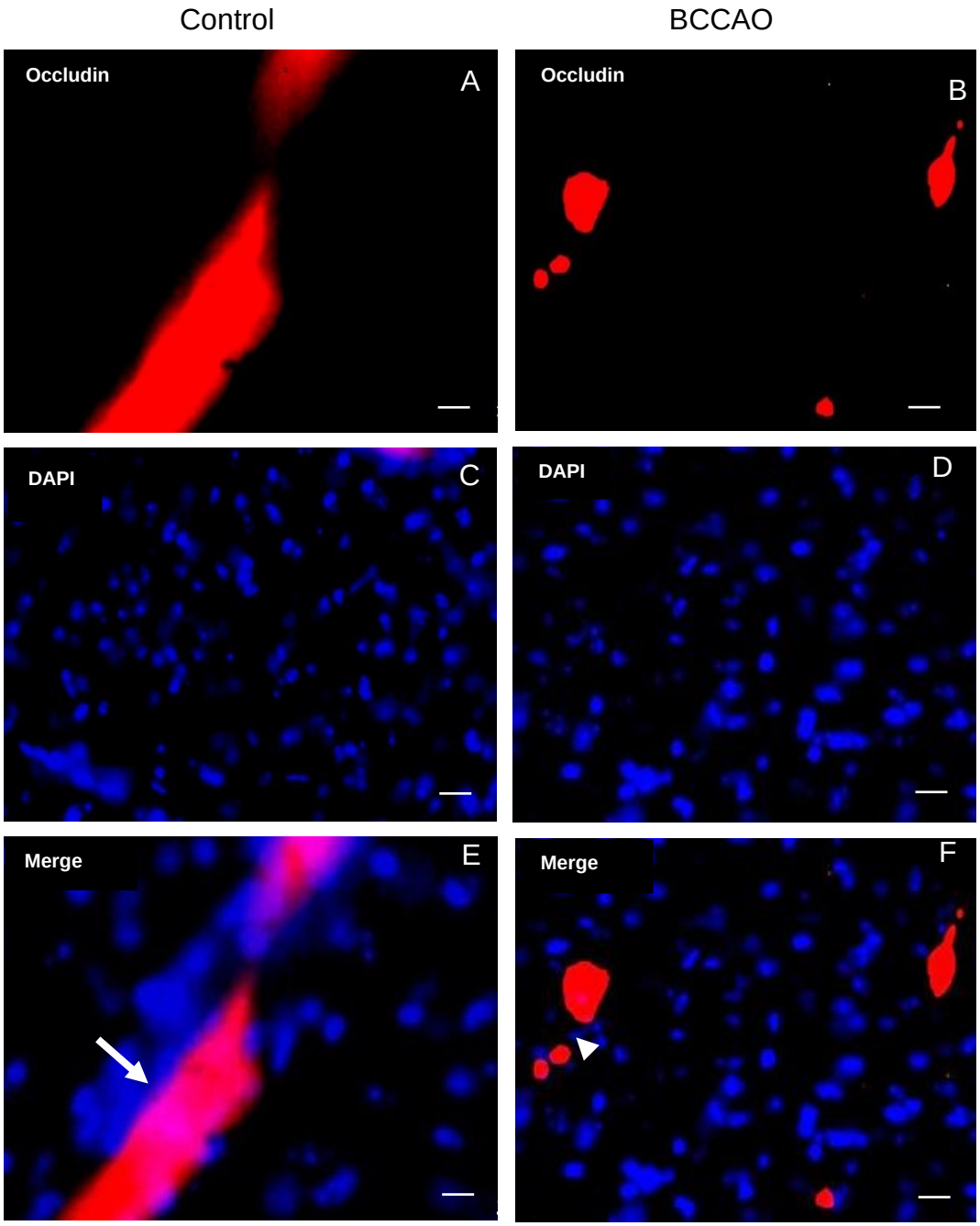

Figure 3.20 Representative photomicrographs showing immunofluorescence staining for Occludin with anti-Occludin and Cy3-conjugated secondary antibodies with DAPI stained nuclei in the hippocampus in sham (A, C, E) and BCCAO stroke brains (B, D, F). The labelled TJs are disrupted in stroke brain (arrowhead) compared to the intact ones in the control (arrow). (Scale bar=10um). (The images are taken at the level of Bregma-2.06mm). (Slice thickness=50um).

3.1.7.3 Claudin-5 immunostaining results

Claudin-5 is one of the integral components of the BBB TJ that controls the BBB permeability (Nitta et al., 2003; Ohtsuki et al., 2007). Moreover, it is reported to be one of the main TJ component in endothelial cells of the brain (Jia et al., 2014). Coronal sections of the brains were assessed using fluorescence labelling in relation to Claudin-5 immunoreactivity in the hippocampus of BCCAO and control brains. The best optimal dilution was 1:500, diluted in PBS-T since it achieved the strongest labelling of specific antigens in correlation with low non-specific staining for the background. Negative controls were performed to define the specificity of the binding of primary and secondary antibodies. Brain sections at the level of the hippocampus were captured using florescence microscope with 60 X magnification objectives. The immunostaining results showed disruption of Claudin-5 immunoreactive profiles in BCCAO and reperfusion mice in comparison with intact profiles in the sham-operated mice (Figure 3.21).

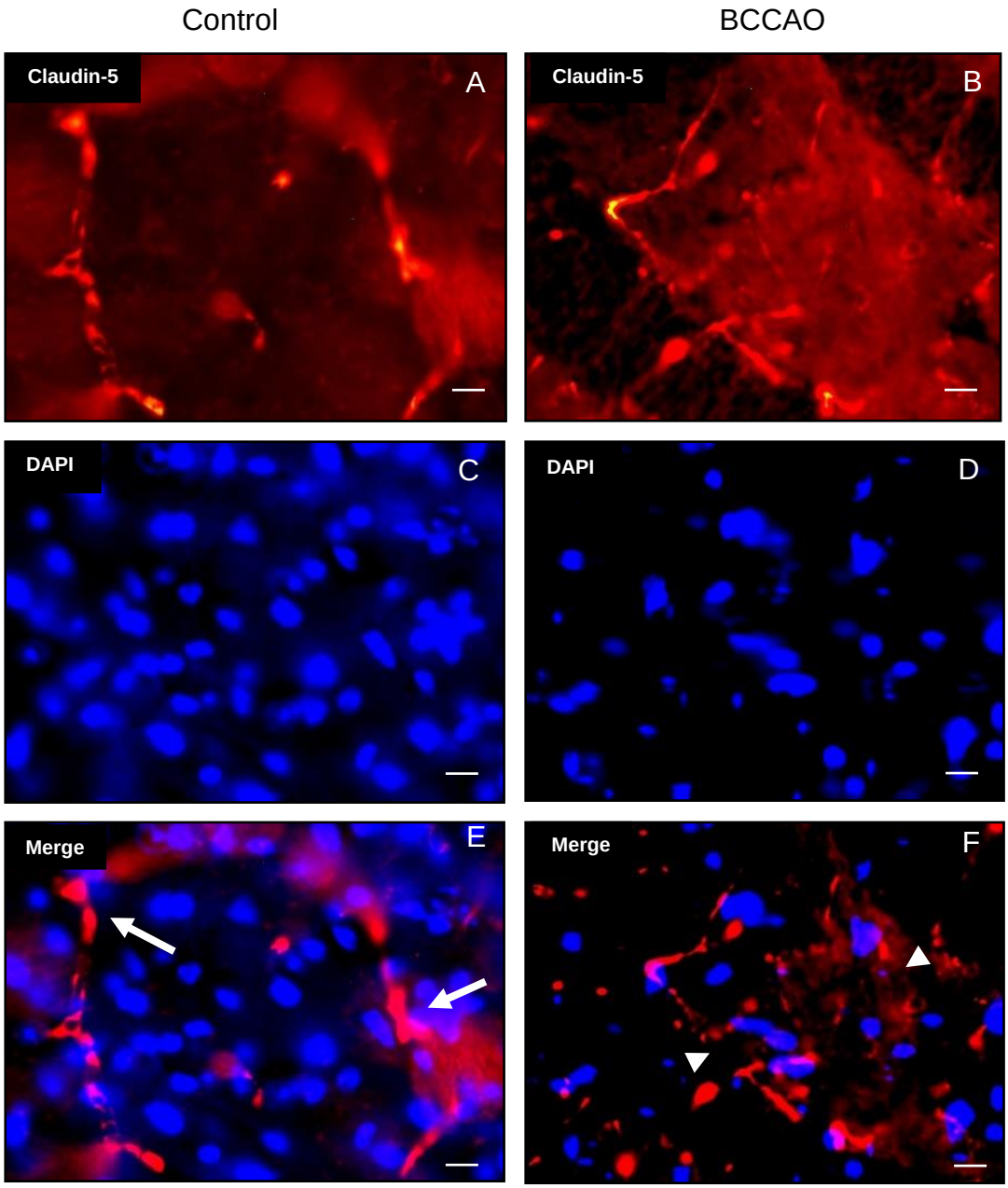

Figure 3.21 Representative photomicrographs showing immunofluorescence staining for Claudin-5 with anti-Claudin-5 and Cy3-conjugated secondary antibodies with DAPI stained nuclei in the hippocampus in sham (A, C, E) and BCCAO stroke brains (B, D, F). The labelled TJs are disrupted in stroke brain (arrowheads) compared to the intact ones in the control (arrows). (Scale bar=10um). (The images are taken at the level of Bregma-2.06mm). (Slice thickness=50um).

3.1.8 Double staining immunohistochemistry staining

3.1.8.1 BCCAO induced morphological changes in endothelial cells and TJ disruption

Changes in endothelial cells of blood vessels following cerebral ischaemic stroke were examined by IHC using specific antibodies against CD31. These changes were correlated with TJ proteins: Occludin, ZO-1 and Claudin-5 to assess disruption of TJ of BBB following stroke and to determine changes in BBB cells in a BCCAO model of cerebral ischaemia and reperfusion. To confirm the expression of the TJ proteins within the endothelial cells profile, double labelling was done by incubation of brain sections with primary antibodies against CD31 and one of the TJ proteins.

First, to find out if the TJ protein (Occludin) is expressed in the endothelial cells profile, dual-immunofluorescence (dual-IF) using anti-CD31 to label endothelial cells and anti-Occludin to detect TJ integrity was done. The results showed that TJ protein (Occludin) is expressed within endothelial cell profile which was expected. CD31 labelling was observed in endothelial cells in stroke and control brains in hippocampus and cortex. The Occludin positive TJs were also stained in stroke and control brains in hippocampus and cortex. Data showed a decrease in Occludin immunoreactive TJ profiles in the hippocampus and cortex due to TJ disruption in stroke brains compared to control brains. Moreover, the results revealed distortion in morphology in the CD31 immunoreactive profiles of endothelial cells with some dilatation throughout the hippocampus and cortex compared to preserved morphology of endothelial cells in sham brains as shown in Figure 3.22 and Figure 3.23.

Because no difference in staining results was seen between 50um microtome brain sections and 20um cryostat brain sections, all the following immunostainings were done in 20um brain sections. Also, this thickness gives better resolution under the microscope.

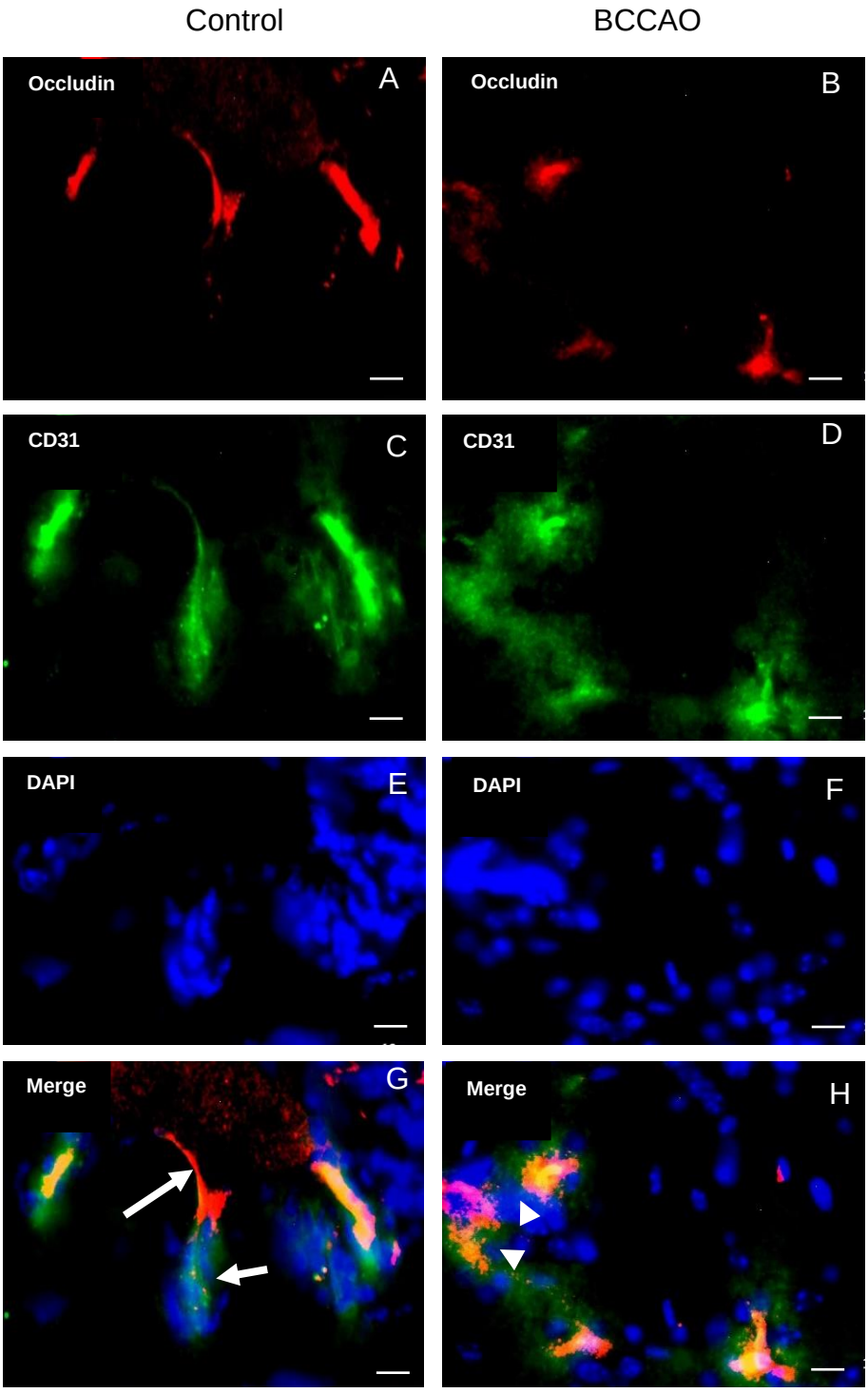

Figure 3.22 Representative photomicrographs showing double immunofluorescence staining for Occludin and CD31 with anti-Occludin (A,B-red) and anti-CD31 (C, D-green) and DAPI stained nuclei (E, F-blue) in the hippocampus area in BCCAO model of stroke (B,D,F,H) compared to control (A,C,E,G). The labelled TJs with anti-Occludin showing disruption of TJs in stroke brain (arrowheads) compared to the intact ones in the control (arrows). The labelled endothelial cells with anti-CD31 showing morphological changes with some dilatation in the stroke brain (arrowheads) compared to control (arrows). (Scale bar=10um). (The images are taken at the level of Bregma-2.06mm). (Slice thickness=20um).

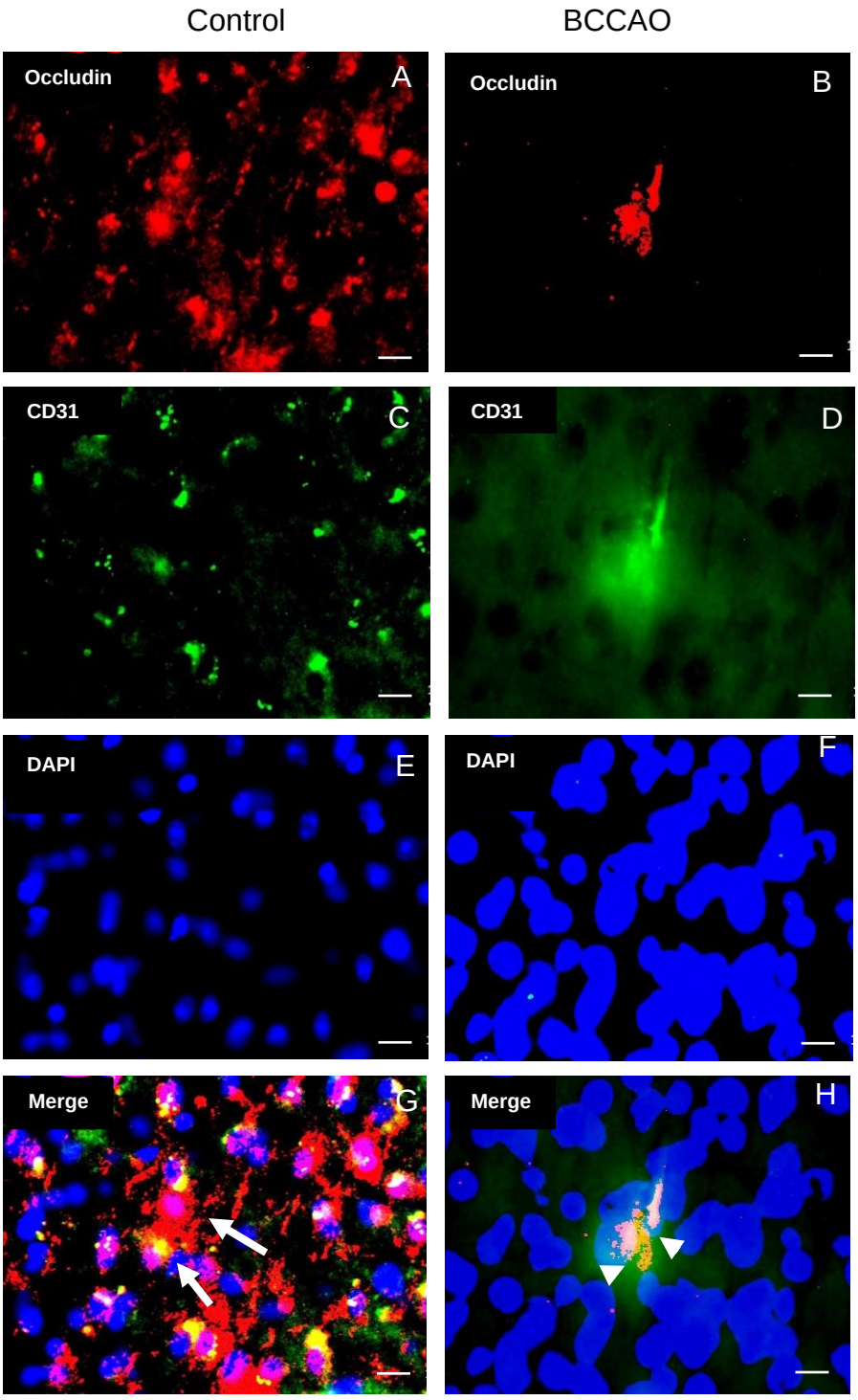

Figure 3.23 Representative photomicrographs showing double immunofluorescence staining for Occludin and CD31 with anti-Occludin (A,B-red) and anti-CD31(C,D-green) and DAPI stained nuclei (E,F-blue) in the cortical area in BCCAO model of stroke (B,D,F,H) compared to control (A,C,E,G). The labelled TJs with anti-Occludin showing disruption of TJs in stroke brain (arrowheads) compared to the intact ones in the control (arrows). The labelled endothelial cells with anti-CD31 showing morphological changes with some dilatation in the stroke brain (arrowheads) compared to control (arrows). (Scale bar=10um). (The images are taken at the level of Bregma 1.54 mm). (Slice thickness=20um).

The impact of ischaemia on BBB damage was examined also by dual-IF using anti-CD31 to label endothelial cells and anti-ZO-1 to detect TJ integrity and to confirm that TJ protein (ZO-1) is expressed in the endothelial cells profile. The results showed that TJ protein (ZO-1) is expressed within the CD31 labelled endothelial cell profile which was expected. The results showed that the labelled TJ with anti-ZO-1 are disrupted in the hippocampus and the cortex area in stroke mice compared to the intact ones in the control mice as shown in Figure 3.24 and Figure 3.25 respectively. In BCCAO mice brains, data showed a decrease in ZO-1 immunoreactive TJ profiles in the hippocampus and cortex compared to control brains. Moreover, the results revealed morphological changes with some dilatation in the CD31 immunoreactive profiles of endothelial cells throughout the hippocampus and cortex in stroke brains compared to preserved morphology of endothelial cells in sham brains.

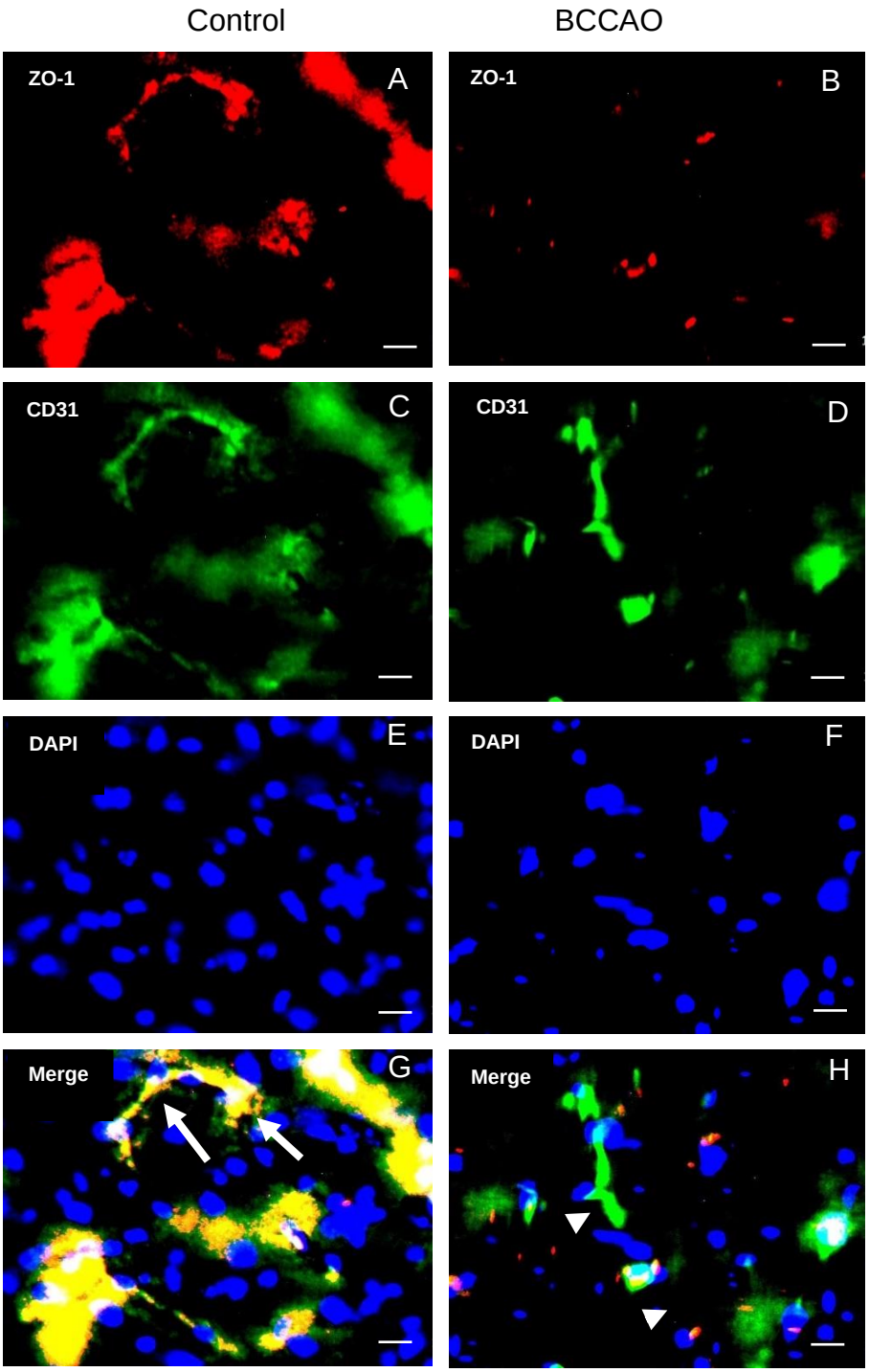

Figure 3.24 Representative photomicrographs showing double immunofluorescence staining for ZO-1 and CD31 with anti-ZO-1 (A,B-red) and anti-CD31(C,D-green) and DAPI (E,F-blue) stained nuclei in the hippocampus area in BCCAO model of stroke (B,D,F,H) compared to control (A,C,E,G). The labelled TJs with anti-ZO-1 showing disruption of TJs in stroke brain (arrowheads) compared to the intact ones in the control (arrows). The labelled endothelial cells with anti-CD31 showing morphological changes with some dilatation in the stroke brain (arrowheads) compared to control (arrows). (Scale bar=10um). (The images are taken at the level of Bregma-2.06mm). (Slice thickness=20um)

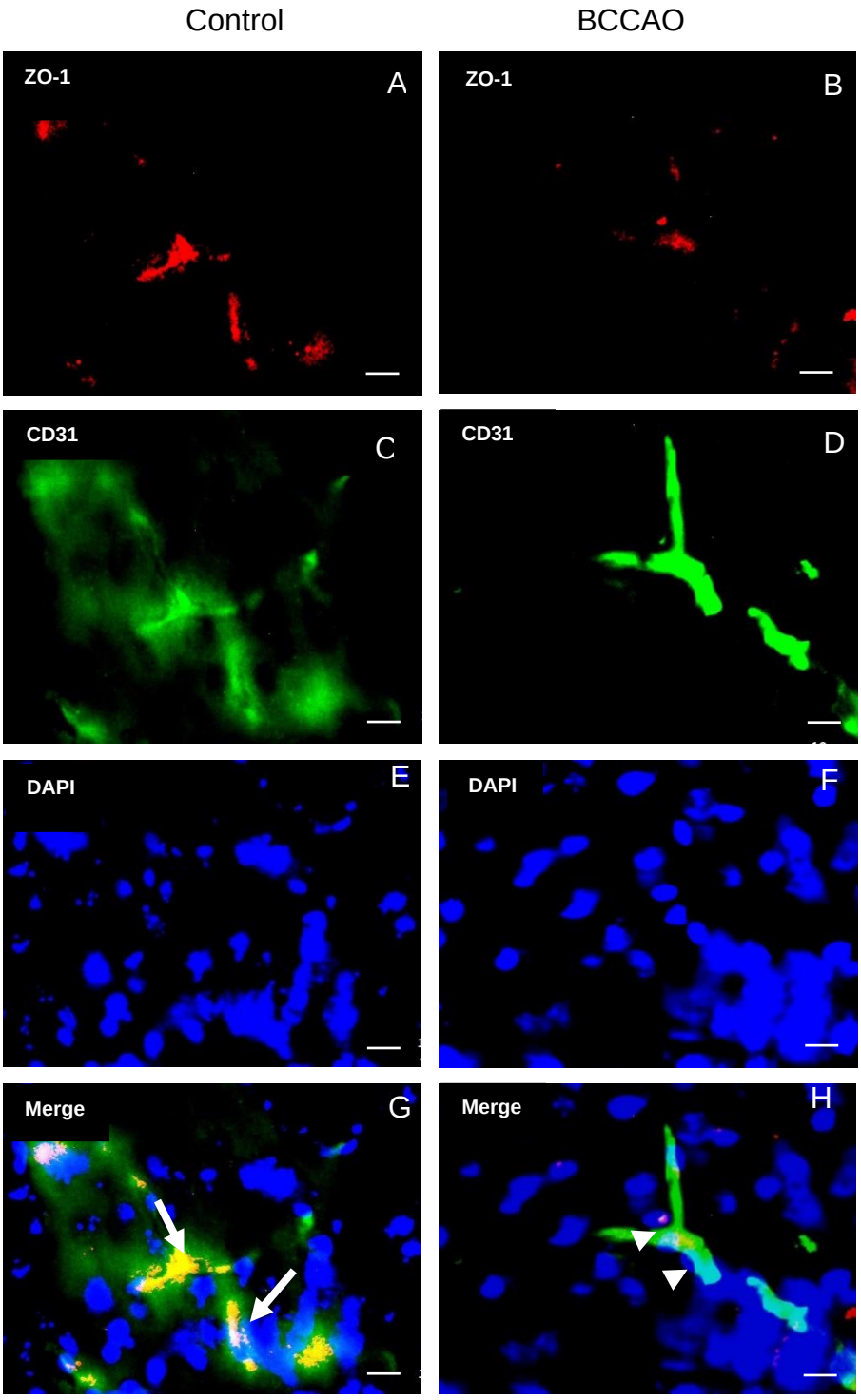

Figure 3.25 Representative photomicrographs showing double immunofluorescence staining for ZO-1 and CD31 with anti-ZO-1 (A,B-red) and anti-CD31(C,D-green) and DAPI (E,F-blue) stained nuclei in the cortical area in BCCAO model of stroke (B,D,F,H) compared to control (A,C,E,G). The labelled TJs with anti-ZO-1 showing disruption of TJs in stroke brain (arrowheads) compared to the intact ones in the control (arrows). The labelled endothelial cells with anti-CD31 showing morphological changes with some dilatation in the stroke brain (arrowheads) compared to control (arrows). (Scale bar=10um). (The images are taken at the level of Bregma 1.54 mm). (Slice thickness=20um).

The changes in endothelial cells of BBB following cerebral global ischaemic stroke were examined using anti-CD31 and correlated with another TJ protein: Claudin-5 to assess the disruption of TJ of BBB following stroke. This double labelling has been done also to confirm that TJ protein (Claudin-5) is expressed within the endothelial cells profile. The results confirmed that TJ protein (Claudin-5) is expressed in endothelial cell profile which was expected. Claudin-5 immunoreactivity was present in TJ in both BCCAO and control mice in hippocampus and cortex. The staining of TJ by anti-Claudin-5 was observed. In stroke brains, data showed a decrease in Claudin-5 immunoreactive TJ profiles compared to control brains. When compared to the labelled intact TJs with anti-Claudin-5 in the control models, the labelled TJs with anti-Claudin-5 are disrupted in the stroke model compared to the control in both hippocampus and cortical regions as shown in Figure 3.26 and Figure 3.27 respectively. Furthermore, in both hippocampus and cortical regions, the labelled endothelial cells with anti-CD31 showed morphological alterations with dilatation in the BCCAO stroke brains compared to comparable control brains.

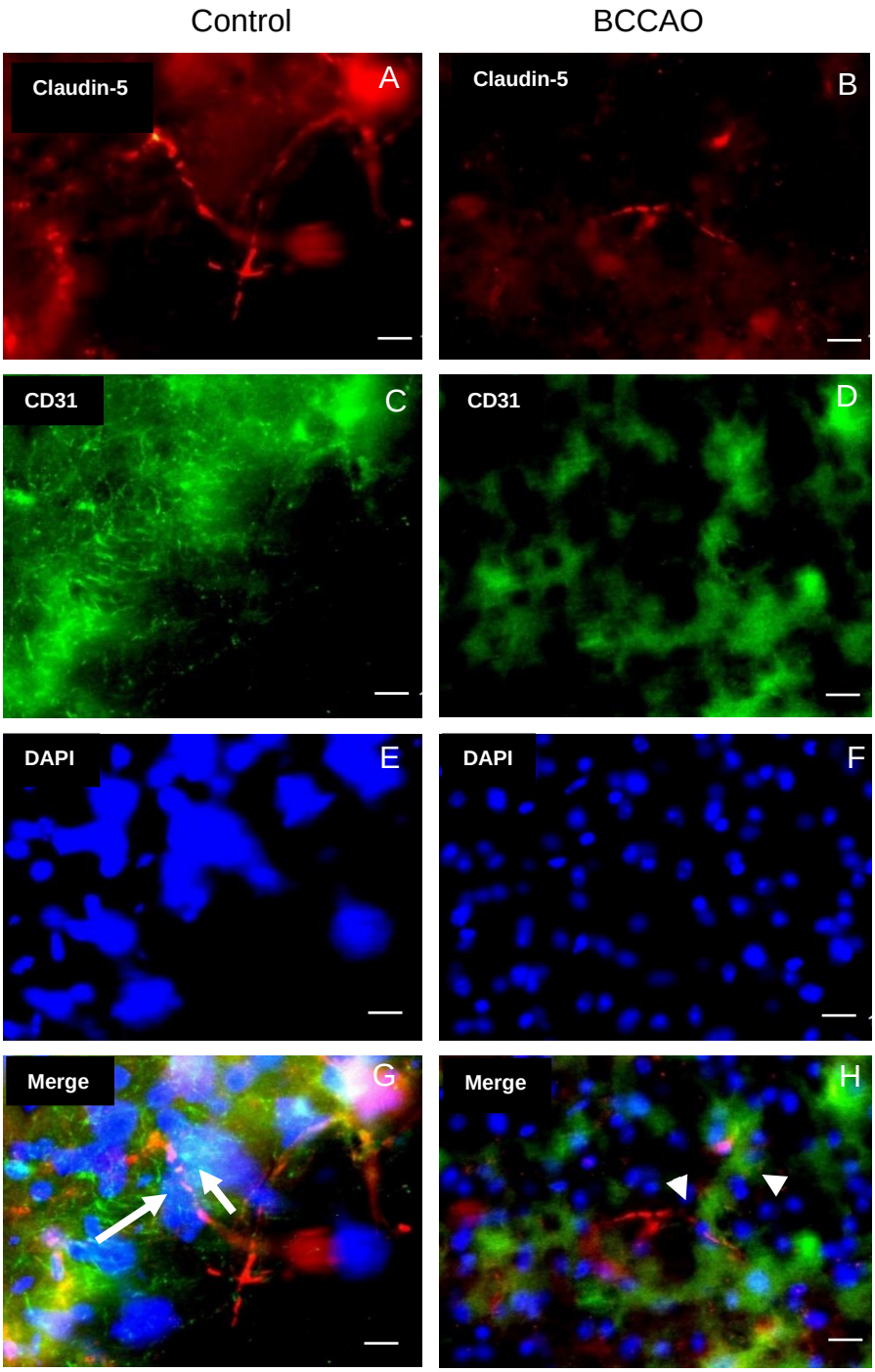

Figure 3.26 Representative photomicrographs showing double immunofluorescence staining for Claudin-5 and CD31 with anti-Claudin-5 (A,B-red) and anti-CD31(C,D-green) and DAPI (E,F-blue) stained nuclei in the hippocampus area in BCCAO model of stroke (B,D,F,H) compared to control (A,C,E,G). The labelled TJs with anti-Claudin-5 showing disruption of TJs in stroke brain (arrowheads) compared to the intact ones in the control (arrows). The labelled endothelial cells with anti-CD31 showing morphological changes with some dilatation in the stroke brain (arrowheads) compared to control (arrows). (Scale bar=10um). (The images are taken at the level of Bregma-2.06mm). (Slice thickness=20um).

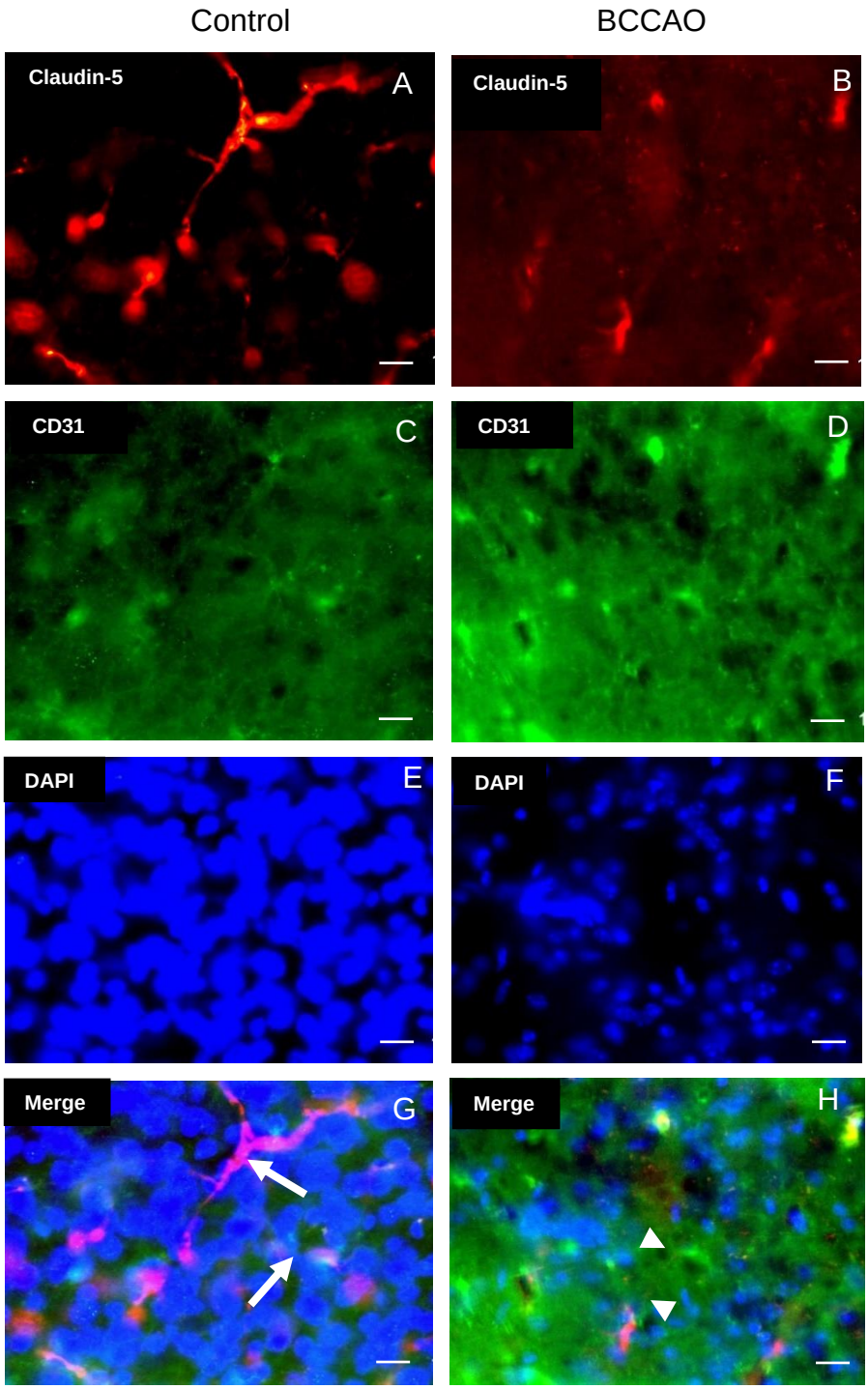

Figure 3.27 Representative photomicrographs showing double immunofluorescence staining for Claudin-5 and CD31 with anti-Claudin-5 (A,B-red) and anti-CD31(C,D-green) and DAPI (E,F-blue) stained nuclei in the cortical area in BCCAO model of stroke (B,D,F,H) compared to control (A,C,E,G). The labelled TJs with anti-Claudin-5 showing disruption of TJs in stroke brain (arrowheads) compared to the intact ones in the control (arrows). The labelled endothelial cells with anti-CD31 showing morphological changes with some dilatation in the stroke brain (arrowheads) compared to control (arrows). (Scale bar=10um). (The images are taken at the level of Bregma 1.54 mm).(Slice thickness=20um).

3.1.8.2 BCCAO induced neuronal death and TJ disruption

The impact of ischaemia on neurons and TJ was examined by dual-IF using anti-NeuN to label neuron cells correlated with anti-ZO-1 to label and detect TJ integrity. Also, to investigate that TJ proteins are not expressed in the neuronal cells, this double labelling was performed. The results confirmed that neurons and TJ protein are stained in separated profiles. NeuN immunoreactivity was observed in neuronal cells in the stroke mice and control mice in both examined anatomical areas of the brain. The neuronal reduction due to death was observable in stroke mice in the hippocampus area (Figure 3.28) and in cortical area (Figure 3.29) compared to the control mice. The labelled TJs with anti-ZO-1 in the BCCAO mice were disrupted and immunoreactivity was decreased compared to the control mice in both cortex and hippocampus.

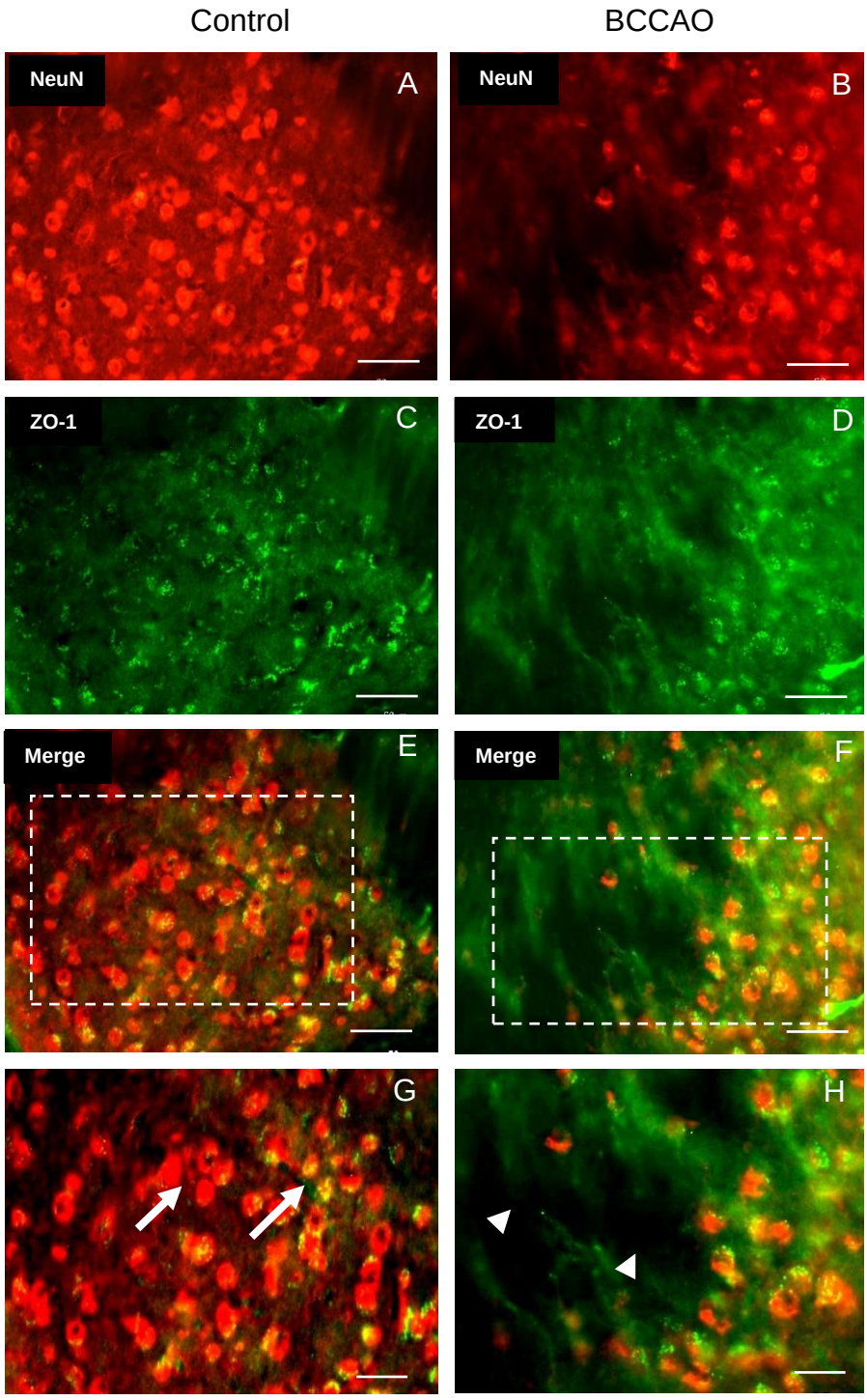

Figure 3.28 Representative photomicrographs showing double immunofluorescence staining for NeuN and ZO-1 using anti-NeuN (A,B-red) and anti-ZO-1 (C,D-green) in the hippocampus in BCCAO model of stroke (B,D,F,H) compared to control (A,C,E,G). The labelled TJs with anti-ZO-1 are disrupted in stroke brain (arrowheads) compared to the control (arrows). The labelled neuron cells with anti-NeuN show neuronal death following stroke (arrowheads) compared to control (arrows). (Scale bar= 20um and 50um). (The images are taken at the level of Bregma -2.06mm). (Slice thickness=20um).

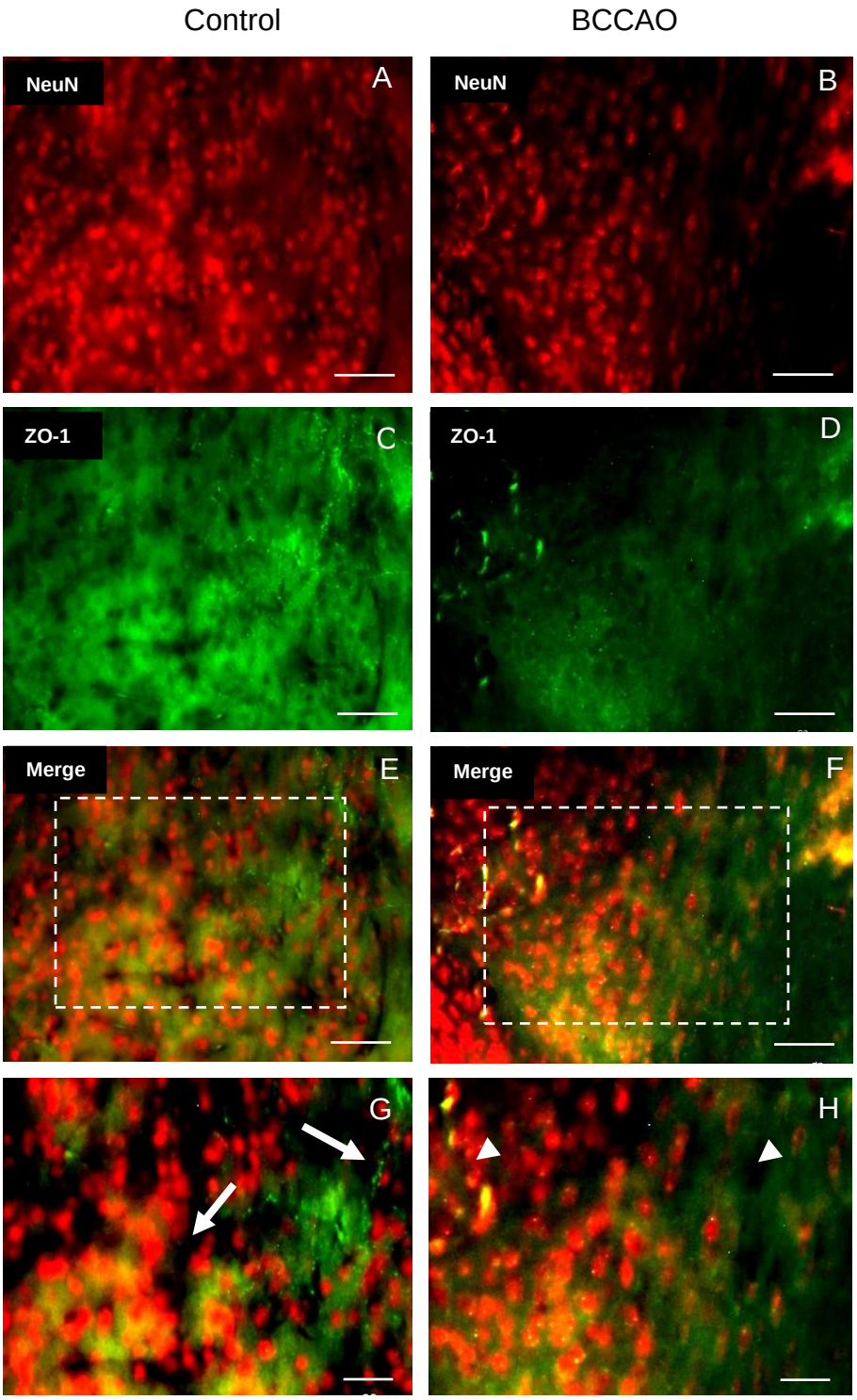

Figure 3.29 Representative photomicrographs showing double immunofluorescence staining for NeuN and ZO-1 with using anti-NeuN (A,B-red) and anti-ZO-1 (C,D-green) in the cortical area in BCCAO model of stroke (B,D,F,H) compared to control (A,C,E,G). The labelled TJs with anti-ZO-1 are disrupted in stroke brain arrowheads) compared to the control (arrows). The labelled neuron cells with anti-NeuN show neuronal death following stroke (arrowheads) compared to control (arrows). (Scale bar=20um and 50um). (The images are taken at the level of Bregma 1.54mm). (Slice thickness=20um).

3.1.8.3 BCCAO induced astrogliosis and TJ disruption

To investigate that TJ proteins are not expressed in the astrocytes, dual-IF using anti-GFAP to label astrocytes correlated with anti-ZO-1 to detect TJ integrity was done. The results confirmed that antibodies to TJ protein (ZO-1) and GFAP for astrocytes stained the separate profiles as was expected. The labelled TJs with anti-ZO-1 are disrupted in stroke mice compared to the control mice in cortical and hippocampal areas as shown in Figure 3.30 and Figure 3.31 respectively. The labelled astrocytes and processes with anti-GFAP become more and thicker due to astrocytes activation following stroke in stroke mice compared to control mice in the hippocampus and cortex.

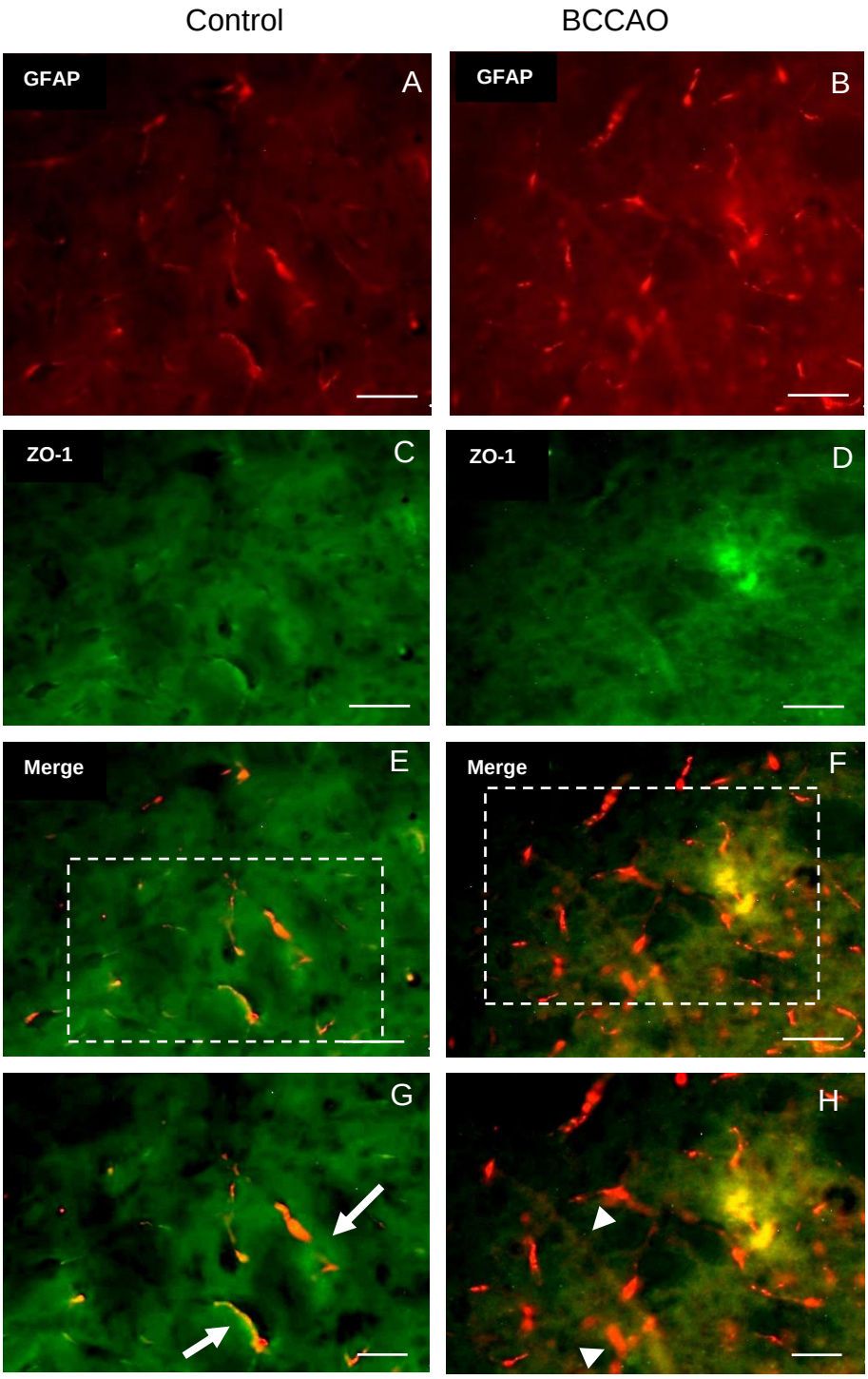

Figure 3.30 Representative photomicrographs showing double immunofluorescence staining for GFAP and ZO-1 with anti-GFAP (A,B-red) and anti-ZO-1 (C,D-green) in the hippocampus in BCCAO model of stroke (B,D,F,H) compared to control (A,C,E,G). The labelled TJs with anti-ZO-1 are disrupted in stroke brain (arrowheads) compared to the control (arrows). The labelled astrocytes and processes with anti-GFAP become more and thicker due to astrocytes activation following stroke (arrowheads) compared to control (arrows). (Scale bar=20um and 50um). (The images are taken at the level of Bregma -2.06mm). (Slice thickness=20um).

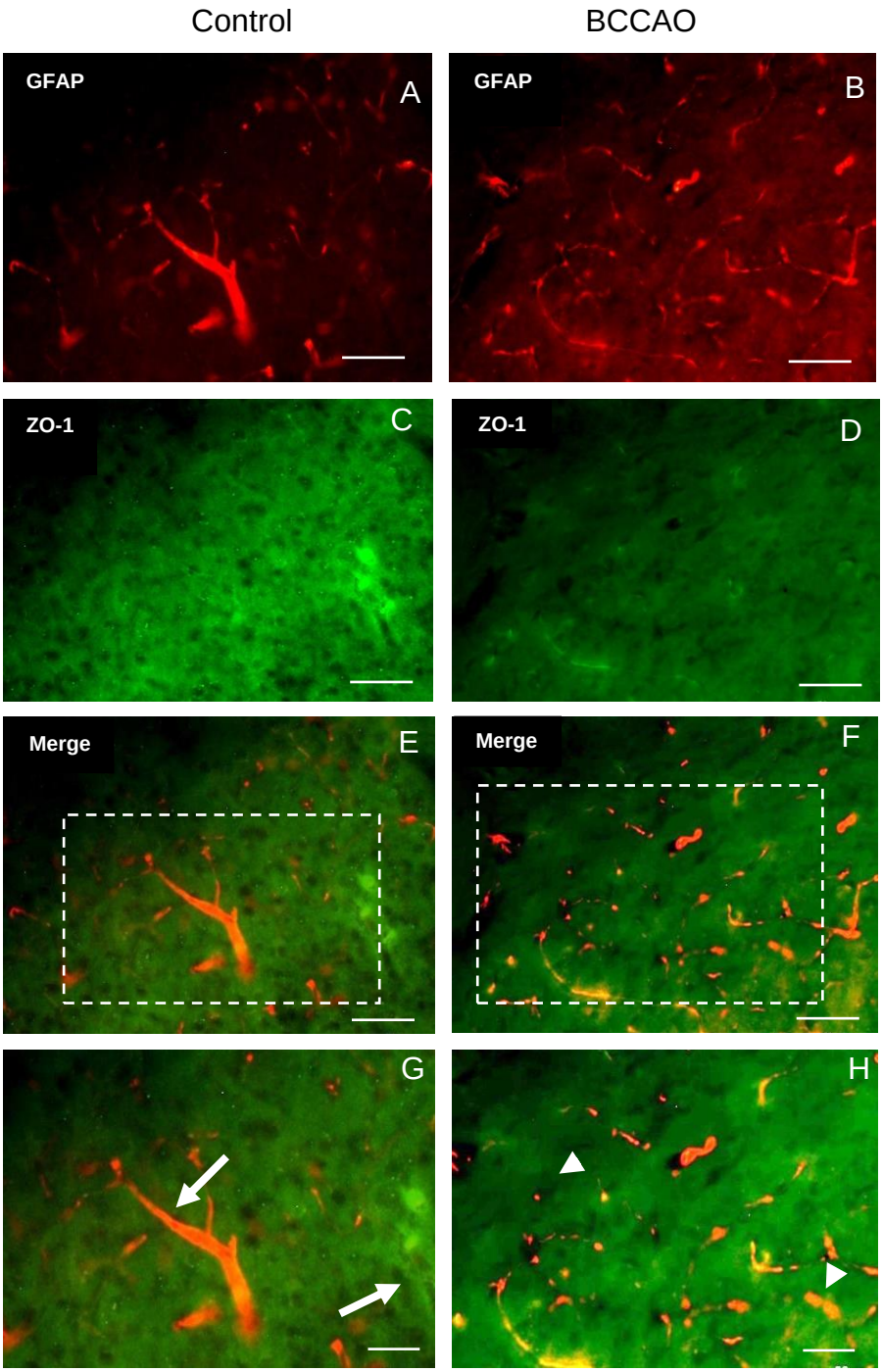

Figure 3.31 Representative photomicrographs showing double immunofluorescence staining for GFAP and ZO-1 with anti- GFAP (A,B-red) and anti- ZO-1 (C,D-green) in the cortical area in BCCAO model of stroke (B,D,F,H) compared to control (A,C,E,G). The labelled TJs with anti-ZO-1 are disrupted in stroke brain (arrowheads) compared to the control (arrows). The labelled astrocytes and processes with anti-GFAP become more and thicker due to astrocytes activation following stroke (arrowheads) compared to control (arrows). (Scale bar=20um and 50um). (The images are taken at the level of Bregma 1.54mm). (Slice thickness=20um).

3.1.9 Western blotting

Six brain tissues from controls and BCCAO model were harvested, and specific glial cell protein (GFAP) and BBB TJ proteins (Occludin, ZO-1 and Claudin-5) expressions were measured. The bicinchoninic acid assay (BCA) is used to determine the total concentrations of protein in samples. The standard serial dilution is shown in (Figure 3.32). The results showed a significant increase in protein concentrations in the ischaemic brains compared to control brains ($p<0.0001$- Unpaired Student's t-test, n=6) as displayed in (Figure 3.33). This suggested that the protein concentration is approximately double in the BCCAO ischaemic brains compared to control.

The difference between the bands in the control tissues and the ischaemic tissues using these specific antibodies were shown in the following section. All proteins bands were found in the correct level of molecular weights (kDa) as shown in the following section.

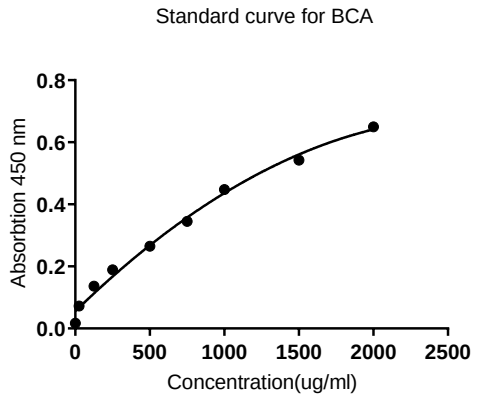

Figure 3.32 Bicinchoninic acid assay (BCA) standard dilution.

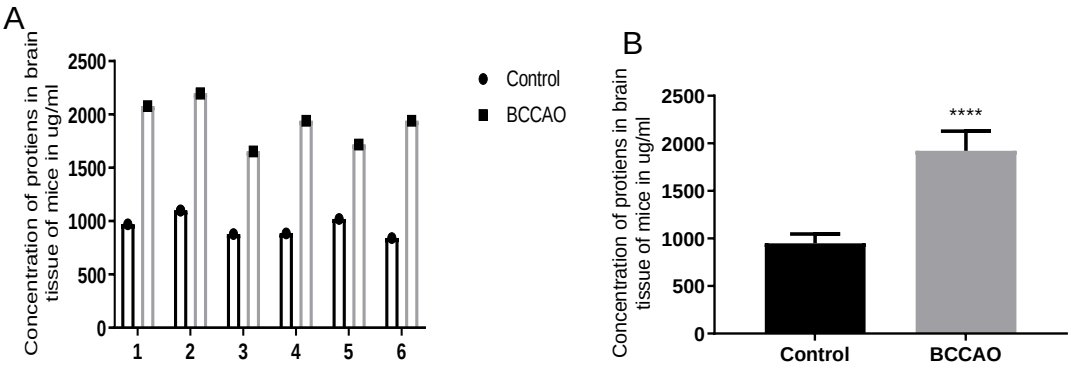

Figure 3.33 Quantitative analysis shows a very significant increase of proteins level (**$p<0.0001$, Unpaired Student's t-test, n=6) in BCCAO as compared to control mice individually (n=6) (A) and as mean ± SD (B).**

3.1.9.1 Protein expression of GFAP after ischaemia

GFAP as mentioned previously is the major intermediate filament protein in astrocytes (Liem and Messing, 2009). GFAP expression up-regulation is known as a reliable and sensitive marker of astrocytes reactivation (Sofroniew, 2009). To further investigate whether BCCAO and reperfusion affected the astrocytes' activity and to assess the changes in the expression of GFAP, WB was used to measure the expression of GFAP in BCCAO ischaemic brains compared to sham brains in hippocampus tissues. Also, to confirm the astrocytes activity, that observed in hippocampus in IHC results, this WB experiment was conducted. Quantitative WB analysis of GFAP expression following BCCAO and reperfusion showed a significant increase of GFAP protein (p=0.002- Mann-Whitney U test, n=6/ group) in hippocampus tissues in ischaemic mice brains compared to the control brains (Figure 3.34), thereby confirming the IHC observations. Normality and lognormality tests were performed and reported that the data set is not normally distributed according to Kolmogorov-Smirnov test. Beta actin was used as a loading control.

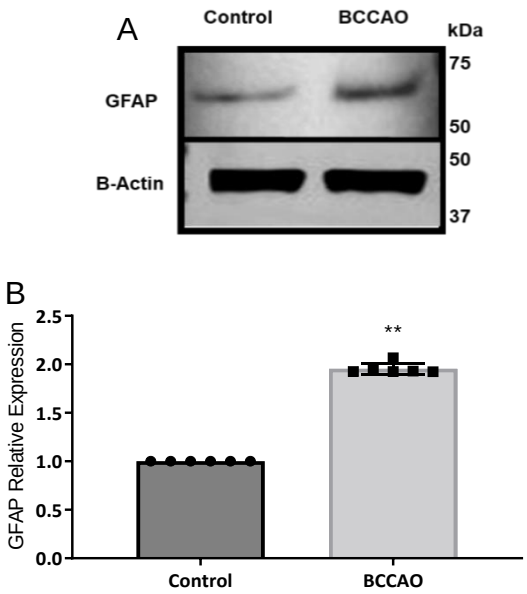

Figure 3.34 WB analysis of GFAP expression in the hippocampus of sham-operated and BCCAO mice. A) GFAP band density is greatly increased in the hippocampus of BCCAO models as compared to control. B) Quantitative analysis of GFAP band density relative to ß-actin shows a significant increase (p=0.002, Mann-Whitney U test, n= 6/group) in GFAP expression in BCCAO mice as compared to control. (Data presented as mean ± SD). (Control group was set as 1.0 as comparison to BCCAO).**

3.1.9.2 Protein expression of Occludin, ZO-1 and Claudin-5 after ischaemia

TJ is the BBB's most significant barrier structure. TJ is fundamentally made up of Claudins, Occludin, and ZO-1 (Sweeney et al., 2019). As observed previously in IHC results, TJ is distributed with loss of intact and continuity, as well as reduced the intensity of staining of these proteins in BCCAO model. To assess if cerebral ischaemia-induced BBB breakdown, the same antibodies to TJ proteins (Occludin, ZO-1 and Claudin-5) were used for WB analysis to measure quantitatively the expression levels of these proteins in the ischaemic hippocampus tissues compared to the sham-operated hippocampus tissues.

Occludin, ZO-1 and Claudin-5 expressions levels were considerably reduced after global ischaemia (BCCAO model). Quantitative WB analysis revealed that the expression levels of Occludin, ZO-1 and Claudin-5 after BCCAO in ischaemic hippocampus were significantly lower than the sham operated animals (n= 6/group) (p=0.002- Mann-Whitney U test,Figure 3.35), (p=0.002- Mann-Whitney U test,Figure 3.36) and (p=0.002- Mann-Whitney U test,Figure 3.37) respectively consistent with the IHC results. Normality and lognormality tests were done and confirmed that the data set is not normally distributed based on Kolmogorov-Smirnov test. Beta actin was used as a loading control.

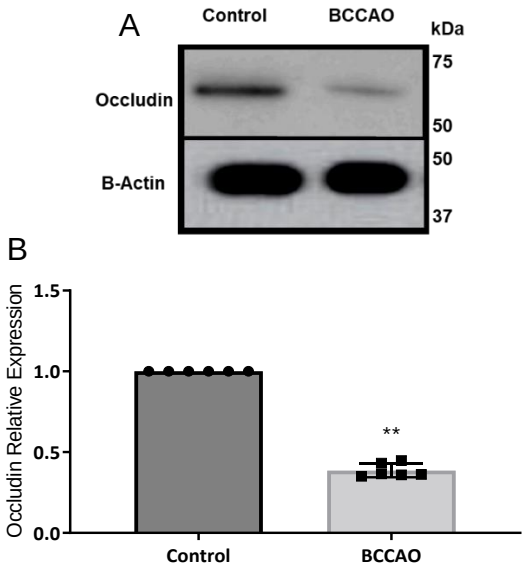

Figure 3.35 WB analysis of Occludin expression in the hippocampus of sham-operated and BCCAO mice. A) Occludin band density is greatly decreased in the hippocampus of BCCAO models as compared to control. B) Quantitative analysis of Occludin band density relative to ß-actin shows a significant decrease (p=0.002, Mann-Whitney U test, n= 6/group) in Occludin expression in hippocampus of BCCAO mice as compared to control. (Data presented as mean ± SD). (Control group was set as 1.0 as comparison to BCCAO).**

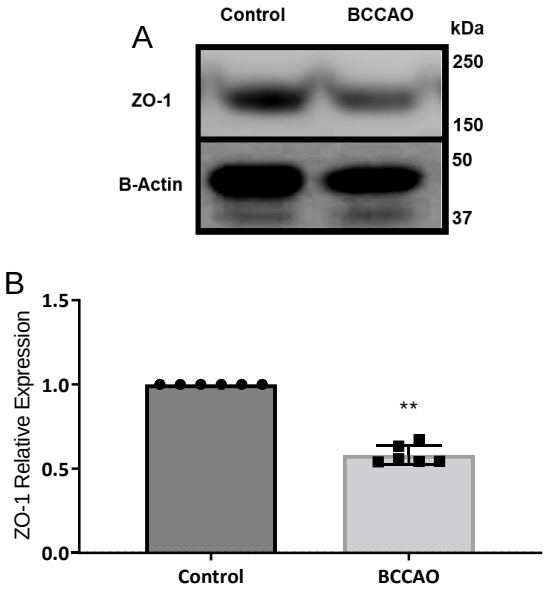

Figure 3.36 WB analysis of ZO-1 expression in the hippocampus of sham-operated and BCCAO mice. A) ZO-1 band density is greatly decreased in the hippocampus of BCCAO models as compared to control. B) Quantitative analysis of ZO-1 band density relative to ß-actin shows a significant decrease (p=0.002, Mann-Whitney U test, n = 6/group) in ZO-1 expression in hippocampus of BCCAO mice as compared to control. (Data presented as mean ± SD). (Control group was set as 1.0 as comparison to BCCAO).**

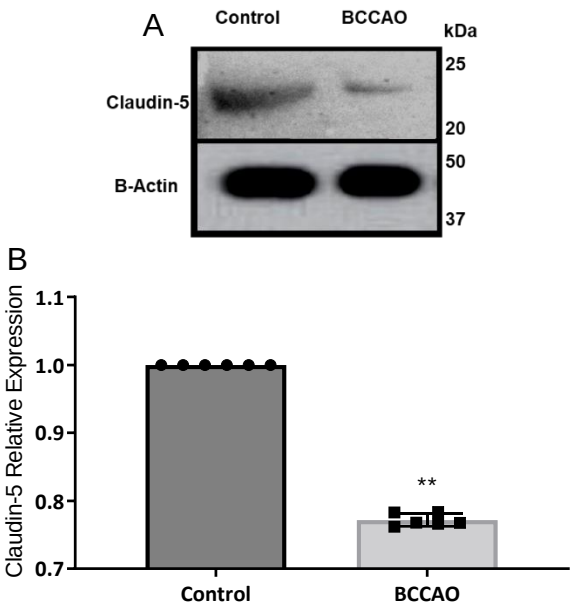

Figure 3.37 WB analysis of Claudin-5 expression in the hippocampus of sham-operated and BCCAO mice. A) Claudin-5 band density is greatly decreased in the hippocampus of BCCAO models as compared to control. B) Quantitative analysis of Claudin-5 band density relative to ß-actin shows a significant decrease (p=0.002, Mann-Whitney U test, n = 6/group) in Claudin-5 expression in hippocampus of BCCAO mice as compared to control. (Data presented as mean ± SD). (Control group was set as 1.0 as comparison to BCCAO).**

3.1.10 Analysis of markers in blood serum

Eight serum samples (n=8) from control and BCCAO ischaemic models were measured. Concentration on serum samples, mainly, was made as it excludes clotting factors of blood (Sotelo-Orozco et al., 2021) which may interrupt with intended protein detection. The majority of studies measured the biomarkers in serum due to the same reason. Some labelling problems with plasma samples also have been found.

3.1.10.1 GFAP

GFAP levels in serum samples from control and BCCAO were measured and compared. The levels of GFAP in blood serum elevated significantly with nearly 1.5-fold in BCCAO models and reperfusion (p=0.0002- Unpaired Student's t- test, n=8/group,Figure 3.38), which is consistent well with immunohistochemical results.

3.1.10.2 Occludin

The levels of Occludin in serum samples from BCCAO and sham operated mice as well as their corresponding control mice were quantified. The quantitative statistical analysis showed a 1.3-fold significant increase in Occludin levels in the BCCAO ischaemia group as compared to the sham operated one ($p<0.0001$ - Unpaired Student's t-test, n=8/group**),** (Figure 3.39).

3.1.10.3 ZO-1

The levels of ZO-1 in serum samples from BCCAO cerebral ischaemic models and controls were measured. The statistical analysis illustrated a significant 3-fold increase in the ZO-1 serum levels in the ischaemia group as compared to the control one with ($p<0.0001$- Unpaired Student's t-test, n= 8/group,Figure 3.40).

3.1.10.4 Claudin-5

The concentrations of Claudin-5 in serum samples from the control and BCCAO ischaemic model were measured and compared. The data displayed a significant increase in the Claudin-5 serum levels by~3.6-fold in the ischaemia group as compared to the sham operated group with ($p<0.0001$- Unpaired Student's t-test, n=8/ group, Figure 3.41).

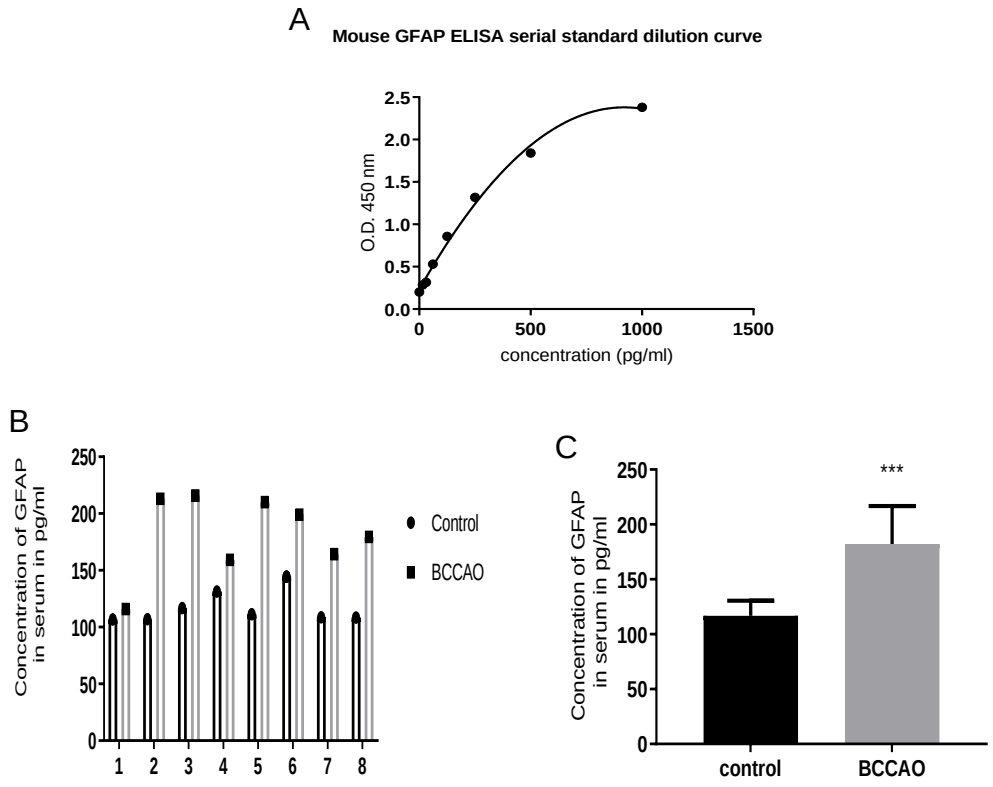

Figure 3.38 ELISA analysis showing serum GFAP levels between control and BCCAO stroke models. A) Mouse GFAP serial standard dilution vs optimal density in 450nm. B) Serum GFAP levels in control and BCCAO ischaemic models (n=8) individually. C) Significant increase in the serum protein levels in BCCAO ischaemic serum group compared to the control group (p=0.0002 - Unpaired Student's t-test).

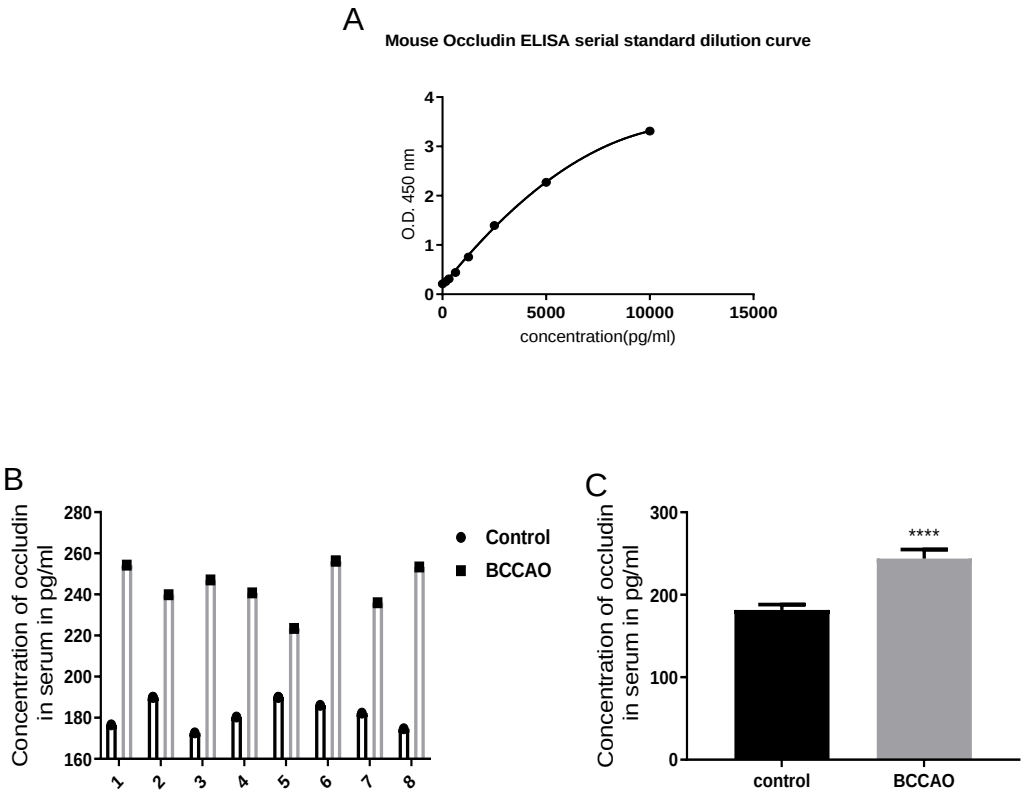

Figure 3.39 ELISA analysis showing serum Occludin levels between control and BCCAO stroke models. A) Mouse Occludin serial standard dilution vs optimal density in 450nm. B) Serum Occludin levels in control and BCCAO ischaemic models (n=8) individually. C) Significant increase in the serum protein levels in BCCAO ischaemic serum group compared to the control group (p<0.0001 - Unpaired Student's t-test).

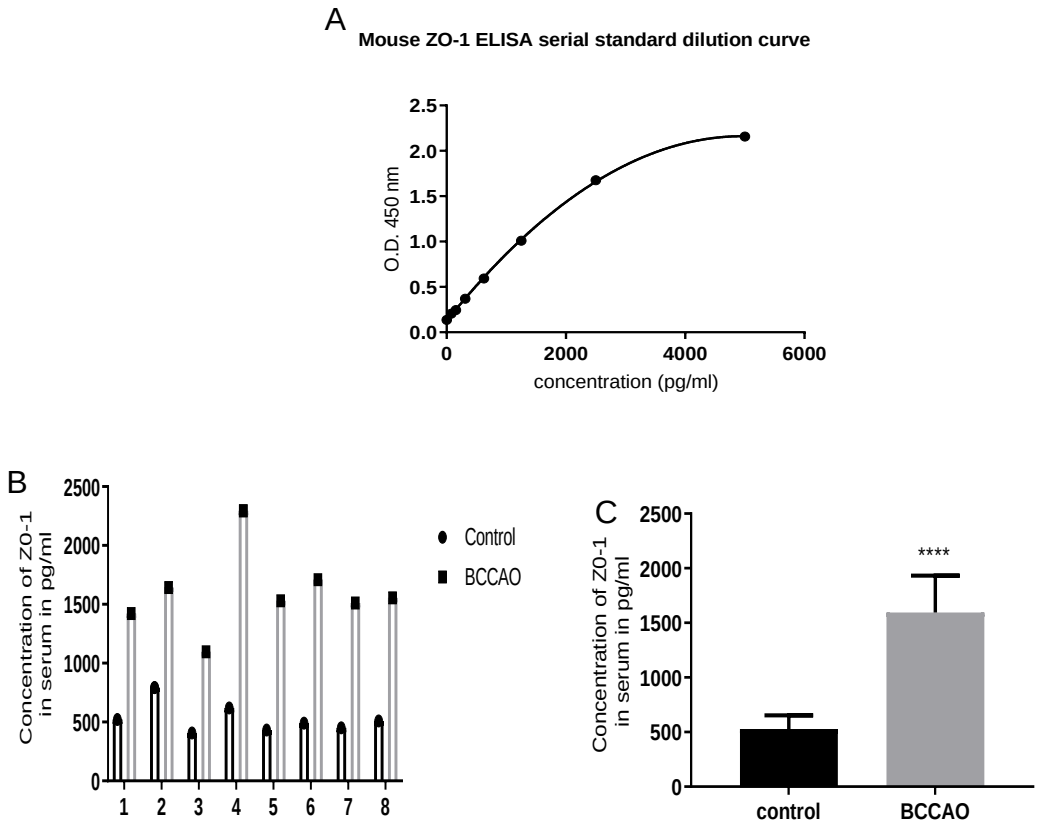

Figure 3.40 ELISA analysis showing serum ZO-1 levels between control and BCCAO stroke models A) Mouse ZO-1serial standard dilution vs optimal density in 450nm. B) Serum ZO-1 levels in control and BCCAO ischaemic models (n=8) individually. C) Significant increase in the serum protein levels in BCCAO ischaemic serum group compared to the control group ($p<0.0001$- Unpaired Student's t-test).

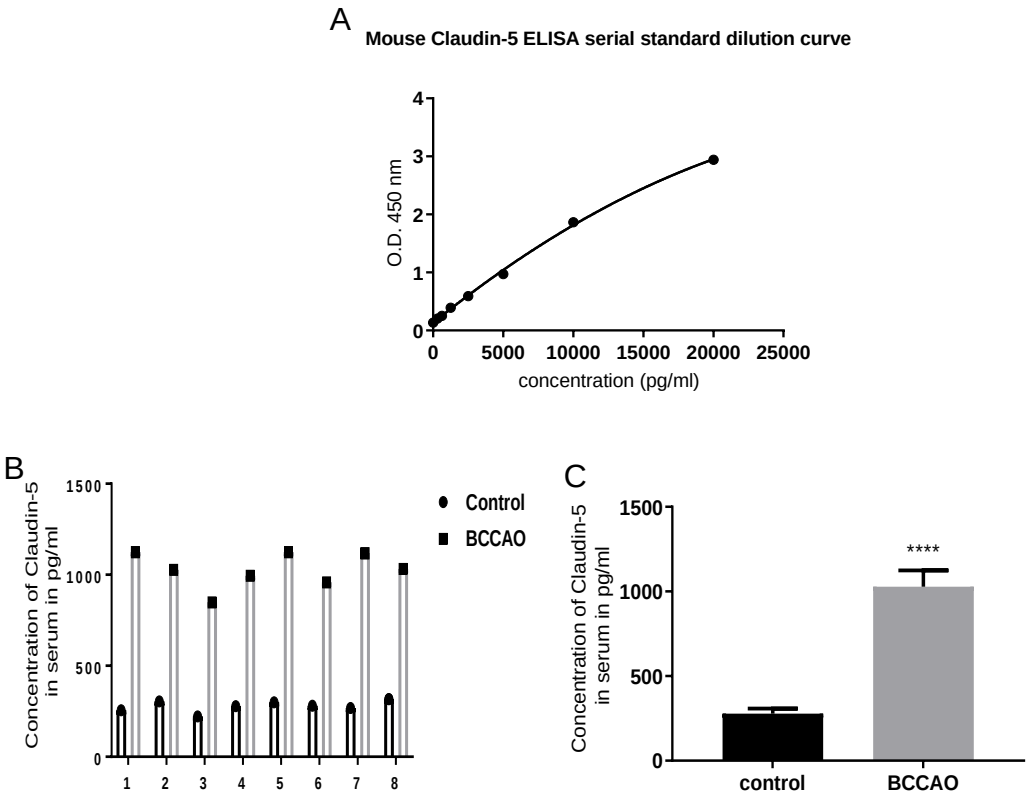

Figure 3.41 ELISA analysis showing serum Claudin-5 levels between control and BCCAO stroke models. A) Mouse Claudin-5 serial standard dilution vs optimal density in 450nm. B) Serum Claudin-5 levels between control and BCCAO ischaemic models (n=8) individually. C) Significant increase in the serum protein levels in BCCAO ischaemic serum group compared to the control group ($p<0.0001$- Unpaired Student's t-test).

3.1.11 Correlation between expression of markers in serum and brain

An investigation whether serum GFAP level is correlated to the expression of GFAP in the hippocampal tissue in the brain was done. The results of the Spearman correlation indicated a significant very strong positive correlation between GFAP expression and serum GFAP level after BCCAO (r = 0.943, p=0.017) (Figure 3.42-A) indicating that blood GFAP level could well reflect GFAP release from the hippocampal ischaemic brain. However, in simple linear regression analysis, it lost its significant (95% confidence interval, R SQUARED = 0.319, p=0.243).

In addition, this study tested whether serum TJ proteins (Occludin, ZO-1 and Claudin-5) levels are correlated to the expressions of these proteins in the hippocampal tissue in the brain after BCCAO. In fact, results of the Spearman correlation and linear regression indicated a significant very strong negative correlation between Occludin WB expression and serum Occludin level after BCCAO (r = -0.886, p=0.033)(95% confidence interval, R SQUARED = 0.545, p=0.009) respectively as shown in (Figure 3.42-B). This indicated that blood Occludin level could well reflect Occludin expression from the hippocampal global ischaemic brain.

On the other hand, the results indicated no association between ZO-1 WB expression and serum ZO-1 level after BCCAO (r = 0.029, p >0.999) and (95% confidence interval, R SQUARED = 0.004, p=0.912) (Figure 3.42-C). Similarly, results of the Spearman correlation and results of the simple linear regression showed no association between Claudin-5 WB expression and serum Claudin-5 level after BCCAO (r = 0.435, *p*=0.389) and (95% confidence interval, R SQUARED = 0.197, p=0.378) respectively as displayed on (Figure 3.42-D).

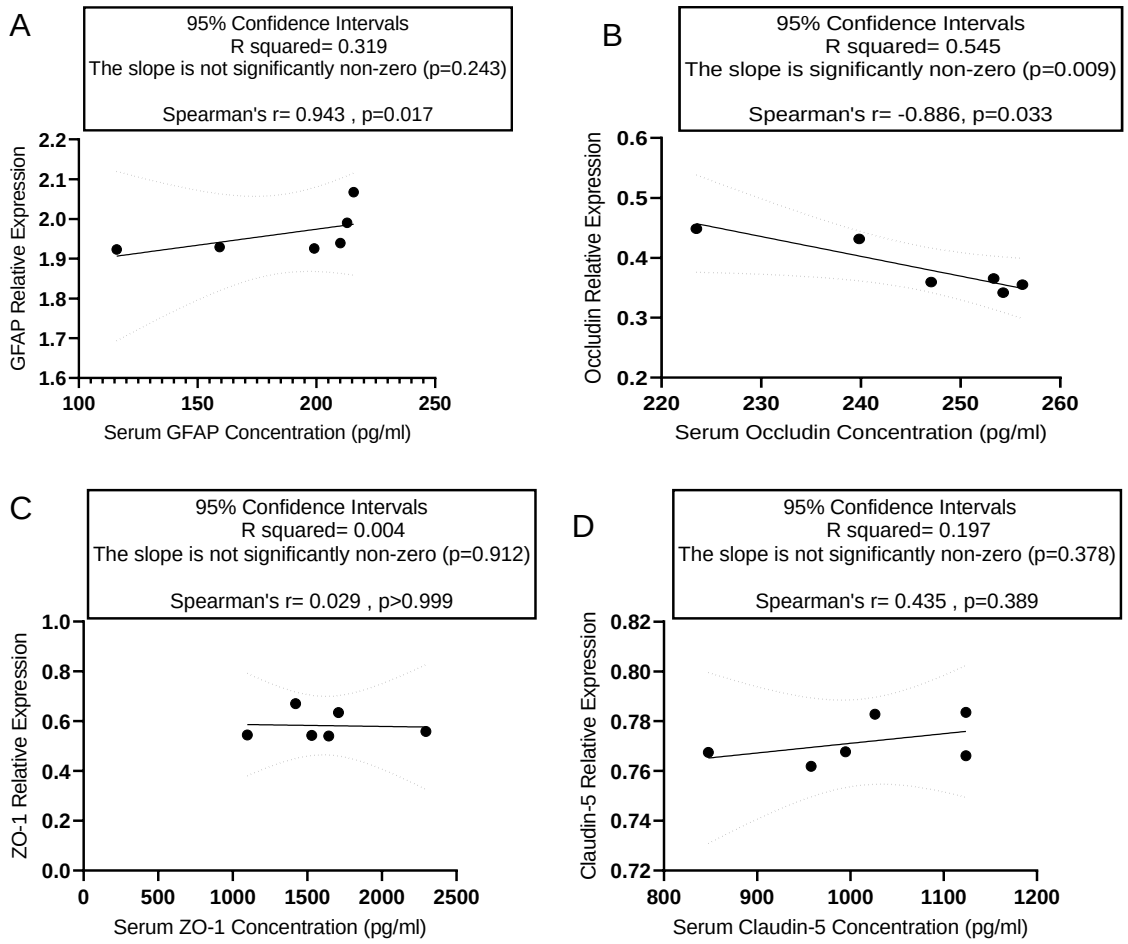

Figure 3.42 Correlation analysis between serum A: GFAP, B: Occludin, C: ZO-1 and D: Claudin-5 levels and these proteins' expressions in hippocampal tissue of the brain in BCCAO using Spearman correlation and simple linear regression. Proteins expressions in hippocampal brain tissue of the brain were quantitatively assessed by WB. Serum proteins levels were quantified by ELISA. A: Spearman correlation showing a significant very strong positive correlation between GFAP expression in the brain and serum GFAP level; (r=0.943, p=0.017). Linear regression analysis showing non-significant association GFAP expression in the brain and serum GFAP level ;(R SQUARED = 0.319, p=0.243). B: Spearman correlation and linear regression showing a significant very strong negative correlation between Occludin expression in the brain and serum Occludin level; (r = -0.886, p=0.033) and (95% confidence interval, R SQUARED = 0.545, p=0.009) respectively. C: Spearman correlation analysis and simple linear regression analysis showing no association between serum ZO-1 level and ZO-1 expression in hippocampal tissue of the brain; (r = 0.029, *p*>0.999) and (R SQUARED = 0.004, p=0.912) respectively. D: Spearman correlation analysis and simple linear regression analysis showing no association between serum Claudin-5 level and Claudin-5 expression in hippocampal tissue of the brain; (r = 0.435, p=0.389) and (R SQUARED = 0.197, p=0.378) respectively.

3.2 Changes in neuronal, glial cell and blood brain barrier proteins in middle cerebral artery occlusion (MCAO)

This study aimed to investigate brain damage using antibodies of the specific neuronal and glial cell as well as examine BBB marker of specific TJ in MCAO model of cerebral ischaemia and reperfusion in a comparison with sham operated mice using single and double staining (as per section 2.1.5 and 2.1.7) respectively. Quantification of NeuN and GFAP immunolabelled profiles was achieved as per section 2.1.9. Quantification of NG2, PDGFR and IBA-1 immunolabelled profiles was done only after BCCAO and not after MCAO in this study since there have been achieved in earlier studies as shown in Table 1.4-B.

Additionally, the expressions of (GFAP, Claudin-5, Occludin and ZO-1) in the hippocampus using quantitative WB analysis were determined and compared between control and MCAO mice as per section 2.1.12.

Lastly, the levels of circulating biomarkers (GFAP, Claudin-5, ZO-1, Occludin) by ELISA method in this model compared to the corresponding control were determined as per section 2.1.14. Correlation analysis between WB analysis and ELISA of blood biomarkers was done as per section 2.1.15.

For more details about the antibodies used in IHC staining and the optimal dilution, refer to the results chapter of BCCAO.

3.2.1 Histochemistry - Cresyl violet staining results

Light microscopy imaging of the hippocampus revealed ischaemic damage. Data showed chromatolytic changes in the hippocampus in the MCAO group (n=3) due to cellular damage following stroke, as compared to the control group(n=3),(Figure 3.43).

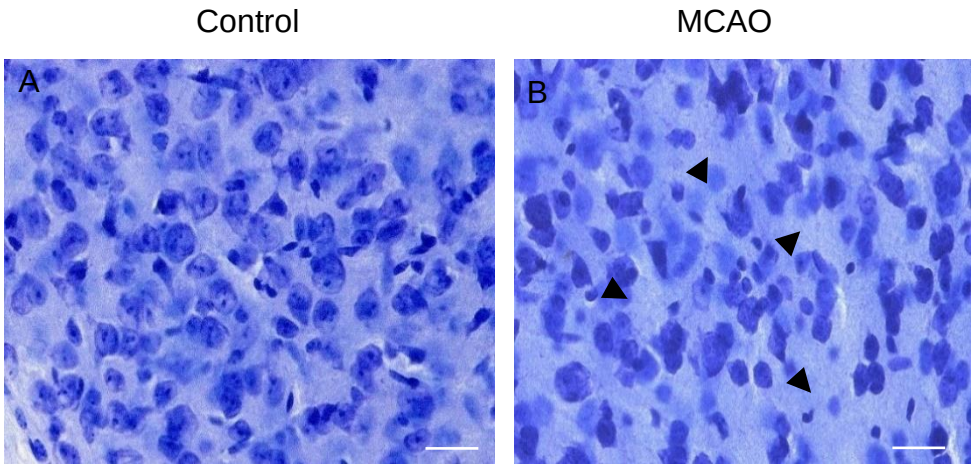

Figure 3.43 Representative photomicrographs showing cresyl violet staining of neuron cell nuclei in the hippocampus in control (A) and MCAO (B) brains. The staining shows chromatolytic changes in the stroke brain compared to the control brain due to cellular damage following MCAO induced stroke (arrowheads). (Scale bar=20um). (The images are taken at the level of Bregma -2.06mm).

3.2.2 NeuN immunostaining and quantitative analysis

This section aimed to examine neuronal damage following focal ischaemia induced by MCAO as compared to sham operated mice using IHC staining methods. Similar to the study in BCCAO mice, antibodies to NeuN to stain neuronal cells in ischaemic and sham brains was used (Refer to section 3.1.2 for more staining details).

Data from NeuN IHC in MCAO brains and sham brains showed loss of neurones in the hippocampus (CA1), M1 (primary motor cortex), M2 (2nd motor cortex), the granular insular cortex area and striatum as shown in Figure 3.44. Quantitative analysis showed that the NeuN positive cells were significantly decreased in ischaemic brains compared to control brains (n=3) in the striatum, M1 and M2 motor cortex. The highest significant decrease was in the striatum (paired Student's t-test, p=0.0010), followed by M2 with (p= 0.0017) and M1 with (p=0.0392). However, no statistically significant difference was seen in hippocampus (p=0.1141) and the granular insular cortex area (p= 0.080) as shown in Figure 3.45.

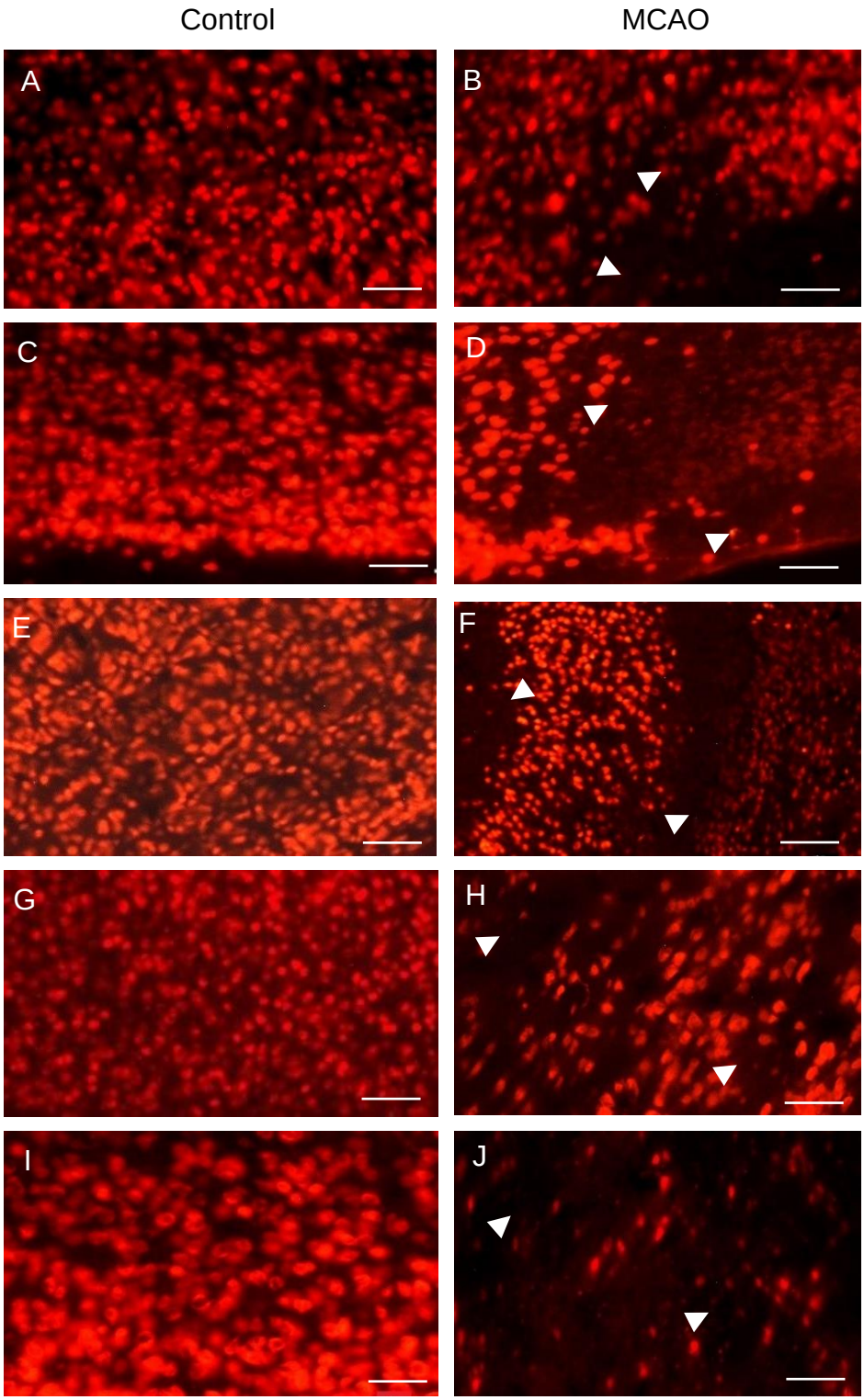

Figure 3.44 Representative photomicrographs showing immunofluorescence staining of NeuN labelled cell nuclei in the M1 motor cortex (A-B), the M2 motor cortex (C-D), granular insular Cortex (E-F), hippocampus (CA1) (G-H) and striatum area (I-J) of control (left column) and MCAO stroke (right column). NeuN labelled cells are fewer in stroke mice than in the controls due to neuronal cells death following stroke (arrowheads). (Scale bar=50um). (The images are taken at the level of Bregma 1.54 or -2.06mm). (Slice thickness=20um).

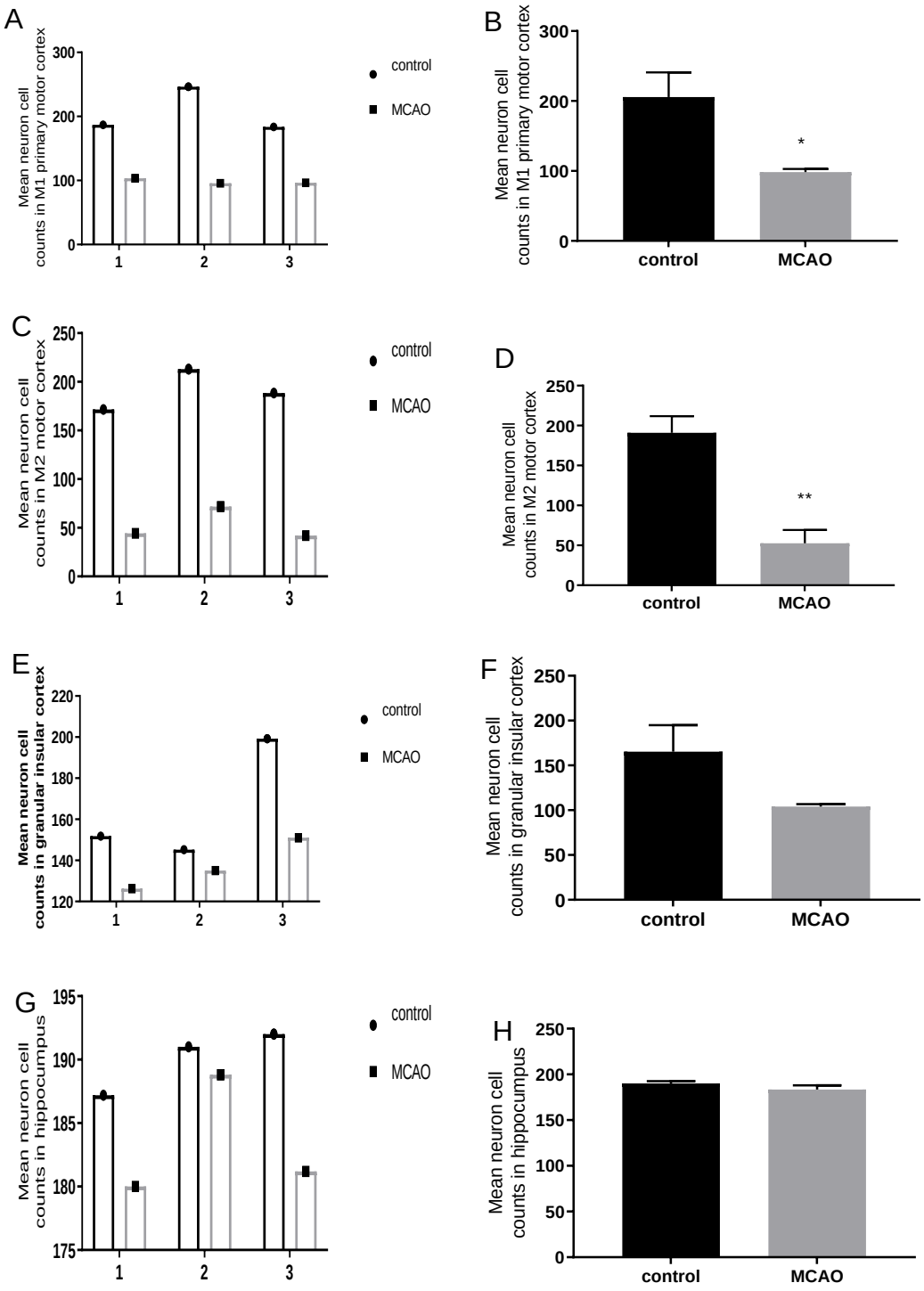
A
Mean neuron cell counts in M1 primary motor cortex
300
200
100
0
1
2
3
control
MCAO
B
Mean neuron cell counts in M1 primary motor cortex
300
200
100
0
*
control
MCAO
C
Mean neuron cell counts in M2 motor cortex
250
200
150
100
50
0
1
2
3
control
MCAO
D
Mean neuron cell counts in M2 motor cortex
250
200
150
100
50
0
**
control
MCAO
E
Mean neuron cell counts in granular insular cortex
220
200
180
160
140
120
1
2
3
control
MCAO
F
Mean neuron cell counts in granular insular cortex
250
200
150
100
50
0
control
MCAO
G
Mean neuron cell counts in hippocumpus
195
190
185
180
175
1
2
3
control
MCAO
H
Mean neuron cell counts in hippocumpus
250
200
150
100
50
0
control
MCAO

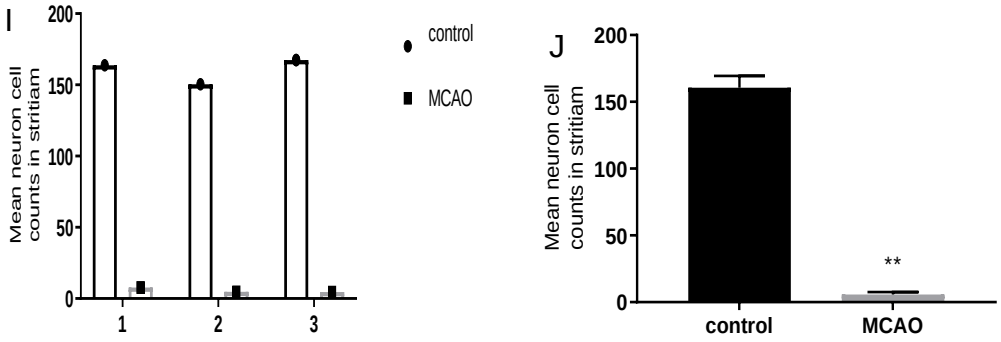

Figure 3.45 Quantitative analysis shows significant differences (*p< 0.05, ,p ≤ 0.01 - paired Student's t-test, n=3) in the number of NeuN-positive nuclei between sham-operated and MCAO mice in the M1 motor cortex (A-B, p=0.0392), the M2 motor cortex (C-D, p=0.0017) and striatum area (I-J, p=0.0010), but not in granular insular Cortex (E-F, p=0.080) and hippocampus (CA1) (G-H, p=0.1141).**

3.2.3 GFAP immunostaining and quantitative analysis

GFAP as a glial cells specific protein was used to stain glial cells and processes (For additional IHC details, refer to section 3.1.3). Data from GFAP IHC staining in MCAO brains in a comparison with sham brains revealed an active astrogliosis as shown in (Figure 3.46) under 20 and 40 X magnification objectives. Quantitative analysis of the number of GFAP immunostained cells in the hippocampus (CA1) showed significant elevation in the astrocyte's cells and processes in the MCAO stroke model brains (n=3) compared to the control brains with (paired Student's t-test-p=0.0497) and (p=0.0485) respectively as displayed in Figure 3.47.

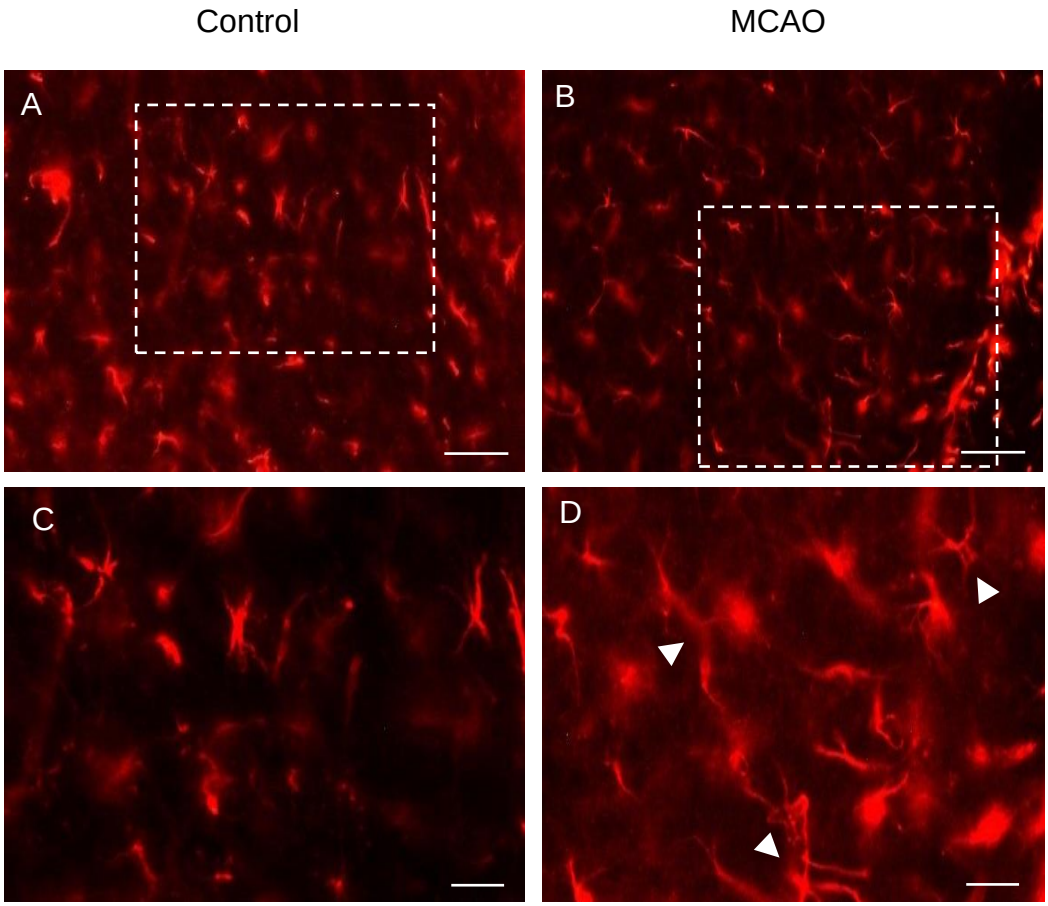

Figure 3.46 Representative photomicrographs showing immunofluorescence staining of GFAP labelled astrocytes in the hippocampus of control (A, C) and MCAO stroke (B, D) brains. The GFAP labelled cells and processes becomes thicker and more due to astrocytes activation following stroke (arrowheads). (Scale bar=50um:A,B and 20um:C,D). (The images are taken at the level of Bregma -2.06mm). (Slice thickness=20um).

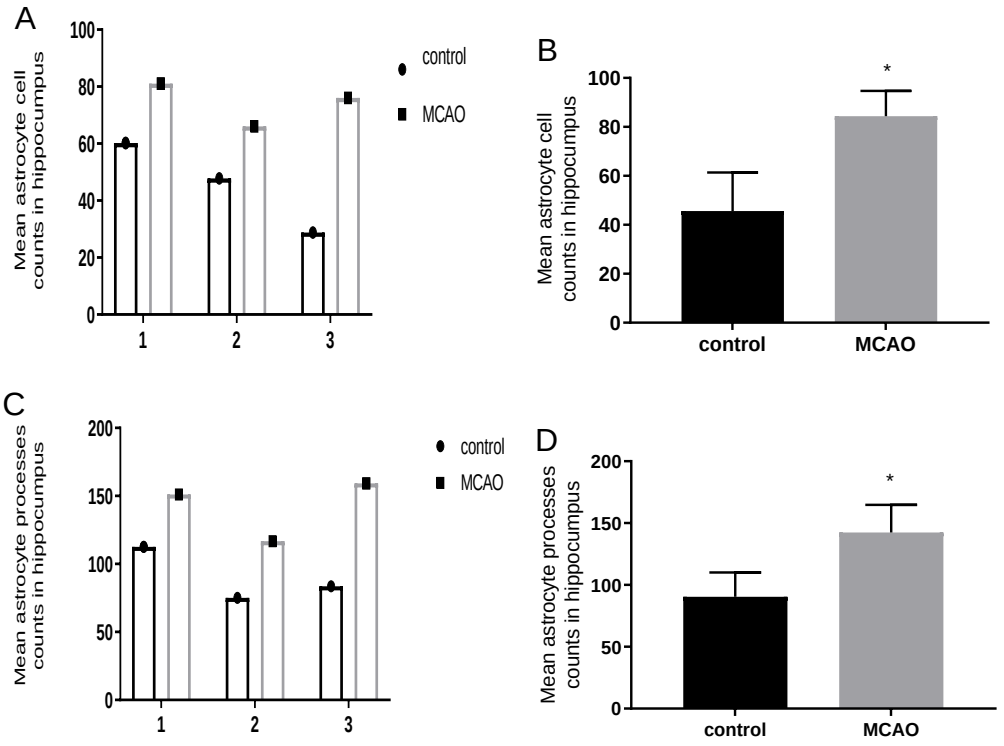

Figure 3.47 Quantitative analysis shows significant increases (*p < 0.05 - paired Student's t-test, n=3) in the number of GFAP labelled astrocyte cells (A,B-*p=0.0497) and profiles processes (C,D-*p=0.0485) in MCAO mice compared to sham in hippocampus (CA1).

3.2.4 Disruption of TJ of BBB

In order to investigate BBB damage in murine model of focal ischaemia, antibodies to ZO-1, Occludin and Claudin-5 were used in IHC. The immunostaining results are presented in the following section.

3.2.4.1 ZO-1 immunostaining results

This staining aimed to examine the changes on TJ of BBB integrity following focal ischaemic stroke. ZO-1; one of the junctional BBB proteins was used to compare the changes in TJ between MCAO brains and corresponding controls brains. At the hippocampus level (Bregma -2.06mm), brain sections were stained and imaged using 60 X magnification objectives. The IHC results showed that labelled TJs of BBB are disrupted in MCAO brains in a comparison with the intact ones in the corresponding sham brains as shown in Figure 3.48.

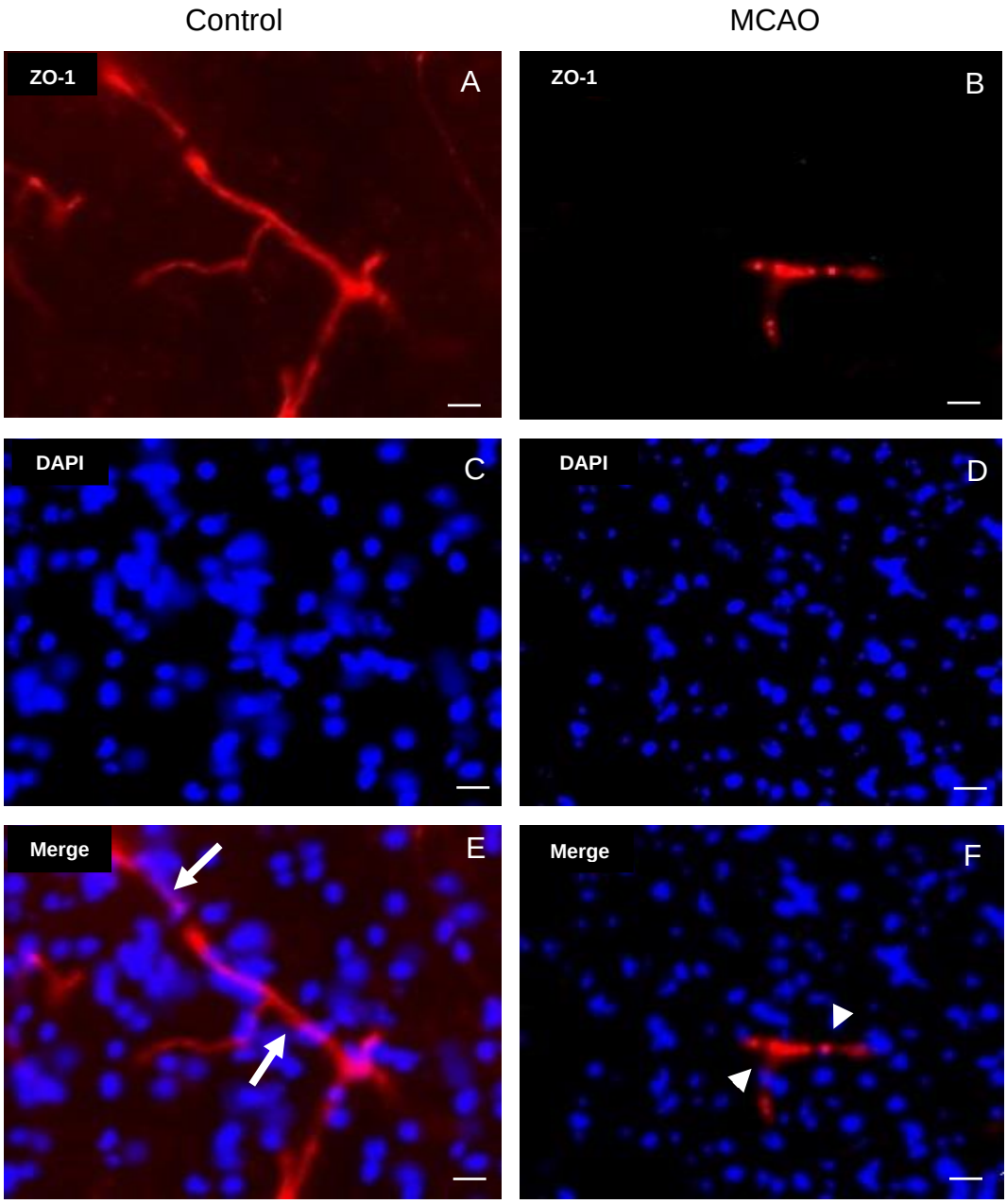

Figure 3.48 Representative photomicrographs showing immunofluorescence staining for ZO-1 using anti-ZO-1 and Cy3-conjugated secondary antibodies with DAPI stained nuclei in the hippocampus in sham (A, C, E) and MCAO stroke brains (B, D, F). The labelled TJs are disrupted in stroke brain (arrowheads) compared to the intact ones in the control (arrows). (Scale bar=10um). (The images are taken at the level of Bregma-2.06mm). (Slice thickness=20um).

3.2.4.2 Occludin immunostaining results

Antibody to Occludin was used in IHC to examine the changes in TJ of BBB in MCAO. The staining was conducted at the level of hippocampus and imaged using 60 X magnification objectives. The data showed disruption of Occludin immunoreactive TJ profiles in the hippocampus of ischaemic mice as compared to sham-operated mice as shown in Figure 3.49.

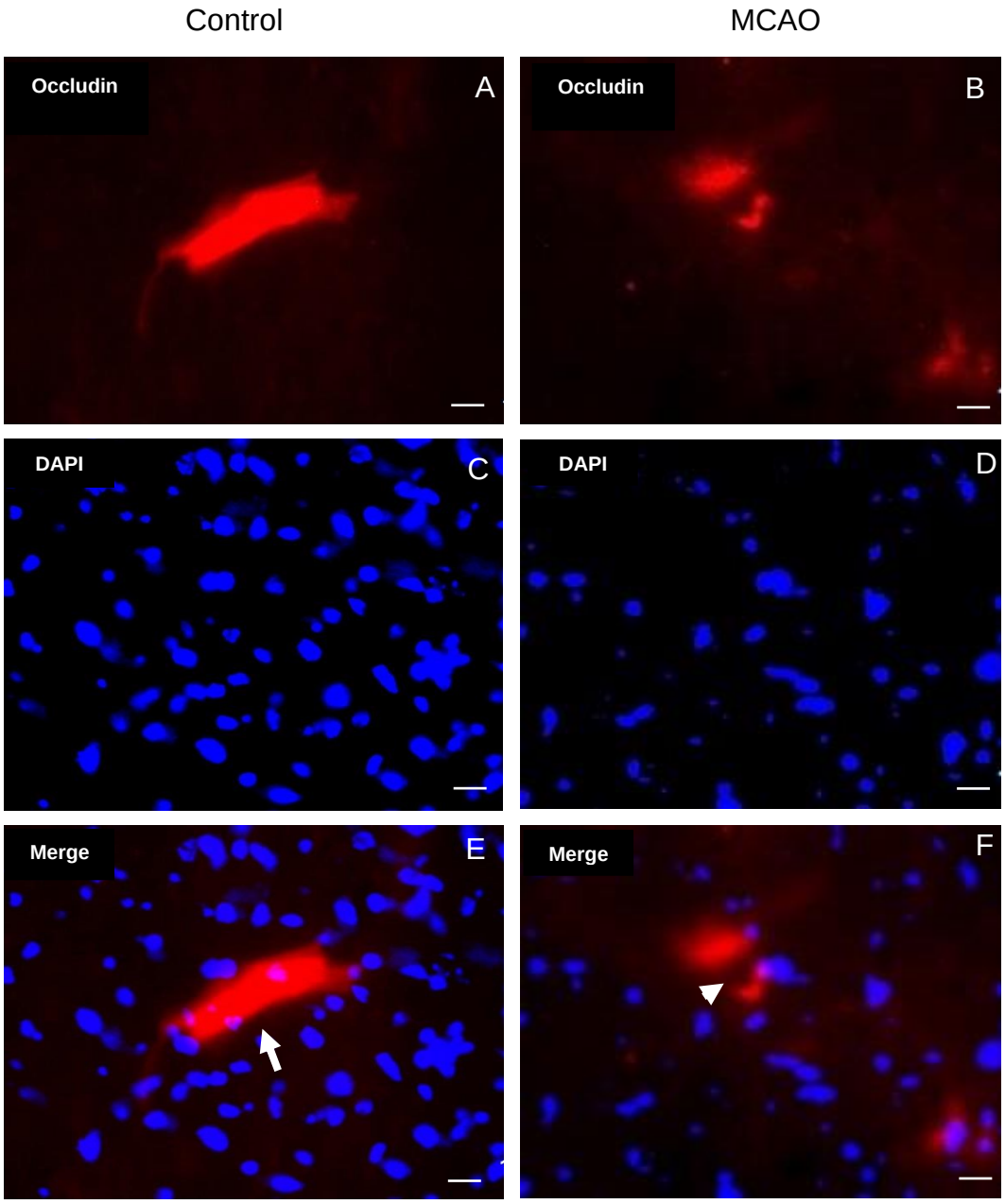

Figure 3.49 Representative photomicrographs showing immunofluorescence staining for Occludin using anti-Occludin and Cy3-conjugated secondary antibodies with DAPI stained nuclei in the hippocampus in sham (A,C,E) and MCAO stroke brains (B,D,F). The labelled TJs are disrupted in stroke brain (arrowhead) compared to the intact ones in the control (arrow). (Scale bar= 10um). (The images are taken at the level of Bregma-2.06mm). (Slice thickness=20um).

3.2.4.3 Claudin-5 immunostaining results

To also investigate the BBB damage following focal ischaemia, anti-Claudin-5 was used. Claudin-5 as mentioned previously is one of the TJ of the endothelial cells of BBB specific proteins. IHC staining results revealed showed disruption of Claudin-5 immunoreactive TJ profiles in MCAO stroke brain mice compared to the sham brain in the hippocampus under using 60 X magnification objectives, Figure 3.50.This confirms that TJs are disrupted following MCAO and reperfusion as compared to intact TJs in the sham brains.

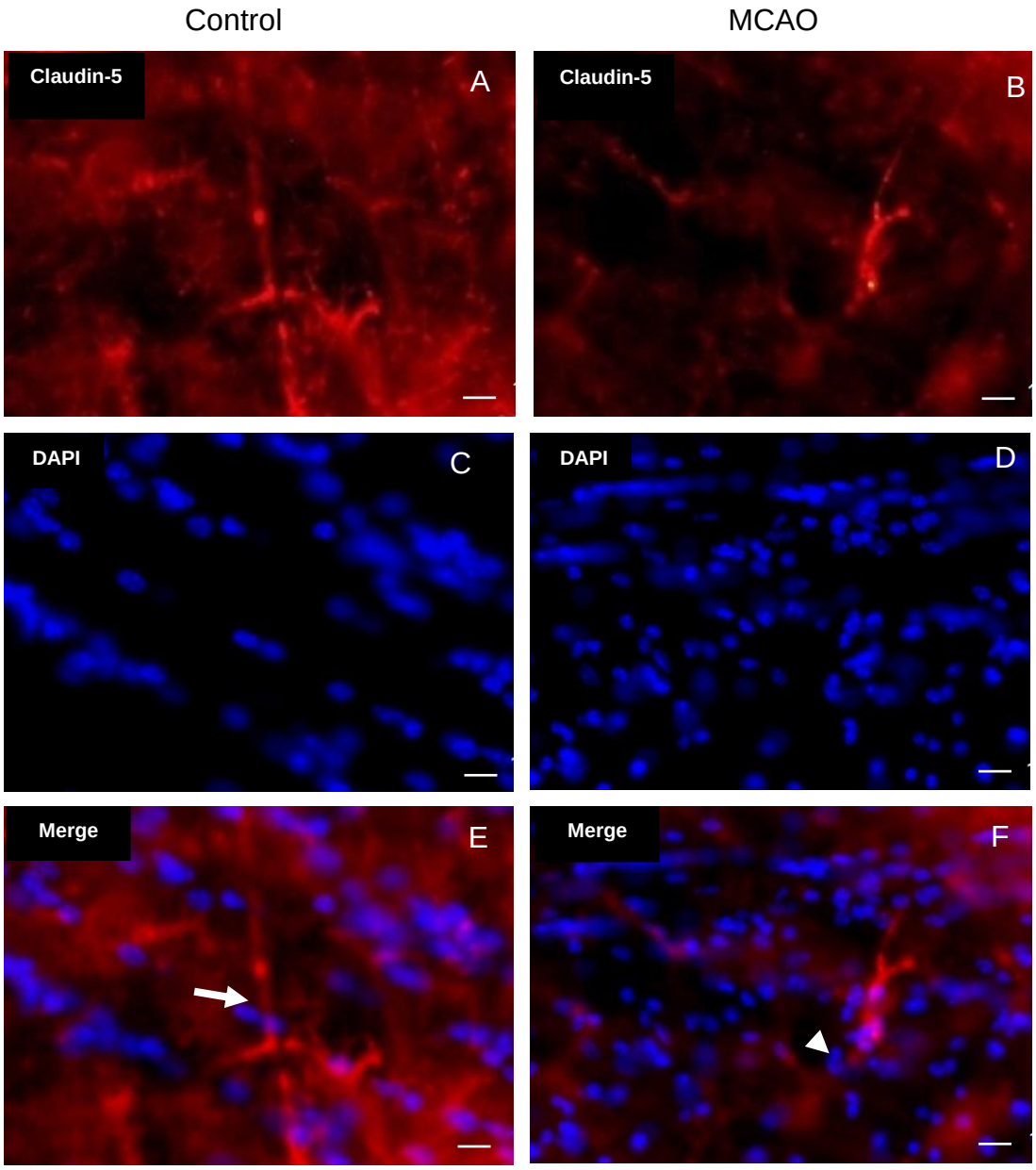

Figure 3.50 Representative photomicrographs showing immunofluorescence staining for Claudin-5 using anti-Claudin-5 and Cy3-conjugated secondary antibodies with DAPI stained nuclei in the hippocampus in sham (A, C, E) and MCAO stroke brains (B, D, F). The labelled TJs are disrupted in stroke brain (arrowhead) compared to the intact ones in the control (arrow). (Scale bar=10um). (The images are taken at the level of Bregma-2.06mm). (Slice thickness=20um).

3.2.5 Brain cells damage and TJ disruption in MCAO and BCCAO models

To determine the brain cell damage and TJ disruption following cerebral ischaemia in both MCAO and BCCAO models, immunohistochemical staining using antibodies to (NeuN, GFAP, ZO-1, Occludin, Claudin-5, CD31, PDGFR, NG2 and IBA-1) was performed. The immunostaining results were concentrated on the hippocampus, area known as one of the most vulnerable and affected areas in ischaemia, thus, most of the IHC staining results in this study were conducted in this area based on earlier studies. Also, the hippocampus is the area where some of these proteins' expressions were analysed using WB. The results are shown alongside each other in the following section to achieve a clear vision.

As mentioned previously, antibody to neuronal nuclei (NeuN), has been utilized widely to determine neurons. Data from NeuN IHC in BCCAO and MCAO ischaemic and sham brains showed that both models induce loss of neurones in the hippocampus in stroke brains compared to control brains as shown in Figure 3.51.

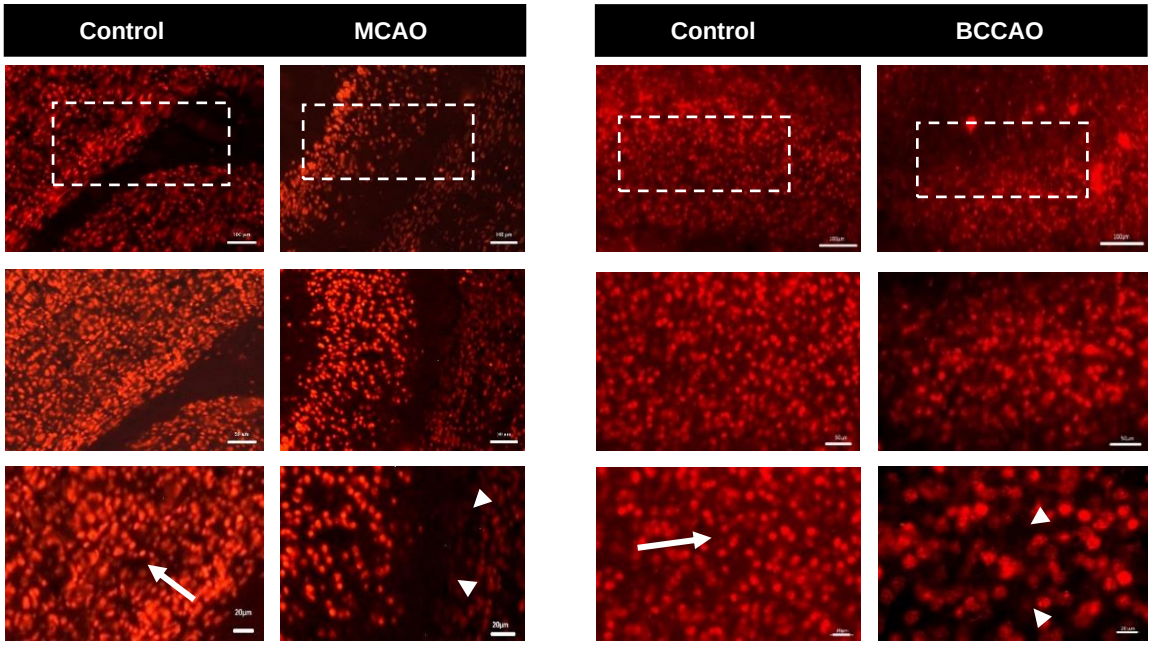

Figure 3.51 Representative photomicrographs showing immunofluorescence staining for NeuN using anti-NeuN in the hippocampus of MCAO stroke model and BCCAO stroke model. For both models, the left panel side represents the control brains, while the right panel side represents the stroke brains. NeuN labelled cells are fewer in stroke models (arrowheads) than in the controls (arrows). (Scale bar=100um: upper row,50um:middle row and 20um:lower row). (The images are taken at the level of Bregma -2.06mm). (Slice thickness = 20 um).

A large portion of astroglia was demonstrated by immunolabelling of GFAP in hippocampus. Data from astrocytes cells and processes labelled by GFAP IHC in BCCAO and MCAO showed an increase in astrocytes cells and processes in the hippocampus in both stroke brains compared to the control brains as shown in Figure 3.52.

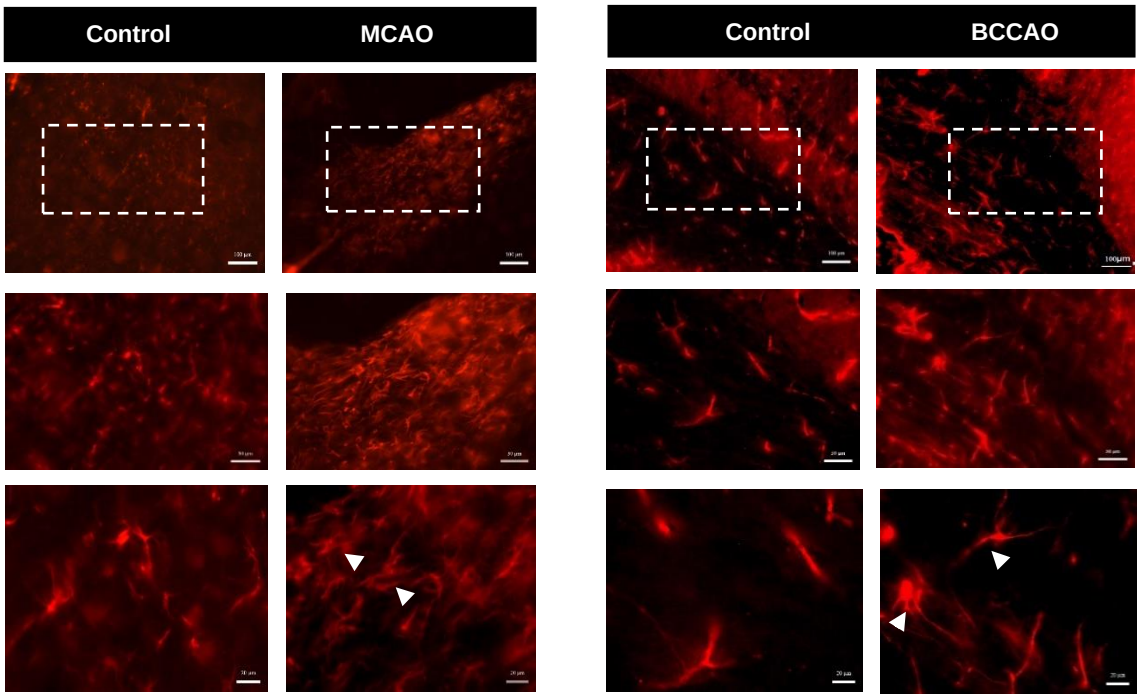

Figure 3.52 Representative photomicrographs showing immunofluorescence staining for GFAP using anti-GFAP in the hippocampus area of MCAO stroke model and BCCAO stroke model. For both models, the left panel side represents the control brains, while the right panel side represents the stroke brains. In the stroke brains, the GFAP labelled cells and processes are thicker and higher in number due to astrocytes activation following stroke (arrowheads). (Scale bar=100um: upper row,50um:middle row and 20um:lower row). (The images are taken at the level of Bregma -2.06mm). (Slice thickness=20um).

Moreover, to define TJ of BBB structural alterations during ischaemia, an IHC analysis of TJ proteins (Occludin, ZO-1 and Claudin-5) in BCCAO and MCAO brains was performed. Immunofluorescence staining using antibodies to Occludin, ZO-1 and Claudin-5 in the hippocamps area are shown in Figure 3.53, Figure 3.54 and Figure 3.55 respectively. The immunostaining results illustrated disruption of TJ labelled profiles in the hippocampus following BCCAO and MCAO compared to the intact ones in the controls.

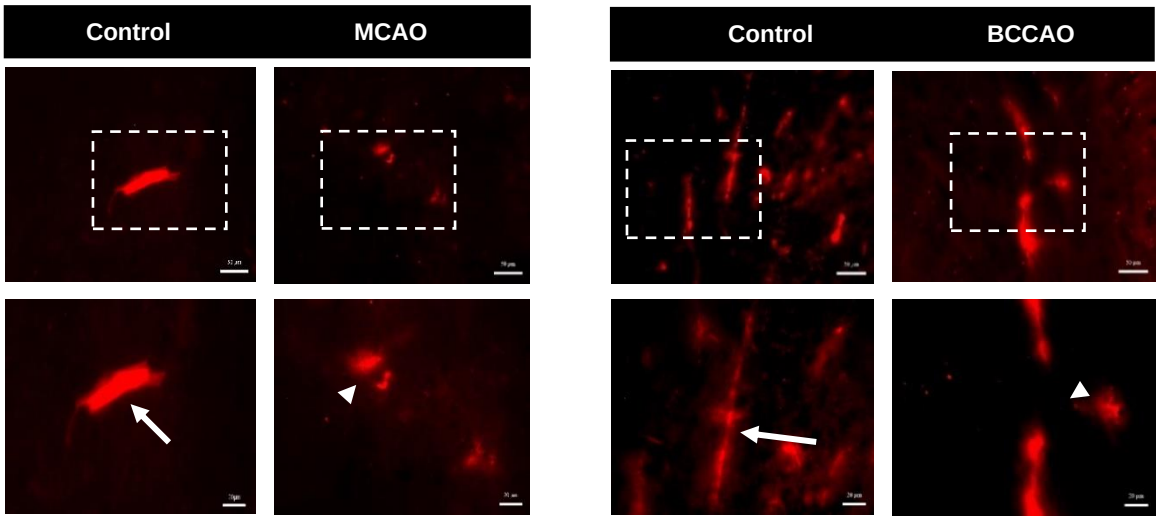

Figure 3.53 Representative photomicrographs showing immunofluorescence staining for Occludin using anti-Occludin in the hippocampus area of MCAO stroke model and BCCAO stroke model. For both models, the left panel side represents the control brains, while the right panel side represents the stroke brains. In the stroke brains, the labelled TJs are disrupted (arrowheads) compared to the intact ones in the control brains (arrows). (Scale bar= 50um:upper row and 20um:lower row). (The images are taken at the level of Bregma -2.06mm). (Slice thickness=20um).

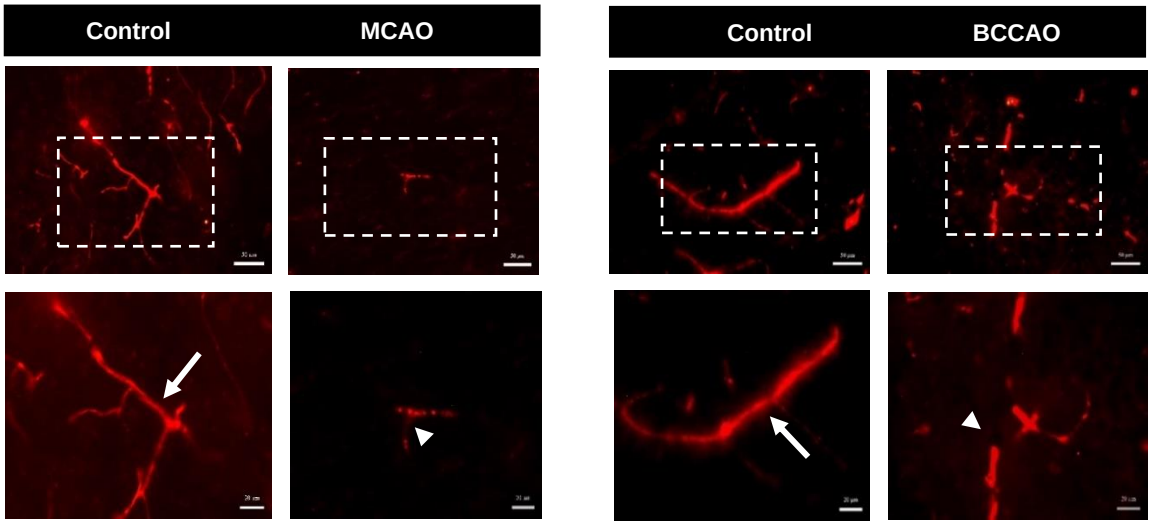

Figure 3.54 Representative photomicrographs showing immunofluorescence staining for ZO-1 using anti-ZO-1 in the hippocampus area of MCAO stroke model and BCCAO stroke model. For both models, the left panel side represents the control brains, while the right panel side represents the stroke brains. In the stroke brains, the labelled TJs are disrupted (arrowheads) compared to the intact ones in the control brains (arrows). (Scale bar= 50um:upper row and 20um:lower row). (The images are taken at the level of Bregma-2.06mm). (Slice thickness=20um).

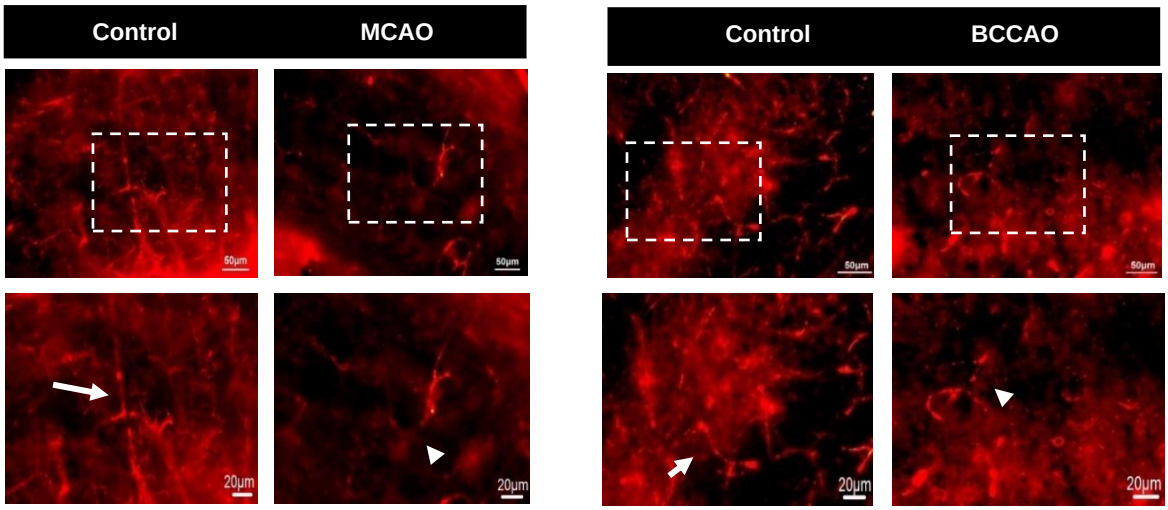

Figure 3.55 Representative photomicrographs showing immunofluorescence staining for Claudin-5 using anti-Claudin-5 in the hippocampus area of MCAO stroke model and BCCAO stroke model.For both models, the left panel side represents the control brains, while the right panel side represents the stroke brains. In the stroke brains, the labelled TJs are disrupted (arrowheads) compared to the intact ones in the control brains (arrows). (Scale bar= 50um:upper row and 20um:lower row). (The images are taken at the level of Bregma-2.06mm). (Slice thickness=20um).

To investigate the changes on endothelial cells following ischaemia in BCCAO and MCAO models, immunofluorescence staining using anti-CD31 and Alexa488-conjugated secondary antibodies in the hippocampus area was achieved. The results illustrated that the endothelial labelled cells showed morphological changes with some dilatations in both ischaemic models compared to sham as revealed in Figure 3.56.

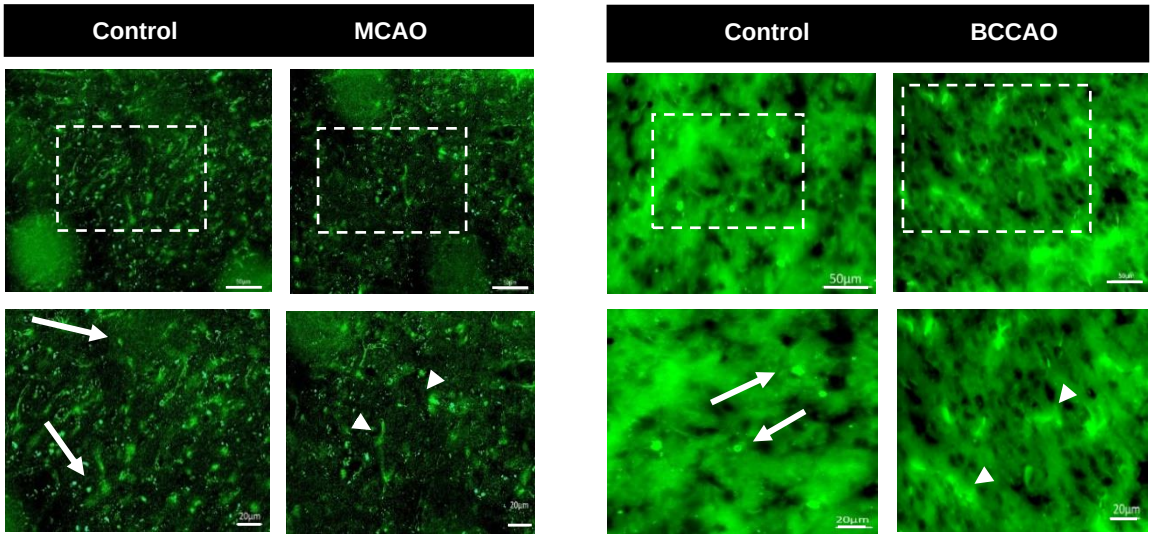

Figure 3.56 Representative photomicrographs showing immunofluorescence staining for CD-31 using anti-CD31 in the hippocampus area of MCAO stroke model and BCCAO stroke model. For both models, the left panel side represents the control brains, while the right panel side represents the stroke brains. In the stroke brains, the endothelial labelled cells showing morphological changes with some dilatations (arrowheads) compared to control (arrows). (Scale bar= 50um:upper row and 20um:lower row). (The images are taken at the level of Bregma -2.06mm). (Slice thickness=20um).

IBA-1 as mentioned previously is actin-binding protein that is expressed in all microglia (Imai et al., 1996). To determine the difference on microglia in the hippocampus area in MCAO stroke model and BCCAO stroke model, immunofluorescence staining using anti-IBA-1 was done. The results showed an increase in microglia processes in the stroke brains compared control brains as shown in Figure 3.57.

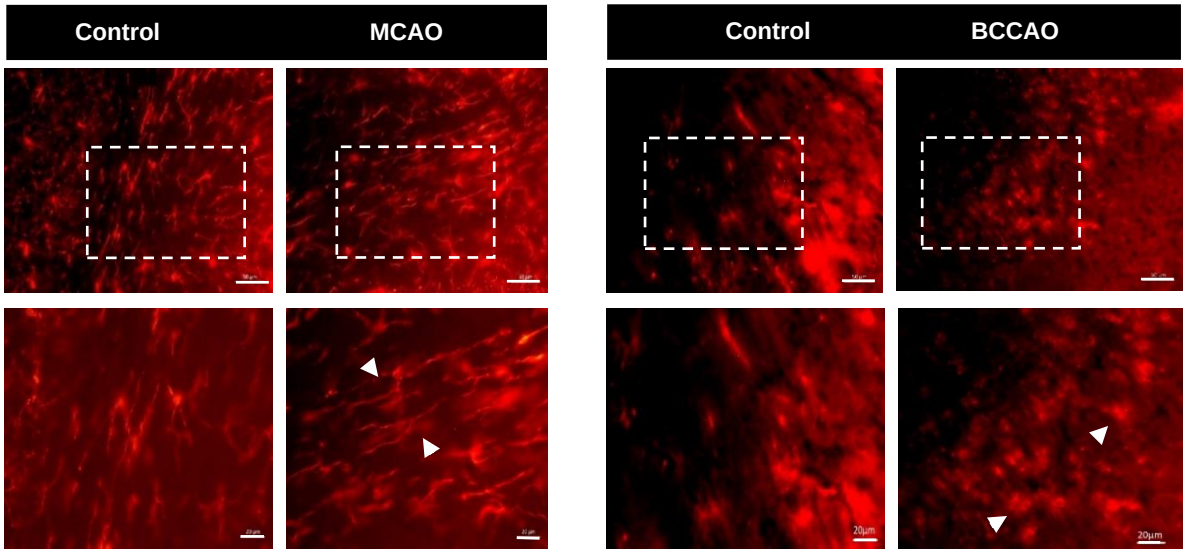

Figure 3.57 Representative photomicrographs showing immunofluorescence staining for IBA-1 using anti-IBA-1 in the hippocampus area of MCAO stroke model and BCCAO stroke model. For both models, the left panel side represents the control brains, while the right panel side represents the stroke brains. The IBA-1 labelled cells and processes are more in stroke brains than in the control brains following stroke (arrowheads). (Scale bar= 50um:upper row and 20um:lower row). (The images are taken at the level of Bregma -2.06mm). (Slice thickness=20 um).

To examine changes in pericytes cells after focal and global ischaemia, antibodies to PDGFR and NG2 were used in IHC staining. Results of IHC staining using anti-PDGFR (Figure 3.58) and anti-NG2 (Figure 3.59) in the hippocampus showed that labelled pericytes are changed morphologically and showed some reduction following stroke in both MCAO and BCAAO.

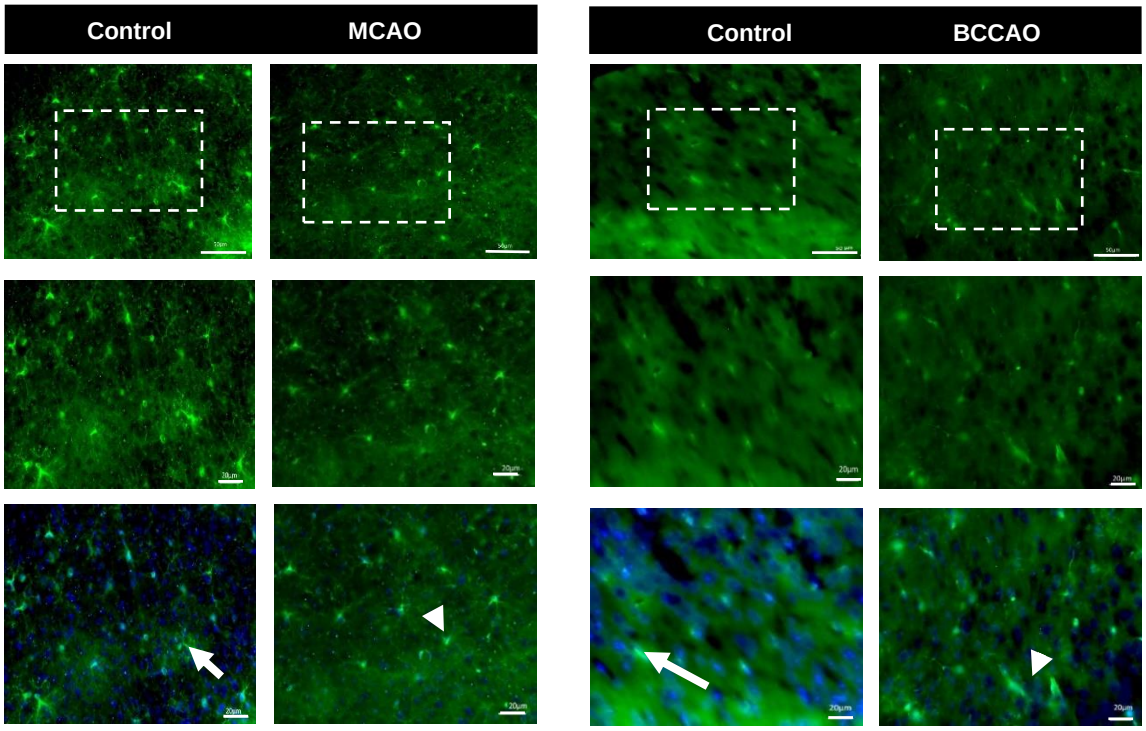

Figure 3.58 Representative photomicrographs showing immunofluorescence staining for PDGFR using anti-PDGFR and Alexa488 conjugated secondary antibodies with DAPI stained nuclei in the hippocampus of MCAO stroke model and BCCAO stroke model. For both models, the left panel side represents the control brains, while the right panel side represents the stroke brains. The labelled pericytes show morphological changes with some reduction in the stroke brains (arrowheads) compared to control (arrows). (Scale bar= 50um:upper row and 20um:middle and lower rows). (The images are taken at the level of Bregma -2.06mm). (Slice thickness=20 um).

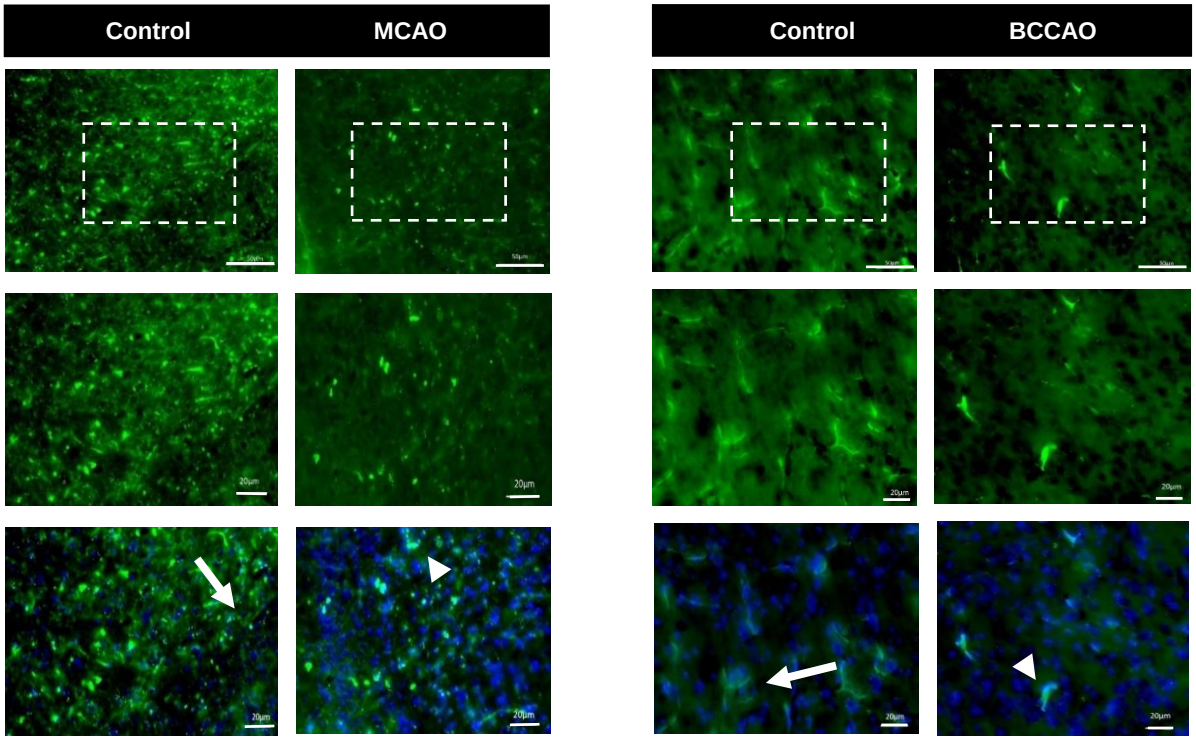

Figure 3.59 Representative photomicrographs showing immunofluorescence staining for NG2 using anti-NG2 and Alexa488 conjugated secondary antibodies with DAPI stained nuclei in the hippocampus of MCAO stroke model and BCCAO stroke model. For both models, the left panel side represents the control brains, while the right panel side represents the stroke brains. The labelled pericytes show morphological changes and some reduction in the stroke brains (arrowheads) compared to control (arrows). (Scale bar= 50um:upper row and 20um:middle and lower rows). (The images are taken at the level of Bregma -2.06mm). (Slice thickness=20 um).

3.2.6 Double staining immunohistochemistry staining

3.2.6.1 MCAO induced morphological changes in endothelial cells and TJ disruption

Changes in endothelial cells following focal cerebral ischaemic stroke were investigated by IHC using specific antibodies against CD31. These changes were correlated with TJ proteins: Occludin, ZO-1 and Claudin-5 to evaluate disruption of TJ of BBB following stroke in MCAO model of cerebral ischaemia and reperfusion in the cortical and hippocampal areas. Moreover, to confirm that the TJ proteins are expressed within the endothelial cells profile, double labelling with primary antibodies against CD31 and one of the TJ proteins was done.

First, double labelling using the anti-CD31 to label endothelial cells correlated with anti-Occludin to label TJ and detect the TJ integrity of BBB was done in order to confirm that TJ protein (Occludin) is expressed in the endothelial cells profile. The results confirmed that TJ protein is expressed within the endothelial cells profile which was expected. The labelling of TJ with anti-Occludin and the labelling of endothelial cells with anti-CD31 were seen in the hippocampus area and cortical area as shown in Figure 3.60 and Figure 3.61 respectively. The results illustrated disruption of TJ labelled with anti-Occludin in stroke brains compared to the intact ones in the control brains. Furthermore, morphological changes of the endothelial cells labelled with anti-CD31 were observed in the MCAO stroke brains.

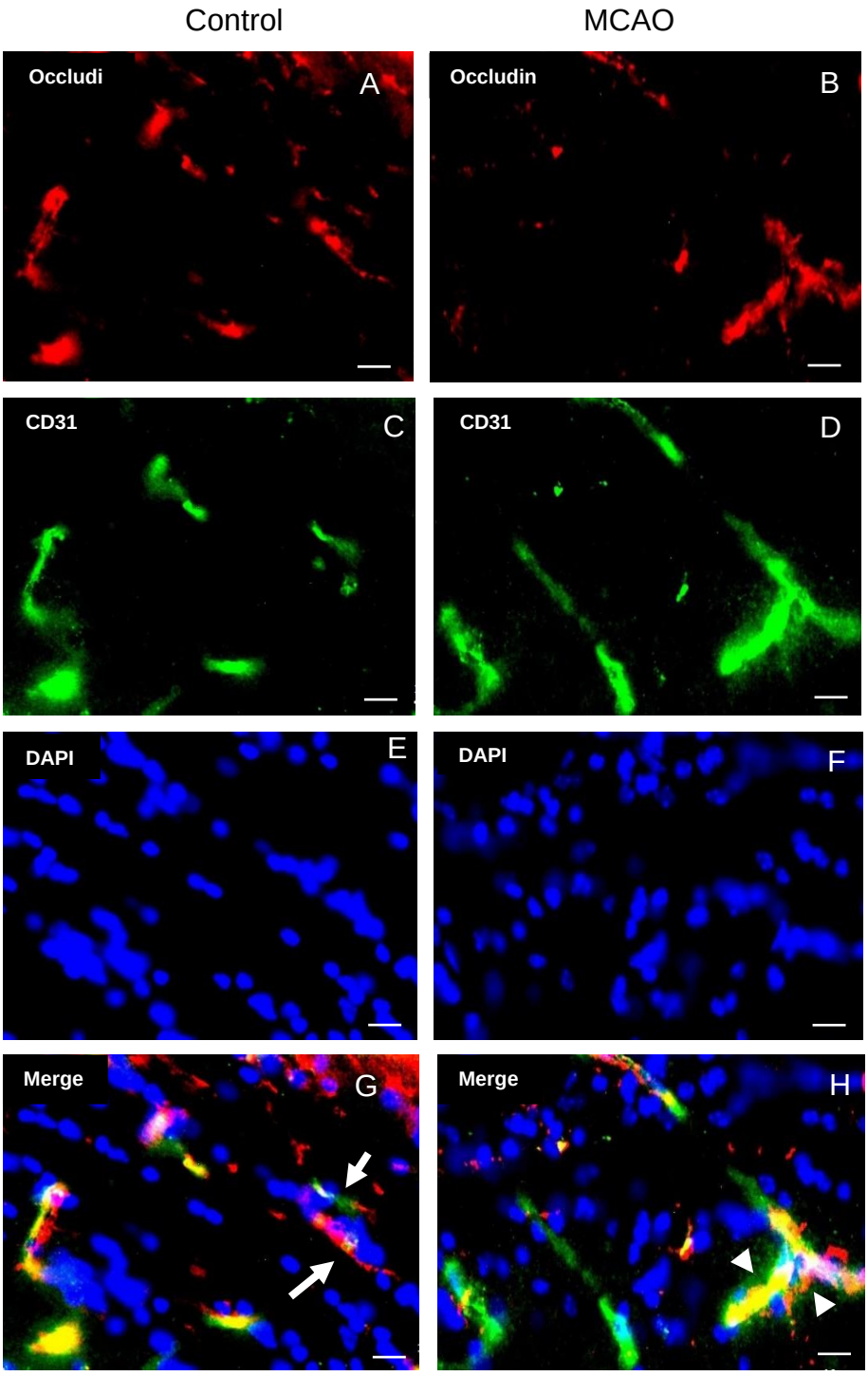

Figure 3.60 Representative photomicrographs showing double immunofluorescence staining for Occludin and CD31 with anti-Occludin (A,B-red) and anti-CD31(C,D-green) and DAPI (E,F-blue) stained nuclei in the hippocampus area in MCAO model of stroke (B,D,F,H) compared to control (A,C,E,G). The labelled TJs with anti-Occludin showing disruption of TJs in stroke side (arrowheads) compared to the intact ones in the control (arrows). The labelled endothelial cells with anti-CD31 showing morphological changes in the stroke brain (arrowheads) compared to control (arrows). (Scale bar=10um). (The images are taken at the level of Bregma -2.06mm). (Slice thickness=20um).

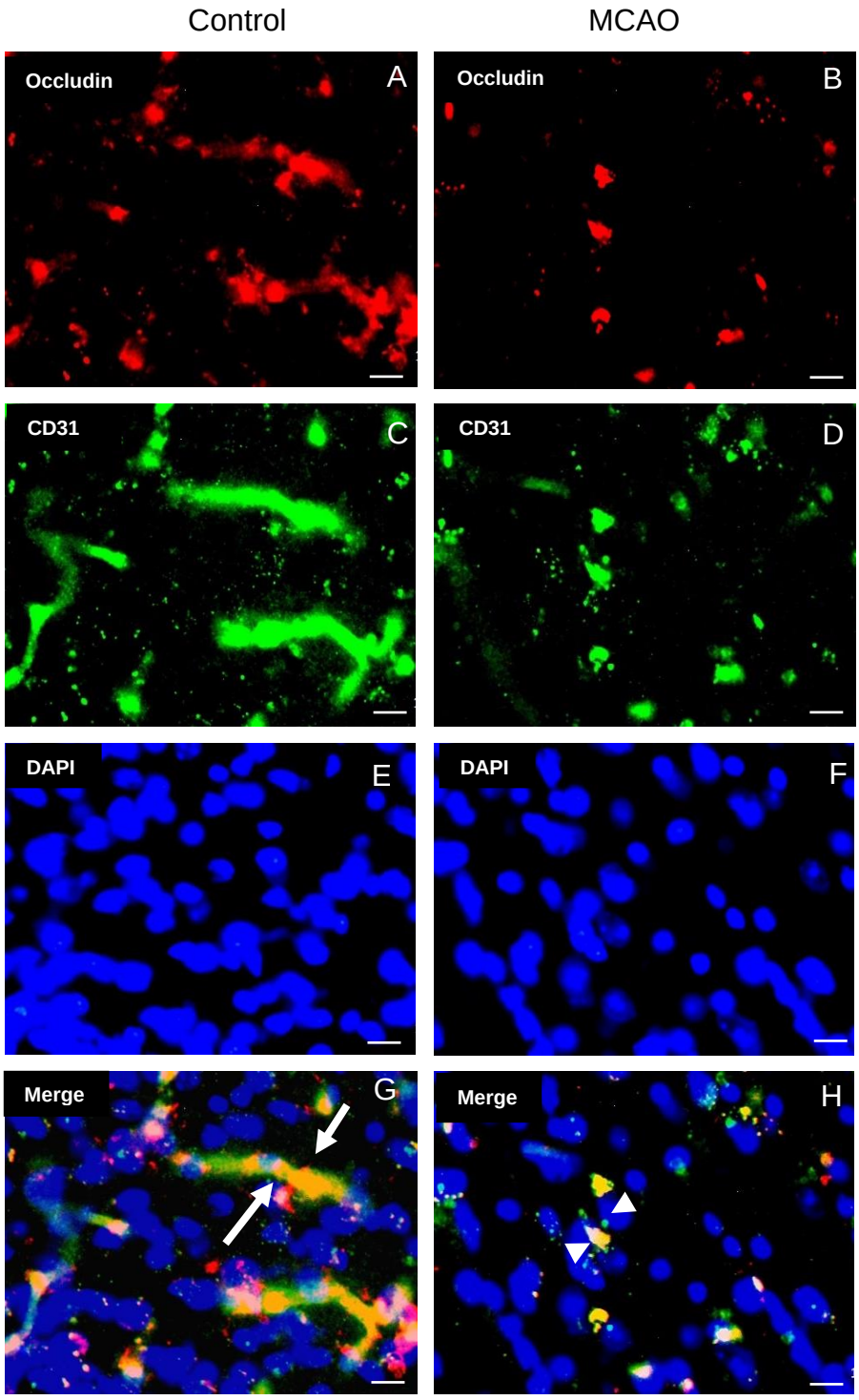

Figure 3.61 Representative photomicrographs showing double immunofluorescence staining for Occludin and CD31 with anti-Occludin (A,B-red) and anti-CD31(C,D-green) and DAPI (E,F-blue) stained nuclei in the cortical area in MCAO model of stroke (B,D,F,H) compared to control (A,C,E,G). The labelled TJs with anti-Occludin showing disruption of TJs in stroke side (arrowheads) compared to the intact ones in the control (arrows). The labelled endothelial cells with anti-CD31 showing morphological changes in the stroke brain (arrowheads) compared to control (arrows). (Scale bar= 10um). (The images are taken at the level of Bregma 1.54 mm). (Slice thickness=20um).

Dual-IF using antibody to CD31 to label endothelial cells and antibody to ZO-1 to label TJ was carried out in order to detect TJ integrity and to confirm the expression TJ protein (ZO-1) within the endothelial cells profile. The results showed that TJ protein (ZO-1) is expressed within endothelial cell profile which was expected. The results showed that endothelial cells of BBB were labelled with anti-CD31 in both hippocampus and cortex area in stroke mice and control mice as shown in Figure 3.62 and Figure 3.63. In addition, the results showed that the TJs were labelled with anti-ZO-1 in both hippocampus and cortex area in stroke mice and control mice. The labelled TJs with anti-ZO-1 are disrupted in stroke mice compared to the intact ones. The labelled endothelial cells with anti-CD31 showed morphological changes in the MCAO stroke brains compared to preserved morphology of endothelial cells in the control brains in hippocampus and cortex areas.

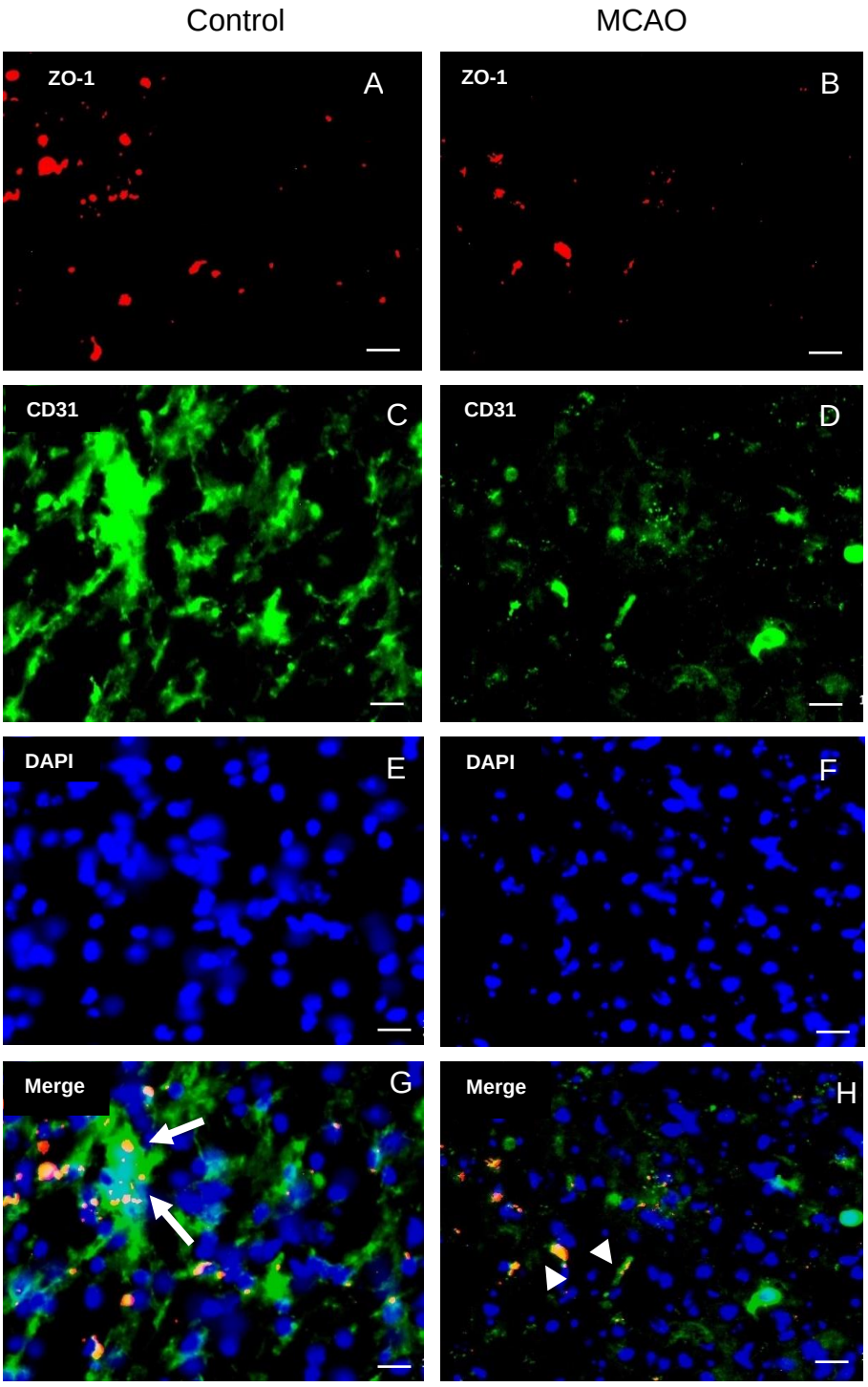

Figure 3.62 Representative photomicrographs showing double immunofluorescence staining for ZO-1 and CD31 with using anti-ZO-1 (A,B-red) and anti-CD31(C,D-green) and DAPI (E,F-blue) stained nuclei in the hippocampus area in MCAO model of stroke (B,D,F,H) compared to control (A,C,E,G). The labelled TJs with anti-ZO-1 showing disruption of TJs in stroke side (arrowheads) compared to the intact ones in the control (arrows). The labelled endothelial cells with anti-CD31 showing morphological changes in the stroke brain (arrowheads) compared to control (arrows). (Scale bar=10um). (The images are taken at the level of Bregma -2.06mm). (Slice thickness=20um).

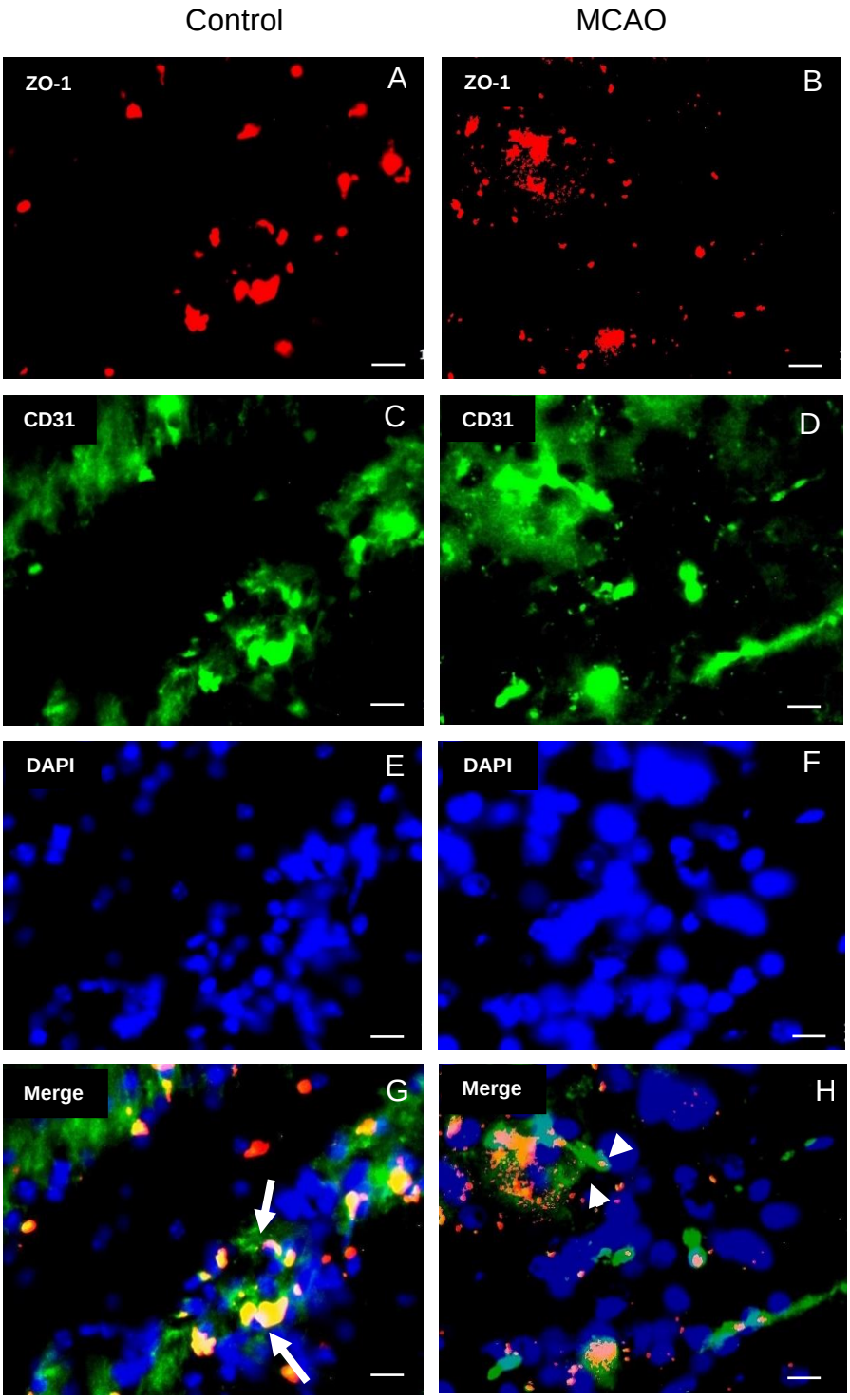

Figure 3.63 Representative photomicrographs showing double immunofluorescence staining for ZO-1 and CD31 with anti- ZO-1 (A,B-red) and anti-CD31(C,D-green) and DAPI (E,F-blue) stained nuclei in the cortical area in MCAO model of stroke (B,D,F,H) compared to control (A,C,E,G). The labelled TJs with anti-ZO-1 showing disruption of TJs in stroke side (arrowheads) compared to the intact ones in the control (arrows). The labelled endothelial cells with anti-CD31 showing morphological changes in the stroke brain (arrowheads) compared to control (arrows). (Scale bar=10um). (The images are taken at the level of Bregma 1.54 mm). (Slice thickness=20um).

Furthermore, to find out that TJ proteins are expressed in the endothelial cells profile, double labelling was conducted by using antibody to CD31 to label endothelial cells and antibody to Claudin-5 to label TJ of BBB. The results confirmed that TJ protein (Claudin-5) is expressed within endothelial cell profile as was expected. Data showed the Claudin-5 immunoreactivity in TJ in the hippocampal and cortical areas in both MCAO and control mice. Also, the stained endothelial cells with anti-CD31 were seen in hippocampus and cortex in MCAO brains and sham brains. The results showed that focal ischaemia and reperfusion induced disruption of TJs in the MCAO stroke mice compared to the intact ones in the control mice in both hippocampus and cortical regions. Moreover, the endothelial cells stained with anti-CD31 are changed morphologically in the stroke brains in both hippocampus and cortex as shown in Figure 3.64 and Figure 3.65 respectively.

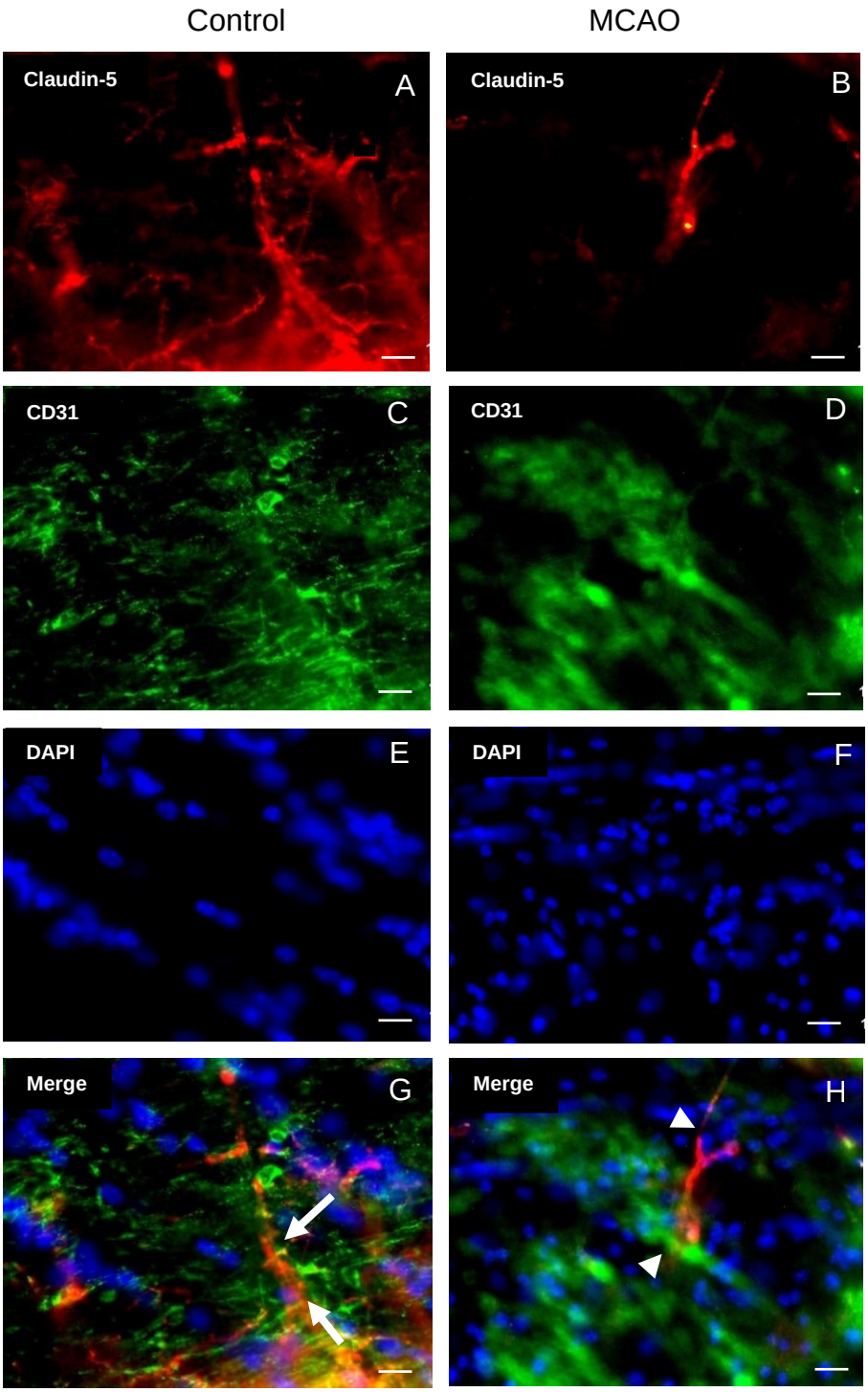

Figure 3.64 Representative photomicrographs showing double immunofluorescence staining for Claudin-5 and CD31 with anti-Claudin-5 (A,B-red) and anti-CD31(C,D-green) and DAPI (E,F-blue) stained nuclei in the hippocampus area in MCAO model of stroke (B,D,F,H) compared to control (A,C,E,G). The labelled TJs with anti-Claudin-5 showing disruption of TJs in stroke side (arrowheads) compared to the intact ones in the control (arrows). The labelled endothelial cells with anti-CD31 showing morphological changes in the stroke brain (arrowheads) compared to control (arrows). (Scale bar=10um). (The images are taken at the level of Bregma -2.06mm). (Slice thickness=20um).

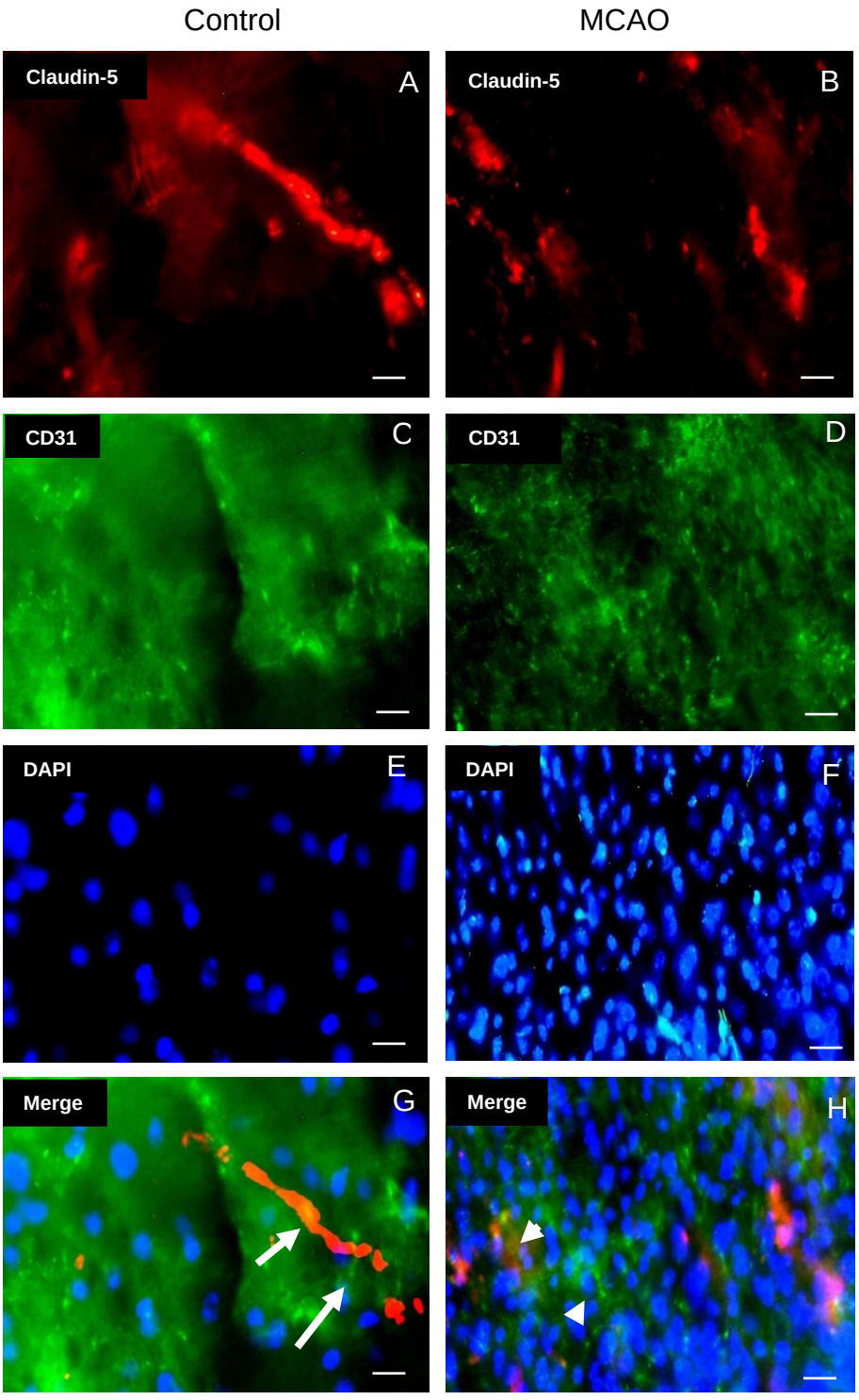

Figure 3.65 Representative photomicrographs showing double immunofluorescence staining for Claudin-5 and CD31 with anti-Claudin-5 (A,B-red) and anti-CD31(C,D-green) and DAPI (E,F-blue) stained nuclei in the cortical area in MCAO model of stroke (B,D,F,H) compared to control (A,C,E,G). The labelled TJs with anti-Claudin-5 showing disruption of TJs in stroke side (arrowheads) compared to the intact ones in the control (arrows). The labelled endothelial cells with anti-CD31 showing morphological changes in the stroke brain (arrowheads) compared to control (arrows). (Scale bar=10um). (The images are taken at the level of Bregma 1.54 mm). (Slice thickness=20um).

3.2.6.2 MCAO induced neuronal death and TJ disruption

Dual labelling was conducted using anti-NeuN to label neuron cells correlated with anti-ZO-1 to label TJ of BBB. This was done to determine if focal ischaemia and reperfusion induced changes on neurons and TJ. Also, to investigate that TJ proteins are not expressed in the neuronal cells, this double labelling was achieved. The results confirmed that neurons and TJ protein are labelled in separated profiles. In both the cortical and hippocampal areas, NeuN immunoreactivity was seen in neuronal cells in the stroke mice and control mice. Neuronal decrease due to death of neurons was detected in the stroke mice compared to the control mice. The ZO-1 immunoreactivity was observed in TJ in the stroke mice and control mice. The labelled TJs with anti-ZO-1 are disrupted in MCAO brains compared to control brains in hippocampus and cortex as shown in (Figure 3.66) and (Figure 3.67) respectively.

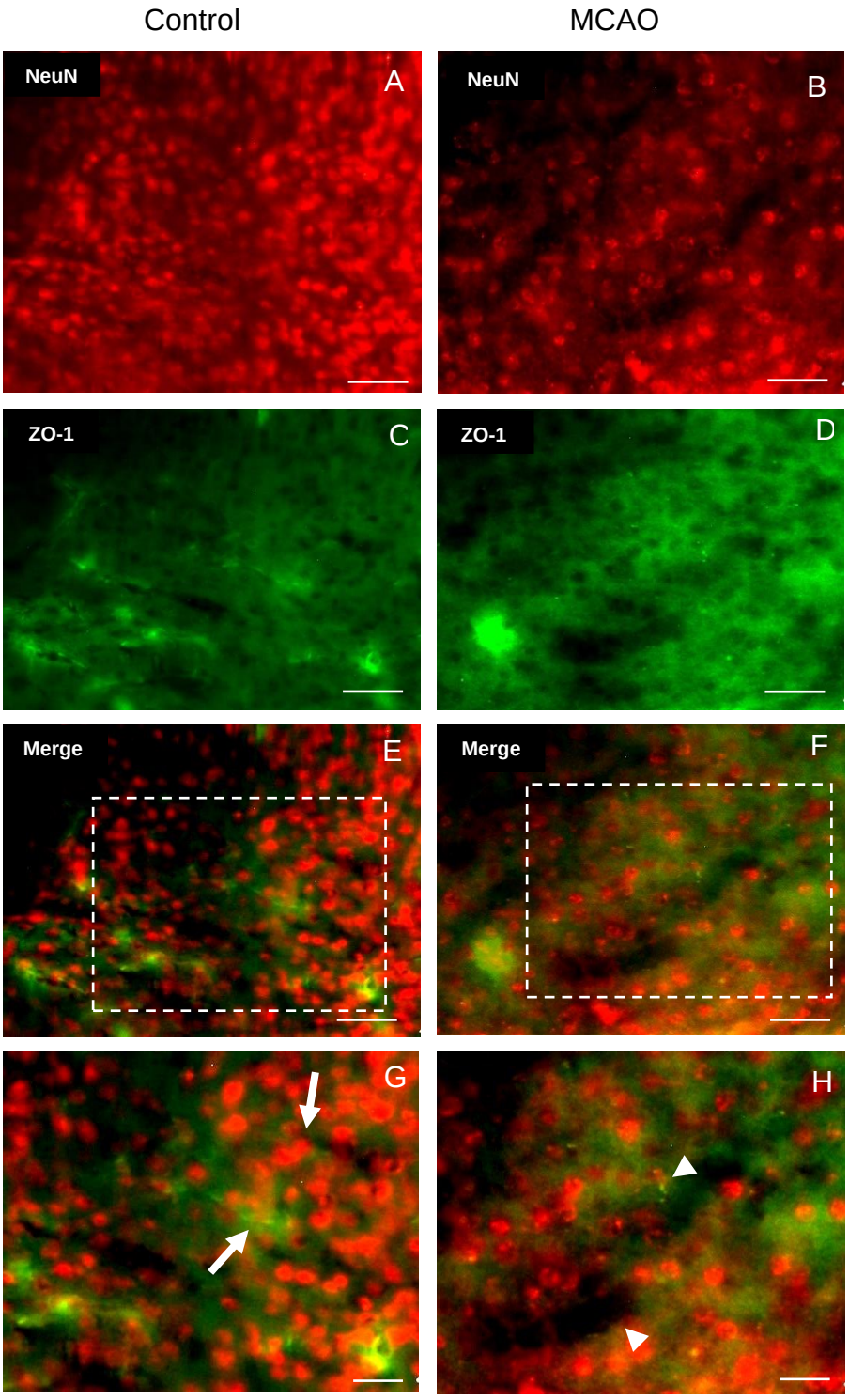

Figure 3.66 Representative photomicrographs showing double immunofluorescence staining for NeuN and ZO-1 with using anti- NeuN (A,B-red) and anti-ZO-1 (C,D-green) in the hippocampus in MCAO model of stroke (B,D,F,H) compared to control (A,C,EG). The labelled TJs with ant-ZO-1 are disrupted in stroke side (arrowheads) compared to the control (arrows). The labelled neuron cells with anti-NeuN show neuronal death following stroke (arrowheads) compared to control (arrows). (Scale bar=20um and 50um). (The images are taken at the level of Bregma-2.06mm). (Slice thickness=20um).

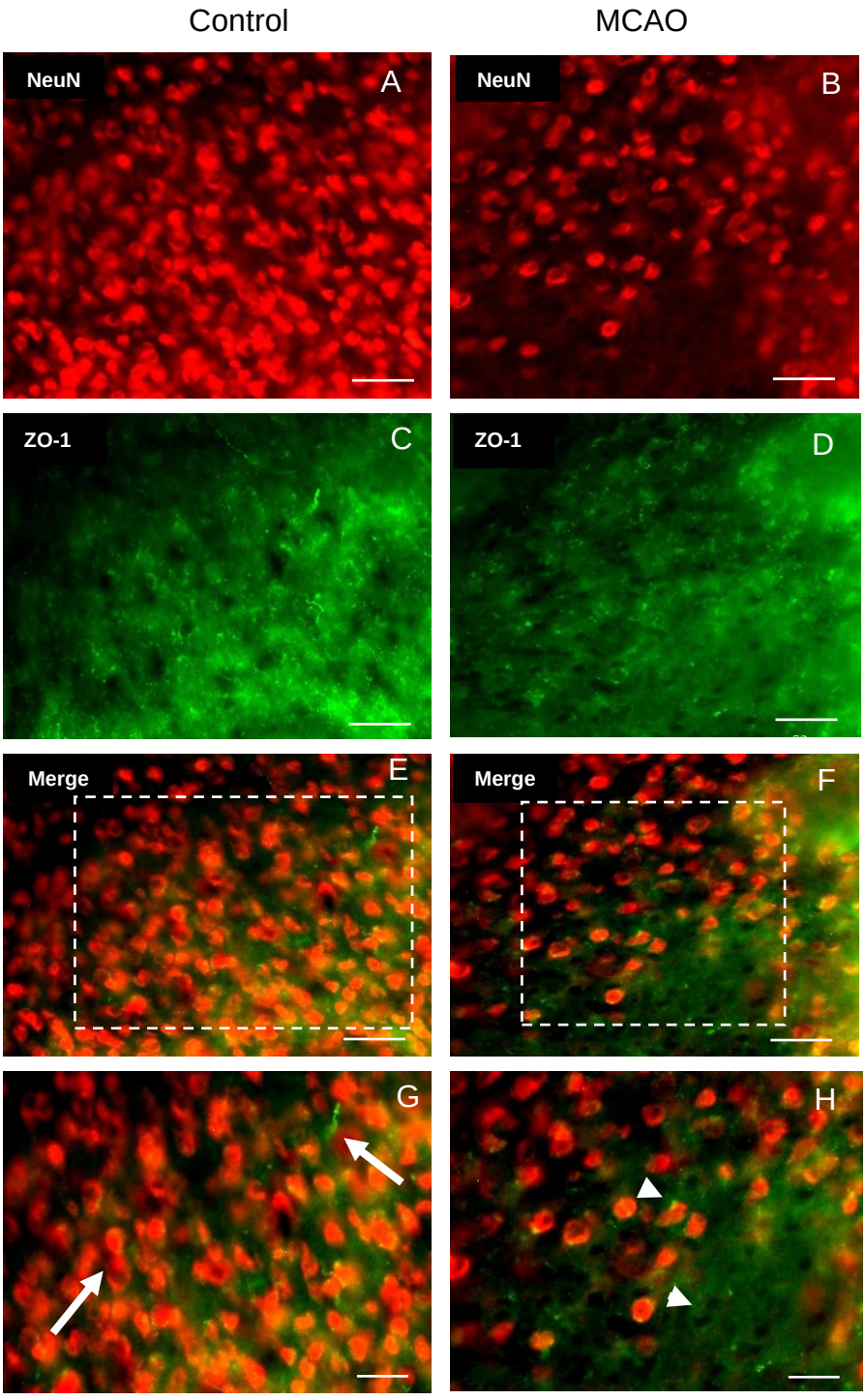

Figure 3.67 Representative photomicrographs showing double immunofluorescence staining for NeuN and ZO-1 with anti-NeuN (A,B-red) and anti-ZO-1 (C,D-green) in the cortical area in MCAO model of stroke (B,D,E,H) compared to control (A,C,EG). The labelled TJs with anti-ZO-1 are disrupted in stroke side (arrowheads) compared to the control (arrows). The labelled neuron cells with anti-NeuN show neuronal death following stroke (arrowheads) compared to control (arrows). (Scale bar= 20um and 50um). (The images are taken at the level of Bregma 1.54mm). (Slice thickness=20um).

3.2.6.3 MCAO induced astrogliosis and TJ disruption

To investigate that TJ proteins are not expressed in the astrocytes, dual-IF using anti-GFAP to label astrocytes correlated with anti-ZO-1 to label TJ was done. This was done also to investigate changes on astrocytes and TJ in MCAO mice brains in a comparison with control in both hippocampus and cortex area. The results confirmed that TJ protein (ZO-1) and astrocytes stained the separate profiles as was expected. The results showed that the labelled TJs with anti-ZO-1 are disrupted in stroke brain compared to the intact ones in the control brain in the hippocampus and cortex as revealed in Figure 3.68 and Figure 3.69 respectively. Furthermore, the labelled astrocytes and processes with anti-GFAP are more and thicker following focal ischaemia due to astrocytes activation compared to control in both cortex and hippocampus. These confirmed that focal ischaemia and reperfusion induced astrogliosis and TJ disruption as seen in the previous IHC results.

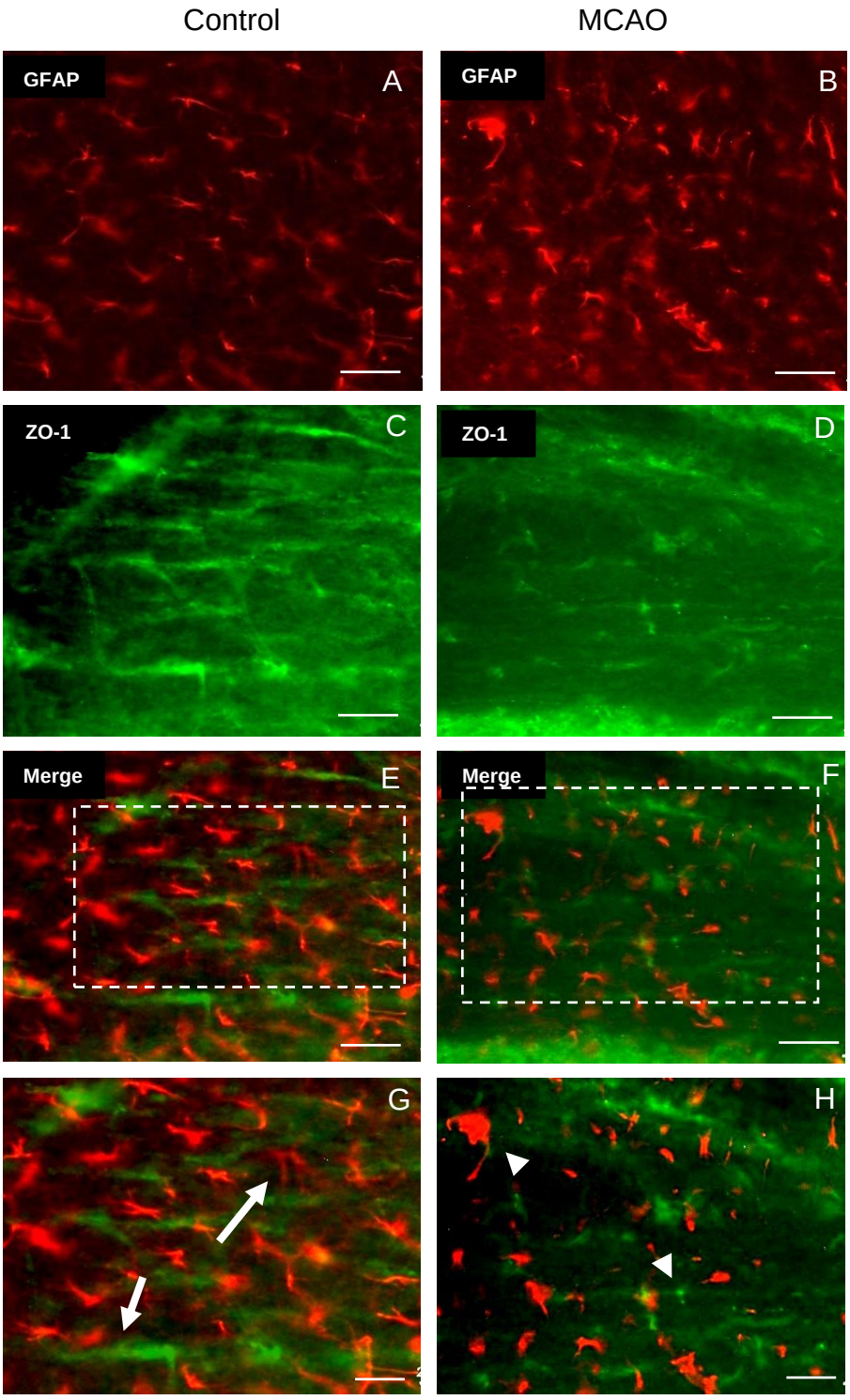

Figure 3.68 Representative photomicrographs showing double immunofluorescence staining for GFAP and ZO-1 with anti-GFAP (A,B-red) and anti-ZO-1 (C,D-green) in the hippocampus in MCAO model of stroke (B,D,F,H) compared to control (A,C,E,G). The labelled TJs with anti-ZO-1 showing disruption of TJs in stroke side (arrowheads) compared to the intact ones in the control (arrows). The labelled astrocytes and processes with anti-GFAP become more and thicker due to astrocytes activation following stroke (arrowheads) compared to control (arrows). (Scale bar= 20um and 50um). (The images are taken at the level of Bregma-2.06mm). (Slice thickness=20um).

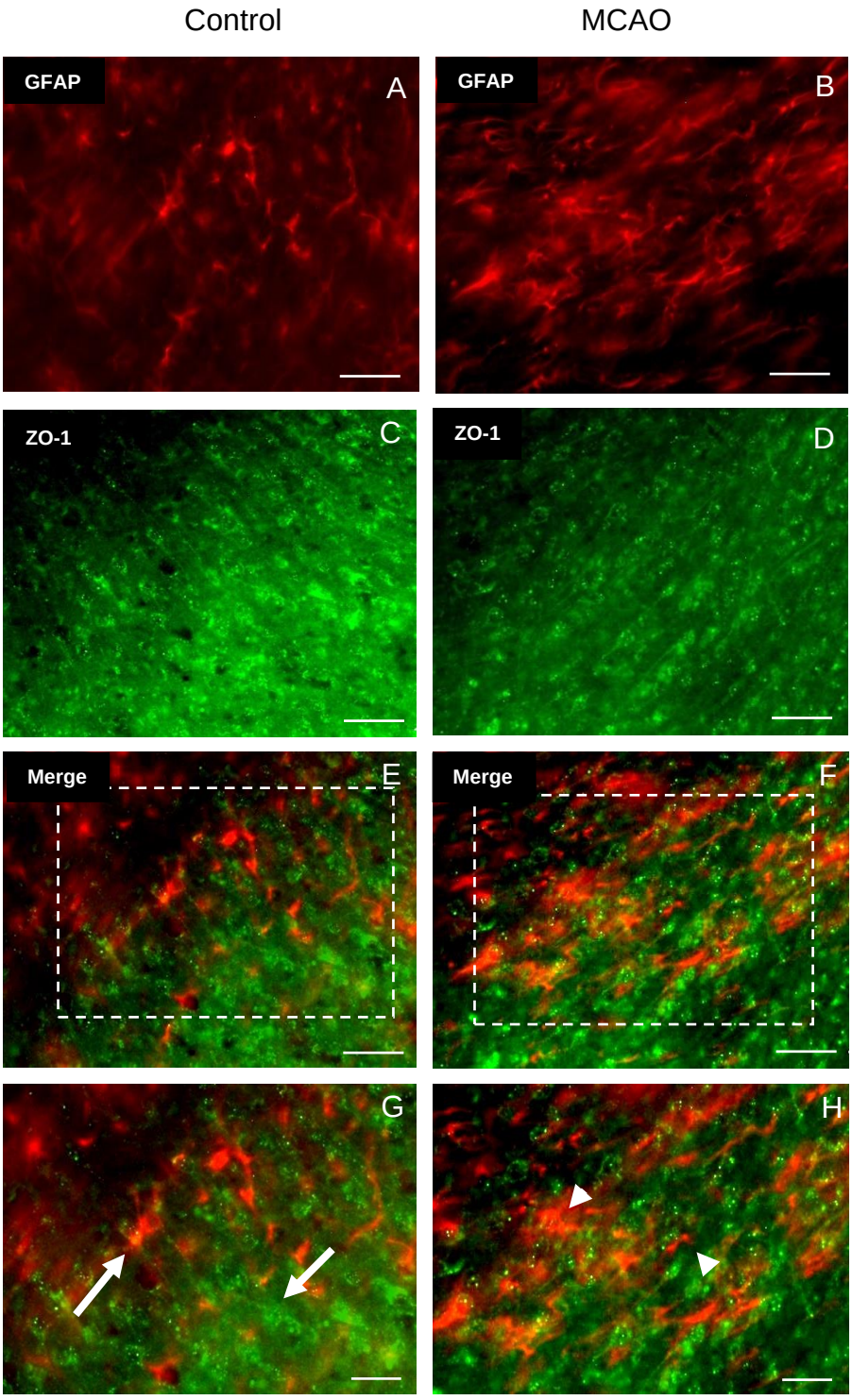

Figure 3.69 Representative photomicrographs showing double immunofluorescence staining for GFAP and ZO-1 with anti-GFAP (A,B-red) and anti-ZO-1 (C,D-green) in the cortical area in MCAO model of stroke (B,D,F,H) compared to control (A,C,E,G). The labelled TJs with anti-ZO-1 showing disruption of TJs in stroke side (arrowheads) compared to the intact ones in the control (arrows). The labelled astrocytes and processes with anti-GFAP become more and thicker due to astrocytes activation following stroke (arrowheads) compared to control (arrows). (Scale bar=20um and 50um). (The images are taken at the level of Bregma 1.54mm). (Slice thickness=20um).

3.2.7 Western blotting

To determine the protein concentrations in focal ischaemia mice as compared to corresponding control mice, six brain tissues from MCAO mice and six control mice were harvested, and GFAP, Occludin, ZO-1 and Claudin-5 expressions were quantified. To find out the total protein concentrations in samples, bicinchoninic acid assay (BCA) is used as shown in (Figure 3.70). A significant increase in the concentrations of protein in MCAO brains in a comparison with control brains (p=0.0001- paired Student's t-test, n=6) (Figure 3.71).

In the next section, the differences between the bands in control and MCAO tissues were demonstrated by utilising these particular antibodies (GFAP and TJ proteins). All of the protein bands were confirmed to be at the right molecular weights (kDa).

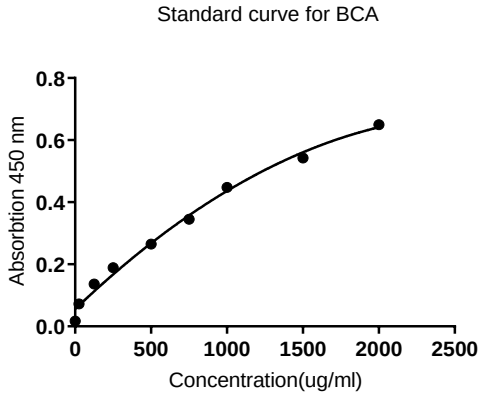

Figure 3.70 Standard dilution curve of bicinchoninic acid assay (BCA).

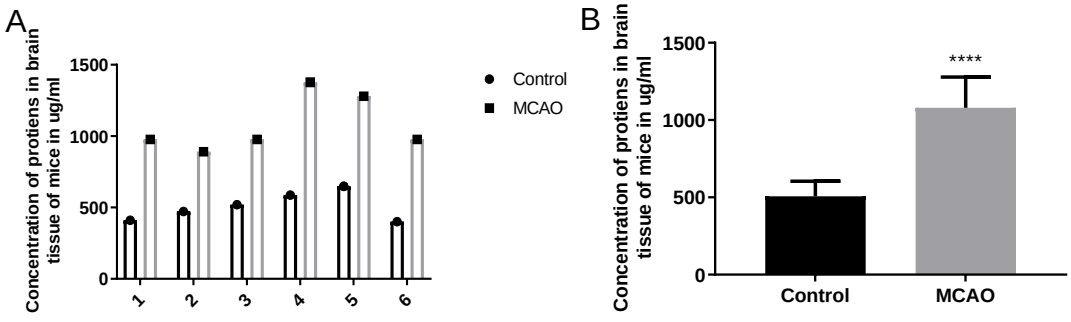

Figure 3.71 Quantitative analysis shows a very significant increase of proteins level (p=0.0001- paired Student's t-test, n=6) in MCAO as compared to control mice individually (n=6) (A) and as mean ± SD (B).

3.2.7.1 Protein expression of GFAP after ischaemia

GFAP as mentioned previously is a glial cells specific marker. To determine whether MCAO model induced astrocytes' activity and changes in GFAP expression after MCAO and reperfusion, WB was used. Quantitative analysis of GFAP expressions showed a significant rise in GFAP protein (p=0.031 - Wilcoxon matched-pairs signed rank test, n=6/ group,Figure 3.72) in hippocampus tissues in ischaemic mice brains compared to the control corresponding brains consistent with the IHC results. Normality and lognormality tests were done and confirmed that the data set is not normally distributed based on Kolmogorov-Smirnov test. Beta actin was used as a loading control.

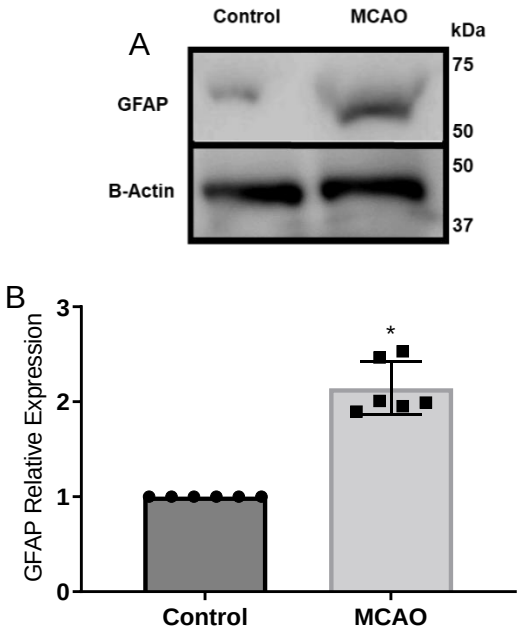

Figure 3.72 WB analysis of GFAP expression in the hippocampus of sham-operated and MCAO mice. A) GFAP band density is greatly increased in the hippocampus of MCAO models as compared to control. B) Quantitative analysis of GFAP band density relative to ß-actin shows a significant increase (*p=0.031, Wilcoxon matched-pairs signed rank test, n= 6/group) in GFAP expression in MCAO mice as compared to control. (Data presented as mean ± SD). (Control group was set as 1.0 as comparison to MCAO).

3.2.7.2 Protein expression of Occludin, ZO-1 and Claudin-5 after ischaemia

To determine whether focal cerebral ischaemia induced BBB breakdown, WB with antibodies to TJ proteins (Occludin, ZO-1 and Claudin-5) was used to quantify the difference in expression levels of these TJ of BBB proteins in MCAO ischaemic hippocampus tissues compared to the control hippocampus tissues.

The results showed that the expressions of the TJ proteins: {Occludin, ZO-1 and Claudin-5} were significantly decreased in MCAO model as compared to the corresponding control. Occludin, ZO-1 and Claudin-5 expression's levels in the hippocampus of MCAO model ischaemic were significantly lower in comparison to the corresponding control brains (n=6/ p=0.031 - Wilcoxon matched-pairs signed rank test, Figure 3.73), (n=6/ p=0.031, Figure 3.74) and (n=6/ p=0.031,Figure 3.75) respectively, consistent with the IHC results. Normality and lognormality tests were performed and showed that the data set is not normally distributed (Kolmogorov-Smirnov test). Beta actin was used as a loading control.

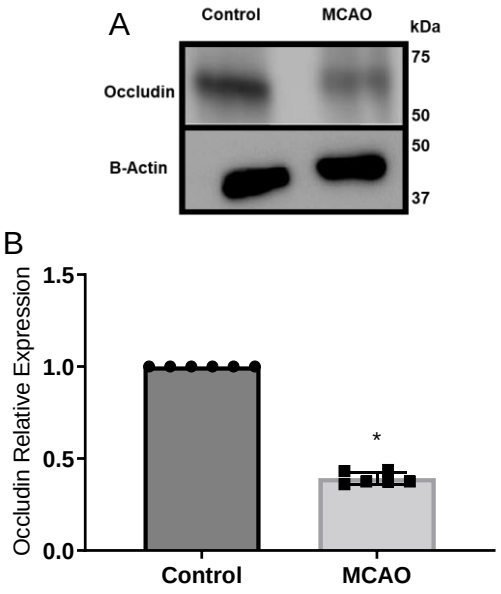

Figure 3.73 WB analysis of Occludin expression in the hippocampus of sham-operated and MCAO mice. A) Occludin band density is greatly decreased in the hippocampus of MCAO models as compared to control. B) Quantitative analysis of Occludin band density relative to ß-actin shows a significant decrease (*p=0.031, Wilcoxon matched-pairs signed rank test, n= 6/group) in Occludin expression in hippocampus area of MCAO mice as compared to control. (Data presented as mean ± SD). (Control group was set as 1.0 as comparison to MCAO).

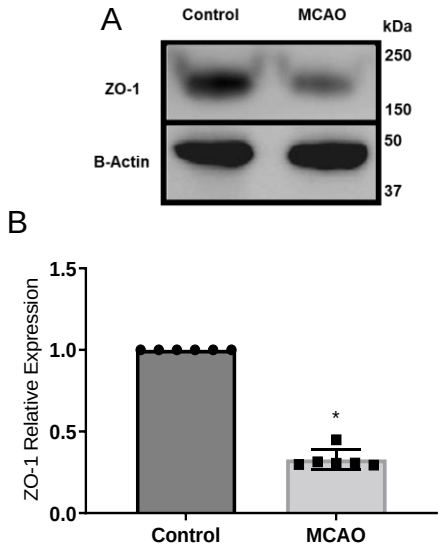

Figure 3.74 WB analysis of ZO-1 expression in the hippocampus of sham-operated and MCAO mice. A) ZO-1 band density is greatly decreased in the hippocampus of MCAO models as compared to control. B) Quantitative analysis of ZO-1 band density relative to ß-actin shows a significant decrease (*p=0.031, Wilcoxon matched-pairs signed rank test, n = 6/group) in ZO-1 expression in hippocampus of MCAO mice as compared to control. (Data presented as mean ± SD). (Control group was set as 1.0 as comparison to MCAO).

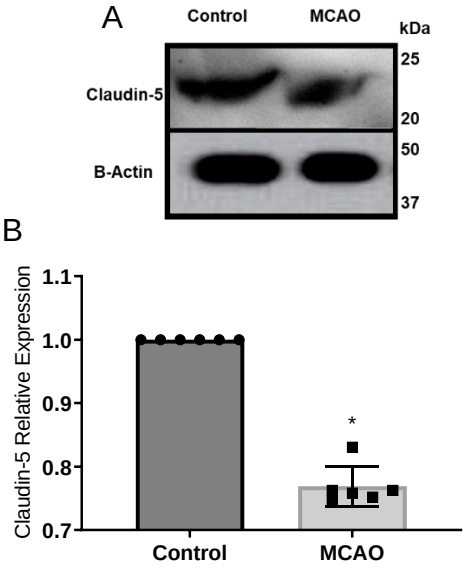

Figure 3.75 WB analysis of Claudin-5 expression in the hippocampus of sham-operated and MCAO mice. A) Claudin-5 band density is greatly decreased in the hippocampus of MCAO models as compared to control. B) Quantitative analysis of Claudin-5 band density relative to ß-actin shows a significant decrease (*p=0.031, Wilcoxon matched-pairs signed rank test, n = 6/group) in Claudin-5 expression in hippocampus area of MCAO mice as compared to control. (Data presented as mean ± SD). (Control group was set as 1.0 as comparison to MCAO).

3.2.8 Analysis of markers in blood serum

Ten serum samples (n=10) from control and (n=10) MCAO ischaemic models were measured. In this study, the concentration on serum samples was done as justified in BCCAO chapter.

3.2.8.1 GFAP

The levels of GFAP in serum samples from MCAO and control operated mice were quantified. The GFAP levels of serum of MCAO model increased significantly compared to sham samples (Unpaired Student's t-test, p=0.0060, n=10/group,Figure 3.76). The GFAP concentrations in stroke samples were 1.1-fold higher than the concentrations in the control.

3.2.8.2 Occludin

Occludin levels in serum samples from MCAO mice as compared to control were quantified**.** The quantitative statistical analysis showed a significant increase in Occludin levels in the MCAO ischaemia group compared to the control operated one with almost 1.1-fold of increase (Unpaired Student's t-test, p=0.0051, n=10/group) as shown in (Figure 3.77).

3.2.8.3 ZO-1

ZO-1 levels in serum samples from MCAO cerebral focal ischaemic model and controls were measured. The levels of ZO-1 in serum samples from MCAO models and controls increased significantly in the MCAO group as compared to the corresponding control one with 1.2-fold increase (Unpaired Student's t-test, p=0.0136, n= 10/group,Figure 3.78).

3.2.8.4 Claudin-5

The concentrations of serum Claudin-5 from control and MCAO ischaemic models were measured and compared. The data showed that the Claudin-5 concentrations in serum samples from MCAO ischaemic models increased significantly compared to the sham, (Unpaired Student's t-test, p=0.0137, n=10/ group,Figure 3.79). The Claudin-5 concentrations showed the highest fold of increase with 1.6-fold in stroke samples compared to the concentrations in control samples.

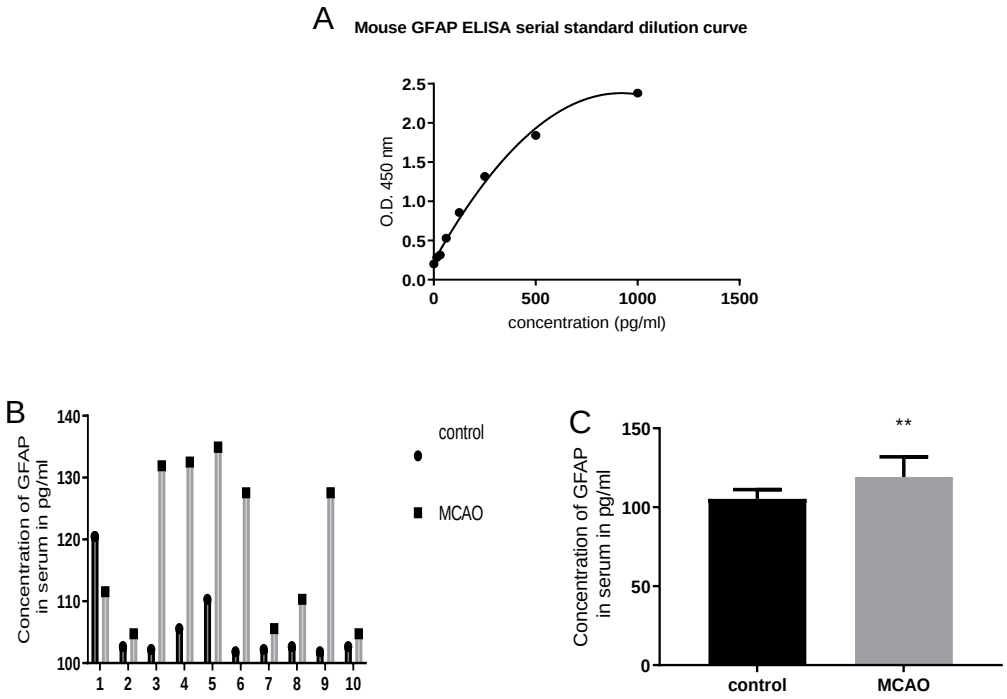

Figure 3.76 ELISA analysis showing serum GFAP levels between control and MCAO stroke models. A) Mouse GFAP serial standard dilution vs optimal density in 450nm. B) Serum GFAP levels in control and MCAO ischaemic models (n=10) individually. C) Significant increase in the serum protein levels in MCAO group compared to the control group (p=0.0060 -Unpaired Student's t-test).

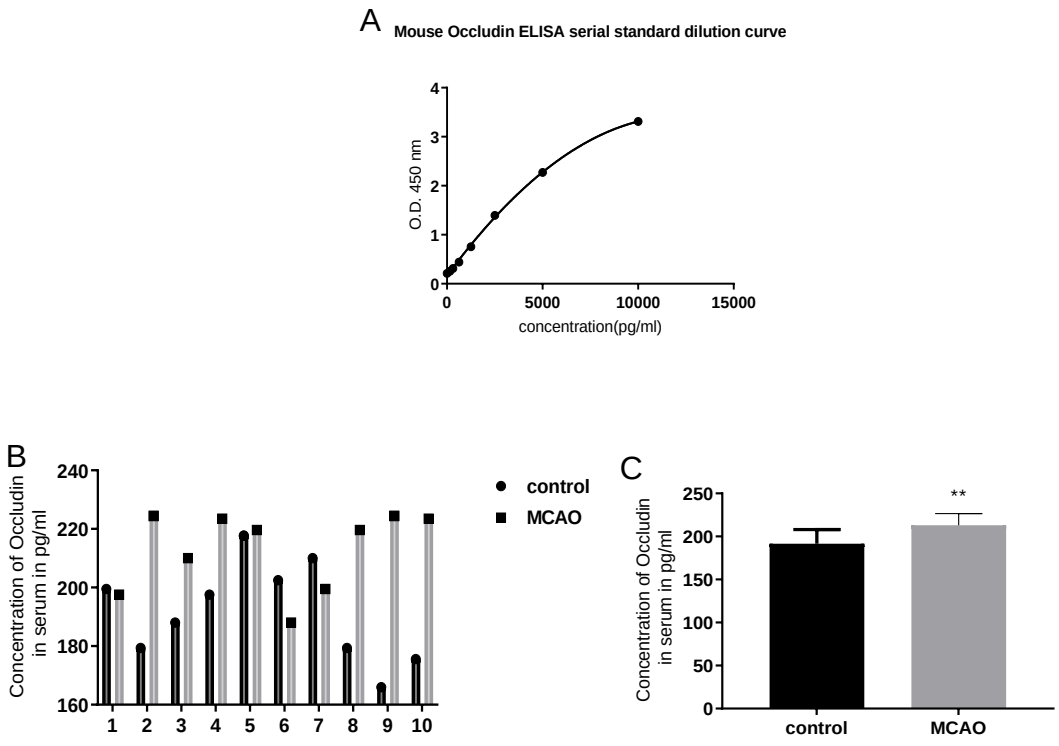

Figure 3.77 ELISA analysis showing serum Occludin levels between control and MCAO stroke models. A) Mouse Occludin serial standard dilution vs optimal density in 450nm. B) Serum Occludin levels in control and MCAO ischaemic models (n=10) individually. C) Significant increase in the serum protein levels in MCAO group compared to the control group (p=0.0051-Unpaired Student's t-test).

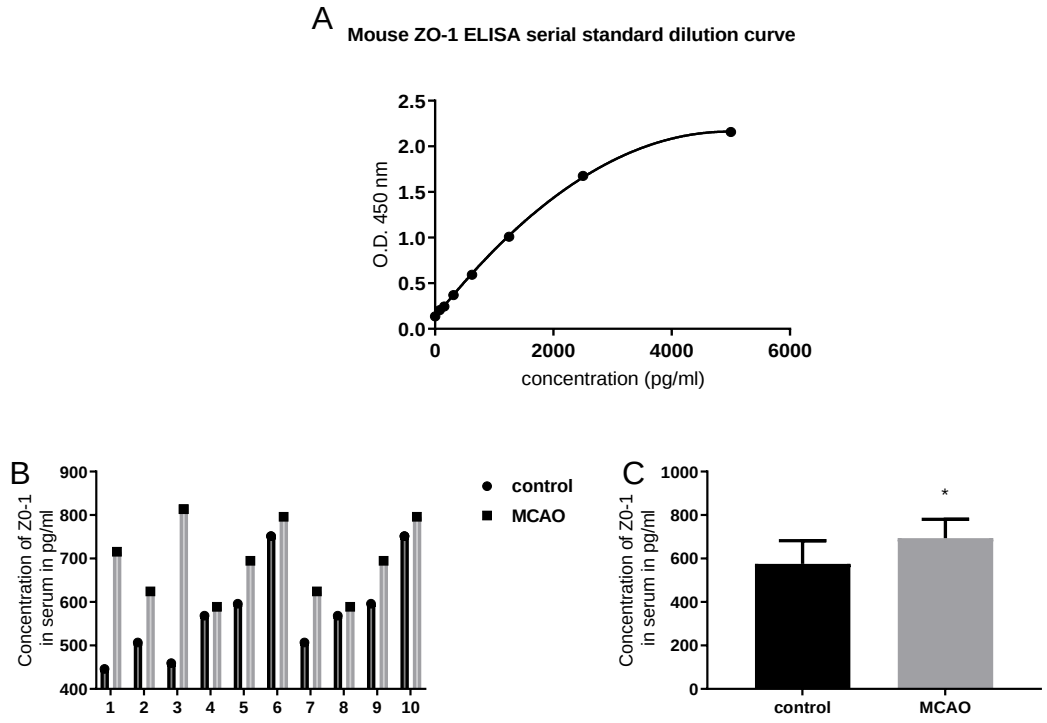

Figure 3.78 ELISA analysis showing serum ZO-1 levels between control and MCAO stroke models. A) Mouse ZO-1serial standard dilution vs optimal density in 450nm. B) Serum ZO-1 levels in control and MCAO ischaemic models (n=10) individually. C) Significant increase in the serum protein levels in MCAO group compared to the control group (p=0.0136-Unpaired Student's t-test).

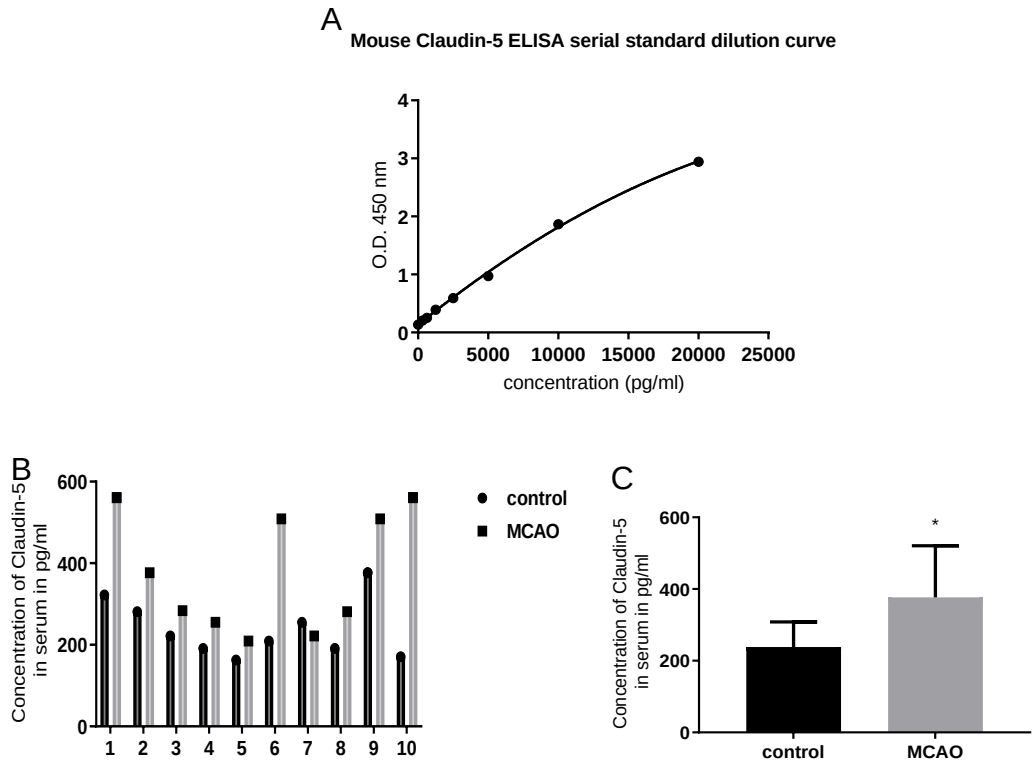

Figure 3.79 ELISA analysis showing serum Claudin-5 levels between control and MCAO stroke models. A) Mouse Claudin-5 serial standard dilution vs optimal density in 450nm. B) Serum Claudin-5 levels in control and MCAO ischaemic models (n=10) individually. C) Significant increase in the serum protein levels in MCAO group compared to the control group (p=0.0137-Unpaired Student's t-test).

3.2.9 Correlation between expression of markers in serum and brain

This section examined the correlation between circulating serum biomarkers determined by ELISA and the expression of corresponding biomarkers in the hippocampus tissues in the brain determined by WB after MCAO. Regarding GFAP, results of the Spearman correlation and results of the simple linear regression indicated no association between GFAP expression and serum GFAP level after MCAO ($r = -0.257$, $p=0.658$) and (95% confidence interval, R SQUARED = 0.028, $p=0.771$) respectively (Figure 3.80-A).

Furthermore, it has been examined whether serum TJ proteins (Occludin, ZO-1 and Claudin-5) levels were correlated with the WB results after MCAO. Results of the Spearman correlation analysis and simple linear regression analysis indicated that there was a negative strong significant association between serum Occludin level and the Occludin expression in hippocampal tissue in the brain ($r = -1.00$, $p=0.003$) and (95% confidence interval, R SQUARED = 0.950, $p=0.001$) respectively as shown in (Figure 3.80-B). Thus, the results indicated that Occludin level was a significant predictor for Occludin expression in the brain in this model.

On the other hand, the results of ZO-1 indicated no association between ZO-1 WB expression and serum ZO-1 level after MCAO ($r = 0.086$, $p=0.919$) and (95% confidence interval, R SQUARED = 1.157e-006, $p=0.998$) (Figure 3.80-C). Similarly, results of Claudin-5 showed no association between Claudin-5 WB expression and serum Claudin-5 level after MCAO ($r = 0.200$, $p=0.714$) and (95% confidence interval, R SQUARED = 0.323, $p=0.239$) as displayed on (Figure 3.80-D).

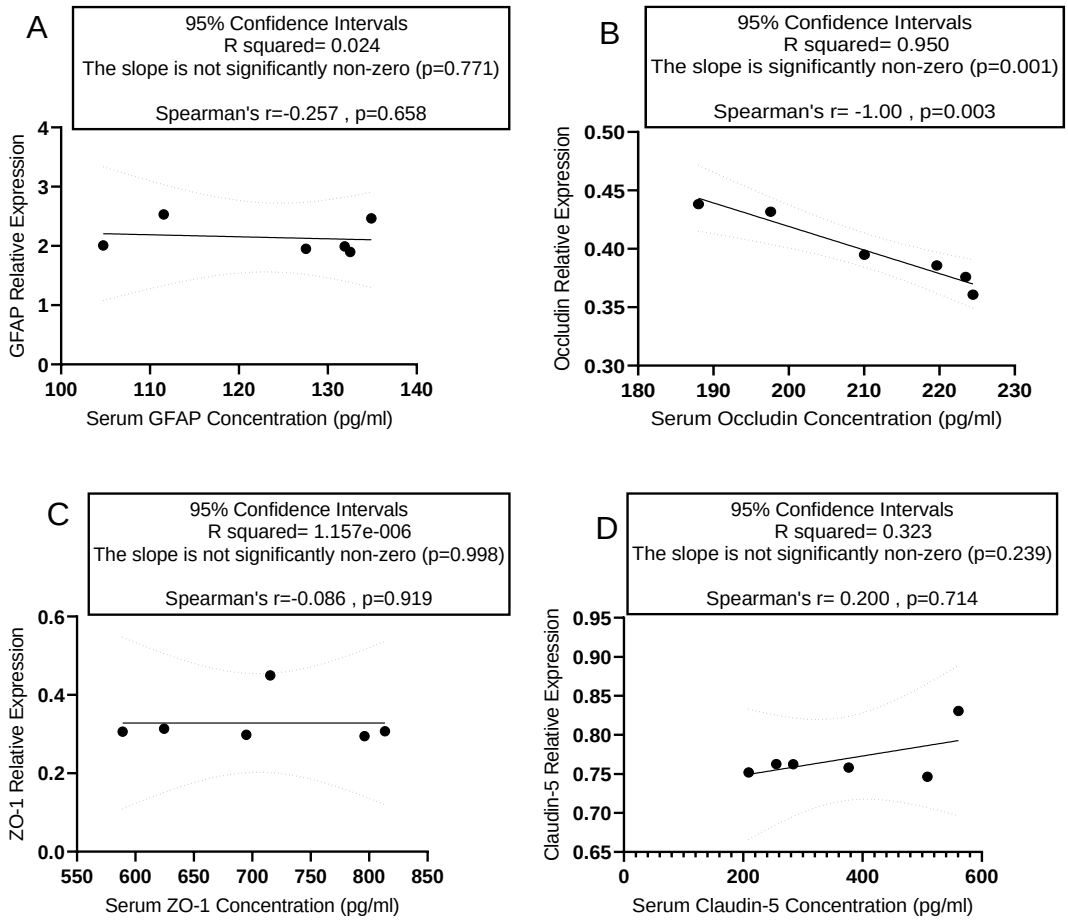

Figure 3.80 Correlation analysis between serum A: GFAP, B: Occludin, C: ZO-1 and D: Claudin-5 levels and these proteins' expressions in hippocampal tissue of the brain in MCAO using Spearman correlation and simple linear regression. Proteins expressions in hippocampal brain tissue of brain were quantitatively assessed by WB. Serum proteins levels were quantified by ELISA. A: Spearman correlation analysis and simple linear regression analysis showing no association between serum GFAP level and GFAP expression in hippocampal tissue of the brain; (r = -0.257, *p*=0.658) and (R SQUARED = 0.028, p=0.771) respectively. B: Spearman correlation and simple linear regression showing a significant negative correlation between serum Occludin level and the Occludin expression in hippocampal tissue in the brain; (r =- 1.00, p=0.003) and (95% confidence interval, R SQUARED = 0.950, p=0.001) respectively. C: Spearman correlation analysis and simple linear regression analysis showing no association between serum ZO-1 level and ZO-1 expression in hippocampal tissue of the brain; (r = 0.086, p=0.919) and (R SQUARED = 1.157e-006, p=0.998) respectively. D: Spearman correlation analysis and simple linear regression analysis showing no association between serum Claudin-5 level and Claudin-5 expression in hippocampal tissue of the brain; (r = 0.200, p=0.714).and (R SQUARED = 0.323, p=0.239) respectively.

3.2.10 Summary and main findings

- Neuronal cell death in specific areas of the brain in BCCAO and MCAO stroke models.
- Astrogliosis in the hippocampus of both BCCAO and MCAO stroke models.
- TJ disruption in the hippocampus in stroke models.
- Significant increase in GFAP and a significant decrease in ZO-1, Occludin and Claudin-5 expressions relative to ß-actin in BCCAO and MCAO stroke mice brains compared to the sham operated brains.
- Significant increase in serum circulating biomarkers (GFAP, Claudin-5, ZO-1 and Occludin) levels in BCCAO and MCAO mice compared to the corresponding control mice.
- Serum GFAP and Occludin levels in BCCAO were correlated with their expressions in brain tissue, whereas, in MCAO only serum Occludin level was correlated with its expression in brain tissue.

3.2.11 Discussion

The present study is the first systematic study investigating detailed changes in neuronal, glial cells and BBB junctional proteins in the hippocampus in the forebrain using both IHC and WB following BCCAO as well as MCAO and reperfusion in C57BL/6J mice. This novel study also examined the expression of GFAP together with three BBB junctional proteins (Occludin, Claudin-5 and ZO-1) in the hippocampus and correlated these proteins expressions in the brain using quantitative WB with their blood serum concentrations using quantitative ELISA in both models.

Over the last four decades, different animal stroke models have been established aiming to identify the mechanisms of cerebral ischaemia and develop a new therapeutic strategy. The BCCAO model for global cerebral ischaemia has been used as recent previous study in our lab (Khan et al., 2018) and others earlier work (Yang et al., 1997; Murakami et al., 1998) and have reported that C57BL/6 mice subjected to BCCAO developed selective neuronal death in the forebrain including hippocampus and cortex with a higher survival rate. On the other hand, models that occlude MCA can mimic human ischaemic stroke (Tamura et al., 1981; Koizumi et al., 1986; Longa

et al., 1989). Therefore, the MCAO model for focal cerebral ischaemia has been used as this is known to produce neuronal damage in the cortex, hippocampus and striatum both in mice and rats (Rao et al., 2001; McColl et al., 2007; Ketheeswaranathan et al., 2011). Corresponding with other studies using the MCAO model (Butler et al., 2002; McColl et al., 2004), this study also consistently detected neuronal degeneration not only in the striatum but also in M2 and M1 motor cortex following 1 hour MCAO and 24 hours reperfusion in this study as reported also in the previous studies in our lab (Ketheeswaranathan et al., 2011).

The effect of ischaemia on the studied groups was noticeable, although the damage amount was more remarkable in BCCAO than in MCAO. The experiments demonstrated the death of neuronal cells in the M1 and M2 motor cortex, somatosensory cortex, granular insular cortex and hippocampus in the BCCAO model and reperfusion. In agreement, a previous study in our lab (Khan et al., 2018) observed that these mice produced the consistent and selective loss of neurones in the hippocampus and the motor and somatosensory cortex. In MCAO, the quantitative immunohistochemical analysis suggested that NeuN labelled neuron cells in the striatum, M1 and M2 cortex are reduced significantly in ischaemic brains compared to sham-operated brains. The reduction in the number of neuron cells in the stroke groups was due to the high sensitivity of neurons to ischaemic effects and the blood supply reduction, causing neuronal death in these areas (Kudabayeva et al., 2017). While in BCCAO models, six control brains and six stroke induced brains were used during this study, however, in MCAO only three control brains and three stroke induced brains were used due to time limitations and COVID-19 restrictions which negatively contributed to the number of experiments conducted in the lab. Ideally, additional replicates would be required to increase the power of statistics.

Additionally, this study reported the astrocyte changes after cerebral ischaemia injury. Interestingly, astrogliosis in the hippocampus was detected in both models with IHC and confirmed with quantitative analysis of GFAP positive cell profiles. Astrocytes play an important and major role in the maintenance and formation of the brain cytoarchitecture, maintaining the supply of energy to neurones, controlling synaptic function and neurotransmitters recycling (Papa et al., 2014). In addition, astrocytes interact with brain blood vessels' endothelial cells through their end feet and regulate the brain blood flow as well as control BBB (Mishra et al., 2016). Quantitative IHC

analysis revealed a significant increase in the astrocytes processes and astrocytes cells in the hippocampus following BCCAO consistent with a previous study in our lab using these mice (Khan et al., 2018). Similar results have been observed in MCAO mice. This may be due to glial cells activation following ischaemia (Pekny et al., 1999). GFAP up-regulation is one of the most important features of astrogliosis; an abnormal increase in the astrocytes number following the ischaemia results in the glia cells's activation (Pekny et al., 1999). Following cerebral ischaemia, processes of astrocytes, as identified by GFAP IHC, appeared to have become thicker and rearranged, which is an indication of reactive gliosis (Pekny and Nilsson, 2005; Burda and Sofroniew, 2014; Papa et al., 2014; Choudhury and Ding, 2016). This may lead to CNS circuit dysfunction, defining maladaptive synaptic plasticity in the glial-neuronal network and causing abnormal synaptic transmission (Papa et al., 2014). The results confirmed previous studies that reported the altered morphology of astrocytes directly after stroke is related to the increased expression of GFAP (Lebkuechner et al., 2015). This includes the upregulation of GFAP which leads to significant hypertrophy of astrocyte cell bodies and processes (Silver and Miller, 2004; Sofroniew, 2009).

The present study also investigates changes in TJ proteins in both ischaemic models using IHC as a very few studies on these proteins were performed using either of these models. By comparing the IHC results between sham and ischaemic stroke models, the results showed that there are considerable disruptions of BBB TJ in the ischaemic brains compared to the sham brains. During the ischaemic stroke, the BBB is damaged, which is a result correlated with alternations in the distributions and concentrations of TJ proteins and other BBB components (Lasek-Bal et al., 2020).

A previous study using brain microvessl endothelial cells showed that dissociation of ZO-1 from the TJ complex has been linked to increased permaeability of BBB suggesting that the ZO-1 tranmembrane protein connection is crucial for TJ stablitiy and function (Fischer et al., 2002). Pan et al. (2017) have reported loss of Occludin from microvessles after ischaemia using IHC. Similarly, disruptions in Claudin-5 expression are linked to a large increase in paracellular solute permeability in previous experimental rat MCAO stroke models using IHC (Liu et al., 2012).

This present study assessed brain damage using the antibody of specific pericytes cell markers (PDGFR and NG2) in murine stroke models as compared to sham operated mice. The findings were consistent with other previous results (Arimura et

al., 2012) as the stained pericytes showed dilatation and morphological changes with loss of cell bodies in cortical and hippocampal areas in the stroke brains compared to control brains. This study also investigated quantitative analysis of PDGFR and NG2 labelled pericytes cells. The results showed that cerebral ischaemia significantly decreased the pericytes profiles in the hippocampus in the stroke brains compared to the control brains. In agreement with this study result, a previous study by Fernández-Klett et al. (2013) also reported that the density of PDGFR cells in acute stroke lesions was reduced significantly.

This study also determined brain damage using the antibody of specific microglia cells (IBA-1) in murine stroke models as compared to sham operated mice. The results showed that the IBA-1 labelled cells and processes are significantly more expressed in the hippocampus of stroke mice than that in the controls due to microglia's activation following stroke. In agreement, a recent study revealed that the amount of IBA-1-immunoreactive microglia cells were significantly higher in both 15 min and 5 min occlusion of BCCAO in all hippocampal regions (Lee et al., 2019).

This study investigated the expression of the TJ proteins within the endothelial cells profile in both stroke models using double immunohistochemical staining by incubation of brain sections with primary antibodies against (NeuN, GFAP and CD31) correlating with TJ proteins: Occludin, ZO-1 and Claudin-5. There are not sufficient studies examining the changes of TJ of endothelial cells of BBB after both global and focal ischaemia comparing it with control using TJ proteins and correlating that with endothelial cell marker (CD31). First, the present study investigated double labelling of immunoreactive CD31 antibodies with TJ proteins. Then, double labellings of immunoreactive of NeuN and GFAP antibodies with TJ proteins were investigated. As expected, the results confirmed that TJ proteins are localised in CD31 labelled endothelial cells and not in the NeuN and GFAP labelled neurones and astrocytes respectively. Ghori et al. (2017) showed by immunostainings of TJ and endothelial cells, decrease the expression of Claudin-5 and Occludin with endothelial cell loss labelled with CD31 following MCAO compared to unaltered TJ in control. This present study also revealed similar results in the cortical and hippocampal areas in BCCAO and MCAO ischaemic mouse brains indicating that TJs are likely disrupted under ischaemic conditions as well as confirming that Occludin, ZO-1, Claudin-5 are expressed within the endothelial cell profile.

This study has also assessed the expressions of the major glial (GFAP) and TJ proteins (ZO-1, Occludin, and Claudin-5) in the hippocampus of the global ischaemic brains and focal ischaemic brains using WB. In support of the IHC results, GFAP, ZO-1, Occludin and Claudin-5 expressions relative to ß-actin show significant changes in the hippocampus in BCCAO and MCAO stroke mouse brain compared to the sham operated brains. GFAP is expressed by astrocytes and the WB shows that the expression of GFAP in the hippocampus in both models' brains is increased significantly compared to the control mice brains confirming the astrocyte astrogliosis due to astrogliosis which also correlates well with the glial cell's changes in the IHC observation. The significant reduction in TJ proteins expressions following focal and global ischaemia observed in this study confirming the IHC staining results and was consistent with previously reported findings (Ren et al., 2015), which indicates that the expression levels of ZO-1, Occludin and Claudin-5 using WB are decreased in rat brain tissue in MCAO of ischaemia, however, no significant changes have been reported in that previous study in Claudin-5 and ZO-1 (Ren et al., 2015). Recently, a study has been done on a rat model of focal cerebral ischaemia to examine variations in the TJ proteins including ZO-1, Occludin and Claudin-5 (Jiao et al., 2011). The levels of these proteins expression were detected in that study by WB with extracted microvessel fragments of rat brain tissues and the study has shown that the levels of ZO-1, Occludin and Claudin-5 are significantly decreased in brain microvessels in all of the ischaemic reperfusion groups (Jiao et al., 2011). Moreover, in alignment with this study findings, a previous study by Shi et al. (2017) and Liu et al. (2018) observed a decrease in the expression level of Occludin in rat brains after ischaemia in MCAO. Yang and Rosenberg (2011) have shown a significant decline of Claudin-5 expression in rat brains after MCAO and reperfusion. Therefore, the present study findings strongly suggest that the disruption of TJ is associated with increased BBB breakdown following stroke.

This novel preclinical study confirms the increased levels of GFAP in blood mice after BCCAO and MCAO. According to a previous literature study, the serum level of GFAP seems to be the ideal stroke specific biomarker (Schiff et al., 2012). Multiple clinical research studies investigated the role of serum GFAP as a diagnostic tool for ischaemic stroke patients by showing increased GFAP levels in ischaemic patients (Ren et al., 2016; Luger et al., 2017). The present study confirmed a significant

increase in the serum GFAP level in the ischaemic mice as compared to control ones. Regarding the level of Occludin following focal and global ischaemia, the major finding is that the ischaemic mice groups had significantly higher Occludin serum levels as compared to matched control groups. Previous works have also observed higher serum levels of Occludin within the first 24 hours after ischaemia in rat MCAO (Pan et al., 2017), thus strongly supporting this present study's findings. Pan et al. (2017) have also investigated the concentrations of Occludin and Claudin-5 in rat serum following MCAO using ELISA and have shown that the blood levels of Claudin-5 did not change considerably during the first 4.5 hours of cerebral ischaemia. However, the present study reported a significant increase in the serum level of Claudin-5 in both stroke models as compared to the controls. The present study also showed a significant increase in the ZO-1 level in serum of both stroke models compared to the respective controls. This increase in ZO-1 concentration in blood is consistent with the disarrangement of the ZO-1 in the TJs in the brain suggesting that BBB opening and damage after ischaemia lead to the release of these proteins into the blood (Petty and Wettstein, 2001). It is worth noting that, the significant difference in terms of concentrations of studied biomarkers was more prominent after BCCAO than MCAO, which might be explained by the difference in the amount of damage. However, this needs further investigation.

The correlation analysis in this study interestingly showed a significant correlation between circulating GFAP and the expression of this protein in the brain of BCCAO mice as determined by Spearman correlation. Moreover, this study obtained a negative good correlation between circulating Occludin and the expression of Occludin in the brain after BCCAO and MCAO. It suggests that the observed blood Occludin levels after BCCAO and MCAO may represent the TJ disruption by releasing Occludin from the ischaemic brain, which might be closely related to early BBB disruption confirming earlier results in rat MCAO (Liu et al., 2009).

Further studies using these biomarkers and these models are required to understand the mechanisms of ischaemia-induced BBB damage.

In summary, the present study findings suggest that GFAP and TJ proteins levels might be useful biomarkers for differentiating between ischaemic stroke and controls and can be translated into identifying acute stroke patients from mimics.

Chapter 4 CT and MRI imaging biomarkers in clinical samples

4.1 Retrospective study - Can quantitative CT and MRI biomarkers improve the prediction of outcomes after mechanical thrombectomy? A cross-sectional pilot study

This chapter presented a pilot study, which aimed to test a hypothesis that the absolute values of CTP and MRI imaging biomarkers can improve the prediction of outcomes in MT. This can inform a longitudinal study design in the future by correlating the imaging results with blood biomarkers in MT. However, due to the small sample size, only a comparison of CTP biomarkers, MRI ADC values, the volume of infarct and functional outcomes between the MT group and the non-MT group was conducted.

This study showed if the CTP markers are significantly different between ischaemic and non-ischaemic side as well as between the MT group and the non-MT group (as per section 2.2.3 and section 2.2.4).

Furthermore, this chapter presented as MRI analysis comparing the ischaemic side and non-ischaemic side using ADC values as well as quantifying the volume of infarct in the MT group and the non-MT group (as per section 2.2.6 and section 2.2.7).

Lastly, the functional outcomes were determined and compared between the two groups (as per section 2.2.8).

Data were obtained from two groups: a group who had been treated with MT (MT group) and a group who had not been treated with MT (non-MT group).

4.1.1 Computed tomography perfusion (CTP) scan results

4.1.1.1 Imaging biomarkers in the MT treated group

Altogether, 15 patients were identified. Typical images from a patient with an ischaemic stroke are shown in Figure 4.1. In the CTP, mean (SD) in ischaemic and non-ischaemic WM and GM areas are presented in Table 4-1. All patients have a reduced CBF in the ischaemic WM and GM areas (ratio from 0.40 to 0.99) and (ratio from 0.11 to 0.66) respectively. A significant difference between CBF values in ischaemic and non-ischaemic WM areas was seen (Paired Student's t-test - p= 0.0001). Moreover, CBF values in GM areas on ischaemic side was significantly lower compared to non-ischaemic side with p<0.0001. CBV values in ischaemic WM were lower than the one in non-ischaemic side with no significant variations (p= 0.1218). Interestingly, 44% have an increased CBV (ratio from 1.26 to 2.33) and 66% have a reduced CBV (ratio from 0.28 to 0.90) in ischaemic WM areas as shown in Figure 4.2. Whereas 70% have an increased CBV (ratio from 1.02 to 2.97) and 30% have a reduced CBV (ratio from 0.11 to 0.46) in ischaemic GM areas without any significant differences (p=0.479). Regarding MTT, all patients have an increased MTT in the ischaemic WM and GM areas (ratios from 0.31 to 2.48 and 0.57 to 16.72) respectively. Interestingly, the significant difference in MTT was seen only in GM areas (p=0.0003) as displayed in Figure 4.2. An example of a CT scan for one MT patient is shown in Figure 4.3.

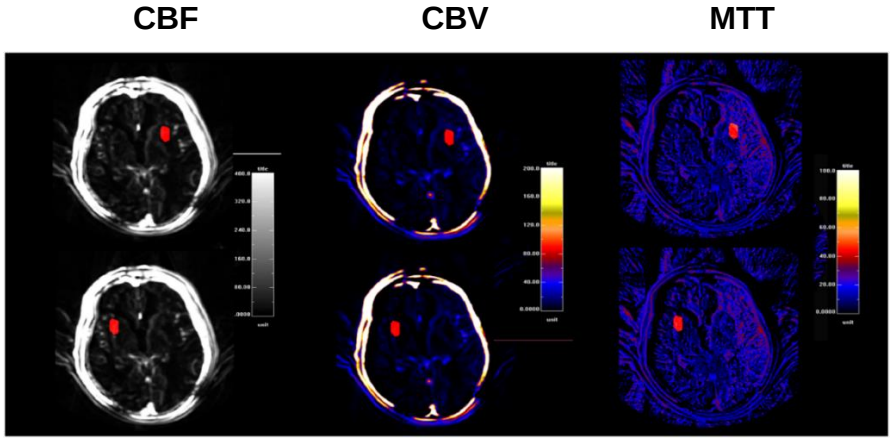

Figure 4.1 CTP CBF (left), CBV (middle) and MTT (right) maps in a typical ischaemic stroke patient. Red areas show the location of ROIs in WM ischaemic (upper row) and non-ischaemic areas (bottom row).

Table 4-1 A comparison of CTP parameters between ischaemic and non-ischaemic WM and GM areas in the MT group (n=15). Data are shown as mean (SD).

	Tissue (WM or GM)	Ischaemic area			Non-ischaemic area		
		CBF (ml/min/100g)	CBV (ml/100g)	MTT (Second)	CBF (ml/min/100g)	CBV (ml/100g)	MTT (Second)
Mean (SD)	WM	20.94 (12.61)	2.24 (1.02)	8.29 (4.77)	29.76 (16.18)	2.90 (1.41)	7.19 (4.12)
	GM	16.09 (9.14)	2.33 (1.38)	10.21 (6.31)	61.40 (11.36)	2.02 (1.13)	1.99 (1.17)

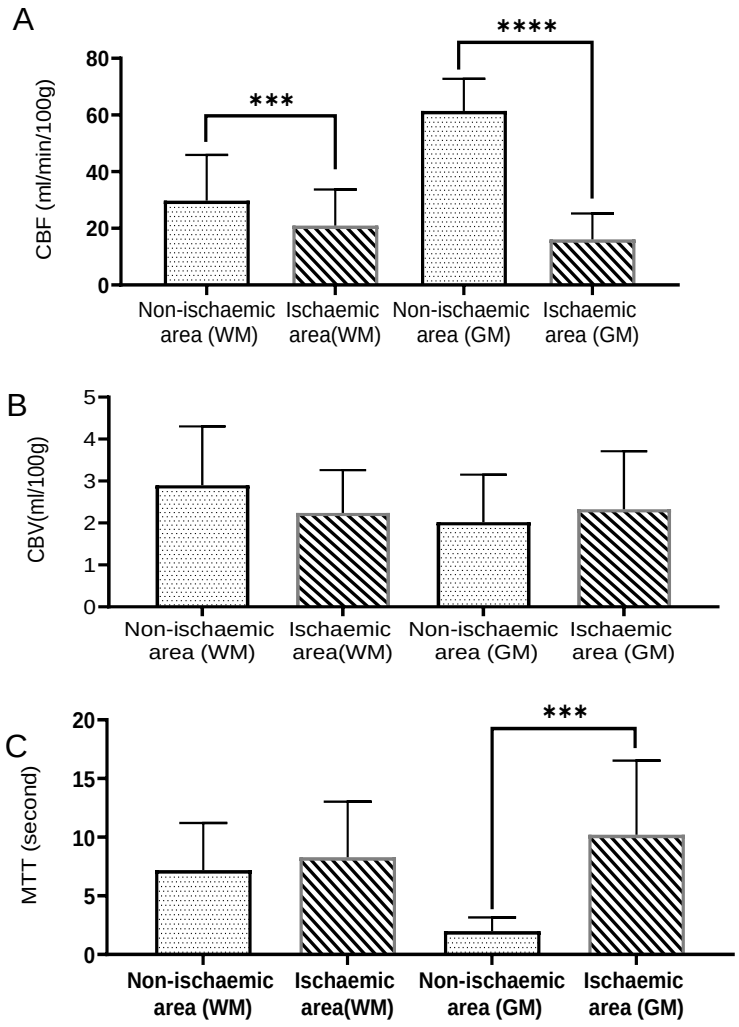

Figure 4.2 CTP CBF (A), CBV (B) and MTT(C) values in ischaemic and non-ischaemic WM and GM areas in the MT group (n=15), (Paired Student's t-test - A: CBF in WM p=0.0001 and in GM p<0.0001), (C: MTT in GM p=0.0003).

A

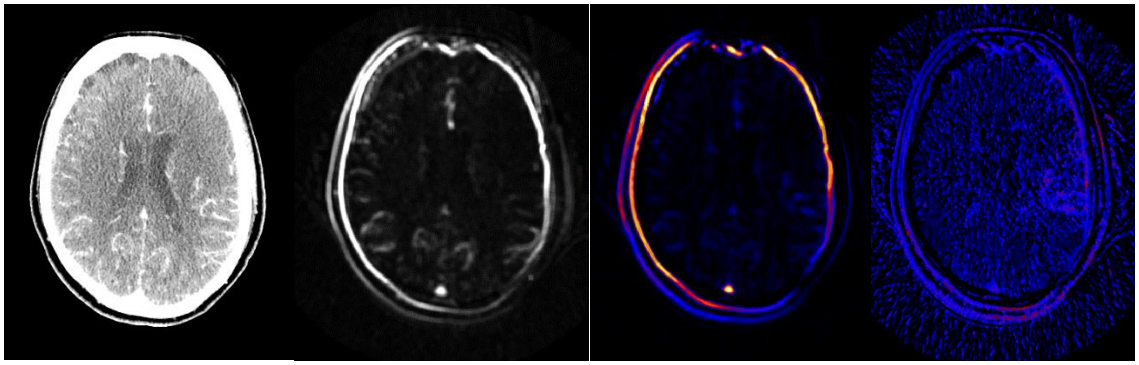

B

	CBF(WM) ml/min/100g	CBV(WM) ml/100g	MTT(WM) seconds
Ischaemic side	11.37	1.74	9.16
Non-ischaemic side	20.24	2.27	6.72

C

	CBF(GM) ml/min/100g	CBV(GM) ml/100g	MTT(GM) seconds
Ischaemic side	35.42	2.90	4.92
Non-ischaemic side	53.35	5.76	4.00

Figure 4.3 A) CTP images of right-side MCA infarct in a patient, who received MT directly after the CTP scan. Also, CBF, CBV and MTT maps are shown. B) CBF, CBV and MTT values for the ischaemic and non-ischaemic sides in WM and C) CBF, CBV and MTT values for the ischaemic and non-ischaemic sides in GM.

4.1.1.2 Imaging biomarkers in the non-MT treated group

Altogether 15 patients were selected in the group, not treated with MT. In this group, the mean (SD) in ischaemic and non-ischaemic WM and GM areas are presented in Table 4-2. All patients have a significant reduction in CBF in the ischaemic WM and GM areas (Paired Student's t-test - $p=0.0031$, ratio from 0.49 to 1.22 and $p<0.0001$, ratio from 0.11 to 0.58) respectively. CBV values in ischaemic WM and GM areas were significantly lower than these in non-ischaemic side with ($p = 0.0269$) in the former areas and ($p= 0.0350$) in the latter areas. In depth, 27% have an increased CBV in ischaemic WM areas (ratio from 1.05 to1.44) and 73% have a reduced CBV (ratio from 0.10 to 0.91). Similarly, regarding CBV in ischaemic GM areas, 20% have an increased CBV in ischaemic WM areas (ratio from 1.11 to 2.25) and 80% have a reduced CBV (ratio from 0.10 to 0.95). It is interesting to note that, no significant

difference was seen in MTT between the WM ischaemic and the non-ischaemic areas (ratio from 0.13 to 1.64), whereas, a significant rise in the MTT values in GM ischaemic areas was observed compared to the corresponding areas (ratio from 0.17 to 14.02), (p=0.0011), Figure 4.4. An example of a CT scan for non-MT patients is shown in Figure 4.5.

Table 4-2 A comparison of CTP parameters between ischaemic and non-ischaemic WM and GM areas in the non-MT group (n=15). Data are shown as mean (SD).

	Tissue (WM or GM)	Ischaemic area			Non-ischaemic area		
		CBF (ml/min/100g)	CBV (ml/100g)	MTT (Second)	CBF (ml/min/100g)	CBV (ml/100g)	MTT (Second)
Mean (SD)	WM	17.59 (9.75)	2.00 (1.42)	7.36 (4.48)	21.90 (11.43)	2.69 (1.59)	7.74 (3.52)
	GM	17.28 (8.80)	2.23 (1.74)	8.02 (4.54)	66.59 (9.55)	3.44 (2.81)	3.15 (2.51)

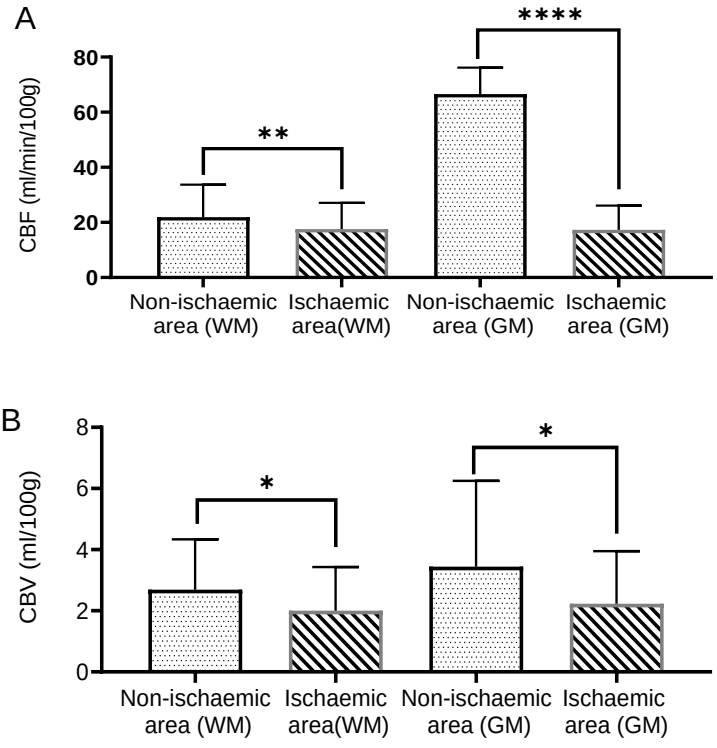

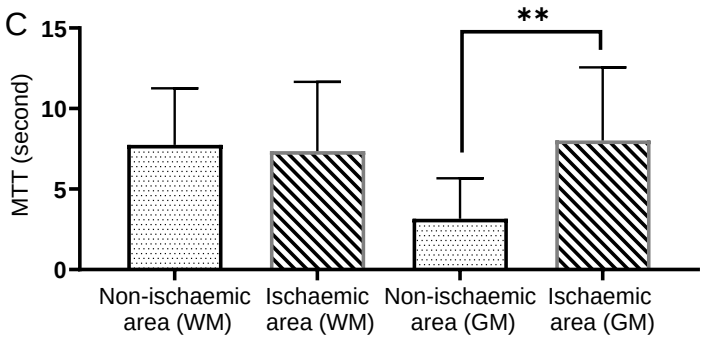

Figure 4.4 CTP CBF (A), CBV (B) and MTT (C) values in ischaemic and non-ischaemic WM and GM areas in the non-MT group (n=15), (Paired Student's t-test - A: CBF in WM p=0.0031 and in GM p<0.0001), (B: CBV in WM p = 0.0269 and CBV in GM p= 0.0350) and (C: MTT in GM p=0.0011).

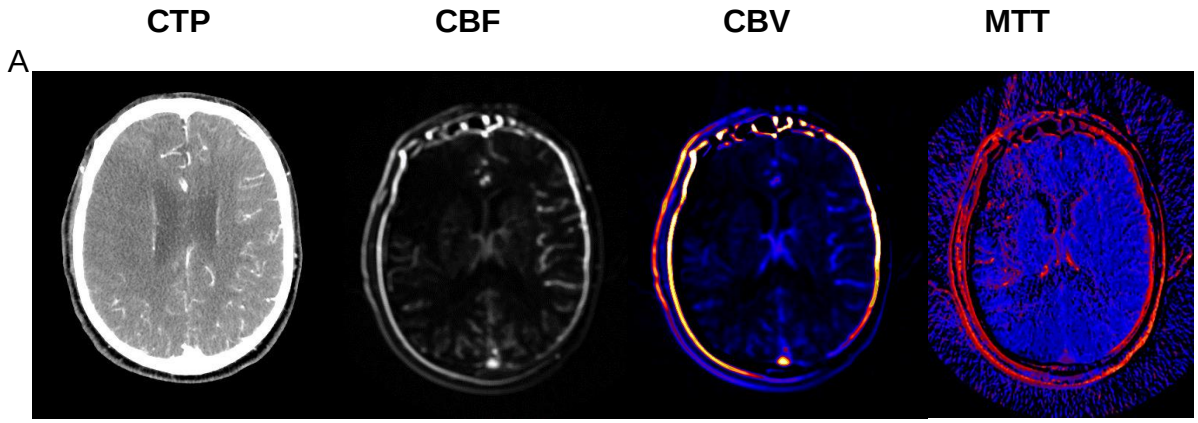

B

	CBF(WM) ml/min/100g	CBV(WM) ml/100g	MTT(WM) seconds
Ischaemic side	17.87	0.29	0.97
Non-ischaemic side	23.56	2.90	7.39

C

	CBF(GM) ml/min/100g	CBV(GM) ml/100g	MTT(GM) seconds
Ischaemic side	21.02	0.14	0.40
Non-ischaemic side	56.31	5.15	4.29

Figure 4.5 A) CTP images for a patient with a massive right MCA territory ischaemia who couldn't receive MT after the CTP scan due to delay from stroke onset to hospital arrival. Also, CBF, CBV and MTT maps are shown. B) CBF, CBV and MTT values for the ischaemic and non-ischaemic sides in WM and C) CBF, CBV and MTT values for the ischaemic and non-ischaemic sides in GM.

4.1.1.3 Compare CTP imaging biomarkers between the MT treated group and the non-MT treated group

In this section, the CTP biomarkers between the MT group and the non-MT group were compared from the previous results, which showed both groups developed a considerable reduction in CBF in the ischaemic WM and GM areas compared to the non-ischaemic side areas.

Therefore, by looking at the amount of reduction of CBF in terms of the ratio (ischaemic/non-ischaemic area) of the mean value, the following considerable findings were stated. The MT treated group has a decreased WM CBF ratio (0.71) compared to the non-MT treated group (0.80) (Figure 4.6, A). Furthermore, an increased WM CBV ratio (0.98) was conducted in the MT group in a comparison with (0.76) in the non-MT one (Figure 4.6, B). Regarding MTT, all the MT treated patients have a higher WM MTT ratio (1.36) in contrast with the non-treated group (0.97), (Figure 4.6, C).However, no statistical changes were seen in CTP parameters in WM between the two groups (Mann-Whitney U test).

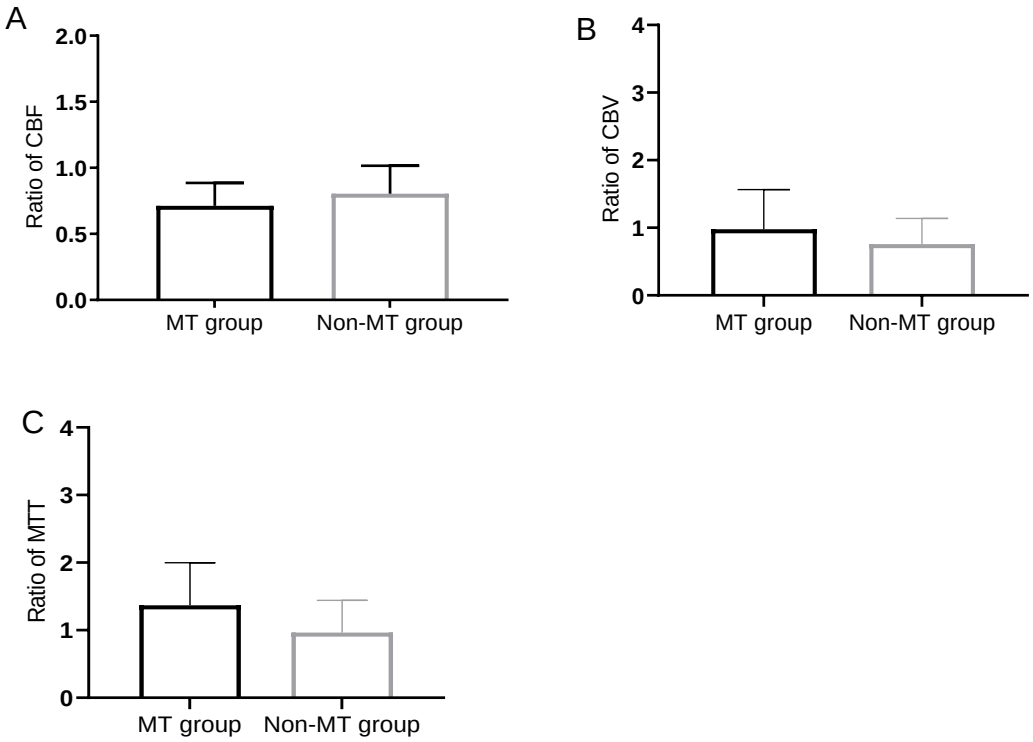

Figure 4.6 The analysis of WM CBF (A), CBV (B) and MTT (C) ratio between the MT group (n=15) and the non-MT group (n=15). No significant difference was seen between the two groups (Mann-Whitney U test).

On the other hand, no significant difference in the GM CBF ratio between the MT treated group (0.28) and the non-MT treated group (0.26) was observed (Figure 4.7, A). Interestingly, a significant increase in the GM CBV ratio (1.45) was observed in the MT group in comparison with (0.77) the non-MT one (Mann-Whitney U test -p=0.041), (Figure 4.7, B). Finally, all the MT treated patients appeared to have a higher GM MTT ratio (6.91) in comparison with the non-treated group (3.59) but the results were not statistically significant (Figure 4.7, C).

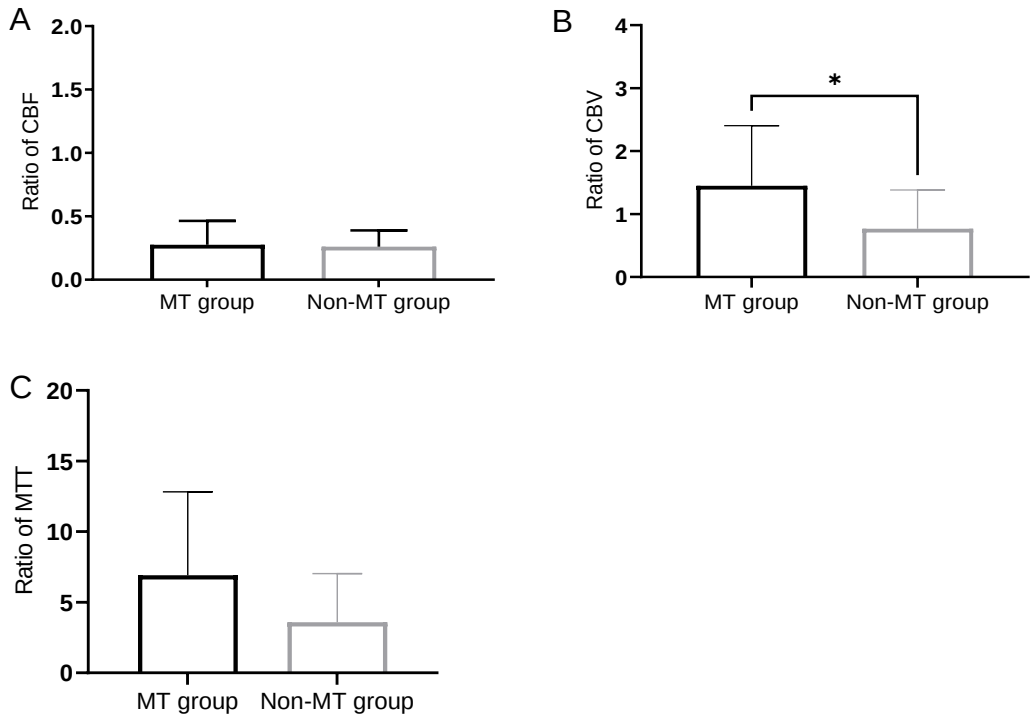

Figure 4.7 The analysis of GM CBF (A), CBV (B) and MTT (C) ratio between the MT group (n=15) and the non-MT group (n=15). Only CBV ratio showed significant difference between the two groups (Mann-Whitney U test -p=0.041).

4.1.2 Follow-up MRI results

4.1.2.1 Imaging biomarkers in the MT treated group

In the ADC map of MRI, 7 patients who received MT were identified. Mean (SD) in ischaemic and non-ischaemic WM and GM areas are shown in Table 4-3. All patients have an increased ADC value in ischaemic WM and GM areas (ratio from 0.70 to 2.31) and (ratio from 0.93 to 1.90) respectively, Figure 4.8. However, no significant results were seen in both areas (Paired Student's t-test -p=0.129 for the

former and p=0.221 for the latter). An example of an MRI scan for one MT patient is shown in Figure 4.9.

Table 4-3 A comparison of ADC map values in MRI DWI between ischaemic and non-ischaemic WM and GM areas in the MT group (n=7). Data are shown as mean (SD).

	Tissue (WM or GM)	Ischaemic area ADC ($*10^{-6}$ mm^2/s)	Non-ischaemic area ADC ($*10^{-6}$ mm^2/s)
Mean (SD)	WM	1245.72 (559.32)	901.18 (134.52)
	GM	1289.68 (373.01)	1136.04 (313.86)

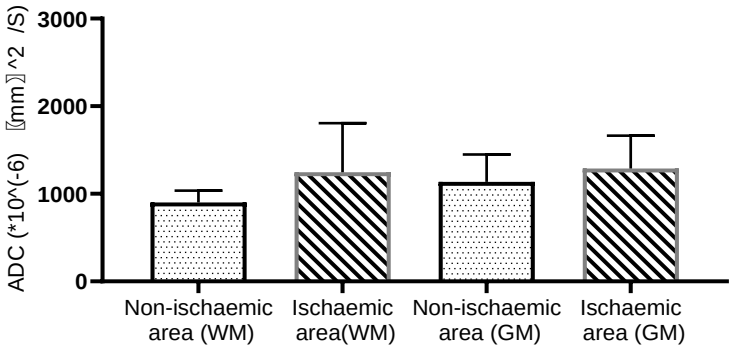

Figure 4.8 ADC map values in MRI DWI in ischaemic and non-ischaemic WM and GM areas in the MT group (n=7).

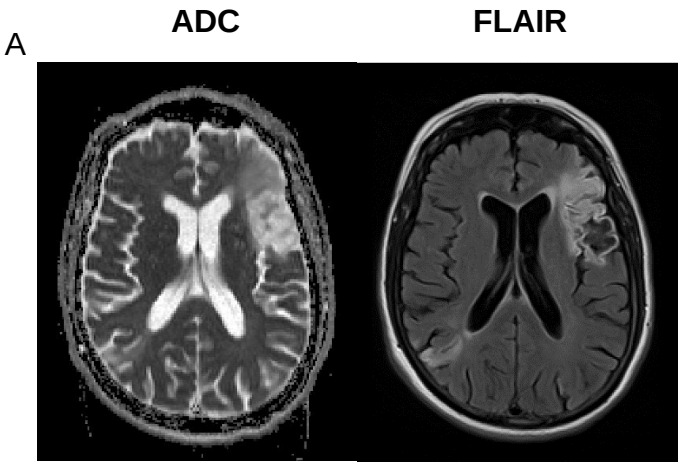

B

	ADC (WM) (x 10^{-6} mm^2/s)	ADC (GM) (x 10^{-6} mm^2/s)
Ischaemic side	1234.90	1237.90
Non-ischaemic side	928.75	1019.20

Figure 4.9 A) MRI ADC map and fluid-attenuated inversion recovery (FLAIR) of left hemisphere anterior circulation stroke in a patient, who received MT. B) ADC values for the ischaemic and non-ischaemic areas in WM and GM. The stroke is shown as hyperintense in the ADC map as the scan has done after more than a month from the stroke onset.

4.1.2.2 Imaging biomarkers in the non-MT treated group

In the ADC map of MRI, 8 patients who have not received MT were identified. Mean (SD) in ischaemic and non-ischaemic WM and GM areas are shown in

Table **4-4**. All patients have considerably significant increased ADC value in ischaemic WM and GM areas (ratio from 0.60 to 2.40, Paired Student's t-test - p=0.047) and (ratio from 1.25 to 2.37, p=0.0016) respectively, Figure 4.10. An example of an MRI scan for one non-MT patient is shown in Figure 4.11.

Table 4-4 A comparison of ADC map values in MRI DWI between ischaemic and non-ischaemic WM and GM areas in the non-MT group (n=8). Data are shown as mean (SD).

	Tissue (WM or GM)	**Ischaemic area ADC (*10^{-6} mm^2 /s)**	**Non-ischaemic area ADC (*10^{-6} mm^2 /s)**
Mean (SD)	WM	1293.35(642.59)	780.80(63.64)
	GM	1763.90(375.35)	1062.85(184.08)

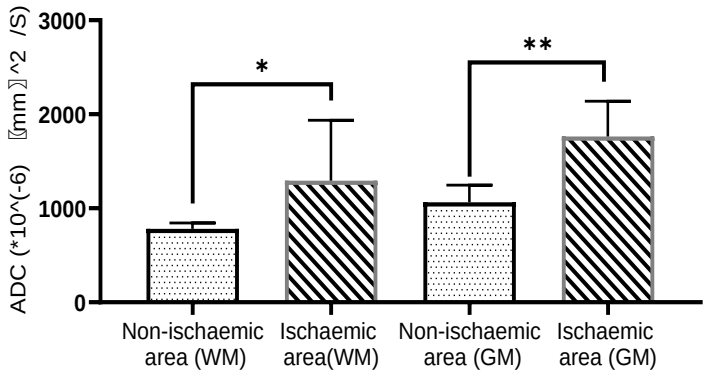

Figure 4.10 ADC map values in MRI DWI in ischaemic and non-ischaemic WM and GM areas in the non-MT group (n=8), (Paired Student's t-test - in WM p=0.047 and in GM p=0.0016).

A

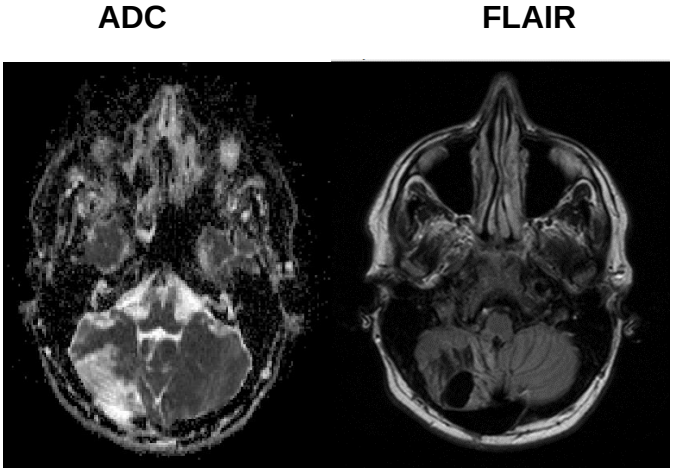

B

	ADC (WM) (x 10^{-6} mm^2/s)	ADC (GM) (x 10^{-6} mm^2/s)
Ischaemic side	1135.33	1317.50
Non-ischaemic side	710.63	1050.20

Figure 4.11 A) MRI ADC map and fluid-attenuated inversion recovery (FLAIR) of pons infarct and right cerebral infarct in a patient, who couldn't receive MT. B) ADC values for the ischaemic and non-ischaemic areas in WM and GM. The stroke is shown as hyperintense in the ADC map as the scan has done after more than a month from the stroke onset.

4.1.2.3 Compare imaging biomarkers between the MT treated group and the non-MT treated group

From the follow-up MRI results, the ratio of ADC WM and GM values in the MT treated group was lower than the ones in the non-MT treated group. The non-MT treated group has an increased ADC WM ratio (1.66) compared to the MT treated group (1.38) with no statistically significant results observed (Mann-Whitney U test). Interestingly, a significant increased ADC GM ratio (1.66) was observed in the non-MT group in a comparison with (1.14) in the MT one (p=0.009) as shown in Figure 4.12.

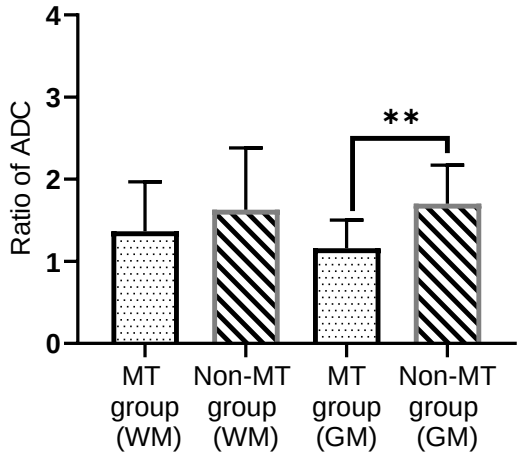

Figure 4.12 The analysis of ADC WM and GM ratio between the MT group (n=7) and the non-MT group (n=8), (Mann-Whitney U test – in GM p=0.009).

4.1.2.4 Compare of the volume of infarct area between the MT treated group and the non-MT treated group

Volumes of infarct (ml) were calculated. Mean (SD) were 1254.71 (329.08) and 1319.24 (447.71) for the volume of infarct in the MT group and the non-MT group respectively. It is worth mentioning that the volume of infarct in ml in the MT treated group (28.18ml) is smaller than the one in the non-MT treated group (30.91ml). However, no significant difference was shown (Mann-Whitney U test - p= 0.8545), Figure 4.13. Typical images from two ischaemic stroke patients, one has received MT treatment while the other does not receive MT are shown in Figure 4.14 and Figure 4.15 respectively.

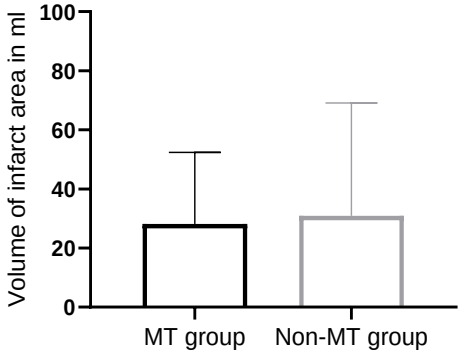

Figure 4.13 A comparison between the infarct volume in ml between the MT group (n=7) and the non-MT group (n=8).

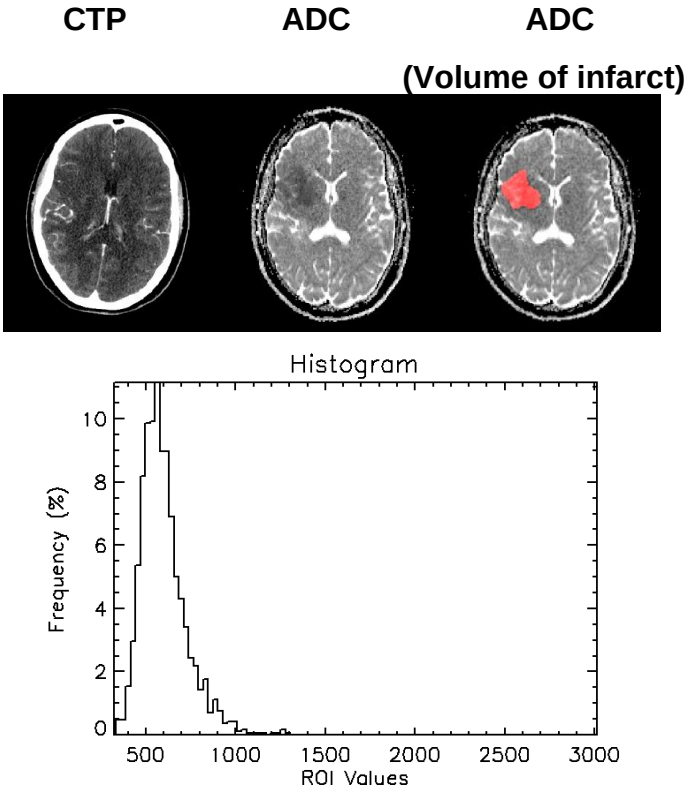

Figure 4.14 CTP and ADC images for a patient with acute stroke in the right MCA occlusion who received MT directly after the CTP scan (left panel). The middle panel represents an ADC map on follow-up MRI. The volume of infarct was calculated in ml according to the ROI volume (right panel, red). The histogram shows the number of pixels in the infarct area with been used to calculate the volume of infarct in ml (11.80ml).

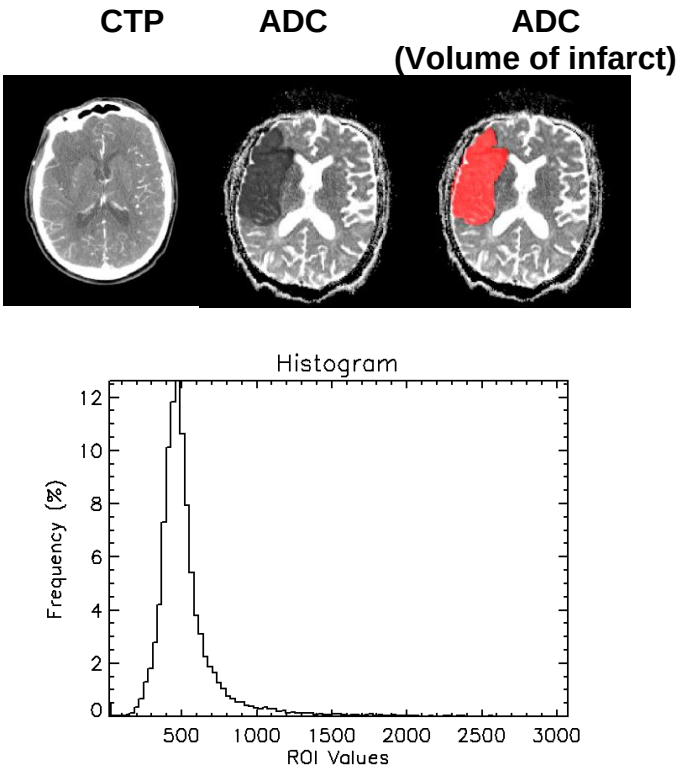

Figure 4.15 CTP and ADC images for a patient case with acute stroke with a massive infarction in the right MCA occlusion who couldn't receive MT after the CTP scan (left panel). The middle panel represents an ADC map on follow-up MRI. The volume of infarct was calculated in ml according to the ROI volume (right panel, red). The histogram shows the number of pixels in the infarct area with been used to calculate the volume of infarct in ml (110.79ml).

4.1.3 Functional outcomes

Functional outcomes at 90 days (mRS) was collected for each patient who received MT and did not receive MT then the score was divided into "good outcome" (mRS≤2) or "bad outcome" (mRS>2). It is worth noting that, because of the limited sample size, correlation analysis between baseline imaging biomarkers and mRS was not performed. Instead, only a comparison of functional outcomes between MT group and non- MT group was conducted. Interestingly, 13 patients out of 15 in MT group showed a good outcome (varied from 0 to 2) whereas only two patients out of the 15 patients showed bad outcomes (varied from 4 to 5) as shown in Table 4-5 and Figure 4.16, left panel. However, only 6 out of 15 expected good outcomes while the majority (9 out of 15) expected bad outcomes (varied from 4 to 5) in those did not treated with MT as shown in Table 4-5 and Figure 4.16, right panel.

Table 4-5 Individual mRS at 3 months in the MT group (n=15) and the non-MT group (n=15), "good outcome" (mRS≤2) or "bad outcome" (mRS>2).

Patient number	mRS at 3 months in MT group	mRS at 3 months in non-MT group
Pt#1	0	1
Pt#2	0	1
Pt#3	5	3
Pt#4	4	3
Pt#5	2	3
Pt#6	0	5
Pt#7	2	4
Pt#8	0	1
Pt#9	0	4
Pt#10	0	1
Pt#11	1	3
Pt#12	1	1
Pt#13	0	5
Pt#14	1	3
Pt#15	1	1

(MT group)	good outcomes	bad outcomes
Number of patients	13	2

(Non-MT group)	good outcomes	bad outcomes
Number of patients	6	9

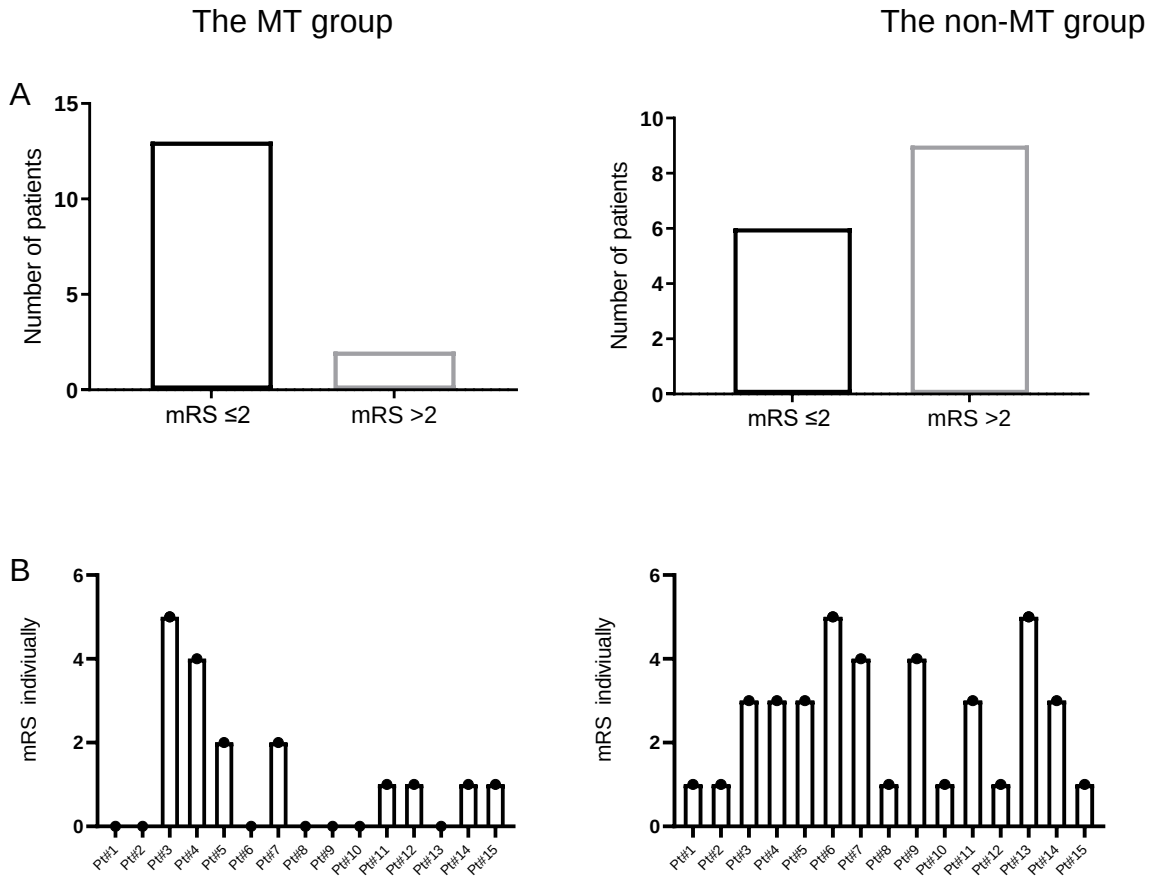

Figure 4.16 A) A comparison between the number of patients with "good oucome" (mRS≤2) and "bad outcome" (mRS>2) in the MT group (left) and the non-MT group (right). B) Individual mRS at 3 months in the MT group in the left (n=15) and the non-MT group in the right (n=15).

4.1.4 Summary and main findings

This study presented here the results of a pilot study aiming to test a hypothesis that can inform a longitudinal study design in the future. As seen from the result of the CTP biomarkers, the non-treated group in this study suffered from irreversible infarction, as both CBF and CBV significantly dropped. The CTP biomarkers results of the treated patients, on the other hand, confirm reversible ischaemia, as the CBF reduced dramatically while the CBV remained stable or rose.

In summary:

- CTP parameters are feasible in acute stroke patients undergoing MT.
- MT is a useful treatment in acute stroke to improve favourable outcomes.

4.1.5 Discussion

4.1.5.1 CTP imaging biomarkers in the MT treated group and the non-MT treated group.

This pilot study aimed to determine if the CTP and MRI imaging biomarkers or parameters have the potential to improve the prediction of outcomes in MT. However, this aim could not be achieved due to the small sample size. Instead, only comparisons of CTP biomarkers, MRI ADC values, volume of infarct and functional outcomes between MT group and non-MT group were conducted.

From CTP, this study compared the values of CBV, CBF, and MTT between the ischaemic areas and the non-ischaemic areas (mirror side zone) in WM and GM in both MT and non-MT groups. Since, previous studies showed that GM and WM have various perfusion and diffusion values for ischaemic areas in acute stroke patients (Arakawa et al., 2006; Chen et al., 2019), this study quantified the imaging biomarkers in both WM and GM.

Relevant CTP parameters can reflect the patient's collateral circulation and the abnormal perfusion of hemodynamic in brain tissues, so it gives a basis for clinical treatment (Xu et al., 2019). Using a quantitative CTP perfusion method, a significant decreased in CBF in ischaemic WM and GM areas in both groups; patients treated with MT and patients not treated with MT was observed. The absolute CBF values have been obtained in both WM and GM ischaemic areas in MT group in this study were consistent with previous CTP studies such as (Khandelwal, 2008). This provides further evidence for the CBF measurements' validity using this quantitative CTP technique. According to Yu et al. (2016), if the CBF decreases slightly, it indicates that the cerebral circulation reserve is decompensated. However, a significant decline indicates that the patient might develop a cerebral infarction if not treated (Yu et al., 2016).

This study found no significant difference in WM's and GM's CBV between the ischaemic and non-ischaemic areas in the MT group which indicates the preserved CBV. Also, the majority of patients have an increase CBV in ischaemic GM areas which might refer to the vasodilatation sign following early blood reduction. According to Khandelwal et al (2008), when CBF is reduced, cerebral autoregulation guarantees appropriate CBV by generating capillary dilation, which increases MTT and CBV. CTP

biomarkers result in the MT group in this study indicates a reversible ischaemia which is characterized by a reduction in CBF with a steady or increasing CBV on CTP (Tomandl et al., 2003; Srinivasan et al., 2006). Moreover, increased CBV in the penumbra region is due to the brain's direct autoregulatory mechanism in order to preserve CBF by expanding the collateral vessels as a response to decreased the pressure of perfusion (Powers et al.,1984).

On the other hand, in the non-MT group, mean values of WM's and GM's CBV were significantly lower in ischaemic regions compared to the collateral ones. This decrease in CBV with the decrease in CBF is because of autoregulation failure in response to massive cerebral hypoperfusion (Powers et al.,1984). According to Tomandl et al. (2003) and Srinivasan et al. (2006), irreversible infarction occurs when both CBF and CBV fall critically below the critical level (usually 20% of the normal level).

In both groups, this study did not observe a significant change in the WM's MTT between both sides. However, this study observed significant increases in GM's MTT in ischaemic areas compared to the collateral side regions in the treated and the non-treated groups. The MTT is the ratio of CBV/CBF which indicates the pressure of local perfusion (Schumann et al., 1998). Increased or delayed MTT indicates impaired perfusion reserve and a deduced cerebral perfusion pressure which all can be an indicator of the patient's collateral circulation condition (Yu et al., 2016).

In addition, comparing the ratio of CTP biomarkers between the MT group and the non-MT group, a considerable rise in the WM and GM CBV in the MT group compared to the non-MT group with a significant difference observed only in the GM areas. It is worth noting that CBV has been proposed as the best predictor of infarct core (Wintermark et al., 2006). This study results are consistent with a previous study that reported that a preserved or increased CBV suggests penumbra after MT in acute stroke patients (Austein et al., 2016). Furthermore, the noticed significant CBV difference between the MT and the non-MT groups in the GM areas might be because of the neurochemical responses variations to ischaemia in the brain's WM and GM areas (Stys et al., 1990; Dohmen et al., 2001). A previous study showed that laminar necrosis in the cerebral cortex (GM) and severe ischaemia abnormalities in the basal ganglia (GM) in individuals who survived a brief period of cardiac arrest, yet there were only slight WM changes (Sawada et al., 1990). Furthermore, Arakawa et al. (2006) showed that GM is more susceptible to ischaemia than WM.

All in all, according to the CTP biomarkers findings, the non-treated group suffered from irreversible infarction as both the CBF and CBV decreased significantlly. However, the treated patient's CTP biomarkes results confirm a reversible ischaemia as the CBF decreased significantly while the CBV was steady or increased. This confirms previous studies results (Koenig et al., 2001: Munich et al., 2016), that showed the CTP biomarkers are significantly different between ischaemic and non-ischaemic sides.

4.1.5.2 Follow-up MRI imaging biomarkers in the MT treated group and the non-MT treated group.

On the follow-up MRI scan, this study found that all patients have an increased ADC value in the ischaemic WM and GM areas compared to the non-ischaemic area in the MT group and the non-MT group. However, only significant increases in ADC values in the ischaemic areas compared to the non-ischaemic areas in the non-MT group on the follow-up MRI scan was observed. Furthermore, a significant increase in the mean ADC ratio (ischaemic/non-ischaemic) in GM areas in the non-MT treated group compared to the ones in the MT treated group was found. The ADC map in the brain is reduced quickly 30 min after ischaemia, this reduction continues during the first to fourth days after ischaemia (Gouhar and Taha, 2010). This is because of cytotoxic oedema correlated with reduced diffusion; thus, the occluded lesion in early scans shows on ADC map as hypointense and on DWI as hyperintense (Gouhar and Taha, 2010). However, after more than two weeks from ischaemia (follow-up MRI, as in this study), supranormal ADC values are started to be seen, and it is referred to increase the extracellular water, gliosis and tissue cavitation. Consequently, the occluded lesion shows as on ADC map as hyperintense and on DWI as hypointense (Gouhar and Taha, 2010). Similarly, an earlier study showed a gradual increase in the ADC from the 7th day to the 90th day in stroke patients (Sui et al., 2016). In particular, this study results agreed with the previous studies (Moon et al., 2005; Kim et al., 2005; Gouhar and Taha, 2010) about the increase of ADC in later ischaemia on follow-up MRI.

Regarding the volume of infarct, this study observed that the infarct volume in the MT treated group is non significantly smaller than the one in the no treated group. Friedrich et al. (2014) found that the volume of infarct after good recanalization with MT was significantly smaller. However, this study results did not show any significant

differences between the MT group and the non-MT group. One possible explanation might be due to the small sample size.

4.1.5.3 Functional outcomes

Functional outcomes at 90 days (mRS) showed promising results as 13 patients out of 15 in the MT group have a good outcome (varied from 0 to 2). The 2 patients with bad outcomes in the MT group might be due to clot size or inaccurate measurement of the clot. However, only 6 patients out of 15 in the non-MT group have good outcomes. Consequently, this study demonstrated that interventional treatment with MT results in favourable functional outcomes in ischaemic patients.

Furthermore, the earlier observed increase or perseverance in CBV in the MT group on CTP in this study could predict good outcomes in the MT group and this might be confirmed in future work with larger sample size. Van Seeters et al. (2015) found in a study of suspected acute ischaemic stroke patients, the CTP parameters at admission have a strong predictive value on patients with poor clinical outcomes prognosis and therefore can be applied to predict long-term clinical outcomes. The present study results showed that MT treated patients exhibits good outcomes compared to non-treated patients. However, future study with outcomes correlation is highly recommended.

However, not all of the patients recruited came for the follow-up MRI scan and functional outcomes collection appointments given to them and because of this, it has impacted the MRI's final study sample size (n=7: MT group vs n=8 non-MT group). Additionally, all the MRI scans have been done without intravenous contrast, thus, the analyses of the routine MRI head scan including the ADC values and the volume of infarct were the only possible analyses. Thus, further studies carrying these results with larger samples are required to confirm these results.

A larger prospective study on hyperacute stroke patients undergoing MT with outcome data collection was planned to verify this hypothesis and then correlate the results with blood biomarkers in MT. However, due to COVID-19, it was not able to do prospective research CT and MRI scans including perfusion scans obtained on stroke patients undergoing MT and correlate the perfusion imaging biomarkers results with blood biomarkers results. Thus, this pilot study would help future work.

In conclusion, the results of the current study confirmed previous studies results regarding the feasibility of CTP parameters in acute stroke patients undergoing MT diagnosis. MT is known to be a valuable treatment in acute stroke which has the potential to improve functional outcomes. These pilot study data, however, need validation with a larger sample size. This pilot study might help future studies comparing MT with non-MT.

Chapter 5 Biomarkers in clinical samples

5.1 Cross-Sectional study – Comparison of circulating biomarkers between stroke and stroke mimics

Despite a lot of research that has been pursued in the search for blood-based biomarkers as an indicator of brain damage, there is no single circulating biomarker that can be used at hospitals to detect the stroke onset and to help differentiate between stroke patients and stroke mimics. Different specific circulating biomarkers have been studied in the last decade using preclinical models and in a small number of stroke patients. However, these studies have produced variable results and lack a correlation between the level of circulating biomarkers with imaging biomarkers. Thus, this study for the first time aimed to assess the ability of the blood-based biomarkers (specific to neuronal and glial cell injury and BBB damage) to distinguish between ischaemic stroke patients and stroke mimics as defined by clinical scoring as well as CT and MRI imaging data to improve stroke diagnosis.

The selected circulating biomarkers in this study's panel were: GFAP, NSE, NfL, Occludin, Claudin-5 and ZO-1. These biomarkers were selected based on of the preclinical studies (as detailed in Chapter 3) and other published studies on stroke biomarkers.

5.1.1 Demographic results

A total of 94 patients were included in this study, of whom 70 had acute ischaemic strokes and 24 had stroke mimics. Baseline characteristics and demographic data are displayed in Table 5-1. In ischaemic patients, 48 patients were male and 22 were female. In mimics, 15 patients were male and 9 were female. Mean (SD) age of the ischaemic patients was 60 (13.4) and stroke mimics 64 (15). The time (in day) between stroke onset and blood sample collection was 2.37 (1.65) in the ischaemic patients and 2.66 (1.74) in the mimics. Clinical stroke severity score defined by NIHSS at arrival was 3.51 (3.29) in the ischaemic patients and 2.16 (2.03) in the mimics.

Table 5-1 Baseline characteristics of the included patients including age, gender, type of stroke, time difference between stroke and blood sample collection, NIHSS on arrival. Data are presented as mean (SD).

	Ischaemic stroke	Mimics
Sample size, number	70	24
Age	60 (13.4)	64 (15)
Gender: Male **Female**	Male n= 48 Female n=22	Male n= 15 Female n=9
Time between stroke onset and blood sample collection (day)	2.37 (1.65)	2.66 (1.74)
NIHSS on arrival	3.51 (3.29)	2.16 (2.03)

5.1.2 Different in biomarkers levels between serum and plasma

Blood samples were obtained from 94 patients (70 acute ischaemic patients and 24 stroke mimics). Data were collected from Leeds Teaching Hospitals NHS Trust as explained in section 2.3.1 to section 2.3.3. Blood samples were prepared as per section 2.3.4. Measurement of circulating biomarkers was done using ELISA as per section 2.3.5. Statistical data analysis was done as per section 2.3.6.

The levels of GFAP, NSE, Occludin, Claudin-5 and ZO-1 concentrations in both serum and in plasma samples received from the first 25 patients (n=20 ischaemic, n=5 mimics). No significant difference in the concentrations of biomarkers was found between serum and plasma in the stroke group and the mimics group (paired Student's t-test), as seen in (Figure 5.1). Thus, the subsequent studies were

performed on blood serum in consistent with the preclinical study as it excludes blood clotting factors (Sotelo-Orozco et al., 2021).

A.1

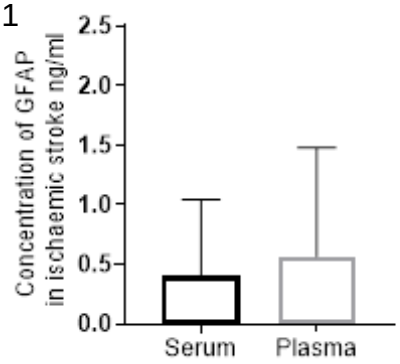

A.2

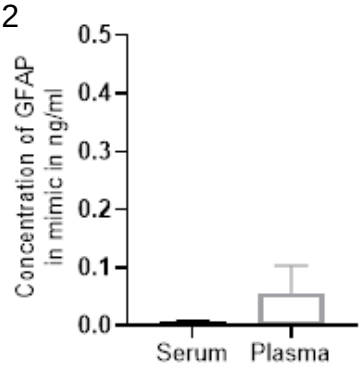

B.1

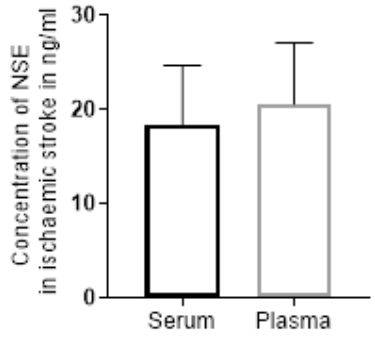

B.2

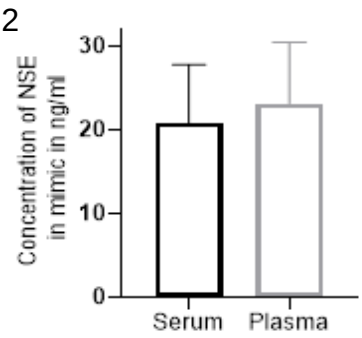

C.1

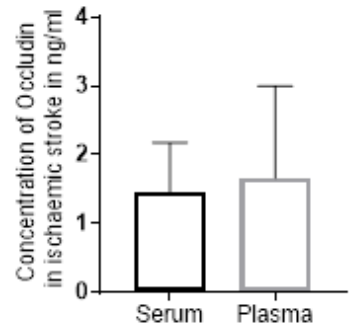

C.2

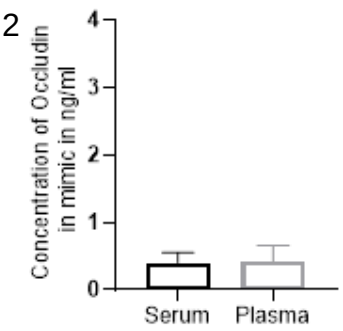

D.1

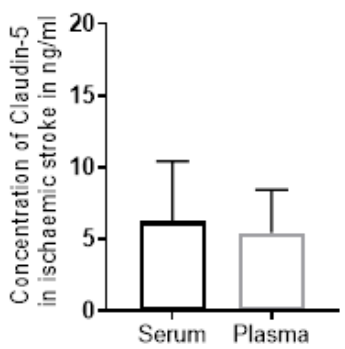

D.2

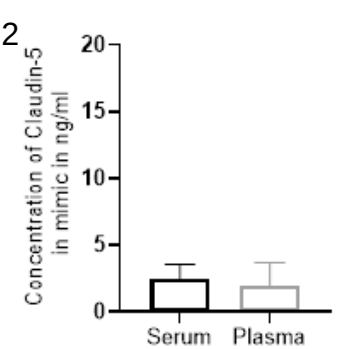

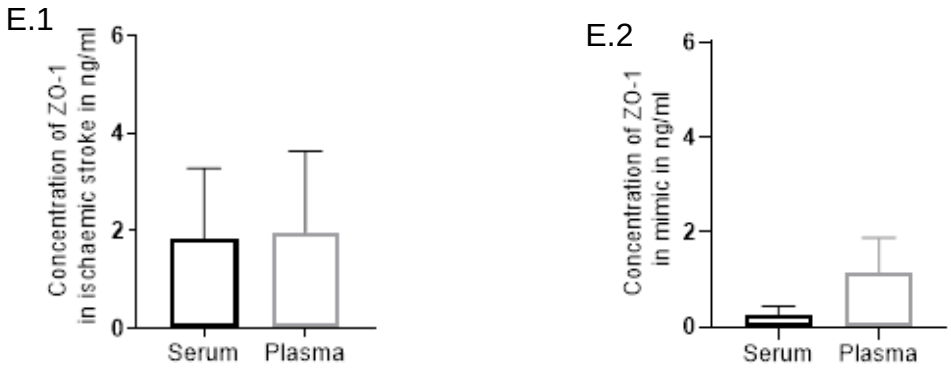

Figure 5.1 The difference in (A) GFAP, (B) NSE, (C) Occludin, (D) Claudin-5 and (E) ZO-1 levels between serum and plasma in the ischaemic group (n=25) and the mimics group (n=5). No significant changes were found, (Paired Student's t-test).

5.1.3 Serum biomarkers levels to distinguish between the stroke patients and the stroke mimic

Table **5-2** shows the range, mean and median of serum concentrations of GFAP, NSE, NfL, Occludin, Claudin-5 and ZO-1 in the ischaemic stroke patients and the stroke mimics. NfL was included later in this study since recent studies showed NfL as a promising biomarker for stroke diagnosis (Tiedt et al., 2018; Uphaus et al., 2019).

The concentrations of serum GFAP were significantly higher in the ischaemic stroke patients as compared to the mimics with 4-fold increase (range 0.02-2.41 vs 0.01-1.20 ug/ml) ($p<0.0001$, Mann-Whitney U test) as shown in Figure 5.2-A. While, the concentrations of NSE in the serum of the stroke patients were not significantly different as compared to the mimics (range 9.29-28.42 vs 12.38-27.43 ng/ml) ($p = 0.075$), (Figure 5.2-B). Thus, analysis of NSE was discontinued at n=60. Serum NfL concentrations were 1.33-fold significantly higher in the ischaemic patients compared to the mimics (range 0.03-0.05 vs 0.03-0.04 ng/ml, respectively, $p<0.0001$) (Figure 5.2-C).The range of serum Occludin in the stroke group was significantly 2.24-fold higher compared to the mimics group (range 0.19 - 3.18 vs. 0.25 - 1.66 ng/ml, $p<0.0001$) (Figure 5.2-D). Serum Claudin-5 concentrations were significantly 1.40-fold higher in the ischaemic patients than the mimics (range 0.57 - 17.10 vs. 0.74 - 14.99 ng/ml, respectively, $p<0.0001$) (Figure 5.2-E). In the ischaemic patients,

the mean serum ZO-1 levels were significantly higher compared to the stroke mimics with a 3.31-fold of increase (0.01 - 5.12 vs. 0.07 - 3.70 ng/ml, respectively, p<0.0001), (Figure 5.2-F).

Table 5-2 The range, mean and median of serum GFAP, NSE, NfL, Occludin, ZO-1 and Claudin-5 concentrations in the ischaemic stroke group (n=70) and the mimics group (n=24).

Biomarker		Ischaemic stroke (ng/ml)	Mimics (ng/ml)
GFAP	Mean	0.32	0.08
	Minimum	0.02	0.01
	Maximum	2.41	1.20
	Median	0.26	0.02
NSE	Mean	19.64	21.47
	Minimum	9.29	12.38
	Maximum	28.42	27.43
	Median	20.54	23.66
Claudin-5	Mean	5.09	3.65
	Minimum	0.57	0.74
	Maximum	17.10	14.99
	Median	5.51	2.96
Occludin	Mean	1.59	0.71
	Minimum	0.19	0.25
	Maximum	3.18	1.66
	Median	1.64	0.62
ZO-1	Mean	2.02	0.61
	Minimum	0.01	0.07
	Maximum	5.12	3.70
	Median	2.57	0.42
NfL	Mean	0.04	0.03
	Minimum	0.03	0.03
	Maximum	0.05	0.04
	Median	0.04	0.03

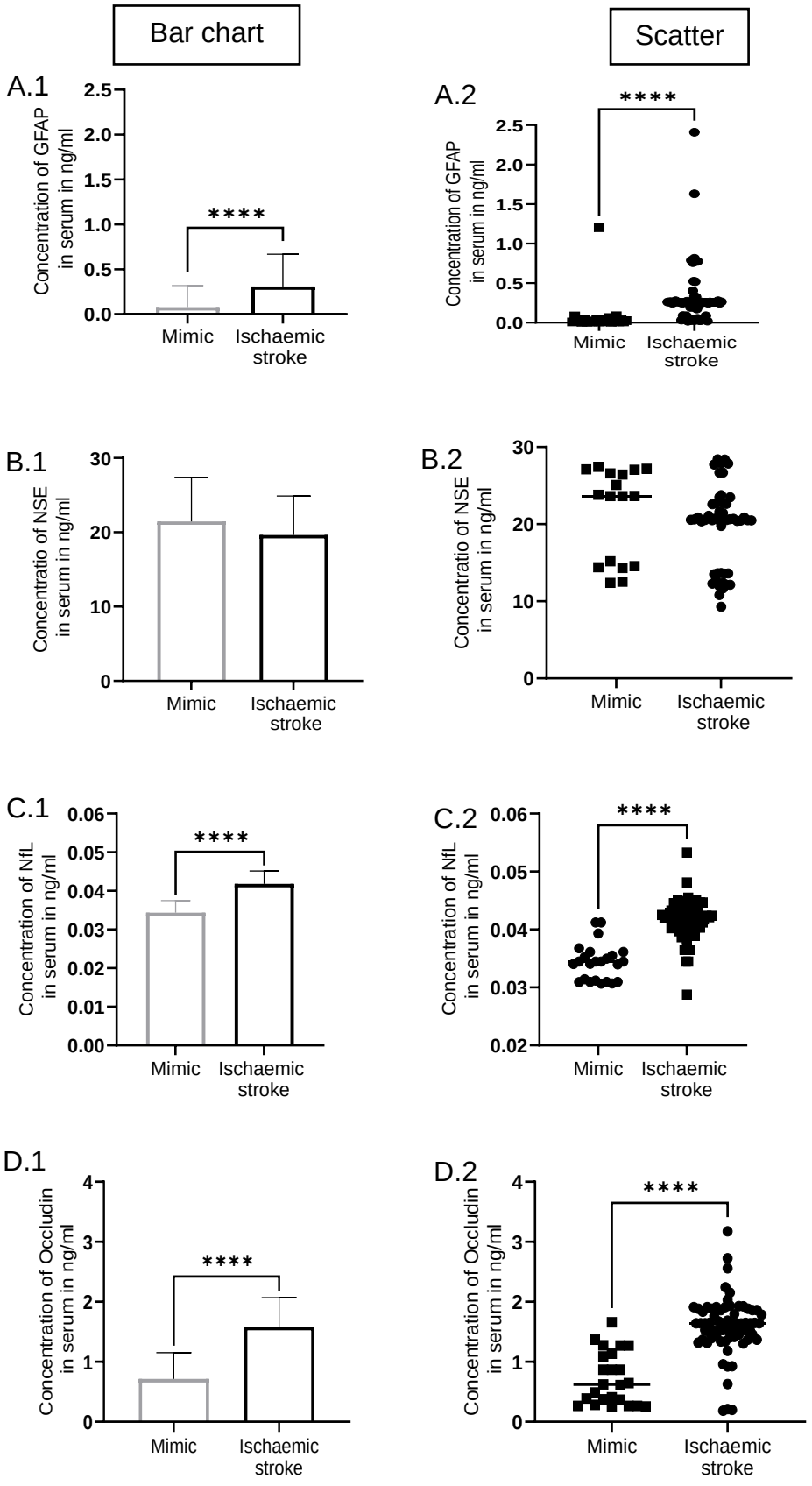
Bar chart
Scatter
A.1
A.2
Concentration of GFAP in serum in ng/ml
****
Mimic
Ischaemic stroke
B.1
B.2
Concentratio of NSE in serum in ng/ml
C.1
C.2
Concentration of NfL in serum in ng/ml
D.1
D.2
Concentration of Occludin in serum in ng/ml

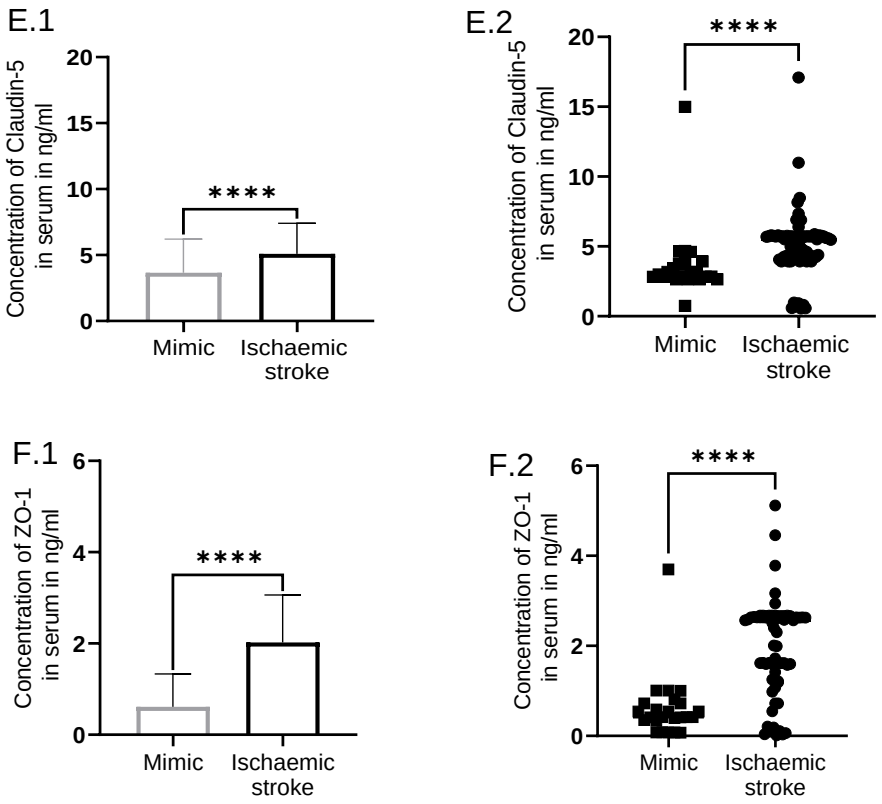

Figure 5.2 The levels of serum (A) GFAP, (B) NSE, (C) NfL, (D) Occludin, Claudin-5 (E) and ZO-1 (F) levels in the ischaemic patients (n=70) compared to the mimics (n=24). A significant increase has been observed in the concentrations of biomarkers except NSE in the ischaemic group compared to the mimics. GFAP: p<0.0001, NfL: p<0.0001, Occludin: p<0.0001, Claudin-5: p<0.0001 and ZO-1: p<0.0001. (Mann-Whitney U test, p≤0.0001: **).**

5.1.4 Difference between gender and biomarkers levels

In both the ischaemic and the mimics groups, patients were classified according to gender (male or female). Out of 70 ischaemic patients, 48 were male and 22 were female. Out of 24 mimics, 15 were male and 9 were female.

No significant difference in gender specific between males and females was found in GFAP, NSE, NfL, Occludin, Claudin-5 and ZO-1 levels in the same group.

The serum GFAP concentrations in males were significantly higher in the ischaemic group as compared to the mimics group (p=0.0001, Mann-Whitney U test). Similarly, the serum GFAP concentrations in females in the ischaemic were also higher significantly compared to the mimics group (p<0.0001,Figure 5.3-A). However, there was a non-significant decrease in the serum NSE concentrations in males (p=0.095)

and in females (p=0.212) in the ischaemic patients as compared to the mimics as displayed in Figure 5.3-B. There was a significant increase in the serum NfL, Occludin, Claudin-5 and ZO-1 in males (p<0.0001, p<0.0001, p<0.0001 and p=0.0001 respectively) as well as in females (p=0.0007, p<0.0001, p=0.001 and p=0.002 respectively) in the ischaemic patients as compared to the mimics as shown in Figure 5.3-C,D,E, F respectively.

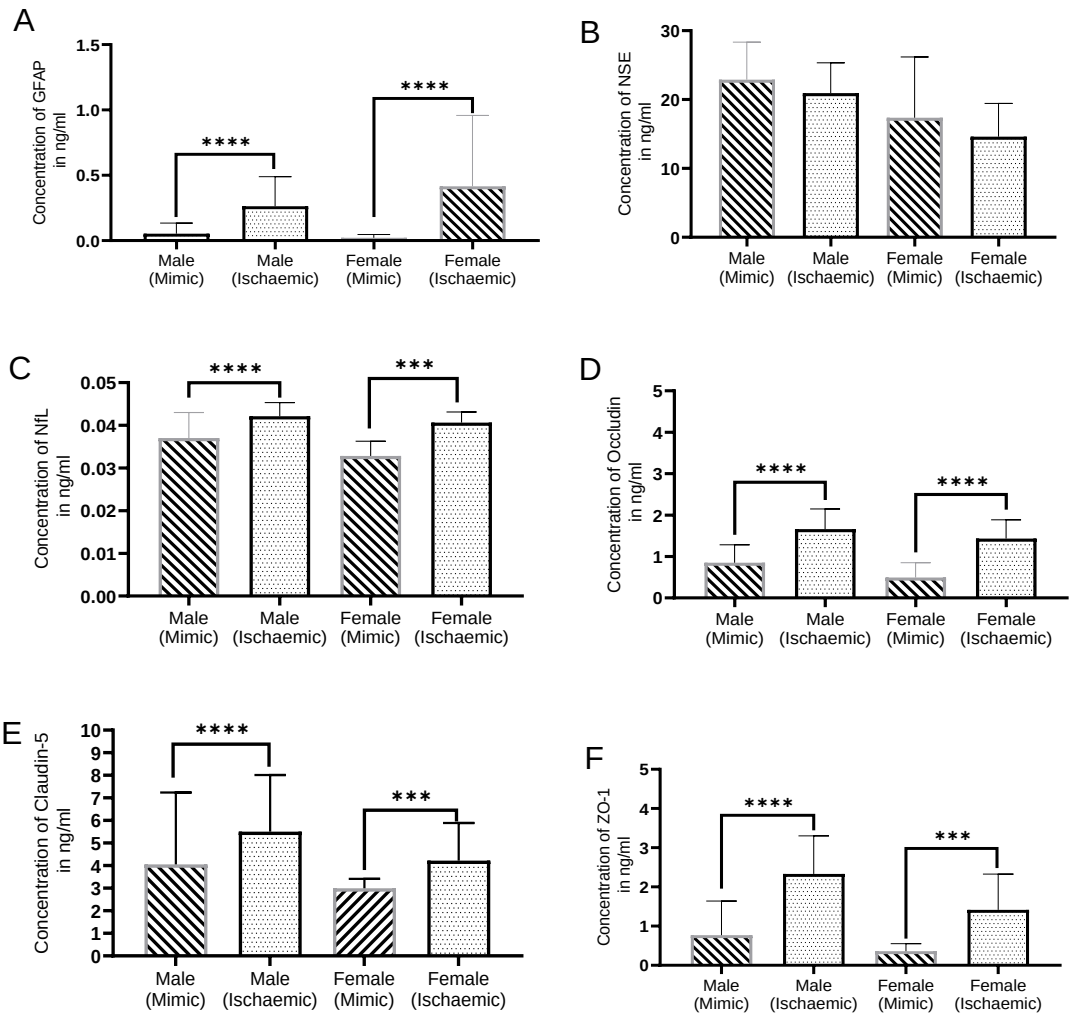

Figure 5.3 The difference in serum (A) GFAP, (B) NSE, (C) NfL, (D) Occludin, Claudin-5 (E) and ZO-1(F) levels between the ischaemic group and the mimics group based on the gender. (Mann-Whitney U test, p≤0.001: ***, p≤0.0001: **). (Ischaemic male: n=48 and female: n=22) (Mimics male: n=15 and female: n=9).**

5.1.5 Difference between the day of blood collection and biomarkers levels

Patients in each group (ischaemic or mimics) were classified into two subgroups based on the day of blood collection from the time of stroke onset. One subgroup is where the blood samples were collected before or at 2 days from the stroke onset and in the other subgroup where the blood samples were collected after 2 days from the stroke onset. Out of 70 ischaemic patients, the blood was collected at ≤2 days from 44 patients and > 2 days from 26 patients. Out of 24 mimics, the blood was collected at ≤2 days from 13 patients and > 2 days from 11 patients.

The serum GFAP concentrations at ≤2 days were significantly higher in the ischaemic group as compared to the mimics group (p=0.0001, Mann-Whitney U test). Similarly, the serum GFAP concentrations at >2 days in the ischaemic were also higher significantly compared to the mimics group (p<0.0001, Figure 5.4-A). It is worth mentioning that there was a non-significant decrease in the serum NSE concentrations at ≤2 days (p=0.071) and at >2 days (p=0.482) in the ischaemic patients as compared to the mimics as displayed in Figure 5.4 -B. There was a significant increase in the serum NfL, Occludin, Claudin-5 and ZO-1 at ≤2 days (p<0.0001, p<0.0001, p=0.0005 and p=0.0004 respectively) as well as >2 days (p=0.0002, p<0.0001, p=0.0003 and p=0.0002 respectively) in the ischaemic patients as compared to the mimics as shown in Figure 5.4-C,D,E, F respectively.

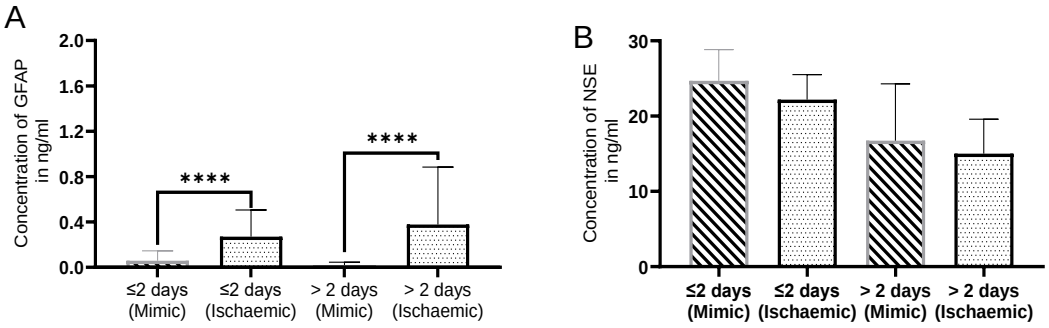

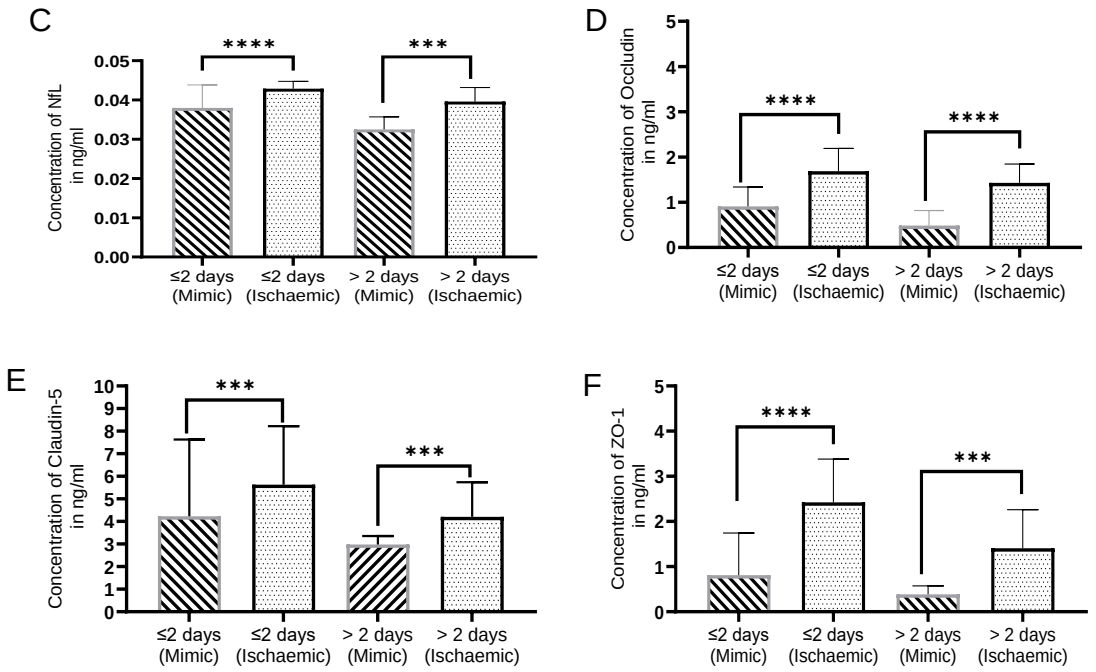

Figure 5.4 The difference in serum (A) GFAP, (B) NSE, (C) NfL, (D) Occludin, Claudin-5 (E) and ZO-1(F) levels between the ischaemic group and the mimics group based on the day of blood collection. (Mann-Whitney U test, p≤0.001: ***, p≤0.0001: **). (Ischaemic ≤2 days: n=44 and >2 days: n=26) (Mimics ≤2 days: n=13 and >2 days: n=11).**

5.1.6 Difference in biomarkers levels between the severity of stroke and the mimics

The NIHSS score runs from 0 to 42 as mentioned previously (Refer to section1.1.8). Based on the NIHSS score on arrival, the ischaemic patients were classified as mild stroke (NIHSS ≤ 7) and moderate to severe stroke (NIHSS > 7).

Out of 70 ischaemic patients, 60 patients had NIHSS ≤ 7 and 10 patients had NIHSS > 7. When comparing the relationship between the ischaemic and the mimics groups and the severity of a stroke, it has been found that the ischaemic patients had significantly higher serum GFAP concentrations with NIHSS ≤ 7 ($p<0.00001$, Mann-Whitney U test) as well as NIHSS> 7 ($p=0.003$) as compared to the mimics (Figure 5.5-A). Serum NSE concentrations were non-significantly different in both groups (NIHSS ≤ 7: $p=0.285$ and NIHSS >7: $p=0.158$) as compared to mimics (Figure 5.5-B). When compared serum NfL concentrations between the ischaemic and the mimics, the ischaemic patients appeared to have a significantly higher level of serum NfL in

both cases (NIHSS≤ 7 and > 7) compared to the mimics, ($p < 0.00001$ and $p=0.002$ respectively) (Figure 5.5-C). The ischaemic stroke patients with mild (NIHSS ≤ 7) as well as moderate to severe stroke (NIHSS >7) had significantly higher concentrations of serum Occludin than that of the mimics ($p < 0.0001$ and $p=0.001$ respectively) (Figure 5.5-D). A similar pattern was also found for the serum Claudin-5 and ZO-1 concentrations in both groups (NIHSS ≤ 7 and NIHSS >7) compared to the mimics (Claudin-5: $p < 0.00001$ and $p=0.001$ respectively) and (ZO-1: $p < 0.00001$ and $p=0.002$ respectively), (Figure 5.5-E, F).

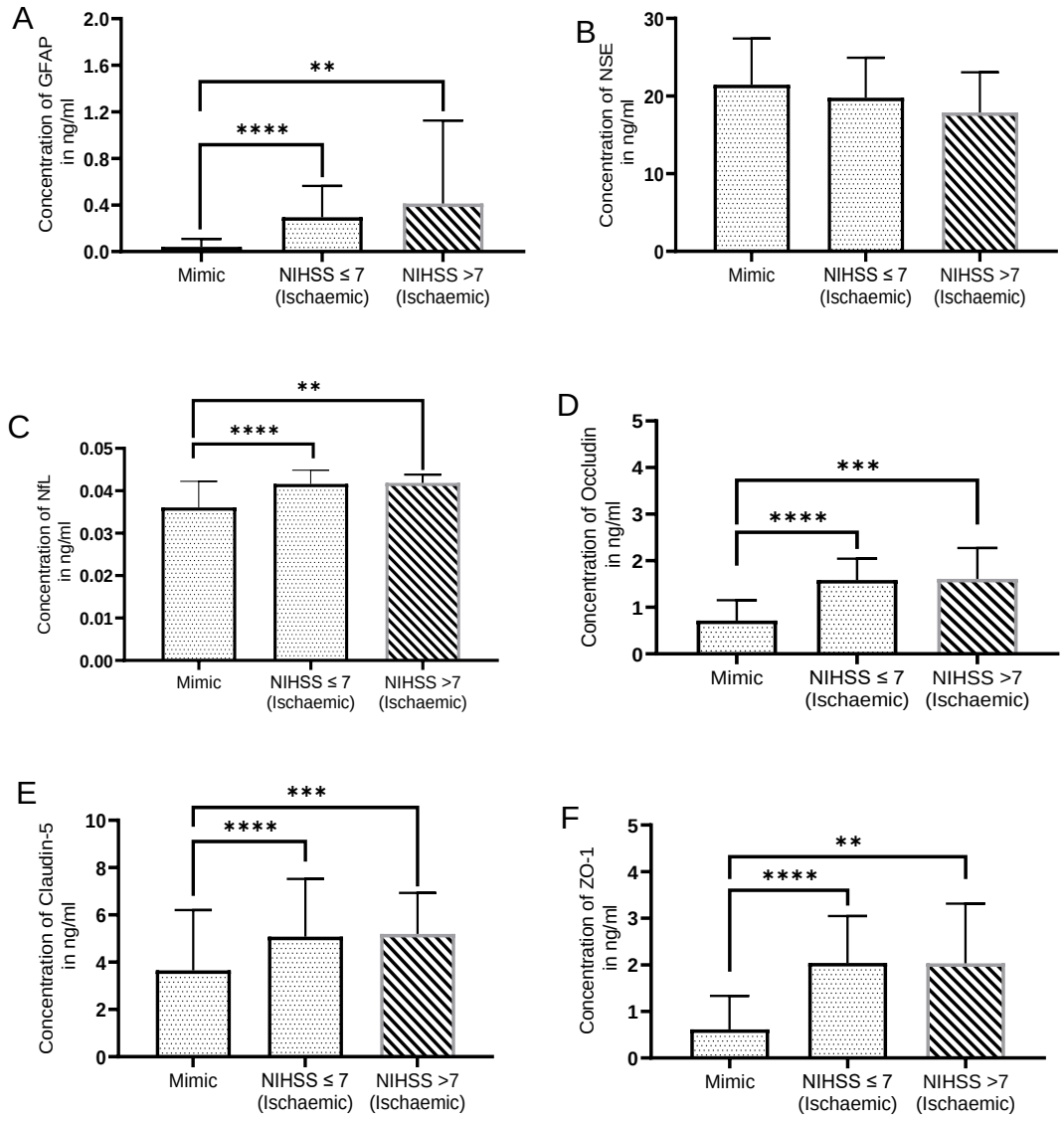

Figure 5.5 The difference in serum (A) GFAP, (B) NSE, (C) NfL, (D) Occludin, Claudin-5 (E) and ZO-1(F) levels based on the severity of stroke. (Mann -Whitney U test, p≤0.01: **, p≤0.001: ***, p≤0.0001: **). (NIHSS $\leq$ 7: n=60, NIHSS >7:n=10 and mimics: n=24).**

5.1.7 Difference in biomarkers levels between the location of occlusion and the mimics

Based on the location of occlusion in ischaemic patients, the patients were classified as anterior cerebral occlusion (ACO, n=45) or posterior cerebral occlusion (PCO, n=25).

Both the ACO and the PCO groups had significantly higher concentrations of GFAP as compared to the mimics (Mann-Whitney U test, p <0.00001 and p <0.00001 respectively) (Figure 5.6-A). Serum NSE concentrations were similar in the both categories of the ischaemic patients with no significant variations between those and the mimics (ACO: p=0.204 and PCO: p=0.352) (Figure 5.6-B). Moreover, both the ACO and the PCO groups had significantly higher NfL and Occludin concentrations as compared to the mimics (NfL: p <0.00001 and p <0.00001) (Occludin: p <0.00001 and p <0.00001) (Figure 5.6-C, D). The ACO and the PCO groups had significantly higher serum Claudin-5 and ZO-1 concentrations than the mimics (Claudin-5: p <0.00001 and p=0.0002) (ZO-1: p <0.00001 and p <0.00001) respectively (Figure 5.6-E, F).

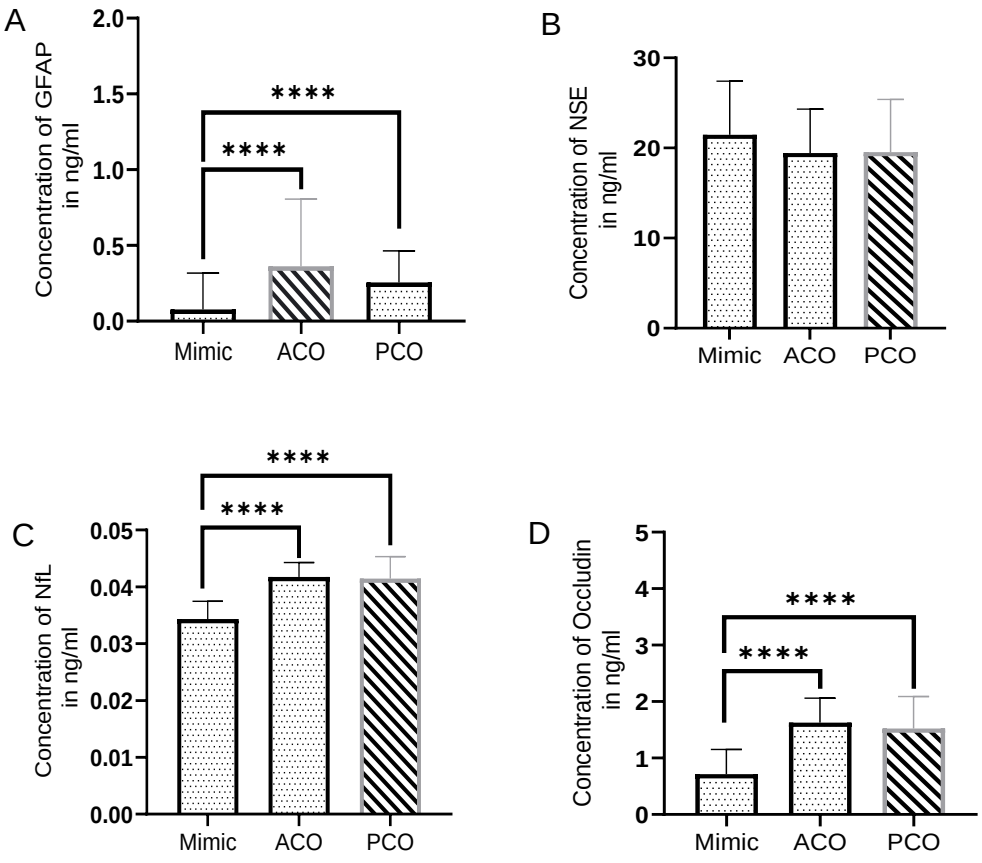

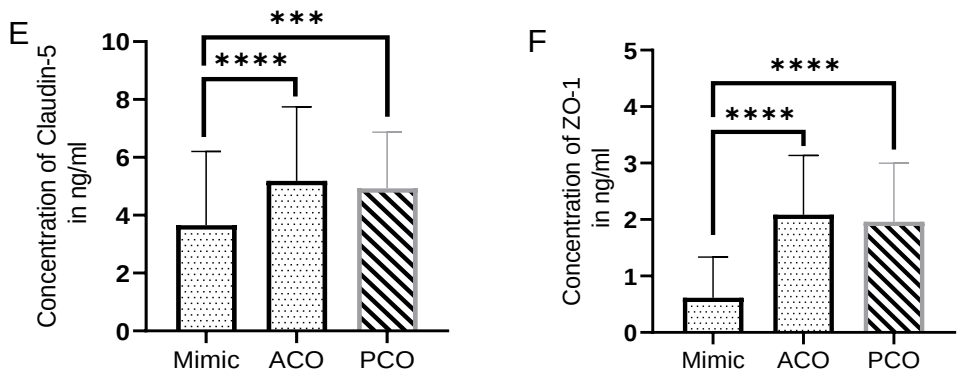

Figure 5.6 The difference between serum (A) GFAP, (B) NSE ,(C) NfL, (D) Occludin, Claudin-5 (E) and ZO-1(F) levels in the ACO (n=45) and the PCO (n=25) in a comparison with the mimics (n=24). (Mann-Whitney U test, p≤0.001: ***, p≤0.0001: **).**

5.1.8 Ratio of GFAP to other biomarkers in the ischaemic group with relation to the mimics

To investigate the connection between the serum levels of glial cell marker (GFAP) and neuronal markers (NSE, NfL) in the ischaemic stroke patients and the mimics, the ratio of GFAP to NSE or NfL was calculated. The ratio of (GFAP/NSE) in serum showed significantly higher values for the ischaemic patients compared to the mimics (Mann-Whitney U test, p <0.0001) (Figure 5.7-A). The ratio of serum (GFAP/NfL) was also significantly higher in the ischaemic patients compared to the mimics (p <0.00001) (Figure 5.7-B).

To investigate the relation of the serum levels of glial cell marker (GFAP) versus BBB TJ proteins, the ratio of GFAP to each TJ protein (Occludin, Claudin-5 or ZO-1) was analysed. The results showed the ratio of (GFAP/Occludin) in serum was significantly higher in the ischaemic patients in comparison to the mimics (p <0.00001) (Figure 5.7-C). Similarly, the ratio of (GFAP/Claudin-5) in serum was significantly higher in the ischaemic group compared to the mimics (p <0.00001), (Figure 5.7-D). The ratio of (GFAP/ZO-1) in serum was also found significantly higher in the ischaemic patients in comparison to the mimics (p=0.0006) (Figure 5.7-E).

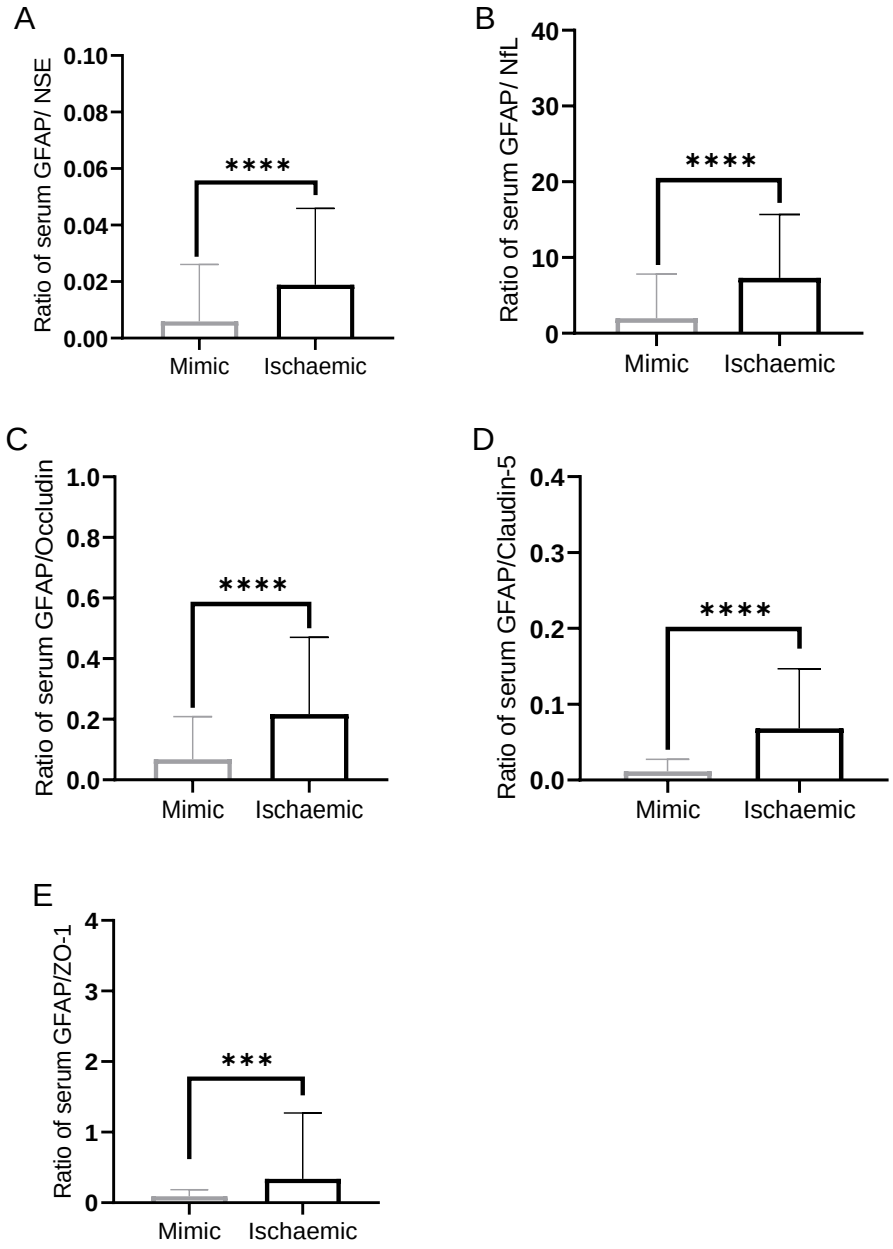

Figure 5.7 The ratio of serum A) GFAP/NSE, B) GFAP/NfL C) GFAP/Occludin D) GFAP/Claudin-5 and E) GFAP/ZO-1 in the ischaemic patients (n=70) compared to the mimics (n=24). (Mann-Whitney U test, p≤0.001: ***, p≤0.0001: **).**

5.1.9 Summary and main findings

- Significant increase in serum GFAP, NfL, Occludin, ZO-1 and Claudin-5 but not NSE in stroke patients compared to mimics.
- These biomarkers are able to differentiate between stroke patients and mimics even after classifying the patients according to the gender, time of blood collection, the severity of stroke (NIHSS), location of occlusion in ischaemic patients and ratio of GFAP to other biomarkers in the panel.

5.2 Cross sectional study - Comparison of CT and MRI imaging biomarkers between stroke and stroke mimics

Imaging biomarker as defined previously is a marker for both pathological and biological processes (Atkinson et al., 2001) acquired from imaging tools (Mitterhauser and Wadsak, 2014). Thus, to avoid unnecessary acute therapy, it is critical to appropriately recognise the stroke mimics quickly. This chapter presented the ability of the CT and MRI imaging biomarkers in differentiating between acute ischaemic stroke and stroke mimics. Specifically, this study compared HU values of ASPECTS between ischaemic side and non-ischaemic side in ischaemic patients. Since all the patients received NCCT scan, the only possible analysis was analysing the HU values (CT density) of ASPECTS. Also, compared HU values of ASPECTS between right side and left side in mimics. Comparisons between MRI ADC values and T2 signal intensity between ischaemic side and non-ischaemic side in some ischaemic patients were also achieved. Similar comparisons were done between right side and left side in mimics. Comparisons between MRI ADC values and T2 signal intensity between ACO and PCO patients were done. Finally, volume of infarct was compared with NIHSS as well as with location of occlusion.

5.2.1 CT scan ASPECTS analysis

5.2.1.1 Comparing ischaemic and non-ischaemic side in the ischaemic group

Imaging data from some of the recruited patients who were selected for collection blood samples, were obtained from Leeds Teaching Hospitals NHS Trust as explained in section 2.3.7. Altogether, CT results were obtained from 49 acute stroke patients and 16 mimics. CT data analysis was done as per section 2.3.9. MRI data analysis was done as per section 2.3.12. Statistical analysis was achieved as per section 2.3.10 for CT data.

This study included n=49 patients with acute ischaemic stroke in the CT analysis. The demographic characteristics of the patients were shown previously in Table 5-1. A Head NCCT scan was done as soon as the patients arrived at the emergency.

Mean (SD) of HU values for the 10 ASPECTS regions obtained from the ischaemic side were compared with the respective HU values of the non-ischaemic side.

Table 5-3 shows the mean (SD) of HU values of 10 regions of ASPECTS on the ischaemic side and the non-ischaemic side of the stroke patients (n=49). All the patients have a significantly reduced HU value (Paired Student's t-test, $p < 0.0001$) in all 10 regions in the ischaemic side as compared to the non-ischaemic side as shown in Figure 5.8. A NCCT scan for one ischaemic patient showing the 10 regions of ASPECTS is presented in Figure 5.9.

Table 5-3 The mean (SD) of HU values (densities) obtained from 10 regions of ASPECTS in the ischaemic side and the non-ischaemic side in the ischaemic stroke patients (n=49).

	Mean (SD) of HU									
	M1	**M2**	**M3**	**M4**	**M5**	**M6**	**C**	**I**	**IC**	**L**
Ischaemic side	31.92 (8.25)	31.77 (3.68)	32.13 (4.23)	31.17 (3.24)	31.36 (3.51)	32.32 (4.18)	31.64 (3.55)	31.58 (2.73)	31.45 (2.61)	31.22 (3.47)
Non-ischaemic side	33.28 (2.99)	32.87 (3.14)	33.38 (3.71)	32.80 (3.79)	32.62 (3.21)	33.73 (3.63)	33.28 (3.62)	32.75 (2.42)	32.82 (2.47)	32.55 (3.35)

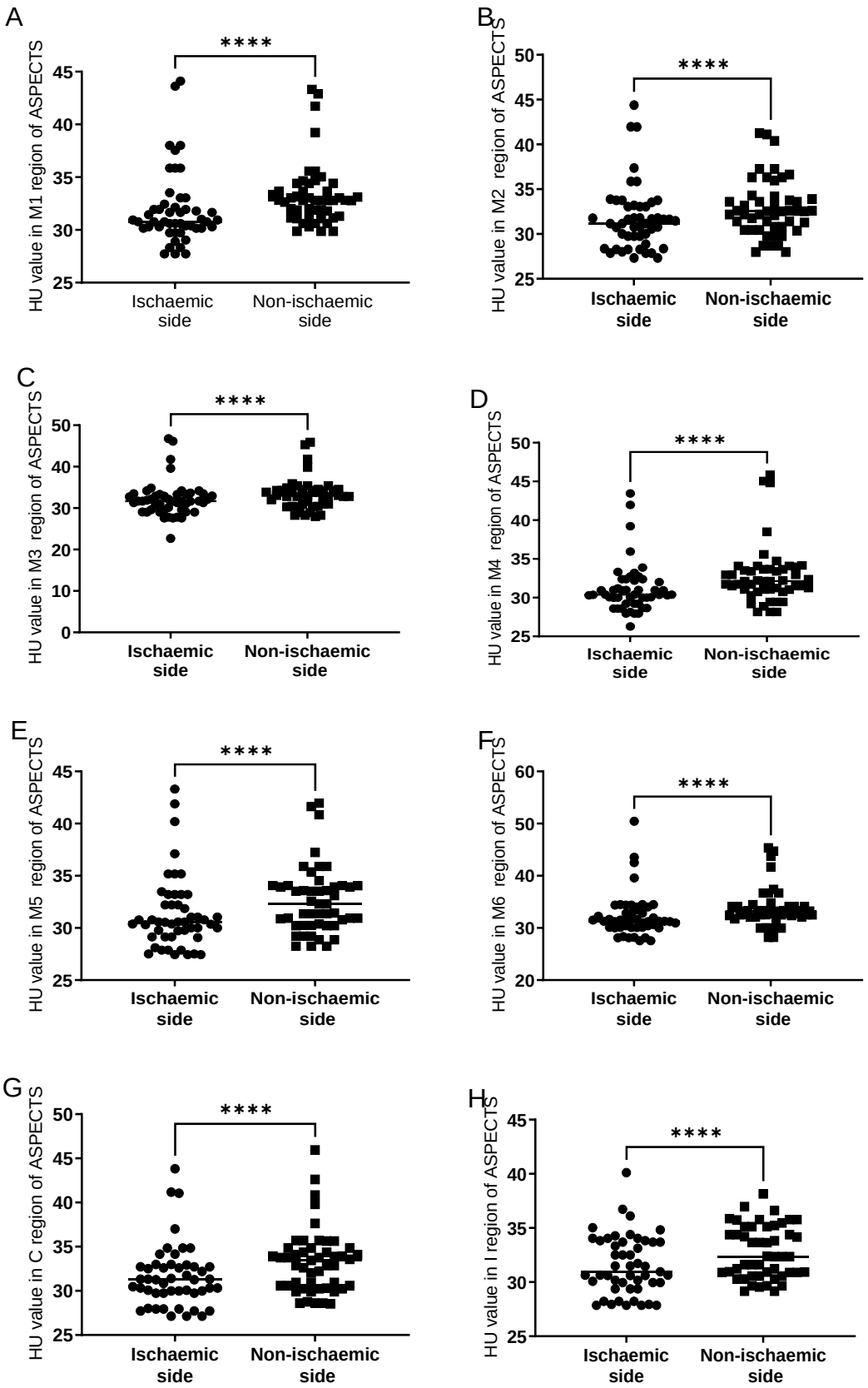
A
HU value in M1 region of ASPECTS
****
45
40
35
30
25
Ischaemic side
Non-ischaemic side
B
HU value in M2 region of ASPECTS
****
50
45
40
35
30
25
Ischaemic side
Non-ischaemic side
C
HU value in M3 region of ASPECTS
****
50
40
30
20
10
0
Ischaemic side
Non-ischaemic side
D
HU value in M4 region of ASPECTS
****
50
45
40
35
30
25
Ischaemic side
Non-ischaemic side
E
HU value in M5 region of ASPECTS
****
45
40
35
30
25
Ischaemic side
Non-ischaemic side
F
HU value in M6 region of ASPECTS
****
60
50
40
30
20
Ischaemic side
Non-ischaemic side
G
HU value in C region of ASPECTS
****
50
45
40
35
30
25
Ischaemic side
Non-ischaemic side
H
HU value in I region of ASPECTS
****
45
40
35
30
25
Ischaemic side
Non-ischaemic side

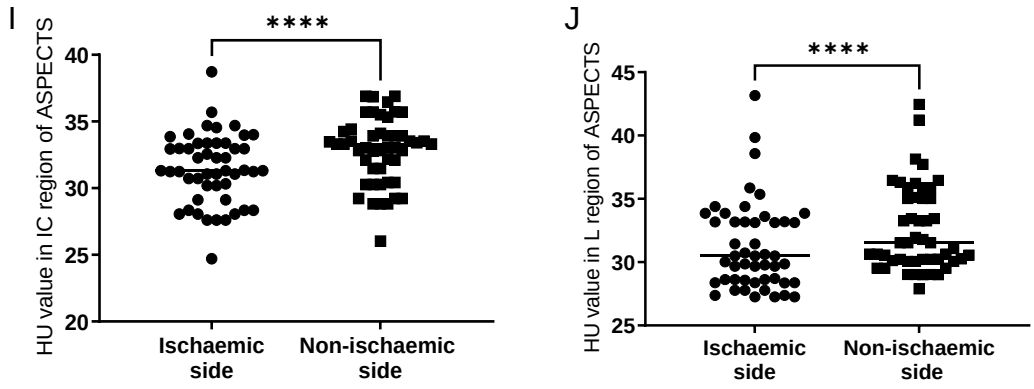

Figure 5.8 The difference in HU values (densities) of 10 regions of ASPECTS between the ischaemic side and the non-ischaemic side in the ischaemic stroke patients (n=49), (Paired Student's t-test; p<0.0001: **).**

A

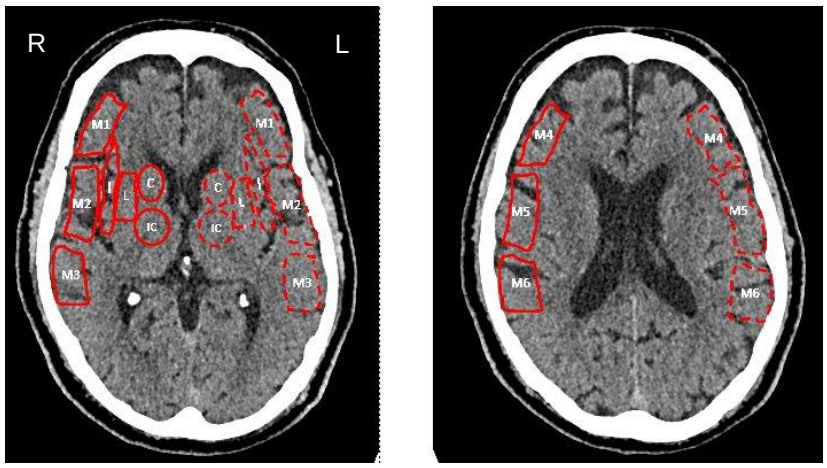

B

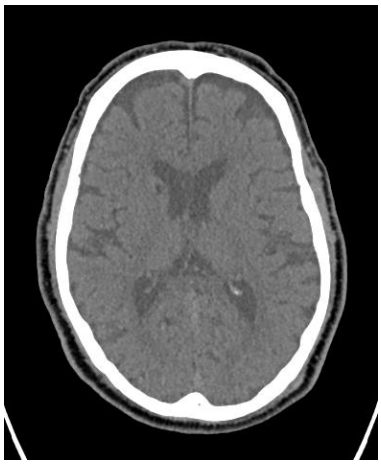

C

	M1	M2	M3	M4	M5	M6	C	I	IC	L
Ischaemic side	31.45	28.00	32.89	26.28	29.08	28.19	28.54	33.34	32.01	29.77
Non-ischaemic side	33.36	30.37	34.51	28.87	30.37	30.06	30.07	34.16	34.47	31.07

Figure 5.9 A) initial axial CT head images at two different levels, (left: basal ganglia level) and (right: corona radiata level) show where the 10 ASPECTS ROIs are drawn manually. Solid line regions represent the ischaemic side, and the dashed line regions represent the non-ischaemic side. L = lentiform nucleus; C = caudate head; I = insular ribbon; IC = internal capsule; M1 = anterior MCA cortical region; M2 = MCA cortical region located lateral to insular ribbon; M3 = posterior MCA cortical region; M4, M5 and M6 about 2 cm superior to M1, M2, and M3 regions respectively. B) NCCT head for a patient with chronic lacunar infarction in the right caudate head. C) (HU) values of the 2 hemispheres (Rt: the ischaemic side and Lt: the non-ischaemic side).

5.2.1.2 Comparing left side and right side in the mimic group

Altogether n=16 stroke mimics were included in this CT analysis. The mean (SD) of HU for the 10 ASPECTS regions obtained from the right and the left sides of the head scan were compared.

Table 5-4 displays the mean (SD) of HU values of 10 regions of ASPECTS obtained from the left and the right sides of brain scan of the mimics. As expected, no significant changes between the HU values of the left side and the right side of the brain have been observed (Figure 5.10). An NCCT scan for one mimic patient showing the 10 regions of ASPECTS is displayed in Figure 5.11.

Table 5-4 The mean (SD) of HU values (densities) obtained from 10 regions of ASPECTS in the left side and the right side of brain in the mimics (n=16).

	Mean (SD) of HU									
	M1	**M2**	**M3**	**M4**	**M5**	**M6**	**C**	**I**	**IC**	**L**
Left side	33.34 (8.46)	34.66 (3.37)	33.16 (3.07)	33.21 (3.13)	32.06 (3.48)	34.29 (3.93)	33.51 (2.98)	32.67 (9.91)	34.42 (3.56)	33.00 (2.76)
Right side	33.26 (2.45)	33.70 (3.01)	32.34 (3.25)	33.86 (3.60)	31.73 (2.77)	34.12 (3.31)	32.17 (3.67)	34.07 (9.75)	34.11 (3.26)	33.86 (2.79)

A

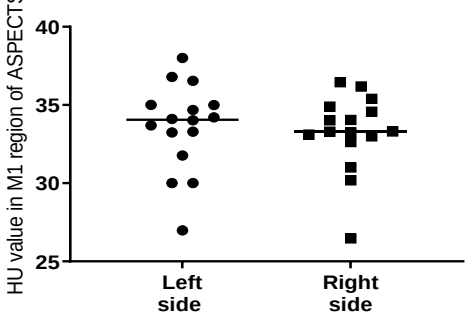
HU value in M1 region of ASPECTS
40
35
30
25
Left side
Right side

B

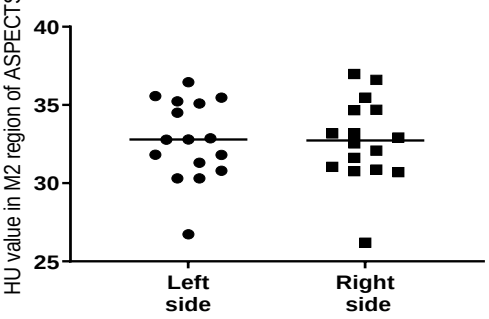
HU value in M2 region of ASPECTS
40
35
30
25
Left side
Right side

C

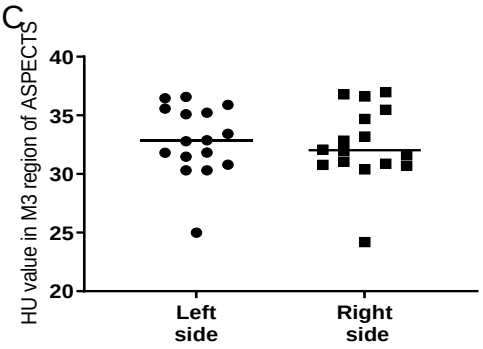
HU value in M3 region of ASPECTS
40
35
30
25
20
Left side
Right side

D

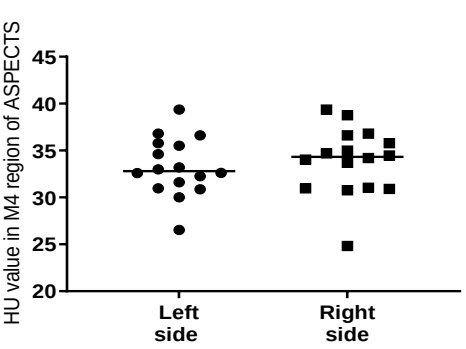
HU value in M4 region of ASPECTS
45
40
35
30
25
20
Left side
Right side

E

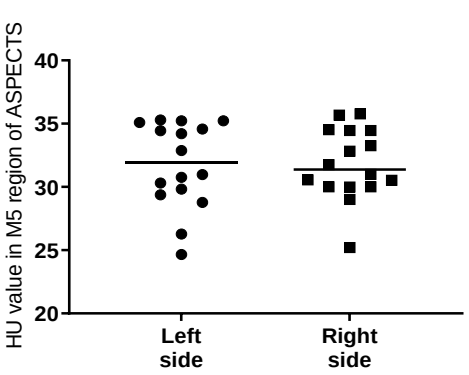
HU value in M5 region of ASPECTS
40
35
30
25
20
Left side
Right side

F

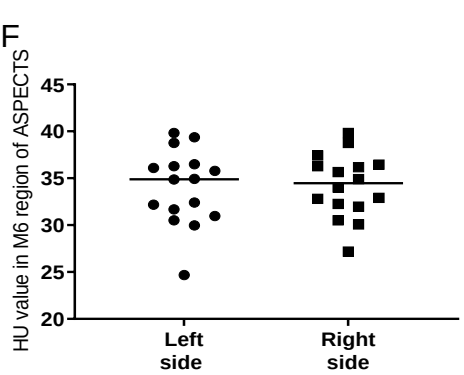
HU value in M6 region of ASPECTS
45
40
35
30
25
20
Left side
Right side

G

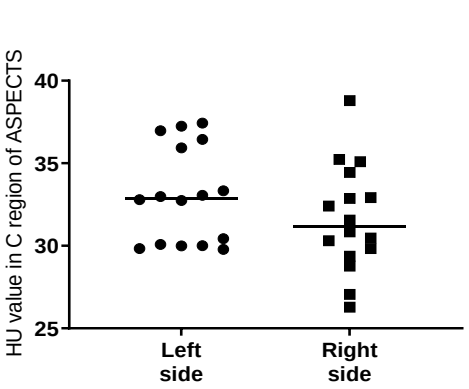
HU value in C region of ASPECTS
40
35
30
25
Left side
Right side

H

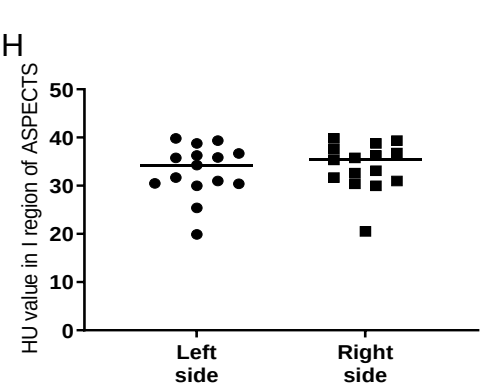
HU value in I region of ASPECTS
50
40
30
20
10
0
Left side
Right side

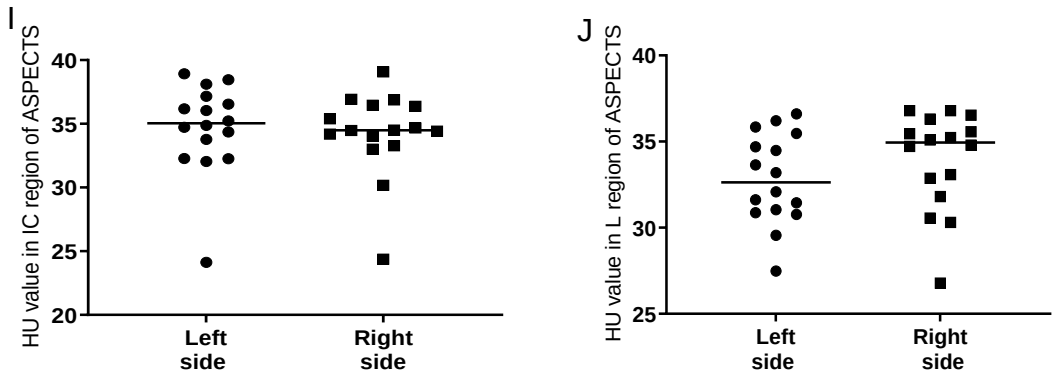

Figure 5.10 The difference between HU values (densities) of 10 regions of ASPECTS in the right and the left side of brain in the mimics (n=16). No statistical difference was seen (Paired Student's t-test).

A

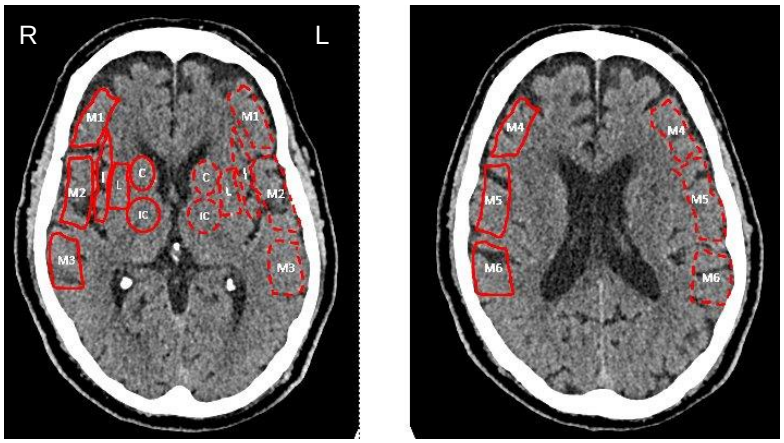

B

C

	M1	M2	M3	M4	M5	M6	C	I	IC	L
Right side	34.99	34.97	31.82	34.62	34.58	32.17	30.43	30.39	34.72	33.65
Left side	34.05	35.40	30.71	34.99	34.45	32.26	30.47	30.40	34.68	33.08

Figure 5.11 A) initial axial CT head images at two different levels, (left: basal ganglia level) and (right: corona radiata level) show where the 10 ASPECTS ROIs are drawn manually. Solid line regions represent the right side, and the dashed line regions represent the left side. L = lentiform nucleus; C = caudate head; I = insular ribbon; IC = internal capsule; M1 = anterior MCA cortical region; M2 = MCA cortical region located lateral to insular ribbon; M3 = posterior MCA cortical region; M4, M5 and M6 about 2 cm superior to M1, M2, and M3 regions respectively. B) NCCT head for a stroke mimics. This patient has a generalised hyperdensity of intracranial vessels which could be due to dehydration. C) (HU) values of the 2 hemispheres (right side and left side).

5.2.2 CT ASPECTS and circulating biomarkers

The CT ASPECTS runs from 0 to 10 as mentioned previously (Refer to section 1.1.11.1 and section 2.3.9). Based on the ASPECTS obtained from the NCCT, the ischaemic patients were classified as moderate to severe stroke (ASPECTS ≤ 7) and mild stroke (ASPECTS > 7). In order to predict functional reliance in patients who had thrombolysis within 3 hours of the beginning of symptoms, an ASPECTS cut off of 7 on the first NCCT was suggested by the previous group (Barber et al., 2000). Previous studies also reported that patients with ASPECTS ≤ 7 are more likely to have haemorrhagic transformation and have a poorer prognosis (Puetz et al., 2009; Padroni et al., 2016). Furthermore, in the Penumbra Pivotal Stroke Trial, when compared to the ASPECTS ≤ 7 group, the ASPECTS >7 group had significantly more favourable outcomes (The Penumbra Pivotal Stroke Trial Investigators, 2009).

Out of 49 ischaemic patients, 33 patients had ASPECTS ≤ 7 and 16 patients had ASPECTS > 7. The results showed that serum GFAP concentrations were significantly higher in ASPECTS ≤ 7 and ASPECTS > 7 group than the mimics (Mann-Whitney U test, $p < 0.0001$ and $p = 0.023$) respectively (Figure 5.12 -A). Serum GFAP levels were found to be higher in ASPECTS ≤ 7 group compared to ASPECTS > 7 group. In addition, serum NSE concentrations were non-significantly different in both subgroups as compared to the mimics (ASPECTS ≤ 7 : $p=0.234$ and ASPECTS > 7 : $p=0.313$) (Figure 5.12-B). Serum NfL and Occludin concentrations were significantly higher in both subgroups as compared to the mimics (NfL: ASPECTS ≤ 7 : $p < 0.0001$ and ASPECTS > 7 : $p=0.002$) (Occludin: ASPECTS ≤ 7 : $p < 0.0001$ and ASPECTS > 7: $p = 0.0001$) (Figure 5.12-C,D). Serum Claudin-5 and ZO-1 concentrations were also significantly higher in ASPECTS ≤ 7 and ASPECTS $>$

7 groups as compared to the mimics ($p < 0.0001$ and $p = 0.003$) ($p < 0.0001$ and $p = 0.041$) respectively (Figure 5.12-E, F).

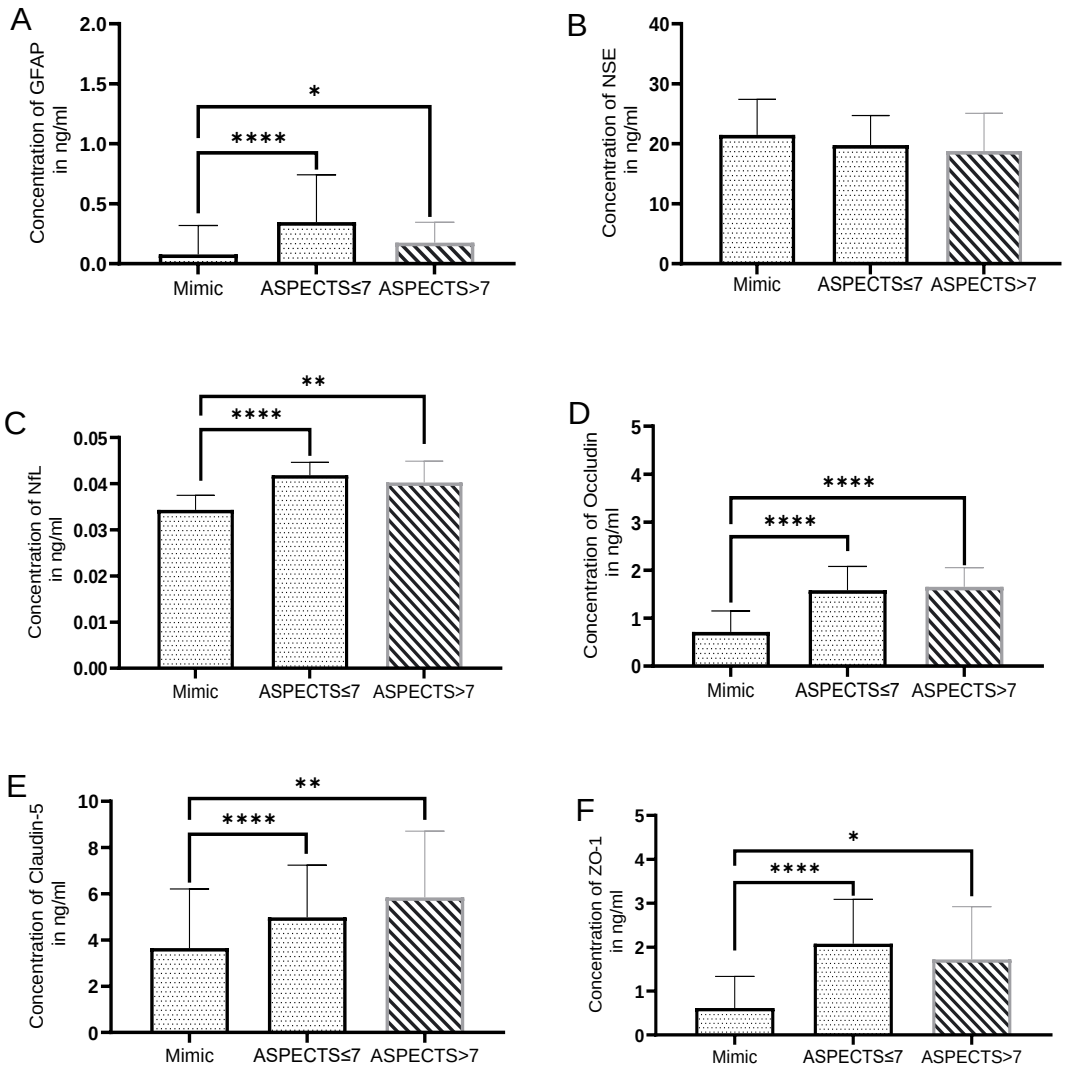

Figure 5.12 The difference between serum (A) GFAP, (B) NSE, (C) NfL, (D) Occludin, Claudin-5 (E) and ZO-1(F) levels according to ASPECT score in the ischaemic group in a comparison with the mimics. (ASPECTS ≤ 7, n=33), (ASPECTS > 7, n=16) and mimics (n=24). (Mann-Whitney U test, p>0.05: *, p≤0.01: **, p≤0.0001: **).**

5.2.3 MRI results

5.2.3.1 Comparison of ADC in WM and GM of the ischaemic patients

Follow-up head MRI scans were performed on a small group of the patients before discharge. MRI results were obtained from 9 acute stroke patients and 13 mimics. Statistical analysis was achieved as per section 2.3.13 for MRI data

A total of 9 patients with acute ischaemic stroke were included in the MRI analysis. The MRI ADC map was analysed and mean ADC values for the WM and GM of the ischaemic side were compared with those of the non-ischaemic side. Mean WM's ADC value in the ischaemic side of the brain was 1300.63 $*10^{-6}$ mm^2/s and in the non-ischaemic sides of brains was 881.81 $*10^{-6}$ mm^2/s. Similarly, the mean GM's ADC value in the ischaemic and the non-ischaemic sides of brains were 1480.88 $*10^{-6}$ mm^2/s and 1013.13 $*10^{-6}$ mm^2/s, respectively as shown in Table 5-5.

The results showed that all the ischaemic stroke patients have a significant rise in ADC values following stroke both in the ischaemic WM and GM areas as compared to their corresponding values in the non-ischaemic regions of the brains (Paired Student's t-test, p=0.002 and p=0.002) respectively as shown in Figure 5.13. An MRI scan for one ischaemic patient showing the difference in the ADC values between the ischaemic and the non-ischaemic sides is shown in Figure 5.14.

Table 5-5 ADC values of the ischaemic and the non-ischaemic WM and GM areas in the ischaemic patients (n=9). Data are shown as mean (SD).

Mean (SD)	Tissue (WM or GM)	Ischaemic area ADC ($*10^{-6}$ mm^2/s)	Non-ischaemic area ADC ($*10^{-6}$ mm^2/s)
	WM	1300.63 (245.15)	881.81 (91.62)
	GM	1480.88 (242.42)	1031.13 (32.38)

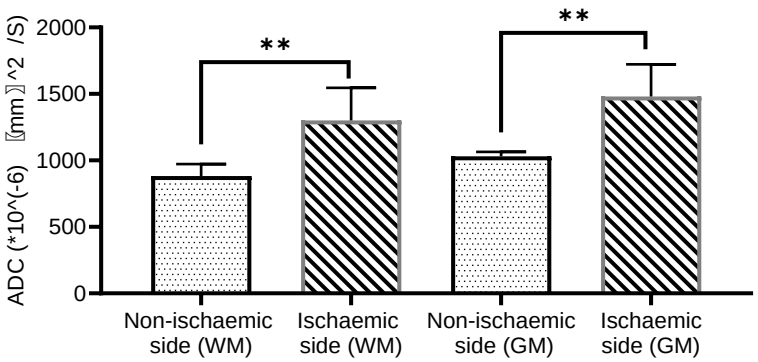

Figure 5.13 ADC values in MRI DWI in the ischaemic and the non-ischaemic WM and GM areas in the ischaemic patients (n=9), (Paired Student's t-test, in WM p=0.002 and in GM p=0.002).

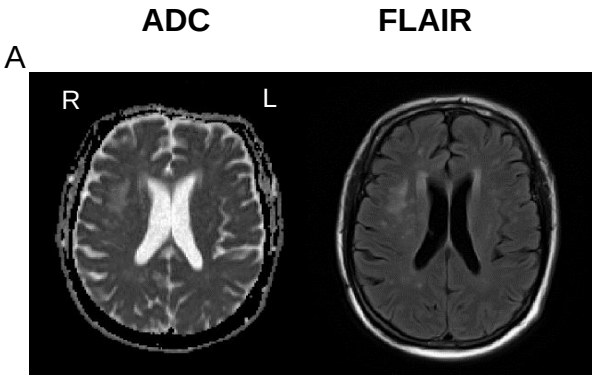

B

	ADC (WM) (x 10^{-6} mm^2/s)	ADC (GM) (x 10^{-6} mm^2/s)
Ischaemic side	1224.00	1267.42
Non-ischaemic side	882.80	1068.14

Figure 5.14 An MRI head scan for a patient with acute right MCA territory infarct. A) MRI ADC map (left) and fluid-attenuated inversion recovery (FLAIR)(right). B) ADC values of the 2 hemispheres (the ischaemic side and the non-ischaemic side) in both WM and GM.

5.2.3.2 Comparison of ADC in WM and GM in the stroke mimics

In the MRI analysis, 13 mimics were included. Follow-up head MRI was performed before discharge. The MRI ADC map was analysed and the mean ADC values for the right side were compared with the left side. The mean WM's ADC value on the right sides was 742.80*10^{-6} mm ^{2}/s and on the left sides was 734.46 *10^{-6} mm^2/s. Similarly,

the mean GM's ADC values on the right sides and the left sides were 1015.01 *10^{-6} mm^2/s and 985.39 *10^{-6} mm^2/s, respectively Table 5-6.

The results showed no significant difference between the ADC values in WM and GM of the left and the right side of the brain in the mimics as expected (Figure 5.15). An MRI scan for one mimic patient showing the ADC values between the right and the left sides is shown in Figure 5.16.

Table 5-6 ADC values in the left side and the right side WM and GM areas in the mimics (n=13). Data are shown as mean (SD).

Mean (SD)	Tissue (WM or GM)	Left side ADC (*10^{-6} mm^2/s)	Right side ADC (*10^{-6} mm /s)
	WM	734.46 (67.32)	742.80 (77.52
	GM	985.39 (93.42)	1015.01 (93.67)

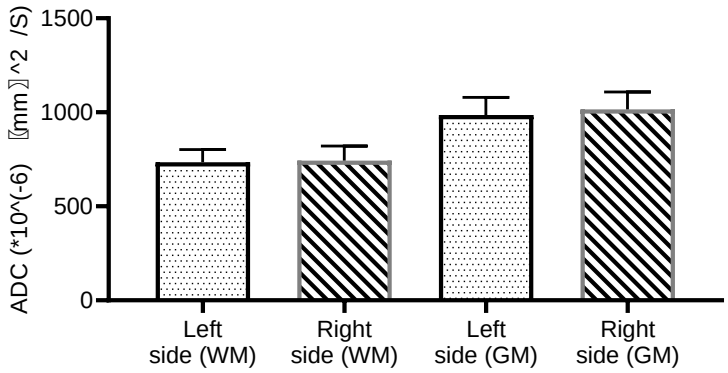

Figure 5.15 ADC map values in the left side and the right side WM and GM areas in the mimics (n=13). No significant difference was observed between the two sides (Paired Student's t-test).

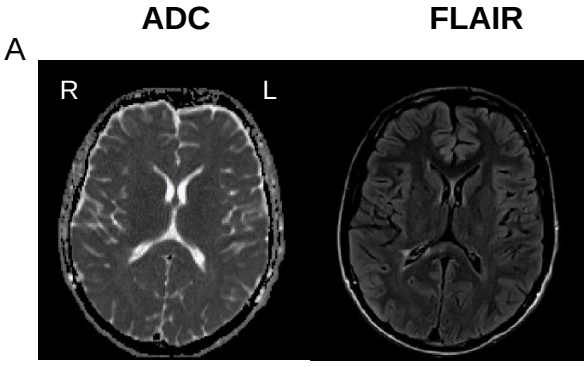

B

	ADC (WM) (x 10^{-6} mm^2/s)	ADC (GM) (x 10^{-6} mm^2/s)
Right side	668.73	842.55
Left side	621.35	822.33

Figure 5.16 An MRI head scan for a stroke mimics A) MRI ADC map (left) and fluid-attenuated inversion recovery (FLAIR)(right). B) ADC values of the 2 hemispheres (the right side and the left side) in both WM and GM.

5.2.3.3 Ratio of T2 signal intensity of WM and GM in the ischaemic patients

This analysis has been done on 9 patients with acute ischaemic stroke. T2-weighted images were analysed and the ratio of T2 signal intensity (ischaemic /non-ischaemic) in WM and GM regions are shown in Table 5-7. The results showed that the ratio of T2 signal intensity (ischaemic side to the non-ischaemic side) was significantly different in WM (One sample t-test, p=0.05) and GM areas of the brain (One t test, p=0.05) as displayed in Figure 5.17. An example of MRI scan for an ischaemic patient scan where the ratio of T2 signal intensity was used is shown in Figure 5.18.

Table 5-7 Ratio of T2 signal intensity (ischaemic side/non-ischaemic side) in WM and GM in the ischaemic group (n=9). Data are shown as mean (SD).

Ratio of T2 signal intensity	Tissue (WM or GM)	(Ischaemic area / non-ischaemic)
	WM	1.84 (0.61)
	GM	1.36 (0.28)

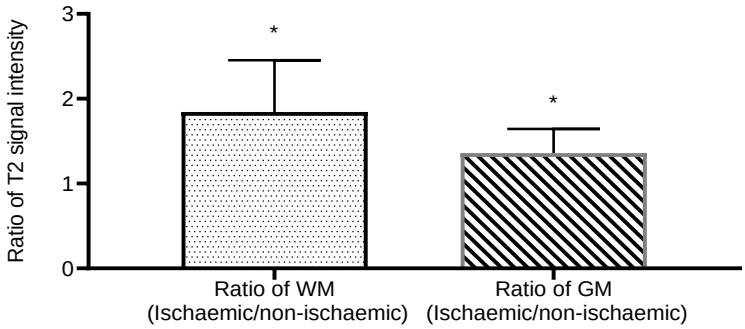

Figure 5.17 Ratio of T2 signal intensity different from 1 in WM and GM areas in the ischaemic patients (n=9). (One sample t-test, in WM p=0.05 and in GM p=0.05).

A

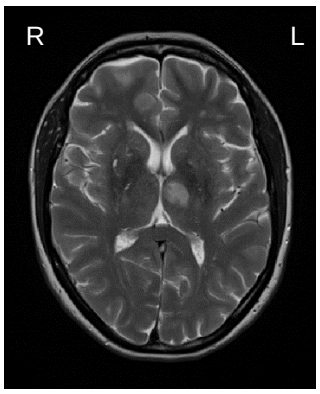

B

	Ratio of T2 signal intensity (Ischaemic side / non-ischaemic side)
WM	2.18
GM	1.04

Figure 5.18 Follow-up MRI head scan for a patient with atypical ischaemic in the left thalamus. A) T2-weighted image. B) the ratio of T2 signal intensity (the ischaemic side / the non-ischaemic side) in both WM and GM.

5.2.3.4 Ratio of T2 signal intensity in WM and GM in the mimics

This analysis has been done from 13 mimics. The mean (SD) of ratios of T2 signal intensity (left /right side) of WM and GM regions in the stroke mimics are shown in Table 5-8. As expected, no significant changes in the ratio of T2 signal intensity in WM and GM in the mimics (Figure 5.19) were found. An example of MRI scan for one mimic patient where the ratio of T2 signal intensity was used is shown in Figure 5.20.

Table 5-8 Ratio of T2 signal intensity (left side of brain/right side of the brain) in WM and GM in the mimics (n=13). Data are shown as mean (SD).

Ratio of T2 signal intensity	Tissue (WM or GM)	(Left side / right side)
	WM	1.05 (0.09)
	GM	1.02 (0.09)

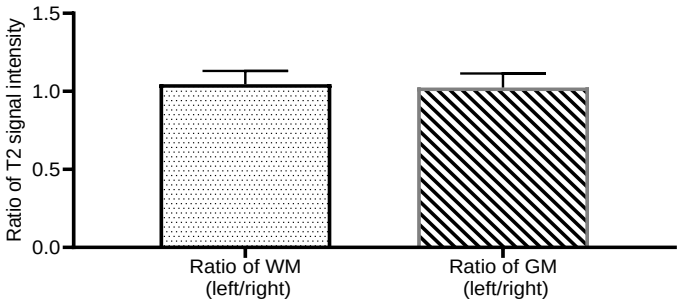

Figure 5.19 Ratio of T2 signal intensity different from 1 in WM and GM areas in mimics (n=16). No significant difference was observed between the two sides of the brain.

A

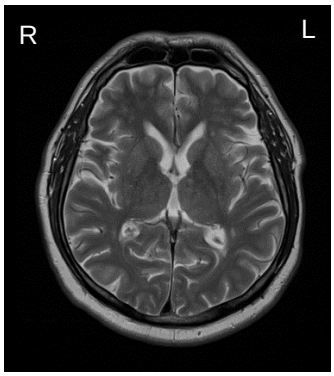

B

	Ratio of T2 signal intensity (Left side / right side)
WM	1.21
GM	1.13

Figure 5.20 Follow-up MRI head scan for stroke mimics. A) T2-weighted image. B) the ratio of T2 signal intensity (the left side / the right side) in both WM and GM.

5.2.3.5 Difference in biomarkers between anterior circulation occlusion vs posterior circulation occlusion in WM and GM

Out of the 9 ischaemic patients, 5 patients had occlusion in the anterior circulation (ACO) and 4 patients in the posterior circulation (PCO). All the PCO patients had an increased ADC value in both WM and GM compared to the ACO patients with no significant changes (Figure 5.21, A). Similarly, while all the PCO patients had an increased ratio of T2 signal intensity in both WM and GM compared to the ACO

patients in which no significant changes were seen (Figure 5.21, B), suggesting the possible ability of these imaging biomarkers to differentiate between the ACO and the PCO.

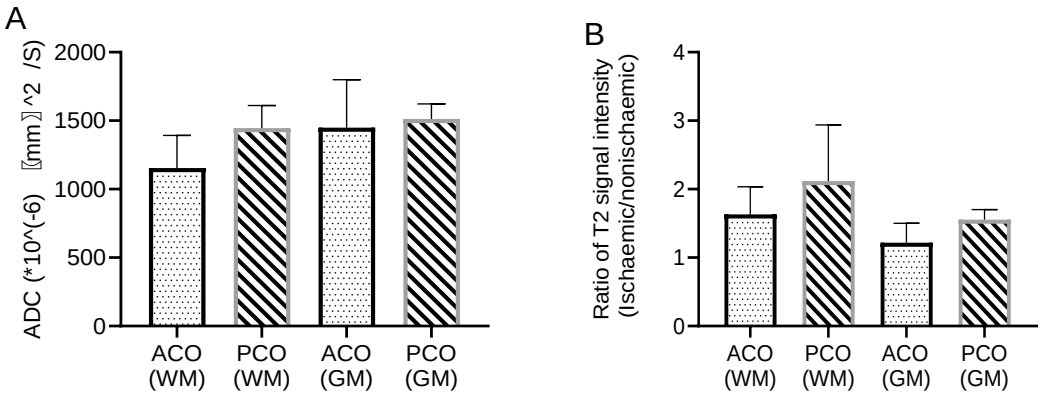

Figure 5.21 Difference of A) ADC values and B) ratio of T2 signal intensity between (ACO:n=5) and (PCO:n=4) in WM and GM. No significant difference was observed in both groups, (Unpaired Student's t-test t).

5.2.3.6 Volume of infarct area and NIHSS

Volumes of infarct (ml) were measured in each ischaemic patient. The mean (SD) of the volume of infarct was 5.82 ml (8.04). Figure 5.22 shows the analysis results of the volume of infarct individually. Volume of infarct was compared with NIHSS. Seven patients had NIHSS ≤ 7, while two patients had NIHSS > 7. However, clot volume was not a significant predictor of the difference in NIHSS score in this sample. Data showed that NIHSS ≤ 7's patients had a larger volume of infarcts than NIHSS > 7 's patients with no significant difference (Mann-Whitney U test- p=0.884) as shown in Figure 5.23.

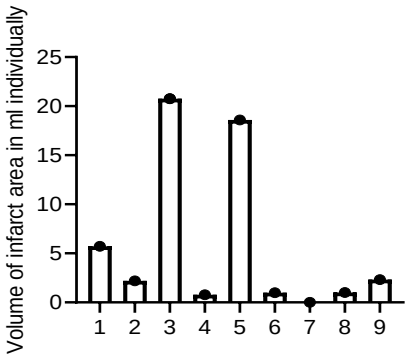

Figure 5.22 An individual volume of infarct volume ml in each patient.

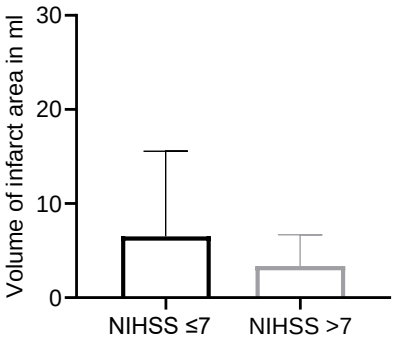

Figure 5.23 A comparison between the volume of infarct and NIHSS ($NIHSS \leq 7$, n=7) ($NIHSS > 7$, n=2). (Mann-Whitney U test- p=0.884).

5.2.3.7 Volume of infarct and the location of occlusion

Volume of infarct was compared with the location of the occlusion. Five patients had ACO, while four patients had PCO. The results showed that infarct volume was not a significant predictor of the difference in the location of the occlusion. Specifically, no significant difference in the volume of infarct between ACO and PCO patients was seen as shown in Figure 5.24, (Mann-Whitney U test- p=0.713).

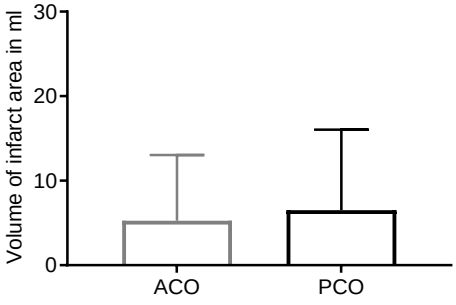

Figure 5.24 A comparison of the volume of infarct volume in ml between the anterior circulation occlusion (ACO:n=5) and the posterior circulation occlusion (PCO:n=4). (Mann-Whitney U test- p=0.713).

5.2.4 Summary and main findings

- The imaging biomarkers: CT HU values of ASPECTS, MRI ADC values and T2 signal intensity are significantly different between the ischaemic side and the non-ischaemic side in the ischaemic patients.
- These imaging biomarkers are not significantly different between the left side and the right side in the mimics patients.
- Serum GFAP, NfL, Occludin, Claudin-5 and ZO-1 but not NSE are able to differentiate between ischaemic patients with ASPECTS ≤ 7 and mimics as well as between ischaemic patients with ASPECTS >7 and mimics.

5.3 Cross sectional study – Added value of imaging biomarkers to circulating biomarkers for improving stroke diagnosis

In this project, the levels of blood biomarkers with CT and MRI imaging biomarkers (Chapter 5.2) to distinguish between ischaemic stroke and stroke mimics were assessed. There are very few studies that correlated the levels of circulating biomarkers with CT and MRI imaging biomarkers. Thus, this chapter presented the added value of imaging biomarkers to circulating biomarkers to improve stroke diagnosis by studying the correlation between the blood biomarker results and CT or MRI results.

5.3.1 ASPECTS correlated with biomarkers levels

Data were collected from Leeds Teaching Hospitals NHS Trust as explained in section 2.3.2 and section 2.3.3. Blood samples were prepared and analysed, as per section 2.3.4 and section 2.3.5 respectively. CT ASPECTS data analysis was done as per section 2.3.9. Statistical correlation analysis was similar to section 3.3.14.
Both Spearman correlation and simple linear regression analyses were applied to determine the association between the studied biomarkers concentrations (GFAP, NSE, NfL, Occludin, Claudin-5 and ZO-1) and CT ASPECTS in the ischaemic patients.

The Spearman correlation analysis indicated a significant negative association between GFAP concentrations and ASPECTS obtained from the stroke patients (n=49), (r=- 0.273, p =0.023). Also, in the simple linear regression analysis, a significant association was observed between GFAP concentrations and ASPECTS in these patients (95% confidence interval, R SQUARED = 0.074, p=0.023), (Figure 5.25-A).

The neuronal markers (NSE and NfL) concentrations did not show any correlations with ASPECTS in the Spearman correlation analysis (NSE: r=0.034; p=0.821, Figure 5.25-B) and (NfL: r =- 0.120; p=0.325, Figure 5.25-C). The simple linear regression analysis also did not show any associations between these two markers and the ASPECT score (NSE:95% confidence interval, R SQUARED = 0.003, p=0.736) and NfL:95% confidence interval, R SQUARED = 0.028, p=0.166).

The Spearman's rank correlation coefficient between TJ proteins (Occludin, Claudin-5 and ZO-1) and ASPECTS revealed no correlations between these two parameters in the ischaemic patients, (Occludin: r=- 0.087, p=0.475, Figure 5.25-D), (Claudin-5: r=0.066, p=0.593, Figure 5.25-E) and (ZO-1: r=- 0.221, p=0.068, Figure 5.25-F). Similar results were found in the simple linear regression analysis (Occludin: 95% confidence interval, R SQUARED = 0.006, p=0.542), (Claudin-5:95% confidence interval, R SQUARED = 0.005, p=0.551) and (ZO-1:95% confidence interval, R SQUARED = 0.026, p=0.190).

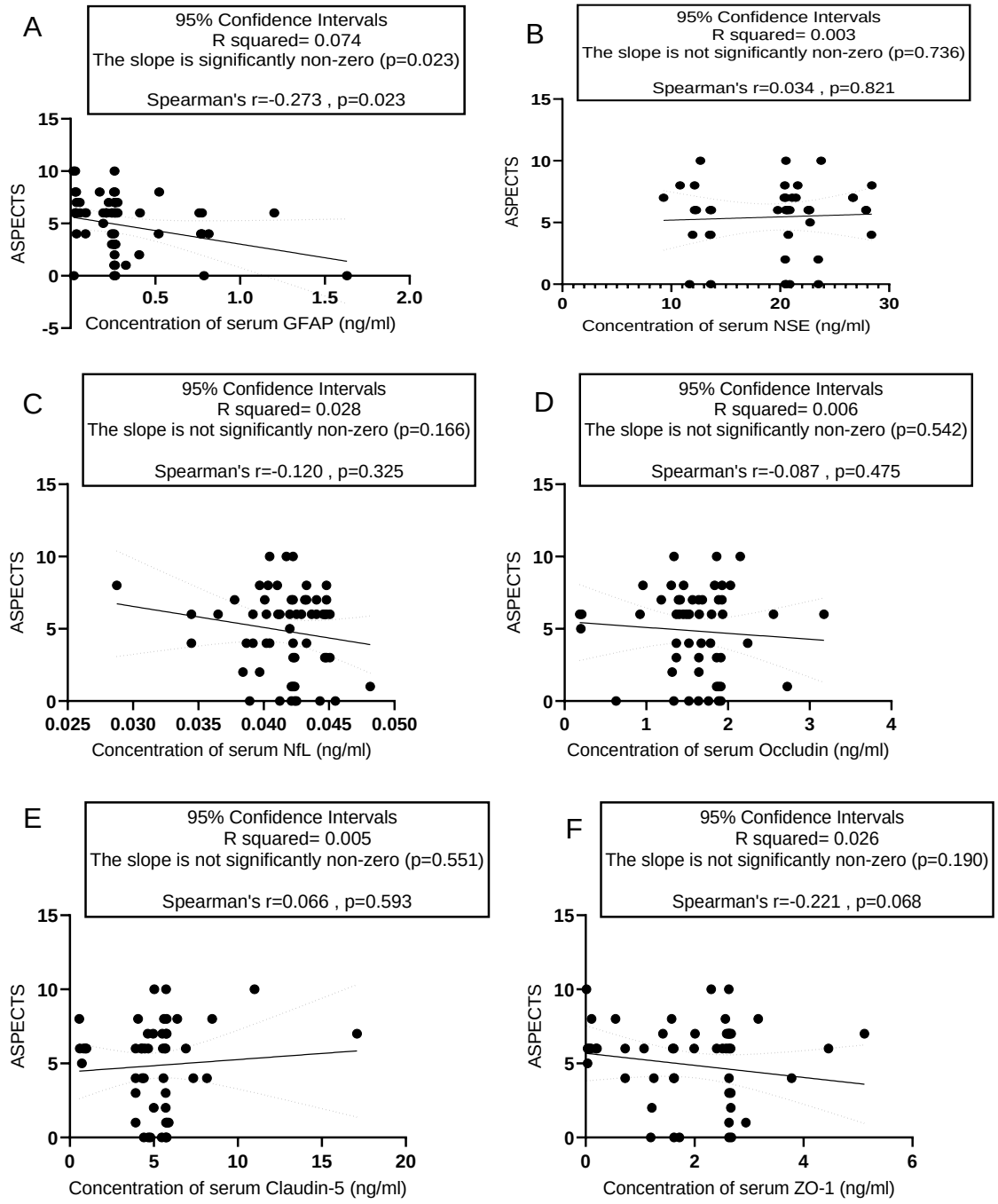

Figure 5.25 Correlation analysis between serum A: GFAP, B: NSE C: NfL, D: Occludin, E: Claudin-5 and F: ZO-1 levels and ASPECTS using Spearman correlation and simple linear regression (n=49). Only GFAP level (A) showed a significant negative association with ASPECTS (r= - 0.273, p =0.023).

5.3.2 ADC values correlated with biomarkers levels

MRI data analysis was done as per section 2.3.12. Statistical correlation analysis was similar to section 3.3.14.

To investigate if MRI ADC values in the WM and GM are correlated with biomarkers levels, the Spearman correlation test and simple linear regression analyses were also used.

Results of the Spearman correlation indicated that there were no significant associations between GFAP, NSE and NfL levels and ADC values in WM (n=9), (GFAP: r= 0.150, p= 0.708, Figure 5.26-A; NSE: r= 0.250, p=0.521, Figure 5.26-B; and NfL: r= - 0.083, p=0 .843, Figure 5.26-C). Similarly, results of the simple linear regression indicated that there were no significant effects between the GFAP, NSE and NfL levels and ADC values in WM (GFAP:95% confidence interval, R SQUARED = 0.002, p =0.911), (NSE:95% confidence interval, R SQUARED = 0.085, p=0 .448) and (NfL:95% confidence interval, R SQUARED = 0.00, p=0 .955).

The Spearman correlation also indicated that there were no significant associations between GFAP, NSE and NfL levels and ADC values in GM (GFAP: r= - 0.367, p=0.336, Figure 5.26-A;NSE: r= 0.083, p=0 .843, Figure 5.26-B and NfL: r= - 0.517, p=0 .162, Figure 5.26-C). Similarly, results of the simple linear regression indicated that there were no collective significant effects between the GFAP, NSE and NfL levels and ADC values in GM (GFAP:95% confidence interval, R SQUARED = 0.146, p=0 .309), (NSE:95% confidence interval, R SQUARED = 0.037, p=0 .620) and (NfL:95% confidence interval, R SQUARED = 0.099, p= 0.407).

The link between the three TJ proteins levels and ADC values in WM and GM was examined using the Spearman's rank correlation coefficient and the simple linear regression analysis. Results of the Spearman correlation showed that there were no significant correlations between Occludin, Claudin-5 and ZO-1 with ADC values in WM (Occludin: r= 0.133, p= 0.744, Figure 5.26-D), (Claudin-5: r= - 0.183, p=0 .644, Figure 5.26-E) and (ZO-1: r= - 0.083, p=0 .843, Figure 5.26-F). Similarly, results of the simple linear regression indicated that there were no collective significant effects between the Occludin, Claudin-5 and ZO-1 with ADC values in WM (Occludin:95% confidence interval, R SQUARED = 0.00, p =0.972), (Claudin-5:95% confidence interval, R

SQUARED =5.558e-005, p=0 .985) and (ZO-1:95% confidence interval, R SQUARED = 0.003, p=0 .884).

The Spearman correlation showed that there were no significant correlations between Occludin, Claudin-5 and ZO-1 with ADC values in GM (Occludin: r= 0.167, p= 0.677, Figure 5.26-D), (Claudin-5: r= -0.083, p=0.843, Figure 5.26-E) and (ZO-1: r= 0.066, p=0.880, Figure 5.26-F). Similarly, results of the simple linear regression indicated that there were no collective significant effects between the Occludin, Claudin-5 and ZO-1 with ADC values in GM (Occludin:95% confidence interval, R SQUARED = 0.002, p =0.907), (Claudin-5:95% confidence interval, R SQUARED = 0.091, p=0 .430) and (ZO-1:95% confidence interval, R SQUARED = 0.024, p=0.694).

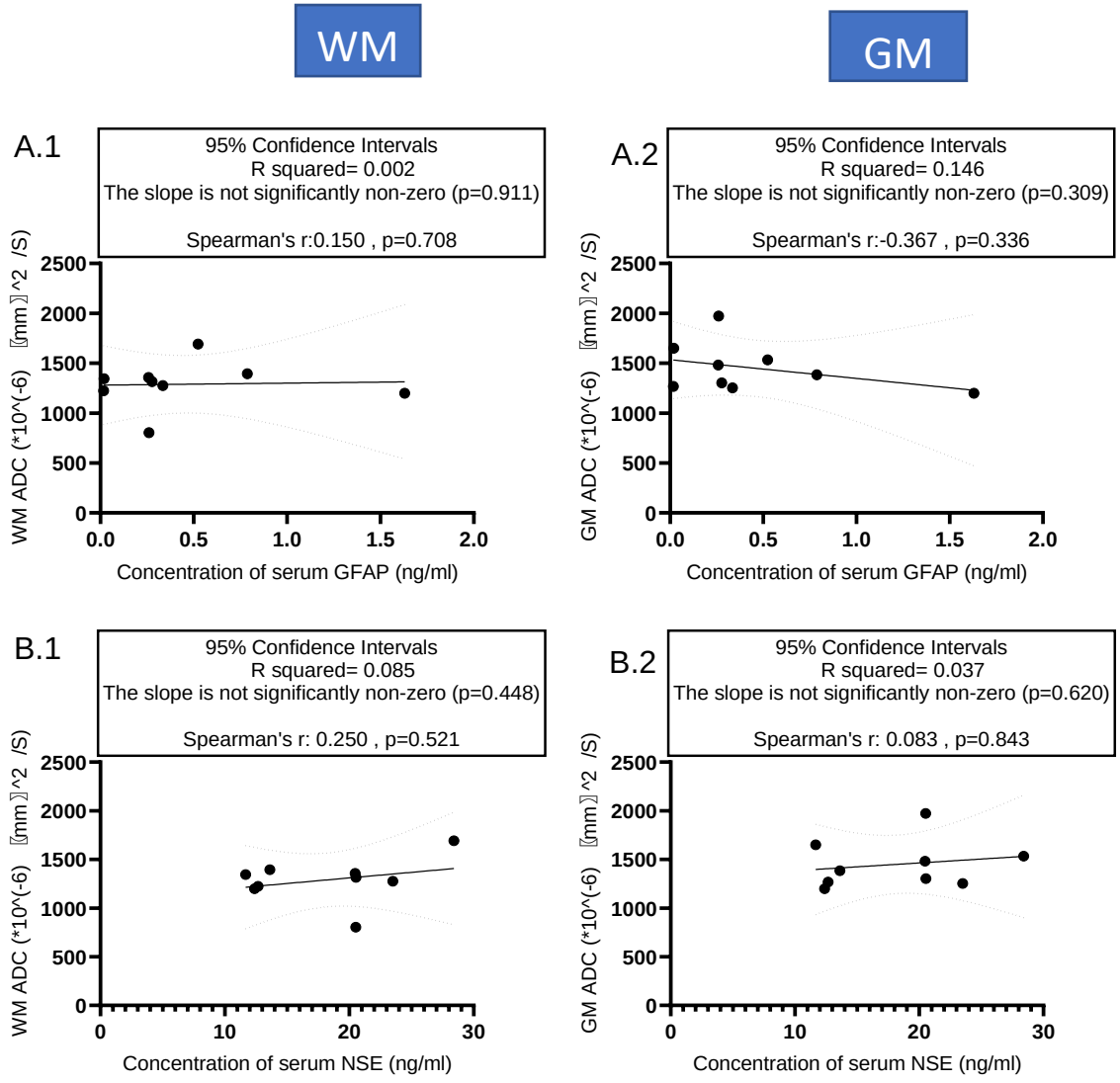

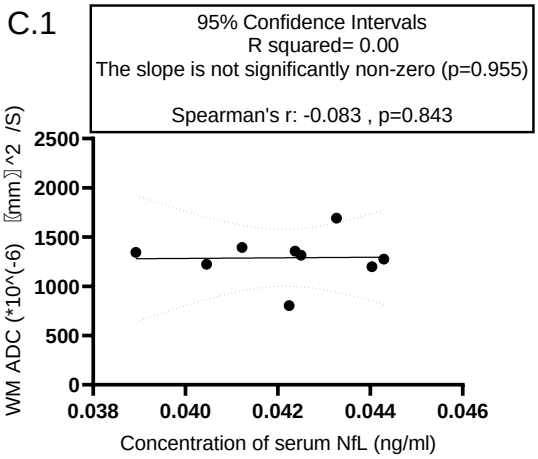
C.1
95% Confidence Intervals
R squared= 0.00
The slope is not significantly non-zero (p=0.955)
Spearman's r: -0.083 , p=0.843
WM ADC (*10^(-6) ⟦mm⟧^2 /S)
2500
2000
1500
1000
500
0
0.038
0.040
0.042
0.044
0.046
Concentration of serum NfL (ng/ml)

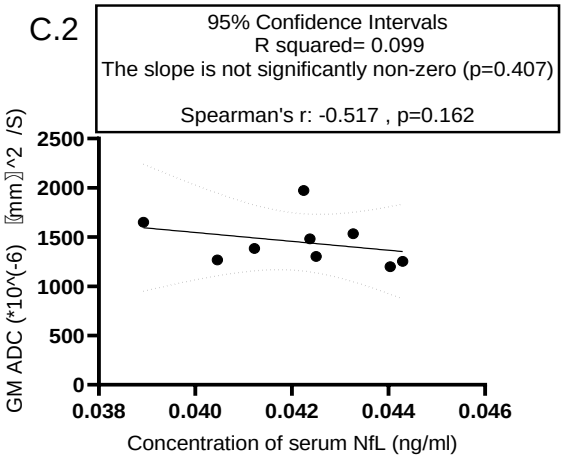
C.2
95% Confidence Intervals
R squared= 0.099
The slope is not significantly non-zero (p=0.407)
Spearman's r: -0.517 , p=0.162
GM ADC (*10^(-6) ⟦mm⟧^2 /S)
2500
2000
1500
1000
500
0
0.038
0.040
0.042
0.044
0.046
Concentration of serum NfL (ng/ml)

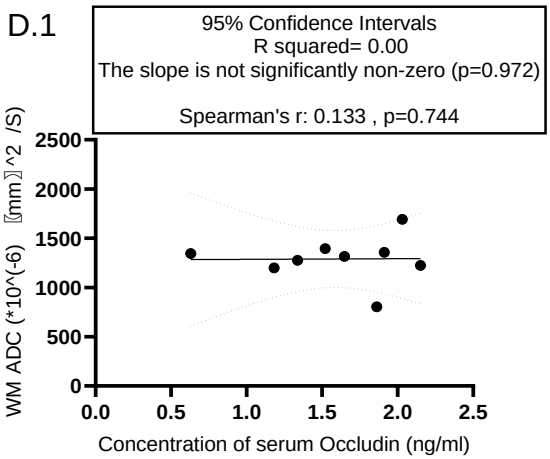
D.1
95% Confidence Intervals
R squared= 0.00
The slope is not significantly non-zero (p=0.972)
Spearman's r: 0.133 , p=0.744
WM ADC (*10^(-6) ⟦mm⟧^2 /S)
2500
2000
1500
1000
500
0
0.0
0.5
1.0
1.5
2.0
2.5
Concentration of serum Occludin (ng/ml)

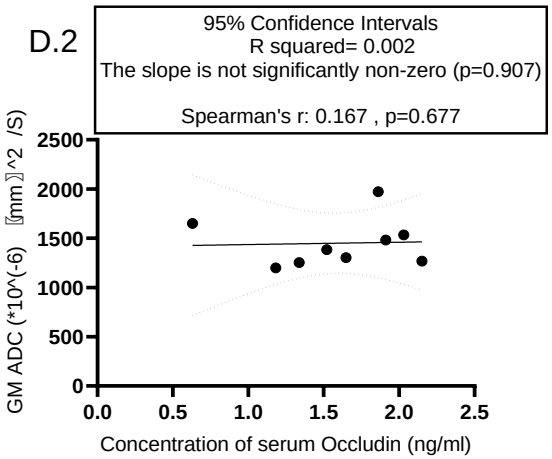
D.2
95% Confidence Intervals
R squared= 0.002
The slope is not significantly non-zero (p=0.907)
Spearman's r: 0.167 , p=0.677
GM ADC (*10^(-6) ⟦mm⟧^2 /S)
2500
2000
1500
1000
500
0
0.0
0.5
1.0
1.5
2.0
2.5
Concentration of serum Occludin (ng/ml)

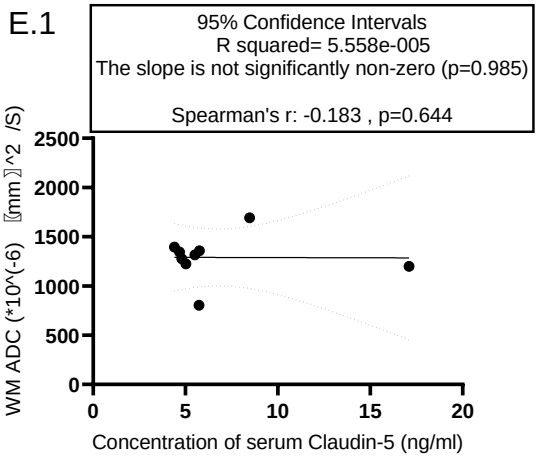
E.1
95% Confidence Intervals
R squared= 5.558e-005
The slope is not significantly non-zero (p=0.985)
Spearman's r: -0.183 , p=0.644
WM ADC (*10^(-6) ⟦mm⟧^2 /S)
2500
2000
1500
1000
500
0
0
5
10
15
20
Concentration of serum Claudin-5 (ng/ml)

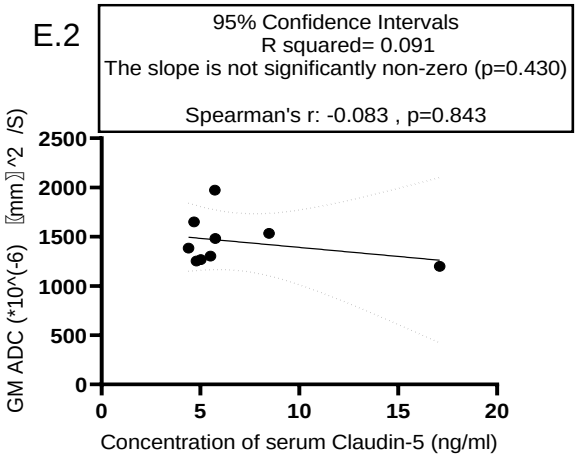
E.2
95% Confidence Intervals
R squared= 0.091
The slope is not significantly non-zero (p=0.430)
Spearman's r: -0.083 , p=0.843
GM ADC (*10^(-6) ⟦mm⟧^2 /S)
2500
2000
1500
1000
500
0
0
5
10
15
20
Concentration of serum Claudin-5 (ng/ml)

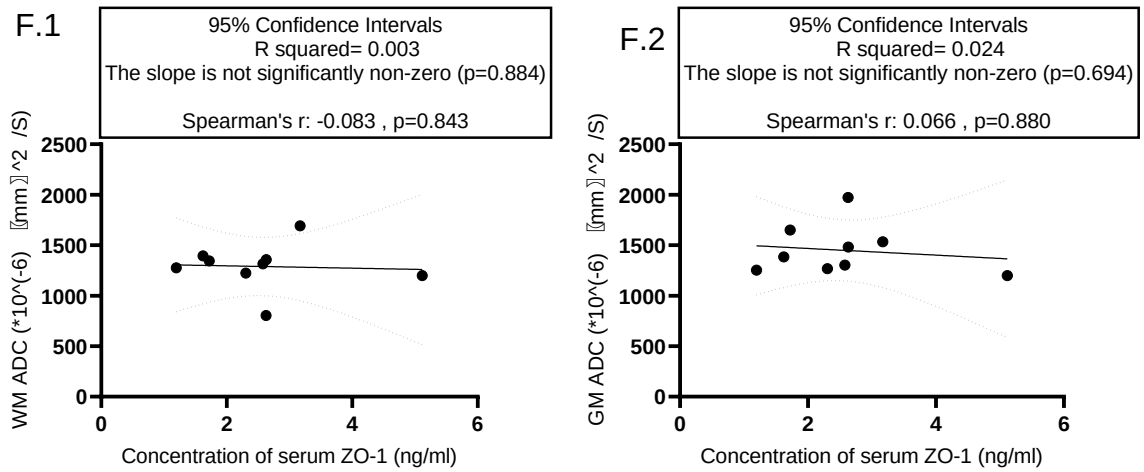

Figure 5.26 Correlation analysis between serum A: GFAP, B: NSE C: NfL, D: Occludin, E: Claudin-5 and F: ZO-1 levels and ADC values in MRI using Spearman correlation and simple linear regression (n=9). None of the biomarkers were correlated with ADC values.

5.3.3 T2 signal intensity correlated with biomarkers levels

To investigate if the T2 signal intensities in MRI in ischaemic WM and GM are correlated with the investigated biomarkers' concentrations, the Spearman correlation analysis and simple linear regression were performed.

Results of the Spearman correlation indicated that there was no significant association between GFAP and T2 signal intensity in WM (n=9), (r= 0.383, p= 0.313, Figure 5.27-A). Similarly, the results of the simple linear regression indicated that there was no collective significant effect between the GFAP and T2 signal intensity in WM (95% confidence interval, R SQUARED = 0.009, p =0.811). Regarding GM, results of the Spearman correlation indicated that there was also no significant association between GFAP and T2 signal intensity in GM in both the Spearman correlation analysis (r= 0.167, p=0.677, Figure 5.27-A) and the linear regression analysis (95% confidence interval, R SQUARED = 0.009, p=0.809).

However, positive significant associations between the neuronal marker, NSE and T2 signal intensity both in WM (r= 0.733, p=0 .031, Figure 5.27-B) (95% confidence interval, R SQUARED = 0.647, p=0 .009) and in GM was observed (r= 0.733, p=0.031, Figure 5.27-B) (95% confidence interval, R SQUARED = 0.560, p=0.020).

The other neuronal marker (NfL) also showed a positive significant correlation with WM T2 signal intensity using the Spearman correlation (r= 0.967, p=0.0002, Figure 5.27-C) and the linear regression analysis (95% confidence interval, R SQUARED = 0.497, p=0.034). In GM also, results revealed a significant association between NfL and T2 signal intensity (r= 0.817, p=0.011, Figure 5.27-C) (95% confidence interval, R SQUARED = 0.659, p=0.008).

Results of the Spearman correlation showed that there were no significant correlations between Occludin, Claudin-5 and ZO-1 with T2 signal intensity in the WM (Occludin: r= 0.217, p= 0.581, Figure 5.27-D), (Claudin-5: r=0.600, p=0.097, Figure 5.27-E) and (ZO-1: r= 0.483, p=0.194, Figure 5.27-F) as well as in the GM (Occludin: r= 0.167, p= 0.677, Figure 5.27-D), (Claudin-5: r= 0.117, p=0.776 Figure 5.27-E) and (ZO-1: r= 0.050, p=0.912, Figure 5.27-F). Similarly, the results of the simple linear regression indicated that there were no collective significant effects between the Occludin, Claudin-5 and ZO-1 with T2 signal intensity in the WM (Occludin:95% confidence interval, R SQUARED = 0.095, p =0.420), (Claudin-5:95% confidence interval, R SQUARED = 0.025, p=0.682) and (ZO-1:95% confidence interval, R SQUARED = 0.054, p=0.545) and in the GM (Occludin:95% confidence interval, R SQUARED = 0.059, p =0.528), (Claudin-5:95% confidence interval, R SQUARED = 0.046, p=0.581) and (ZO-1:95% confidence interval, R SQUARED = 0.070, p=0.490).

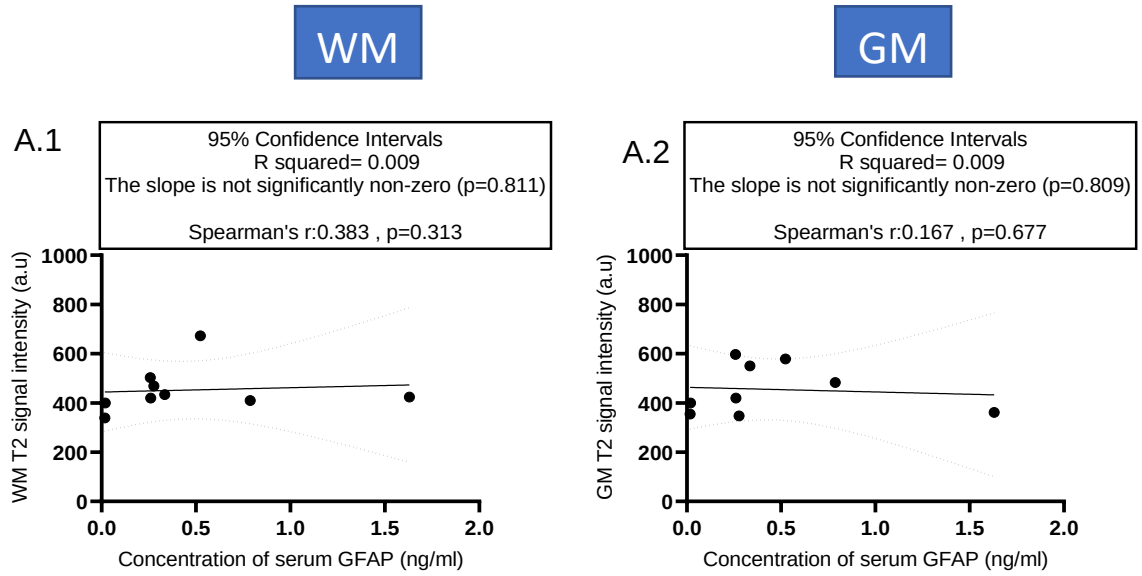

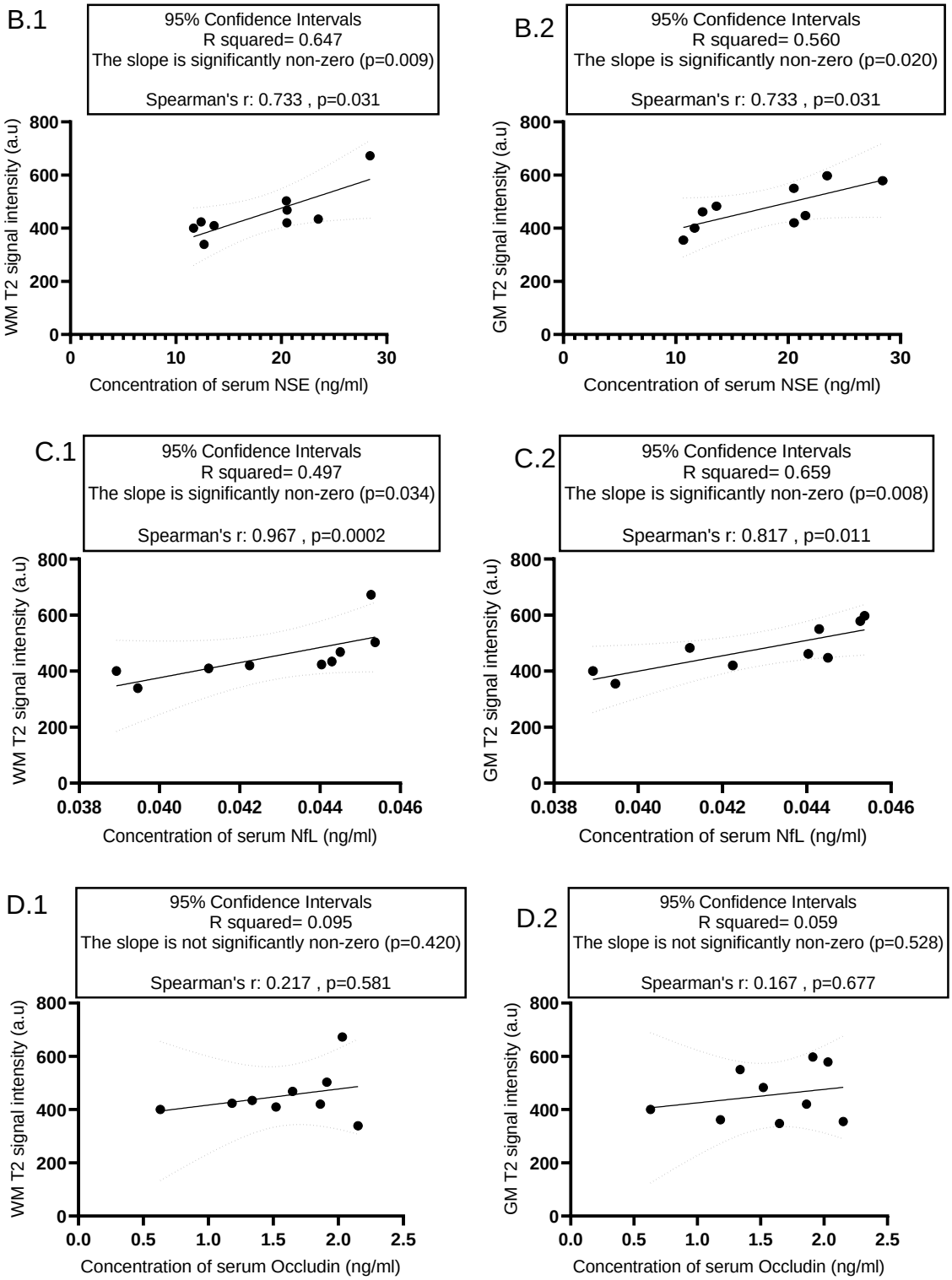
B.1
95% Confidence Intervals
R squared= 0.647
The slope is significantly non-zero (p=0.009)
Spearman's r: 0.733 , p=0.031
WM T2 signal intensity (a.u)
Concentration of serum NSE (ng/ml)
B.2
95% Confidence Intervals
R squared= 0.560
The slope is significantly non-zero (p=0.020)
Spearman's r: 0.733 , p=0.031
GM T2 signal intensity (a.u)
Concentration of serum NSE (ng/ml)
C.1
95% Confidence Intervals
R squared= 0.497
The slope is significantly non-zero (p=0.034)
Spearman's r: 0.967 , p=0.0002
WM T2 signal intensity (a.u)
Concentration of serum NfL (ng/ml)
C.2
95% Confidence Intervals
R squared= 0.659
The slope is significantly non-zero (p=0.008)
Spearman's r: 0.817 , p=0.011
GM T2 signal intensity (a.u)
Concentration of serum NfL (ng/ml)
D.1
95% Confidence Intervals
R squared= 0.095
The slope is not significantly non-zero (p=0.420)
Spearman's r: 0.217 , p=0.581
WM T2 signal intensity (a.u)
Concentration of serum Occludin (ng/ml)
D.2
95% Confidence Intervals
R squared= 0.059
The slope is not significantly non-zero (p=0.528)
Spearman's r: 0.167 , p=0.677
GM T2 signal intensity (a.u)
Concentration of serum Occludin (ng/ml)

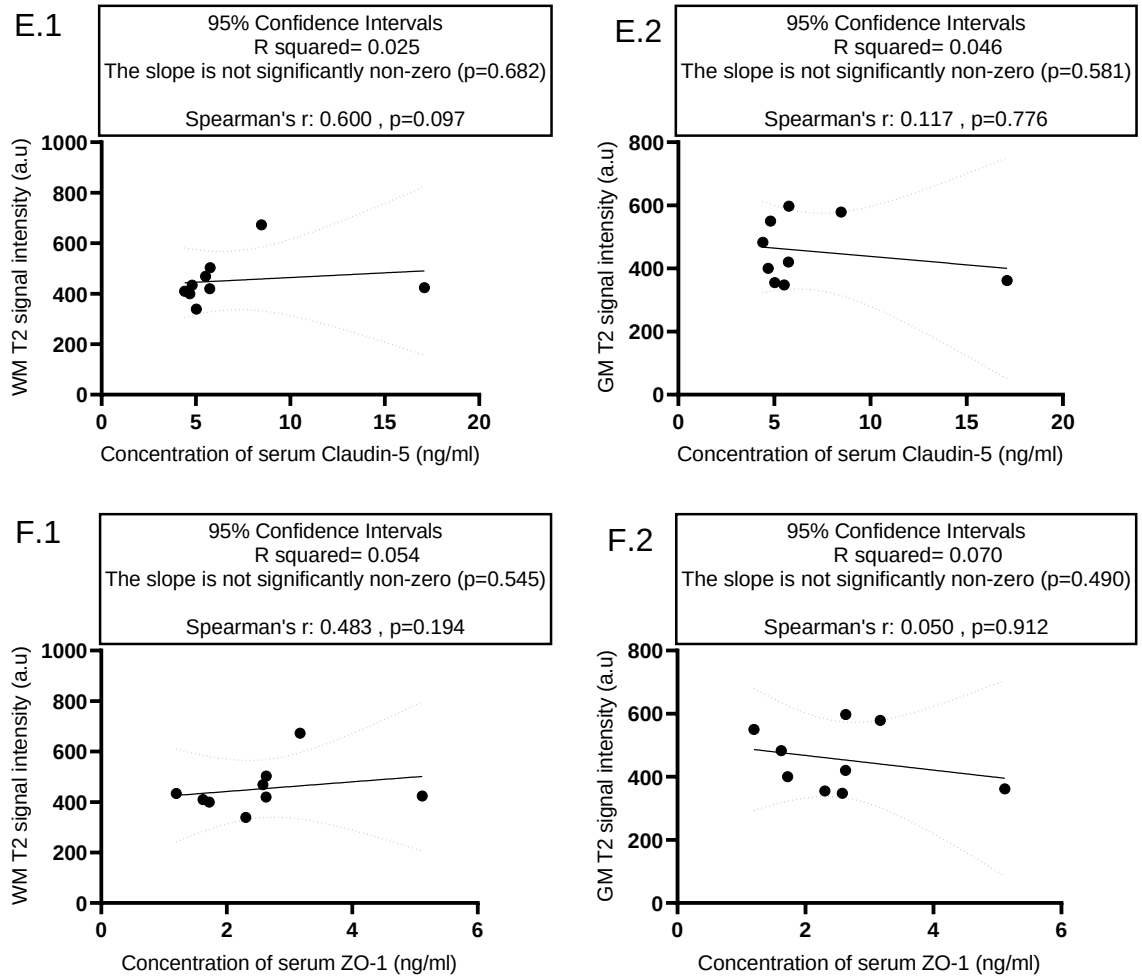

Figure 5.27 Correlation analysis between serum A: GFAP, B: NSE C: NfL, D: Occludin, E: Claudin-5 and F: ZO-1 levels and the of T2 signal intensity in MRI using Spearman correlation and simple linear regression (n=9). NSE level (B) and NfL level (C) were correlated positively with T2 signal intensity in both WM and GM.

5.3.4 Volume of infarct correlated with biomarkers levels

The results revealed no correlation between GFAP concentrations and the volume of infarct (n=9), (r= -0.383, p =0.313). Similar results were observed with the simple linear regression as the results showed no association between the two variables, (95% confidence interval, R SQUARED = 0.023, p=0.695), (Figure 5.28-A).

Regarding neuronal markers, interestingly, results of the simple linear regression indicated that there was a collective positive significant effect between NSE concentrations and the volume of infarct obtained from the linear regression analysis (95% confidence interval, R SQUARED =0.647, p=0.009, Figure 5.28-B). Moreover,

results of the Spearman correlation analysis showed a significant association between the two variables (r =0.717; p=0.037). On the other hand, the Spearman correlation analysis and the simple linear regression analysis did not indicate any correlation between NfL and the volume of infarct (r =0.184; p=0.634) (95% confidence interval, R SQUARED = 0.238, p=0.183), (Figure 5.28-C).

The Spearman's rank correlation coefficient revealed no correlations between TJ proteins (Occludin, Claudin-5 and ZO-1) and the MRI volume of infarct in the ischaemic patients (Occludin: r=0.500, p=0.178, Figure 5.28-D), (Claudin-5: r=0.017, p=0.982, Figure 5.28-E) and (ZO-1: r=-0.133, p=0.744, Figure 5.28-F). Similar results were found in the simple linear regression analysis (Occludin: 95% confidence interval, R SQUARED = 0.048, p=0.569), (Claudin-5:95% confidence interval, R SQUARED = 0.009, p=0.801) and (ZO-1:95% confidence interval, R SQUARED = 0.048, p=0.570).

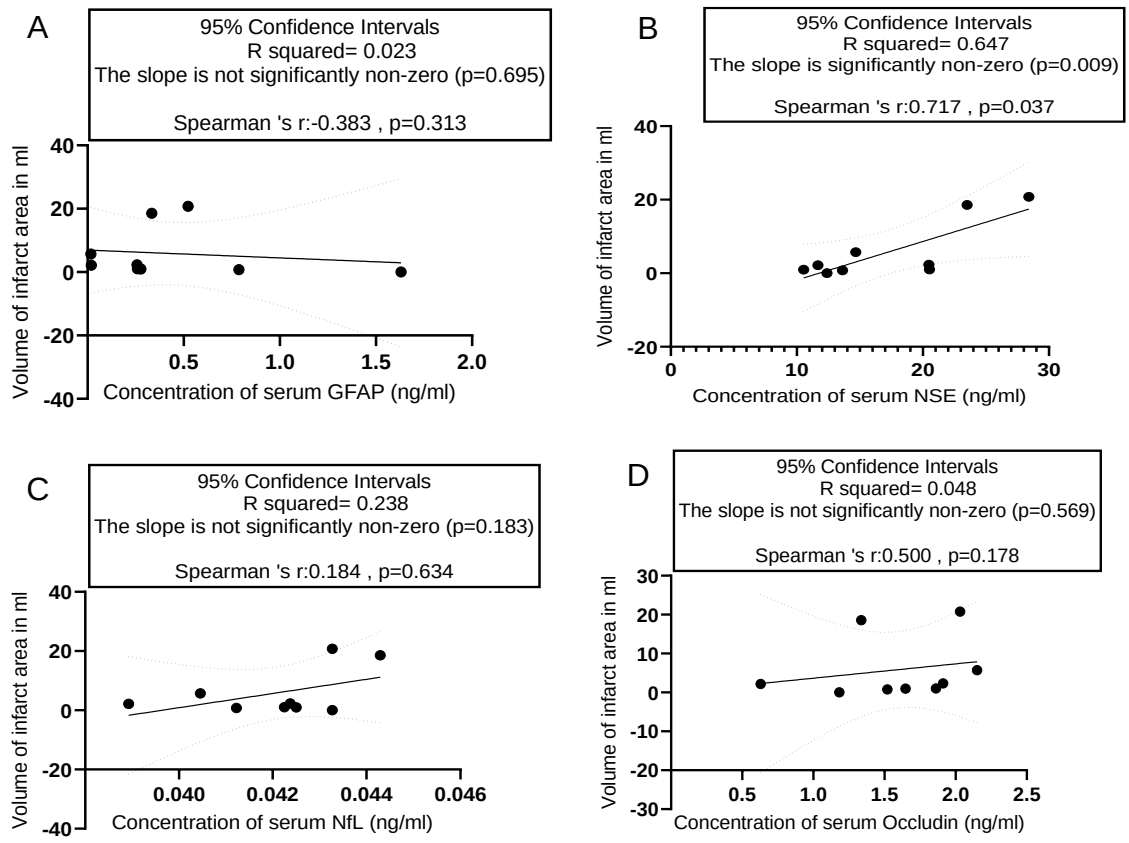

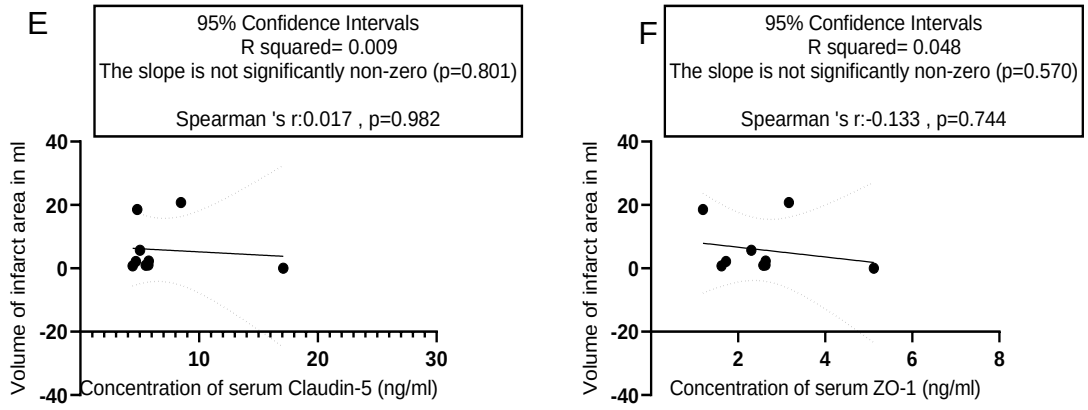

Figure 5.28 Correlation analysis between serum A: GFAP, B: NSE C: NfL, D: Occludin, E: Claudin-5 and F: ZO-1 levels and the volume of infarct in MRI using Spearman correlation and simple linear regression (n=9). Only NSE level (B) showed a significant positive association with the volume of infarct (r =0.717; p=0.037).

5.3.5 NIHSS correlated with biomarkers levels

Both the Spearman correlation and the simple linear regression tests were used to find out if there was an association between the biomarkers' levels in the ischaemic patients and the stroke severity identified by NIHSS at arrival. It is worth noting that, this correlation analysis doesn't include any imaging biomarkers results as it was between circulating biomarkers and the neurological deficit scale (NIHSS). But, the results have been included in this chapter since the same correlation analysis methods were used.

Following an acute stroke, results of the Spearman correlation indicated no association between GFAP concentrations and NIHSS, (n=70), (r= - 0.141, p =0.245). Results of the simple linear regression also indicated no association between the two variables, (95% confidence interval, R SQUARED = 0.002, p=0.691), (Figure 5.29-A).

NSE concentration in the stroke patients did not show any correlation with the severity of stroke (NIHSS) at the time of arrival (r = -0.181; p=0.291) (95% confidence interval, R SQUARED = 0.042, p=0.164), (Figure 5.29-B). However, NfL level has a significant positive correlation with NIHSS in the Spearman correlation (r =0.441; p=0.0001) and the linear regression (95% confidence interval, R SQUARED = 0.141, p=0.002) (Figure 5.29-C).

The link between TJ proteins (Occludin, Claudin-5 and ZO-1) and NIHSS was examined using both the Spearman's rank correlation coefficient and the simple linear regression analysis, which revealed no correlations between these biomarkers and NIHSS in the ischaemic patients, (Spearman's rank correlation; Occludin: r=- 0.0115, p=0.348, Figure 5.29-D), (Claudin-5: r=- 0.032, p=0.797, Figure 5.29-E) and (ZO-1: r=- 0.227, p=0.060, Figure 5.29-F), (Simple linear regression; Occludin: 95% confidence interval, R SQUARED = 4.053e-005, p=0.959), (Claudin-5:95% confidence interval, R SQUARED = 5.398e-005, p=0.952) and (ZO-1:95% confidence interval, R SQUARED = 0.012, p=0.373).

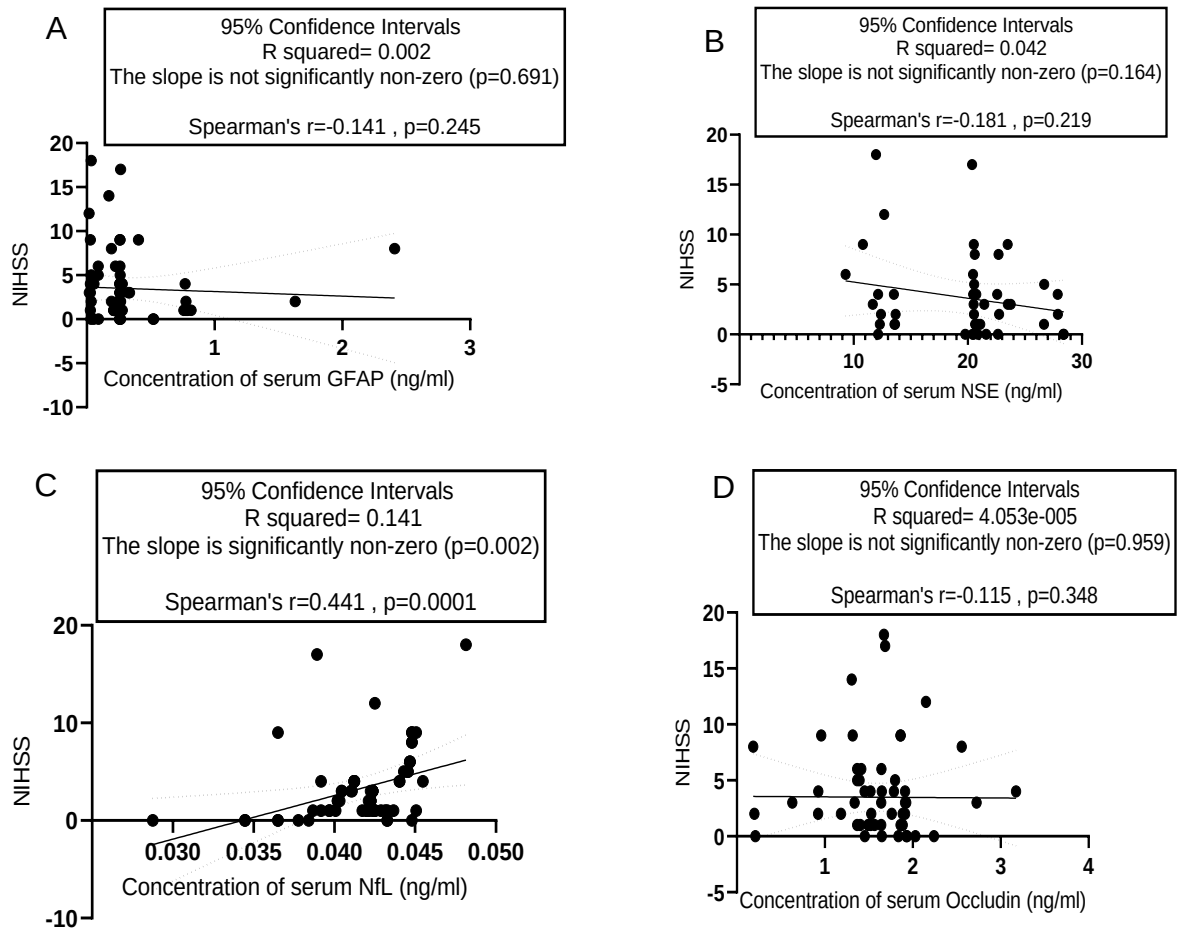

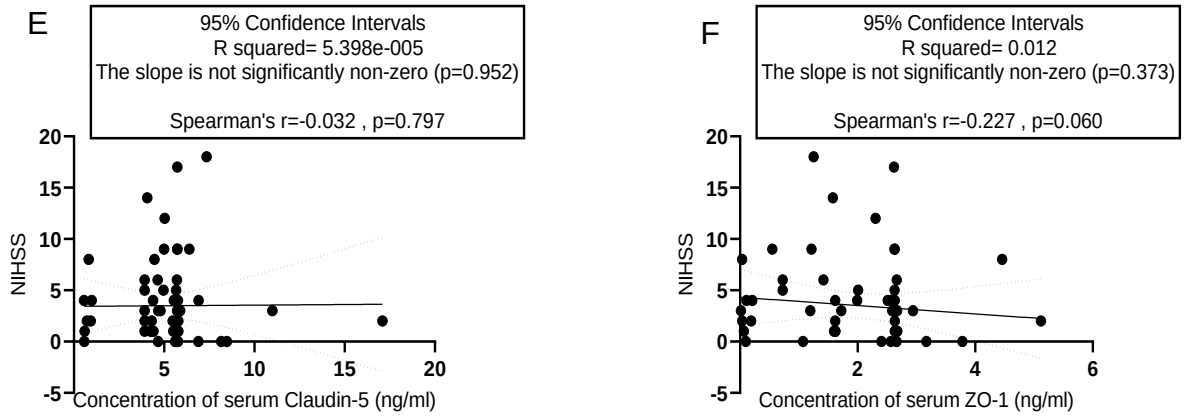

Figure 5.29 Correlation analysis between serum A: GFAP, B: NSE C: NfL, D: Occludin, E: Claudin-5 and F: ZO-1 levels and NIHSS at arrival using Spearman correlation and simple linear regression (n=70). Only NfL levels (C) showed a significant positive correlation with NIHSS (r =0.441; p=0.0001).

5.3.6 Summary and main findings

- GFAP level has a significant negative association with ASPECTS in the ischaemic patients.
- None of the blood biomarkers are correlated with ADC values.
- Neuronal markers (NSE and NfL) levels are correlated positively with MRI T2 signal intensity in both WM and GM.
- NSE level has a significant positive association with the MRI volume of infarct.
- NfL level has a significant positive association with NIHSS.

5.3.7 Discussion

5.3.7.1 Comparison of circulating biomarkers between stroke and stroke mimics

This study aimed to assess the ability of the selected blood-based biomarkers to distinguish between ischaemic stroke patients and stroke mimics as defined by clinical scoring systems as well as imaging data to improve stroke diagnosis. Different comparisons with multiple categories were done to investigate the ability of the selected circulating biomarkers to differentiate between acute stroke patients and mimics. This study compared the biomarkers concentrations between ischaemic and mimics in terms of different classifications: gender, time of blood collection, the

severity of stroke, the location of the occlusion, CT ASPECTS and the ratio of GFAP to other markers. On the basis of the preclinical results, GFAP and TJ proteins were included in the panel of biomarkers to find out if these biomarkers are able to distinguish between ischaemic stroke and mimics. The panel also included neuronal makers (NSE and NfL) based on previous work. The results suggested that GFAP, NfL, Occludin, Claudin-5 and ZO-1 can differentiate stroke from mimics. However, NSE did not distinguish between stroke and stroke mimics. To my knowledge, this is the first study of comparisons of the selected biomarkers between ischaemic stroke and stroke mimics identified by both neurological scoring and the imaging data and also using different classifications.

This study used ELISA method to detect the biomarkers in serum samples obtained from ischaemic and mimics. A variety of commonly used clinical tests depended on the principles of sandwich ELISA, in which a target protein is initially captured to the assay device's surface and then detected by a second antibody carrying an easily detected label. The rapid assay of biomarker detection could be adapted for stroke diagnosis in conjunction with neurological scores and imaging data (Alhajj and Farhana, 2022).

Initially, the biomarkers in both blood serum and plasma samples were measured but did not obtain any significant differences between biomarker concentration in plasma and serum. Thus, the subsequent measurement of proteins in this project was conducted on serum only as serum eliminates fibrinogen and most clotting factors, (Busher, 1990) which may interfere with biomarker detection in a lower concentration. This is also consistent with this project's preclinical study.

In the present study, serum GFAP level in the ischaemic patients was significantly higher than in the mimics confirming its ability to distinguish between stroke and mimics. Previous studies have shown that GFAP might be utilised as a blood biomarker to distinguish between ischaemic stroke and intracerebral haemorrhagic stroke in the acute stage (Foerch et al., 2006; Foerch et al., 2015; Luger et al., 2020). Moreover, an earlier study has found a significant increase in serum GFAP levels in haemorrhagic stroke patients compared to ischaemic stroke or stroke mimics patients (Luger et al., 2017).

Previous studies have compared the levels of NSE between ischaemic stroke patients and healthy control and found that NSE serum concentrations were substantially higher in stroke patients than in controls (Missler et al., 1997; Wunderlich et al., 2004; 2006; Singh et al., 2013). This present study found that serum NSE concentrations were not significantly different between the ischaemic patients and the mimics suggesting that it may not be an appropriate marker to discriminate between ischaemic stroke patients and mimics. However, previous studies have compared the levels of NSE between ischaemic stroke patients and healthy control and found that NSE serum concentrations were substantially higher in stroke patients than in health controls (Missler et al., 1997; Wunderlich et al., 2004; 2006; Singh et al., 2013). In the present study, clinically defined mimics have been recruited rather than healthy subjects, which, may not be appropriate controls for studying biomarkers for stroke.

In consistent with previous studies (Onatsu et al., 2019 ; Uphaus et al., 2019; Zheng et al., 2021) that measured serum NfL levels using Simoa, the present study found that the level of serum NfL measured with ELISA was significantly higher in the ischaemic patients compared to the mimics. This may be due to the increased release of NfL following axonal injury or neuronal degeneration (Gaiottino et al., 2013).

Previous research has showed that, the BBB is disrupted during a stroke, resulting in alterations in the concentrations and distributions of Claudin-5, Occludin, ZO-1, and other BBB building blocks (Jie et al., 2011; 2012). The evidence is strengthened by the results of the preclinical study in this project, as well as the findings in this clinical study which showed that TJ proteins concentrations are significantly higher in the ischaemic patients in comparison with the mimics suggesting that disruption in the integrity of the BBB after stroke leads to increase in the release of these TJ proteins in blood.

In the sample, there were more males than females as shown in Table 5-1 reflecting the worldwide epidemiology of ischaemic stroke (Appelros et al., 2009). However, this study did not observe a significant gender specific difference in the biomarkers' levels in the same group. The majority of previous investigations were carried out with stroke severity and neurological impairments, which were used as the uncorrected baseline parameters. There was no sex difference in the severity of stroke in these investigations which might reflect the reason behind this study findings (Kapral et al., 2005; Madsen et al., 2015). The studied biomarkers except NSE showed the ability to

differentiate between the ischaemic and the mimics patients even after classifying the patients according to the gender. Therefore, GFAP, NfL and TJ proteins were able to differentiate between male ischaemic and male mimics as well as between female ischaemic and female mimics.

The levels of GFAP, NfL and TJ biomarkers are significantly increased both at ≤2 days and >2 days of the onset of cerebral ischaemia. This indicated that the selected biomarkers are released early in blood after stroke suggesting a quick and early way for stroke diagnosis. The significant increase of the proteins levels even after 2 days indicates that these proteins may still exist in a higher level which make it detectable in blood with a very simple way of analysis and able to differentiate between ischaemic patients and mimics even in later stages of stroke. Due to COVID-19 restrictions, this study was not able to recruit hyperacute stroke or obtain blood collection at different time point. However, blood was collected as soon as possible once it was confirmed that the patient had tested negative for COVID-19 and consent was obtained.

The biomarkers tested except NSE showed their ability to differentiate between NIHSS ≤ 7 and the mimics as well as between NIHSS >7 and the mimics. The classification of the severity of stroke in the ischaemic patients into two groups based on NIHSS score of ≤ 7 or >7 was selected on the basis of previous studies (DeGraba et al., 1999; Wouters et al., 2018). According to DeGraba et al. (1999), based on the first NIHSS score of 7, a clinical difference was indicated. Also, clinical deterioration and worsening were detected sharply with an initial NIHSS score above 7, and the likelihood of worsening was much higher in this group than the one with a NIHSS score below 7 (DeGraba et al., 1999). Moreover, Wouters et al. (2018) expressed that the score of NIHSS < 7 was associated with good functional outcomes.

In this study, a novel finding was that, the acute ischaemic stroke patients with the ACO or the PCO had significantly higher GFAP, NfL, Occludin, Claudin-5 and ZO-1 levels compared to the mimic.

The combined ratios of serum GFAP to other biomarkers in the panel to study the relationship between astrogliosis and neuronal death or between astrogliosis and TJ breakdown in ischaemic stroke patients and mimics were also determined. Although no significant difference in the NSE levels between the ischaemic and the mimics was observed, the ratio of GFAP/NSE showed a significant difference between the

ischaemic stroke and the mimics. This implied that by combining NSE and GFAP, the role of NSE in distinguishing between ischaemic stroke and stroke mimic might be strengthened. A significant elevation of the serum (GFAP/NfL) in the ischaemic patients compared to the mimic patients was observed. The findings assume that the significant increase in GFAP and NfL might represent neuronal damage and reactive astrogliosis due to ischaemia. This study, for the first time, demonstrated that the ratios of GFAP/Occludin, GFAP/Claudin-5 and GFAP/ZO-1 might be able to differentiate between ischaemic stroke and mimics. It has been reported that, during cerebral ischaemia the TJ proteins are readily released into the circulation (Kazmierski et al., 2012), indicating TJ disintegration which disrupts the BBB's integrity.

It is worth noting that, the possible variations (although non-significant) in concentrations between patients in the same group might be due to difference in clinical history, hospital arrival time, blood collecting time, NIHSS score, vascular disease and ischaemic size, ischaemic volume or severity among patients. Furthermore, the recruitment process was carried out without knowing the final diagnosis which was confirmed later after radiology report, physician opinion, blood results and clinical investigation. Even the mimics groups showed some variations in concentrations of biomarkers, which might be due to some having brain damage, some being normal, and some having an infection.

In conclusion, this study suggests that circulating serum GFAP, NfL, Occludin, Claudin-5, and ZO-1 levels might be valuable tools to differentiate between ischaemic and mimics as defined by clinical scoring systems. These differences were observed irrespective of the gender, time of blood collection, the severity of stroke (NIHSS), the location of occlusion in ischaemic patients and even based on the ratio of GFAP to other biomarkers in the panel.

5.3.7.2 Comparison of CT and MRI imaging biomarkers between stroke and stroke mimics

In CT data analysis, since all the patients received routine CT head protocol, the only possibilities could be analyses were HU values of ASPECTS regions. ASPECTS as explained previously is a quantitate CT score that measures the extent of early ischaemic changes (Mokin et al., 2017). All the ischaemic patients have a significantly reduced HU value in the 10 points on the ischaemic side compared to the non-

ischaemic side. This is because in acute ischaemic stroke, variations in x-ray attenuation reflect the ischaemic brain tissue's water absorption which is due to the excessive water uptake (Dzialowski et al., 2004). Therefore, this study demonstrated that CT density (Hus) is a good biomarker to distinguish between the ischaemic and the non-ischaemic areas.

On the other hand, the present study showed no significant difference in the HU values across ASPECTS regions between the left side and the right side in the mimics. This is what was expected before the analysis was performed as the mimics are free from brain ischaemic changes. In Agreement, Hand et al. (2006) found that 75% of stroke mimics had normal brain imaging. Moreover, Buck et al. (2021) stated that the physician should be made aware of the likelihood of a stroke mimics by the existence of normal CT, CTA, and CTP.

Few research studies have tested the relationship of the circulating biomarkers concerning CT imaging biomarkers for improved stroke diagnosis; hence this study was designed to investigate specific brain and BBB damaged biomarkers in CT defined stroke patients and mimics. The subgroups based on score 7 was chosen based on previous published studies (Barber et al., 2000; Puetz et al., 2009; The Penumbra Pivotal Stroke Trial Investigators, 2009; Padroni et al., 2016). This study results showed that GFAP, NfL and TJ biomarkers can distinguish between ischaemic patients with ASPECTS≤ 7 or ASPECTS>7 and mimics. Therefore, these blood protein biomarkers can be proposed as quick available diagnostic biomarkers for acute stroke. Interestingly, serum GFAP levels were higher in ASPECTS ≤ 7 group compared to ASPECTS > 7 group suggesting that the moderate to severe stroke patients had a higher concentration of this biomarker than the patients with minor stroke, but these need further investigation with a larger sample size.

Regarding MRI results, as all of the MRI scans are routine MRI head, so only the analyses of the DWI and T2 images were able to be done in the present study. Microstructural and metabolic changes have been proven to be detectable using quantitative MR methods (Collorone et al., 2021). To identify changes in signal intensity caused by tissue abnormalities, quantitative MR imaging parameters such as ADC and T2 values, each contributing to various tissue features, are required.

ADC reflects the diffusion speed of water molecules, and the fast diffusion of water molecules could be revealed with a larger ADC value in the image (Shen et al., 2011). The significantly higher ADC values on the ischaemic side were noticed in this study results. This could be purely due to the time when the MRI was done. All the recruited patients did not receive the MRI scan as soon as they were admitted, and they received the MRI scan within a week to 14 days from admission. Since, ADC value depends on the time of the scan as it increases as time passed (Shen et al., 2011), these ADC values in ischaemic side were observed. As previously stated by Soinne et al. (2003), ADC increase might be related to vasogenic oedema.

In this study, significant differences between the ratio of T2 signal intensity in WM and GM were found. These significant differences were consistent with the differences observed in ADC values in the identical regions. According to Knight et al. (2019), the increase in T2 signal intensity correlated with water increase with time. Moreover, they have stated that T2 intensity might be helpful to determine lesion age if the time of stroke onset is unknown (Knight et al., 2019).

This study, on the other hand observed, no changes in ADC values and T2 signal intensity in mimics as expected. In support, a recent study have reported similar results, as they found no statistically significant changes between right and left hippocampal T2 values in seizure (Andrews et al., 2021).

The non-significant increase in ADC values and T2 signal intensity in the PCO compared to the ACO might suggested that ADC values and T2 signal intensity might be able to differentiate between the different locations of stroke which requires further studies with a larger sample size.

The infarct volume was not a significant predictor of the difference in NIHSS score or the location of the occlusion. A prior study by Yaghi et al. (2017) has shown that some patients with massive infarcts initially had a relatively low NIHSS score. Furthermore, they stated that if their infarct is worsened by considerable cytotoxic oedema, clinical deterioration may have taken place (Yaghi et al., 2017). Duan et al. (2015), stated that small subcortical infarcts, for instance, might result in significant clinical impairment. Other research findings have produced contradictory results (Tong et al., 1998; Lövblad et al., 1997). Therefore, further research with a larger sample size is needed.

In conclusion, this study results showed that CT ASPECTS and MRI ADC values and T2 signal intensity are significantly different between the two sides in the ischaemic patients but not in the stroke mimics confirming the ability of these imaging biomarkers to distinguish between these patients. The selected panel of blood biomarkers except NSE show promising results in terms of differentiating between ischaemic stroke and mimics identified by imaging score (ASPECTS) but this needs further investigation.

5.3.7.3 The added value of imaging biomarkers to circulating biomarkers for improving stroke diagnosis

With the recent attention to blood biomarkers and the advances in imaging technology, still there are few studies has been investigated the correlation between blood biomarkers with CT and MRI imaging biomarkers in acute stroke for stroke diagnosis improvement. This study investigated the correlation between the six serum biomarkers with CT and MRI imaging biomarkers as well as the severity of stroke identified by NIHSS.

Some novel correlations between circulating biomarkers and CT and MRI imaging biomarkers were observed, which can help improve the diagnosis of ischaemic stroke from stroke mimics. This study found that GFAP level is negatively associated with ASPECTS in ischaemic patients. This might indicate a clear significance of GFAP level in stroke diagnosis improvement which may add value to CT scanning in ischaemic patients. The correlation results confirm the GFAP potential to predict the extent and severity of stroke obtained from CT ASPECTS. According to Vos et al. (2010), high levels of GFAP have been shown to link with overall outcome and prognosis in people who have had a brain injury. Recent study has studied S100B, NSE, GFAP, NfL, Tau and UCLH-L1 biomarkers which were measured with Simoa in traumatic brain injury and found that CT positive abnormalities were substantially predicted by serum GFAP levels in the first 24 hours after injury (Czeiter et al., 2020). Thus, they studied the correlation between biomarkers and CT positivity but they did not study ASPECTS (Czeiter et al., 2020). Other researchers have studied the correlation of several different biomarkers and found that only plasma adiponectin levels are correlated with ASPECTS in acute stroke (MOURÃO et al., 2020), however, they did not study the biomarkers analysed in this study. This is the first study, to the extent of my knowledge, to identify the association between GFAP and the stroke extension in brain measured by CT ASPECTS in acute ischaemic patients.

This study found that NSE level is positively associated with the volume of infarct obtained from MRI in the acute ischaemic patients. This might indicate the additional value of NSE level to MRI scan for ischaemic patients. The findings showed that higher levels of NSE are correlated with larger infarct reflecting the significant role of measuring the NSE levels in stroke patients using a quick and simple way to define the amount of brain damage especially in patients who have contraindicated for MRI scans. However, this finding requires further future study with a larger sample size. These findings are consistent with the study conducted by Oh et al. (2003), that serum NSE levels were found to be associated positively with the volume of infarction obtained from MRI. Furthermore, multiple previous studies have reported a positive correlation between CT volume of infarct and NSE concentration (Missler et al., 1997; Wunderlich et al., 2006; Brea et al., 2009; Zaheer et al., 2013; Khandare et al., 2022) in accord with the present study findings.

This study found a correlation between serum NfL measured by ELISA and the stroke severity measured by the NIHSS at arrival. Thus, NfL levels could reflect the clinical deficits following an ischaemic stroke. These findings were consistent with earlier studies (Duering et al., 2018; Uphaus et al., 2019) that showed a strong association between serum NfL measured by Simoa and NIHSS. Thus, this study differed than others in terms of measuring the serum NfL using ELISA.

There are no studies which have examined the correlation between neuronal, glial and TJ specific biomarkers with the ADC values and T2 signal intensity obtained from MRI. This study was the first study to examine these correlations. None of the panel biomarkers analysed in this study were correlated with ADC values. This might be explained by the small sample size (n=9). Moreover, the results of correlations suggested that both imaging and blood biomarkers may be used to indicate two different useful information for stroke diagnosis. In detail, the blood biomarkers as shown in the prior section are able to differentiate between ischaemic stroke and mimics and other studied factors using a very simple and quick techniques in a remote area. The ADC values obtained from MRI indicate the amount of damage in the brain. Therefore, this study's correlation results might be useful in the future in terms of the techniques complementing each other to give important diagnostic information.

Interestingly, the novel findings which showed that both neuronal markers (NSE and NfL) levels are positively correlated with MRI T2 signal intensity in both WM and GM

adding value to clinical factors considered in MRI scan. This indicates the significance of using neuronal biomarkers in stroke diagnosis improvement reflecting also the strength of these results. The role of NSE and NfL might add value to MRI scanning in ischaemic patients. The correlation results might confirm these biomarkers potential to predict the increase in T2 signal intensity obtained from MRI. The increase in T2 signal intensity might reflect that vasogenic oedema (Alexander et al., 1996) which also are reported to reflect irreversible brain damage (Noguchi et al., 1997). However, these findings need further investigation with a larger sample size.

In conclusion, despite the limited sample size in this study, the data suggest that circulating GFAP is correlated with CT ASPECTS in ischaemic patients. Neuronal markers (NSE and NfL) levels are correlated with MRI T2 signal intensity in both WM and GM. NSE is correlated with the MRI volume of infarct size. NfL level is correlated with NIHSS in ischaemic patients.

Chapter 6 Discussion, conclusions and future work

In this project, the focus was on improving the diagnosis of stroke aiming firstly to assess the circulating biomarkers in mouse models of stroke compared to sham operated mice and then to examine the circulating biomarkers in acute stroke patients compared to mimics as defined by clinical scoring systems as well as CT and MRI scans. The experimental approaches to achieve these aims were to first study the circulating biomarkers in two different murine models of stroke (BCCAO and MCAO), then to study the circulating biomarkers and CT and MRI imaging biomarkers in recruited acute stroke patients and stroke mimics. The objectives to achieve these aims were first to determine brain damage in stroke mice as compared to sham operated mice by single and double IHC using antibodies to specific markers of brain cells and BBB TJ proteins, and then to determine the expressions of biomarkers (GFAP, Claudin-5, ZO1, Occludin) in the brain using WB. The levels of circulating biomarkers (GFAP, Claudin-5, ZO1, and Occludin) were also determined in the blood serum of stroke and control mice by ELISA method. Subsequently, these circulating biomarkers (GFAP, NSE, NfL, Occludin, Claudin-5 and ZO-1) were studied in blood serum of ischaemic stroke patients and stroke mimics as identified by clinical scoring systems as well as by analysing CT and MRI scans to improve stroke diagnosis. In a retrospective study, the CTP, MRI biomarkers and functional outcomes in the MT group and the non-MT group were compared. In a cross-sectional study, the ability of CT and MRI biomarkers in distinguishing stroke and mimics was also determined. Finally, the correlation between the circulating biomarkers with CT and MRI imaging biomarkers for improved stroke diagnosis was studied.

6.1 Overview on the results

To achieve the aims of this project, the planned objectives were followed and studied. The following section will briefly mention the overall results that have been obtained from the preclinical study and clinical study in this project.

6.1.1 Results from preclinical study

In the preclinical study, brain damages in the cortex and the hippocampus were studied using antibodies of specific neuronal (NeuN), glial cell (GFAP), microglial cell (IBA-1), pericytes (PDGFR and NG2) and endothelial cells (CD31) in both BCCAO

and MCAO model of cerebral ischaemia and reperfusion as compared to sham operated mice. Additionally, BBB specific TJ markers (Occludin, Claudin-5 and ZO-1) were assessed in both models using single and double immunolabelling. The data from the IHC staining and quantification results showed neuronal cell death and changes in astrocytes, pericytes and microglial cells in specific areas of the brain in both BCCAO and MCAO models of stroke. The IHC results also showed morphological changes in endothelial cells, pericytes and TJ proteins in the hippocampus of these models.

The levels of GFAP, ZO-1, Occludin and Claudin-5 expressions relative to ß-actin were tested using WB. The results showed significant changes in stroke mice brains compared to the sham operated brains. Finally, circulating biomarkers (GFAP, Claudin-5, ZO1, Occludin) were determined by ELISA method in BCCAO and MCAO mice compared to corresponding controls followed by correlations test between ELISA results and WB results. The selection of biomarkers was based on the literature review of earlier studies. The results showed that the selected circulating biomarkers can differentiate between mouse stroke models and controls. The correlation tests showed that serum GFAP and Occludin levels in BCCAO were correlated with their expression in the brains tissue, whereas, in MCAO only serum Occludin level was correlated with its expression in the brain tissue. The overall results from the preclinical study suggest that GFAP and TJ proteins' levels might be useful biomarkers for identifying acute stroke patients at high risk of BBB damage. Consistent with these findings, a clinical study was done.

6.1.2 Results from retrospective study (A pilot study)

The CTP and MRI imaging biomarkers were tested in a pilot study in two groups (MT and non-MT) to test a hypothesis that can inform a longitudinal study in the future and then correlate the results with blood biomarkers. This pilot study aimed to find out if the CTP and MRI imaging biomarkers or parameters can improve the prediction of outcomes in MT. However, due to the small sample size, only comparisons of CTP biomarkers, MRI ADC values, the volume of infarct and functional outcomes between the MT group and the non-MT group was conducted. The results confirmed previous studies regarding the feasibility of CTP parameters in acute stroke patients undergoing MT. MT is a useful treatment in acute stroke to improve favourable outcomes.

A larger prospective study with outcome data collection was planned to verify this hypothesis. However, due to COVID-19, it was not able to do prospective research on CTP and MR perfusion scans obtained from stroke patients undergoing MT and correlate the perfusion imaging biomarkers results with blood biomarkers results. The results of this pilot study were discussed in detail in the results chapter (Chapter 4).

6.1.3 Results from cross sectional study

Blood samples from ischaemic stroke patients and stroke mimics were collected from the Leeds Teaching Hospitals NHS Trust to study the ability of the blood-based biomarkers (GFAP, NSE, NfL, Occludin, Claudin-5 and ZO-1) to distinguish between ischaemic patients and stroke mimics in order to improve stroke diagnosis. The biomarkers have been looked at were selected based on this project's preclinical work and other earlier works. The results showed a significant increase in serum GFAP, NfL, Occludin, ZO-1 and Claudin-5 but not NSE in the stroke patients compared to the mimics. The results revealed that the selected panel of biomarkers except NSE showed promising results in terms of differentiating between ischaemic stroke and mimics. However, this needs further investigation with larger number of patients in the future. This is also observed after classifying the patients according to the gender, time of blood collection, the severity of stroke and the location of occlusion in the ischaemic patients. Furthermore, the biomarkers showed the distinguish ability even based on CT ASPECTS and the ratio of GFAP to other biomarkers in the panel.

From the same recruited patients, the ability of the CT and MRI imaging biomarkers in differentiating between the ischaemic stroke patients and the stroke mimics was tested. The results showed that CT HU values of ASPECTS, MRI ADC values and T2 signal intensity are significantly different between the ischaemic side and the non-ischaemic side in the ischaemic patients. These imaging biomarkers are not significantly different between the left side and the right side in the mimics patients as expected. Moreover, in the ischaemic patients, no significant differences were observed between the infarct volume and NIHSS score as well as between the infarct volume and the location of occlusion.

Finally, the added value of imaging biomarkers to circulating biomarkers for improving stroke diagnosis was studied by testing the correlation between the blood biomarker results with CT and MRI imaging results. The data from all correlations and linear

regression tests suggested that GFAP level is correlated with CT ASPECTS in the ischaemic patients. Data showed that none of the studied biomarkers was correlated with ADC values. NSE and NfL are correlated with T2 signal intensity in MRI. A significant association between NSE level and the MRI volume of infarct obtained from MRI was observed. Lastly, NfL was reported to be correlated with the severity of stroke. The results suggest that each of the biomarker studied except NSE can differentiate between the stroke patients and the stroke mimics identified by combined neurological scores and imaging data. However, different biomarkers may be predictive of different outcomes of stroke patients as identified by imaging markers.

6.2 General Discussion

6.2.1 Biomarkers in preclinical models

The current study is the first systematic study examining detailed changes in neuronal, glial cell, endothelial cells, pericytes and BBB TJ proteins in the forebrain using single and double IHC and WB following both BCCAO and MCAO and reperfusion in C57BL/6J mice. Furthermore, this is the first study to investigate the expression of GFAP and TJ proteins in the hippocampus and correlated that with serum protein concentrations in both models.

Since BCCAO caused selective neuronal death in the forebrain, including the hippocampus and cortex in C57BL/6 mice with a greater survival rate, this model has been used first to get consistent results following cerebral ischaemia (Yang et al., 1997; Murakami et al., 1998). This study on BCCAO mice demonstrated the significant death of neuronal cells in M1 and M2 motor cortex, somatosensory cortex, granular insular cortex and hippocampus. These results agreed with previous studies conducted in our lab (Khan et al., 2018). On the other hand, because focal cerebral ischaemia is known to cause neuronal injury in the cortex, hippocampus and striatum of both mice and rats (Rao et al., 2001; McColl et al., 2007; Ketheeswaranathan et al., 2011) and represents the majority of human stroke, the MCAO model has been used to confirm the brain damage and biomarker results in this model as have been obtained in the BCCAO model in this study. Corresponding with previous studies in our lab (Ketheeswaranathan et al., 2011) and other studies (Butler et al., 2002; McColl et al., 2004), this study also consistently detected neuronal degeneration in MCAO not only in the striatum but also in the M1 and M2 motor cortex, the granular insular cortex

and the hippocampus. The reduction in neuron cells number in the stroke group was due to the high sensitivity of neurons to ischaemic effects and the blood supply reduction, causing neuronal death in this area (Kudabayeva et al., 2017). While six control brains and six stroke-induced brains were used in the BCCAO models for this study, only three control brains and three stroke-induced brains were used in the MCAO models because of time constraints and COVID-19 restrictions.

The IHC and WB results showed significant increases in the expressions of GFAP in the hippocampus in both models compared to control mice. In agreement, Liu et al. (2018) showed that GFAP expression level using WB at a different time point after MCAO in rat were significantly higher compared to the control. GFAP up-regulation is one of the most important features of astrogliosis (abnormal increase in the astrocytes number following the ischaemia resulting in the glia cells activation) (Pekny et al., 1999). In agreement, recent studies reported the altered morphology of astrocytes directly after stroke related to the expression of GFAP (Lebkuechner et al., 2015). The glial scar is the most characteristic reactive astrogliosis profile which includes upregulation of GFAP and other genes which leads to significant hypertrophy of astrocyte cell bodies and processes (Silver and Miller, 2004; Sofroniew, 2009). Circulating GFAP levels were investigated in this study and the results showed a significant increase in the GFAP levels in both models compared to controls. The measurement of proteins in this project was conducted on serum. This is because after plasma has clotted, serum remains, eliminating fibrinogen and most clotting factors (Busher, 1990). GFAP is a filament protein in the astrocytes, which is specific for brain tissue and not found outside the central nervous system (Svetlov et al., 2010). Thus, according to previous studies, it seems to be ideal stroke specific biomarker (Schiff et al., 2012). Although there is a lack of studies investigating the GFAP levels in animal models of stroke using ELISA which was done in this study, multiple clinical research studies investigated the role of serum GFAP as a diagnostic and prognosis prediction tool for stroke patients (Schiff et al., 2012; Ren et al., 2016).

This study's IHC staining and quantitative analysis results of pericytes and microglia were in agreement with previous studies (Arimura et al., 2012; Fernández-Klett et al., 2013; Lee et al., 2019).

In this study, both IHC and WB results showed significant reductions in the expressions of TJ proteins in the hippocampus in both models compared to corresponding control mice. These findings in mice agree with previous study that suggest that loss of Occludin proteins from the brain's microvessels in rat MCAO model of ischaemic stroke occurs concurrently with the release of Occludin in the blood circulation (Pan et al., 2017). Ren and their colleagues have found that focal ischaemia with rat MCAO and reperfusion induced discontinuous Claudin-5 staining and revealed markable gap formation (Ren et al., 2015). Moreover, they have indicated that the expression levels of ZO-1, Occludin and Claudin-5 using WB are decreased in MCAO, however, no significant changes have been reported in their previous studies on Claudin-5 and ZO-1 (Ren et al., 2015). The present study showed that the WB results were consistent with IHC stainings and reported significant reduction in TJ proteins expressions in the hippocampus in both models. In addition, serum ZO-1, Occludin and Claudin-5 levels were found to be significantly increased in both models compared to controls. Pan et al. (2017) investigated the concentrations of Occludin and Claudin-5 in rat's serum following MCAO using ELISA and showed only a significant increase in Occludin levels but not in Claudin-5. However, this study showed a significant increase in Claudin-5 and Occludin levels not only in MCAO but also in BCCAO compared to controls. Since there is a lack of studies investigating the ZO-1 levels in stroke animal models analysed with ELISA as has been done in this study, the results might indicate the disarrangement of the ZO-1 in the TJs that was observed in IHC and WB leading to BBB opening after ischaemia and releasing these proteins into blood. Further investigation of these has been carried out using clinical samples from stroke and stroke mimics which will be discussed in the following section.

This study examined the expression of the TJ proteins within the endothelial cells profile in both models in the hippocampus and cortex areas using double labelling. There are very few studies examining the changes in TJ proteins of endothelial cells labelled with CD31 following BCCAO and MCAO brains compared to control brains. The results confirms that TJ proteins are localised in CD31 labelled endothelial cells and not in the NeuN and GFAP labelled neurones and astrocytes respectively. Moreover, the double labelling results are consistent with the similar damage that was shown in single labelling. In agreement with previous study findings in MCAO, that the

expression of Claudin-5 and Occludin with loss of endothelial cell labelled with CD31 (Ghori et al., 2017), the present study revealed that TJ proteins are disrupted under ischaemic conditions in both BCCAO and MCAO. Furthermore, the double labelling results of GFAP colocalised with ZO-1 were consistent with Lee et al. (2019) study that reported that GFAP immunoreactivity in the rat hippocampal areas were significantly increased in BCCAO with 15 min occlusion as well as with Hao et al. (2019) study which demonstrated much lower Occludin and ZO-1 expressions in MCAO mice with approximately 30% that of control mice.

To the best of my knowledge, there are no studies that reported the changes of glial cell and BBB TJ proteins after ischaemia using preclinical models of ischaemia with multiple methods such as IHC, and WB and correlate the results of ELISA and WB which have been done in this project. Based on the WB and ELISA results, this study demonstrated a novel correlation between the expression of these biomarkers in hippocampus and their serum levels. According to this study, a substantial significant positive link between circulation and the expression of GFAP in BCCAO was observed as measured by Spearman correlation, indicating astrogliosis after ischaemia (Pekny et al., 1999). Additionally, this study discovered a strong negative association between the expression of Occludin in the brain following BCCAO and MCAO with circulating Occludin levels. It has been stated that blood Occludin concentrations measured after BCCAO may precisely reflect the expression of Occludin released from the hippocampus ischaemic brain, which may be strongly associated with early BBB rupture (Liu et al., 2009). Compared to earlier research in the same field, this study used fewer mice, thus more mice may be required to show significant correlations in other biomarkers.

In conclusion, the data not only verified the induced neurodegeneration, astrogliosis and TJ disruption after stroke in murine models of cerebral ischaemia and reperfusion but also showed the association of expression of GFAP, ZO-1, Occludin and Claudin-5 proteins in the ischaemic brain tissues with an increased level of these proteins in the serum of ischaemic mice as compared to the sham-operated mice. This suggests that GFAP and TJ proteins levels might be useful biomarkers for identifying acute stroke patients at high risk of BBB damage. These results are helpful for further understanding of the mechanisms of stroke and to develop new therapeutic approaches targeting the BBB.

6.2.2 Biomarkers in clinical samples

6.2.2.1 Cross sectional study - Comparison of circulating biomarkers between stroke and stroke mimics

The current study focused to assess the ability of circulating biomarkers (GFAP, NSE, NfL, Occludin, Claudin-5 and ZO-1) in distinguishing between ischaemic stroke and stroke mimics as defined by clinical scoring systems to improve stroke diagnosis. The biomarkers that have been looked at were based on the preclinical work in this project.

The studied biomarkers except NSE were able to differentiate between male ischaemic and male mimics as well as between female ischaemic and female mimics. However, this study did not observe a significant difference in the biomarkers' levels between male and female in the same group. There are few studies investigating the levels of stroke biomarkers in male and female. Specifically, the majority of previous sex difference investigations were carried out with the stroke severity and neurological impairments as the uncorrected baseline parameters. In agreement with this study finding, there was no sex difference in the severity of stroke in previous studies (Kapral et al., 2005; Madsen et al., 2015) which might reflect the reason behind the findings.

GFAP protein, which is an astrocyte's cytoskeleton, is released when astrocytes are destroyed (Puspitasari et al., 2019). Although, most previous studies have shown that GFAP might be used as a blood biomarker to distinguish between ischaemic stroke and intracerebral haemorrhage in the acute stage (Foerch et al., 2015; Misra et al., 2017; Luger et al., 2020), this study showed that GFAP was able to distinguish between the ischaemic patients and the mimics. It is worth noting that, GFAP was included in the panel on the basis of my preclinical results and also to find out if it was able to distinguish between ischaemic and mimics as a large body of evidence suggests its ability to distinguish between ischaemic stroke and haemorrhagic stroke (Foerch et al., 2006; 2015). Kumar et al. (2019) in their meta-analysis suggested that GFAP is a promising biomarker in terms of distinguishing haemorrhagic stroke from ischaemic stroke and mimics. However, in this study, concentration of GFAP was able to distinguish between the acute ischaemic stroke and the mimics in the early stage before haemorrhagic stroke occurs. The higher observed level of GFAP in the ischaemic patients in this study could reflect the reactive astrogliosis following stroke (Pekny et al., 1999).

Despite previous studies found a significantly higher level of NSE in ischaemic stroke patients compared to controls (Missler et al., 1997; Wunderlich et al., 2004; 2006; Singh et al., 2013), this present study did not find any significant difference in the NSE levels between the ischaemic patients and the mimics suggesting that NSE might be not a suitable marker to distinguish between ischaemic and mimics. However, this result works as a positive control supporting the credibility of the used method.

Regarding NfL, this study showed the ability for serum NfL to distinguish between ischaemia and mimics using ELISA confirming previous studies measured NfL level in blood serum using Simoa (Onatsu et al., 2019; Uphaus et al., 2019). Also, previous studies measured NfL level in blood plasma using Simoa (Gendron et al., 2020; Wang et al., 2021). The observed significant higher level of serum NfL in the ischaemic compared to the mimics in this study might be because of axonal injury or neuronal degeneration, which lead to release of NfL in circulation (Gaiottino et al., 2013).

In this project's preclinical study, significant increases in the concentrations of Claudin-5, Occludin, and ZO-1 in the stroke mice compared to the control were observed. Accordingly, investigating the role of these TJ proteins in differentiating stroke from stroke mimics was carried out. The results showed that these biomarkers are increased significantly in the ischaemic stroke compared to the mimics. This might be a significant clinical discovery that corresponds to the preclinical findings in this project indicating that any disruption in the BBB integrity after stroke led to an increase in the permeability of the BBB followed by release of these TJ proteins in the blood (Zhang et al., 2020). The current study findings revealed serum TJ protein levels may indicate the degree of BBB disruption at the early ischaemic stage, implying that measuring the levels of these biomarkers may help to identify acute ischaemic patients who are at high risk of BBB damage and haemorrhaging.

There is a lack of clinical studies reporting the ability of this study's biomarkers panel in differentiating between stroke and mimics ≤ 2 days and >2 days of blood collection. This study has contributed by showing the ability of selected biomarkers except for NSE in distinguishing between ischaemic patients and mimics before 2 days as well as after 2 days of blood collection. The significant increase of the levels of these biomarkers even after 2 days suggest that the biomarkers still exist at high levels which makes them detectable in blood with a very simple way of analysis to differentiate between ischaemic stroke and mimic even in later stages. This implies a significant

discovery in the field of biomarkers in terms of differentiating between stroke and stroke mimics at an early time saving unneeded hospital admission time in order to find out the correct diagnosis.

The choice of classifying the severity of stroke in ischaemic patients identified by NIHSS score of 7 in this study was based on previous studies (DeGraba et al., 1999; Wouters et al., 2018) as explained in the previous chapter. This classification of the ischaemic patients was done in the present project to further test for the first time in the laboratory the ability of the biomarkers panel in differentiating between ischaemic patients and mimics even after identifying by neurological score (NIHSS) . Accordingly, the results showed the ability of GFAP, NfL and TJ proteins to distinguish between the two NIHSS subgroups and mimics indicating the benefits of the suggested biomarkers in stroke diagnosis.

It has been reported in a previous study that GFAP levels in individuals with partial anterior circulation infarcts were considerably higher than the threshold values (Herrmann et al., 2000). Additionally, it has been shown that the mean Occludin and Claudin-5 concentrations are significantly higher in partial anterior cerebral infarct patients compared to posterior cerebral infarct patients (Lasek-Bal et al., 2020). Whereas, in the same study, authors did not find any statistically significant differences in the ZO-1 concentration between the anterior and posterior infarction location groups (Lasek-Bal et al., 2020). However, this present study focused on the ability to distinguish between the different location of occlusion in the ischaemic patients and the mimics, and showed that serum GFAP, NfL and TJ proteins can distinguish between the ACO and the mimics as well as between the PCO and the mimics.

This study tested the ratio of serum GFAP to other biomarkers in the panel to find out whether there was a link between astrogliosis, neurons and TJ breakdown after ischaemic stroke, and to find out if there were any significant differences in these ratios between the ischaemic stroke and the mimic patients. The results showed that GFAP/NSE, GFAP/NfL, GFAP/Occludin, GFAP/Claudin-5 and GFAP/ZO-1 are able to differentiate between the ischaemic stroke and the mimics. While NSE alone was not able to differentiate between the ischaemic and the mimics, the ratio of GPAP to NSE did differentiate between the two groups. This suggested that the role of NSE in differentiating between ischaemic stroke and stroke mimic is strengthened by combining it with GFAP. This supports with previous study interpretation, that proteins

are released from brain cells in response to neuronal and glial cells damage and then enter the systemic circulation, either directly through the disrupted BBB or indirectly through release into the CSF followed by absorption through the intraventricular choroid plexus or via arachnoid villi into the cerebral sinuses (Vos et al., 2006). In addition, a significant elevation of serum GFAP/NfL ratio in the ischaemic patients compared to the mimic patients was found assuming that the significant increase in GFAP and NfL represent neuronal damage and reactive astrogliosis due to ischaemia. It has been reported previously in ischaemic stroke patients that blood levels of Claudin-5, Occludin, and Claudin-5/ZO-1 ratios can be utilised to test for clinical worsening caused by haemorrhagic transformation (Wunderlich et al., 2006). Additionally, it has been stated that GFAP release kinetics are thought to be linked to patient clinical impairments and infarct volume (Wunderlich et al., 2006), which agreed with the present study outcomes. However, no previous study combined the ratio of GFAP and TJ proteins as in this study did and tested that on ischaemic patients and mimics. Interestingly, this study showed that GFAP/Occludin, GFAP/Claudin-5 and GFAP/ZO-1 succeeded to differentiate between ischaemic and mimics. These findings indicate that GFAP and TJ proteins might be released into the serum once BBB destruction reaches a higher level in stroke patients making these biomarkers suitable candidates to differentiate between stroke patients and mimics.

In conclusion, this study showed the ability of serum GFAP, NfL and TJ proteins levels in differentiating between ischaemic patients and mimics which also has been observed after classifying the patients based on gender, time of blood collection, the severity of stroke (NIHSS), the location of occlusion in ischaemic patients and the ratio of GFAP to other biomarkers in the panel.

6.2.2.2 Cross sectional study - Comparison of CT and MRI imaging biomarkers between stroke and stroke mimics

One objective of the current study focused to determine the CT and MRI biomarker's ability in distinguish between stroke and mimics. It is worth mentioning that, HU values analysis of ASPECTS regions is the only possible analysis that could be done as all recruited patients have received NCCT. In agreement with (Mokin et al., 2017; Maegerlein et al., 2019) results, this study showed that all the ischaemic patients have a significant reduced HU value in the 10 points in the ischaemic side compared to the non-ischaemic side. This is related to the fact that in acute ischaemic stroke, changes

in x-ray attenuation reflect the water absorption of the ischaemia brain tissue, which is brought on by the excessive water uptake (Dzialowski et al., 2004). Since, the infarcted tissue's water uptake is represented by the HU value, thus, the HU value drops as the water intake rises (Zhu et al., 2021). Thus, this result confirmed that CT density (HUs) is a good biomarker to distinguish between the ischaemic and the non-ischaemic areas. Regarding mimics patients, as expected no significant difference was found in the HU values across ASPECTS regions between the left and the right side as the mimics patients are free from ischaemic changes. This result is consistent with a previous study by Hand et al. (2006) that found that 75% of mimics patients had normal brain imaging. Additionally, Buck et al. (2021) stated that the physician should expect the stroke mimic likelihood by the existence of normal CT, CTA, and CTP.

Moreover, the selected panel of biomarkers except NSE show promising results in terms of differentiating between ischaemic stroke and mimics identified by CT ASPECTS. The choice of classifying the CT ASPECTS in ischaemic patients on 7 was based on previous studies (Barber et al., 2000; Puetz et al., 2009; The Penumbra Pivotal Stroke Trial Investigators, 2009; Padroni et al., 2016) as explained previously. This classification of ischaemic patients was performed for the first time in the laboratory in the present project to further assess the discriminations' ability of the studied biomarkers panel between ischaemic patients and mimics based on CT ASPECTS. Accordingly, this ability existed with significantly higher levels of GFAP, NfL and TJ proteins in the ischaemic patients compared to the mimics. This might indicate the strong ability of the studied biomarkers in stroke diagnosis in terms of differentiating between ischaemic and mimics as the current ability of CT ASPECTS by using a quick available blood test.

It has been found that the reduced NCCT attenuation corresponds with the ADC value on DWI MRI (Kucinski et al., 2002) and with the observed DWI MRI lesion (Barber et al., 1999). This study was able to analyse the ADC values obtained from DWI and analyse T2 images because all of the follow-up MRI scans were only routine MRI head. The results showed a significant increase in the ADC values in the ischaemic side compared to the non-ischaemic side in the ischaemic patients. This might only be a result of the time the MRI was performed. The MRI scan was not given to every patient who was recruited right away; instead, it was given to them between a week and 14 days after admission. The results explain that ADC value depends on the scanning

time as it increases as time passed (Shen et al., 2011). Similarly, a previous study has shown that in the hyperacute and acute stroke stages, ADC levels rose over time in 8 to 14 days, and in the chronic stage, ADC values rose higher than normal (Shen et al., 2011). Also, according to Soinne et al. (2003), an increase in ADC might be related to vasogenic oedema.

The observed significant difference in the ratio of T2 signal intensity from 1 was consistent with the significant difference in ADC values in the ischaemic patients. In agreement, a previous study has discovered in no recanalization patients the mean quantitative T2-values assessed in follow-up MRI scans were considerably greater than similar values observed in acute scans (Siemonsen et al., 2012). A possible explanation for the present study findings is due to vasogenic oedema, which, unlike cytotoxic oedema, is more likely to be reversible, leaving no irreparably injured brain tissue. The ADC and T2 non-significant results observed in the mimics were expected and in agreement with a previous study result (Andrews et al., 2021).

The non-significant increase in ADC values and T2 signal intensity in the PCO compared to the ACO may indicate that these imaging biomarkers might distinguish between the different locations of stroke, necessitating further research with a larger sample size in the future.

This study showed that NIHSS ≤ 7's patients had a larger volume of infarct than NIHSS > 7 's patients however, no significant difference was observed. In similar results to what has been achieved, the authors found that some patients with massive infarcts initially had a relatively low NIHSS score (Yaghi et al., 2017). It has been claimed that clinical deterioration may have occurred if their infarct was made worse by a significant amount of cytotoxic oedema (Yaghi et al., 2017). It also has been stated by Duan et al. (2015) that small subcortical infarcts might result in significant clinical impairment. Even though other research' findings were controversial (Lövblad et al., 1997; Tong et al., 1998). This also might be due to the difference in the time between MRI scan and performing the NIHSS. Specifically, the MRI scan has been done within a week to 14 days from admission while the NIHSS was performed upon arrival. Thus, further research with a larger sample size is highly recommended.

In conclusion, this study showed that CT ASPECTS, MRI ADC values and T2 signal intensity are able to differentiate between ischaemic patients and mimics. The selected

panel of blood biomarkers except NSE show promising results in terms of differentiating between ischaemic stroke and mimics identified by imaging score (ASPECTS) but this needs further investigation. This study might add benefit to the literature by including all these results in one study obtained from ischaemic and mimics patients and correlating the imaging results with blood results.

6.2.2.3 Cross sectional study – Added value of imaging biomarkers to circulating biomarkers for improving stroke diagnosis.

This study is the first to test a connection between all 6 serum biomarkers with CT as well as MRI imaging biomarkers following ischaemic stroke to improve stroke diagnosis. The results found that GFAP level is related negatively to ASPECTS in the ischaemic patients. Although a previous study found a correlation between CT positivity abnormalities and GFAP measured with Simoa in traumatic brain injury (Czeiter et al., 2020), however, they did not test CT ASPECTS as this present study did. Another study found a correlation between plasma adiponectin levels and ASPECTS in acute stroke (MOURÃO et al., 2020). Rahmig et al. (2021) found that NfL measured with Simoa is correlated with ASPECTS. This study finding supports the ability of GFAP to predict the scope and the severity of stroke as determined by CT ASPECTS by using a simple and quick test. Thus, this might potentially extend the utility of serum GFAP as a marker for ischaemic stroke diagnosis. To my knowledge, this is the first study to identify that GFAP is associated with CT ASPECTS, suggesting an added value of GFAP levels to CT ASPECTS with a quick and simple test.

The correlation results indicated that higher levels of NSE are correlated with larger infarct. This was consistent with Oh et al. (2003) results. Moreover, other studies showed similar results while the volume of infarct obtained from CT (Missler et al., 1997; Wunderlich et al., 2006; Brea et al., 2009; Zaheer et al., 2013; Khandare et al., 2022). This study result demonstrated that the NSE levels might add usefulness for ischaemic patients even though it failed to distinguish between the ischaemic patients and the mimic which could be explained by it is not a suitable marker for that differentiation. Thus, the result may demonstrate a crucial role in detecting NSE levels in stroke patients in a rapid and easy approach to identify the degree of brain damage, particularly in individuals for whom MRI scans are contraindicated. However, no other correlation between the studied biomarkers and the volume of infarct was observed. This may be due to a small sample size.

This study showed a correlation between serum NfL measured by ELISA and the NIHSS at arrival. Thus, NfL levels might add value to the clinical neurological assessments regarding the severity of stroke using a biomarker test. The findings agreed with earlier studies findings while the authors analysed NfL by Simoa (Duering et al., 2018; Uphaus et al., 2019; Pedersen et al., 2019; Rahmig et al., 2021).

As far as known, this is the first study to examine any correlation between MRI T2 signal intensity and the studied blood biomarkers. The levels of both neuronal markers (NSE and NfL) are positively associated with MRI T2 signal intensity in both the WM and GM. This may demonstrate the value of using neuronal biomarkers to improve stroke diagnosis. The correlational findings support these biomarkers' capacity to forecast the rise in T2 signal intensity measured by MRI which could reflect irreversible brain damage (Noguchi et al., 1997) due to vasogenic oedema (Alexander et al., 1996).

No correlations were significant in this study between any of the 6 biomarkers and the MRI imaging biomarker (ADC values). Despite the fact that, this is the first study testing if there any correlation exists, this result might indicate that circulating biomarkers and MRI imaging biomarkers give different useful information for stroke diagnosis. Specifically, the proposed blood biomarkers may be able to differentiate between ischaemic stroke and mimics using very simple, affordable and quick techniques in a remote area. While, MRI even though is relatively expensive and time consuming, it allows the detection of DWI hyperintensity (Moseley et al., 1990) and alterations in ADC values (Reith et al., 1995) within minutes of the beginning of ischaemia. Thus, this present result might indicate that blood biomarkers and imaging biomarkers may each function independently to provide crucial diagnostic data. It is worth noting that, in the MRI data set there were not enough patients. Thus, studies with larger cohort is required.

Altogether, this study suggests that the combination of circulating biomarkers except NSE in acute stroke patients with neurological scores as well as CT and MRI imaging data can improve the diagnosis of stroke.

6.3 Final Conclusions

In conclusion, the preclinical studies in the present project for the first-time confirmed brain damage together with changes in circulatory markers in murine models of stroke. The experimental data showed the association between astrogliosis and TJ disruption with an increased level of specific proteins in blood serum in ischaemic mice as compared to sham-operated mice, suggesting that these proteins can be used as potential biomarkers for determining ischaemic stroke. These data, however, need further validation.

Consistent with the preclinical findings, this novel clinical study confirms the preclinical results and suggests that blood biomarkers in combination with neurological scores and imaging data might offer valuable tools for differentiation between ischaemic stroke and mimics and assessing the severity of ischaemic stroke.

All in all, this study suggests the possible added value of the studied circulating biomarkers except NSE to neurological scores and the imaging data for improvement of stroke diagnosis. The study findings encourage further research into developing circulating biomarkers for use in clinical practice and evaluating the potential of measuring specific biomarkers in addition to imaging techniques as a diagnostic method for ischaemic stroke. These data, however, need more validation with a larger sample and the effectiveness of the use of biomarkers has to finally be proven in additional multi-centre clinical trials.

6.4 Project limitations

Difficulties with this research started from the first step of brain tissue staining, a series of experimental repeats were done to achieve the optimal working dilution of used antibodies, especially the TJ proteins before the successful IHC staining were produced. Throughout the immunohistochemical studies, this study found the staining quality was affected by the concentrations of primary antibodies, incubation time, diluent, protocol modification and temperature. Thus, to achieve the optimal result, these variables needed to be optimized to obtain specific staining with low background. The optimization process is undertaken by changing the antibody concentration while maintaining a constant temperature and incubation time to verify the optimal dilution. Furthermore, changing the Triton concentration from 0.01% to 0.1% helped the staining by maximising the antibody penetration to the tissue

sections. Treating the sections with L.A.B. Solution assisted in the elimination of excessive fixative and minimisation of protein cross-linking.

Next, in quantitative positive cells analysis, only three control brains and three stroke-induced brains were available from MCAO models because of time constraints and COVID-19 restrictions. Thus, the power of statistics should ideally be increased by requiring more replicates. For WB, huge multiple experimental repeats were performed to achieve the clear bands from the 4 proteins in both models which was a very long and costly process that concluded with the presented results in this project. Some experiments such as fluorescence imaging microscopy were difficult to repeat due to booking unavailability of the microscope.

The MT pilot study aimed to identify a hypothesis that can inform a longitudinal study design in the future by correlating the imaging results with blood biomarkers in MT. The specific aim was to determine if the absolute values of CTP and MRI imaging biomarkers can improve the prediction of outcomes in MT. However, due to the limited sample size available, only a comparison of CTP biomarkers, MRI ADC values, the volume of infarct and functional outcomes between the MT group and the non-MT group was conducted. Furthermore, this pilot study was planned to carry on with a larger prospective study with outcome data collection, however, due to COVID-19, I was not able to get prospective research CTP and MR perfusion scans obtained from stroke patients undergoing MT and correlate the perfusion imaging biomarkers results with blood biomarkers results.

The clinical findings must be evaluated in light of the study's limitations, which include limited sample size and stringent selection of inclusion criteria that restrict generalizability. Additionally, there is a wide range of diagnostic criteria in the biomarkers' thresholds utilised across investigations, raising concerns regarding the clinical application. Many factors could contribute to this variability, including patient characteristics, differences in sample type (plasma vs. serum), and time points, as well as a lack of standardisation, analytical factors (different ELISA kits, laboratory equipment and procedures), and the lack of validated reference methods. The discovery and standardisation of optimal cut-off values will require more rigorous and consistent quality control research in the future. On the other hand, the study's biomarkers panel, which included several specificities, processes and pathways, may be considered a strength.

One of the most important limiting factors in this project was the recruitment process of stroke patients and stroke mimics from the hospital during COVID-19 phase, which results in a relatively smaller sample size. Collecting patients' data including completed CRF, CT scan CDs and MRI scan CDs after recruitment was not easy. Struggling a lot was exist during the clinical study to reach these results. Another major difficulty is that not all of the recruited patients undergo MRI scan thus small sample size in MRI results. To cope with that, it has been tried to recruit patients from Bradford General Infirmary Hospital but unfortunately, the process of transporting the blood and data including imaging CDs was delayed.

This research recruited acute stroke phase only as it was not able to recruit hyperacute phase from the accident and emergency (A&E) department due to COVID-19 restrictions. However, the best was tried to collect the blood ASAP from the hospital once the researcher was informed that the patients tested negative for COVID-19, consent was completed and blood samples from patients were obtained. This study was not able to monitor the biomarkers levels from the same patients at different time points due to COVID-19 restrictions and ethical issues, thus, the blood collection in this study had been done at only one-time point. However, the presence of selected biomarkers was detectable up to 7 days from stroke onset which may be considered a strength. Further research testing these biomarkers at different time points is highly recommended.

Identification of the ischaemic side in all patients has been confirmed by looking at patients' records, whereas, identification of volume of infarct has been done by image visualisation, thus, it is influenced by intrinsic biases and subjectivity. As a result, further work regarding this aspect is highly recommended. There are other variables, which may also affect the values of imaging biomarkers such as scanning equipment, software and protocol.

This study was carried out using ELISA methods which have good sensitivity, but it might be better to use higher sensitive methods that measure the biomarkers in smaller units.

6.5 Clinical relevance and future direction

Detection of the biomarker in ischaemic stroke is potentially a very important area of research. Although beyond the aim of this research, understanding the mechanism of

stroke and BBB damage more broadly in preclinical and clinical work could assist to explore the additional detailed understanding of stroke and BBB cells damages to determine a quick way for stroke diagnosis and to develop new therapeutic approaches targeting the BBB.

The results of this study propose that circulating biomarkers in acute stroke patients concerning neurological scores, CT and MRI imaging data might improve the diagnosis of stroke. Further research in this field is highly recommended.

This research recruited acute stroke phase only as it was not able to recruit hyper acute stroke due to COVID-19 restrictions. It is believed that some of these biomarkers might also be specific to be picked up during the hyperacute phase.

Also, future work is needed to find out what is the best time point for blood collection that shows the best result. Moreover, finding out which time point of blood biomarkers that gives an idea about the stroke infarct size is also important.

Finally, this study used ELISA for analysis of biomarkers level. It has good sensitivity, but one recommended direction is to measure the biomarkers and compare the results using other techniques like mass spectrometry, Olink, laser spectroscopy or microRNA sequencing technique.

In conclusion, the proposed circulating biomarker could become a useful and faster potential tool for stroke diagnosis which could combine with imaging biomarkers, however, further research in this field is highly recommended.

References

Abels, B., Klotz, E., Tomandl, B.F., Kloska, S.P. and Lell, M.M. 2010. Perfusion CT in acute ischemic stroke: A qualitative and quantitative comparison of deconvolution and maximum slope approach. *American Journal of Neuroradiology*. **31**(9), pp.1690–1698.

Achrol, A.S. and Steinberg, G.K. 2016. Personalized Medicine in Cerebrovascular Neurosurgery: Precision Neurosurgical Management of Cerebral Aneurysms and Subarachnoid Hemorrhage. *Frontiers in Surgery*. **3**.

Adams, H.P., Del Zoppo, G., Alberts, M.J., Bhatt, D.L., Brass, L., Furlan, A., Grubb, R.L., Higashida, R.T., Jauch, E.C., Kidwell, C., Lyden, P.D., Morgenstern, L.B., Qureshi, A.I., Rosenwasser, R.H., Scott, P.A. and Wijdicks, E.F.M. 2007. Guidelines for the early management of adults with ischemic stroke: a guideline from the American Heart Association/American Stroke Association Stroke Council, Clinical Cardiology Council, Cardiovascular Radiology and Intervention Council, and the Atherosclerotic Peripheral Vascular Disease and Quality of Care Outcomes in Research Interdisciplinary Working Groups: the American Academy of Neurology affirms the value of this guideline as an educational tool for neurologists. *Stroke*. **38**(5), pp.1655–1711.

Ahmed, Z., Shaw, G., Sharma, V.P., Yang, C., McGowan, E. and Dickson, D.W. 2007. Actin-binding proteins coronin-1a and IBA-1 are effective microglial markers for immunohistochemistry. *Journal of Histochemistry and Cytochemistry*. **55**(7), pp.687–700.

Ahn, J.H., Song, M., Kim, H., Lee, T.K., Park, C.W., Park, Y.E., Lee, J.C., Cho, J.H., Kim, Y.M., Hwang, I.K., Won, M.H. and Park, J.H. 2019. Differential regional infarction, neuronal loss and gliosis in the gerbil cerebral hemisphere following 30 min of unilateral common carotid artery occlusion. *Metabolic Brain Disease*. **34**(1), pp.223–233.

Akbarzadeh, M.A., Sanaie, S., Kuchaki Rafsanjani, M. and Hosseini, M.S. 2021. Role of imaging in early diagnosis of acute ischemic stroke: a literature review. *Egyptian Journal of Neurology, Psychiatry and Neurosurgery*. **57**(1), pp.1–8.

Al-Otaiby, M.A., Al-Amri, H.S. and Al-Moghairi, A.M. 2011. The clinical significance of

cardiac troponins in medical practice. *Journal of the Saudi Heart Association*. **23**(1), pp.3–11.

Alexander, J.A., Sheppard, S., Davis, P.C. and Salverda, P. 1996. Adult cerebrovascular disease: role of modified rapid fluid-attenuated inversion-recovery sequences. *AJNR: American Journal of Neuroradiology*. **17**(8), p.1507.

Alhajj, M. and Farhana, A. 2022. Enzyme Linked Immunosorbent Assay. *StatPearls*.

Anand, N. and Stead, L.G. 2005. Neuron-specific enolase as a marker for acute ischemic stroke: A systematic review. *Cerebrovascular Diseases*. **20**(4), pp.213–219.

Andreucci, M., Solomon, R. and Tasanarong, A. 2014. Side Effects of Radiographic Contrast Media: Pathogenesis, Risk Factors, and Prevention. *BioMed Research International*. **2014**.

Andrews, A.E., Perumpalath, N., Puthiyakam, J. and Mekkattukunnel, A. 2021. Hippocampal magnetic resonance imaging in focal onset seizure with impaired awareness—descriptive study from tertiary care centre in southern part of India. *Egyptian Journal of Neurology, Psychiatry and Neurosurgery*. **57**(1), pp.1–7.

Antje, B., Tobias, M., Christian, B., Ingmar A.F.M, H., CT, B., T, Derfuss, J, K. and T, Daikeler 2018. Serum neurofilament light chain: a biomarker of neuronal injury in vasculitic neuropathy. *Annals of the rheumatic diseases*. **77**(7), pp.1093–1094.

Appelros, P., Stegmayr, B. and Terént, A. 2009. Go Red for Women Sex Differences in Stroke Epidemiology A Systematic Review.

Arakawa, S., Wright, P.M., Koga, M., Phan, T.G., Reutens, D.C., Lim, I., Gunawan, M.R., Ma, H., Perera, N., Ly, J., Zavala, J., Fitt, G. and Donnan, G.A. 2006. Ischemic Thresholds for Gray and White Matter. *Stroke*. **37**(5), pp.1211–1216.

Argaw, A.T., Asp, L., Zhang, J., Navrazhina, K., Pham, T., Mariani, J.N., Mahase, S., Dutta, D.J., Seto, J., Kramer, E.G., Ferrara, N., Sofroniew, M. V. and John, G.R. 2012. Astrocyte-derived VEGF-A drives blood-brain barrier disruption in CNS inflammatory disease. *Journal of Clinical Investigation*. **122**(7), pp.2454–2468.

Argaw, A.T., Gurfein, B.T., Zhang, Y., Zameer, A. and John, G.R. 2009. VEGF-mediated disruption of endothelial CLN-5 promotes blood-brain barrier breakdown. *Proceedings of the National Academy of Sciences of the United*

States of America. **106**(6), pp.1977–1982.

Arimura, K., Ago, T., Kamouchi, M., Nakamura, K., Ishitsuka, K., Kuroda, J., Sugimori, H., Ooboshi, H., Sasaki, T. and Kitazono, T. 2012. PDGF receptor β signaling in pericytes following ischemic brain injury. *Current neurovascular research*. **9**(1), pp.1–9.

Ashish 2017. Circle Of Willis: Anatomy, Diagram And Functions » Science ABC. [Accessed 3 June 2020]. Available from: https://www.scienceabc.com/humans/circle-of-willis-anatomy-diagram-and-functions.html.

Atkinson, A.J., Colburn, W.A., DeGruttola, V.G., DeMets, D.L., Downing, G.J., Hoth, D.F., Oates, J.A., Peck, C.C., Schooley, R.T., Spilker, B.A., Woodcock, J. and Zeger, S.L. 2001. Biomarkers and surrogate endpoints: Preferred definitions and conceptual framework. *Clinical Pharmacology & Therapeutics*. **69**(3), pp.89–95.

Austein, F., Riedel, C., Kerby, T., Meyne, J., Binder, A., Lindner, T., Huhndorf, M., Wodarg, F. and Jansen, O. 2016. Comparison of Perfusion CT Software to Predict the Final Infarct Volume after Thrombectomy. *Stroke*. **47**(9), pp.2311–2317.

Bansal, S., Sangha, K.S. and Khatri, P. 2013. Drug [1] S. Bansal, K.S. Sangha, P. Khatri, Drug Treatment of Acute Ischemic Stroke, Am. J. Cardiovasc. Drugs. 13 (2013) 57–69. doi:10.1007/s40256-013-0007-6.Treatment of Acute Ischemic Stroke. *American Journal of Cardiovascular Drugs*. **13**(1), pp.57–69.

Barber, P., Demchuk, A.M., Zhang, J. and Buchan, A.M. 2000. Validity and reliability of a quantitative computed tomography score in predicting outcome of hyperacute stroke before thrombolytic therapy. ASPECTS Study Group. Alberta Stroke Programme Early CT Score. *Lancet (London, England)*. **355**(9216), pp.1670–1674.

Barber, P.A., Darby, D.G., Desmond, P.M., Gerraty, R.P., Yang, Q., Li, T., Jolley, D., Donnan, G.A., Tress, B.M. and Davis, S. 1999. Identification of major ischemic change. Diffusion-weighted imaging versus computed tomography. *Stroke*. **30**(10), pp.2059–2065.

Barro, C., Chitnis, T. and Weiner, H.L. 2020. Blood neurofilament light: a critical review of its application to neurologic disease. *Annals of Clinical and Translational*

Neurology. **7**(12), p.2508.

Bederson, J.B., Pitts, L.H., Tsuji, M., Nishimura, M.C., Davis, R.L. and Bartkowski, H. 1986. Rat middle cerebral artery occlusion: Evaluation of the model and development of a neurologic examination. *Stroke*. **17**(3), pp.472–476.

Berger, A. 2002. How does it work?: Magnetic resonance imaging. *BMJ : British Medical Journal*. **324**(7328), p.35.

Bergers, G. and Song, S. 2005. The role of pericytes in blood-vessel formation and maintenance. *Neuro-Oncology*. **7**(4), pp.452–464.

Bharosay, A., Bharosay, V.V., Varma, M., Saxena, K., Sodani, A. and Saxena, R. 2012. Correlation of brain biomarker neuron specific enolase (NSE) with degree of disability and neurological worsening in cerebrovascular stroke. *Indian Journal of Clinical Biochemistry*. **27**(2), pp.186–190.

Birenbaum, D., Bancroft, L.W. and Felsberg, G.J. 2011. Imaging in Acute Stroke. *Western Journal of Emergency Medicine*. **12**(1), p.67.

Bjarnegård, M., Enge, M., Norlin, J., Gustafsdottir, S., Fredriksson, S., Abramsson, A., Takemoto, M., Gustafsson, E., Fässler, R. and Betsholtz, C. 2004. Endothelium-specific ablation of PDGFB leads to pericyte loss and glomerular, cardiac and placental abnormalities. *Development (Cambridge, England)*. **131**(8), pp.1847–57.

Bloem, J.L., Reijnierse, M., Huizinga, T.W.J. and Van Der Helm-Van Mil, A.H.M. 2018. MR signal intensity: staying on the bright side in MR image interpretation. *RMD Open*. **4**(1).

Bogousslavsky, J., Melle, G. Van and Regli, F. 1988. The lausanne stroke registry: Analysis of 1,000 consecutive patients with first stroke. *Stroke*. **19**(9), pp.1083–1092.

Borst, J., Berkhemer, O.A., Roos, Y.B.W.E.M., Van Bavel, E., Van Zwam, W.H., Van Oostenbrugge, R.J., Van Walderveen, M.A.A., Lingsma, H.F., Van Der Lugt, A., Dippel, D.W.J., Yoo, A.J., Marquering, H.A. and Majoie, C.B.L.M. 2015. Value of computed tomographic perfusion-based patient selection for intra-arterial acute ischemic stroke treatment. *Stroke*. **46**(12), pp.3375–3382.

Bradley, A., Bertrand, L., Rao, D.B., Greg Hall, D. and Sharma, A.K. 2018. Brain *In*:

Boorman's Pathology of the Rat [Online]. Academic Press, pp.191–215. [Accessed 3 November 2022]. Available from: https://linkinghub.elsevier.com/retrieve/pii/B9780123914484000137.

Brea, D., Sobrino, T., Blanco, M., Cristobo, I., Rodríguez-González, R., Rodríguez-Yañez, M., Moldes, O., Agulla, J., Leira, R. and Castillo, J. 2009. Temporal profile and clinical significance of serum neuron-specific enolase and S100 in ischemic and hemorrhagic stroke. *Clinical Chemistry and Laboratory Medicine*. **47**(12), pp.1513–1518.

Brown, L.S., Foster, C.G., Courtney, J.-M., King, N.E., Howells, D.W. and Sutherland, B.A. 2019. Pericytes and Neurovascular Function in the Healthy and Diseased Brain. *Frontiers in Cellular Neuroscience*. **13**, p.282.

Buck, B.H., Akhtar, N., Alrohimi, A., Khan, K. and Shuaib, A. 2021. Stroke mimics: incidence, aetiology, clinical features and treatment. *Annals of Medicine*. **53**(1), p.420.

Burda, J.E. and Sofroniew, M. V. 2014. Reactive gliosis and the multicellular response to CNS damage and disease. *Neuron*. **81**(2), pp.229–248.

Buscemi, L., Price, M., Bezzi, P. and Hirt, L. 2019. Spatio-temporal overview of neuroinflammation in an experimental mouse stroke model. *Scientific Reports*. **9**(1), pp.1–13.

Busher, J.T. 1990. Serum Albumin and Globulin *In*: *Clinical Methods: The History, Physical, and Laboratory Examinations* [Online]. Boston: Butterworths. [Accessed 10 August 2022]. Available from: https://www.ncbi.nlm.nih.gov/books/NBK204/.

Bustamante, A., López-Cancio, E., Pich, S., Penalba, A., Giralt, D., García-Berrocoso, T., Ferrer-Costa, C., Gasull, T., Hernández-Pérez, M., Millan, M., Rubiera, M., Cardona, P., Cano, L., Quesada, H., Terceño, M., Silva, Y., Castellanos, M., Garces, M., Reverté, S., Ustrell, X., Marés, R., Baiges, J.J., Serena, J., Rubio, F., Salas, E., Dávalos, A. and Montaner, J. 2017. Blood Biomarkers for the Early Diagnosis of Stroke: The Stroke-Chip Study. *Stroke*. **48**(9), pp.2419–2425.

Butler, T.L., Kassed, C.A., Sanberg, P.R., Willing, A.E. and Pennypacker, K.R. 2002. Neurodegeneration in the rat hippocampus and striatum after middle cerebral artery occlusion. *Brain Research*. **929**(2), pp.252–260.

Cabezas, R., Ávila, M., Gonzalez, J., El-Bachá, R.S., Báez, E., García-Segura, L.M., Coronel, J.C.J., Capani, F., Cardona-Gomez, G.P. and Barreto, G.E. 2014. Astrocytic modulation of blood brain barrier: Perspectives on Parkinson's disease. *Frontiers in Cellular Neuroscience*. **8**(AUG), p.211.

Caldemeyer, K.S. and Buckwalter, K.A. 1999. The basic principles of computed tomography and magnetic resonance imaging. *Journal of the American Academy of Dermatology*. **41**(5 I), pp.768–771.

Campbell, B.C.V., Yassi, N., Ma, H., Sharma, G., Salinas, S., Churilov, L., Meretoja, A., Parsons, M.W., Desmond, P.M., Lansberg, M.G., Donnan, G.A. and Davis, S.M. 2015. Imaging selection in ischemic stroke: Feasibility of automated CT-perfusion analysis. *International Journal of Stroke*. **10**(1), pp.51–54.

Chan, Y.H. 2003. Biostatistics 104: Correlational Analysis. *Singapore Med J*. **44**(12), pp.614–619.

Chen, C., Bivard, A., Lin, L., Levi, C.R., Spratt, N.J. and Parsons, M.W. 2019. Thresholds for infarction vary between gray matter and white matterin acute ischemic stroke: A CT perfusion study. *Journal of Cerebral Blood Flow & Metabolism*. **39**(3), p.536.

Choudhury, G.R. and Ding, S. 2016. Reactive astrocytes and therapeutic potential in focal ischemic stroke. *Neurobiology of Disease*. **85**, pp.234–244.

CIRSE 2022. Endovascular treatment of stroke. [Accessed 12 June 2022]. Available from: https://www.cirse.org/patients/ir-procedures/endovascular-treatment-of-stroke/.

Collorone, S., Prados, F., Kanber, B., Cawley, N.M., Tur, C., Grussu, F., Solanky, B.S., Yiannakas, M., Davagnanam, I., Wheeler-Kingshott, C.A.M.G., Barkhof, F., Ciccarelli, O. and Toosy, A.T. 2021. Brain microstructural and metabolic alterations detected in vivo at onset of the first demyelinating event. *Brain*. **144**(5), pp.1409–1421.

Colonna, M. and Butovsky, O. 2017. Microglia function in the central nervous system during health and neurodegeneration. *Annual Review of Immunology*. **35**, pp.441–468.

Czeiter, E., Amrein, K., Gravesteijn, B.Y., Lecky, F., Menon, D.K., Mondello, S.,

Newcombe, V.F.J., Richter, S., Steyerberg, E.W., Vyvere, T. Vande, Verheyden, J., Xu, H., Yang, Z., Maas, A.I.R., Wang, K.K.W. and Büki, A. 2020. Blood biomarkers on admission in acute traumatic brain injury: Relations to severity, CT findings and care path in the CENTER-TBI study. *EBioMedicine*. **56**, p.102785.

Dagonnier, M., Donnan, G.A., Davis, S.M., Dewey, H.M. and Howells, D.W. 2021. Acute Stroke Biomarkers: Are We There Yet? *Frontiers in Neurology*. **12**, p.73.

Daneman, R. and Prat, A. 2015. The blood–brain barrier. *Cold Spring Harbor Perspectives in Biology*. **7**(1).

Debette, S., Compter, A., Labeyrie, M.-A., Uyttenboogaart, M., Metso, T.M., Majersik, J.J., Goeggel-Simonetti, B., Engelter, S.T., Pezzini, A., Bijlenga, P., Southerland, A.M., Naggara, O., Béjot, Y., Cole, J.W., Ducros, A., Giacalone, G., Schilling, S., Reiner, P., Sarikaya, H., Welleweerd, J.C., Kappelle, L.J., Borst, G.J. de, Bonati, L.H., Jung, S., Thijs, V., Martin, J.J., Brandt, T., Grond-Ginsbach, C., Kloss, M., Mizutani, T., Minematsu, K., Meschia, J.F., Pereira, V.M., Bersano, A., Touzé, E., Lyrer, P.A., Leys, D., Chabriat, H., Markus, H.S., Worrall, B.B., Chabrier, S., Baumgartner, R., Stapf, C., Tatlisumak, T., Arnold, M. and Bousser, M.-G. 2015. Epidemiology, pathophysiology, diagnosis, and management of intracranial artery dissection. *The Lancet Neurology*. **14**(6), pp.640–654.

DeGraba, T.J., Hallenbeck, J.M., Pettigrew, K.D., Dutka, A.J. and Kelly, B.J. 1999. Progression in Acute Stroke. *Stroke*. **30**(6), pp.1208–1212.

Delisser, H.M., Newman, P.J. and Albelda, S.M. 1993. Platelet endothelial cell adhesion molecule (CD31). *Current topics in microbiology and immunology*. **184**, pp.37–45.

DenOtter, T.D. and Schubert, J. 2022. Hounsfield Unit *In*: *Radiopaedia.org* [Online]. StatPearls Publishing. [Accessed 22 December 2022]. Available from: https://www.ncbi.nlm.nih.gov/books/NBK547721/.

Derex, L. and Cho, T.H. 2017. Mechanical thrombectomy in acute ischemic stroke. *Revue Neurologique*. **173**(3), pp.106–113.

deSouza, N.M., Achten, E., Alberich-Bayarri, A., Bamberg, F., Boellaard, R., Clément, O., Fournier, L., Gallagher, F., Golay, X., Heussel, C.P., Jackson, E.F., Manniesing, R., Mayerhofer, M.E., Neri, E., O'Connor, J., Oguz, K.K., Persson,

A., Smits, M., van Beek, E.J.R. and Zech, C.J. 2019. Validated imaging biomarkers as decision-making tools in clinical trials and routine practice: current status and recommendations from the EIBALL* subcommittee of the European Society of Radiology (ESR). *Insights into Imaging*. **10**(1), pp.1–16.

Dias, A., Silva, I., Pinto, I.M. and Maia, L.F. 2021. Timely and blood-based multiplex molecular profiling of acute stroke. *Life*. **11**(8), pp.1–17.

Dohmen, C., Kumura, E., Rosner, G., Heiss, W.D. and Graf, R. 2001. Adenosine in relation to calcium homeostasis: Comparison between gray and white matter ischemia. *Journal of Cerebral Blood Flow and Metabolism*. **21**(5), pp.503–510.

Duan, Z., Fu, C., Chen, B., Xu, G., Tao, L., Tang, T., Hou, H., Fu, X., Yang, M., Liu, Z. and Zhang, X. 2015. Lesion patterns of single small subcortical infarct and its association with early neurological deterioration. *Neurological sciences : official journal of the Italian Neurological Society and of the Italian Society of Clinical Neurophysiology*. **36**(10), pp.1851–1857.

Duering, M., Konieczny, M.J., Tiedt, S., Baykara, E., Tuladhar, A.M., Leijsen, E. van, Lyrer, P., Engelter, S.T., Gesierich, B., Achmüller, M., Barro, C., Adam, R., Ewers, M., Dichgans, M., Kuhle, J., Leeuw, F.-E. de and Peters, N. 2018. Serum Neurofilament Light Chain Levels Are Related to Small Vessel Disease Burden. *Journal of Stroke*. **20**(2), p.228.

Dzialowski, I., Weber, J., Doerfler, A., Forsting, M. and Kummer, R. Von 2004. Brain Tissue Water Uptake after Middle Cerebral Artery Occlusion Assessed with CT. *Journal of Neuroimaging*. **14**(1), pp.42–48.

Emberson, J., Lees, K.R., Lyden, P., Blackwell, L., Albers, G., Bluhmki, E., Brott, T., Cohen, G., Davis, S., Donnan, G., Grotta, J., Howard, G., Kaste, M., Koga, M., Von Kummer, R., Lansberg, M., Lindley, R.I., Murray, G., Olivot, J.M., Parsons, M., Tilley, B., Toni, D., Toyoda, K., Wahlgren, N., Wardlaw, J., Whiteley, W., Del Zoppo, G.J., Baigent, C., Sandercock, P. and Hacke, W. 2014. Effect of treatment delay, age, and stroke severity on the effects of intravenous thrombolysis with alteplase for acute ischaemic stroke: A meta-analysis of individual patient data from randomised trials. *The Lancet*. **384**(9958), pp.1929–1935.

Engedal, T.S., Hjort, N., Hougaard, K.D., Simonsen, C.Z., Andersen, G., Mikkelsen, I.K., Boldsen, J.K., Eskildsen, S.F., Hansen, M.B., Angleys, H., Jespersen, S.N.,

Pedraza, S., Cho, T.H., Serena, J., Siemonsen, S., Thomalla, G., Nighoghossian, N., Fiehler, J., Mouridsen, K. and Østergaard, L. 2018. Transit time homogenization in ischemic stroke – A novel biomarker of penumbral microvascular failure? *Journal of Cerebral Blood Flow and Metabolism*. **38**(11), pp.2006–2020.

Evans, M.R.B., White, P., Cowley, P. and Werring, D.J. 2017. Revolution in acute ischaemic stroke care: A practical guide to mechanical thrombectomy. *Practical Neurology*. **17**(4), pp.252–265.

Feldman, G.J., Mullin, J.M. and Ryan, M.P. 2005. Occludin: Structure, function and regulation. *Advanced Drug Delivery Reviews*. **57**(6), pp.883–917.

Fernández-Klett, F., Potas, J.R., Hilpert, D., Blazej, K., Radke, J., Huck, J., Engel, O., Stenzel, W., Genové, G. and Priller, J. 2013a. Early loss of pericytes and perivascular stromal cell-induced scar formation after stroke. *Journal of Cerebral Blood Flow and Metabolism*. **33**(3), pp.428–439.

Fernández-Klett, F., Potas, J.R., Hilpert, D., Blazej, K., Radke, J., Huck, J., Engel, O., Stenzel, W., Genové, G. and Priller, J. 2013b. Early loss of pericytes and perivascular stromal cell-induced scar formation after stroke. *Journal of Cerebral Blood Flow and Metabolism*. **33**(3), pp.428–439.

Fiebach, J.B., Schellinger, P.D., Jansen, O., Meyer, M., Wilde, P., Bender, J., Schramm, P., Jüttler, E., Oehler, J., Hartmann, M., Hähnel, S., Knauth, M., Hacke, W. and Sartor, K. 2002. CT and diffusion-weighted MR imaging in randomized order: Diffusion-weighted imaging results in higher accuracy and lower interrater variability in the diagnosis of hyperacute ischemic stroke. *Stroke*. **33**(9), pp.2206–2210.

Fischer, S., Wobben, M., Marti, H.H., Renz, D. and Schaper, W. 2002. Hypoxia-induced hyperpermeability in brain microvessel endothelial cells involves VEGF-mediated changes in the expression of zonula occludens-1. *Microvascular research*. **63**(1), pp.70–80.

Fisher Scientific 2022. Evacuated Blood Tubes | Phlebotomy | Fisher Scientific. *Fisher Scientific*. [Online]. [Accessed 10 October 2022]. Available from: https://www.fishersci.co.uk/gb/en/products/I9C8KT8G/evacuated-blood-tubes.html.

Flottmann, F., Broocks, G., Faizy, T.D., Ernst, M., Forkert, N.D., Grosser, M., Thomalla, G., Siemonsen, S., Fiehler, J. and Kemmling, A. 2017. CT-perfusion stroke imaging: a threshold free probabilistic approach to predict infarct volume compared to traditional ischemic thresholds. *Scientific Reports 2017 7:1*. **7**(1), pp.1–10.

Foerch, C., Curdt, I., Yan, B., Dvorak, F., Hermans, M., Berkefeld, J., Raabe, A., Neumann-Haefelin, T., Steinmetz, H. and Sitzer, M. 2006. Serum glial fibrillary acidic protein as a biomarker for intracerebral haemorrhage in patients with acute stroke. *Journal of neurology, neurosurgery, and psychiatry*. **77**(2), pp.181–184.

Foerch, C., Luger, S. and Group, B.F.S. 2015. Glial fibrillary acidic protein (GFAP) plasma levels distinguish intracerebral hemorrhage from cerebral ischemia in the early phase of acute stroke. *Journal of the Neurological Sciences*. **357**, p.e430.

Fred, H.L. 2004. Drawbacks and Limitations of Computed Tomography: Views from a Medical Educator. *Texas Heart Institute Journal*. **31**(4), p.345.

Friedrich, B., Kertels, O., Bach, D., Wunderlich, S., Zimmer, C., Prothmann, S. and Förschler, A. 2014. Fate of the penumbra after mechanical thrombectomy. *American Journal of Neuroradiology*. **39**(5), pp.972–977.

Fu, J.H., Chen, Y.K., Chen, X.Y., Mok, V. and Wong, K.S. 2010. Coexisting Small Vessel Disease Predicts Poor Long-Term Outcome in Stroke Patients with Intracranial Large Artery Atherosclerosis. *Cerebrovascular Diseases*. **30**(5), pp.433–439.

Furuse, M., Itoh, M., Hirase, T., Nagafuchi, A., Yonemura, S., Tsukita, S. and Tsukita, S. 1994. Direct association of occludin with ZO-1 and its possible involvement in the localization of occludin at tight junctions. *The Journal of cell biology*. **127**(6 Pt 1), pp.1617–26.

Gaiottino, J., Norgren, N., Dobson, R., Topping, J., Nissim, A., Malaspina, A., Bestwick, J.P., Monsch, A.U., Regeniter, A., Lindberg, R.L., Kappos, L., Leppert, D., Petzold, A., Giovannoni, G. and Kuhle, J. 2013. Increased Neurofilament Light Chain Blood Levels in Neurodegenerative Neurological Diseases. *PLoS ONE*. **8**(9), p.75091.

Gao, J., Parsons, M.W., Kawano, H., Levi, C.R., Evans, T.J., Lin, L. and Bivard, A.

2017. Visibility of CT Early Ischemic Change Is Significantly Associated with Time from Stroke Onset to Baseline Scan beyond the First 3 Hours of Stroke Onset. *Journal of Stroke*. **19**(3), pp.340–346.

Gendron, T.F., Badi, M.K., Heckman, M.G., Jansen-West, K.R., Vilanilam, G.K., Johnson, P.W., Burch, A.R., Walton, R.L., Ross, O.A., Brott, T.G., Miller, T.M., Berry, J.D., Nicholson, K.A., Wszolek, Z.K., Oskarsson, B.E., Sheth, K.N., Sansing, L.H., Falcone, G.J., Cucchiara, B.L., Meschia, J.F. and Petrucelli, L. 2020. Plasma neurofilament light predicts mortality in patients with stroke. *Science Translational Medicine*. **12**(569).

Ghadimi, M. and Sapra, A. 2022. Magnetic Resonance Imaging Contraindications *In*: *StatPearls* [Online]. StatPearls Publishing. [Accessed 1 July 2022]. Available from: https://www.ncbi.nlm.nih.gov/books/NBK551669/.

Ghori, A., Freimann, F.B., Nieminen-Kelhä, M., Kremenetskaia, I., Gertz, K., Endres, M. and Vajkoczy, P. 2017. EphrinB2 Activation Enhances Vascular Repair Mechanisms and Reduces Brain Swelling After Mild Cerebral Ischemia. *Arteriosclerosis, Thrombosis, and Vascular Biology*. **37**(5), pp.867–878.

Glushakova, O.Y., Glushakov, A. V, Miller, E.R., Valadka, A.B. and Hayes, R.L. 2016. Biomarkers for acute diagnosis and management of stroke in neurointensive care units. *Brain Circulation*. **2**(1), p.28.

González-García, S., González-Quevedo, A., Fernández-Concepción, O., Peña-Sánchez, M., Menéndez-Saínz, C., Hernández-Díaz, Z., Arteche-Prior, M., Pando-Cabrera, A. and Fernández-Novales, C. 2012. Short-term prognostic value of serum neuron specific enolase and S100B in acute stroke patients. *Clinical Biochemistry*. **45**(16–17), pp.1302–1307.

Gordon, Y., Partovi, S., Müller-Eschner, M., Amarteifio, E., Bäuerle, T., Weber, M.-A., Kauczor, H.-U. and Rengier, F. 2014. Dynamic contrast-enhanced magnetic resonance imaging: fundamentals and application to the evaluation of the peripheral perfusion. *Cardiovascular diagnosis and therapy*. **4**(2), pp.147–14764.

Gouhar, G.K. and Taha, T.F. 2010. MR exponential image in ischemic stroke: A preliminary evaluation. *Egyptian Journal of Radiology and Nuclear Medicine*. **41**(3), pp.401–409.

Gundersen, H.J.G. 1977. Notes on the estimation of the numerical density of arbitrary profiles: the edge effect. *Journal of Microscopy*. **111**(2), pp.219–223.

Gusel'nikova, V. V and Korzhevskiy, D.E. 2015. NeuN As a Neuronal Nuclear Antigen and Neuron Differentiation Marker. *Acta naturae*. **7**(2), pp.42–7.

Hacke, W., Kaste, M., Bluhmki, E., Brozman, M., Dávalos, A., Guidetti, D., Larrue, V., Lees, K.R., Medeghri, Z., Machnig, T., Schneider, D., von Kummer, R., Wahlgren, N. and Toni, D. 2008. Thrombolysis with Alteplase 3 to 4.5 Hours after Acute Ischemic Stroke. *New England Journal of Medicine*. **359**(13), pp.1317–1329.

Hall, C.N., Reynell, C., Gesslein, B., Hamilton, N.B., Mishra, A., Sutherland, B.A., Oâ Farrell, F.M., Buchan, A.M., Lauritzen, M. and Attwell, D. 2014. Capillary pericytes regulate cerebral blood flow in health and disease. *Nature*. **508**(1), pp.55–60.

Hand, P.J., Kwan, J., Lindley, R.I., Dennis, M.S. and Wardlaw, J.M. 2006. Distinguishing between stroke and mimic at the bedside: The brain attack study. *Stroke*. **37**(3), pp.769–775.

Hao, F. li, Han, X. fang, Wang, X. li, Zhao, Z. ru, Guo, A. hong, Lu, X. jian and Zhao, X. fei 2019. The neurovascular protective effect of alogliptin in murine MCAO model and brain endothelial cells. *Biomedicine and Pharmacotherapy*. **109**, pp.181–187.

Hasan, N., McColgan, P., Bentley, P., Edwards, R.J. and Sharma, P. 2012. Towards the identification of blood biomarkers for acute stroke in humans: a comprehensive systematic review. *British Journal of Clinical Pharmacology*. **74**(2), pp.230–240.

Hawkins, B.T. and Davis, T.P. 2005. The blood-brain barrier/neurovascular unit in health and disease. *Pharmacological Reviews*. **57**(2), pp.173–185.

Heart & Stroke 2022. What is stroke? *Heart and Stroke Foundation*. [Online]. [Accessed 12 June 2022]. Available from: https://www.heartandstroke.ca/stroke/what-is-stroke.

Helenius, J., Soinne, L., Perkiö, J., Salonen, O., Kangasmäki, A., Kaste, M., Carano, R.A.D., Aronen, H.J. and Tatlisumak, T. 2002. Diffusion-Weighted MR Imaging in Normal Human Brains in Various Age Groups.

Henriksen, K., O'Bryant, S.E., Hampel, H., Trojanowski, J.Q., Montine, T.J., Jeromin,

A., Blennow, K., Lönneborg, A., Wyss-Coray, T., Soares, H., Bazenet, C., Sjögren, M., Hu, W., Lovestone, S., Karsdal, M.A. and Weiner, M.W. 2014. The future of blood-based biomarkers for Alzheimer's disease. *Alzheimer's and Dementia*. **10**(1), pp.115–131.

Herrmann, M., Vos, P., Wunderlich, M.T., de Bruijn, C.H.M.M. and Lamers, K.J.B. 2000. Release of Glial Tissue–Specific Proteins After Acute Stroke. *Stroke*. **31**(11), pp.2670–2677.

Hol, E.M. and Pekny, M. 2015. Glial fibrillary acidic protein (GFAP) and the astrocyte intermediate filament system in diseases of the central nervous system. *Current Opinion in Cell Biology*. **32**, pp.121–130.

Hossmann, K.-A. 1991. Animal Models of Cerebral Ischemia. 1. Review of Literature. *Cerebrovascular Diseases*. **1**(1), pp.2–15.

Hoving, J.W., Marquering, H.A., Majoie, C.B.L.M., Yassi, N., Sharma, G., Liebeskind, D.S., Lugt, A. van der, Roos, Y.B., Zwam, W. van, Oostenbrugge, R.J. van, Goyal, M., Saver, J.L., Jovin, T.G., Albers, G.W., Davalos, A., Hill, M.D., Demchuk, A.M., Bracard, S., Guillemin, F., Muir, K.W., White, P., Mitchell, P.J., Donnan, G.A., Davis, S.M. and Campbell, B.C.V. 2018. Volumetric and Spatial Accuracy of Computed Tomography Perfusion Estimated Ischemic Core Volume in Patients With Acute Ischemic Stroke. *Stroke*. **49**(10), pp.2368–2375.

Imai, Y., Ibata, I., Ito, D., Ohsawa, K. and Kohsaka, S. 1996. A novel gene iba1 in the major histocompatibility complex class III region encoding an EF hand protein expressed in a monocytic lineage. *Biochemical and Biophysical Research Communications*. **224**(3), pp.855–862.

Investigators, T.P.P.S.T. 2009. The penumbra pivotal stroke trial: safety and effectiveness of a new generation of mechanical devices for clot removal in intracranial large vessel occlusive disease. *Stroke*. **40**(8), pp.2761–2768.

Itoh, M. and Bissell, M.J. 2003. The organization of tight junctions in epithelia: Implications for mammary gland biology and breast tumorigenesis. *Journal of Mammary Gland Biology and Neoplasia*. **8**(4), pp.449–462.

Jahng, G.H., Li, K.L., Ostergaard, L. and Calamante, F. 2014. Perfusion Magnetic Resonance Imaging: A Comprehensive Update on Principles and Techniques.

Korean Journal of Radiology. **15**(5), p.554.

Jia, W., Lu, R., Martin, T.A. and Jiang, W.G. 2014. The role of claudin-5 in blood-brain barrier (BBB) and brain metastases (Review). *Molecular Medicine Reports*. **9**(3), pp.779–785.

Jiao, H., Wang, Z., Liu, Y., Wang, P. and Xue, Y. 2011. Specific role of tight junction proteins claudin-5, occludin, and ZO-1 of the blood-brain barrier in a focal cerebral ischemic insult. *Journal of Molecular Neuroscience*. **44**(2), pp.130–139.

Jickling, G.C., Liu, D., Stamova, B., Ander, B.P., Zhan, X., Lu, A. and Sharp, F.R. 2014. Hemorrhagic transformation after ischemic stroke in animals and humans. *Journal of Cerebral Blood Flow and Metabolism*. **34**(2), pp.185–199.

Jie, L., X, J., KJ, L. and W, L. 2012. Matrix metalloproteinase-2-mediated occludin degradation and caveolin-1-mediated claudin-5 redistribution contribute to blood-brain barrier damage in early ischemic stroke stage. *The Journal of neuroscience : the official journal of the Society for Neuroscience*. **32**(9), pp.3044–3057.

Jin, R., Zhu, X. and Li, G. 2014. Embolic Middle Cerebral Artery Occlusion (MCAO) for Ischemic Stroke with Homologous Blood Clots in Rats. *Journal of Visualized Experiments : JoVE*. (91), p.51956.

Jin, X., Riew, T.R., Kim, S., Kim, H.L. and Lee, M.Y. 2020. Spatiotemporal Profile and Morphological Changes of NG2 Glia in the CA1 Region of the Rat Hippocampus after Transient Forebrain Ischemia. *Experimental Neurobiology*. **29**(1), p.50.

Jonsson, M., Zetterberg, H., Straaten, E. Van, Lind, K., Syversen, S., Edman, Å., Blennow, K., Rosengren, L., Pantoni, L., Inzitari, D. and Wallin, A. 2010. Cerebrospinal fluid biomarkers of white matter lesions – cross-sectional results from the LADIS study. *European Journal of Neurology*. **17**(3), pp.377–382.

Kaneko, K., Kuwabara, Y., Mihara, F., Yoshiura, T., Nakagawa, M., Tanaka, A., Sasaki, M., Koga, H., Hayashi, K. and Honda, H. 2004. Validation of the CBF, CBV, and MTT Values by Perfusion MRI in Chronic Occlusive Cerebrovascular Disease: A Comparison with 15O-PET. *Academic Radiology*. **11**(5), pp.489–497.

Kapral, M.K., Fang, J., Hill, M.D., Silver, F., Richards, J., Jaigobin, C. and Cheung, A.M. 2005. Sex differences in stroke care and outcomes: Results from the Registry of the Canadian Stroke Network. *Stroke*. **36**(4), pp.809–814.

Kassner, A. and Merali, Z. 2015. Assessment of Blood-Brain Barrier Disruption in Stroke. *Stroke*. **46**(11), pp.3310–3315.

Katan, M. and Elkind, M. 2018. The potential role of blood biomarkers in patients with ischemic stroke: An expert opinion.

Katsanos, A.H., Makris, K., Stefani, D., Koniari, K., Gialouri, E., Lelekis, M., Chondrogianni, M., Zompola, C., Dardiotis, E., Rizos, I., Parissis, J., Boutati, E., Voumvourakis, K. and Tsivgoulis, G. 2017. Plasma Glial Fibrillary Acidic Protein in the Differential Diagnosis of Intracerebral Hemorrhage. *Stroke*. **48**(9), pp.2586–2588.

Kazmierski, R., Michalak, S., Wencel-Warot, A. and Nowinski, W.L. 2012. Serum tight-junction proteins predict hemorrhagic transformation in ischemic stroke patients. *Neurology*. **79**(16), pp.1677–1685.

Keedy, A.W., Fischette, ; W Scott, Soares, B.P., Arora, S., Benison, ;, Lau, C., Magge, R., Bredno, J., Cheng, S. and Wintermark, M. 2012. Contrast Delay on Perfusion CT as a Predictor of New, Incident Infarct A Retrospective Cohort Study.

Keep, R.F., Xiang, J., Ennis, S.R., Andjelkovic, A., Hua, Y., Xi, G. and Hoff, J.T. 2008. Blood-brain barrier function in intracerebral hemorrhage. *Acta Neurochirurgica, Supplementum*. (105), pp.73–77.

Ketheeswaranathan, P., Turner, N.A., Spary, E.J., Batten, T.F.C., McColl, B.W. and Saha, S. 2011. Changes in glutamate transporter expression in mouse forebrain areas following focal ischemia. *Brain Research*. **1418**, pp.93–103.

Khalil, M., Teunissen, C.E., Otto, M., Piehl, F., Sormani, M.P., Gattringer, T., Barro, C., Kappos, L., Comabella, M., Fazekas, F., Petzold, A., Blennow, K., Zetterberg, H. and Kuhle, J. 2018. Neurofilaments as biomarkers in neurological disorders. *Nature reviews. Neurology*. **14**(10), pp.577–589.

Khan, S., Yuldasheva, N.Y., Batten, T.F.C., Pickles, A.R., Kellett, K.A.B. and Saha, S. 2018. Tau pathology and neurochemical changes associated with memory dysfunction in an optimised murine model of global cerebral ischaemia - A potential model for vascular dementia? *Neurochemistry International*. **118**(April), pp.134–144.

Khan, S.U., Zomaya, A.Y. and Abbas, A. 2017. Handbook of Large-Scale Distributed

Computing in Smart Healthcare S. U. Khan, A. Y. Zomaya, & A. Abbas, eds.

Khandare, P., Saluja, A., Solanki, R.S., Singh, R., Vani, K., Garg, D. and Dhamija, R.K. 2022. Serum S100B and NSE Levels Correlate With Infarct Size and Bladder-Bowel Involvement Among Acute Ischemic Stroke Patients. *J Neurosci Rural Pract*. **13**, pp.218–225.

Khandelwal, N. 2008. CT perfusion in acute stroke. *Indian Journal of Radiology and Imaging*. **18**(4), p.281.

Kidwell, C.S. 2013. MRI biomarkers in acute ischemic stroke: A conceptual framework and historical analysis. *Stroke*. **44**(2), pp.570–578.

Kim, H.J., Choi, C.G., Lee, Hee, Lee, Hyun, Kim, S.J. and Suh, D.C. 2005. *High-b-Value Diffusion-Weighted MR Imaging of Hyperacute Ischemic Stroke at 1.5T*.

Knight, M.J., Damion, R.A., McGarry, B.L., Bosnell, R., Jokivarsi, K.T., Gröhn, O.H.J., Jezzard, P., Harston, G.W.J., Carone, D., Kennedy, J., El-Tawil, S., Elliot, J., Muir, K.W., Clatworthy, P. and Kauppinen, R.A. 2019. Determining T2 relaxation time and stroke onset relationship in ischaemic stroke within apparent diffusion coefficient-defined lesions. A user-independent method for quantifying the impact of stroke in the human brain. *Biomedical Spectroscopy and Imaging*. **8**(1–2), pp.11–28.

Koenig, M., Kraus, M., Theek, C., Klotz, E., Gehlen, W. and Heuser, L. 2001. *Quantitative Assessment of the Ischemic Brain by Means of Perfusion-Related Parameters Derived From Perfusion CT* [Online]. [Accessed 20 March 2020]. Available from: http://ahajournals.org.

Koizumi, Y, Y. and O, N.T. 1986. Experimental studies of ischemic brain edema. 1. A new experimental model of cerebral embolism in rats in which recirculation can be introduced in the ischemic area. *Jpn J Stroke*. **8**, pp.1–8.

Kucinski, T., Väterlein, O., Glauche, V., Fiehler, J., Klotz, E., Eckert, B., Koch, C., Röther, J. and Zeumer, H. 2002. Correlation of Apparent Diffusion Coefficient and Computed Tomography Density in Acute Ischemic Stroke. *Stroke*. **33**(7), pp.1786–1791.

Kudabayeva, M., Kisel, A., Chernysheva, G., Smol'Yakova, V., Plotnikov, M. and Khodanovich, M. 2017. The increase in the number of astrocytes in the total

cerebral ischemia model in rats. *Journal of Physics: Conference Series*. **886**(1).

Kumar, A., Misra, S., Yadav, A.K., Sagar, R., Verma, B., Grover, A. and Prasad, K. 2019. Role of glial fibrillary acidic protein as a biomarker in differentiating intracerebral haemorrhage from ischaemic stroke and stroke mimics: a meta-analysis. *https://doi.org/10.1080/1354750X.2019.1691657*. **25**(1), pp.1–8.

Lai, S.L., Chen, Y.C., Weng, H.H., Chen, S.T., Hsu, S.P. and Lee, T.H. 2005. Bilateral common carotid artery occlusion - A case report and literature review. *Journal of the Neurological Sciences*. **238**(1–2), pp.101–104.

Lasek-Bal, A., Kokot, A., Gendosz de Carrillo, D., Student, S., Pawletko, K., Krzan, A., Puz, P., Bal, W. and Jędrzejowska-Szypułka, H. 2020. Plasma levels of occludin and claudin-5 in acute stroke are correlated with the type and location of stroke but not with the neurological state of patients—preliminary data. *Brain Sciences*. **10**(11), pp.1–11.

Latchaw, R.E., Yonas, H., Hunter, G.J., Yuh, W.T.C., Ueda, T., Sorensen, A.G., Sunshine, J.L., Biller, J., Wechsler, L., Higashida, R. and Hademenos, G. 2003. Guidelines and Recommendations for Perfusion Imaging in Cerebral Ischemia. *Stroke*. **34**(4), pp.1084–1104.

Lebkuechner, I., Wilhelmsson, U., Möllerström, E., Pekna, M. and Pekny, M. 2015. Heterogeneity of Notch signaling in astrocytes and the effects of GFAP and vimentin deficiency. *Journal of Neurochemistry*. **135**(2), pp.234–248.

Ledsam, J. 2021. *Getting started with PMI: Platform for Medical Imaging* [Online]. Leeds. [Accessed 2 June 2021]. Available from: https://sites.google.com/site/plaresmedima/.

Lee, T.K., Kim, Hyunjung, Song, M., Lee, J.C., Park, J.H., Ahn, J.H., Yang, G.E., Kim, Hyeyoung, Ohk, T.G., Shin, M.C., Cho, J.H. and Won, M.H. 2019. Time-course pattern of neuronal loss and gliosis in gerbil hippocampi following mild, severe, or lethal transient global cerebral ischemia. *Neural Regeneration Research*. **14**(8), pp.1394–1403.

León-Moreno, L.C., Castañeda-Arellano, R., Rivas-Carrillo, J.D. and Dueñas-Jiménez, S.H. 2020. Challenges and Improvements of Developing an Ischemia Mouse Model Through Bilateral Common Carotid Artery Occlusion. *Journal of*

Stroke and Cerebrovascular Diseases. **29**(5).

Lever, N.M., Nyström, K. V., Schindler, J.L., Halliday, J., Wira, C. and Funk, M. 2013. Missed Opportunities for Recognition of Ischemic Stroke in the Emergency Department. *Journal of Emergency Nursing*. **39**(5), pp.434–439.

Li, T. and Zhang, S. 2016. Microgliosis in the Injured Brain: Infiltrating Cells and Reactive Microglia Both Play a Role. *Neuroscientist*. **22**(2), pp.165–170.

Li, W., Pan, R., Qi, Z. and Liu, K.J. 2018. Current progress in searching for clinically useful biomarkers of blood–brain barrier damage following cerebral ischemia. *Brain Circulation*. **4**(4), p.145.

Liebner, S., Czupalla, C.J. and Wolburg, H. 2011. Current concepts of blood-brain barrier development. *The International journal of developmental biology*. **55**(4–5), pp.467–476.

Liebner, S., Dijkhuizen, R.M., Reiss, Y., Plate, K.H., Agalliu, D. and Constantin, G. 2018. Functional morphology of the blood–brain barrier in health and disease. *Acta Neuropathologica*. **135**(3), pp.311–336.

Liem, R.K.H. and Messing, A. 2009. Dysfunctions of neuronal and glial intermediate filaments in disease. *Journal of Clinical Investigation*. **119**(7), pp.1814–1824.

Linfante, I., Llinas, R.H., Schlaug, G., Chaves, C., Warach, S. and Caplan, L.R. 2001. Diffusion-Weighted Imaging and National Institutes of Health Stroke Scale in the Acute Phase of Posterior-Circulation Stroke. *Archives of Neurology*. **58**(4), pp.621–628.

Liu, G. and Geng, J. 2018. Glial fibrillary acidic protein as a prognostic marker of acute ischemic stroke. *Human and Experimental Toxicology*. **37**(10), pp.1048–1053.

Liu, J., Jin, X., Liu, K.J. and Liu, W. 2012. Matrix metalloproteinase-2-mediated occludin degradation and caveolin-1-mediated claudin-5 redistribution contribute to blood-brain barrier damage in early ischemic stroke stage. *The Journal of neuroscience : the official journal of the Society for Neuroscience*. **32**(9), pp.3044–3057.

Liu, P., Zhang, R., Liu, D., Wang, J., Yuan, C., Zhao, X., Li, Y., Ji, X., Chi, T. and Zou, L. 2018. Time-course investigation of blood–brain barrier permeability and tight junction protein changes in a rat model of permanent focal ischemia. *Journal of*

Physiological Sciences. **68**(2), pp.121–127.

Liu, W., Hendren, J., Qin, X.J., Shen, J. and Liu, K.J. 2009. Normobaric hyperoxia attenuates early blood-brain barrier disruption by inhibiting MMP-9-mediated occludin degradation in focal cerebral ischemia. *Journal of neurochemistry*. **108**(3), pp.811–820.

Liu, Z. and Chopp, M. 2016. Astrocytes, therapeutic targets for neuroprotection and neurorestoration in ischemic stroke. *Progress in neurobiology*. **144**, pp.103–120.

Lo, E.H., Dalkara, T. and Moskowitz, M.A. 2003. Mechanisms, challenges and opportunities in stroke. *Nature Reviews Neuroscience*. **4**(5), pp.399–414.

Longa, E.Z., Weinstein, P.R., Carlson, S. and Cummins, R. 1989. Reversible middle cerebral artery occlusion without craniectomy in rats. *Stroke*. **20**(1), pp.84–91.

Lövblad, K.O., Baird, A.E., Schlaug, G., Benfield, A., Siewert, B., Voetsch, B., Connor, A., Burzynski, C., Edelman, R.R. and Warach, S. 1997. Ischemic lesion volumes in acute stroke by diffusion-weighted magnetic resonance imaging correlate with clinical outcome. *Annals of neurology*. **42**(2), pp.164–170.

Lu, K., Xu, X., Cui, S., Wang, F., Zhang, B. and Zhao, Y. 2015. Serum neuron specific enolase level as a predictor of prognosis in acute ischemic stroke patients after intravenous thrombolysis. *Journal of the Neurological Sciences*. **359**(1–2), pp.202–206.

De Luca, A., Mariani, M., Riccardi, M.T. and Damiani, G. 2019. The role of the Cincinnati Prehospital Stroke Scale in the emergency department: evidence from a systematic review and meta-analysis.

Luger, S., Jæger, H.S., Dixon, J., Bohmann, F.O., Schaefer, J.H., Richieri, S.P., Larsen, K., Hov, M.R., Bache, K.G. and Foerch, C. 2020. Diagnostic Accuracy of Glial Fibrillary Acidic Protein and Ubiquitin Carboxy-Terminal Hydrolase-L1 Serum Concentrations for Differentiating Acute Intracerebral Hemorrhage from Ischemic Stroke. *Neurocritical care*. **33**(1), pp.39–48.

Luger, S., Witsch, J., Dietz, A., Hamann, G.F., Minnerup, J., Schneider, H., Sitzer, M., Wartenberg, K.E., Niessner, M. and Foerch, C. 2017. Glial Fibrillary Acidic Protein Serum Levels Distinguish between Intracerebral Hemorrhage and Cerebral Ischemia in the Early Phase of Stroke. *Clinical Chemistry*. **63**(1), pp.377–385.

Lutsep, H.L., Albers, G.W., DeCrespigny, A., Kamat, G.N., Marks, M.P. and Moseley, M.E. 1997. Clinical utility of diffusion-weighted magnetic resonance imaging in the assessment of ischemic stroke. *Annals of Neurology*. **41**(5), pp.574–580.

Lv, J., Hu, W., Yang, Z., Li, T., Jiang, S., Ma, Z., Chen, F. and Yang, Y. 2018. Focusing on claudin-5: A promising candidate in the regulation of BBB to treat ischemic stroke. *Progress in Neurobiology*. **161**, pp.79–96.

Ma, Y., Wang, J., Wang, Y. and Yang, G.Y. 2017. The biphasic function of microglia in ischemic stroke. *Progress in Neurobiology*. **157**, pp.247–272.

Maas, M.B. and Furie, K.L. 2009. Molecular biomarkers in stroke diagnosis and prognosis. *Biomarkers in Medicine*. **3**(4), pp.363–383.

Maas, W.J., Lahr, M.M.H., Buskens, E., Van Der Zee, D.J. and Uyttenboogaart, M. 2020. Pathway design for acute stroke care in the era of endovascular thrombectomy: A critical overview of optimization efforts. *Stroke*., pp.3452–3460.

Madsen, T.E., Choo, E.K., Seigel, T.A., Palms, D. and Silver, B. 2015. Lack of gender disparities in emergency department triage of acute stroke patients. *Western Journal of Emergency Medicine*. **16**(1), pp.203–209.

Maegerlein, C., Fischer, J., Mönch, S., Berndt, M., Wunderlich, S., Seifert, C.L., Lehm, M., Boeckh-Behrens, T., Zimmer, C. and Friedrich, B. 2019. Automated Calculation of the Alberta Stroke Program Early CT Score: Feasibility and Reliability. *Radiology*. **291**(1), pp.141–148.

Masuda, T., Croom, D., Hida, H. and Kirov, S.A. 2011. Capillary blood flow around microglial somata determines dynamics of microglial processes in ischemic conditions. *GLIA*. **59**(11), pp.1744–1753.

McColl, B.W., Carswell, H. V., McCulloch, J. and Horsburgh, K. 2004. Extension of cerebral hypoperfusion and ischaemic pathology beyond MCA territory after intraluminal filament occlusion in C57Bl/6J mice. *Brain Research*. **997**(1), pp.15–23.

McColl, B.W., Rothwell, N.J. and Allan, S.M. 2007. Systemic inflammatory stimulus potentiates the acute phase and CXC chemokine responses to experimental stroke and exacerbates brain damage via interleukin-1- and neutrophil-dependent mechanisms. *Journal of Neuroscience*. **27**(16), pp.4403–4412.

Menon, B.K. and Demchuk, A.M. 2011. Computed Tomography Angiography in the Assessment of Patients With Stroke/TIA. *The Neurohospitalist*. **1**(4), pp.187–199.

Mishra, A., Reynolds, J.P., Chen, Y., Gourine, A. V., Rusakov, D.A. and Attwell, D. 2016. Astrocytes mediate neurovascular signaling to capillary pericytes but not to arterioles. *Nature neuroscience*. **19**(12), pp.1619–1627.

Misra, S., Kumar, A., Kumar, P., Yadav, A.K., Mohania, D., Pandit, A.K., Prasad, K. and Vibha, D. 2017. Blood-based protein biomarkers for stroke differentiation: A systematic review. *PROTEOMICS – Clinical Applications*. **11**(9–10), p.1700007.

Missler, U., Wiesmann, M., Friedrich, C. and Kaps, M. 1997. S-100 Protein and Neuron-Specific Enolase Concentrations in Blood as Indicators of Infarction Volume and Prognosis in Acute Ischemic Stroke. *Stroke*. **28**(10), pp.1956–1960.

Mitterhauser, M. and Wadsak, W. 2014. Imaging Biomarkers or Biomarker Imaging? *Pharmaceuticals*. **7**(7), p.765.

Mokin, M., Ansari, S.A., Mctaggart, R.A., Bulsara, K.R., Goyal, M., Chen, M. and Fraser, J.F. 2019. Indications for thrombectomy in acute ischemic stroke from emergent large vessel occlusion (ELVO): report of the SNIS Standards and Guidelines Committee. *J NeuroIntervent Surg*. **11**, pp.215–220.

Mokin, M., Primiani, C.T., Siddiqui, A.H. and Turk, A.S. 2017. ASPECTS (Alberta Stroke Program Early CT Score) Measurement Using Hounsfield Unit Values When Selecting Patients for Stroke Thrombectomy. *Stroke*. **48**(6), pp.1574–1579.

Montaner, J., Mendioroz, M., Ribó, M., Delgado, P., Quintana, M., Penalba, A., Chacón, P., Molina, C., Fernández-Cadenas, I., Rosell, A. and Alvarez-Sabín, J. 2011. A panel of biomarkers including caspase-3 and d-dimer may differentiate acute stroke from stroke-mimicking conditions in the emergency department. *Journal of Internal Medicine*. **270**(2), pp.166–174.

Moon, W.-J., Na, D.G., Ryoo, J.W., Roh, H.G., Byun, H.S., Jeon, Y.H. and Chung, E.C. 2005. Assessment of Tissue Viability Using Diffusion- and Perfusion-Weighted MRI in Hyperacute Stroke. *Korean Journal of Radiology*. **6**(2), p.75.

Moseley, M.E., Cohen, Y., Mintorovitch, J., Chileuitt, L., Shimizu, H., Kucharczyk, J., Wendland, M.F. and Weinstein, P.R. 1990. Early detection of regional cerebral ischemia in cats: Comparison of diffusion- and T2-weighted MRI and

spectroscopy. *Magnetic Resonance in Medicine*. **14**(2), pp.330–346.

MOURÃO, A.M., VICENTE, L.C.C., ABREU, M.N.S., SANT'ANNA, R.V., DE MEIRA, F.C.A., XAVIER, R.M. de B., TANURE, M.T. de A., VIEIRA, E.L.M., DE SOUZA, L.C., MIRANDA, A.S. de, RACHID, M.A. and TEIXEIRA, A.L. 2020. Clinical and molecular correlates of the ASPECTS in the acute phase of stroke. *Arquivos de Neuro-Psiquiatria*. **78**(5), pp.262–268.

Mourik, J.A. van, Leeksma, O.C., Reinders, J.H., de Groot, P.G. and Zandbergen-Spaargaren, J. 1985. Vascular endothelial cells synthesize a plasma membrane protein indistinguishable from the platelet membrane glycoprotein IIa. *The Journal of biological chemistry*. **260**(20), pp.11300–6.

Mu, M., Teng, H., Cho, I.-C., Kao, Y.-H., Chuang, C.-S., Chiu, F.-Y. and Chang, F.-C. 2013. Improvements in the Quantitative Assessment of Cerebral Blood Volume and Flow with the Removal of Vessel Voxels from MR Perfusion Images. *BioMed Research International*. **2013**, p.11.

Müller, N.L. 2002. Computed tomography and magnetic resonance imaging: past, present and future. *European Respiratory Journal*. **19**(35 suppl), pp.3s-12s.

Mullins, M.E., Schaefer, P.W., Sorensen, A.G., Halpern, E.F., Ay, H., He, J., Koroshetz, W.J. and Gonzalez, R.G. 2002. CT and conventional and diffusion-weighted MR imaging in acute stroke: study in 691 patients at presentation to the emergency department. *Radiology*. **224**(2), pp.353–360.

Munich, S.A., Shakir, H.J. and Snyder, K. V. 2016. Role of CT perfusion in acute stroke management. *Cor et Vasa*. **58**(2), pp.e215–e224.

Murakami, K., Kondo, T., Kawase, M. and Chan, P.H. 1998. The development of a new mouse model of global ischemia: Focus on the relationships between ischemia duration, anesthesia, cerebral vasculature, and neuronal injury following global ischemia in mice. *Brain Research*. **780**(2), pp.304–310.

Musuka, T.D., Wilton, S.B., Traboulsi, M. and Hill, M.D. 2015. Diagnosis and management of acute ischemic stroke: speed is critical. *CMAJ : Canadian Medical Association Journal*. **187**(12), p.887.

My-MS.org 2022. MRI - Brain and Spinal Cord Cross-Sections. *My-MS.org*. [Online]. [Accessed 28 June 2022]. Available from: https://my-ms.org/mri_sections.htm.

Nitta, T., Hata, M., Gotoh, S., Seo, Y., Sasaki, H., Hashimoto, N., Furuse, M. and Tsukita, S. 2003. Size-selective loosening of the blood-brain barrier in claudin-5-deficient mice. *Journal of Cell Biology*. **161**(3), pp.653–660.

Nogles, T.E. and Galuska, M.A. 2022. Middle Cerebral Artery Stroke - StatPearls - NCBI Bookshelf *In*: National Library of Medicine. [Accessed 22 June 2022]. Available from: https://www.ncbi.nlm.nih.gov/books/NBK556132/.

Noguchi, K., Ogawa, T., Inugami, A., Fujita, H., Hatazawa, J., Shimosegawa, E., Okudera, T., Uemura, K. and Seto, H. 1997. MRI of acute cerebral infarction: a comparison of FLAIR and T2-weighted fast spin-echo imaging. *Neuroradiology*. **39**(6), pp.406–410.

O'Connell, G.C., Alder, M.L., Smothers, C.G., Still, C.H., Webel, A.R. and Moore, S.M. 2020. Diagnosis of ischemic stroke using circulating levels of brain-specific proteins measured via high-sensitivity digital ELISA. *Brain research*. **1739**, p.146861.

Oh, S.H., Lee, J.G., Na, S.J., Park, J.H., Choi, Y.C. and Kim, W.J. 2003. Prediction of Early Clinical Severity and Extent of Neuronal Damage in Anterior-Circulation Infarction Using the Initial Serum Neuron-Specific Enolase Level. *Archives of Neurology*. **60**(1), pp.37–41.

Ohtsuki, S., Sato, S., Yamaguchi, H., Kamoi, M., Asashima, T. and Terasaki, T. 2007. Exogenous expression of claudin-5 induces barrier properties in cultured rat brain capillary endothelial cells. *Journal of Cellular Physiology*. **210**(1), pp.81–86.

Onatsu, J., Vanninen, R., Jäkälä, P., Mustonen, P., Pulkki, K., Korhonen, M., Hedman, M., Zetterberg, H., Blennow, K., Höglund, K., Herukka, S.K. and Taina, M. 2019. Serum Neurofilament Light Chain Concentration Correlates with Infarct Volume but Not Prognosis in Acute Ischemic Stroke. *Journal of stroke and cerebrovascular diseases : the official journal of National Stroke Association*. **28**(8), pp.2242–2249.

Padroni, M., Bernardoni, A., Tamborino, C., Roversi, G., Borrelli, M., Saletti, A., De Vito, A., Azzini, C., Borgatti, L., Marcello, O., D'Esterre, C., Ceruti, S., Casetta, I., Lee, T.Y. and Fainardi, E. 2016. Cerebral Blood Volume ASPECTS Is the Best Predictor of Clinical Outcome in Acute Ischemic Stroke: A Retrospective, Combined Semi-Quantitative and Quantitative Assessment. *PloS one*. **11**(1).

Pan, R., Yu, K., Weatherwax, T., Zheng, H., Liu, W. and Liu, K.J. 2017. Blood Occludin Level as a Potential Biomarker for Early Blood Brain Barrier Damage Following Ischemic Stroke. *Scientific Reports*. **7**(1), p.40331.

Pandey, A., Shrivastava, A.K. and Saxena, K. 2014. Neuron Specific Enolase and C-reactive Protein Levels in Stroke and Its Subtypes: Correlation with Degree of Disability. *Neurochemical Research 2014 39:8*. **39**(8), pp.1426–1432.

Papa, M., De Luca, C., Petta, F., Alberghina, L. and Cirillo, G. 2014. Astrocyte-neuron interplay in maladaptive plasticity. *Neuroscience and biobehavioral reviews*. **42**, pp.35–54.

Paxinos, G. and Franklin., K.B.J. 2012. *The Mouse Brain in Stereotaxic Coordinates, 4th Edition-Braintree Scientific, Inc* [Online] 4th Editio. [Accessed 23 March 2020]. Available from: https://www.braintreesci.com/prodinfo.asp?number=mous-dlx4.

Peacock, W.F. 2017. Where Are the Stroke Markers? *Clinical Chemistry*. **63**(1), pp.252–254.

Pedersen, A., Stanne, T.M., Nilsson, S., Klasson, S., Rosengren, L., Holmegaard, L., Jood, K., Blennow, K., Zetterberg, H. and Jern, C. 2019. Circulating neurofilament light in ischemic stroke: temporal profile and outcome prediction. *Journal of Neurology*. **266**(11), pp.2796–2806.

Pekna, M. and Pekny, M. 2012. The Neurobiology of Brain Injury. *Cerebrum: the Dana Forum on Brain Science*. **2012**, p.9.

Pekny, M., Eliasson, C., Siushansian, R., Ding, M., Dixon, S.J., Pekna, M., Wilson, J.X. and Hamberger, A. 1999. The impact of genetic removal of GFAP and/or vimentin on glutamine levels and transport of glucose and ascorbate in astrocytes. *Neurochemical Research*. **24**(11), pp.1357–1362.

Pekny, M. and Nilsson, M. 2005. Astrocyte activation and reactive gliosis. *Glia*. **50**(4), pp.427–434.

Petty, M.A. and Wettstein, J.G. 2001. Elements of cerebral microvascular ischaemia. *Brain research. Brain research reviews*. **36**(1), pp.23–34.

Piorntek, J., Winkler, L., Wolburg, H., Müller, S.L., Zuleger, N., Piehl, C., Wiesner, B., Krause, G. and Blasig, I.E. 2008. Formation of tight junction: determinants of homophilic interaction between classic claudins. *The FASEB Journal*. **22**(1),

pp.146–158.

Pitkanen, A., Schwartzkroin, P. and Moshe, S. 2006. *Models of Seizures and Epilepsy*. Elsevier Inc.

PixelMed 2019. How to use DicomCleaner. *PixelMed Publishing*. [Online]. [Accessed 22 October 2019]. Available from: https://www.dclunie.com/pixelmed/software/webstart/DicomCleanerUsage.html.

Powers, W.J., Grubb, R.L. and Raichle, M.E. 1984. Physiological responses to focal cerebral ischemia in humans. *Annals of Neurology*. **16**(5), pp.546–552.

Prakash, R. and Carmichael, S.T. 2015. Blood−brain barrier breakdown and neovascularization processes after stroke and traumatic brain injury. *Current Opinion in Neurology*. **28**(6), pp.556–564.

Proescholdt, M.A., Jacobson, S., Tresser, N., Oldfield, E.H. and Merrill, M.J. 2002. Vascular endothelial growth factor is expressed in multiple sclerosis plaques and can induce inflammatory lesions in experimental allergic encephalomyelitis rats. *Journal of Neuropathology and Experimental Neurology*. **61**(10), pp.914–925.

Puetz, V., I, D., MD, H. and AM, D. 2009. The Alberta Stroke Program Early CT Score in clinical practice: what have we learned? *International journal of stroke : official journal of the International Stroke Society*. **4**(5), pp.354–364.

Puig, B., Brenna, S. and Magnus, T. 2018. Molecular communication of a dying neuron in stroke. *International Journal of Molecular Sciences*. **19**(9).

Purushotham, A., Campbell, B.C. V., Straka, M., Mlynash, M., Olivot, J.-M., Bammer, R., Kemp, S.M., Albers, G.W. and Lansberg, M.G. 2015. Apparent diffusion coefficient threshold for delineation of ischemic core. *International journal of stroke : official journal of the International Stroke Society*. **10**(3), p.348.

Purves, D., Augustine, G.J., Fitzpatrick, D., Katz, L.C., LaMantia, A.-S., McNamara, J.O. and Williams, S.M. 2001. The Blood Supply of the Brain and Spinal Cord.

Puspitasari, V., Yani Gunawan, P., Dwiputra Wiradarma, H. and Hartoyo, V. 2019. Glial Fibrillary Acidic Protein Serum Level as a Predictor of Clinical Outcome in Ischemic Stroke. *Macedonian Journal of Medical Sciences*. **7**(9), p.1471.

Rahmig, J., Akgün, K., Simon, E., Gawlitza, M., Hartmann, C., Siepmann, T., Pallesen,

L.P., Barlinn, J., Puetz, V., Ziemssen, T. and Barlinn, K. 2021. Serum neurofilament light chain levels are associated with stroke severity and functional outcome in patients undergoing endovascular therapy for large vessel occlusion. *Journal of the Neurological Sciences*. **429**, p.118063.

Rao, V.L.R., Bowen, K.K. and Dempsey, R.J. 2001. Transient focal cerebral ischemia down-regulates glutamate transporters GLT-1 and EAAC1 expression in rat brain. *Neurochemical Research*. **26**(5), pp.497–502.

Reith, W., Hasegawa, Y., Latour, L.L., Dardzinski, B.J., Sotak, C.H. and Fisher, M. 1995. Multislice diffusion mapping for 3-D evolution of cerebral ischemia in a rat stroke model. *Neurology*. **45**(1), pp.172–177.

Ren, C., Kobeissy, F., Alawieh, A., Li, Na, Li, Ning, Zibara, K., Zoltewicz, S., Guingab-Cagmat, J., Larner, S.F., Ding, Y., Hayes, R.L., Ji, X. and Mondello, S. 2016. Assessment of Serum UCH-L1 and GFAP in Acute Stroke Patients. *Nature Publishing Group*.

Ren, C., Li, N., Wang, B., Yang, Y., Gao, J., Li, S., Ding, Y., Jin, K. and Ji, X. 2015. Limb ischemic perconditioning attenuates blood-brain barrier disruption by inhibiting activity of MMP-9 and occludin degradation after focal cerebral ischemia. *Aging and Disease*. **6**(6), pp.406–417.

Rostrup, E., Knudsen, G.M., Law, I., Holm, S., Larsson, H.B.W. and Paulson, O.B. 2005. The relationship between cerebral blood flow and volume in humans. *NeuroImage*. **24**(1), pp.1–11.

Roth, C.K., Westbrook, C.; and Talbot, J. 2005. *MRI in Practice* [Online] Third edit. [Accessed 30 December 2020]. Available from: https://www.abebooks.co.uk/servlet/BookDetailsPL?bi=30582444421&searchurl=an%3Dwestbrook%2Bcatherine%2Bkaut%2Broth%2Bcarolyn%26sortby%3D17&cm_sp=snippet-_-srp1-_-title1.

Roth, J.M. 2011. Recombinant tissue plasminogen activator for the treatment of acute ischemic stroke. *Proceedings (Baylor University. Medical Center)*. **24**(3), p.257.

Roth, M., Gaceb, A., Enström, A., Padel, T., Genové, G., Özen, I. and Paul, G. 2019. Regulator of G-protein signaling 5 regulates the shift from perivascular to parenchymal pericytes in the chronic phase after stroke. *FASEB Journal*. **33**(8),

pp.8990–8998.

Rousselet, E., Kriz, J. and Seidah, N.G. 2012. Mouse model of intraluminal MCAO: cerebral infarct evaluation by cresyl violet staining. *Journal of visualized experiments : JoVE*. (69).

Saenger, A.K. and Christenson, R.H. 2010. Stroke Biomarkers: Progress and Challenges for Diagnosis, Prognosis, Differentiation, and Treatment. *Clinical Chemistry*. **56**(1), pp.21–33.

Sandelius, Å., Zetterberg, H., Blennow, K., Adiutori, R., Malaspina, A., Laura, M., Reilly, M.M. and Rossor, A.M. 2018. Plasma neurofilament light chain concentration in the inherited peripheral neuropathies. *Neurology*. **90**(6), pp.518–524.

Sandercock, P., Wardlaw, J.M., Lindley, R.I., Dennis, M., Cohen, G., Murray, G., Innes, K., Venables, G., Czlonkowska, A., Kobayashi, A., Ricci, S., Murray, V., Berge, E., Slot, K.B., Hankey, G.J., Correia, M., Peeters, A., Matz, K., Lyrer, P., Gubitz, G., Phillips, S.J., Arauz, A., Baigent, C., Chadwick, D., Tyrrell, P., Lowe, G., Collins, R., Bath, P., Van Gijn, J., Gray, R., Hart, R., Yusuf, S., Clark, A., Perry, D., Soosay, V., Buchanan, D., Grant, S., Sakka, E., Drever, J., Walker, P., Herath, I., Brown, A.L., Chmielnik, P., Armit, C., Walton, A., Hautvast, M., Lewis, S., Heron, G., Odusanya, S., Linksted, P., Kane, I., Whiteley, W., Sellar, R., White, P., Keston, P., Farrell, A., Morris, Z., Miranda, H. and Blackwell, L. 2012. The benefits and harms of intravenous thrombolysis with recombinant tissue plasminogen activator within 6 h of acute ischaemic stroke (the third international stroke trial [IST-3]): a randomised controlled trial. *Lancet (London, England)*. **379**(9834), pp.2352–2363.

Saver, J.L., Fonarow, G.C., Smith, E.E., Reeves, M.J., Grau-Sepulveda, M. V., Pan, W., Olson, D.W.M., Hernandez, A.F., Peterson, E.D. and Schwamm, L.H. 2013. Time to Treatment With Intravenous Tissue Plasminogen Activator and Outcome From Acute Ischemic Stroke. *JAMA*. **309**(23), pp.2480–2488.

Saver, J.L., Jahan, R., Levy, E.I., Jovin, T.G., Baxter, B., Nogueira, R.G., Clark, W., Budzik, R. and Zaidat, O.O. 2012. Solitaire flow restoration device versus the Merci Retriever in patients with acute ischaemic stroke (SWIFT): A randomised, parallel-group, non-inferiority trial. *The Lancet*. **380**(9849), pp.1241–1249.

Sawada, H., Udaka, F., Seriu, N., Shindou, K., Kameyama, M. and Tsujimura, M. 1990. MRI demonstration of cortical laminar necrosis and delayed white matter injury in anoxic encephalopathy. *Neuroradiology 1990 32:4*. **32**(4), pp.319–321.

Schaefer, P.W., Copen, W.A., Lev, M.H. and Gonzalez, R.G. 2006. Diffusion-Weighted Imaging in Acute Stroke. *Magnetic Resonance Imaging Clinics of North America*. **14**(2), pp.141–168.

Schaefer, P.W., Grant, P.E. and Gonzalez, R.G. 2000. Diffusion-weighted MR imaging of the brain. *Radiology*. **217**(2), pp.331–345.

Schiff, L., Hadker, N., Weiser, S. and Rausch, C. 2012. A Literature Review of the Feasibility of Glial Fibrillary Acidic Protein as a Biomarker for Stroke and Traumatic Brain Injury. *Molecular Diagnosis & Therapy*. **16**(2), pp.79–92.

Schmidt-Kastner, R., Wietasch, K., Weigel, H. and Eysel, U.T. 1993. Immunohistochemical staining for glial fibrillary acidic protein (GFAP) after deafferentation or ischemic infarction in rat visual system: Features of reactive and damaged astrocytes. *International Journal of Developmental Neuroscience*. **11**(2), pp.157–174.

Schober, P., Boer, C. and Schwarte, L.A. 2018. Correlation coefficients: Appropriate use and interpretation. *Anesthesia and Analgesia*. **126**(5), pp.1763–1768.

Schumann, P., Touzani, O., Young, A.R., Baron, J.C., Morello, R. and MacKenzie, E.T. 1998. Evaluation of the ratio of cerebral blood flow to cerebral blood volume as an index of local cerebral perfusion pressure. *Brain*. **121**(7), pp.1369–1379.

van Seeters, T., Biessels, G.J., Kappelle, L.J., van der Schaaf, I.C., Dankbaar, J.W., Horsch, A.D., Niesten, J.M., Luitse, M.J., Majoie, C.B., Vos, J.A., Schonewille, W.J., van Walderveen, M.A., Wermer, M.J., Duijm, L.E., Keizer, K., Bot, J.C., Visser, M.C., van der Lugt, A., Dippel, D.W., Kesselring, F.O., Hofmeijer, J., Lycklama à Nijeholt, G.J., Boiten, J., van Rooij, W.J., de Kort, P.L., Roos, Y.B., van Dijk, E.J., Pleiter, C.C., Mali, W.P., van der Graaf, Y. and Velthuis, B.K. 2015. The Prognostic Value of CT Angiography and CT Perfusion in Acute Ischemic Stroke. *Cerebrovascular Diseases*. **40**(5–6), pp.258–269.

Shaikh, Z., Torres, A. and Takeoka, M. 2019. Neuroimaging in pediatric epilepsy. *Brain Sciences*. **9**(8), pp.1–13.

Shen, J.M., Xia, X.W., Kang, W.G., Yuan, J.J. and Sheng, L. 2011. The use of MRI apparent diffusion coefficient (ADC) in monitoring the development of brain infarction. *BMC Medical Imaging*. **11**, p.2.

Shi, S., Qi, Z., Ma, Q., Pan, R., Timmins, G.S., Zhao, Y., Shi, W., Zhang, Y., Ji, X. and Liu, K.J. 2017. Normobaric Hyperoxia Reduces Blood Occludin Fragments in Rats and Patients With Acute Ischemic Stroke. *Stroke*. **48**(10), pp.2848–2854.

Siemonsen, S., Löbel, U., Sedlacik, J., Forkert, N.D., Mouridsen, K., Østergaard, L., Thomalla, G. and Fiehler, J. 2012. Elevated T2-values in MRI of stroke patients shortly after symptom onset do not predict irreversible tissue infarction. *Brain*. **135**(6), pp.1981–1989.

Silver, J. and Miller, J.H. 2004. Regeneration beyond the glial scar. *Nature Reviews Neuroscience*. **5**(2), pp.146–156.

Singh, H.V., Pandey, A., Shrivastava, A.K., Raizada, A., Singh, S.K. and Singh, N. 2013. Prognostic value of neuron specific enolase and IL-10 in ischemic stroke and its correlation with degree of neurological deficit. *Clinica Chimica Acta*. **419**, pp.136–138.

Sofroniew, M. V. 2009. Molecular dissection of reactive astrogliosis and glial scar formation. *Trends in Neurosciences*. **32**(12), pp.638–647.

Sofroniew, M. V. and Vinters, H. V. 2010. Astrocytes: Biology and pathology. *Acta Neuropathologica*. **119**(1), pp.7–35.

Soinne, L., Helenius, J., Saimanen, E., Salonen, O., Lindsberg, P.J., Kaste, M. and Tatlisumak, T. 2003. Brain diffusion changes in carotid occlusive disease treated with endarterectomy. *Neurology*. **61**(8), pp.1061–1065.

Soria, G., Tudela, R., Márquez-Martín, A., Camón, L., Batalle, D., Muñoz-Moreno, E., Eixarch, E., Puig, J., Pedraza, S., Vila, E., Prats-Galino, A. and Planas, A.M. 2013. The Ins and Outs of the BCCAo Model for Chronic Hypoperfusion: A Multimodal and Longitudinal MRI Approach. *PLoS ONE*. **8**(9).

Sotelo-Orozco, J., Chen, S.Y., Hertz-Picciotto, I. and Slupsky, C.M. 2021. A Comparison of Serum and Plasma Blood Collection Tubes for the Integration of Epidemiological and Metabolomics Data. *Frontiers in Molecular Biosciences*. **8**, p.650.

Sourbron, S., Ingrisch, M., Siefert, A., Reiser, M. and Herrmann, K. 2009. Quantification of cerebral blood flow, cerebral blood volume, and blood-brain-barrier leakage with DCE-MRI. *Magnetic Resonance in Medicine*. **62**(1), pp.205–217.

Speetzen, L.J., Endres, M. and Kunz, A. 2013. Bilateral common carotid artery occlusion as an adequate preconditioning stimulus to induce early ischemic tolerance to focal cerebral ischemia. *Journal of visualized experiments : JoVE*. (75).

Srinivasan, A., Goyal, M., Al Azri, F. and Lum, C. 2006. State-of-the-art imaging of acute stroke. *Radiographics : a review publication of the Radiological Society of North America, Inc*. **26 Suppl 1**(SPEC. ISS.).

Stallcup, W.B. 2002. The NG2 proteoglycan: Past insights and future prospects. *Journal of Neurocytology*. **31**(6/7), pp.423–435.

Stockinger, H., Gadd, S.J., Eher, R., Majdic, O., Schreiber, W., Kasinrerk, W., Strass, B., Schnabl, E. and Knapp, W. 1990. Molecular characterization and functional analysis of the leukocyte surface protein CD31. *Journal of immunology (Baltimore, Md. : 1950)*. **145**(11), pp.3889–97.

Stroke Association 2020. Haemorrhagic stroke | Brain Haemorrhage | Stroke Association. [Accessed 22 November 2020]. Available from: https://www.stroke.org.uk/what-is-stroke/types-of-stroke/haemorrhagic-stroke.

Stroke Association 2018. *State of the Nation Stroke Statistics*.

Stys, P.K., Ransom, B.R., Waxman, S.G. and Davis, P.K. 1990. Role of extracellular calcium in anoxic injury of mammalian central white matter. *Proceedings of the National Academy of Sciences*. **87**(11), pp.4212–4216.

Sui, H.J., Yan, C.G., Zhao, Z.G. and Bai, Q.K. 2016. Prognostic Value of Diffusion-Weighted Imaging (DWI) Apparent Diffusion Coefficient (ADC) in Patients with Hyperacute Cerebral Infarction Receiving rt-PA Intravenous Thrombolytic Therapy. *Medical Science Monitor : International Medical Journal of Experimental and Clinical Research*. **22**, p.4438.

Svetlov, S.I., Prima, V., Kirk, D.R., Gutierrez, H., Curley, K.C., Hayes, R.L. and Wang, K.K.W. 2010. Morphologic and biochemical characterization of brain injury in a

model of controlled blast overpressure exposure. *Journal of Trauma - Injury, Infection and Critical Care*. **69**(4), pp.795–804.

Sweeney, M.D., Zhao, Z., Montagne, A., Nelson, A.R. and Zlokovic, B. V. 2019. Blood-Brain Barrier: From Physiology to Disease and Back. *Physiological reviews*. **99**(1), pp.21–78.

Takizawa, S., Hogan, M. and Hakim, A.M. 1991. The effects of a competitive NMDA receptor antagonist (CGS-19755) on cerebral blood flow and pH in focal ischemia. *Journal of cerebral blood flow and metabolism : official journal of the International Society of Cerebral Blood Flow and Metabolism*. **11**(5), pp.786–93.

Tamura, A., Graham, D.I., McCulloch, J. and Teasdale, G.M. 1981. Focal cerebral ischaemia in the rat: I. Description of technique and early neuropathological consequences following middle cerebral artery occlusion. *Journal of Cerebral Blood Flow and Metabolism*. **1**(1), pp.53–60.

Tatlisumak, T. 2002. Is CT or MRI the method of choice for imaging patients with acute stroke? Why should men divide if fate has united? *Stroke*. **33**(9), pp.2144–2145.

Tenny, S. and Thorell, W. 2022. Intracranial Hemorrhage *In*: *Volpe's Neurology of the Newborn* [Online]. StatPearls Publishing, pp.593-622.e7. [Accessed 22 December 2022]. Available from: https://www.ncbi.nlm.nih.gov/books/NBK470242/.

The Leeds Teaching Hospitals 2022. Radioligy Departments and Services. *The Leeds Teaching Hospitals*. [Online], https://www.leedsth.nhs.uk/a-z-of-services/radiolo. [Accessed 21 October 2019]. Available from: https://www.leedsth.nhs.uk/a-z-of-services/radiology/radiology-departments/.

The Mouse brain Library 2003. The Mouse Brain Library - Search the library. [Accessed 7 July 2021]. Available from: http://www.mbl.org/.

Tiedt, S., Duering, M., Barro, C., Boeck, A.G.J., Bode, F.J., Klein, M., Dorn, F., Gesierich, B., Kellert, L., Ertl-Wagner, B., Goertler, M.W., Petzold, G.C., Kuhle, J., Wollenweber, F.A., Peters, N. and Dichgans, M. 2018. Serum neurofilament light: A biomarker of neuroaxonal injury after ischemic stroke. *Neurology*. **91**(14), pp.E1338–E1347.

Tofts, P.S. 2010. T1-weighted DCE Imaging Modelling, Acquisition and Analysis.

Tomandl, B.F., Klotz, E., Handschu, R., Stemper, B., Reinhardt, F., Huk, W.J., Eberhardt, K.E. and Fateh-Moghadam, S. 2003. Comprehensive imaging of ischemic stroke with multisection CT. *Radiographics : a review publication of the Radiological Society of North America, Inc*. **23**(3), pp.565–592.

Tong, D.C., Yenari, M.A., Albers, G.W., O'Brien, M., Marks, M.P. and Moseley, M.E. 1998. Correlation of perfusion- and diffusion-weighted MRI with NIHSS score in acute (. *Neurology*. **50**(4), pp.864–870.

Tong, E., Hou, Q., Fiebach, J.B. and Wintermark, M. 2014. The role of imaging in acute ischemic stroke. *Neurosurgical Focus*. **36**(1).

Tsalafoutas, I.A. and Koukourakis, G. V 2010. Patient dose considerations in computed tomography examinations. *World Journal of Radiology*. **2**(7), p.262.

Uphaus, T., Bittner, S., Gröschel, S., Steffen, F., Muthuraman, M., Wasser, K., Weber-Krüger, M., Zipp, F., Wachter, R. and Gröschel, K. 2019. NfL (Neurofilament Light Chain) Levels as a Predictive Marker for Long-Term Outcome After Ischemic Stroke. *Stroke*. **50**(11), pp.3077–3084.

Vilela, P. 2017. Acute stroke differential diagnosis: Stroke mimics. *European Journal of Radiology*. **96**, pp.133–144.

Vos, P.E., Van Gils, M., Beems, T., Zimmerman, C. and Verbeek, M.M. 2006. Increased GFAP and S100β but not NSE serum levels after subarachnoid haemorrhage are associated with clinical severity. *European Journal of Neurology*. **13**(6), pp.632–638.

Vos, P.E., Jacobs, B., Andriessen, T.M.J.C., Lamers, K.J.B., Borm, G.F., Beems, T., Edwards, M., Rosmalen, C.F. and Vissers, J.L.M. 2010. GFAP and S100B are biomarkers of traumatic brain injury: an observational cohort study. *Neurology*. **75**(20), pp.1786–1793.

Vu, D., González, R.G. and Schaefer, P.W. 2006. Conventional MRI and MR Angiography of Stroke *In*: *Acute Ischemic Stroke* [Online]. Berlin/Heidelberg: Springer-Verlag, pp.115–137. [Accessed 21 October 2019]. Available from: http://link.springer.com/10.1007/3-540-30810-5_6.

Vymazal, J., Rulseh, A.M., Keller, J. and Janouskova, L. 2012. Comparison of CT and MR imaging in ischemic stroke. *Insights into Imaging*. **3**(6), pp.619–627.

Wahul, A.B., Joshi, P.C., Kumar, A. and Chakravarty, S. 2018. Transient global cerebral ischemia differentially affects cortex, striatum and hippocampus in Bilateral Common Carotid Arterial occlusion (BCCAo) mouse model. *Journal of chemical neuroanatomy*. **92**, pp.1–15.

Wang, H., Song, G., Chuang, H., Chiu, C., Abdelmaksoud, A., Ye, Y. and Zhao, L. 2018. Portrait of glial scar in neurological diseases. *International Journal of Immunopathology and Pharmacology*. **31**, pp.1–6.

Wang, Y., Peng, F., Xie, G., Chen, Z.Q., Li, H.G., Tang, T. and Luo, J.K. 2016. Rhubarb attenuates blood-brain barrier disruption via increased zonula occludens-1 expression in a rat model of intracerebral hemorrhage. *Experimental and Therapeutic Medicine*. **12**(1), pp.250–256.

Wang, Z., Wang, R., Li, Y., Li, M., Zhang, Y., Jiang, L., Fan, J., Wang, Q. and Yang, D. 2021. Plasma Neurofilament Light Chain as a Predictive Biomarker for Post-stroke Cognitive Impairment: A Prospective Cohort Study. *Frontiers in Aging Neuroscience*. **0**, p.41.

Weber, R.A., Chan, C.H., Nie, X., Maggioncalda, E., Valiulis, G., Lauer, A., Hui, E.S., Jensen, J.H. and Adkins, D.A.L. 2017. Sensitivity of diffusion MRI to perilesional reactive astrogliosis in focal ischemia. *NMR in Biomedicine*. **30**(7).

Whiteley, W., Tseng, M.C. and Sandercock, P. 2008. Blood biomarkers in the diagnosis of ischemic stroke: A systematic review. *Stroke*. **39**(10), pp.2902–2909.

Whiteley, W.N., Emberson, J., Lees, K.R., Blackwell, L., Albers, G., Bluhmki, E., Brott, T., Cohen, G., Davis, S., Donnan, G., Grotta, J., Howard, G., Kaste, M., Koga, M., von Kummer, R., Lansberg, M.G., Lindley, R.I., Lyden, P., Olivot, J.M., Parsons, M., Toni, D., Toyoda, K., Wahlgren, N., Wardlaw, J., del Zoppo, G.J., Sandercock, P., Hacke, W. and Baigent, C. 2016. Risk of intracerebral haemorrhage with alteplase after acute ischaemic stroke: a secondary analysis of an individual patient data meta-analysis. *The Lancet Neurology*. **15**(9), pp.925–933.

Williams, R.W. and Rakic, P. 1988. Three-dimensional counting: An accurate and direct method to estimate numbers of cells in sectioned material. *The Journal of Comparative Neurology*. **278**(3), pp.344–352.

Winkler, E.A., Sengillo, J.D., Bell, R.D., Wang, J. and Zlokovic, B. V. 2012. Blood-

spinal cord barrier pericyte reductions contribute to increased capillary permeability. *Journal of Cerebral Blood Flow and Metabolism*. **32**(10), pp.1841–1852.

Wintermark, M., Flanders, A.E., Velthuis, B., Meuli, R., van Leeuwen, M., Goldsher, D., Pineda, C., Serena, J., van der Schaaf, I., Waaijer, A., Anderson, J., Nesbit, G., Gabriely, I., Medina, V., Quiles, A., Pohlman, S., Quist, M., Schnyder, P., Bogousslavsky, J., Dillon, W.P. and Pedraza, S. 2006. Perfusion-CT assessment of infarct core and penumbra: receiver operating characteristic curve analysis in 130 patients suspected of acute hemispheric stroke. *Stroke*. **37**(4), pp.979–85.

Wouters, A., Nysten, C., Thijs, V. and Lemmens, R. 2018. Prediction of outcome in patients with acute ischemic stroke based on initial severity and improvement in the first 24 h. *Frontiers in Neurology*. **9**(MAY), p.308.

Wunderlich, Michael T., Lins, H., Skalej, M., Wallesch, C.W. and Goertler, M. 2006. Neuron-specific enolase and tau protein as neurobiochemical markers of neuronal damage are related to early clinical course and long-term outcome in acute ischemic stroke. *Clinical Neurology and Neurosurgery*. **108**(6), pp.558–563.

Wunderlich, M.T., Wallesch, C.-W. and Goertler, M. 2004. Release of neurobiochemical markers of brain damage is related to the neurovascular status on admission and the site of arterial occlusion in acute ischemic stroke. *Journal of the Neurological Sciences*. **227**(1), pp.49–53.

Wunderlich, M. T., Wallesch, C.W. and Goertler, M. 2006. Release of glial fibrillary acidic protein is related to the neurovascular status in acute ischemic stroke. *European Journal of Neurology*. **13**(10), pp.1118–1123.

Xiong, L., Yang, Y., Zhang, M. and Xu, W. 2015. The use of serum glial fibrillary acidic protein test as a promising tool for intracerebral hemorrhage diagnosis in Chinese patients and prediction of the short-term functional outcomes. *Neurological sciences : official journal of the Italian Neurological Society and of the Italian Society of Clinical Neurophysiology*. **36**(11), pp.2081–2087.

Xu, S., Wang, L. and Zhao, L. 2019. Clinical application value of brain CT perfusion imaging in the treatment of acute ischemic stroke thrombolytic therapy. *Experimental and Therapeutic Medicine*.

Yaghi, S., Herber, C., Boehme, A.K., Andrews, H., Willey, J.Z., Rostanski, S.K., Siket, M., Jayaraman, M. V., McTaggart, R.A., Furie, K.L., Marshall, R.S., Lazar, R.M. and Boden-Albala, B. 2017. The Association between Diffusion MRI-Defined Infarct Volume and NIHSS Score in Patients with Minor Acute Stroke. *Journal of neuroimaging : official journal of the American Society of Neuroimaging*. **27**(4), p.388.

Yang, G., Kitagawa, K., Matsushita, K., Mabuchi, T., Yagita, Y., Yanagihara, T. and Matsumoto, M. 1997. C57BL/6 strain is most susceptible to cerebral ischemia following bilateral common carotid occlusion among seven mouse strains: Selective neuronal death in the murine transient forebrain ischemia. *Brain Research*. **752**(1–2), pp.209–218.

Yang, Q., Tress, B.M., Barber, P.A., Desmond, P.M., Darby, D.G., Gerraty, R.P., Li, T. and Davis, S.M. 1999. Serial study of apparent diffusion coefficient and anisotropy in patients with acute stroke. *Stroke*. **30**(11), pp.2382–2390.

Yang, Y., Estrada, E.Y., Thompson, J.F., Liu, W. and Rosenberg, G.A. 2007. Matrix metalloproteinase-mediated disruption of tight junction proteins in cerebral vessels is reversed by synthetic matrix metalloproteinase inhibitor in focal ischemia in rat. *Journal of Cerebral Blood Flow and Metabolism*. **27**(4), pp.697–709.

Yang, Y. and Rosenberg, G.A. 2011. MMP-mediated disruption of claudin-5 in the blood-brain barrier of rat brain after cerebral ischemia. *Methods in Molecular Biology*. **762**, pp.333–345.

Yew, K.S. and Cheng, E. 2009. Acute Stroke Diagnosis. *American family physician*. **80**(1), p.33.

Yu, Y., Han, Q., Ding, X., Chen, Q., Ye, K., Zhang, S., Yan, S., Campbell, B.C.V., Parsons, M.W., Wang, S. and Lou, M. 2016. Defining Core and Penumbra in Ischemic Stroke: A Voxel- and Volume-Based Analysis of Whole Brain CT Perfusion. *Scientific Reports*. **6**.

Yuan, S., Liu, K. and Qi, Z. 2020. Occludin regulation of blood–brain barrier and potential therapeutic target in ischemic stroke. *Brain Circulation*. **6**(3), p.152.

Zaheer, S., Rizvi, I., Islam, N., Ullah, E., Beg, M. and Akhtar, N. 2013. Correlation

between serum neuron specific enolase and functional neurological outcome in patients of acute ischemic stroke. *Annals of Indian Academy of Neurology*. **16**(4), p.504.

Zaitsev, M., Maclaren, J. and Herbst, M. 2015. Motion Artefacts in MRI: a Complex Problem with Many Partial Solutions. *Journal of magnetic resonance imaging : JMRI*. **42**(4), p.887.

Zamanian, J.L., Xu, L., Foo, L.C., Nouri, N., Zhou, L., Giffard, R.G. and Barres, B.A. 2012. Genomic Analysis of Reactive Astrogliosis. *The Journal of Neuroscience*. **32**(18), p.6391.

Zhang, S. 2019. Microglial activation after ischaemic stroke. *Stroke and Vascular Neurology*. **4**(2), pp.71–74.

Zhang, W., Zhu, L., An, C., Wang, R., Yang, L., Yu, W., Li, P. and Gao, Y. 2020. The blood brain barrier in cerebral ischemic injury – Disruption and repair. *Brain Hemorrhages*. **1**(1), pp.34–53.

Zhao, B., Yin, Q., Fei, Y., Zhu, J., Qiu, Y., Fang, W. and Li, Y. 2020. Research progress of mechanisms for tight junction damage on blood–brain barrier inflammation. *https://doi.org/10.1080/13813455.2020.1784952*.

Zheng, Y.-S., Sun, C., Wang, R., Chen, N., Luo, S.-S., Xi, J.-Y., Lu, J.-H., Zhao, C.-B., Li, Y.-X., Zhou, L. and Lin, J. 2021. Neurofilament light is a novel biomarker for mitochondrial encephalomyopathy, lactic acidosis, and stroke-like episodes. *Scientific Reports 2021 11:1*. **11**(1), pp.1–7.

Zhu, Z., Zhang, R., Ren, K., Cong, R., Zhu, X., Zhu, L. and Wang, T. 2021. The prognosis prediction significance of Hounsfield unit value for stroke patients treated by intravenous thrombolysis. *BMC Medical Imaging*. **21**(1), pp.1–9.

Zlokovic, B. V. 2008. The Blood-Brain Barrier in Health and Chronic Neurodegenerative Disorders. *Neuron*. **57**(2), pp.178–201.

Chapter 7 Appendices

UNIVERSITY OF LEEDS

NHS
The Leeds Teaching Hospitals
NHS Trust

A study of Stroke Diagnosis and Prognosis to improve outcomes

PARTICIPANT CONSENT FORM

Version 2.1: Date: 20/10/2021 IRAS Reference No: 50831

Participant Number:

Please initial every box if you agree

1. I confirm that I have read and understood the patient information sheet (Version 2.1 dated 20/10/2021) for the above study including potential risks of additional tests. ☐

2. I have had the opportunity to ask questions and I have had any questions answered satisfactorily. ☐

3. I understand that my participation is voluntary and that I am free to withdraw at any time without giving any reason and that this will not affect my treatment. ☐

4. I understand that any data I provide, will be confidential and my anonymity will be preserved in any reports or publications arising from the study, sharing data with other researchers, new research, educational activity, or commercial purposes. ☐

5. I understand that relevant sections of my healthcare electronic medical records will be accessed by the researchers to record clinical data. I give permission for access to my records for this purpose. ☐

6. I agree to my GP being informed on my participation in the study and a referral being made in the event of any incidental findings arising in the course of this study that require further investigation. ☐

7. I understand the research team will keep a copy of my consent form. ☐

8. I understand that should I lose the capacity to consent during the course of the study, that data and samples collected up to that point will continue to be used in the research and routinely collected outcome data also will be used. ☐

9. I understand that I **may** undergo an additional MRI of brain and legs for research purposes at zero and 3 months, and this will involve the injection of a dye. MRI scans are optional. ☐

10. I agree that my blood samples collected for the study are stored at the University of Leeds in anonymised form and under secure conditions, for 25 years after study finishes. ☐

11. I agree to take part in the above study. ☐

12. I agree to my contact details being kept for future research. ☐

UNIVERSITY OF LEEDS

NHS
The Leeds Teaching Hospitals

Name: **Date**

Signature

Researcher's name: **Date**

Signature

When completed: 1(original) to be kept in care record, 1 copy for the patient, 1 for researcher site file

SOPs for CT perfusion parameters using PMI program

standard operating procedure

PMI is a program used to view and analysis any radiological images. PMI runs only on windows operating system. It is the program that used to do CTP images post-processing in this thesis.

To do the post-processing operation:

1- It is important to ensure that all the patient's information has been wiped and anonymized for patients' privacy.
2- After opening the PMI program, create a new study (study > new) and give it a name such as: image analyzed
3- Import data (Serious > import > DICOM) "import from the top folder of the original patient study images.
4- Select the serious and sort the image by: (Slice location + image number)

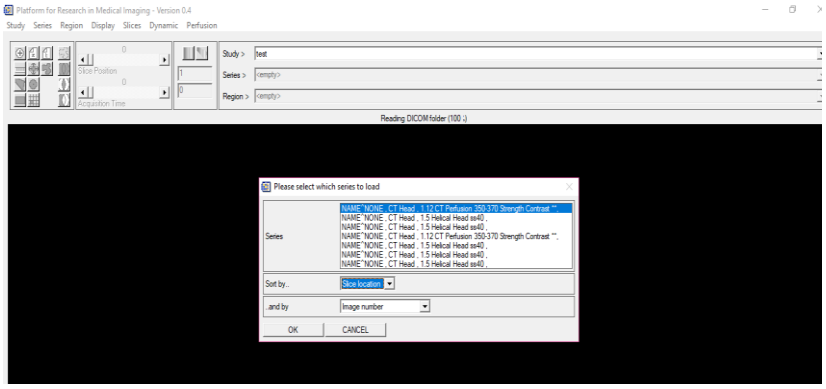

5- Try to move between the seriouses and check if any artifacts or head motion are visible.
6- If there are any interrupted or shifted slices which may affect the analysis results, try to extract them. (Serious > extract > enter the beginning slice number and the end slice number)
7- Before start doing the perfusion analysis, time resolution needs to be edited (Serious > edit > time resolution) enter start of measurements(sec)=0 while the temporal resolution (sec)=1.

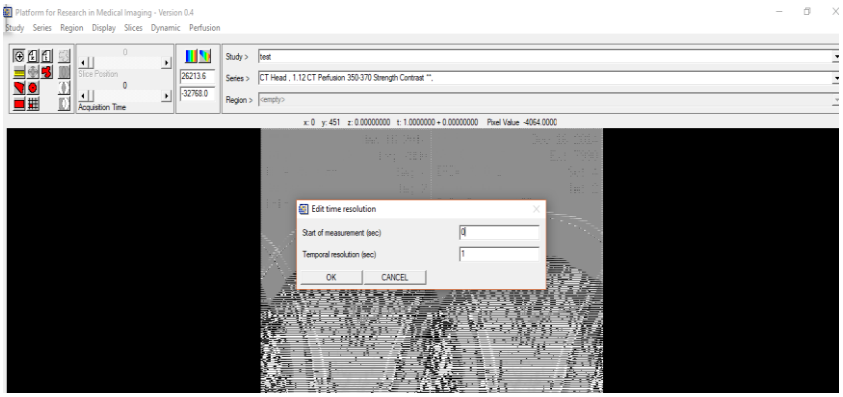

8- Select the CT perfusion serious and view the serious in 1D + 2D (Display > 1D +2D) to view the wash in- wash out curve. By put the crosser on the MCA or ACA and track the time when the contrast arrives.

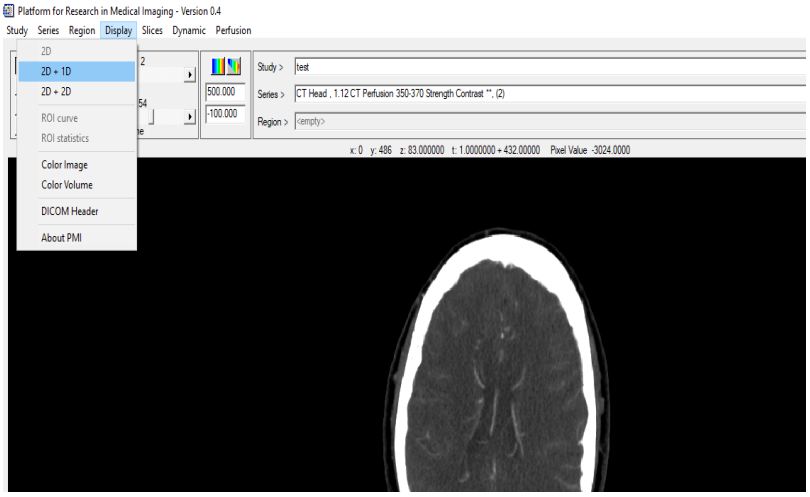

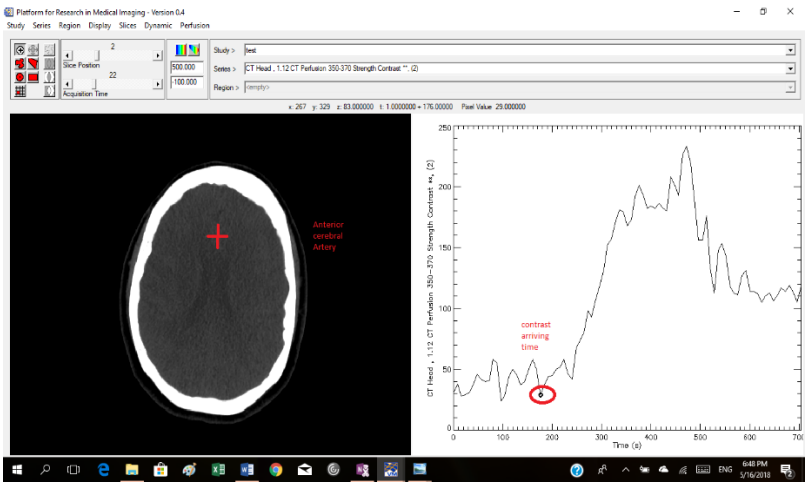

9- From the main bar go (perfusion > semi-quantitive (pixels) and enter the arriving contrast time in the (Length of baseline) (# of dynamics) as shown in the screen shots.

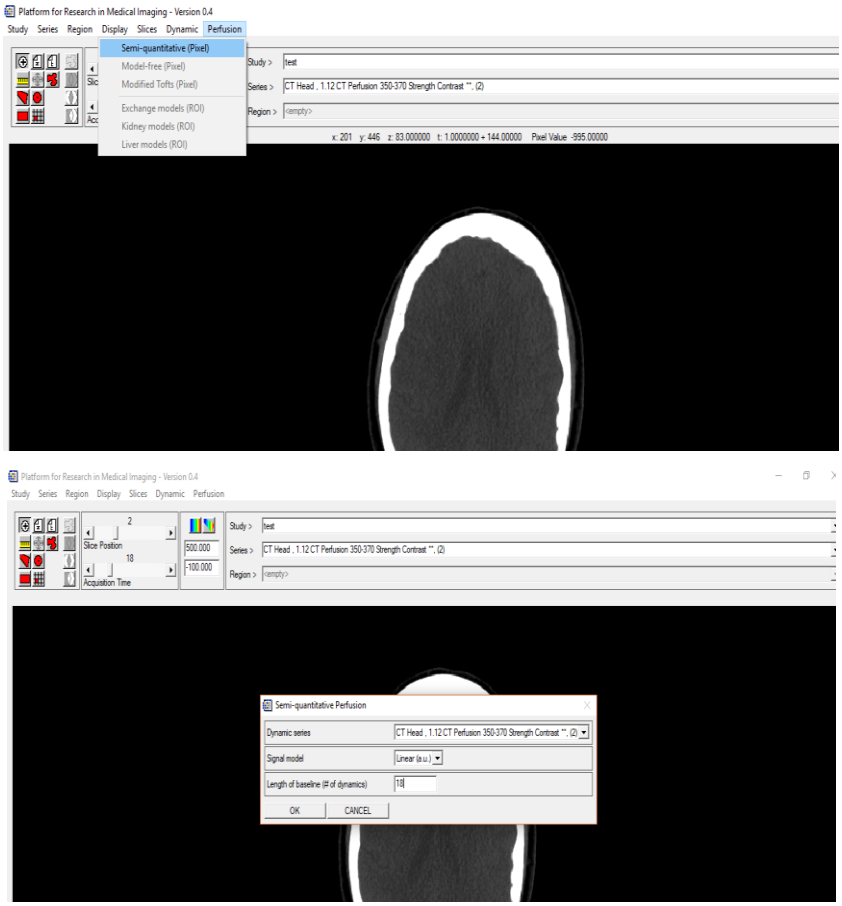

10-Three maps are generated:

_ Maximum (a.u) which shows the maximum signal change image

_ Area Under the Curve (a.u)

_ Area: Maximum (sec)

11-Open the Maximum (a.u) image and define either the ACA or MCA, go (Region > threshold) in order to define arterial input function (AIF) as shown in the screen shots.

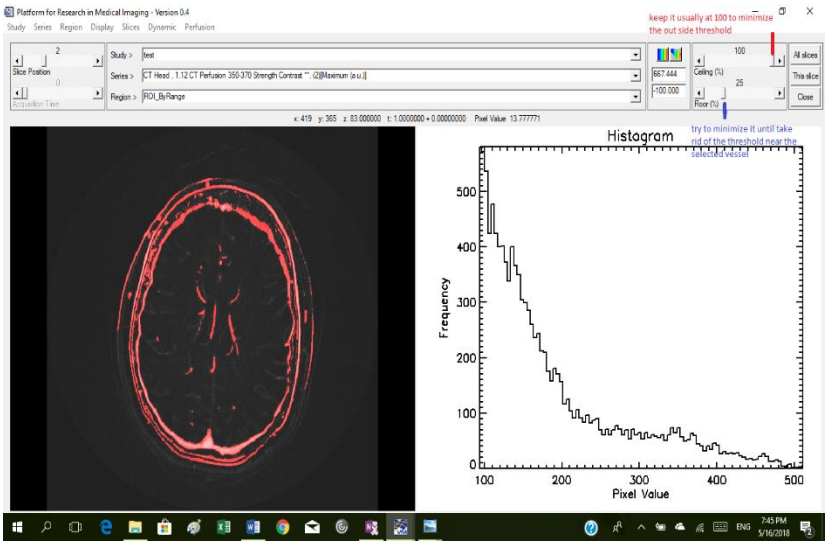

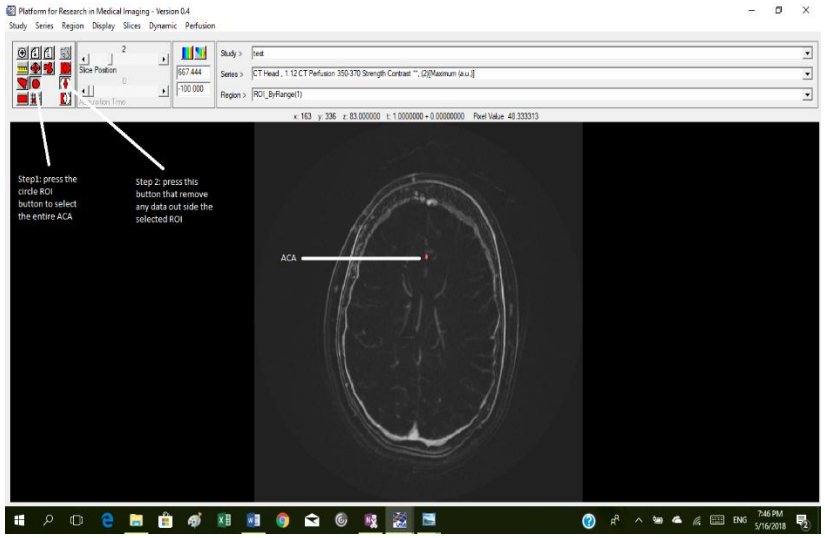

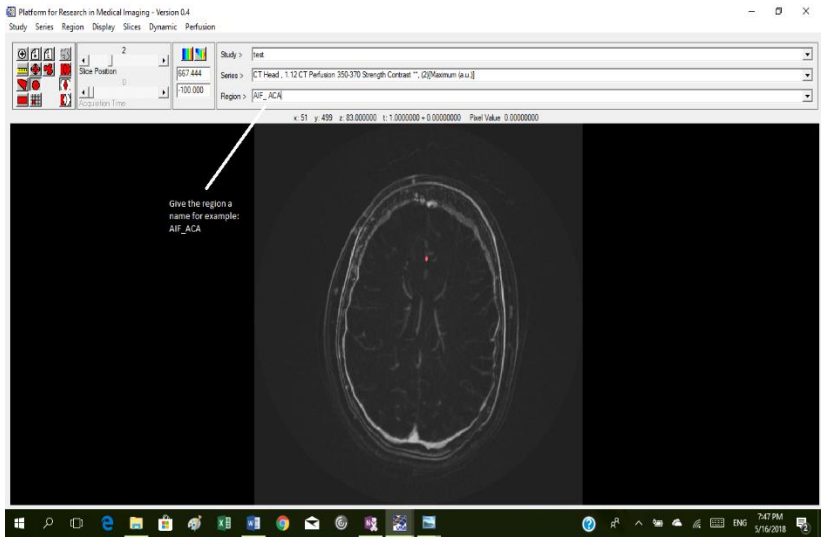

12-To generate the three perfusion maps:

_Plasma flow (ml/100ml/min)

_Extracellular volume (ml/100ml)

_Extracellular MTT (sec)

Go (perfusion > model free (pixel)) and follow the screenshot instructions.

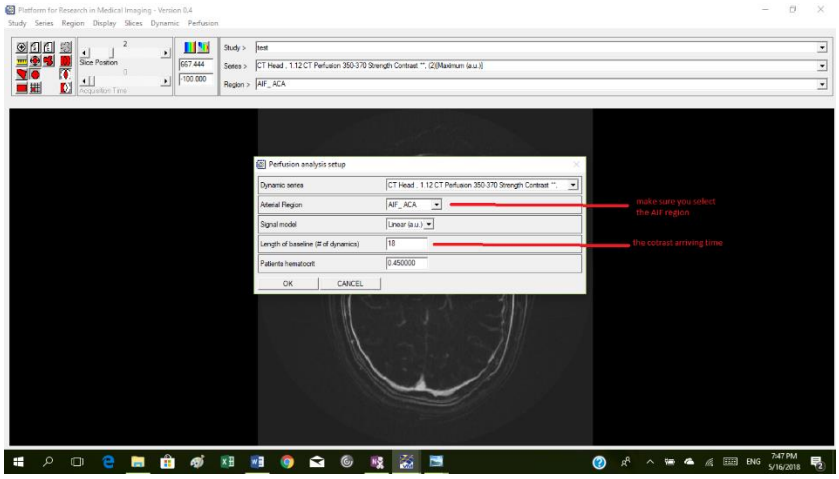

13- Different ROIs need to be drawn: (right side white matter area, left side white matter area, right side grey matter area and left side grey matter area).Open the plasma flow map then view it as coloured map then draw a white matter ROI on right side as the screen shot images below shown to follow the steps to draw the ROI on the opposite side as shown in the screen shots.

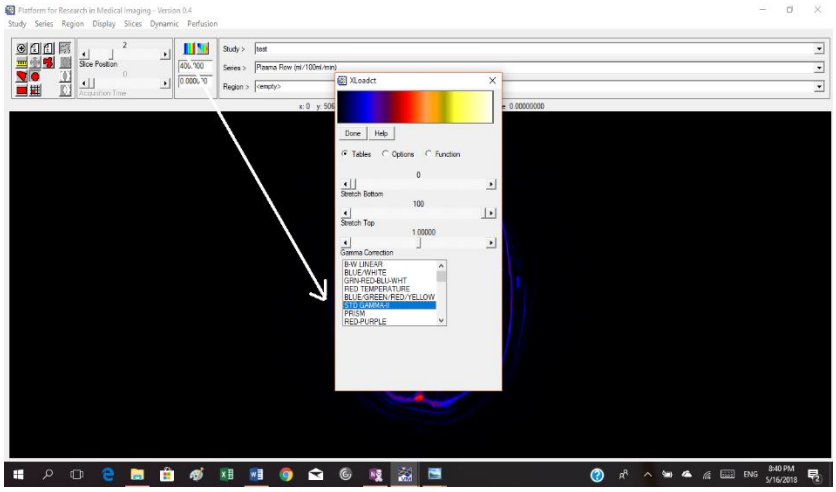

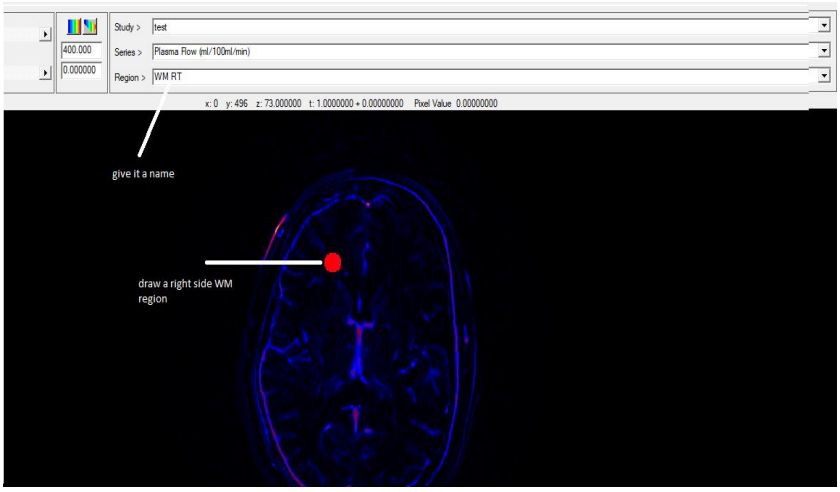

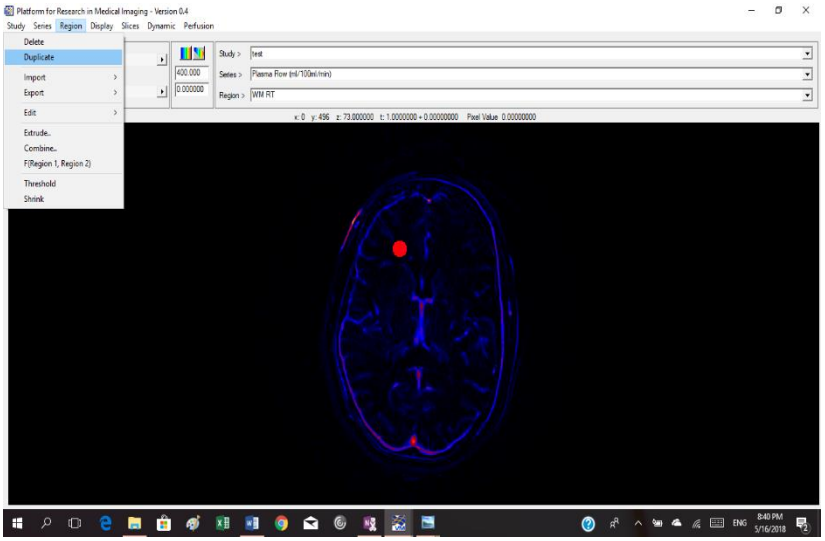

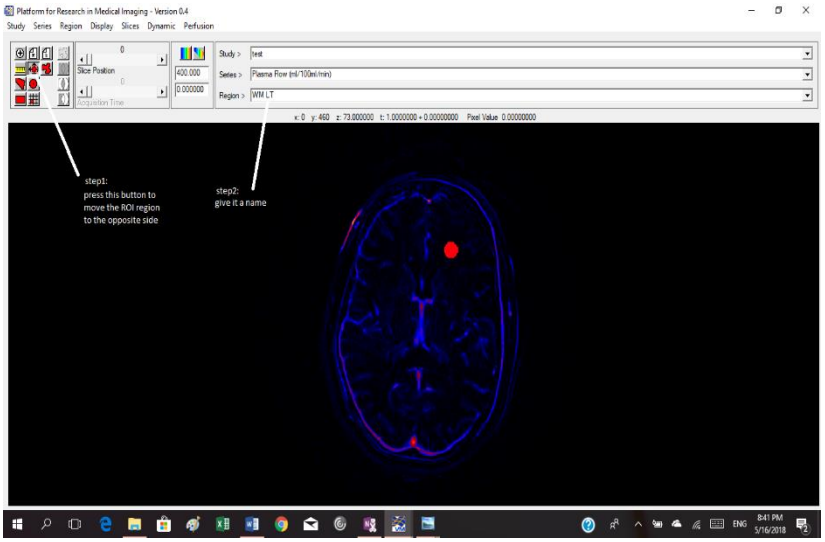

On the same slice, it is possible to draw the grey matter area on the Basal ganglia on both sides according to the steps on the images below:

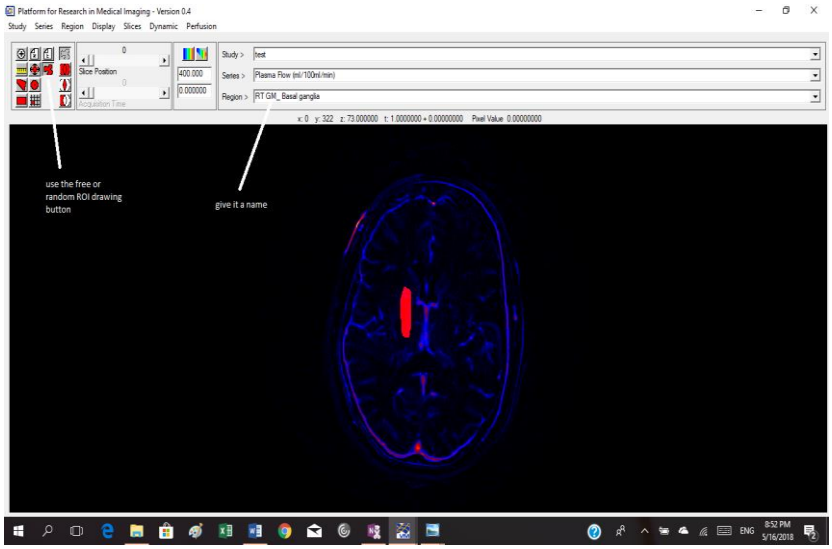

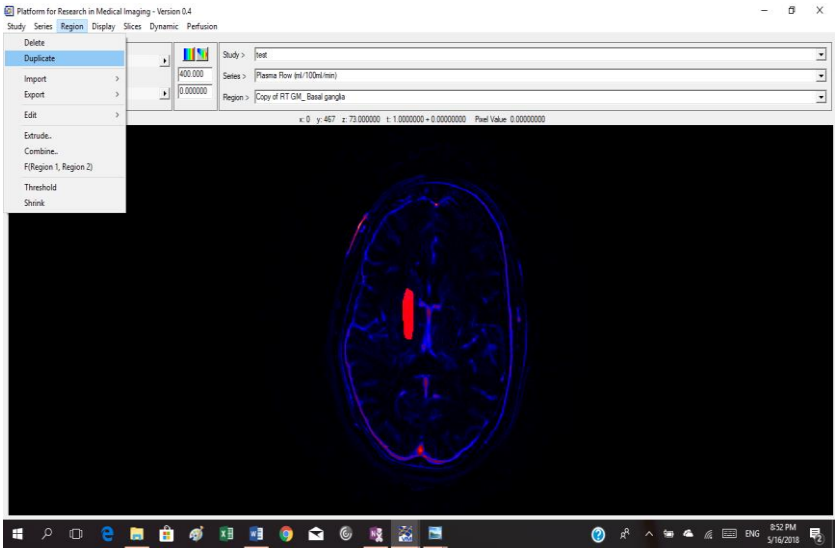

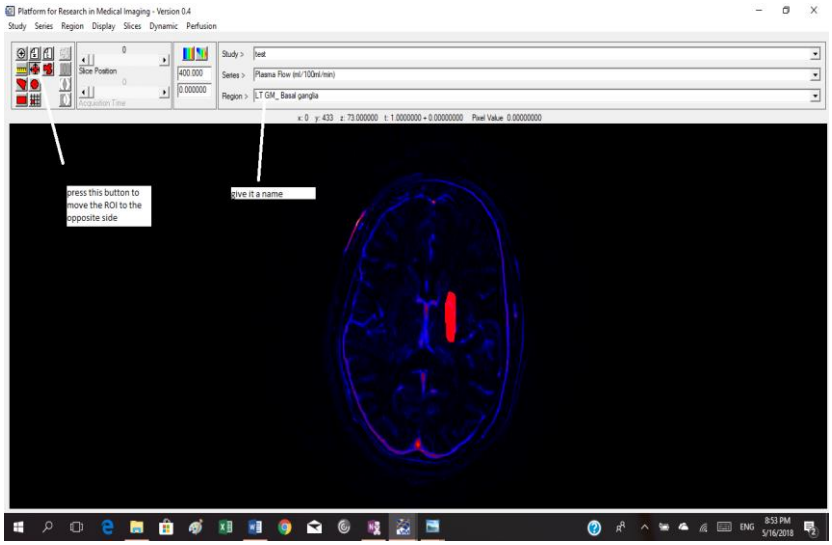

14- Some perfusion maps need to be filtered or smoothed to enhance the signal to noise, go (Slices > uniform soothing) or (Slices > Median filtering).

15- It is possible to view the values of each ROI such as: mean, median, standard deviation. To see that, go (Display > ROI Statistics).

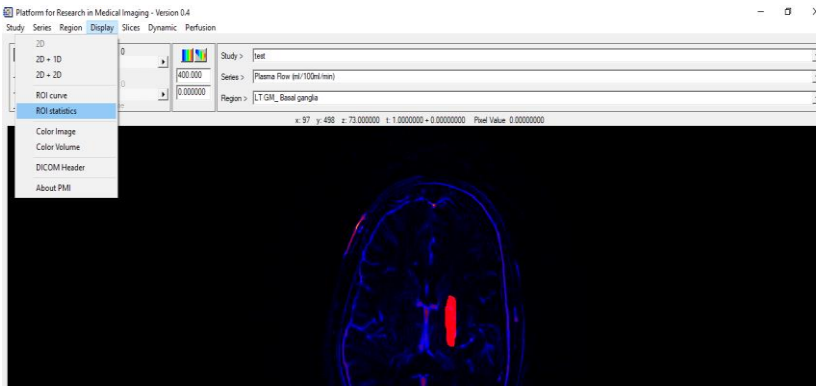

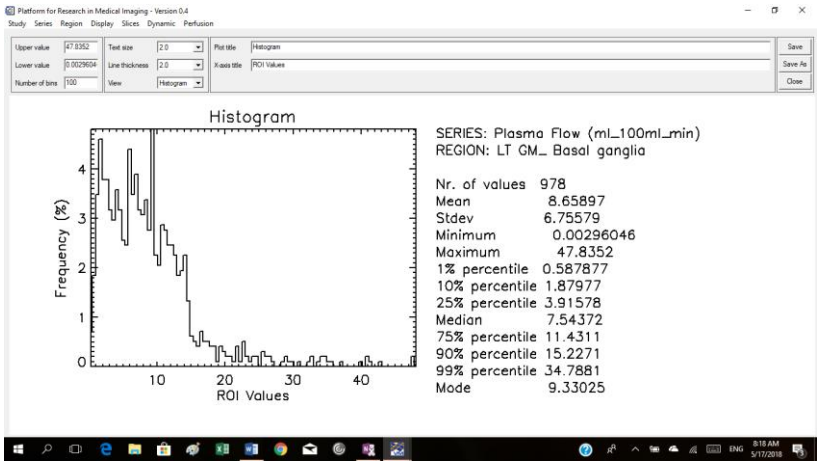

16- It is recommended, partial volume correction factor (PVC). It modifies volume-of-interest statistics or ROI statistics in order to compensate the Partial Volume Effect. It ensures the proper quantification of objects considering spill-over and spill-in between regions.To do that, open the extracellular volume “without filter or smoothing”, find a clear slice with the superior sagittal sinuses, the go (Region > threshold),then the ROI statistics can be displayed (follow the screen shot steps below) :

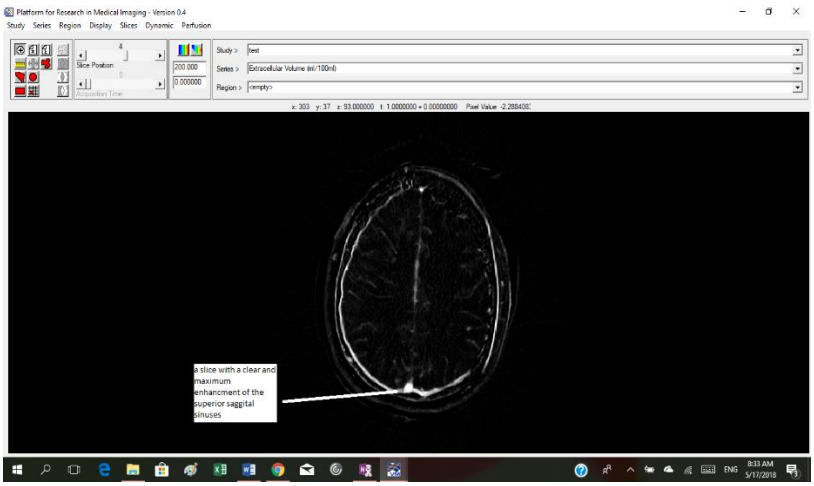

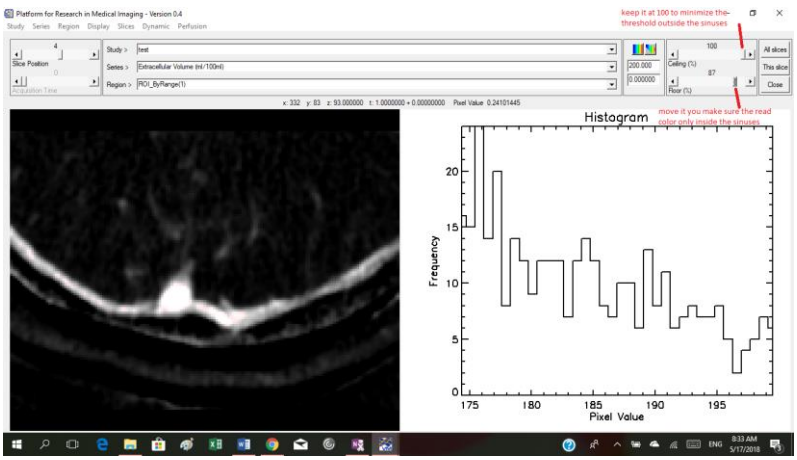

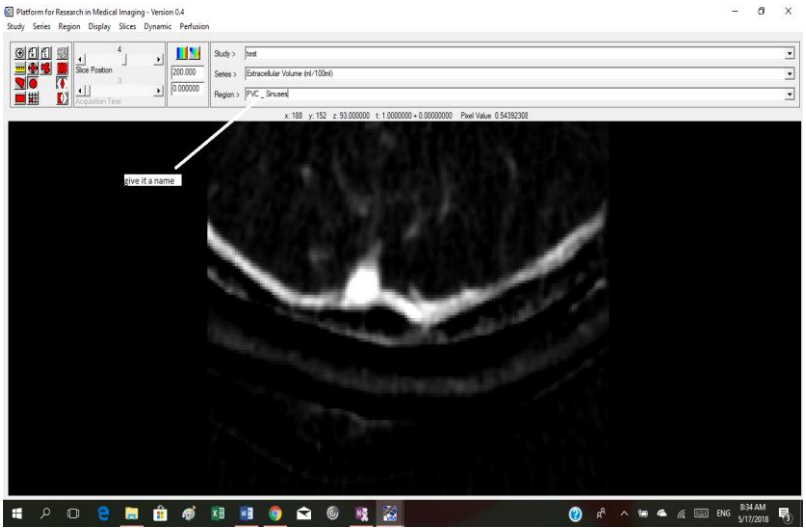

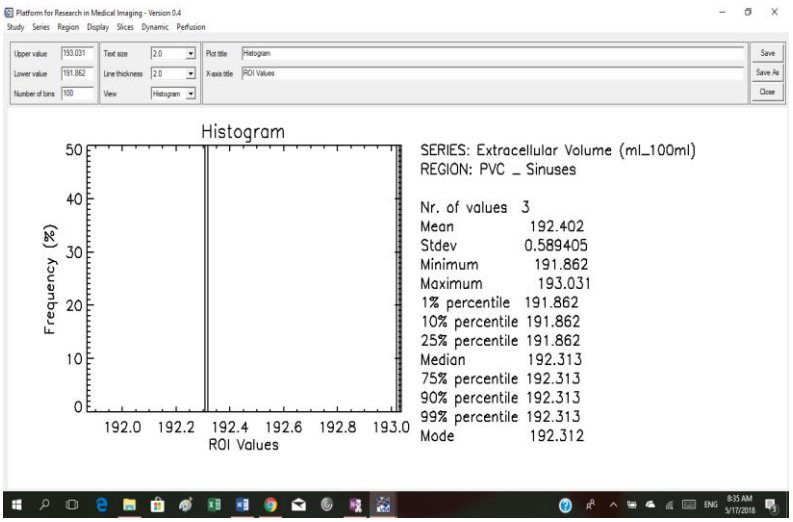

It is worth mentioning that, PVC = 0.55 / the mean ROI value

17- Once all the studies have been analysed and data has been collected, Excel sheet needs to be created included the CT perfusion three parameters mean and standard deviation values for each ROI region. It is worth mentioning that, the PMI program gives the plasma value instead of blood value. Therefore, to get the blood value for each parameter, small calculation needs to be done.

<u>To calculate Cerebral blood flow ”CBF” from the plasma flow:</u>

((Plasma flow = (1 – hematocrit) * CBF))

known that: hematocrit = 0.45

>> CBF = Plasma flow \ 0.55

To calculate Cerebral blood volume from the extracellular volume:

((extracellular volume = (1 – hematocrit) * CBV))

known that: hematocrit = 0.45

>> CBV = extracellular volume \ 0.55

To calculate Mean Transit Time from the Extracellular MTT:

MTT= CBV / CBF (the result is shown in minute unit according to the CBV and CBF units. In order to make the MTT more reliable, it is recommended to converted into second unit.

Note that, each CBF and CFV values should be corrected with the partial volume correction factor (PVC). To do that the value has to multiply with the PVC value.

18-A final step to do in Excel sheet, is to calculate the average, mean, standard deviation and median for each value of the parameters.